DOWN-REGULATION OF *PAX3* GENE EXPRESSION IN RHABDOMYOSARCOMA AND MELANOMA

AHMED A MASHUD

A thesis submitted as part of the requirement of the Manchester Metropolitan University for the award of the degree of Doctor of Philosophy in Biomedical Science

School of Healthcare Science
Faculty of Science and Engineering
The Manchester Metropolitan University
United Kingdom

2014

To

My wife Jamilatu

and

Children

DEDICATION

I dedicate this thesis to my family and friends for their support, prayer and best wishes throughout my PhD career.

DECLARATION

I declare that this work has not already been accepted for any degree and is not being currently submitted in support of an application for any degree in any higher learning institution, other than the degree of Doctor of Philosophy in Biomedical Science of the Manchester Metropolitan University.

AHMED A MASHUD

2014

ACKNOWLEDGEMENTS

Firstly, my humble acknowledgement goes to the ALMIGHTY for blessing, guiding, and protecting me throughout the journey of my PhD education. My special appreciation to the Government of Ghana for sponsoring my PhD cancer biology medical research programme in the United Kingdom for the development of my professional career. I extend my appreciation to the Ghana high commission in London for processing my tuition fees and stipends, as a representative of the Government of Ghana. I also recognise the support given to me by the Ghana Ministry of health, Korle-Bu Teaching Hospital of Ghana and the Head of department of pathology, University of Ghana Medical School for processing my sponsorship and study leave.

I wish to express my profound gratitude to my supervisors, Professor Patricia Kumar, Professor Shant Kumar, Dr. Lisa Lee-Jones and Dr. Qiuyu Wang for their guidance, support, constructive criticisms and advice throughout my research studies. I extend my special gratitude and appreciation to Professor Patricia Kumar and Professor Shant Kumar for their assistance and care given to my family and me throughout the difficult times in my research studies. Without this parental support, finishing my research work would have been more difficult for me.

I extend my special thanks to my wife for her support and encouragement as well as caring for the children in the UK, which has given me some peace of mind during my studies.

I would like to acknowledge my research colleagues Dr. Minche chen, Dr. Alexandra Bosutti, Dr. Faizan Abdul and Dr. Sabine Matou for their expert advice, suggestions, encouragement and keen interest in my research work. I also extend my special appreciation to the technical team including Ms Helen Sutton, Mr. Mike Head, Dr. Muhammad Saeed Ahmad, and Mr. Glen Ferris, all of the School of Healthcare Science of the Manchester Metropolitan University, for their technical support and assistance during my studies.

I would like to extend my special thanks to members of staff at the University of Manchester including, Dr. Leo Zeef, Dr. Mulle Smidge and Ms. Leanne Wordleworth

for assisting and running my microarray analysis (Microarray Analysis facility, University of Manchester, UK). My special thanks to Dr. Fiona Marriage for running my quantitative RT-PCR analysis (Manchester Institute of Biotechnology, University of Manchester, UK). I would also like to extend my special thanks to Dr. Jeff Barry and Dr. Mike Hughes for running my flow cytometry analysis (Paterson Institute for Cancer Research, University of Manchester, UK). My special thanks to Dr. Paul Fullwood and Ms Kimberley Swinton for sequencing my PBabe plasmid DNA (Sequencing Facility, University of Manchester, UK).

Finally but not the least, my special thanks to my parents and friends for their love, prayers and best wishes during my studies.

TABLE OF CONTENTS

ABSTRACT

The *PAX3* gene as a member of the paired homeodomain family of transcription factors plays a crucial role during embryonal development by regulating the early development of neural structures, derivatives of the neural crest and skeletal muscles. Following embryonal development, the *PAX3* expression is switched off. Mutations in the *PAX3* gene are commonly associated with Waardenburg's syndrome and in Craniofacial-hand syndrome. Aberrant re-expression of *PAX3* after embryogenesis plays a key role in the onset, growth, survival and progression of rhabdomyosarcoma, melanoma and neuroblastoma. Alternative splicing of *PAX3* results in seven transcript variants (*PAX3a, PAX3b, PAX3c, PAX3d, PAX3e, PAX3g* and *PAX3h*), the interactions of which with other downstream targets, make it difficult for manipulation and the development of potent chemotherapeutic regimens to effectively treat malignant tumours including rhabdomyosarcoma, melanoma and neuroblastoma which have unfavourable prognostic outcomes.

This research was aimed at down-regulating *PAX3* gene expression in human rhabdomyosarcoma and melanoma cell lines, subsequently identifying the downstream target genes of *PAX3* and determining the effects on cell growth and survival. The expression of *PAX3* in human rhabdomyosarcoma and human melanoma cell lines was significantly down-regulated using novel pre-designed *PAX3* small interference RNA molecules, at a final concentration of 0.5µM in an *in vitro* transient transfection. The three prime Affymetrix microarray analyses showed more than a four-fold and a two-fold down-regulation of *PAX3* gene expression in the human JR1 embryonal rhabdomyosarcoma and RH30 alveolar rhabdomyosarcoma cell lines respectively, whilst in the human A375 melanoma cell line, over an eight-fold down-regulation of *PAX3* expression was demonstrated relative to negative control cells. A quantitative RT-PCR analysis, which was used in validating results of the Affymetrix array, confirmed the knockdown of *PAX3* in both human rhabdomyosarcoma and melanoma cell lines. A semi-quantitative RT-PCR analysis of gene expression revealed at least 90% down-regulation of all *PAX3* variant expression in JR1, RH30 and A375 cell lines relative to negative controls cells. Higher levels of gene silencing were observed in the JR1 cell line than in either RH30 or A375 cell lines. Western blotting analysis, which

quantified the level of *PAX3* gene knockdown, indicated a 98%, 92% and 90% reduction of *PAX3* protein in JR1, RH30 and A375 cell lines respectively. This down-regulation of *PAX3* expression significantly inhibited tumour cell growth, proliferation, migration, adhesion, invasion, and induced apoptosis of JR1, RH30 and A375 cell lines *in vitro*. These results were explainable by the particular genes that were up- or down-regulated by *PAX3*, which were correlated with the microarray results and the quantitative RT-PCR experiments. The expression of *PAX3* gene has been previously demonstrated to promote tumourigenesis of rhabdomyosarcoma and melanoma. Results of this present study suggest that down-regulation of *PAX3* might inhibit the progression of rhabdomyosarcoma and melanoma and *PAX3* thus could be a suitable target for the development of potent chemotherapy.

Silencing of *PAX3* in these cell lines resulted in the alteration of expression of a host of downstream target genes, which *PAX3* uses in the modulation of cellular activities, including cell growth, proliferation, migration, adhesion, metastatic invasion and apoptosis of the rhabdomyosarcoma and melanoma cell lines.

Publications and Presentations

Publications

Fang, W. H., Wang, Q., Li, H. M., Ahmed, M., Kumar, P., Kumar, S. (2014). '*PAX3* in neuroblastoma: oncogenic potential, chemosensitivity and signalling pathways'. J. Cell Mol, Med., vol.18, issue 1, pp. 38-48.

Fang, W. H., Ahmed, M., Wang, Q., Li, H.M., Kumar, P., Kumar, S. (2013). '*PAX3* promotes tumour progression via CD105 signaling'. Microvasc Res., vol. 86, pp.42-3.

Oral/ Poster Presentations

Ahmed, M., Wang, Q., Lee-Jones, L., Kumar, S., Kumar, P. (2010). 'Down-regulation of *PAX3* gene expression in rhabdomyosarcoma. Postgraduate Researchers in Science Medicine Conference, Prism 2010, Lancaster University, United Kingdom, 23/09/2010.

Ahmed, M., Wang, Q., Lee-Jones, L., Kumar, S., Kumar, P. (2010). 'Down-regulation of *PAX3* gene expression in melanoma'. 1st Faculty of Science and Engineering Research and Development Day at Manchester Metropolitan University, April 2010, United Kingdom.

Ahmed, M., Wang, Q., Kumar, S., Kumar, P., Lee-Jones, L. (2012). 'Down-regulation of *PAX3* gene expression in rhabdomyosarcoma and melanoma'. National Cancer Research Conference, NCRI November 2012, pp.263, Liverpool, United Kingdom.

Ahmed, M., Wang, Q., Kumar, S., Kumar, P. (2009). 'Down-regulation of *PAX3* gene expression in melanoma'. Postgraduate Researchers in Science Medicine Conference, Prism 2010, Lancaster University, United Kingdom, 23/09/2010.

Conferences Attended

National Cancer Research, Institute Cancer Conference, Liverpool, November 2012, United Kingdom.

Manchester Cancer Research Centre Conference, University of Manchester, Manchester, January 2010, United Kingdom.

Postgraduate Researchers in Science Medicine, Prism 2009, University of Manchester, Manchester, October 2009, United Kingdom.

List of Figures

List of Tables

List of Abbreviations

A375	Malignant melanoma cell line
ADAM23	ADAM metallopeptidase domain 23
ACTB	Actin, beta
AEN	Apoptosis enhancing nuclease
AKT	V-AKTmurine thymoma viral homolog 3 oncogene
ARMS	Alveola rhabdomyosarcoma
AS	Alternative Slicing
ANAPC5	Anaphase promoting complex subunit 5
BAX	BCL2-associated X protein
BCL2	B-Cell lymphoma 2
BIRC5	Baculoviral IAP repeating containing 5 (survivin)
BNIP1	BCL2/adenovirus E1B 19kDa interacting protein 1
BNIP3	BCL2/adenovirus E1B19kDa interacting protein 3
bp	Base pair
BRCA1	Breast cancer 1
BRCA2	Breast cancer 2
β2M	Beta-2-microglobulin
Brn-2	POU domain transcription factor 2
BSA	Bovine serum albumin
BTG2	B-cell translocation gene 2
BUB1	Budding uninhibited by benzimidazoles 1
CALM3	Calmodulin 3
CAPRIN1	Cell cycle associated protein 1
CASP3	Caspase 3, apoptosis-related cysteine peptidase
CASP4	Caspase 4, apoptosis-related cysteine peptidase
CASP7	Caspase 7, apoptosis-related cysteine peptidase
CCNA	Cyclin A
CCNA2	Cyclin A2
CCNBI	Cyclin B1
CCND1	Cyclin D1
CCND2	Cyclin D2
CCND3	Cyclin D3
CCNE1	Cyclin E1
CDC25A	Cell division cyclin 25 homolog A
CDC25B	Cell division cycle 25 homolog B
CDC25C	Cell division cycle 25 homolog C
CDC42EP3	CDC42 effector protein (Rho GTPase binding)
CDC42SE1	CDC42 small effector 1
CDC7	Cell division cycle 7 homolog
CDCA3	Cell cycle associated 3
CDCA7	Cell division cycle association 7
CDH2	Cadherin 2, type 1 N-cadherin (neuronal)
CDK1	Cyclin-dependent kinase 1
CDK2	Cyclin-dependant kinase 2
CDK4	Cyclin-dependant kinase 4
CDK5	Cyclin-dependent kinase 5

CDK6	Cyclin-dependent kinase 6
CDKN1A	Cyclin-dependent kinase inhibitor 1A
CDKN2C	Cyclin-dependent kinase inhibitor 2C (p18)
CDKN3	Cyclin-dependent kinase inhibitor 3
cDNA	Complementary DNA
CGRRF1	Cell growth regulator with ring finger 1
CHEK1	CHK1 checkpoint homolog (S. pombe)
CHEK2	CHK2 checkpoint homolog (S. pombe)
CIB1	Calcium and integrin binding 1
CITED2	Cbp/p300-interacting transactivator with Glu/Asp-rich carboxy-terminal domain2,
C-MY	C-myc binding protein
COL1A1	Collagen type I, alpha 1
COL3A1	Collagen type III, alpha 1
CXCR4	Chemokine (C-X-C motif) receptor
CYB5B	Cytochrome b5 type B
DAPI	Diamidino-2-phenylindole
DAXX	Death-domain associated protein
DDB2	Damage-specific DNA binding protein 2, 48kDa domain 2,
DHFR	Dihydrofolate reductase
DDH2O	Double distilled water
DMSO	Dimethyl sulphoxide
DNA	Deoxyribonucleic acid
E2F2	E2F transcription factor 2
E2F7	E2F transcription factor7
E2F8	E2F transcription factor 8
ECM	Extracellular matrix
EDN3	Endothelin 3
ENDRA	Endothelin receptor type A
ETS1	V-ETS erythroblastosis virus E26 oncogene
et al	And others
FAIM	Fas apoptotic inhibitory molecule
FGD4	FYVE, Rho GEF and PH domain containing 4
FNDC5	Fibronectin containing sub-unit 5
FOXO1	Forkhead box O1
FOXO3	Forkhead box O3
FSCN1	Fascin homolog 1, actin bunding protein
FYVE	RhoGEF and PH domain containing 4
GADDβ45	Growth arrest and DNA-damage-inducible, beta
GAPDH	Glyceraldehyde-3-phosphate dehydrogenase
GAS1	Growth arrest-specific 1
GINS1	GINS complex subunit 1(Psf1 homolog)
GRK6	G protein coupled receptor 6 kinase
GTSE1	G-2 and S-phase expressed 1
HES1	Hairy and enhancer of split 1
HD	Homeodomain
HIRA	HIR histone cell cycle regulation defective homolog

HMOX1	Heme oxygenase 1
HMBS	Hydroxymethylbilane synthase
HP1γ	Heterochromatin protein Lambda binding 1,
hr	Hour
H-RAS	V-Ha-ras Harvey rat sarcoma oncogene
HUS1	Hus1 checkpoint homolog
ID3	Inhibitor of DNA binding 3
IGFβP3	Insulin-like growth factor binding protein 3
IGFβP5	Insulin-like growth factor binding protein 5
IPO13	Importin 13
IR	Infrared
ITGβ1	Integrin beta 1
ITGβ5	Integrin beta 5
JAK2	Janus kinase 2
JAM2	Junctional adhesion molecule 2
JR1	Embryonal rhabdomyosarcoma cell line
JUN	Jun oncogene
KAP1	Kinase A anchor protein 1
KITLG	Kit ligand
LAMA1	Laminin alpha 1
Lb	Luria Bertani
LOC	Similar to C-Jun
MAP1A	Microtubule-associated protein 1A
MAPK 3	Mitogen-activated protein kinase 3
MAPK9	Mitogen-activated protein kinase 9
MCAM	Melanoma cell adhesion molecule
MCL1	Myeloid cell leukemia sequence 1 (BCL2-related)
MCM3	Minichromosone maintenance complex 3
MDM2	Mdm2 p53 binding protein homolog
MELK	Maternal Embryonic leucine zipper kinase
MITF	Microphthalmia associated transcription factor
MKNK2	MAP kinase interacting serine/threonine kinase 2
MMP2	Matrix metallopeptidase 2 A (pseudo)
MRPL16	Mitochondria ribosomal protein L16
MSH2	Muts homolog 2
MSX1	Msh homeobox 1
MTSS1	Metastasis suppressor 1
MXRA7	Matrix-remodelling associated 7
MYC	V-myc myelocytomatosis viral oncogene
MYOD1	Myogenic differentiation 1
MYOG4	Myogenin (myogenic factor 4)
NAMPT	Nicotinamide phosphoribosyl transferase
NCAPH	Barren homolog 1
NDRG1	N-myc downstream regulated 1
NID1	Nidogen 1
NC	Neural crest
NC-siRNA	Scrambled non-targeting siRNA negative control
NUSAP1	Nucleolar and spindle associated protein 1

OP	Octapeptide domain
P15	Cyclin-dependent kinase inhibitor 2B
P16	Cyclin-dependent kinase inhibitor 2A
P300	CREB binding protein E1A binding protein
PAK2	P21 protein (Cdc42/Rac)-activated kinase 2
PAX3	Paired box3
PAX3-siRNA	Pre-designed siRNA targeting PAX3
PBK	PDZ binding kinase
PCDH18	Proto cadherin 18
PCDH7	Proto cadherin 7
PCNA	Proliferating cell nuclear antigen
PDRG1	P53 and DNA-damage regulated 1
POLA2	Polymerase (DNA directed alpha 2)
pRB	Phosphorylated Retinoblastoma
PRM 2	Protein arginine methyltransferase 2
PTEN	Phosphatase and tensin homolog
RAB27B	RAB27B, member RAS oncogene family
RASA2	RAS p21 protein activator 2
RB	Retinoblastoma
RH30	Alveola rhabdomyosarcoma cell line
RBBP4	Retinoblastoma binding protein 4
RECK	Reversion-inducing-cysteine-rich protein K
RMS	Rhabdomyosarcoma
RNA	Ribonucleic acid
ROCK2	Rho-associated, coiled-coil containing protein kinase 2
RPL32	Ribosomal protein L32 pseudogene 3
	flavoprotein pseudogene 1
RPL13A	Ribosomal protein L13a
HPRT1	Hypoxanthine phosphoribosyltransferase 1
RXA	Retinoid X receptor alpha
SAM68	Src-associated in mitosis with a molecular weight of 68 kDa
SDHA	Succinate dehydrogenase complex, subunit A,
Sec	Seconds
SELPLG	Selectin P ligand
SENP5	SUMO1/sentrin specific peptidase
SHC4	Src homology 2 domain member 4
siRNA	Small interfering ribonucleic acid
SKP2	S-phase kinase- Associated protein 2(p45)
SMAD2	SMAD family member 2
SMC1	Structural maintenance of chromosomes 4
SMEK1	SMEK homolog 1, suppressor of mek1
SOSTDC1	Selerostin domain containing 1
SPCS3	Signal peptidase receptor complex subunit 3
SRY 10	Sex determining region-box 10
SRY 9	Sex determining region-box 9
TA	Transactivating domain
TAZ	Tafazzin
TBX18	T-box 18

TFDP1	Transcription factor DP-1
TGFβ2	Transforming growth factor, beta 2
TGFβ3	Transforming growth factor beta 3
TMBIM4	Transmembrane BAX inhibitor motif containing 4
TNC	Tenascin
TNFRSF19	Tumour necrosis factor receptor superfamily member 19
TP53	Tumour protein p53 inducible protein
TRAF1	TNF receptor-associated factor 1
TRIB3c	Tribbles homolog 3
TUBB2 C	Tubulin beta 2c
UV	Ultraviolet
VCAN	Versican
VEGFA	Vascular endothelial growth factor A
ZEB2	Zinc finger E-box binding homolog 2

CHAPTER 1

INTRODUCTION

CHAPTER 1: INTRODUCTION

1.1. Overview of Cancer

Human physiological activity depends on the normal function of cells, which are the building blocks and functional units of life in all living organisms. At the cellular molecular level, genes contained in the DNA of cells regulate and control normal cellular function including cell cycle, proliferation, migration, adhesion, cell-cell communication and apoptosis which govern normal organ physiology (Marchetti *et al.,* 2012). Gene activities in living organisms are often determined by investigating gene expression, which represent the transcription of DNA into RNA and translation of RNA into protein (Hebert and Molinari, 2007). Inappropriate gene expression patterns, resulting from malformation of structural components of DNA motifs, may lead to mutational abnormalities and sometimes cancer with impairment of cell function (Damm *et al.,* 2012; Michael *et al.,* 2012).

Cancer is a disease of cell abnormality characterised by uncontrollable cell growth, cell cycle, proliferation, migration, adhesion, evasion of apoptosis and aggregation of cells to form tumours in organs and body cavities. Cancer cells in the body fails to respond to stimuli and allow continual cell growth, proliferation and inhibition of apoptosis to outgrow normal cells, which in contrast respond to stimuli for normal functional activity. Many different forms of cancer can develop in virtually any organ or tissue of the body. Some of the cancers of various organs of the body include rhabdomyosarcoma, melanoma, Ewing's carcoma, neuroblastoma, medulloblastoma, leukaemia, Hodgkin's lymphoma, non-Hodgkin's lymphoma, breast cancer, lung cancer, cervical cancer, prostate cancer, colon cancer, kidney cancer, liver cancer, ovarian cancer, testicular cancer, thyroid cancer and uterine cancer (Moscow and Cowan, 2011).

Several contributory risk factors of cancer include genetic mutation; carcinogens such as benzene, excessive alcohol, and other chemicals; environmental toxins; ultra-violet radiation; excessive sunlight; smoking; viruses and other unknown factors. These factors cause damage or mutations to DNA, which leads to uncontrolled cell growth because of abnormal activation of the cell division and apoptosis genes. During DNA damage in normal cells, the DNA controls oncogenes in cell division and tumour suppressor genes

to inhibit cell division to allow the DNA-repair genes to effectively repair the damaged DNA, whilst the apoptosis regulatory genes are directed to induce cell apoptosis if the DNA damage is beyond repair. In cancer cells however, mutations inhibit the normal function of oncogenes, tumour suppressor genes, and apoptosis genes leading to uncontrollable cell growth. Gene mutations renderer cells unable to correct DNA damage and unable to induce apoptosis (Thun and Jemal, 2011).

Various cancers present varying signs and symptoms depending on the type and location of the cancer. For instance, lung cancer is associated with coughing, breathing difficulty, and chest pain while in colon cancer, diarrhoea, constipation and bloody stools are commonly seen. Generally, many cancers present symptoms such as fever, fatigue, chills, loss of appetite, malaise, night sweats and weight loss. Symptoms of some cancers are observed at the advanced stage of the disease, whilst other cancers are symptomless (Munde *et al*., 2014).

Several diagnostic tools for cancer include histological examination of tumour and bone marrow biopsies, molecular biological diagnosis of specific tumour markers, full blood cell counts, liver function tests, magnetic resonance imaging, positron emission tomography, computed tomography or, ultrasound scans and chest x-ray. Available treatment schemes for various cancers depend on the type, stage, and location of the cancer and include surgery, radiation and chemotherapy (Carrillo *et al.,* 2014).

Cancer cells continue to evade apoptosis, which makes treatment unsuccessful in most malignant cases after several treatment cycles, and this pose a great challenge to medical research. Currently, new treatment modalities aim at treatment of cancer cells at the molecular level by targeting cancer specific genes or proteins using targeted genetherapy, booster of patient's immune system using immunotherapy and modulation of patient's hormonal activities using hormonetherapy, as well as nanoknife tumour treatment using electric current are being studied (Carrillo *et al.,* 2014).

1.2. The Paired Box (*PAX*) Genes

Paired box (*PAX*: human*) / (Pax*: mouse*)* genes, encode important developmental transcriptional factors and belong to the homeobox (*HOX*) family of developmental genes (Li[1] and Eccles, 2012). *PAX/Pax* genes have individual functions and therefore differ from other members of the *HOX* family of developmental genes, which perform functions in temporal or partial combination (Kumar, 2009; Kang *et al*., 2011). The *PAX/Pax* family which was initially identified in *Drosophila* and later found to be conserved across species, has an evolutionarily conserved amino-terminal 128 amino-acid DNA-binding paired domain (PD) (384 base pairs), which facilitates *PAX/Pax* binding to DNA sequences during transcription (Martin and Wang, 2011). Apart from the PD, several *PAX* proteins have a homeodomain (HD) for DNA interaction (Martin and Wang, 2011).

Nine *PAX* family members, crucial in embryonic and postembryonic development, have been described in vertebrates (Li[1] and Eccles, 2012). *PAX* transcription factors residing on different chromosomal locations have been described in man (*PAX1-PAX9*) and mice (*Pax1–Pax9*) with orthologous genes occurring in worms, flies, fish and birds (Li[1] and Eccles, 2012).

The mammalian PAX protein has sequence homology to the Pax protein identified in the *Drosophila,* segmentation pair-rule class proteins (prd), the *Drosophila* segmentation polarity class protein gooseberry proximal (gsb-p) and gooseberry distal (gsb-d) and the *Drosophila* proteins, pox-meso and pox-neuro (Ravasi *et al.,* 2010). There is 98% sequence homology of amino acids in human and mouse. Quail has 95% sequence similarity with humans and mice, with slight variation in intron 8 (Moretti *et al.,* 2012).

1.2.1. The *PAX/Pax* Gene Ancestral Family

PAX/Pax is sub-divided into five large sub-groups of *Drosophila* / vertebrate genes including *Pax1-9/meso, PAX/PaxD/3-7/ paired/gooseberry, PAX/Pax6-4/eyeless, PAX/PaxB/2-5-8/sparkling* and *PAX/PaxA/neuro* (Aradhya *et al*., 2011). *PAX/Pax* has been cloned from a variety of other metazoans such as arthropods, nematodes and several vertebrates (Kusakabe *et al.,* 2011; Mudge *et al.,* 2011). Ruzickova *et al.* (2009) which has demonstrated that their roles are highly conserved across the animal kingdom. *PAX/Pax* homologues, which are found in simple organisms include *PAX/PaxA* and *PAX/PaxB* in *hydra, PAX/PaxA, PAX/PaxB* and *PAX/PaxD* in corals and *PAX/PaxB/2-5-8/sparkling*-homologue in sponges. Over 100 *PAX/Pax* genes are accessible in scientific databases (Chuang *et al*., 2012). *PAX/PaxA* genes containing only a paired box, underwent double autonomous homeobox capturing events producing the *PAX/PaxB/2-5-8/sparkling* and *PAX/Pax1-9/3-7/4-6* family groups based on an analysis of their HD. Reports indicate that the initial capturing event occurred in advance of sponge evolution whereas the subsequent event happened ahead of the triploblast split among crucians (Jo *et al.,* 2011). This scenario has been represented as an evolutionary tree, comprising *PAX/PaxC* that is an ancestral form of *PAX/Pax1* and *9/meso*, *PAX/Pax3* and *7/gooseberry/paired* and *PAX/Pax4* and *6/eyeless* (Birrane *et al*., 2009).

1.2.2. *PAX/Pax* Gene Structure

PAX/Pax interacts with DNA using a PD made up of two helix-turn-helix (HTH) motifs and a β-hairpin major domain. Mutations and other abnormalities occur in these in both mice and humans (Aggarwal *et al.,* 2011). The defining common feature of the *PAX/Pax* PD (Apuzzo and Gros, 2006), which contains a 128-amino-acid DNA-binding motif consisting of two discrete subdomains, which act together to distinguish specific DNA sequences (Chuang *et al.,* 2012). In *Drosophila*, the PD has a bipartite domain, comprising an amino-terminal subdomain (NTD or PAI) and a carboxyl-terminal subdomain (CTD or RED) (**Fig. 1.1**), (Devi *at al.,* 2009).

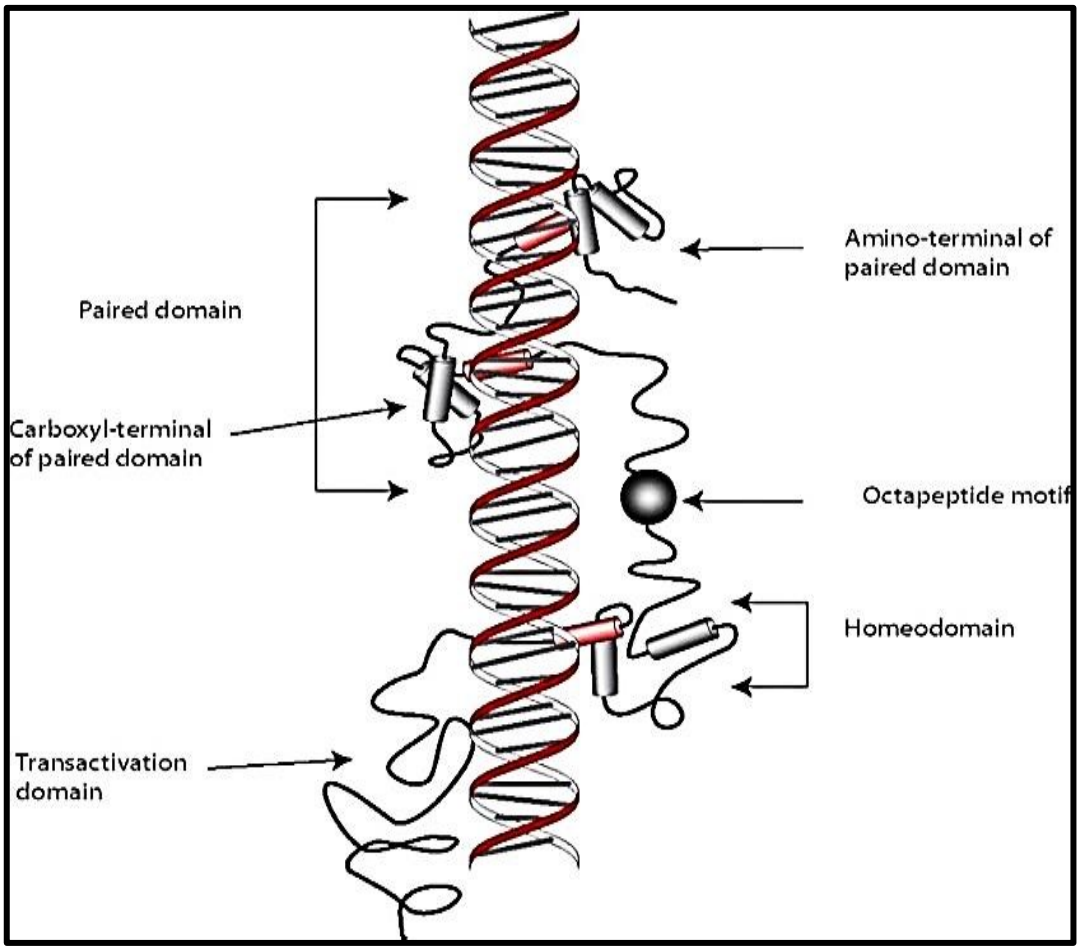

Figure 1.1 Molecular crystal structural domains of *PAX* gene family (Blake and Ziman 2003**).** Structural domains of PAX/Pax protein are: PD, HD, TA and octapeptide (OP).

The two sub-domains, which interact with each other, each comprise three α-helices, which accumulate to form HTH patterns (Sergio and Philippe, 2007). Conversely, identification of the helix (α3) side chains using the amino-terminal sub-domain anchorage at the DNA major-groove, binding to the DNA in a particular fashion, is suggestive of binding of a λ repressor with the DNA (Gregory, 2006). Reports indicate that the HD of NTD sub-domain comprises an N-terminal β-turn, β-hairpin known as Wing, which can also contribute to DNA-binding, allowing the linker molecule to bind the DNA minor-groove (Sergio and Philippe, 2007). In paired protein, the binding of DNA with protein is controlled by the NTD sub-domain (Narayansingh and Ouellette, 2011). However, in other *PAX/Pax* proteins, the CTD subdomain seems to induce modulation of binding specificity at the NTD subdomain. *PAX/Pax* genes encoding a carboxyl-terminal transactivating domain (TA) have the PD located in the NTD, while

HD and octapeptide regions (OP) occur in both the CTD and the serine-threonine-proline-rich C-terminus (Corry *et al.,* 2010). *PAX/Pax* proteins with a HD interact with an ATTA sequence (Wang[2] *et al.,* 2011). In addition, the *PAX/Pax* proteins can bind as dimers through their HD to a palindromic motif with the consensus sequence TAAT (N2-3)/ATTA (P2 or P3 sites respectively) and other targets are likely to exist for the CTD sub-domain (Birrane *et al.,* 2009). Therefore, some *PAX/Pax* proteins have at least three distinct means of binding DNA (Apuzzo and Gros, 2006).

Furthermore, different *PAX/Pax* proteins and their alternatively spliced isoforms use different subdomains for DNA-binding to mediate the specificity of sequence recognition (Buckingham[1], 2007). The amino acid composition of the NTD sub-domain residues (42, 44 and 47) is essential in determining the specificity of DNA sequence recognition (Apuzzo and Gros, 2006; Sergio and Philippe, 2007) by *PAX5/Pax5* and *PAX6/Pax6* (Rowan *et al.,* 2010). Biochemical analysis revealed that the CTD of certain *PAX/Pax* proteins, such as *PAX5/Pax5,* directly links DNA on other binding sites (Fujita and Fujii, 2011). Apart from linking the amino and carboxyl terminal regions, DNA interaction is further enhanced by a linker that induces substantial interactions with the minor-groove phosphodiester backbone (Apuzzo and Gros, 2006; Birrane *et al.,* 2009). Several developmental irregularities, which arise from missense mutations in both the β-hairpin and β-turn motifs of the PD, demonstrate their functional significance in the Pax protein (Sergio and Philippe, 2007; Birrane *et al.,* 2009).

The PD contains three sub-domains, which show differences in DNA-binding, enabling the PD protein to act as an activator or repressor (Chao *et al.,* 2013). Another important feature of PD-DNA interactions is their relatively relaxed nucleotide sequence specificity allowing *PAX/Pax* proteins to mediate transcriptional activation or repression (Robson *et al.,* 2006; Corry *et al*., 2010). The role of *PAX/Pax* protein as transcriptional activators or repressors has been demonstrated through their interaction with other transcription factors to induce target promoters (Buchberger *et al.,* 2007). Many *PAX/Pax* proteins, including *PAX1/Pax1, PAX2/Pax2, PAX3/Pax3, PAX6/Pax6* and *PAX8/Pax8* have similar sequence recognition enabling different Pax proteins to identify similar downstream targets (Chao *et al.*, 2013). Furthermore, PAX/Pax proteins which

show great flexibility in DNA-binding, interact with several sequences that are not related (Liu[2] and Xue, 2011). Identification of several downstream targets by PAX/Pax proteins is mediated through flexible interaction of either PAI and RED subdomains or the HD to induce gene modulation. Interaction of Pax proteins with several transcription factors is facilitated by their ability to identify inconsistent sequences (Shin *et al.,* 2012).

Following embryonic development, *PAX* gene expression is switched off. Few tissues show continual expression of *PAX* in adult life or re-expression (Kusakabe *et al.,* 2011). In adult tissues, *PAX/Pax* directs organ-specific regenerative events and prevents stress-induced cell death (Zhang[1] *et al*., 2012). The cellular functions of PAX/Pax proteins, including apoptosis resistance and repression of terminal differentiation, may possibly be subverted during the progression of a number of specific malignancies (Ozcan *et al.,* 2011).

1.2.3. Function of *PAX/Pax* Genes

Generally, PAX/Pax proteins act as transcription factors, regulating diverse signal transduction pathways and organogenesis during embryonic development by influencing cell proliferation and self-renewal, resistance to apoptosis, embryonic precursor cell migration, coordination of specific differentiation programmes and prevention of terminal differentiation (Hayashi *et al*., 2011; Liu *et al.,* 2012). PAX/Pax proteins influence the development of many tissues and organs in mammals, including muscle, thymus, thyroid, pancreas, neurons, eyes and kidney (Singh *et al.,* 2011). Recent studies have identified the role of PAX/Pax proteins in specific stem cell or progenitor cell populations and of PAX3/Pax3 in particular in differentiation of neural crest cells, myoblasts, melanocytes, B-lymphocytes and neurogenesis (Murdoch *et al.,* 2012; Sanchez-Ferras *et al.,* 2012). PAX/Pax proteins are sub-grouped into four groups (I-IV) based on structural similarities. The number of exons, the bases and amino acid composition identify the various PAX/Pax groups (**Table 1.1**) (Haldeman-Englert *et al*., 2012).

Table 1.1 Compositions of PAX/Pax groups

Group	PAX/Pax	Number of Exons	Number of Bases	Number of Amino Acid
I	PAX1 PAX9	4 4	1,323 1,644	440 341
II	PAX2 PAX5 PAX8	12 10 11	4,261 3,644 2,526	417 391 451
III	PAX3 PAX7	10 8	7,678 2,260	479 520
IV	PAX4 PAX6	9 12	2,010 5,656	350 422

Various PAX/Pax groups are differenciated from each other because of the differences in structural composition of the number of amino acids, bases and exons. (Adapted from Birrane *et al.,* 2009; http://ghr.nlm.nih.gov/).

Differences in fixed radical amino acids among PAX protein are important for their sequence recognition specificities based in their structural domains (Holland and Short, 2010).

The phylogenetic analysis of PAX proteins demonstrated the existence of four fixed radical amino acid differences between sub-group **I** and sub-group **III**, located exclusively in the N-terminal alpha helices (Hayashi *et al.,* 2011). Similarly, sub-groups **II** and **IV** have three fixed radical amino acid differences in alpha helices, existing at positions different from those of sub-groups **I** and **III**.

1.2.4. *PAX/Pax* Gene Classification and Chromosomal Location

Members of *PAX/Pax* gene family are located on separate chromosomes in mammals (**Fig. 1.2**) (Chuang *et al.,* 2012).

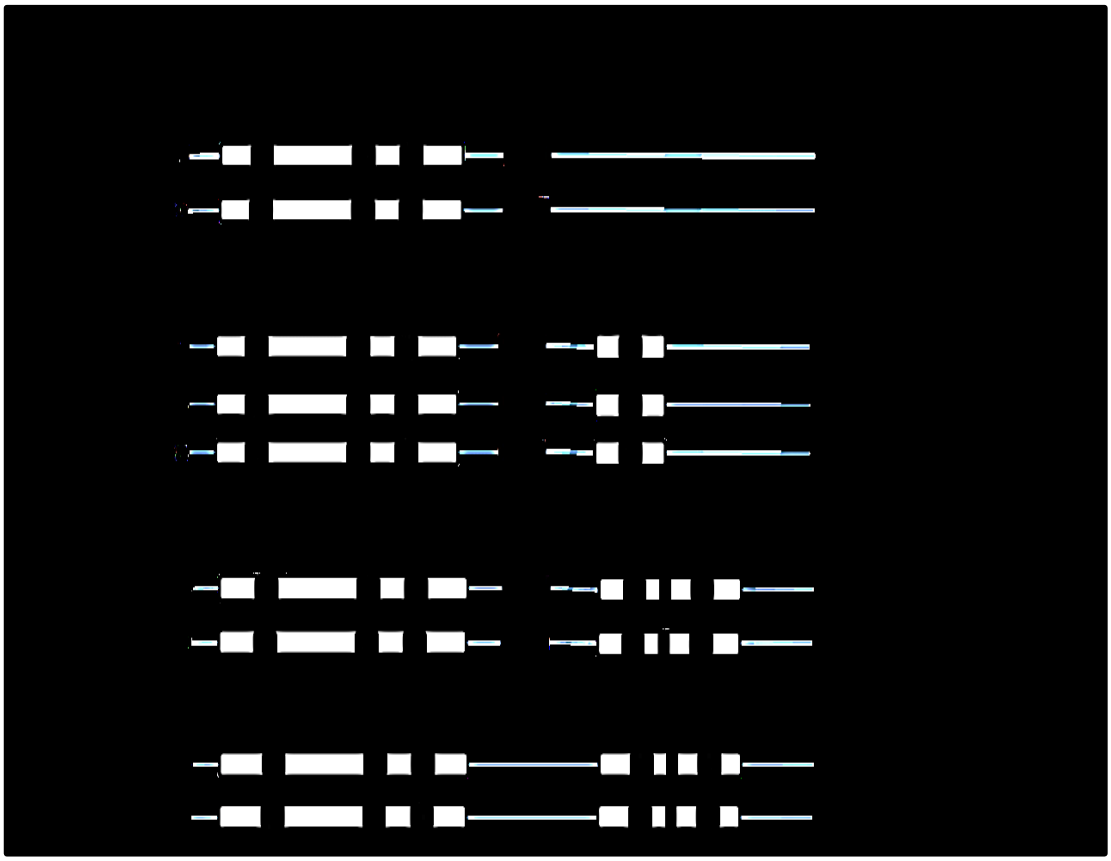

Figure 1.2 Structural domains and chromosomal location of *PAX* genes (adapted from Sergio and Philippe, 2007). The PD is present in all PAX/Pax groups but other domains may not be present.

Group I

This PAX group comprising PAX1/Pax1 and PAX9/Pax9 has a PD and an OP but without a HD (Bouchard *et al*., 2010) (**Fig. 1.2**). PAX1/Pax1 and PAX9/Pax9 both contribute to skeletal development during embryogenesis (Zhao *et al.,* 2007). Pax1 regulates vertebral column development (Chuang *et al.,* 2012). A study of Pax1-deficient 'undulated' mice, demonstrated that Pax1 is a facilitator of notochordal signals during sclerotome differentiation (Capellini *et al.,* 2010). PAX1/Pax1 expression has been demonstrated in both the developing sclerotome and intervertebral discs (Capellini *et al.,* 2010). PAX1/Pax1 in adult thymus epithelium promotes the thymus microenvironment, which is vital for normal maturation of T cells (Inami *et al.,* 2011).

PAX9/Pax9 regulates cell proliferation, resistance to apoptosis and cell migration. It is expressed in adult thymus and is essential for permanent tooth and skeletal formation (Suda *et al.,* 2011). It occurs in developing somites, specifically in the posterior ventrolateral areas, where cells are in the process of epithelial-mesenchymal transition, with subsequent enhancement of cell migration (Walter *et al.,* 2011). Migration of these cells, results in the formation of the lateral sclerotome, which develops into ribs and neural arches (Mues *et al.,* 2009). Furthermore, PAX9/Pax9 is essential in craniofacial and limb development by decreasing cell proliferation and increasing apoptosis in areas that normally form the vertebral column components (Hsu *et al.,* 2011).

Group II

Sub-group II comprises PAX2/Pax2, PAX5/Pax5 and PAX8/Pax8 structurally characterised by a PD sequence, a truncated HD and an OP (Bouchard *et al*., 2010) (**Fig. 1.2**). PAX2/Pax2 is important for development of the urogenital tract, eyes and central nervous system (CNS) (Barembaum and Bronner- Fraser, 2010; Bouchard *et al.,* 2010). Its expression occurs in adult kidney medulla, transitional urothelium of the ureter, bladder wall, the epithelial lining of female fallopian tube and in the ejaculatory duct epithelium of male rats (Burger *et al*., 2012). In female mice, Pax2 expression observed during puberty in the mammary tubular epithelium is essential for progesterone-dependent mammary development, where it forms a complex with an oestrogen receptor to modulate the erythroblastic leukemia viral oncogene homolog 2 promoter (Silberstein *et al.,* 2006). PAX2/Pax2 has been demonstrated in pancreas and optic tectum in mice (Samimi *et al.*, 2008). PAX2/Pax2*,* which occurs during development of the inner ear, is repressed upon terminal differentiation (Bouchard *et al.,* 2010).

Re-expression of all known PAX/Pax isoforms is essential for repair and regeneration of tissue (Samimi *et al.,* 2008). PAX2/Pax2 expression is mostly reduced in the adult kidney cortex following kidney injury, but during early stage of tubular regeneration, its brief expression is observed (Negrisolo *et al.,* 2011; Ozcan *et al*., 2011).

This demonstrates an anti-apoptotic function role of PAX2/Pax2 during tubular regeneration (Karafin *et al.,* 2011). In male mice, castration induced the androgen-dependent re-expression of Pax2 (Chen[3] *et al*. 2010).

PAX5 is expressed during B lymphopoiesis in the development of early B, pre-B and pro-B lymphocytes predominantly in the regulatory pathway of the V-to-DJ recombination (Firtina *et al.,* 2012). Intriguingly, re-programming of mature B-lymphocytes to pluripotency entails inhibiting PAX5 and inducing expression of other regulatory genes including octamer-binding transcription factor 4, sex determining region Y-box 2 (Sox2), Kruppel-like factor 4 and Myc (c-Myc) (Fujita *et al.,* 2011; Herbeck *et al.,* 2011). PAX8 expression, occuring in kidney, adult thyroid and developing thyroid, regulates the expression of thyroglobulin thyroid peroxidase and sodium/iodide symporter that are required for thyroid hormone synthesis (Narumi *et al*., 2010). PAX8 expression in adult kidneys is in the Bowman's capsule and medullary areas (Hu *et al*., 2012).

Group III

This group comprising PAX3 and PAX7 contains all three complete structural domains: a PD, a HD and an OP (Du *et al,* 2005; Dumont *et al,* 2012) (**Fig. 1.2**). PAX3/Pax3 is crucial in embryogenesis as subsequently discussed in detail below (see sections **1.3 and 1.3.7**). Expression of Pax7 has been observed in adult muscle stem cell pools, (satellite cells) which are essential for tissue repair and regeneration after muscle injury (Liao *et al.,* 2009; Xynos *et al.,* 2010). Pax7 is crucial for maintaining the survival and proliferation of postnatal satellite cells (Shin *et al.,* 2012).

Group IV

This group comprising PAX4 and PAX6 contains a PD and a HD without an OP (Rath *et al,* 2009) (**Fig. 1.2**). Even though few studies have implicated PAX4 in adult and cancer tissues, re-expression of PAX4 has been demonstrated to prevent pancreatic β-cells apoptosis (Plengvidhya *et al*., 2007; Liang *et al.,* 2011). Apart from increasing β-cell

replicative potential, mitogen-induced PAX4 expression further protects cells from apoptosis by activating *C-MYC* and B-cell lymphoma-extra large (*BCL-XL*) (Brun *et al*., 2008; Collombat *et al*., 2009). Increased PAX4 expression occurs in human insulinomas and inhibition of apoptosis in rat insulinomas cells occurs via up-regulation of Bcl-xl (Brun *et al.,* 2007; Bai *et al.,* 2011).

Re-expression of PAX6 observed in corneal epithelium, induced corneal wound repair, while decreased PAX6 expression during corneal wound repair, decreased corneal epithelial cell adhesion and corneal neuronal migration, but increased cell proliferation and stromal cell apoptosis (Smith[1] *et al.,* 2012). Correspondingly, in olfactory epithelial regeneration, transient increased expression of Pax6 induced the globose basal stem cell pool into either neuronal or epithelial cell lineages (Cocas *et al.,* 2011). The levels of PAX6 protein regulates the balance between neural stem cell self-renewal and neurogenesis and hence is regarded as a neuroectodermal cell fate determinant (Jia *et al.,* 2011; Yoo *et al*., 2011). Inhibition of human glioblastoma cell growth by increased expression of PAX6, repressed matrix-metalloproteinase 2 (MMP2) regulated invasiveness and induced glioma cell susceptibility to detachment, oxidative stress and decreased angiogenesis (Wang[3] *et al.,* 2013). However, PAX6 is not apparently mutated in gliomas (Liu *et al.,* 2012).

1.2.5. *PAX/Pax* Gene Mutations and the Development of Cancer

Aberrant expression and mutations in PAX/Pax play a role in the onset of diseases and tumours (Li[1] and Eccles, 2012). PAX/Pax protein expression is up-regulated in several different types of tumour, although the precise role of PAX proteins in cancer is not clearly understood (Gutkovich *et al.,* 2010). The essential roles played by PAX proteins in maintaining tissue-specific stem cells by inhibiting terminal differentiation and apoptosis, has been observed to facilitate the development, survival and progression of specific cancers. Various subgroups display distinct involvement in the development of several cancers, with subgroups II and III functioning as facilitators of tumour development, while subgroups I and IV exhibited neutral or favourable involvement in cancer (Li[1] and Eccles, 2012). PAX/Pax proteins, therefore, serve as tumour markers in

several cancers such as rhabdomyosarcoma, melanoma, neuroblastoma and Ewing's sarcoma (Jothi *et al.,* 2012; Li[1] and Eccles, 2012). For the purpose of development of novel anti-cancer therapies, an understanding of normal developmental pathways regulated by PAX/Pax proteins might contribute to other potentially parallel pathways common in tumours, and result in identifying new molecular targets (Li *et al.,* 2009; Oesch *et al.,* 2009).

PAX1/Pax1 aberrant expression is related to developmental defects of craniofacial structures and teeth, which happen intermittently and the fundamental genetic abnormalities are not well understood, in part due to unknown protein-protein interactions (Militi *et al.,* 2011).

Cell proliferation is reduced, with increased apoptosis, in areas that develop into vertebral column components (Capellini *et al.,* 2010). Pax1 mutant mice had severe developmental abnormalities in the pectoral girdle, involving the fusions of skeletal elements, which normally remain separated, plus defective differentiation of blastemas into cartilaginous structures (Capellini *et al.,* 2011). In mice, Pax1 mutations produced the 'undulated' phenotype described by vertebral malformations along the entire rostro-caudal axis (Capellini *et al.,* 2011). Studies of mice with homozygous mutations in Pax1 or Pax9, showed a complete absence of derivatives of sclerotome, including intervertebral discs, vertebral bodies and proximal ribs because of lack of sclerotome chondrogenesis (Zhu *et al*., 2012). Expression of some *PAX* genes, which has been associated with increase DNA methylation, induced inhibition of tumourigenesis. For instance, *PAX1* tumour suppressor activity through DNA hypermethylation, has been demonstrated in both human cervical and ovarian cancers, and this suggests that lack of PAX1 activity might induce the development of these cancers (Macones *et al.,* 2011; Chao *et al*., 2013).

Aberrant expression and mutation of PAX9/Pax9 are associated with tooth abnormalities in both humans and mice (Zhu *et al.,* 2012). Human PAX9 mutations afford a unique opportunity to investigate how these alterations change gene function and its effects on

normal tooth development (Sull *et al.,* 2009; Zhang[2] *et al.,* 2012). Tooth agenesis has been identified after PAX9/Pax9 autosomal dominant mutations (Brook *et al*., 2009; Mendoza-Fandino *et al.,* 2011). The majority of mutations are situated in the PD (Kapadia *et al.,* 2006). Previous studies of mutations, predicted that mutant proteins resulting from a frameshift or nonsense mutation, shows a total loss of function (Hansen *et al.,* 2007).

Expression of PAX9/Pax9 facilitates oncogene-induced cell survival in oral squamous cell carcinoma (Lee *et al.,* 2008). It is implicated in epithelial dysplasia and oesophageal invasive carcinoma (Zhu *et al*., 2012), being significantly reduced in these compared to levels in normal tissue (Zhao *et al.,* 2005; Wang *et al.,* 2009). Progressive loss of PAX9/Pax9 expression has been associated with enhanced oesophageal tumour malignancy (Hsu *et al.,* 2011; Haldeman-Engler *et al.,* 2012). Increased levels of PAX/Pax9 expression may be a useful prognostic indicator of favourable outcome in oesophageal invasive carcinoma (Kist *et al.,* 2005; Hu *et al.,* 2011). Lung cancer tissues showed increased PAX9/Pax9 expression (Militi *et al*., 2011).

Aberrant expression of PAX2/Pax2 is frequently identified in tumour cell lines including those from lymphoma, breast, ovarian, lung, prostate, colon and in primary tumour tissue samples (Quick *et al.,* 2010; Davis *et al.,* 2013). PAX2/Pax2 promotes the survival of ovarian, renal cell and bladder carcinomas and has been proposed as a marker for renal neoplasms (Carney *et al*., 2011; Davis *et al.,* 2013). Apoptosis induced in cell lines following RNA interference to silence PAX2/Pax2 expression, further suggests that endogenous PAX2/Pax2 expression is required for the growth, survival and resistance to apoptosis of cancer cells and could be a suitable target for immunotherapy (Quick[2] *et al.,* 2012; Upson *et al*., 2012). The downstream targets of PAX2/Pax2 are still poorly described, PAX2/Pax2 acts as both transcriptional repressor and activator of both phosphoprotein tumour suppressor 53 (p53) and Wilms tumour protein 1 (Shen *et al.,* 2011). Recently, wingless (Wnt) signaling pathway protein 5a (Wnt-5a) and human beta defensin 1 were identified as PAX2/Pax2 targets (Johnson *et al.,* 2011; Padanad *et al.,* 2012). The expression of PAX2/Pax2 has been demonstrated in breast and prostate tumours and acute myeloid leukemia (Chivukula *et al.,* 2009; Xu *et al.,* 2012).

Interestingly, PAX2/Pax2 maintained oestrogen receptor responsiveness in breast cancer (Chivukula *et al.,* 2009; Li[3] *et al.,* 2013). In addition, PAX2/Pax2 expression induced endometrial cancer malignancy, while tamoxifen inhibition of PAX2/Pax2 expression prevents endometrial carcinogenesis (Monte *et al.,* 2010; Upson *et al.,* 2012).

PAX5 expression is observed in most B-cell neoplasms, including B-cell lymphoma (Lazzi *et al.,* 2009; Moretti *et al.,* 2012). PAX5 is expressed in breast cancer, medulloblastoma and neuroblastoma (Proulx *et al.,* 2010; Moelans *et al.,* 2012). In contrast, PAX5 haploinsufficiency synergizes with signal transducer and activator of transcription 5 (STAT5) activation to induce acute lymphoblastic leukemia (Rafei *et al.,* 2008; Heltemes-Harris *et al*., 2011). PAX5 has been identified as a novel tumour suppressor in hepatocellular carcinoma through interaction with the p53 signaling pathway and an increase in PAX5 induced apoptosis in multiple myeloma cells (Proulx *et al.,* 2010; Liu[2] *et al*., 2011). PAX8 undergoes chromosome rearrangement with peroxisome proliferator-activated receptor (PPAR) in thyroid adenocarcinomas and has been demonstrated as a lineage survival factor for an ovarian cancer cell line (Chia *et al.,* 2010). In renal, ovarian and thyroid tumours, PAX8 is implicated in inducing transcription of the transcription factor E2F1 (E2F1) and maintenance of retinoblastoma tumour suppressor protein (RB) stability (Li[1]. *et al*., 2011; Yang[1]*et al*., 2012). In glioblastoma cell lines, PAX8 regulates telomerase, which is an important factor in cellular ageing and immortalization (Chen *et al.,* 2008).

Aberrant PAX3/Pax3 expression is associated with various mutations and tumours (see sections **1.3.9 and 1.3.10**). In alveolar rhabdomyosarcomas, PAX7 may also undergo chromosomal translocation with forkhead (FKHR) box protein O1 (FOXO1) to form a fusion protein similar to PAX3-FKHR (Dumont *et al.,* 2012; Yang[2] *et al.,* 2012).

Ectopic PAX4 expression in melanoma decreases cell growth, demonstrating a potential tumour suppressor function (Hata *et al.,* 2008; Sultana *et al.,* 2011). Repression of PAX6 in pancreatic adenocarcinoma following terminal cell differentiation induces pancreatic cancer cell progression by activating the mesenchymal epithelial transition

factor (MET) tyrosine kinase receptor (Mascarenhas *et al.,* 2010). PAX6, which stimulates retinoblastoma cell proliferation and inhibits apoptosis, also promotes breast cancer cell proliferation and tumourigenesis (Bai *et al.,* 2011; Li[2] *et al.,* 2011). Increased expression of PAX6 in breast and bladder cancer induced hypermethylation of CpG islands as an indication of tumour progression (Zong *et al.,* 2011; Moelans *et al.,* 2012).

1.3. Paired Box Gene 3

The human paired box gene 3 (*PAX3*), encodes 510 amino acids with several structural domains including a PD, OP, HD and TA, whilst murine Pax3 encoding 479 amino acids, has similar structural domains (Boutet *et al.,* 2010; Gutkovich *et al*, 2010; Okamoto *et al.,* 2012).

PAX3/Pax3 directs development of skeletal muscle, central nervous system, somites and neural crest-derived cells that become cardiac tissue, gastrointestinal enteric ganglia, and melanocytes (Liu *et al.,* 2012; Yvernogeau *et al.,* 2012). The capability of *PAX3/Pax3* to regulate vastly different developmental processes is due to AS and the features of its protein structural domains (Holland and Short 2010; Charytonowicz *et al*., 2011). *PAX3/Pax3* AS modifies the C-terminal end of the HD, causing a frameshift to alter TA activity and produce several *PAX3/Pax3* isoforms (Fernandez *et al.,* 2010). Currently, seven variants of *PAX3/Pax3* have been defined: *PAX3a/Pax3a; PAX3b/Pax3b; PAX3c/Pax3c; PAX3d/Pax3d; PAX3e/Pax3e; PAX3g/Pax3g* and *PAX3h/Pax3h* showing different expression patterns which demonstrates that they have distinct functions (Parker *et al.,* 2004; Wang[2] *et al*., 2008; Charytonowicz *et al.,* 2011).

PAX3/Pax3 protein domains, which facilitate binding interactions with a host of factors in different combinations, induce either activation or repression of downstream target promoters (Gutkovich *et al.,* 2010; Berlin *et al.,* 2012). PAX3/Pax3 interacts with other proteins that act as co-activators or co-repressors of transcription (Boutet *et al.,* 2010; Lagha *et al.,* 2010). These binding interactions modulate the development and activities of melanocytes in both embryo and adult (Li[3] *et al*., 2011; Medic *et al*., 2011).

PAX3/Pax3 controls cell proliferation, differentiation and apoptosis to maintain equilibrium between cell proliferation and differentiation (Berlin *et al*., 2012; Dong *et al*., 2013).

1.3.1. Regulation of *PAX3/Pax3* Activation and Functional Modulation

Several protein interactions that regulate PAX3/Pax3 function subsequently induce terminal differentiation of cells. The binding of Pax3 to DNA regulatory elements or Pax3 protein degradation may be inhibited by molecular obstruction. For instance, Pax3 binding to DNA is inhibited by calmyrin (Sidhu *et al.,* 2010). Increased expression of calmyrin and decreased expression levels of Pax3 were demonstrated in differentiated cells, compared to their initial expression levels in undifferentiated myoblasts (Sidhu *et al.,* 2010). The transcriptional and DNA-binding activities of Pax3 were both inhibited by the direct interaction of calmyrin with Pax3 PD (Christova *et al.,* 2010). The mechanism of binding in melanocytes and melanoblasts is not fully understood (Dedeic *et al*., 2011). Using the first two helices of the HD, Pax3 directly interacts with the N-terminal domain of Rb and other related proteins such as p107 and p130 (Wiggan *et al.,* 2006). The HD of Rb interacts with E2F to form an E2F-Rb complex, which in turn inhibits PAX3 activation of the Met promoter by an unknown mechanism (Grabellus *et al.,* 2010). The interaction of Rb with other Pax proteins such as (Pax2, 5, and 8), promotes Pax3 transcriptional inhibition, repression, or co-activation (Jain *et al.,* 2011). The effects of Rb on Pax downstream transcriptional activities depends on the cell type involved, transcriptional target and a direct interaction of phosphorylated Rb-Pax3 complex with death-domain associated protein (Daxx) (Kaneko *et al*., 2007). Daxx protein, acts as both pro-and anti-apoptotic regulator. It can repress transcription factors in the nucleus. Promyelocytic leukaemia protein inhibits functional activities of Daxx with subsequent conversion of the latter into nuclear bodies. The passage of Daxx into nuclear bodies prevents its inhibition of Pax3 (Yamaguchi *et al.,* 2007). The ability of Pax3 to activate promoters is inhibited through binding of Daxx at both the HD and the OP (Yamaguchi *et al.,* 2007; Fenby *et al.,* 2008). Inhibition of Pax3 by Daxx further inhibits Pax3 downstream targets such as Met (Mascarenhas *et al.,* 2010).

Direct interaction of HIR histone cell cycle regulation defective homolog (HIRA) with Pax3 at their C-terminal domains induces senescence, which is related to heterochromatin foci induced by wide dynamic repeat-containing chromatin regulator (Lorain *et al.,* 2001; Charytonowicz *et al.,* 2011). Cellular senescence is induced by heterochromatin-associated protein HP1complex (Hong and Saint-Jeannet, 2007). A brief transfer of both HP1 and HIRA to promyelocytic leukaemia protein bodies has been demonstrated during cell senescence. Direct interaction of Pax3 with Grg4, which functions as a repressor is analogous to Pax3-HIRA interaction (Zibat *et al*., 2010). Interaction of HP1 with both Pax3 and HIRA, facilities the transfer of HP1 to promoters, which subsequently inhibits the transcriptional activity of Pax3 (Christova *et al.,* 2010). The fact that HIRA activity requires promyelocytic leukaemia protein indicates that the binding pattern of Pax3-HIRA is similar to Daxx-Pax3 induced inhibition (Zeng *et al.,* 2009).

The influence of the binding interaction of Pax3 and POU domain transcription factor 2 (Brn-2) on their downstream targets observed in melanocytes and melanoma cells has not been elucidated (Betters *et al*., 2010). The development of the central nervous system, neural crest and neuronal differentiation requires the expression of Brn-2 (Betters *et al*., 2010). High Brn-2 expression has been demonstrated in melanoma compared to insignificant Brn-2 expression in melanocytes (Bosserhoff *et al.,* 2011). In aggressive melanomas, a mutant B-Raf, V600E, can increase Brn-2 expression (Betters *et al*., 2010). Response elements of both Pax3 and Sox10 induce Brn-2 expression in order to activate Mitf.

In normal melanocytes and melanoma cells, the interaction of Brn-2 and Pax3 induces alteration of Mitf and downstream target gene expression (He[1] *et al.,* 2011). Mono-ubiquitination facilitates Pax3 regulation and proteasomal degradation (Boutet *et al.,* 2007). Proteasomal degradation of Pax3 induced by poly-ubiquitination involves ubiquitin and protein receptor recognition. Mono-ubiquitinated substrate for proteasomal breakdown is formed by the direct interaction of Pax3 with UV excision repair protein RAD23 homolog B (Rad23B) (Boutet *et al*., 2007). Rad23B links Pax3 and the intrinsic ubiquitin receptor protein S5a as a complex. In myoblasts, muscle differentiation is

impeded owing to inhibition of this pathway, signifying that Pax3 is capable of sustaining an undifferentiated state of cells and its degradation permits cell terminal differentiation (Hosoyama *et al.,* 2011).

Pax3 interaction with other factors not typically found in pigment cells has been demonstrated (Thomas *et al.,* 2009; Nitzan *et al.,* 2013). For instance, binding of muscle segment homeobox 1 (Msx1) with MyoD1 inhibits Pax3 transcriptional activation, facilitated by both the Pax3 PD and Msx1 HD (Miller *et al.,* 2007). Mesenchyme homeobox (Mox)1 and 2, (also known as Meox1 and 2), which are primarily expressed in mesodermal structures interact with the Pax3 HD (Woodruff *et al.,* 2007; Zhang[1] and Liu, 2009). Pax3 directly interacts with importin 13 (IPO13) via the HD and basic amino acid C-terminal domain (Beaudin *et al.,* 2011). Several protein interactions with Pax3 are vital for modulating Pax3 as an effective transcriptional regulator of melanocyte cellular function, morphological characteristics and change of gene expression pattern (Tedesco *et al.,* 2010; Djian-Zaouche *et al.,* 2012).

In mice, Bradshaw *et al*. (2009) and Marie *et al.* (2010) found that the proximal 1.6kb *Pax3* promoter fragment used to induce *Pax3* expression in the neural crest (NC) was sufficient to rescue all of the NC defects in *Pax3*-deficient Splotch embryos, including cardiac defects. Increased *Pax3* expression in this region was not associated with developmental abnormalities (Curchoe *et al.,* 2010; Sanchez-Ferras *et al.,* 2012). These reports demonstrate that the proximal 1.6kb upstream of the *Pax3* promoters contained sequences sufficient to mediate functional expression of *Pax3* in the NC (Nelms *et al*., 2011; Singh *et al*., 2011). PAX3/Pax3 expression has been found in somite compartments forming embryonic skeletal muscle progenitors, which subsequently produce skeletal muscle in the growing limb buds (Cairns *et al*., 2012) and in muscle proliferative cells in skeletal muscle development (Wan *et al*., 2011).

1.3.2. Functional Biological Activities of *PAX3/Pax3*

PAX3/Pax3 possesses four structural domains: the PD, HD, OP and TA have unique DNA binding patterns. In **figure 1.3,** each group of letters with a similar colour represents a specific amino acid sequence acting as a protein interaction epitope (Sergio and Philippe, 2007; Farin *et al*., 2008; Corry *et al.,* 2010). The PD, so-called for the two HTH motif-containing sub-domains (PAI and RED) contain 128 amino acids, which are located at the N-terminal of Pax3.

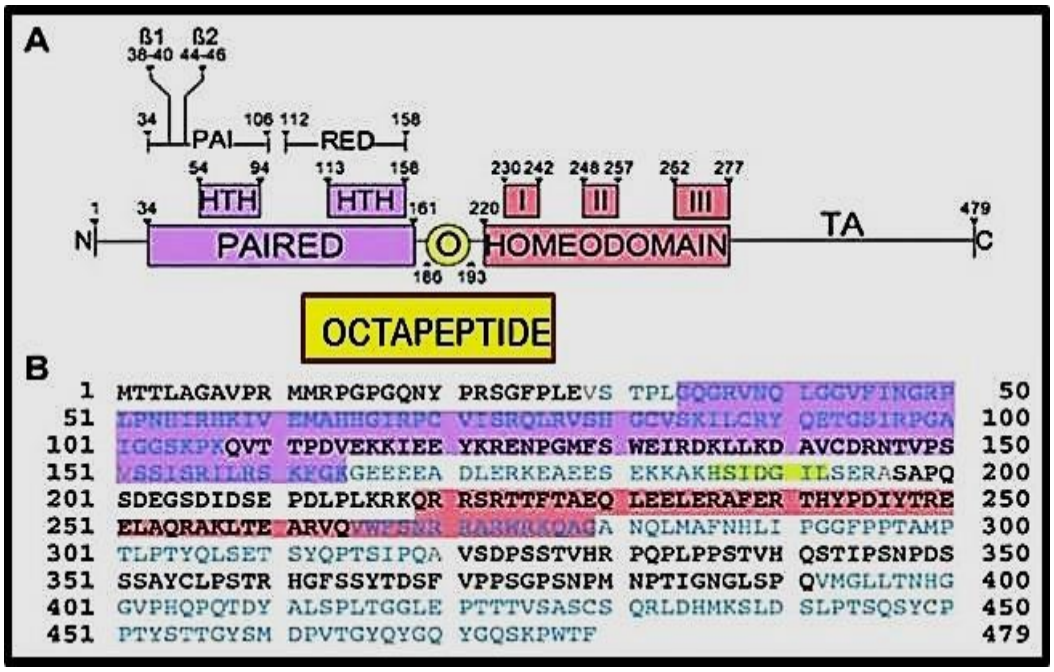

Figure 1.3 Structural domains of PAX3/Pax3 protein (Taken from Kubic *et al.,* 2008). **A:** Four domains of Pax3 protein: PD, lavender (composed of PAI, RED, HTH and HTH motifs); HD, pink (composed of three helices I, II and III); OP, yellow (located in between PD and HD); TA (located at C terminal). **B:** Letters denots Pax3 amino acid sequence in the PD, HD and OP and the numbers represent the number of exons.

HD interaction with other proteins modulates Pax3 activity (Olaopa *et al.,* 2011). For instance, binding to Rb represses Pax3 transcriptional activation (Pallafacchina *et al.,* 2010; Zibat *et al*., 2010). Co-repressors, including HIRA and Daxx, interact with DNA by binding to the HD (Thomas e*t al.,* 2009). The three different DNA-binding motifs of the Pax3 HD permit several patterns of DNA binding sites, which allow the co-ordination required for regulation of developmental processes (Thomas e*t al.,* 2009).

The PAI is composed of two beta-sheets, a HTH motif which binds with DNA to accelerate the association of Pax3 protein with downstream proteins (Farin *et al*., 2008; Corry *et al.,* 2010). The N-terminal HTH motif has been demonstrated to be responsible for interaction with the consensus sequence (G)T(T/C)(C/A)(C/T)(G/C)(G/C), several of which exist as target sites in the DNA (Corry *et al.,* 2010; Gutkovich *et al.,* 2010). Although the PAI HTH motif has been demonstrated to enhance DNA binding at the C-terminal end, the role of the RED HTH is uncertain. The latter motif is not involved in enhancing DNA binding capability since it does not bind DNA (Christova *et al.,* 2010). The RED subdomain increases DNA binding potentials in relation to downstream targets (Makawita *et al.,* 2009). The PD interacts with other structural motifs, such as SOX and calmyrin downstream of the HD in order to modulate the functional activity of Pax3 (Xia *et al.,* 2009; Cairns *et al.,* 2012). For instance, calmyrin represses functions by inhibiting Pax3 binding to DNA (Hsieh *et al*., 2006; Conrad *et al.,* 2009). Binding of Pax3 to SOX10 induces synergistic activation of ret proto-oncogene (c-Ret) and microphthalmia-associated transcription factor (Mitf) (Wahlbuhl *et al*., 2012; Zhang[1] *et al*., 2012).

The HD is 60 amino acids in length and comprises three HTH motifs, which include helices I, II and III. Helices I and II induced binding with downstream proteins, whereas helix III identifies and facilitates DNA sequence (TAAT) binding (Soleimani *et al.*, 2012). The DNA binding capability of the PD is modulated by the HD (Christova *et al.,* 2010). The HD further functions as a boundary between Pax3 and DNA as well as downstream targets in order to prevent other molecules from binding (Soleimani *et al.,* 2012). Pax3 binds to DNA via the consensus sequences of the PD and HD so that they synergistically activate downstream target genes (Goljanek-Whysall *et al.,* 2011). Direct interaction of the OP with calmyrin produces a complex that inhibits Pax3 DNA binding capability (Miller *et al.,* 2007). Pax3-DNA binding integrity is facilitated by the TA, which is rich in S/G/T and located at the carboxyl-terminal end (Charytonowicz *et al*., 2011). To ensure sequence specificity in the absence of either PD or HD reactive elements, the TA inhibits the binding of the HD to DNA (Cao *et al.,* 2005). These reports indicate that the TA binds DNA directly alongside both the PD and HD (Himeda *et al.,* 2013).

Even though Pax3 transcriptional regulatory mechanisms are not well known, post-translational modifications of Pax3 have been demonstrated in several studies (Wan *et al*., 2011). Reports indicate that protein kinase C (PKC), containing eight recognised sites for S/T phosphorylation, regulate the function of Pax3 during embryonic myogenesis (Brunelli *et al*., 2007). In rhabdomyosarcoma, decreased Pax3/FKHR transcriptional activity induced by the kinase inhibitor PKC412 suggests that complete activity of Pax3/FKHR requires phosphorylation (Amstutz *et al.,* 2008; Dietz *et al.,* 2011). In myoblast precursor cells, an unknown kinase is reported to phosphorylate Pax3 on serine 205 (Miller *et al.,* 2008; Iyengar *et al*., 2012). Terminal differentiation of myogenic progenitors requires decreased levels of *Pax3* mRNA and the phosphorylated state is lost swiftly after onset of differentiation (Dietz *et al.,* 2009; Lagha *et al.,* 2013). During myogenic development and adult stem cell differentiation, Pax3 activity is modulated by the ubiquitination-proteasomal degradation pathway (Boutet *et al.,* 2010; Wang[2] *et al*., 2011).

1.3.3. Binding Partners of PAX3/Pax3

Interaction of PAX3/Pax3 with other molecules is augmented through the direct binding of many co-activators and repressors in order to obtain greater influence on downstream targets (Lai *et al*., 2010; Sumegi *et al*., 2010). Both Sox10 and tafazzin (TAZ) augment Pax3 transcriptional activity (Cairns *et al*., 2012). Pax3 and Sox10 interact directly through their DNA binding domains (Zhang[1] *et al.,* 2012).

The expression of Sox9 and Sox10 has been demonstrated in both melanoblasts and melanocytes (Bosserhoff *et al*., 2011). In neural crest melanocyte precursors, increased expression levels of Sox9, which were observed initially, decreased before migration, while Sox10 expression was increased during migration (Wahlbuhl *et al.,* 2012). Melanoblasts show increased levels of Sox10 while differentiated cells exhibit decreased levels of Sox10 (Cairns *et al.,* 2012). During mouse development, the expression of Sox10 induces melanoblast maturity whilst Sox10 inhibition leads to pigmentation defects (Pingault *et al.,* 2010) and Sox9 is essential in differentiating melanocytes (Cairns *et al.,* 2012). Mitf, crucial for melanogenesis, is activated by increased levels of

both Sox9 and Sox10 (Chen[1] *et al.,* 2010; Hou *et al.,* 2008). Interaction between Pax3 and Sox10 can activate c-Ret (Kubic *et al.,* 2008; Leon *et al*., 2009).

Expression of both Mitf and C-Ret promoters is induced by Pax3 and Sox10 (Tshori *et al.,* 2006). The direct DNA binding of Pax3 induces the c-Ret enhancer whereas activation of Sox10 requires protein-protein binding. The genomic *cis* regulatory site requires protein binding to induce the Mitf promoter (Wan *et al.,* 2011). Sox10 induces the activation of dopachrome tautomerase (Dct) while Mitf represses Dct by means of an enhancer sequence similar to that used by Pax3 to induce repression of Dct (Jiao *et al*., 2006). Many Sox10 melanocytic targets including Mitf and Dct are activated by Sox9. Direct interaction of Pax3 with TAZ (also known as WW domain-containing transcriptional regulator 1 or WWTR1), has been demonstrated (Ravasi *et al.,* 2010). Multiple domains induced direct interaction of WW domain in TAZ protein with Pax3. In a luciferase assay system, TAZ presents as an effective transcriptional co-activator of Pax3 promoters, such as the promoter that activates Mitf. Conversely, the expression of TAZ in the melanocytic lineage is not well established (He[1] *et al*., 2011).

Interactions of the Pax3 TA domain with other proteins enable synergistic activation of downstream targets (Kennedy *et al.,* 2009; Zhao[3] *et al.,* 2013). Pax3 is an effective repressor of gene expression in the presence of some cofactor repressor molecules such as KRAB associated protein 1 (KAP1), heterochromatin protein 1 (HP1), groucho protein 4 (Grg4) and T-box (Tbx) family proteins (Farin *et al.,* 2008). Binding of Pax3 to both KAP1 and HP1 stimulates HP1 protein to induce heterochromatin inhibition of gene expression (Bae *et al.,* 2013). Numerous transcriptional repressors, including KAP1, directly bind to and recruit HP1 to regulatory enhancers (Hsieh *et al.,* 2006; Degenhart *et al.,* 2010).

Pax3 interacts with other transcription factors through its PD and recruits them to target promoters. Both HP1 and KAP1 compete for Pax3 interaction to regulate its transcriptional activities, HP1 inhibits Pax3 transcriptional repression, whereas KAP1 enhances it (Hsieh *et al*., 2006). The Tbx1 subfamily of T-box proteins, including

Tbx18, 15 and 22, interacts directly with Pax3 (Farin *et al.,* 2008). All T-box genes contain T-domains required for binding DNA and interaction with protein. The binding interactions between the Tbx proteins and Pax3 occur via the T domain and PD (Tsumagari *et al.,* 2013). The expression of T-box proteins in the neural crest, which induces cell pigmentation, has not been demonstrated to be affected by the binding interactions (Tsumagari *et al.,* 2013). For instance, Tbx15 mutations induce changes in the dorso-ventral pigmentation pattern and the expression of tyrosinase-like protein 1 is repressed by Tbx2 (Liu[2] *et al*., 2013). A segment of Pax3 protein composed of the first 90 amino acids can enhance the capability of Pax3 to repress downstream targets singly or with co-repressors (Hsieh *et al*., 2006; Sanchez-Ferras *et al.,* 2012).

1.3.4. *PAX3/Pax3* Downstream Target Genes

Expression of the C-Ret tyrosine kinase receptor is essential for neural crest-derived cell migration, survival, proliferation and differentiation (Hauswirth *et al.,* 2012). A link between Pax3 and C-Ret was deduced from the study of C-Ret expression in Splotch homozygous-deficient embryos, which died during midgestation accompanied with defective cardiac and neural tube because of diffecient Pax3 and C-Ret expression (Greene *et al.,* 2009). Induction of neural crest enteric ganglia formation was induced by Pax3 while suppression of Pax3 blocked intestinal ganglia formation (Sommer, 2011). Restoration of Pax3, which stimulated enteric ganglia formation and induced high levels of C-Ret expression, established c-Ret as a downstream target of Pax3 (Bradshaw *et al.,* 2009). Synergistic activation of Sox10 facilitated by chromosomal acetylation is induced by the direct interaction of Pax3 with c-Ret promoter enhancer element (Griffith *et al*., 2009; Reichek *et al.,* 2011). Cellular activities including proliferation, differentiation, migration and apoptosis require transforming growth factor-beta 2 (TGFβ2) expression (Ichi[1] *et al.,* 2010). TGFβ2 is required for the development of neural crest derivatives. In mice, developmental defects in heart, craniofacial structures, skeleton, ear and the urogenital system have been induced by homozygous TGFβ2 mutation (Nakazaki *et al.,* 2009). The interaction of TGFβ2 promoter *cis* regulatory elements with both the PD and HD of Pax3, established TGFβ2 as a direct downstream target of Pax3 (Mayanil *et al.,* 2006). A significantly diminished

TGFβ2 expression in mouse embryos can be correlated with inhibition of Pax3 (Morgan *et al.,* 2008).

Proliferation of NC and its subsequent migration and differentiation is induced by Wnt proteins (Zhao *et al*., 2009). In both Wnt1 and Wnt3a, double mutant mice, the overall Wnt signaling pathway induced poor NC development, indicated as a reduced number of neural crest cells (Su[3] *et al*., 2013). Increased expression of Wnt1 induced an increased number of dorsal neural tubes with subsequent induction of premature migratory neural crest cells. The latter decreased after diminished Wnt1 expression (Minchin and Hughes, 2008). A decreased expression level of Wnt1 in the dorsal neural tube, observed in Pax3-deficient mouse embryos, further demonstrates Wnt1 as a Pax3 downstream target (Wu *et al.,* 2008). During NC development, Pax3 directly regulates Wnt1 by activating Wnt1 enhancer elements (Fenby *et al.,* 2008). Acceleration of proliferation, migration and survival of NC cells are regulated by Pax3 (Sanchez-Ferras *et al.,* 2012).

1.3.5. *PAX3/Pax3* Control of Cell Growth and Survival

PAX3/Pax3 expression in cells imparts anti-apoptotic features to these cells, aiding survival (Walter *et al*., 2011; Ciarapica *et al.,* 2013). High Pax3/FKHR expression in rhabdomyosarcoma cells inhibits apoptosis (Ren *et al*., 2008), where as siRNA silencing of Pax3/FKHR expression in rhabdomyosarcoma cells induced significant cell apoptosis (Zeng *et al.,* 2009). Inhibition of Pax3 in mouse embryos induces neural tube defects, including spina bifida and exencephaly with accompanying high apoptosis in the unfused areas of the neural tube, demonstrating the crucial role of Pax3 in inhibiting apoptosis (Chappell *et al.,* 2009). Increased Pax3 expression in rhabdomyosarcoma, melanoma and neuroblastoma cell lines induced increased expression of Bcl-XL, which inhibited apoptosis (Medic *et al.,* 2011). Interaction of Pax3 HD with the enhancer element upstream of Bcl-XL activates Bcl-XL (Taylor *et al.,* 2006). Inhibition of apoptosis is further enhanced by Pax3 repression of phosphatase and tensin homolog (PTEN), while increased expression of PTEN induces apoptosis (Bhattacharya *et al.,* 2006; Li *et al.,* 2007). PTEN plays contributory roles in many pathways, but acts as a negative regulator of the phosphatidylinositide 3-kinase (PI3K) / v-Akt murine thymoma

viral oncogene homolog (AKT) signal transduction pathway, modulating cell proliferation and apoptosis (Li *et al.,* 2007). Pax3 expression in rhabdomyosarcoma and melanoma cell lines is inversely proportional to PTEN expression (Li *et al.,* 2007; Medic *et al.,* 2011). Similarly, increased levels of Pax3-FKHR fusion protein can increase PTEN (Xia *et al*., 2009). Suppression of Pax3-FKHR in cells, which induced increased cell apoptosis, demonstrated that Pax3 promotes survival of cells through modulation of PTEN (Li *et al*., 2007). Interaction of Pax3 with a recognised HD binding motif of the PTEN promoter, revealed a mechanism by which Pax3 regulates PTEN to inhibit apoptosis (Li *et al*., 2007).

1.3.6. *PAX3/Pax3* and Embryonal Development

During embryogenesis, *PAX3/Pax3* is essential in regulating and promoting cell proliferation, migration and differentiation (Berlin *et al.,* 2012). *PAX3/Pax3* is associated with cell transformation as demonstrated in the chromosomal translocation t(2;13) (q35q14) PAX3-FKHR which characterises the solid tumour, alveolar rhabdomyosarcoma (ARMS) (Cao *et al.,* 2010). The *PAX3/Pax3* regulates cell migration from the NC or dorsal dermomyotome, during myogenesis/ melanogenesis or neurogenesis. During development, *PAX3/Pax3* plays an essential role in proper development of neural, cardiovascular, endocrine and musculature systems in humans and mice (Olaopa *et al.,* 2011; Singh *et al.,* 2011). Cells derived from the neural crest ultimately form the peripheral nervous system (PNS), including sensory and motor nerves, as well as the pigment cells of the skin, hair, and inner ear, enteric ganglia, adrenomedullary cells, cardiac smooth muscle and mesenchyme (Wiese *et al.,* 2012).

1.3.6.1. *PAX3/Pax3* and Neural Crest Development

In developing embryos, the functional role of *PAX3/Pax3* has been well demonstrated during the development of the neural crest (Betters *et al*., 2010). The expression of initial neural crest indicators such as Pax3, Wnt1, Slug and Snail have the potential to induced tissue-tissue interactions between neural ectoderm and epidermis (Sanchez-Ferras *et al*., 2012). The neural crest consists of differentiated cells originating from the dorsal region of the neural tube (Edgar *et al.,* 2013) (**Fig. 1.4**).

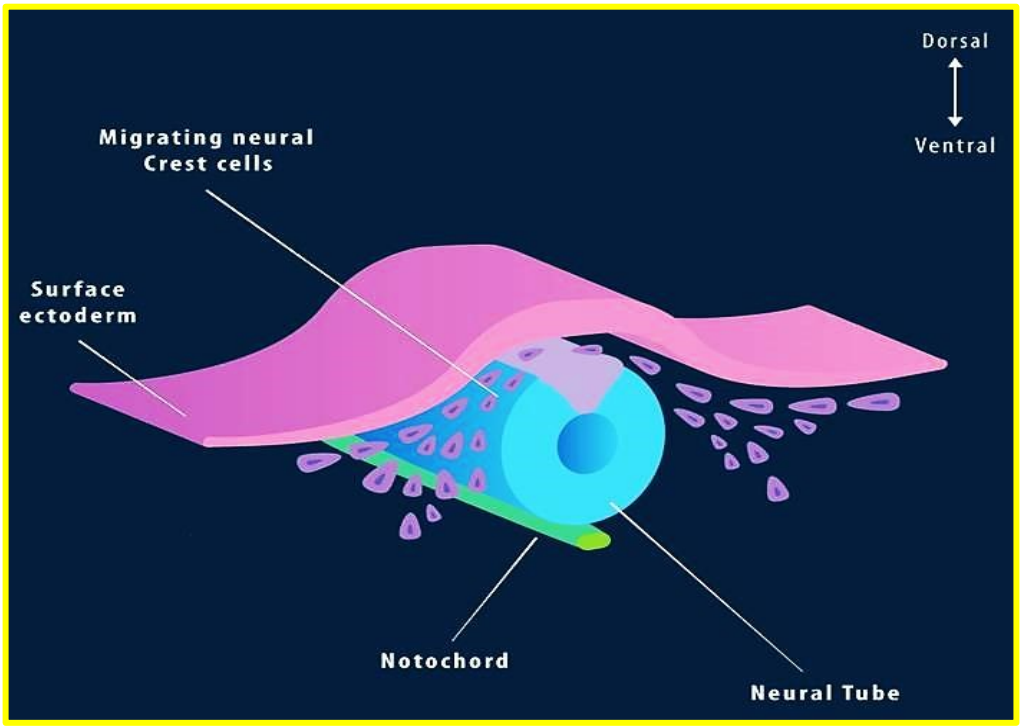

Figure 1.4 NC arises from the dorsal ectoderm (Taken http:/discovery.lifemapsc.com/ Edgar *et al.,* 2013). During embryonic development of the NC, cells are differentiated into many different cell types.

Pax3 expression within the neural tube and dorsal neural groove commences at approximately embryonic day (E) 8.5 in the mouse embryo, climaxes between E9 and E12 then decreases from E13 and reduces to insignificant levels by E17 (Stoller *et al.,* 2008). Expression of *Pax3* at E9 occurs in neuroepithelium of the neural tube and then in the somites (Stoller *et al*., 2008). Pax3 expression on E10 continues the full length of the dorsal half of the embryonic spinal cord and diminishes at E13 (Degenhardt *et al,* 2010; Murdoch *et al.,* 2012). Following NC development, continual expression of Pax3 has been established in the brain, spinal cord of the central nervous system (CNS) and melanocyte stem cells of the neural crest (Gutkovich *et al.,* 2010; Sommer, 2011).

Neural crest development, which commences between the non-neural ectoderm and the neural plate, spreads to new sites within the embryo (Lagha *et al.,* 2010). Cells of NC which pause at various sites, are differentiated into a sizeable group of cellular diversity

including melanocytes, cardiac NC, dorsal root and sympathetic ganglia and thymus (**Fig. 1.5**)

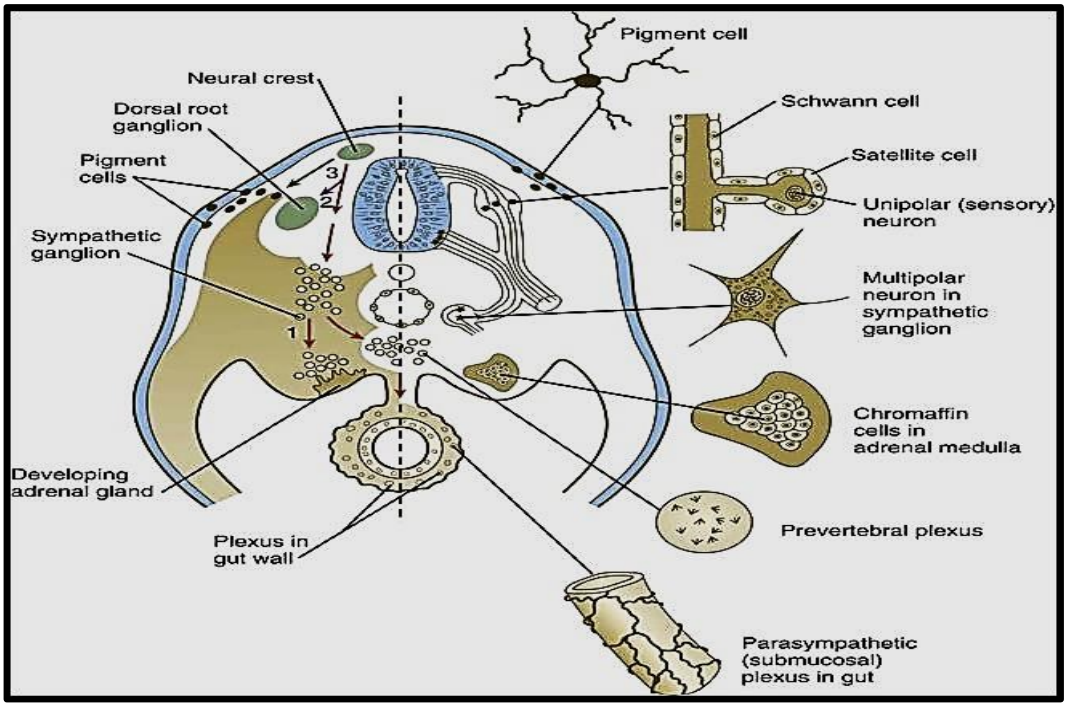

Figure 1.5 Differentiated NC cells originated from the dorsal ectoderm
(Taken from Carlson, 2013).

The migration pattern of the crest has been categorised into two parts. Initially, the dorsoventral cell migration, which occurs between the neural tube and the somites, develops into neural structures (Schmidt *et al.,* 2008). Finally, NC cells migrate mediolaterally dorsal to the somites, underneath the superficial ectoderm and develop into melanoblasts (Medic[1] and Ziman, 2010, Minchin *et al.,* 2013). Migrating NC cells from the dorsal ectoderm are collected on either side of the neural tube and are known as the fourth germ layer because their cells go through a key developmental (epithelial-mesenchymal) transition, to become migratory cells separating along specific pathways in the developing embryo (Betters *et al.,* 2010; Carlson, 2013). The development of the neural crest, which depends on normal function of *PAX3/Pax3*, is well demonstrated in humans and mice, which have deficient *PAX3/Pax3* expression (Kubic *et al*., 2008; Nakazaki *et al*., 2009).

Isolated single NC cells from pre-migratory trunk NC induced by neuregulin-1 proliferate and differentiate into Schwann cells (Ichi[2] *et al.,* 2010; Murdoch *et al.,* 2012). **Table 1.2** is a list of NC derived cells (Barraud *et al.,* 2010; Nagoshi *et al*., 2009). Interestingly, these same cells differentiate into smooth muscle cells in the presence of TGFβ1 (Singh *et al.,* 2011; Dong[2] *et al.,* 2012).

Table 1.2 Derivatives of the neural crest (adopted from Barraud *et al.*, 2010).

Derivatives	Cell type or structure derived
Peripheral nervous System (PNS)	Neurons (sensory ganglia, sympathetic and parasympathetic ganglial and plexuses). Neuroglial cells Schwann cells.
Endocrine	Adrenal medulla
Paraendocrine derivatives	Calcitonin-secreting cells. Carotid body type 1 cells.
Pigment cells	Epidermal pigment cells.
Facial cartilage and Bone	Facial and anterior ventral skull cartilage and bones.
Connective tissue	Corneal endothelium and stroma. Tooth papillae. Dermis, smooth muscle and adipose tissue of skin of head and neck. Connective tissue of salivary, lachrymal and thymus, thyroid and pituitary glands. Connective tissue and smooth muscle in arteries of aortic arch origin

Derivatives of NC cells include: (1) sympathetic and parasympathetic nervous systems, sensory neurons and glial cells; (2) epinephrine-producing adrenal medullar cells; (3) pigment-containing cells of the epidermis; (4) skeletal and connective tissue components of the head (Carlson, 2013; Nitzan *et al.,* 2013). Differentiation of NC cells in the embryo occurs in two main pathways: (1) the "ventral" pathway, which produces PNS neurons and glial cells; (2) The "dorsolateral" pathway, which forms pigment-producing cells (Agoston *et al.,* 2012). Pigment precursor cells (melanoblasts) initially migrate to the dermis where they differentiate and further migrate to the epidermis (Eigelshoven *et*

al., 2009; Singh *et al.,* 2011). Cells of NC expressing neurotrophic tyrosine kinase receptor type 3 become neurons or glial cells, while cells expressing Kit become melanocytes (Thomas *et al,* 2009). *PAX3/Pax3* homozygous and heterozygous mutations produced aberrations in several cells originating from the neural crest (Singh *et al*, 2011).

1.3.6.2. *PAX3/Pax3* and Neurogenesis

In murine embryos, *Pax3* is expressed during early neurogenesis in the developing nervous system (Boshnjaku *et al.,* 2011). *Pax3* expression identified in day 8.5 mouse embryos is restricted to the dorsal neuroepithelium and segmented dermomyotome (Boshnjaku *et al.,* 2011). Detection of *Pax3* expression during early neurogenesis was demonstrated only in the ventricular zone mitotic cells of embryonic spinal cord and in specific areas of the diencephalons, midbrain and hindbrain (Murdoch *et al.,* 2012). *Pax3* expression occurred in E10-E12 embryos in the NC cells of developing spinal ganglia (Wiese *et al.,* 2012). Neural differentiation requires *Pax3* expression (Dong[1] *et al.,* 2012).

Pax3 mRNA expression which occurs in early and later phases of the Schwann cell lineage, modulates myelin basic protein expression (Conrad *et al.,* 2009). Early detection of *Pax3* mRNA expression in NC cells was confined to neurons (Boshnjaku *et al.,* 2011). Cultures of NC cells, which demonstrated significant increases in *Pax3* mRNA expression in the presence of fibroblast growth factor (FGF), indicated induction of neurogenesis. Sensory neurons produced from precursors arising in the NC are regulated by *Pax3* expression (Lassiter *et al*., 2010). Antisense oligonucleotide inhibiting *Pax3* expression in sensory neuron precursors of normal mice resulted in 80-90% inhibition of sensory neuron formation relative to controls (Thompson *et al.,* 2008). In cell cultures of NC from splotch mice, five-fold fewer sensory-like neurons were produced compared with numerous sensory-like neurons observed in normal mice. The role of *Pax3* in the differentiation pathway of peripheral neurons was demonstrated through the insignificant modulatory influence of antisense *PAX3* on the survival of sensory neurons and precursor cells (Yamauchi[2] *et al.,* 2009).

Enteric ganglia formation requires *Pax3* expression (Wiese *et al.,* 2012). In man, an enteric ganglia defect arising from lack of *Pax3* expression, triggers gastrointestinal migration disorders, including Hirschprung's disease (Boshnjaku *et al*., 2011). *Pax3* regulates transcription of the Hirschsprung's disease gene, Ret, by binding and modulating the PD in the Ret promoter, adjacent to a Sox10-binding site (Fenby *et al.,* 2008). Neural progenitors arising from differentiation of embryonic stem cells, had increased expression of *Pax3* and other neural-related genes such as *Pax6* and mammalian achaete-scute homologue 1 (Gee *et al.,* 2011).

1.3.6.3. *PAX3/Pax3* in Melanocyte Stem Cell Development

The essential role of *Pax3* in developing neural crest-derived melanocytes is shown by the pigmentation anomalies of both humans and mice observed, having *PAX3/Pax3* mutations (Zhang[1] *et al*., 2012). Even though the commencement of neural crest development into the melanocytic lineage is seemingly unrelated to *Pax3* expression, *Pax3* is required for proliferation of embryonic melanoblasts and prevention of differentiation of melanoblast precursor cells to melanocytes (Medic[2] and Ziman, 2010). During melanogenesis, the survival of melanoblast and migration into developing hair follicles of skin required the expression of *Mitf* (Dong[2] *et al.,* 2012; Wan *et al.,* 2011). Certain features of neural crest precursors are maintained in adult melanocytes since melanocyte stem cells have the ability to migrate (Kubic *et al*., 2008). This attribute is a contributory factor for potential development of metastatic melanoma (Medic[1] and Ziman, 2010).

Melanocytes are pigment-producing cells of the skin produced by the NC. Melanocyte stem cells give rise to temporary amplifying cells and differentiated melanocytes (Kubic *et al.,* 2008). While the expression of *PAX3/Pax3* promotes proliferation of melanocytes, it is insufficient to maintain differentiated melanocytes (Sommer, 2011; Wahlbuh *et al*., 2012). Kubic *et al.,* (2008) reported that *PAX3/Pax3* expression, which induced melanocyte lineage progression, concurrently inhibited melanocyte differentiation, via activation of *MITF* and *SOX10.* (**Fig. 1.6**).

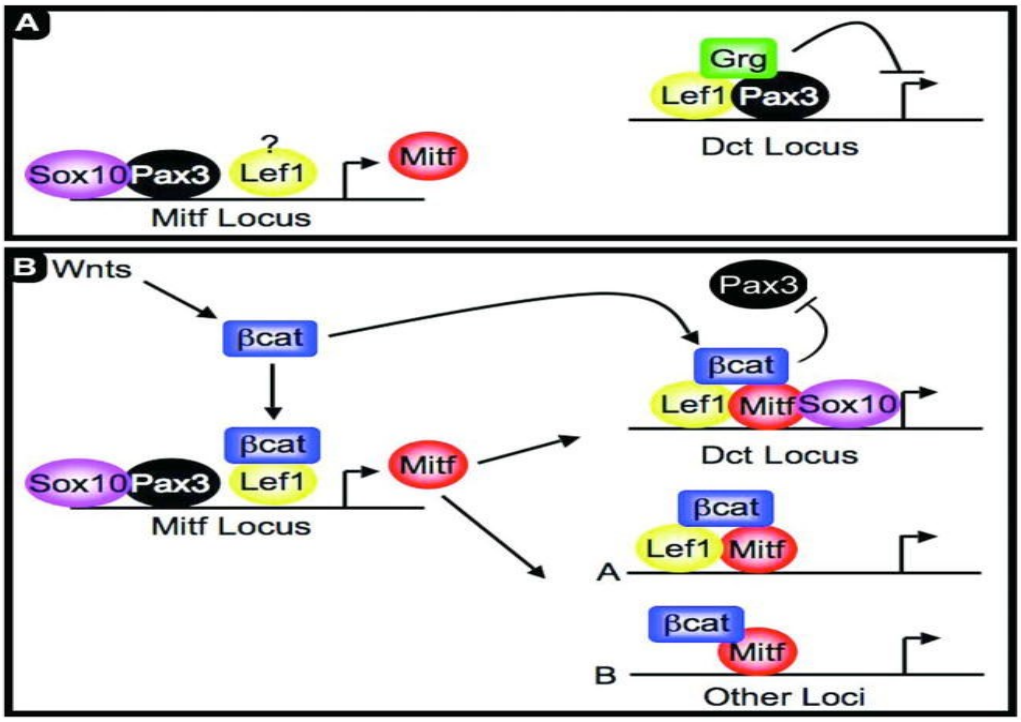

Figure 1.6 Melanogenesis. **A,** Concurrent activation of Mitf and inhibition of Dct expression induced by *Pax3* and *Sox10.* The expression of *Sox10* and *Pax3* modulate the expression patterns of *Dct* and *Mitf.* **B**, changes in melanocyte gene expression patterns are induced by Wnt signaling (taken from Kubic *et al.,* 2008).

In the mature mouse skin, stem cells are controlled to preserve multipotency, prevent apoptosis and remain dormant, pending requirement for daughter cells (Lacosta *et al.,* 2007; Medic *et al.,* 2011). In mice, melanocyte stem cells are located in specific areas within the lower part of the hair follicle bulge (Yang *et al.,* 2008). This area is composed of numerous skin stem cells, including follicular stem cells and keratinocytes (Djian-Zaouche *et al.,* 2012). Cultured cells isolated from bulge areas grew into cell lineages similar to those of adult skin (Qiu *et al.,* 2010). The cell migratory capability and flexibility demonstrated in related studies indicated that the niche melanocyte stem cells maintained the characteristics of their neural crest origin (Yamaguchi[1] and Hearing, 2009). Colonization of neighbouring hair follicle bulge regions occurs by melanocyte stem cells after leaving their primary location and then migrating to the epidermis (Gad *et al.,* 2008; Curchoe *et al.,* 2010). Pigment-producing offspring are produced in this area by melanocyte stem cells (Zhao *et al.,* 2009; Nishimura, 2011). In human and mouse skin, isolated neural crest-derived cells characterised as skin-derived precursor

cells, have the potential to differentiate into neural and mesodermal cell lineages (Gianakopoulos *et al.,* 2011).

The expression of both *Dct* and *Pax3* has been identified in isolated melanocyte stem cells without the expression of other melanocyte indicators such as Lymphoid enhancer binding factor 1 (*Lef1*), *Mitf*, tyrosine-protein kinase Kit (*Kit*), *Sox10* and tyrosinase (Tatlidil *et al.,* 2011). Development and differentiation of melanocytes requires the expression of *Pax3, Mitf* and *Sox10* (Chen[2] *et al.,* 2010; Dong[2] *et al.,* 2012). Both *Pax3* and *Sox10* induce activation of *Mitf* (Wan *et al.,* 2011; Hauswirth *et al.,* 2012). This combined regulation of *Mitf* establishes equilibrium between expansion of melanocyte cell proliferation and stem cell type (Sommer, 2011). The promotion of a lineage-restricted stem cell type being *Pax3*(+), *Sox10*(−) and *Mitf*(−), has been demonstrated to be dormant and fail to undergo apoptosis (Djian-Zaouche *et al.,* 2012).

In melanocyte stem cells, the molecular balance of *Mitf, Sox10* and *Pax3* is greatly affected by the Wnt signaling pathway (Sanchez-Ferras *et al.,* 2012). Melanocyte stem cells are directed either to differentiate or to avoid senescence by *Wnt*, or its downstream activator protein beta-catenin (Hutcheson *et al.,* 2009; Wong[1] *et al.,* 2013). The functional modulation of *Pax3* and *Mitf* stimulates beta-catenin to induce differentiation of cells (Mascarenhas *et al.,* 2010). The presence of beta-catenin opposes *Pax3* inhibition of cell differentiation (Hong and Bain, 2012). The repression of *Dct* expression by *Pax3* requires *Grg4* as an upstream enhancer co-repressor (Li *et al.,* 2009). Both *Pax3* and *Dct* expression have been demonstrated in melanocyte stem cells (Jiao *et al.,* 2006). In the nucleus, activated beta-catenin induces the production of a beta-catenin/*Mitf/Lef1* activator complex, which inhibits the *Pax3/Grg4* repressor complex, allowing the expression of *Dct* (Hutcheson *et al.,* 2009; Wong[1] *et al.,* 2013). The production of immature melanoblasts and melanocytes without expression of *Dct* occurs following inhibition of beta-catenin by gene deletion or increased expression of the *Wnt* inhibitor dickkopf-related protein 1 (*DKK1*) (Kennedy *et al*., 2009). Therefore, *Dct* expression in melanocyte precursors expressing Pax3 requires active beta-catenin (Hutcheson *et al.,* 2009; Wong[1] *et al.,* 2013). Activation of *Mitf* expression requires a direct Wnt signaling pathway through downstream signaling of *Wnt3a* via a *Lef1* binding

site located 3' to the *Pax3* response element in the *Mitf* promoter (Sanchez-Ferras *et al.,* 2012). The *Wnt* inhibitors, including disabled homolog 2 (*Dab2*), *DKK3* and *Sfrp1,* can induce repression of this Wnt signaling pathway in melanocyte stem cells (Pallafacchina *et al.,* 2010). Many Wnt inhibitors, including secreted frizzled-related protein 1 (*Sfrp1*), Wnt inhibitory factor 1 (Wif1), *DKK4* and *Dab2* are expressed by melanocyte stem cells (Su[3] *et al.,* 2013). Inhibition of Wnt signaling induces melanocyte differentiation (Mousavi and Jasmin, 2006) and maintains stem cells *Wnt* signaling sustains melanoblasts (Bosserhoff *et al.,* 2011). For instance, embryonic melanoblast development requires *Wnt1* and *Wnt3a* (Fenby *et al.,* 2008). *Pax3* directly activates *Wnt1* expression through a genomic enhancer (Fenby *et al*., 2008). Wnt inhibitors can induce melanocyte stem cells and melanocytes to respond inversely to the Wnt signaling pathway (Li *et al*., 2009; Zhao *et al.,* 2009). Melanocyte proliferation is induced by moderate expression of Mitf, whereas increased *Mitf* expression promotes melanocyte differentiation (Sommer*,* 2011). A *Wnt-Pax3-Mitf* complex model in which *Wnt* signalling was inhibited has been demonstrated to aid dormant type *Pax3* (+), *Mitf* (−) melanocyte stem cell proliferation. Moderate expression of *Wnt* induced expansion of *Pax3*(+), *Mitf*(+) daughter cells, while high expression of *Wnt* stimulated *Pax3*(−), *Mitf*(+) differentiated melanocytes (Kubic *et al.,* 2008; Medic[2] and Ziman, 2010).

Pax3 transcriptional modulation of its direct downstream targets *Mitf, Dct* and tyrosinase-related protein 1 (Tyrp1) can induce inhibition or promotion of melanogenesis in melanocytes (Hou and Pavan, 2008). The capability of *Mitf* to induce activation of several melanocyte-specific genes and to regulate proliferation or differentiation of vital cells means that *Mitf* has been described as a 'master regulator' of melanogenesis (Berlin *et al.,* 2012). The binding of a *Mitf* motif to the M-box induces the activation of the melanocyte differentiation genes, Tyrosinase, *Tyrp1* and *Dct* (Thomas *et al.,* 2009).

Activation of Mitf is induced by binding of Pax3 PD and HD to Mitf transcriptional initiation site via a *cis* regulatory enhancer located upstream (Hirai *et al.,* 2010). *Mitf* is synergistically activated following interaction of both *Sox10* and *Pax3* with the

consensus sites of the Mitf promoter (Bondurand *et al.,* 2007). The activation of *Mitf* by *Pax3* indictaes promotion of melanoblast differentiation to melanocytes.

The expression of *Dct* is activated by *Mitf*, while expression of *Dct* and the binding capability of *Mitf* to the *Dct* promoter is inhibited by *Pax3*. The binding capability of *Mitf* in the *Dct* enhancer sequence, is actively inhibited by *Pax3* repressor complex with *Lef1* and *Grg4*. In the presence of beta-catenin, *Lef1* forms a complex with other binding partners in combination with *Mitf* and beta-catenin, which dislodges *Pax3* from the *Dct* enhancer (Brunelli *et al.,* 2007). In the presence of *Sox10, Mitf* synergistically triggers *Dct* expression (Jiao *et al.,* 2006). *Sox10* in combination with *Pax3* is unable to induce activation of *Dct* in a cell culture system (Mascarenhas *et al*., 2010). Although the molecular pathway that regulates melanocyte development is not recognised in its entirety, *Pax3* modulation of *Lef1, Mitf* and beta catenin is indicative of differentiation of melanocyte stem cells to melanocytes and subsequent cell proliferation and survival (Medic[2] and Ziman, 2010).

1.3.6.4. *PAX3/Pax3* and Cardiac Development

The NC is an essential component of cardiac development. Cells of the cardiac cranial NC migrate from the hindbrain into the outflow tract of the heart where they participate in the division of the septum into pulmonary and aortic channels (Nelms *et al.,* 2011). Cardiac developmental abnormality can cause malfunction in the separation of the outflow, faulty vessels of the pharyngeal arteries and remodelling of the aortic arch (Sambasivan *et al.,* 2009).

Complete cardiac NC cell migration to the developing heart requires normal Pax3 function. Defective neural tube malformation, defective cardiac outflow tract and aortic arches have been demonstrated in Pax3-deficient splotch mice (Morgan *et al*., 2008; Nie *et al.,* 2008). In nitrofen-treated embryos, the expression of Pax3 was significantly decreased in the heart (Gonzalez-Reyes *et al.*, 2006), together with congenital diaphragmatic hernia and other malformations in the offspring after abnormal cardiac development from NC (Olaopa *et al.,* 2011). During tubular heart patterning, the

ladybird-like homeobox (Lbx1) is expressed in cardiac NC cells (Jain *et al.,* 2011). In mice, defective heart loop and changes in gene expression patterns have been observed following inactivation of the Lbx1 (Kumar *et al.,* 2007). The normal differentiation and function of the myocardium during early development of the heart, requires a negative regulatory function of both Pax3 and the Lbx1 (Zhang and Wang, 2011). Expression of *Pax3* and Lbx1 induces a repressor that later inhibits the expression of both *Pax3* and *Lbx1,* depending on the type of tissue and stage of development (Zhao *et al.,* 2009).

Pax3 induces repression of muscle segment homeobox 2 (*Msx2*) expression directly by a preserved *Pax3* interaction site in the *Msx2* promoter (Miller *et al.,* 2007). In splotch mutant mice, increased expression of *Msx2* preventes cardiac development from NC (Patterson *et al*., 2010). Reduced *Pax3* expression and aberrant Pax3 protein induces defective apoptosis in the heart (Gonzalez-Reye *et al.,* 2006; Lacosta *et al.,* 2007). In mice, deficiency of *Pax3* expression, lead to lower numbers of cells migrating into the pharyngeal arch, caused deficiencies in cardiac outflow tract and arterial smooth muscle cells (Nie *et al.,* 2008; Sambasivan, *et al.,* 2009).

1.3.6.5. *PAX3/Pax3* and Myogenesis

PAX3/Pax3 is crucial for the development of skeletal muscles originating from the paraxial mesoderm enclosing the neural tube (Liu *et al.,* 2006). Early restriction of expression of both *PAX3* and *PAX7*, demonstrated in dermomyotome cells, induced the development of cells into dermis or skeletal muscle of the trunk and limb (Lee[1] *et al.,* 2013). Evidence from a study of muscle precursors, suggested that expression of Pax3 induced myoblast migration and expression of the myogenic regulatory transcription factors, myogenic differentiation antigen 1 (*MyoD1*), myogenin (*Myf-4*), myogenic factor-5 (*Myf-5*) and myogenic factor-6 (*Myf-6*) (**Fig. 1.7**) (Simone and Amy, 2010).

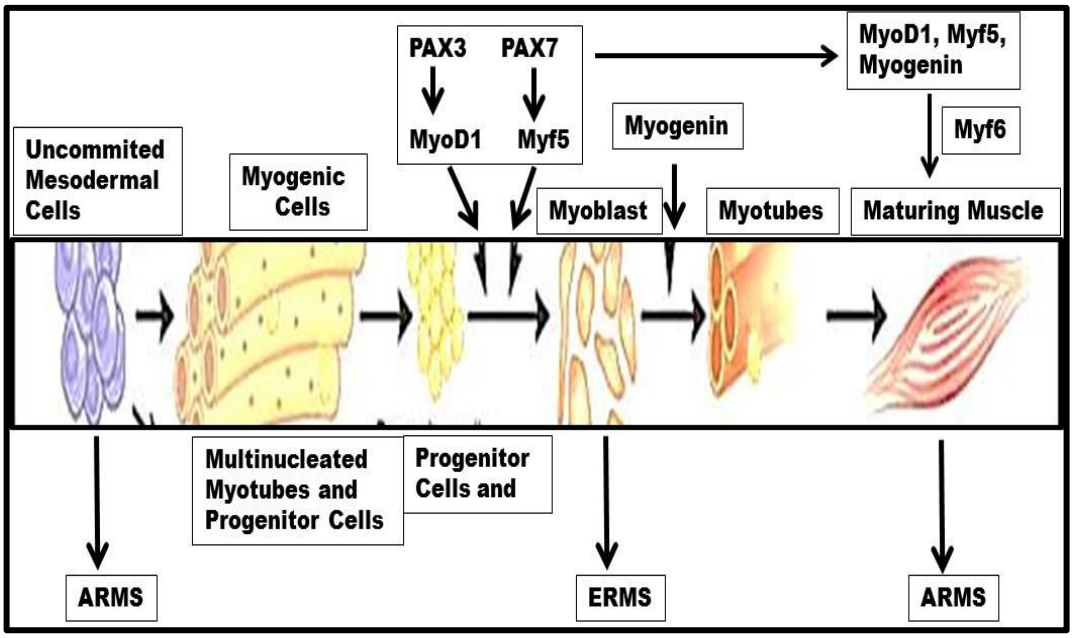

Figure 1.7 *Pax3* and *Pax7* are involved in myogenesis in the embryo and in the adult (taken from Simone and Amy, 2010). Both *PAX3* and *PAX7* activates MyoD1, Myf5, Myf6 and myogenin to promote the development of progenitor cells, myoblast and myotubes into a mature muscle. Aberrant *PAX3* and *PAX7* at various stages of myogenesis leads to ARMS and ERMS.

The myogenic transcription factors (*PAX3, PAX7, MyoD, Myf5,* myogenin and *Myf6*), which direct both embryonic myogenesis and terminal differentiation could lead to embryonal rhabdomyosarcoma (ERMS) and ARMS when aberrantly expressed (Daubas *et al.,* 2013). The expression of *Pax3* decreases during both muscle tissue differentiation and muscle-specific transcription factor activation (Goljanek-Whysall *et al.,* 2011) whilst ectopic expression of *Pax3* has been demonstrated to induce inhibition of myoblast differentiation into myotubes (Scuoppo *et al.,* 2007; Cairns *et al.,* 2012).

In limb muscle development, migration of hypaxial muscle precursors was induced by decreasing *Pax3* expression, thus inhibiting C-Met tyrosine kinase receptor (Boutet *et al.,* 2010). Inhibition of *Pax3* expression in mice, which induced normal myogenesis in the trunk, inhibited myogenesis in the limbs (Hutcheson *et al.* 2009). In a mouse pluripotent stem cell line, increase *Pax3* expression induced cell proliferation and migration necessary for myogenesis (Belay *et al.,* 2010), where as decreased *PAX3* expression inhibits activation of both *MyoD* and myogenin to prevent terminal differentiation (Krskova *et al.*, 2011; Calhabeu *et al.,* 2012). Decreased *Pax3* expression

can prevent differentiation of muscle progenitors also by repressing *Met* expression and migration to sites of muscle terminal differentiation (Grabellus *et al.*, 2010), yet activation of *Pax3* in muscle tumours induces increased expression of *C-Met* (Grabellus *et al.,* 2010). In a study of *P19* murine embryonal carcinoma cells, *Wnt3* induced increased expression of *Pax3,* which in turn activated *Six1, Eya2* and dachshund gene homologue 2 (*Dach2*). This demonstrates that skeletal myogenesis requires *Pax3* transcriptional regulatory activity (Goljanek-Whysall *et al.,* 2011).

During development of the myogenic lineage, *PAX3* and *PAX7* show overlapping co-expression patterns (Bae *et al.,* 2013). Co-expression of both *Pax3* and *Pax7* in mouse myotome at E10.5 demonstrated that approximately 87% of cells were $Pax3^{+}Pax7^{+}$, 10% were *Pax3*+ only, and 3% were $Pax7^{+}$ only (Deries *et al.,* 2010). A spatial and temporal expression difference has been demonstrated in areas where *PAX3* and *PAX7* expressed (Olguín *et al.,* 2011). In skeletal myogenesis, high expression of *Pax3* induces both cell migration and myoblast differentiation (Sousa-Victor *et al.,* 2011). Expression of *Pax3* in the progenitors of adult skeletal muscle signified that *Pax3* is essential for myogenesis after birth (Relaix *et al*, 2005; Boutet *et al.,* 2010). The role of *Pax3* and *Pax7* in myogenesis has been established using mutant mice (Griffith *et al.,* 2009). The complete absence of limb and ventral trunk muscles in Splotch ($Pax3^{-/-}$) mice is suggestive of crucial roles for *Pax3* and *Pax7* (Bradshaw *et al.,* 2009). *PAX3* mutations in man has been demonstrated by Buchberger *et al., (*2007) to be associated with limb muscle hypoplasia in patients with the disorder 'Whole Stomach', since a screene of these patients showed mutation in *PAX3*. The functional activities of *PAX3* and *PAX7* in myogenesis are strongly related but the absence of *PAX3* expression is not counteracted by the presence of *PAX7* (Buckinghan[2] and Relaix, 2007).

1.3.7. *PAX/3Pax3* Gene Alternative Splicing

Alternative splicing (AS) of *PAX3/Pax3* is a major posttranscriptional mechanism in which multiple discrete *PAX3/Pax3* transcripts are generated (Biamonti *et al*., 2012; Chen *et al.,* 2012). PAX/Pax proteins have been demonstrated to modulate transcriptional activity of downstream genes, through binding of DNA promoter

sequences with their highly conserved PD at the amino (N)-terminal end (Martin and Wang, 2011; Berlin *et al.,* 2012). Phosphorylation, which is essential for regulation of binding interactions with other protein binding elements to induce transcription occurrs in the conserved proline-threonine-serine-rich sequence of the TA within the carboxyl (C)-terminal end of the PAX/Pax protein (Wang[1]. *et al.* 2008; Holland and Short, 2010). Various groups of *PAX/Pax* genes, which have been identified to undergo AS, resulted in different isoform, were differentiated by their varying number of exons or length (Holland and Short, 2010). A comparison of *PAX/Pax* in both vertebrates and *amphioxus* demonstrated that 52 variants occur in vertebrates while 23 variants occur in *amphioxus* (Chen[2] *et al.,* 2010). The ancestral functional activities and expression patterns of PAX/Pax proteins are conserved in vertebrates (Chen *et al.,* 2012). The distribution of transcript variants encoding a PD with an alternative carboxyl terminus with enhanced transactivational activity is not well-understood (Hawkins *et al.,* 2010).

Different expression patterns and activities of PAX3 C-terminal variants have been demonstrated in melanocytes and melanoma cell lines. However, in primary myoblasts the most highly expressed isoform is not clear, even though the involvement of full-length variants was investigated (Paternoster *et al.,* 2012). Extra variants of Pax3 in the neural plate of vertebrates have been suggested to allow novel functions (Boutet, *et al*., 2010). Correspondingly, in the case of Pax4 and Pax6, vertebrate-specific AS events occurring on exon 5a are associated with the development of the eye (Holland and Short, 2010). The occurrence of AS at the 3'-end has been demonstrated in PAX7 (Charytonowicz *et al.,* 2011). Exons 1–8 and 1–9, demonstrated in PAX7A and PAX7B respectively indicate that exon 8 is spliced at a conserved site and then joined to exon 9 (Chen *et al.,* 2012). Murine Pax7B and human PAX7B are generally 97% homologous and 100% homologous at the C-terminus, whereas human PAX7A and mouse Pax7A are 96% homologous upstream of the 8th exon but only 7% homologous downstream (Wang[1] *et al.,* 2008; Olguín and Pisconti, 2012).

1.3.7.1. *PAX3/Pax3* Gene Isoforms

PAX3/Pax3 and *PAX7/Pax7*, which are similar in structure, extend to 10 exons (Wang[2] *et al.* 2008; Holland and Short, 2010). During development, AS occurring in the encoding region of the N-terminal PD, induces expression of multiple variants (Paternoster *et al.,* 2012). The diverse DNA-binding events displayed by N-terminal *Pax3/7* variants, are expected to modulate distinct expression patterns of a range of downstream target genes *PAX3* variants demonstrated in humans have different C-termini (Charytonowicz *et al.,* 2011). In humans, mice and other organisms, an extra alternative C-terminal variant of *Pax3* has been demonstrated (Wang *et al.,* 2007). Parker *et al*. (2004) first identified new isoforms. During AS, splicing of the 8th exon to the 9th exon at a conserved point produces the major variants, *PAX3c* and *PAX3d.* The transcription of *Pax3c* and *Pax3d* in mice, produced an extra inactive *Pax3g* deficient in exon 8 (Wang[2] *et al.,* 2008). Studies of *PAX3* structure and developmental roles in human tissues and tumours, identified regular AS events occurring at the 5' end of exon 3, resulting in the inclusion or exclusion of a single codon, encoding a glutamine residue that modifies the PD box to generate two isoforms Q+ and Q- respectively (Short and Holland, 2008; Sumegi *et al.,* 2010). *PAX/Pax3* has the ability to modulate various developmental activities because of AS (Gutkovich *et al.,* 2010) and *PAX3/Pax3* variants play various physiological roles in transcription, sequence-specific DNA binding, embryogenesis, oncogenesis and other biological processes, such as migration of NC cells, neural tube closure and sensory recognition of sound (Castranio and Mishina, 2009). *PAX/Pax3* AS, which generally alters the C-terminal end of the HD, mostly induce a frame shift, which in turn changes the function of the TA (Gutkovich *et al.,* 2010).

Currently seven main AS isoforms of *PAX3* are known in man: *PAX3a, PAX3b, PAX3c, PAX3d, PAX3e, PAX3g* and *PAX3h* isoforms which have different expression patterns, suggesting unique functions and *Pax3d* has been identified as the most functional and active variant in cancer (**Fig. 1.8**), (Parker *et al.,* 2004; Wang *et al.,* 2007).

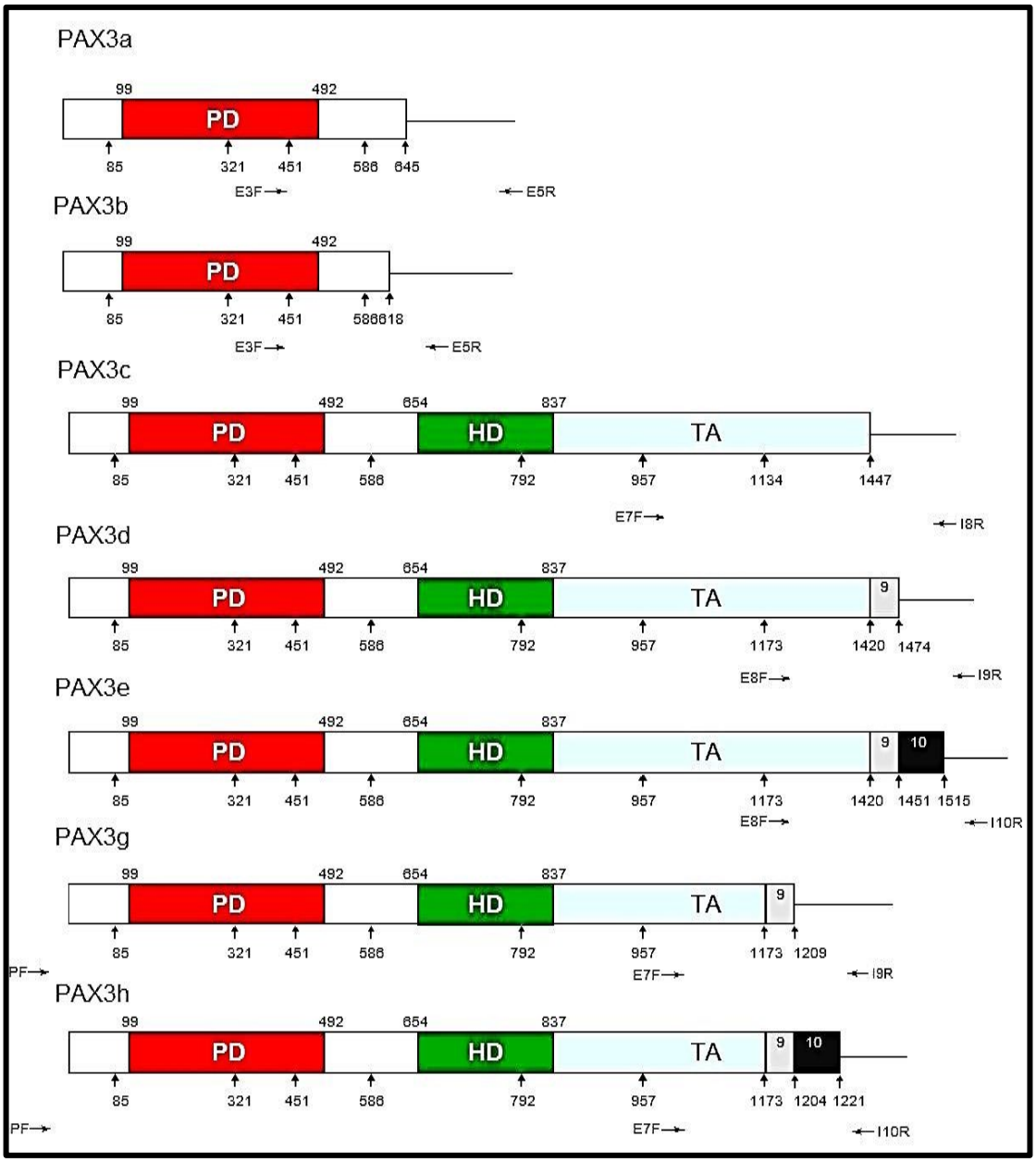

Figure 1.8 The schematic structure of seven alternatively spliced *PAX3* isoforms both *PAX3a* and *PAX3b* were amplified using exon 3 forward and exon 5 reverse primers, contained only PD (Red*); PAX3c* was amplified using exon 7 forward and intron 8 reverse primers, contained PD, HD (green) and TA (ligh aqua); *PAX3d* was amplified using exon 8 forward and intron 9 reverse primers, contained PD, HD and TA; *PAX3e* was amplified using exon 8 forward and intron 10 reverse primers, contained PD, HD and TA; *PAX3g* was amplified using exon 7 forward and intron 9 reverse primers, contained PD, HD and TA; *PAX3h* was amplified using exon 7 forward and intron 10 reverse primers, contained PD, HD and TA (Taken from Parker *et al.,* 2004).

The *PAX3a* transcript extends from exons 1 to 4 whilst *PAX3b,* which extends from exons 1 to 5, is truncated early in intron 4. It lacks the HD and the carboxyl-terminal TA (White *et al.,* 2008; Graveley, 2009). *PAX3a* and *PAX3b* variants vary in the 3' UTR, which includes an alternative segment in the coding region, causing a frameshift and lacks many segments in the 3' coding areas, compared to other *PAX3* variants (Graveley *et al,* 2011). The resulting *PAX3a* and *PAX3b* proteins have distinctly shorter C-termini than other *PAX3* proteins (Charytonowicz *et al.,* 2011). *PAX3b* is highly expressed in most tissues but *PAX3a* occurs only in oesophagus, skeletal muscle and cerebellum (Kang and Krauss, 2010).

Structurally the *PAX3c* transcript consists of a PD, HD and a carboxyl-terminal TA that extends to exon 8. It varies in the 3' UTR and contains an alternative splice site in the 3' coding region that differs from other *PAX3* variants (Graveley, 2009). *PAX3c* interacts with DNA as monomers or as homo-and/or heterodimers in a sequence-specific fashion (Mudge *et al.,* 2011).

The *PAX3d* transcript, which uses an alternative in-frame splice site in the 5' coding region, varies in the 3' UTR and retains an alternative splice site in the 3' coding region, (Graveley, 2009). The resulting *PAX3d* protein, also known as PAX3dQ+*,* structurally consists of a PD, HD and carboxyl-terminal TA that extends to exon 9. *PAX3d* does not contain intron 8 and translation continues from exon 8 to exon 9. The resulting PAX3d protein is longer and has a distinct C-terminus compared to other *PAX3* proteins (Charytonowicz *et al.,* 2011).

Structurally the *PAX3e* transcript, which consists of a PD, HD and a carboxyl-terminal TA, is made up of exons 8, 9 and 10 but lacks introns 8 and 9. It differs in the 3' UTR and contains an alternative splice site in the 3' coding region different from other *PAX3* variants (Paternoster *et al.,* 2012). The resulting PAX3e protein is the longest and has a distinct C-terminus (Charytonowicz *et al.,* 2011).

The *PAX3g* transcript, which consists of a PD and HD, but lacks a carboxyl-terminal TA, extends to exon 8. It is a truncated isoform of *PAX3d* lacking part of the TA encoded by exon 8, varies in the 3' UTR and maintains an alternative splice site in the 3' coding region different from other *PAX3* variants (Zhang[2] *et al.,* 2009). The resulting PAX3g protein is shorter and has a distinct C-terminus (Charytonowicz *et al.,* 2011).

The *PAX3h* transcript consists of a PD and a HD and like *PAX3g* lacks a part of the TA but extends to exon 10. *PAX3h* is a truncated isoform of PAX3e, differs in the 3' UTR and contains a different alternative splice site in the 3' coding region (Zhang[2] *et al*., 2009). The resulting PAX3h protein is shorter and has a distinct C-terminus (Charytonowicz *et al*., 2011).

1.3.8. *PAX3/Pax3* and Development of Disease

Mutations or dysregulation of *PAX3/Pax3* provide a clear understanding of its essential functional activities in embryonic development but also trigger detrimental syndromes (Waardenburg's syndrome and Craniofacial-deafness-hand syndrome). Its aberrant expression results in various cancers including rhabdomyosarcoma, melanoma and neuroblastoma (Zohn, 2012).

1.3.8.1. *PAX3/Pax3* Gene Mutations

Functional defects of *Pax3* occur in Splotch mice and human Waardenburg's syndromes I and III, while *Pax3* overexpression or re-expression occur in neuroblastoma, melanoma, rhabdomyosarcoma and chromosomal translocations are observed in ARMS (Nie *et al.,* 2008; Hayashi *et al.,* 2011). Germ-line mutations of *PAX3* produce Waardenburg's syndrome types I and type III, a non-neoplastic autosomal dominant disorder distinguished by hearing loss and pigmentary defects (Yang[2] *et al.,* 2012). The common feature observed in this abnormality is missense mutations, occuring in encoding regions of the PD or HD (Kohli *et al.,* 2010). Additionally, there are minor deletions, insertions, as well as a few base substitutions at splicing sites, modify the reading frame (Kozawa *et al*., 2009). More than a few cases of substantial deletions and

chromosome 2 translocations in rhabdomyosarcoma and missense mutation in Craniofacial-deafness-hand syndrome have been demonstrated (Nie *et al*., 2008).

1.3.8.2. *Pax3* and the Splotch Mouse

The heterozygous Splotch (Sp) mouse shows an incomplete lack of Pax3 functional activity and is characterised by a white belly spot on the stomach, tail and feet (Greene *et al.,* 2009). Splotch mice possess a Pax3 mutation in the third intron producing four alternative transcripts, three of which result in truncated mRNAs with incomplete or missing domains due to early termination (Thompson *et al,* 2008). The fourth transcript lacks the end of the PD and the OP (exon 4) is spliced out (Bradshaw *et al*., 2009). Homozygous Sp2H mutation, resulting from the deletion of 32bp within exon 3 results in embryonic death by E16. A Pax3 semi-dominant mutation has been demonstrated to produce the Sp2H (Griffith *et al.,* 2009). In mice, both Pax3 and Sp loci were initially tightly mapped together on chromosome 1 and shortly after recognised as an identical gene (Greene *et al*., 2009). In mice, six Splotch mutants, which developed from several *Pax3* deletions or mutations, which induce a variety of phenotypic gravity (Brzóska *et al.,* 2009). The first Splotch (Sp) and the Splotch delayed (Spd) were produced by random mutations within Pax3, while the Sp retarded (Spr), Sp1H, Sp2H and Sp4H mutants were formed after X-irradiation (Griffith *et al.,* 2009; Cabrera[1] *et al.,* 2012).

Sp homozygous with cardiac and neural crest defects, which die mid-gestation exhibit neural tube and neural crest product abnormalities (Davidson *et al*., 2007). Derivatives of the neural crest associated with developmental problems include the CNS, Schwann cells, melanocytes, dorsal root (sympathetic) ganglia, thyroid, thymus, cardiac tissue such as the aortic arches and myotome-derived limb muscles (Snider *et al.,* 2007; Nakazaki *et al*., 2009). Pigmentation malformations occurr owing to inefficient melanocyte precursor (melanoblast) proliferation and migration (Zhou *et al.,* 2008; Bosserhoff *et al.,* 2011). Sp, Sp1H and Sp2H mutants have related phenotypes, which imply that they are all produced from loss of Pax3 functional activity (Bradshaw *et al.,* 2009). The Splotch-delayed (Spd) homozygous mouse was produced because of a spontaneous transversion of glycine to arginine in the PD that permited a full length

protein (Greene *et al*., 2009). Homozygous Spd composed spina bifida, which permited survival until birth. Analysis of the homozygous Spd embryo demonstrates that neural tube defects, which are confined to the posterior end, are different from the whole neural tube defects identified in Sp, Sp1H and Sp2H mutants (Greene *et al.,* 2009). Spd mutants exhibit a decreased size and number of spinal ganglia, in contrast to Sp mice which lack spinal ganglia altogether (Griffith *et al.,* 2009). Spd mice display a reduction in limb bud muscle primordia that mature into the septum of the truncus arteriosis in the heart. Defects caused by Spd mutants are less severe than Sp mutants and indicate that Spd is produced by incomplete loss of *Pax3* functional activity. The homozygous Splotch-retarded mutant (Spr) appears to be a severe phenotype, which induces embryonic death before implantation. Spr is produced by a huge chromosomal deletion of 14-16 centimorgans in *Pax3* (Snider *et al.,* 2007). In heterozygous Spr mice, pigmentation abnormalities and growth retardation have been demonstrated (Griffith *et al.,* 2009). Sp4H is produced by a complete deletion of *Pax3* that induces embryonic death shortly after implantation (Bradshaw *et al.,* 2009).

1.3.8.3. *PAX3/Pax3* and Waardenburg's Syndrome

Waardenburg syndrome (WS), a widespread cause of inherited deafness in infants is an autosomal-dominant disorder characterised by sensorineural hearing loss (of varying severity), dystopia canthorum (lateral displacement of the inner corners of the eye) and pigmentary disorders of the skin, hair and eye (Corry *et al*., 2008; Kapoor *et al.,* 2012). WS is categorised into four variants: WSI, WSII, WSIII and WSIV. WSI and WSIII were the only types of WS previously identified to be linked with *PAX3* mutations until recently, when WSII was demonstrated to be associated with *PAX3* mutations (Hazan *et al.,* 2013; Yang[2] *et al.,* 2013). WSIII is usually connected with deletions of the long arm of chromosome 2 comprising multiple genes including *PAX3,* whereas WSI is commonly linked with intragenic mutations in *PAX3* (Daneshi *et al*., 2005; Wildhardt *et al.,* 2013). WSII is heterogeneous and can also be produced by mutations in the *MITF* gene (Grill *et al*., 2013). WSIV is triggered by mutations in endothelin-3 (*EDN3*), endothelin receptor type B (*EDNRB*) and *SOX10* (Jiang[1] *et al.,* 2011; Fernández *et al.,* 2014).

The similarity between WS types in humans and Splotch mice soon led to the idea that similar genes induced these conditions or they were involved in the same molecular pathways (Demirci *et al.,* 2011; Otręba *et al.,* 2013). Other signs of WSI include a broad nasal bridge and pigmentation defects, which subsequently cause early hair greying, iris heterochromia and patchy skin hypopigmentation (Gad *et al.,* 2008). Diverse *Pax3* mutations, which cause WS, induce missense or frameshift mutations in the highly conserved areas of exon 2, which modifies the DNA binding affinity of the PD causing loss of Pax3 function (Hager *et al*., 2010). WSIII, well- known as Klein-Waardenburg syndrome, presents with symptoms similar to WSI and causes musculoskeletal abnormalities (Wollnik *et al.,* 2003).

1.3.8.4. *PAX3* and Craniofacial-Deafness-Hand Syndrome

Craniofacial-deafness-hand syndrome (CDHS) is an autosomal dominant *PAX3* mutation categorised by distinct facial characteristics, a small, short nose with slit-like nares, hypertelorism, acute hearing loss and short palpebral fissures. Other symptoms include aberrations of hand muscles that can inhibit movement at the wrist and ulnar deviations of the fingers, absence or hypoplasia of the nasal bones and extreme sensorineural deafness (Gad *et al.*, 2008; Sonnesen *et al.,* 2008). Defective neural crest cells result in absence of functional specialisation resulting in overgrowth of craniofacial bones and impairment of muscles and nerve tissues (Haldeman-Englert *et al.,* 2012). A missense mutation in the PD, which was detected in a family of three (a mother and two children), defined this syndrome (Sommer and Bartholomew, 2003). This mutation affects *PAX3* binding to DNA and inhibits *PAX3* regulation of downstream target genes (Mues *et al.,* 2009).

1.3.9. *PAX3/Pax3* in the Development of Cancer

Aberrant *PAX3/Pax3* gene expression, which affects its downstream targets, induces disruption of the various signalling pathways regulated by *PAX3/Pax3* (Sanchez-Ferras *et al.,* 2012). Abnormal *PAX3/Pax3* expression is associated with embryonal rhabdomyosarcoma (ERMS), alveolar rhabdomyosarcoma (ARMS), Ewing's sarcoma and neural-crest-derived tumours including cutaneous melanoma, neuroblastoma and

neuroectodermal tumours such as squamous cell lung carcinomas (Michael *et al.*, 2012). Repression of an aberrant *Pax3* expression prevents inappropriate cellular activities and implicates its direct involvement in tumourigenesis. For instance, repression of *Pax3* expression induced inhibition of cell proliferation both *in vitro* and *in vivo* in young mice (Pham *et al.*, 2012). Knockdown of *pax3* expression by miRNA stimulated increased expression of *MyoD*1 to induce cell apoptosis (Hirai, *et al.,* 2010).

During development, the expression of *PAX3* promotes cell cycle and proliferation of Schwann cells whilst regulating Schwann cell differentiation and inhibition of apoptosis through repression of *TGFβ1* (Doddrell *et al.,* 2012). The oncogenic potential of *PAX3* through modulation of downstream cell cycle and proliferation regulatory genes has been previously demonstrated. For instance, tumour cell proliferation requires the re-expression of *PAX3* whilst inhibition of tumour cell growth entails down-regulation of *PAX3* expression (Xia *et al.,* 2013). Expression of *PAX3* in mouse embryos promotes myogenesis of dermomyotome somitic stem and progenitor cells through regulation of notch signaling, whereas induction of proliferation of muscle progenitors was achieved through repression of *Pitx2c* expression (Lozano-Velasco *et al.,* 2011).

The cell cycle regulatory mechanism under the influence of *Pax3* mRNA expression in neuronal cells has been demonstrated. A serum starvation treatment of mouse ND7 cells for 24 hr, induced a G1 phase cell growth arrest in 89% of the cell population. During that study, the addition of serum to the cell culture medium liberated the cells from this blockade. Intriguingly, the level of *Pax3* mRNA fluctuated throughout the cell cycle and during cell growth arrest, no *Pax3* mRNA expression was detected (Chishti *et al.,* 2013). Conversely, within 1 hr following the addition of serum, the expression of *Pax3* mRNA which was low initially, then increased at 6 hr after serum addition and finally declined as cells entered S phase (Magli *et al.,* 2013). This demonstrates that *Pax3* mRNA expression seems to be cell cycle-dependent, signifying that *Pax3* plays a role in the progression of the cell cycle and/or in directing cell proliferation and differentiation.

1.3.9.1. Rhabdomyosarcoma

Rhabdomyosarcoma, a frequently occurring childhood soft tissue sarcoma, is subdivided into four histological sub-types: ERMS (**Fig. 1.9A**) and ARMS **(Fig. 1.9B**) are the most prevalent variants, while less common are Spindloid and Botryoid variants (Sumegi *et al.,* 2010; Liu *at al*., 2012).

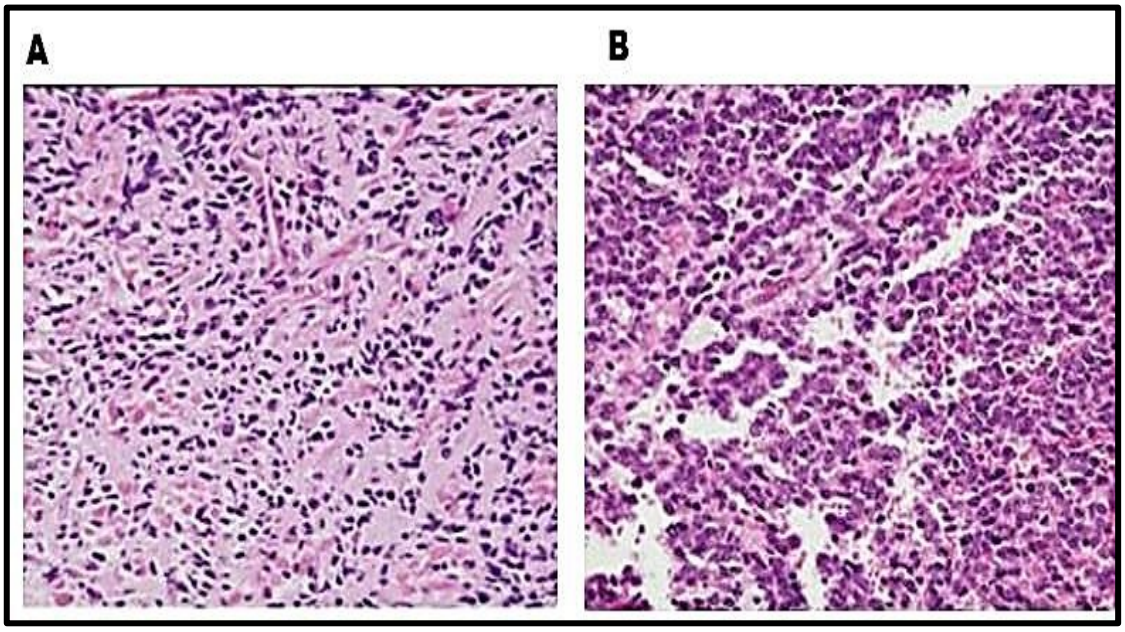

Figure 1.9, X 20 magnification of Haematoxylin and eosin (H&E) of RMS. A, ERMS containing visible irregular elongated, flattened, shrunken and scattered rhabdomyoblasts with eosinophilic cytoplasm. **B**, ARMS with many alveoli spaces lined with numerous rounded granular eosinophilic and swollen rhabdomyoblasts and loss of cellular cohesion (taken from Sumegi *et al.,* 2010).

In contrast to ERMS, which occurs mainly in children, ARMS frequently appears in adolescents and young adults. Although RMS can develop from any organ, the most commonly affected parts of the body include muscle of cheek or lips, head and neck, nose, throat, extremities of arms and legs, genitourinary system including vagina, prostate, bladder and testicles, as well as the eye orbit and parameninges at the base of the skull (Demetri, 2011). Primary rhabdomyosarcomas are usually found in areas of skeletal muscle, including the appendages and trunk (Gallego and Sanchez, 2007; McLean and Castellino, 2008). In most cases, ERMS has a more favourable outcome than ARMS, which has a very poor prognosis (Yu[2] *et al.,* 2012).

1.3.9.1.1. Causes of Rhabdomyosarcoma

Even though the exact aetiology of RMS is unknown, *PAX3* gene mutations occur in addition to other syndromes. Genetic disorders which are associated with the development of RMS include Neurofibromatosis type 1, Li-Fraumeni, Beckwith-Wiedemann, Costello s and Cardio-facio-cutaneous syndromes (Ognjanovic *et al.,* 2010; Lupo *et al.,* 2014). RMS presents varying symptoms, which depend on the location of the primary tumour. Painful or painless tumour masses have been the most usually reported symptom. For instance, the location of tumour in the nose or throat presents with congestion, bleeding and swallowing difficulties. Parameningeal and ear tumours are associated with headaches, facial pain, facial asymmetry, dual vision, and painful ears accompanied with swelling, discharge and hearing loss. A painful and swelling eye with vision difficulty has been observed in patients with an orbital tumour. A firm enlarged painful lesion is commonly seen in patients with a tumour located at the extremities. Genitourinary tumours present with urinating difficulty, poor bowel movement control, haematuria, vaginal bleeding, and vaginal or scrotal mass, whilst the extension of tumours in the brain and spinal cord is depicted by abnormal neurological behaviour (Egas-Bejar and Huh, 2014; Lupo *et al.,* 2014).

1.3.9.1.2. Dignosis of Rhabdomyosarcoma

Although many diagnostic tools are available for the diagnosis of RMS, early diagnosis is essential because of the metastatic potential of RMS. However, diagnosis may be delayed in symptomless RMS. A physical examination of suspected swollen tumour mass under the skin is required, followed by imaging diagnostic techniques including magnetic resonance imaging, positron emission tomography, ultrasound and chest x-ray are usually used to study the stage of RMS (Bánusz *et al*., 2014). These techniques, which determine the size, precise location, and metastasis of RMS to distant sites, are very crucial in the selection of the most effective treatment scheme (Hoffmeier *et al.,* 2014). Finally, cytological diagnosis of fine needle aspirate and histological diagnosis of tumour biopsy for confirmation and identification of RMS variants are essential (Nakib *et al.,* 2014).

1.3.9.1.3. Treatment of Rhabdomyosarcoma

Successful treatment of RMS depends on the variant involved and tumour location. The current treatment schemes, which may not completely cure cancer, but are used to prolong the life of patients, involve surgical removal of the tumour, chemotherapy and radiotherapy (Egas-Bejar *at al.,* 2014). Generally, in most treatment schemes, immediately after surgery, the primary site of the tumour is initially treated by radiotherapy whilst chemotherapy is used for treatment of distant tumour metastatic sites in the body. The first line chemotherapeutic regimens that are currently employed for treatment of RMS include vincristine, dactinomycin, cyclophosphamide, topotecan, irinotecan, etoposide, ifosfamide, doxorubicin, and carboplatin. These chemotherapeutic regimens have been demonstrated to effectively inhibit metastasis of less aggressive ERMS tumours (Bánusz *et al.,* 2014; Hoffmeier *et al.,* 2014). Potent treatment schemes are required for the treatment of recurrent RMS after treatment as frequently observed in aggressive metastatic ARMS, which is resistant to treatment. Targeted treatment schemes including gene therapy, as well as hormonetherapy, and immunotherapy are currently being investigated for effective treatment of resistant RMS (Donahue *et al.,* 2014).

1.3.9.1.4. *PAX3/Pax3* Biological Activity in Rhabdomyosarcoma

A high frequency of chromosomal translocations in ARMS, compared to a pattern of whole chromosome gains and losses in ERMS was demonstrated in a cytogenetic and comparative genomic hybridization study (Stegmaier *et al.,* 2011). Although both ERMS and ARMS originate from dedicated myogenic cells, PAX3-FKHR expression in ARMS activates numerous downstream transcriptional targets that presented a discrete and an aggressive type of tumour, distinct from ERMS (Stegmaier *et al.,* 2011). The usual translocation t(2;13)(q35;q14) and the infrequent translocation t(1;13)(p36;q14) forming the fusion proteins, PAX3-FKHR and PAX7-FKHR respectively, are typical of ARMS (Calhabeu *et al.,* 2012). Marshall[2] *et al.,* (2011) demonstrated that both translocations are fusions of the DNA interacting elements of PAX3/7 with the TA of the forkhead transcription factor (FKHR) and are described as FKHR-disrupting translocations (Hecker *et al.,* 2010). Inefficient transcriptional activation has been

demonstrated in ERMS cell lines expressing wild-type PAX3 that interacts with the same DNA targets as PAX3-FKHR. Occasionally 20% ERMS results from PAX3-FKHR fusion, whereas 80% of ARMS cases are associated with FKHR fusions (Krskova *et al.,* 2011). A non-random chromosomal translocation differentiates ARMS tumours from ERMS and other paediatric solid tumours (**Fig. 1.10)** (O'Connor and Barr, 2008; Shukla *et al.,* 2012)

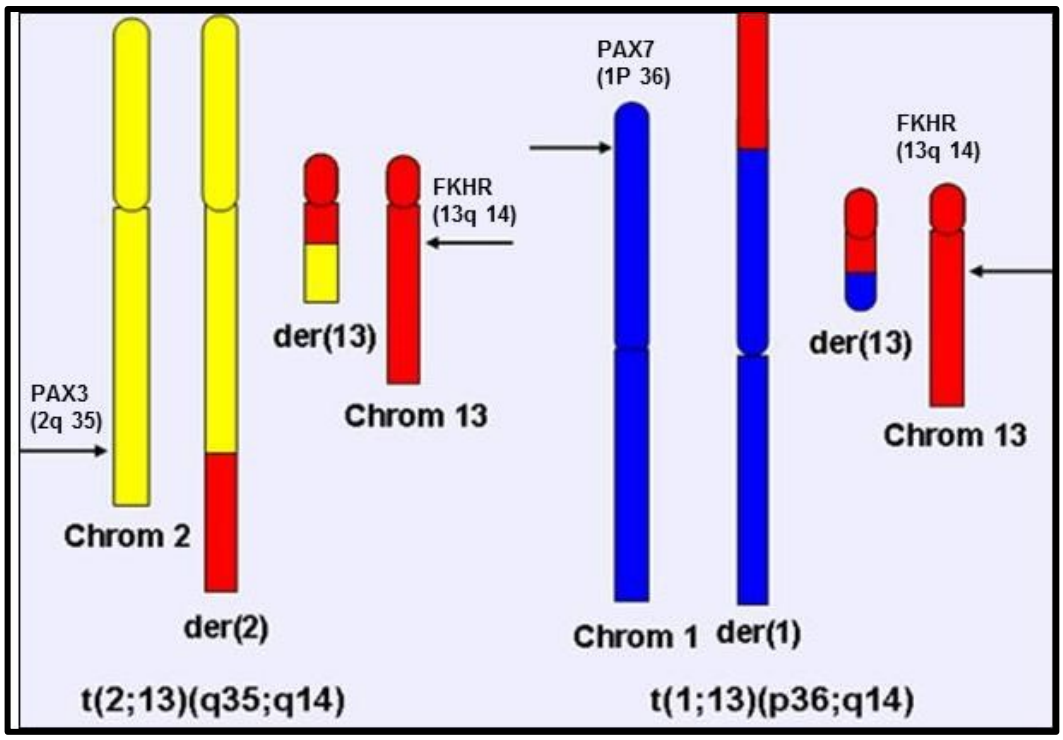

Figure 1.10 Chromosomal translocations in ARMS (taken from O'Connor and Barr, 2008; http//AtlasGeneticsOncology.org/Genes/Foxo1ID83ch13q14.html).

ARMS originates from skeletal muscle precursor (mesenchymal) cells, which can appear in sites other than skeletal muscle (Gallego and Sanchez, 2007; McLean and Castellino, 2008). This generates a protein with the N-terminal end of Pax3, where PD, HD and a part of the TA (first seven exons) are fused to the C-terminal portion of the DNA-binding domain and the TAD (last two exons) of the forkhead protein (FOXO1 or FKHR) **(Fig. 1.11)** (Robson *et al.,* 2006; Reichek *et al.,* 2011). In addition to the chimeric gene produced, a second type of PAX3-FKHR/ PAX3-FOXO1 chimeric gene, which is highly expressed and more stable is found which contains the complete PAX3

N-terminal DNA interacting domain fused to a complete FKHR C-terminal TA (Stegmaier *et al.,* 2011).

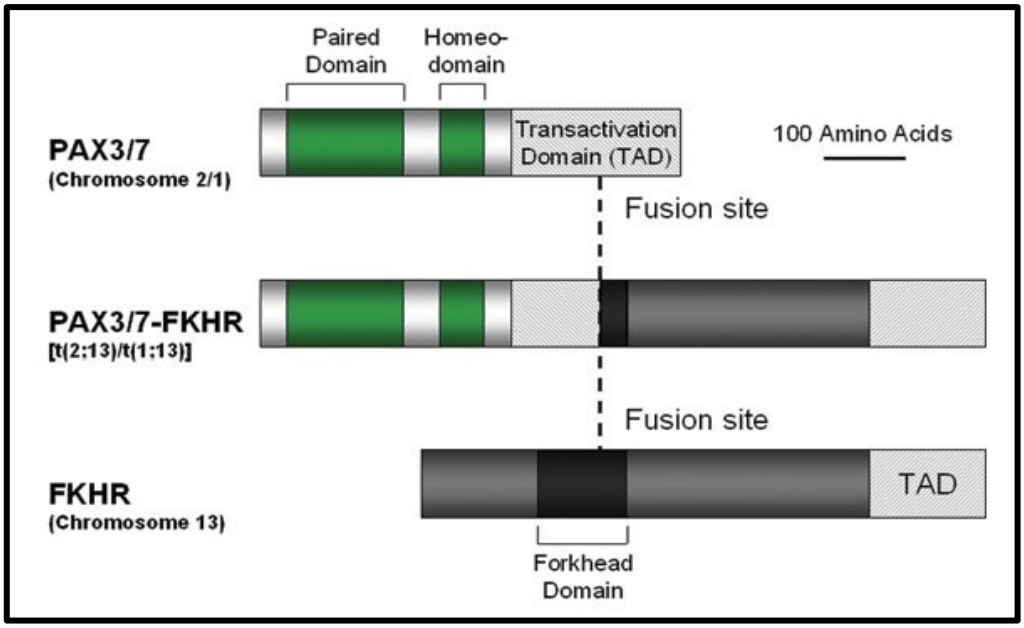

Figure 1.11 Diagram of RMS PAX3/7-FKHR chimeric fusion proteins (taken from Robson *et al.,* 2006). TAD/TA denotes transctivation domain.

The resultant fusion proteins act as malformed transcription factors (Liu[1] *et al.,* 2011). More than 90% of ARMS express a 97 kDa chimeric fusion protein with DNA-binding capabilities analogous to Pax3, functioning as a more potent transcription factor than either Pax3 or FOXO1 (Liu[1] *et al.,* 2011). Pax3-FOXO1 gains oncogenic capacity by dysregulating genes participating in cell proliferation, differentiation, metastasis and apoptosis (Reichek *et al*., 2011). Culture of myoblasts in differentiation medium, demonstrated that Pax3-FOXO1 efficiently inhibited myoblast differentiation into myotubes (Scuoppo *et al.,* 2007; Liu[1] *et al.,* 2011). In ARMS, PAX3 may be combined with an alternative C-terminal partner forkhead box protein O4 (FOXO4). Abnormal Pax3 regulation in either translocations induces equally detrimental effects on paediatric development (Sidhu *et al*., 2010). The expression of both PAX3-FKHR and IGF-II induced cell cycle progression and proliferation of C2C12 myoblasts, whilst inhibiting myogenic differentiation through repression of downstream myogenic factors (Wang *et al.,* 2005). In a related study of ARMS cells, inhibition of *Ink4a/ARF* induced up-

regulation of Cdk4, consequently enhancing the oncogenic potential of PAX3-FOXO1 (Linardic *et al.,* 2007).

Inhibition of PAX3-FKHR in ARM cells induced G1 growth arrest, resulting in fewer cells in S phase while in fibroblasts, ectopic expression of PAX3-FKHR enhanced G0/G1 to S transition and PAX3-FKHR induced degradation of the CDK inhibitor, *P27Kip1* (Stacey *et al.,* 2010). PAX3-FKHR indirectly suppressed the activities of some CDK inhibitors including *P21Cip1* and *P57Kip2* (Li *et al.,* 2007). High expression levels of *P21Cip1* and *P57Kip2* via activation of *EGR-1* were observed during normal myogenesis (Nguyen *et al.,* 2010). In ARMs, proteasomal degradation of EGR-1 induced by PAX3-FKFHR inhibits *EGR-1* activation of *P21Cip1* and *P57Kip2* (Roeb *et al.,* 2007). Interestingly, the suppression of EGR-1 by PAX3-FKHR, which is through protein-protein interactions and not through transcription, signifies that PAX3-FKHR might act as a misfolded protein in association with proteasomes (Hecke *et al.,* 2010). PAX3-FKHR expression has been indicated to collaborate with loss of the CDK inhibitor, *P161NK4a*, stimulating primary myoblasts reach to a tissue culture, induced senescence checkpoint (Linardic *et al.,* 2007; Zhang and Wang, 2011). In recent times, ERMS has been found to harbour one PAX3-NCOA2 translocation. The tumourigenic activity of ERMS has been demonstrated in murine C2C12 myoblasts by transfecting the PAX3-NCOA2 translocated gene. This characteristic of ERMS is comparable with the PAX3-FOXO1 observed in ARMS (Yoshida *et al.,* 2013).

Inhibition of PAX3-FKHR in ARM cells induced G1 growth arrest, resulting in fewer cells in S phase while in fibroblasts, ectopic expression of PAX3-FKHR enhanced G0/G1 to S transition and PAX3-FKHR induced degradation of the CDK inhibitor, *P27Kip1* (Stacey *et al.,* 2010). PAX3-FKHR indirectly suppressed the activities of some CDK inhibitors including *P21Cip1* and *P57Kip2* (Li *et al.,* 2007). High expression levels of *P21Cip1* and *P57Kip2* via activation of *EGR-1* were observed during normal myogenesis (Nguyen *et al.,* 2010). In ARMs, proteasomal degradation of EGR-1 induced by PAX3-FKFHR inhibits *EGR-1* activation of *P21Cip1* and *P57Kip2* (Roeb *et al.,* 2007). Interestingly, the suppression of EGR-1 by PAX3-FKHR, which is through protein-protein interactions and not through transcription, signifies that PAX3-FKHR

might act as a misfolded protein in association with proteasomes (Hecke *et al.,* 2010). PAX3-FKHR expression has been indicated to collaborate with loss of the CDK inhibitor, *P161NK4a*, stimulating primary myoblasts reach to a tissue culture, induced senescence checkpoint (Linardic *et al.,* 2007; Zhang and Wang, 2011). In recent times, ERMS has been found to harbour one PAX3-NCOA2 translocation. The tumourigenic activity of ERMS has been demonstrated in murine C2C12 myoblasts by transfecting the PAX3-NCOA2 translocated gene. This characteristic of ERMS is comparable with the PAX3-FOXO1 observed in ARMS (Yoshida *et al.,* 2013).

Expression of Pax3 has great influence on the metastasis RMS, melanoma and neuroblastoma. Protease degradation of the ECM such as matrix metalloproteinase permits tumour metastasis into distant sites (Hu[1] *et al.,* 2013). *PAX3* directly or indirectly modulates the up-regulation or down-regulation of downstream target genes to induce tumour cell adhesion, migration, and metastasis. For instance, the expression of *pax3* in mouse promotes myoblast cell migration to the limb during colonisation of endothelial and skeletal muscle (Yvernogeau *et al.,* 2012). In ARMS cells (RH2, RH4, RH18, RH30 and RH41) cell lines, the up-regulation of *RasGRF1* induced cell migration whilst shRNA down-regulation of *RasGRF1* inhibited ARMS cell migration (Tarnowski *et al.,* 2012). Alteration of *IGF-1* expression induced F-actin to regulate RH30 cell migration both *in vitro* and *in vivo* (Liu *et al.,* 2008).

PAX3 repression of *ILK* expression decreased basal RMS cell adhesion and in RH18 and RH30 ARMS cell lines, decreased expression of *PAX3* and migratory inhibitory factor, increased cell adhesion and vascularization (Durbin *et al.,* 2009; Maciej, *et al.,* 2010). Likewise, siRNA inhibition of N-cadherin and α9-integrin decreased RMS cell adhesion and invasiveness (Masià *et al.,* 2012). Expression of PAX3-FOXO1 inducing the up-regulation of Cnr1/Cb1 in ARMS and mouse myoblast cells, enhanced cell invasion and metastasis (Marshall[1] *et al.,* 2011). Expression of *MET* and hepatocyte growth factor (*HGF*) in the RH30 cell line induced tumourigenesis and rhabdomyosarcoma metastasis *in vivo*. Similarly, HGF induced up-regulation of CCN1 in a RH30 cell line stimulated rhabdomyosarcoma metastasis (Rees *et al.,* 2006).

In ARMS cells, PAX3-FKHR induced metastasis, accompanied by suppression of immune responses, by interaction with the JAK/STAT pathway (Nabarro *et al.,* 2005).

A reciprocal expression of FKHR-PAX3 in the ARMS RH30 cell line and myoblast cells, which induced inhibition of myogenesis, activated oncogenic pathways by stabilizing PAX3-FKHR expression to enhance cell proliferation, anchorage-independent growth, and matrix adhesion *in vitro*. Additionally, FKHR-PAX3 expression induced tumourigenesis in a xenograft mouse model. On the contrary, FKHR-PAX3 expression negatively affected cell migration, invasion *in vitro* and lung metastasis *in vivo* (Hu[1] *et al.,* 2013). Up-regulation of *PAX* expression in human and murine SHG-44 glioma cell lines, stimulated cell proliferation, enhanced invasion and inhibited apoptosis of the human SHG-44 glioma cell line, whilst inducing tumourigenesis of the mouse SHG-44 glioma cell line *in vivo*. Contrariwise, siRNA repression of *PAX3* expression in the human U87 glioma cell line, suppressed both cell proliferation and invasion and induced apoptosis. Likewise, inhibition of *PAX3* in the mouse U-87MG glioma cell line suppressed tumourigenesis (Xia *et al.,* 2013). PAX3-FKHR siRNA knockdown in ARMS induced inhibition of cell adhesion, migration and invasion through repression of CCN3 (Zhang and Wang, 2011). For instance, in mice, cellular transformation and tumour formation resulting from ectopic expression of PAX3/FOXO1A in murine embyonal myoblasts, suggests that deregulated pax3 protein can induce tumourigenesis (Calhabeu *et al.,* 2013).

Knockdown of fascaplysin expression in a RH30 cell line induced activation of CDK4 and repression of PAX3-FOXO1 expression, inhibiting anchorage-independent growth and cell migration (Lingling *et al.,* 2013). Transfection of C2C12 murine myoblasts with *PAX3* or PAX3-FKHR cDNA induced cell transformation (Lagutina *et al.,* 2002). In NIH3T3 fibroblasts and chicken embryos, PAX3-FKHR expression induced cell transformation, which was demonstrated by the morphological changes of anchorage independent growth and focus formation (Xia *et al.,* 2007).

Mutational expression of *FGFR4* in an ARMS cell line, induced proliferation and transformation of primary mouse myoblasts (Marshall[2] *et al.,* 2012). In mouse ARMS cells, over-expression of P-cadherin as a downstream target of PAX3/7-FOXO1A, supressed myogenic differentiation and stimulated myoblast transformation, migration and invasion. Conversely, hairpin RNA repression of P-cadherin diminished myoblast transformation, migration, and ARMS cell invasion (Thuault *et al*., 2013). Cytogenetic analysis of ERMS patients' tissues, demonstrating malignant cell transformation with increased expression of *PAX3* downstream targets including MyoD1, myogenin and desmin, showed poor prognosis following treatment (Wang *et al.,* 2011). In a related study, histological demonstration of germ cell malignant transformation into ERMS has been reported (Sumerauer *et al.,* 2006). Aberrant expression of *RAS, MYC, P53, SRC* and B-catenin has been demonstrated to induce skeletal muscle precursor cells to undergo malignant transformation (Chen and Langenau, 2011). Likewise, in a related recent case study, Ushida and colleagues (2013), demonstrated rhabdomyosarcoma germ cell tumour transformation in a rhabdomyosarcoma patient. In human rhabdomyosarcoma cell lines, high expression of macrophage migration inhibitory factor, induced cell transformation by activating the chemokine receptors, *CXCR2* and *CD74*, whilst repressing macrophage migration inhibitory factor, and induced massive stromal cell transformation in immunodeficient mice (Maciej *et al*., 2010).

The Rho GTPases that facilitate many integrin-dependent cytoskeletal remodelling that are essential for cell migration are frequently over-expressed in many human cancers (Alan and Lundquist, 2013). For example, the Rho GTPases Rac1 and CDC42 were implicated in the disruption of normal epithelial cell polarization leading to increased motility and invasiveness (Kong *et al.,* 2013). *PAX3* induced mesenchyme-epithelial transition requires appropriate levels of active Rho GTPase (Wiggan *et al.,* 2006). In a related study of RH30 and RD rhabdomyosarcoma cell lines, over-expression of *ELMO1* induced metastatic invasion of rhabdomyosarcoma, whilst repression of *ELMO1* inhibited metastatic invasion (Rapa *et al.,* 2012). Samples from rhabdomyosarcoma patients with distant metastases demonstrated increased expression of *FOXF1* and *ELMO4* and suppression of the latter inhibited metastatic invasion (Armeanu-Ebinger *et al.,* 2011). In the RH30 ARMS cell line, over-expression of *MMP-2* and *VEGFA*

triggered by PAX3-FKHR induced metastatic invasion of these cells (Onisto *et al.,* 2005). The expression of *myf5* in ERMS cells was correlated with the metastatic aggressiveness of a paediatric muscle sarcoma (Myron *et al.,* 2012).

1.3.9.2. Melanoma

Melanoma is a malignant tumour of the skin originating from malignancy of melanocytes under the skin. Melanocytes as dendritic pigment yielding cells originate from NC melanoblasts non-pigmented precursors (Inoue *et al.,* 2013). Development of melanocytes into both cutaneous and ocular melanoma and the development of pigmented ocular tumours induced by retinal pigment epithelium proliferative cells have been confirmed (He[1] *et al.,* 2011). Melanoma affects various parts of the skin on the face, neck, and arms, palms, soles, or under the nails, mouth, and iris of the eye, or retina, vagina, oesophagus, anus, urinary tract, and small intestine (Gajda and Kaminska-Winciorek, 2014). Symptoms of melanoma can present as a mole, sore, lump, or growth on the skin. Additionally a bleeding sore or growth with varying skin colouration may also indicate melanoma. Generally, a flat or slightly raised skin patch or mole with irregular border discoloration may appear as tan, brown, black, red, blue, or white in the trunk or legs or in the upper back of the body (Gajda and Kaminska-Winciorek, 2014; Higgins *et al*., 2014).

Four main variants of melanoma have been identified including cutaneous or superficial malignant metastatic melanoma, as the most common variant, nodular malignant melanoma, lentigo malignant melanoma and a less common variant acral lentiginous melanoma (Gajda and Kaminska-Winciorek, 2014).

1.3.9.2.1. Causes of Melanoma

One of the major risk factor of melanoma is ultraviolet radiation as in prolonged exposure to sunlight and sunburns. Aberrant expression of *PAX3* and *BRAF* have been observed in melanoma. However, other unknown aetiology of melanoma has also been reported in some patients (Arozarena *et al.,* 2014).

1.3.9.2.2. Dignosis of Melanoma

Melanoma is a very malignant tumour with high metastatic index and therefore early diagnosis is important for effective treatment. Melanoma can be diagnosed by examination of a skin lesion or mole using sequential digital dermoscopy imaging. Further diagnostic tool of melanoma include an ultrasound scan of lymph node basins and soft tissue, computed tomography scan of melanoma tumour size, and the use of magnetic resonance imaging or positron emission tomography of surrounding organs and tissues to identify metastatic melanomas (Higgins *et al.,* 2014). Cytological examination of tumour fine needle aspirate and histology of punch, excisional or incisional biopsies are used to confirm and differentiate variants of melanoma (Brauchle *et al.,* 2014). Histologic examination demonstrate that melanoma develops via four different developmental phases beginning from benign naevi to dysplastic naevi, then radial and vertical tumour phases which ultimately results in metastatic melanoma (**Fig. 1.12**) (Smoller, 2006; Mascarenhas *et al.,* 2010).

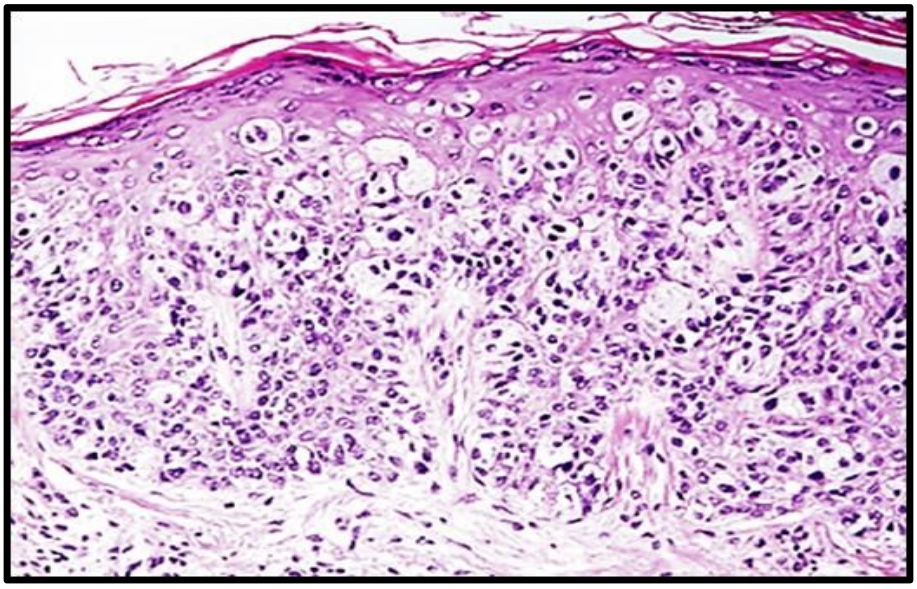

Figure 1.12, X 20 magnification of H & E of skin malignant melanoma. Single and nests of radial melanocytes during invasive growth phase of both epidermis and dermis, with vesicular nuclei and prominent nucleoli. The melanocytes appeared smaller and hyperchromatic with pagetoid extension (taken from Smoller, 2006).

Cutaneous melanoma has been demonstrated to originate from a dysplastic naevus (Medic *et al.,* 2011). It has been universally established that in old men, the frequency

of and death from cutaneous melanoma, has risen 2-3% yearly over the past two decades (Lasfar *et al.,* 2010; Hoshimoto *et al.,* 2012). Clinically, malfunctions observed in numerous melanocyte developmental genes, induced the transformation of melanocytes into melanoma (Nicholl *et al.,* 2011).

1.3.9.2.3. Treatment of Melanoma

Treatment of melanoma depends on the stage of melanoma, size of tumour and location, lymph node involvement, and the age of patient. Melanoma represents a therapeutic challenge with poor prognostic outcome because of its aggressiveness and resistant to treatment schemes with high recurrence index. Currently, combination treatment schemes of melanoma involve the use of radiotherapy, chemotherapy, immunotherapy, and targeted genetherapy after surgery (Deshmane *et al.,* 2014; Mavropoulos and Wang, 2014). Surgical removal of skin lesions or tumours of lymph nodes in patients with local and regional melanoma are first performed (Sondak *et al.,* 2014). Available radiotherapies for the treatment of melanoma include gammaknife, cyberknife, or tomotherapy units are used for treatment of melanoma (La Greca *et al.,* 2014; Tishler, 2014). Currently, chemotherapies use for the treatment of melanoma include bleomicine, dacarbazine, temozolomide, cisplatin, paclitaxel, docetaxel, carmustine, fotemustine, lomustine, vinblastine, carboplatin, and electrochemotherapy (Ashworth *et al.,* 2014; Ricotti *et al.,* 2014). Immunotherapies including ipilimumab, interferon, interleukin-2, aldesleukin, proleukin, sargramostim and tremelimumab are used for the treatment of melanoma (Kaufman *et al.,* 2014; Megahed *et al.,* 2014). Targeted therapies including vemurafenib, dabrafenib, trametinib imatinib, nilotinib and dasatinib have been used to treat melanoma (Laurenz *et al*., 2013; Arozarena *et al.,* 2014).

1.3.9.2.4. *PAX3/Pax3* Biological Activity in Melanoma

Many transcription factors such as *MITF* and *PAX3/Pax3* have been demonstrated to induce transformation of melanocytes (Medic[2] and Ziman, 2010; Berlin *et al.,* 2012). *PAX3/Pax3* is essential for proliferation of dedicated melanoblasts and prevention of premature development of progenitor cells, while Mitf facilitates melanoblast migration from the dorsal neural tube and survival (Ichi[2] *et al.,* 2010). Mechanisms by which

increased levels of Pax3 expression induced the progression of melanoma, through modulation of other genes including *MITF* have been demonstrated (Thomas *et al.,* 2009; Lasfar and Cohen-Solal, 2010). Defects in the mechanism by which *Pax3* retains regulation of melanocyte differentiation, demonstrates that melanoma development requires *Pax3* expression (Maczkowiak *et al.,* 2010; Bosserhoff *et al.,* 2011). *PAX3/Pax3* expression begins before initiation of melanoblast differentiation, which is then stimulated by decreased levels of *PAX3/Pax3* expression (Chen[1] *et al.,* 2010; Michael *et al.,* 2013). This implies that Pax3 promotes melanocyte stem cells into melanocytes, despite the fact that it inhibits terminal differentiation (Djian-Zaouche *et al.,* 2012).

Many transcription factors, including *MITF, PAX3, PTEN, SOX10, C-RET, RAS* and *C-MYC* could perhaps contribute to melanoma pathogenesis (Li *et al.,* 2007; Chen[1] *et al.,* 2010). Recent reports suggest that several melanocytic genes are modulated by *PAX3* (Hauswirth *et al.,* 2012; Yang[2] *et al.,* 2012). Genes that predispose to melanoma include cyclin-dependent kinase inhibitor 2A (*CDKN2A*), cyclin-dependent kinase 4 (*CDK4*), platelet-derived growth factor (*PDGF*), epidermal growth factor (*EGF*), basic fibroblast growth factor (*bFGF*), Mitogen-activated protein kinases (*MAPK*), nodal and *STAT* (Chen *et al.,* 2007; McCabe and Bronner-Fraser, 2008; Dong[2] *et al.,* 2012).

PAX3/Pax3 expression has been demonstrated in primary melanoma and melanoma cells but not in normal adjacent skin tissues (Medic *et al.,* 2011). In the majority of tumours, higher levels of *PAX3/Pax3* expression occur in aggressive melanomas than in less aggressive melanomas (Ryu *et al.,* 2007; Plummer *et al.,* 2008). Regulation of the cell cycle involves potent interaction of *PAX3* with *pRB* (Jothi *et al.,* 2012). In dormant cells, interaction of both RB and phosphorylated retinoblastoma protein (pRB) with E2F inhibits E2F-responsive gene transcription required for cell cycle progression. The significance of Pax3 in sustaining melanoma cells is indicated by experiments where increased Pax3 expression prevented apoptosis and diminished Pax3 induced cell apoptosis (He[1] *et al.,* 2011; Medic *et al.,* 2011). In related studies, antisense *PAX3/Pax3* oligonucleotides induced melanoma cell apoptosis (Hirai *et al.,* 2010). In B16F10.9 melanoma cells, interleukin-6 receptor/interleukin-6, which repressed Pax3 expression,

was associated with a block in glial cell transdifferentiation and proliferation (Hirai *et al*., 2010). Goding *et al.* (2008) attempted to treat mice with melanomas using interleukin-6 receptor/interleukin-6 (IL6R/IL6) as a tumour inhibitor. Pax3 protein and mRNA levels decreased in melanoma cells following IL6R/IL6 treatment (Goding, 2008). Pax3 down-regulation in B16F10.9 melanoma cells after treatment with IL6R/IL6, inhibited cell proliferation and induced cell transdifferentiation to glial cells (Thomas *et al.,* 2009). Decreased Pax3 expression, which promotes defective melanogenesis, diminishes transcriptional activity of Mitf (Wan *et al.,* 2011). Lately, microarray analysis demonstrated that PAX3 modulated the activities of melanoma developmental and susceptibility genes including TGFβ, Ras homolog gene family member C, stem cell factor, metalloproteinase inhibitor and melanoma-progression associated molecule (Nakazaki *et al.,* 2009; He[1] *et al.,* 2011; Hoshimoto *et at.,* 2012). Down-regulation of *Pax3* induced up-regulation of p53 and apoptosis-promoting genes including caspase 3 (He[2] *et al*., 2011; Wang *et al.,* 2011). Increased apoptosis observed in mouse embryos with dysregulated *Pax3,* was to some extent salvaged following crossing of p53 mutant mice with heterozygous Splotch mice (Griffith *et al.,* 2009; Greene *et al.,* 2009). These reports suggest that increased *Pax3* expression allows melanoma progression by evading apoptosis (by repressing both p53 and caspase 3) (Hirai *et al.,* 2010; Wang *et al.,* 2011). It has been demonstrated that Pax3 can inhibit apoptosis by increasing levels of *Bcl-XL* (Taylor *et al.,* 2006; Chappell *et al.,* 2009). These attributes of *Pax3* in melanoma are indicative of the ability of *PAX3* to induce stem cells into tumour formation (Tatlidil *et al.,* 2011; Liu[2] *et al.,* 2013).

In previous study of ERMS and cutaneous malignant melanoma, *PAX3* over-expression induced up-regulation of major cell-surface adhesion molecules, which confer metastatic properties on tumour cells and affect their motility (Oda and Tsuneyoshi, 2009). *PAX3* induced several signaling pathways or downstream targets involved in cell migration including; NCAM, versican*, C-met, LBX1*, connexin-43, ephrin/Eph receptors, the *CXCR4-DSF-1* axis, the Wnt-signalling cascade and the MET-HGF/SF signaling pathway (Wei *et al.,* 2007; Froehlich *et al.,* 2013).

1.3.9.3. *PAX3/Pax3* and Neuroblastoma

Aberrant expression of *PAX3/Pax3* is associated with neuroblastoma, a common paediatric extracranial solid tumour (Murdoch *et al.,* 2012). It is derived from the sympatheticoadrenal lineage of cells with the primary tumours developing from peripheral parasympathetic or sympathetic ganglia (Nelms *et al.,* 2011). Increased *PAX3* expression has been demonstrated in neuroblastoma cell lines and tumours (Xao *et al.,* 2013). Histologic examination of neuroblastoma is shown in **Fig. 1.13**.

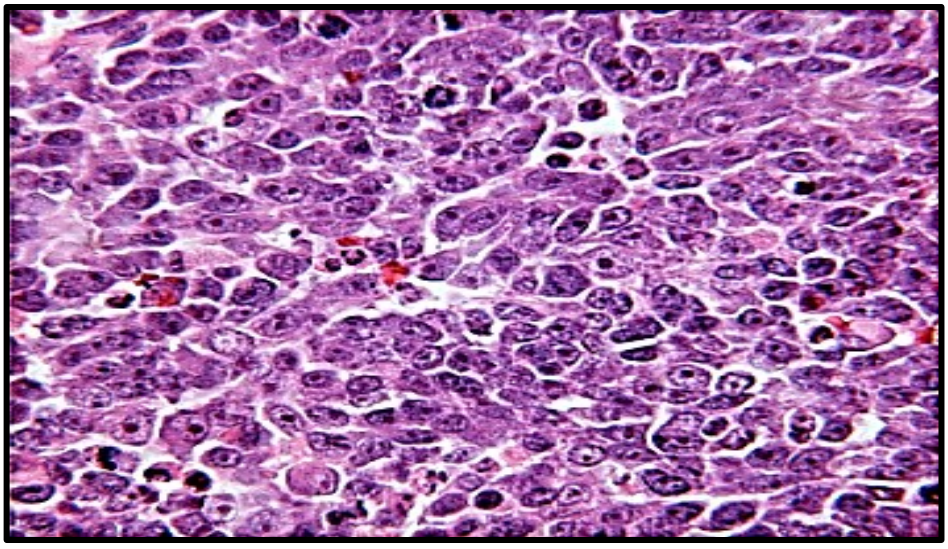

Figure 1.13, X 40 magnification of H & E of neuroblastoma. Tumour cells appeared large with prominent nucleoli (taken from Xao *et al.,* 2013).

Several hereditary malformations associated with neuroblastoma, involve increased expression of N-myc proto-oncogene protein (N-MYC) (Xao *et al.,* 2013). Recent investigations in mice, have demonstrated that increased levels of N-MYC have the potential to stimulate cell transformation. For instance, the development of neuroblastoma in NC tissues has been demonstrated in transgenic mice with increased expression of *N-MYC* (Jain *et al.,* 2011; Dong[2] *et al.,* 2012). Furthermore, in cultured human neuroblastoma cell lines, reduced levels of *N-MYC* induced inhibition of cell proliferation and differentiation (Maczkowiak *et al.,* 2010; Sanchez-Ferras *et al.,* 2012).

Previous mutagenesis and deletion studies demonstrated that Pax3 has a reversed E box sequence CGCGTG (or CACGCG) located within the 5' promoter region which can be

activated by C-Myc or N-Myc, while elevated levels of Pax3 can be induced by N-Myc or C-Myc ectopic expression (Singh *et al.,* 2011; Wentzel and Eriksson., 2011). It is not well understood whether PAX3 alone induces the pathogenesis of neuroblastoma or inhibition of PAX3 by N-MYC results in neuroblastoma. Therefore, this necessitates further research (Sommer*,* 2011; Wahlbuhl *et al.,* 2012). Inhibition of *PAX3* in human neuroblastoma cell lines cells, demonstrated two a fold knockdown of *PAX3* in both SH-SY5Y and SH-EP1 neuroblastoma cell lines with subsequent inhibition of cell cycle, proliferation, migration, adhesion, invasion and induction of apoptosis.

This study identified the expression of *NCAM* in only N-type SH-SY5Y neuroblastoma cells but not S-type SH-EP1 and demonstrated that silencing of *PAX3* in neuroblastoma cells significantly decreased cell attachment to various ECM proteins including fibronection, laminin, collagen 1 and collagen IV (Fang *et al.,* 2013). In a previous study, *NCAM* expression was down-regulated by *PAX3* knockdown via transactivation of the *NCAM* promoter. Decreased *NCAM* expression has been suggested to enhance the metastatic potential of neuroblastoma cells by accelerating cell detachment from primary tumour sites during the first step of metastasis (Bork *et al.,* 2013). Neural cell adhesion molecule has been demonstrated as a marker of neuronal tissue differentiation (Maczkowiak *et al.,* 2010).

Therapies for inducing apoptosis have become a potent tool in the treatment of cancer. *PAX3*, which plays important roles during embryogenesis and has been implicated in the inhibition of rhabdomyosarcoma cell apoptosis, may confer its oncogenic properties by inhibiting apoptosis in order to maintain survival of rhabdomyosarcoma cells (Tonelli *et al.,* 2012; Sarkar *et al.,* 2013). The apoptotic regulatory role of *PAX3* and PAX3-FKHR in development has been demonstrated in RMS and melanoma through modulation of activation of BCL-XL anti-apoptotic gene to induce massive apoptosis. This demonstrates that the anti-apoptotic effect of PAX3 and PAX3-FKHR in ARMS is mediated through BCL-XL (Barr, 2001).

Cell survival and cell cycle progression are negatively regulated by FOXO transcription factors, which act as tumour suppressors (Shi *et al.,* 2010). In hematopoietic cells deprived of growth factors, expression of FOXO proteins induces BIM expression. Up-regulation of FOXO3a by paclitaxel in paclitaxel-sensitive breast cancer inducing increased levels of BIM protein, induced breast cancer cell apoptosis (Chen[5] *et al.,* 2010). In the RH30 ARMS cell line, ectopic expression of PAX3-FKHR was observed following camptothecin siRNA knockdown, which subsequently inhibited cell proliferation and induction of apoptosis (Zeng *et al.,* 2009). Knockdown of FGFR4 in JR1 and RH30 rhabdomyosarcoma cell lines inhibited cell proliferation and induced apoptosis (Li[4] *et al*., 2013). Up-regulation of Noxa in RH30 cells inhibited cell proliferation and induced apoptosis (Marshall *et al.,* 2013). Inhibiting hedgehog activation in RMS induced apoptosis (Uchida *et al.,* 2011). Inhibition of the PI3K/Akt signalling pathway in A204 rhabdomyosarcoma cells and A673 Ewing's sarcoma cells induced apoptosis (Kilic-Eren *et al*., 2013). *PAX3* inhibits melanoma cell apoptosis through the modulation of decreased expression of *PTEN* and increased expression of BCL2 (Kubic *et al.,* 2008). A recent study demonstrates that selumetinib induced apoptosis of A375 cells in mice and fish melanoma xenografts following inhibition of *PAX3* and *MITF* by *SMURF2* (Looi *et al.,* 2013).

In normal myogenic precursor cells, *P57KIP2* prevented progression of cell cycle by inhibiting cyclin E-CDK2 and promoting myogenic differentiation by stabilizing MyoD1 (Bilodeau *et al.,* 2009). Inhibition of *P57KIP2* resulted in Pax3-FOXO1 inhibiting differentiation while promoting proliferation (Sumegi *et al.,* 2010). The functional reliance of Pax3-FOXO1 on decreased levels of *P57KIP2* has been demonstrated to permit uncontrolled growth of undifferentiated cells (Sidhu *et al.,* 2010). Increased cell proliferation rates observed after ectopic expression demonstrates that Pax3-FOXO1 could contribute to tumourigenesis of ARMS since down-regulation of a chimeric gene slowed down proliferation rates (Kikuchi *et al.,* 2008). Another report indicated that Pax3-FOXO1 acts as stimulating factor for proliferation and metastasis in tumours using C-Met as a downstream target (Thuault *et al.,* 2013). Pax3-FOXO1 chimera (Ree *et al.,* 2006) facilitates tumour cell evasion of apoptosis in order to divide. Decreased Pax3 and Pax3-FOXO1 expression, which induced increase in cell

death, suggests that the expression of a chimeric gene may prevent apoptosis (Thuault *et al.,* 2013).

Expression of Pax3 or Pax3-FKHR (Pax3-FOXO1) correlated with increased anti-apoptotic genes, BCL-XL and TFAP2B, further supports the anti-apoptotic role of Pax3-FOXO1 (Davicioni *et al.,* 2009). Knockdown of Pax3-FOXO1 transcripts in ARMS cells resulting in decreased cell migration and diminishing proliferation rates, induced differentiation (Kikuchi *et al.,* 2013). Notwithstanding the vast range of genes modulated by Pax3-FOXO1, which implicates the fusion gene inducing oncogenic behaviours of tumour cells, the introduction of Pax3-FOXO1 into an animal model was insufficient to induce tumour formation. This suggests that the oncogenic capability of Pax3-FOXO1 requires the interaction with other downstream targets to induce tumour growth (Missiaglia *et al*., 2012).

Pax3 has been demonstrated to regulate neural tube development in chick embryos through inhibition of a p53-induced apoptosis during morphogenic embryogenesis (Murko *et al.,* 2013). In neural tube defects, Pax3-dependent apoptosis has been observed (Chappell *et al.,* 2009). A dual inhibitory effect of Pax3 on the activity of p53 has been demonstrated by repression of transcription of p53-dependent genes such as *BAX* and MDM2, and significant decrease of P53 protein through induced degradation of p53 protein (Underwood *et al.,* 2007). Activation of P53 stimulates increased expression of P21 and caspase-3 expression in RMS cell lines, to induce a G1 cell cycle arrest, and p53-dependent apoptosis (Miyachi *et al.,* 2009). Up-regulation of caspase 3 expression in RH4 and RD rhabdomyosarcoma cells as well as SK-N-BE2 and CHLA-20 neuroblastoma cells, induced cell-cycle arrest and apoptosis following inhibition of *PAX3* after Nab-paclitaxel treatment (Zhang[3] *et al.,* 2013). Suppression of *PAX3* in neuroblastoma induced progressive cell apoptosis demonstrated by the appearance of a population of cells with sub-G1 DNA content and Annexin V staining (Fang *et al.,* 2013). Evidence of these findings proposed that the anti-apoptotic function of *PAX3* during embryogenesis and possibly in some human tumours entails the repression of p53-dependent apoptotic pathways. Collectively, these discoveries imply that *PAX3* and PAX3-FKHR have the potential to induce inappropriate cell cycle progression and

proliferation by up-regulating G1/S transition positive regulators as well as repressing cell cycle inhibitors. These studies further establish that suppression of *PAX3* inhibits cell cycle progression by preventing the transition of G1 to S phase. Consequently, inhibition of *PAX3* expression in tumours could possibly be a potential target for therapeutic intervention in tumours including RMS, melanoma and neuroblastoma via inhibition of cell cycle progression.

This current PhD research study is part of a larger research group study, which has been underway for the last twelve years, studying *PAX3/Pax3* up-regulation or down-regulation in different lines of differentiation comparing neural stem cells and neuroblastoma; melanocytes and melanoma; myoblasts and rhabdomyosarcoma. The presently study seeks to inhibit *PAX3* expression in human rhabdomyosarcoma and malignant melanoma cell lines.

1.4. Aim

1. To down-regulate *PAX3* gene expression in human rhabdomyosarcoma and malignant melanoma, in order to determine the effect of *PAX3* knockdown on the tumourigenic characteristics of rhabdomyosarcoma and melanoma *in vitro*.

1.4.1. Objectives

1. To identify the expression of *PAX3* gene in cultured human JR1 and RH30 rhabdomyosarcoma and A375 malignant melanoma cell lines *in vitro*.

2. To confirm the functional tumourigenic characteristics of *PAX3* in cultured human JR1 and RH30 rhabdomyosarcoma and A375 human melanoma cell lines *in vitro* (cell growth, proliferation, migration, adhesion, invasion, transformation, and inhibition of apoptosis).

3. To optimize conditions for *PAX3* gene expression knockdown in cultured human JR1 and RH30 rhabdomyosarcoma and A375 human melanoma cell lines *in vitro* using siRNA silencing.

4. To carry out *in vitro* functional assays for verification of influence of *PAX3* knockdown on the characteristics of JR1 and RH30 rhabdomyosarcoma and A375 melanoma cell lines including cell growth, proliferation, migration, adhesion, invasion, transformation and apoptosis.

5. To evaluate the degree of siRNA knockdown of *PAX3* gene expression in JR1 and RH30 rhabdomyosarcoma and A375 malignant melanoma cell lines *in vitro*.

6. To perform microarray analysis after siRNA knockdown of *PAX3* in the above cell lines.

7. To compare the results of siRNA down-regulation of *PAX3* gene expression in the above rhabdomyosarcoma and melanoma cell lines with the results of previous experiments using siRNA down-regulation of *PAX3* gene expression in neuroblastoma cell lines

CHAPTER 2

MATERIALS AND METHODS

CHAPTER 2: MATERIALS AND METHODS

2.1. Materials

Agar powder (Millipore, UK); Agarose powder (Melford, UK); Ammonium persulfate (APS) (Sigma Aldrich, UK); Anti-Fade solution (Molecular Probes, Sigma Aldrich, UK); BD Falcon 24 and 96-well tissue culture plates (Becton Dickinson, UK); BD BioCoat Matrigel Invasion Chambers (Becton Dickinson); Benchtop DNA ladder (Promega, UK); Bio-Rad dye concentrate (Bio-Rad laboratories, UK); Bis-acrylamide solution (40%) (Sigma Aldrich, UK); Caspase-Glo™ 3/7 buffer and lyophilized Caspase-Glo™ 3/7 substrate (Promega, UK); Cell culture flasks (Corning, USA); Cell transformation kit (Millipore, UK); CellTiter 96® AQueous Non-Radioactive Cell Proliferation Assay kit (Promega, UK); Chemoattractant (5% foetal bovine serum in tissue culture medium) (Sigma Aldrich, UK); Crystal violet staining solution (1%) (Millipore, UK); DeadEnd™ Fluorometric TUNEL System kit (Promega, UK); Dimethyl sulphoxide (Sigma Aldrich, UK); Double distilled water (ddH_2O); DNA Free Turbo (Ambion, UK); DNA loading dye (Bioscience, UK); Dulbecco's Modified Eagle's cell culture Medium (DMEM) supplemented with 4.5g glucose/L (Lonza, Switzerland); ECM array plate (Chemicon International, USA); ECM array kit (Chmicon international, Millipore, UK UK); Eppendorf and microcentrifuge tubes (Netheler, Germany); EDTA solution (200mg/ml, Lonza); Enhanced Chemilumescent (ECL) A and B working detection solutions (GeneFlow, UK); Eukaryote RNA 6000 nano-chip (Millipore, UK); Extracted total RNA and Protein; Ethanol (Sigma Aldrich, UK); Extracted DNA sample; Extraction buffer and Assay buffer (Millipore, UK); Foetal calf serum (FCS) (Labtech international, UK); Fragmentation buffer (5 X) (Qiagen, UK); Gene Chip Sample Clean up Module kit (Affymetrix/QIAGEN, UK); Genechip IVT labeling kit (Affymetrix, USA); Gel matrix, 10X DNAse buffer (Ambion, UK); Giemsa staining solution (Sigma Aldrich, UK); Human genome U133 plus 2.0 Affymetrix GeneChips (Affymetrix, USA); Human rhabdomyosarcoma (JR1 and RH30) and human melanoma (A375) cell lines cells (A kind gift from Professor Patricia Kumar, School of Healthcare Science, Manchester Metropolitan University, UK); Isotone solution (LPD Lab Services Limited, UK); ImProm-IITM cDNA synthesis kit (Promega, UK); Isopropyl alcohol (Sigma Aldrich, UK); Lipofectamine™ RNAiMAX (2mg/ml) (Invitrogen, UK); L-glutamine (200mM) (Lonza, Switzerland); Light Cycler 480 Probes

(Roche, Switzerland); Molecular biological grade chloroform (Sigma Aldrich, UK); MagicMarkTM XP Western Protein standard and Novex® sharp pre-stained protein standard (Invitrogen, UK); Microscope slides, coverslips and immersion oil (Millipore, UK); Methylene blue cell staining solution (0.5%) (Millipore, UK); Nuclease-free water (Promega, UK); Non-fat dry milk (Tesco, UK); Opti-MEM®I reduced serum medium (Invitrogen, UK); Paraformaldehyde fixative (4%) (Sigma Aldrich, UK); PBabe HAER PAX3 plasmid DNA and PBabe HAER empty plasmid DNA (A kind gift from professor); PCR master mix (Promega, UK); Penicillin-streptomycin (10,000U/ml and 10,000µg/ml respectively) (Lonza, Switzerland); Phosphate Buffered Saline (PBS) (PH 7.5) (Oxoid UK); Protein estimation assay kit (Bio-Rad Laboratory, UK); Propedium iodide (PI) (Sigma Aldrich, UK); Pipette tips (Lonza, UK); PCR gel electrophoresis buffer (10X) (Sigma Aldrich, UK); Qiagen mini DNA extraction kit (Qiagen, Ltd Qiagen house, Crewley, RH10 9NQ UK); qRT-PCR primer sets for gene of interest (200µM stock) (Metabion, Germany); Reference 'house-keeping' transcripts: (beta-actin, beta-2 microglobulin, glyceraldehyde 3 phosphate dehydrogenase, hydroxymethyl-bilane synthase, hypoxanthine phosphoribosyl transferase 1, ribosomal protein L13a, ribosomal protein L32, succinate dehydrogenase complex subunit A (Roche, Switzerland); RNA 6000 Nano Assay kit (Agilent Technologies, UK); RNA ladder (Ambion, UK); Radioimmunoprecipitation assay buffer (Sigma Aldrich, UK); R-phycoerythrin conjugated to streptavidin (Molecular Probes, Inc. USA); sqRT-PCR primers (200µM stock) (Invitrogen, UK); (Sterile Tris-EDTA (TE) buffer (PH 8.0) (InVitrogen Ltd, Paisley, PA4 9RF,UK); Shaker incubator (Sigma Aldrich Ltd, Dorset, SP8 4XT UK); Staurosporine stock (1 mM in DMSO) (Sigma Adrich, UK); Super Script IIITM RNase H reverse transcriptase (Invitrogen, UK); siRNA (100µM stock) (Applied Biosystems USA); TEMED (Sigma Aldrich, UK); Thermanox coverslips (13mm) (Nalge Nunc International, U.S.A.); Two-Cycled cDNA Synthesis Kit (Affymerix, USA); Western blotting electrophoresis buffer salts (Sigma Aldrich, UK); Whatman nitrocellulose membrane and 3 mm Whatman chromatographic paper (GeneFlow, UK); White-walled 96-well plate (Millipore, UK); 0.1M Calcium chloride ($CaCl_2$) (Sigma Aldrich Ltd, Dorset, SP8 4XT UK).

2.1.1. Equipments

AGB-75 Laboratory PH meter (Orion, USA); Gene Chip scanner 3000, Affymetrix GCOS (V1.4) software, Agilent 2100 (Agilent, USA); AScorn Ellizer reader (Promega, UK); Automatic plate shaker (Grant Bio, UK); Chanelon Luminometer (Millipore, UK); Bioanalyser (Agilent Technologies, UK); Coulter cell counter (Bio-Rad, UK); Cross power Electrophoresis tank (ATTA, Japan); EukGe W S2v5 program controlled using Affymetrix software; FACS-Calibur Flow (Becton Dickinson, UK); Fluorescence microscope (Thermo Scientific, USA); Gel Electrophoresis tank (Pharmacia, UK); GeNorm software (Primerdesign, UK); Humidified CO2 incubator (Triple Red Lab Technology, UK); G-Box chemiluminescence (Syngene, UK); ImagJ 4.1 software (National Institute of Health, USA); LKB Spectrophotometer (Sigma Aldrich, UK); Microflow class II safety cabinet (Walker, UK); Master Light Cycler® 480 real time PCR machine (Roche, Switzerland); Magnetic stirrer (Heidolph, UK); Inverted light and fluorescent microscopes with camera (Zeiss, Germany); Multiskan Ascent micro plate reader (Millipore, UK); Nanodrop ultra-low-volume, NanoDrop ND-1000 UV-visible spectrophotometer (Thermo scientific, USA); NanoDrop software, Agilent 2100 Bioanalyser (Agilent Technologies, USA); Phase contrast microscope (Zeiss, Germany) Refrigerated centrifuge (4ºC) (Sigma Aldrich, UK); RMA Bioconductor (Agilent Technologies, UK); Spectrophotometer (Pharmacia Biotech, UK); Thermal cycler (PCR Express Hybrid, Australia); Trans-blot SD Semi-Dry Transfer cell (Bio-Rad, UK); Universal Probe Library (Roche Diagnostics, Switzerland); Ultrospec 2000 UV/Visible.

2.2. Cell Culture of Human Rhabdomyosarcoma and Melanoma Cell Lines

The maintenance of viable cells is essential for consistent and reliable experimental results. Cells were revived and maintained for subsequent experiments including transient transfection for gene and protein expression analyses, cell proliferation, migration, adhesion, invasion, transformation and apoptosis assays.

The adherent cell lines (human embryonal rhabdomyosarcoma (JR1), human alveolar rhabdomyosarcoma (RH30) and human malignant melanoma (A375) were used to down-regulate *PAX3* expression. All materials used were sterilized using steam

sterilisation. Cell culture medium was sterilised using membrane filtration (0.02µm pore size, Millipore). All cell culture experimental manipulations requiring sterile conditions were carried out in a sterile microflow class II cell culture safety cabinet using aseptic technique. The JR1, RH30 and A375 cell vials retrieved from liquid nitrogen were briefly thawed in a water bath set at 37^{O}C for 2 min and immediately resuspended in 3ml of DMEM (supplemented with 10% FCS, 100 units/ml penicillin, 100 µg/ml streptomycin and 2mM L-glutamin, Lonza) in complete medium and well mixed. The cells were centrifuged at 300 x g for 5 min and the supernatant discarded.

The cell pellet was resuspended with 5ml of complete DMEM medium and mixed to obtain a homogeneous suspension. An additional 10ml of complete DMEM medium was added to the cell suspension, mixed well and then 2.5ml and 5ml of the cell suspension were transferred into two sterile 25cm^2 and 75cm^2 cell culture flasks (Corning) respectively and incubated at 37^{O}C in a humidified incubator containing 5% atmospheric CO_2 (Tripple Red Lab. Technology, UK). The next day, following adherence of cells to the culture flask substratum, the medium was replaced with fresh complete medium to remove any dead cells. The flasks were examined daily using a phase contrast inverted microscope to monitor the health and growth of the culture. Exhausted medium was replaced with fresh medium until the culture was approximately 70% confluent. The complete medium was discarded and the monolayer was rinsed four times with sterile PBS. Excess PBS was completely removed and 2-3ml of trypsin-EDTA solution (200mg/ml) was added to the monolayer and incubated for 2-5 min at 37^{O}C to trypsinize the cells. Gentle agitation was applied to detach cells from the substratum and the cell layer was intermittently examined microscopically until approximately 90% of the cells were rounded up. Trypsin-EDTA was neutralized by addition of 5ml of complete medium and the cells were mixed well, then centrifuged at 300 x g for 5 min.

The supernatant was discarded and 5ml of complete DMEM was used to resuspend the cell. 100µl of cells were mixed with 20ml Isotone solution and the cells were counted three times using an automated coulter cell counter to estimate the mean concentration of cells. The percentage of cell viability was confirmed by the trypan blue exclusion

technique. The number of cells per ml was calculated using the formula: (**N X 400 cells /ml**), where **N** represents the mean of cell counts. The required cell seeding density to be transferred per well was calculated using a dilution factor formula below.

$$\frac{\textbf{Required cell seeding density per well}}{\textbf{Cell concentration per ml}}$$

Cell stocks were prepared for long storage by centrifuging cells at 300 x g for 5 min and the supernatant medium was discarded. The cell pellet was resuspended in 5ml of 10% DMSO (Sigma Aldrich) in FBS/FCS at 9.5 X 10^6 cells/ml), mixed well and transferred to liquid nitrogen (-190^{o}C) for longer storage.

2.3. Small Interfering RNA Inhibition of *PAX3* Expression in Human Neoplastic Cell Lines

Small interfering RNA (siRNA) are minute regulatory fragments of double-stranded RNA, which are approximately 21 nucleotides elongated, with 3' projections at both ends. These siRNA has the ability of "interfering" or inhibiting protein translation via high binding affinity to and stimulation of degradation of messenger RNA (mRNA) at specific sequences in the nucleus. It is a major biological mechanism in which the cytoplasmic presence of double-stranded RNA (dsRNA) initiates post-transcriptional silencing of homologous genes by targeting sequence-specific inhibition of transcription and degradation of mRNA (Ambesajir *et al;* 2012). This technique was used to silence *PAX3* gene in JR1, RH30, and A375 cells through intracellular degradation and subsequently determine the effects of inhibition of *PAX3* gene on cellular functions.

2.3.1. Transfection with siRNA

The siRNA Silencer® pre-designed *PAX3*-siRNA with three targeting sites on exon four of *PAX3* was used to down-regulate *PAX3* (Applied Biosystems). A scrambled non-targeting siRNA negative control (NC-siRNA) with sequences that do not target any gene product was used for determining transfection efficiency and controlling the effects of siRNA delivery on cells. To monitor the silencing effectiveness of siRNA, NC-siRNA was used in parallel with *PAX3*-siRNA.

Three different pre-designed *PAX3*-siRNA Silencers were tested individually and in combination to select the optimal *PAX3* Silencer (see **table 2.1**).

Table 2.1 Oligonucleotide sequence of *PAX3*-siRNA and NC-siRNA used

siRNA	Sequence
PAX3-siRNA-1	Sense: 5'-GUCGCAUAAUGAGAAGUUUCT-3' Antisense: 5'-CCACGGCUCAGGAUGCUUCTG-3'
PAX3-siRNA-2	Sense: 5'-GUCUCAUCCUGAGCCGUCCUG-3' Antisense: 5'-UCACGUCUCACCAUACUUCTG-3'
PAX3-siRNA-3	Sense: 5'-GCCGCAUCCUGAGAAGUAATT-3' Antisense: 5'-UUACUUCUCAGGAUGCGGCTG-3'
NC-siRNA	Sense: 5'-GAUCCUGUGCAGGUACCAGTT-3' Antisense: 5'-CUGGUACCUGCACAGGAUCCG-3'

JR1, RH30 and A375 cells were seeded in triplicate at a cell concentration of 2.0 x10^5 cells/ml in 24-well plates for subsequent transfection of NC-siRNA and *PAX3*-siRNA (previously called *PAX3*-siRNA-3), alongside non-transfected negative control cells and incubated at 37^{O}C for 24 hr after seeding. When cells were 30%-40% confluent, the medium was discarded and the cells were rinsed three times with 0.5ml sterile Opti-MEM I reduced serum antibiotic-free medium and were maintained in this medium until transfected after 24 hr. The Opti-MEM I reduced serum antibiotic-free medium was completely discarded and 0.5ml freshly prepared siRNA–lipofectamine™ RNAiMAX transfection complex, at a final concentration of 0.5μmol/μl siRNA from a 100μmol/μl stock siRNA (according to the manufacturer's instructions), was added to each well and gently mixed. The plates were then incubated at 37^{O}C in a humidified 5% CO_2 atmosphere for 96 hr. After 24 hr, an additional 0.5ml fresh Opti-MEM I reduced serum antibiotic-free medium was added to each well to prevent medium evaporation during the long incubation. The Opti-MEM I reduced serum antibiotic-free medium was used in growing the cells thoughtout the transfection experiments to achieve a slow cell

growth. All cell lines were transfected for a maximum period of 96 hr prior to cell functional analysis.

2.3.2. Determination of Inhibition of *PAX3* mRNA Expression

To establish the effect of siRNA knockdown on *PAX3* gene expression, total RNA was extracted, reverse transcribed into cDNA and the *PAX3* mRNA expression level was determined by reverse transcription semi-quantitative and quantitative real-time polymerase chain reaction (sqRT-PCR and qRT-PCR respectively), microarrays and western blotting.

2.3.2.1. Extraction of total RNA from Transfected Cells

Total RNA was extracted using TRIzol reagent according to the manufacturer's instructions with a slight modification of prolonged incubation time by 5-10 min extra at the initial incubation stages to ensure complete disruption of cellular components. After transfection, the medium was discarded from the 24-well plates, rinsed with ice-cold PBS four times and excess PBS was completely removed. 1ml of TRIzol reagent was added to each well and incubated for 40 min at room temperature (RT) to homogenise cells and ensure the complete dissociation of nucleoprotein complexes. The cell homogenate mixture was vortexed for 1 min, stored at -80ºC to maintain the integrity of RNA and until ready to extract the cellular total RNA. 0.2ml chloroform was added per ml of TRIzol reagent used in the initial homogenisation, inverted for 15 sec and incubated for 10 min at room RT. The cell homogenate mixture was centrifuged in a refrigerated centrifuge at 12,000 x g for 15 min at 4^{O}C to separate the mixture into a lower red phenol-chloroform phase, a white pellicle interphase and a colourless upper aqueous phase containing pure total RNA. 400µl of the colourless upper aqueous phase was carefully transferred into sterile ice-cold eppendorf tubes and 0.5ml of 100% isopropanol was added (per ml of TRIzol reagent used in the initial homogenisation), vortexed briefly for 1 min and incubated for 10 min at RT to precipitate the total RNA. The precipitated total RNA was centrifuged at 12,000 x g for 10 min at 4^{O}C to pellet isolated total RNA. The supernatant was discarded and the isolated total RNA pellet was washed by adding 1ml of ice-cold 75% ethanol per ml of TRIzol reagent used in the

initial homogenisation, vortexed for 1 min and centrifuged at 7,500 x g for 5 min at 4^{O}C. The supernatant was discarded and the isolated pure total RNA pellet was briefly air-dried for 5 min, resuspended in 15µl ice-cooled nuclease-free-water on ice and stored at -80^{O}C overnight, until ready to use for determination of purity of the isolated RNA and cDNA synthesis.

2.3.2.2. Determination of total RNA Yield and Purity

4µl of RNA was diluted in 996µl of double distilled water (dd H_2O) and the absorbance (OD) at 260nm and 280nm was measured in a spectrophotometer. RNA concentration was calculated according to the absorbance reading at OD_{260} (one absorbance unit at 260nm = 40µg/ml of single-stranded RNA). The value of absorption ratio 260/280 was used to determine the purity of extracted RNA. Ratio of 260/280 values out of (1.6-2.0) range indicates RNA contamination.

2.3.2.3. Complementary DNA Synthesis

Extracted RNA was reverse transcribed into complementary DNA (cDNA) using Promega ImProm-II^{TM} Reverse Transcription System kit according to the manufacturer's instructions. Up to 1µg/µl of target RNA and 1µl of cDNA oligo $(dT)_{15}$ primer (0.5µg/µl) were combined in nuclease-free water to a final volume of 5µl per reverse transcriptase reaction. The target RNA reaction mixture was denatured in a 70^{O}C heat block for 5 min and immediately chilled on ice for 5 min. A reverse transcription reaction mix was prepared on ice by combining 4.5µl Nuclease-free H_2O with 4µl of 25mM $MgCl_2$, 4µl of 5 X Tris-HCl reaction buffer (PH 8.5), 1µl of 10mM dNTP mix, 0.5µl of 2500 units/ml recombinant ribonuclease inhibitor (Rnasin) and 1µl of 50 units/ml Reverse Transcriptase to a final volume of 15µl per reaction. A total volume of 15µl of reverse transcription reaction was mixed with 5µl denatured target RNA. A non-template negative control reaction tube was also set alongside the experimental reaction by combining 2.5µl of 0.5µg oligo $(dT)_{15}$ with 2.5µl nuclease free-H_2O. The reaction tubes were microcentrifuged at 1500 rpm for 2 min and annealed at 25^{O}C for 5 min followed by 1 h extension at 42^{O}C and 15 min at 70^{O}C in a thermal cycler. The synthesized cDNA was stored at -20^{O}C or -80^{O}C.

2.3.2.4. Semi-Quantitative Reverse-Transcription Polymerase Chain Reaction

Semi-quantitative reverse transcription polymerase chain reaction (sqRT-PCR) based on the determination of band intensities of reversed transcribed mRNA on an agarose gel was used to determine the level of *PAX3* mRNA expression knockdown.

RT-PCR analysis of constructed cDNA was performed using a Promega RT-PCR analysis kit according to the manufacturer's instructions. RT-PCR was carried out in ice cooled 0.2ml microcentrifuge tubes by combining 1µl cDNA (1µg/µl) samples with 5µl of 2 X Master mix (composed of 50 units/ml *Taq* DNA polymerase in 5 X Tris-HCl reaction buffer (PH 8.5), 400µM dATP, 400µM dGTP, 400µM dCTP, 400µM dTTP, 3mM $MgCl_2$), 1µl forward/reverse primers (10µM working concentration of each, **table 2.2**) and mixed with 3µl nuclease-free water to a final volume of 10µl per reaction tube.

Table 2.2 RT-sqPCR Oligonucleotide primers used for RT-sqPCR

Primer	Sequence	PAX3 Isoform	Amplicon size (bp)
PAX3a/bF	5'-TCAAGGACGCGGTCTGTGATC-3'	PAX3a	684
PAX3a/bR	5'-ATAAGGCAGCCAATGTGGGGG-3'	PAX3b	277
PAX3E7F	5'-CCGCTTCCTCCAAGTACTGTACACCAAAGC-3'		
PAX3I8R	5'-GATACCGGCATGTGTGCCTTAATCTTGCCTC-3'	PAX3c	532
PAX3E8R	5'GTCAGAGACTAGACCATATGAAGAGCTTGGACAG-3'		
PAX3I9R	5'-CAGAGCAGATTCTTGATATCTAGGCTGCGAAGAC-3'	PAX3d	241
PAX3E8R	5'GTCAGAGACTAGACCATATGAAGAGCTTGGACAG-3'	PAX3d	500
PAX3I10R	5'-GAATTGGGATGTTTTGATATCTAACCATGTGAAA-3'	PAX3e	294
PAX3E7F	5'-CCGCTTCCTCCAAGTACTGTACACCAAAGC-3'	PAX3d	550
PAX3I9R	5'-CAGAGCAGATTCTTGATATCTAGGCTGCGAAGAC-3'	PAX3g	286
PAX3E7F	5'-CCGCTTCCTCCAAGTACTGTACACCAAAGC-3'	PAX3d	750
PAX3I10R	5'-GAATTGGGATGTTTTGATATCTAACCATGTGAAA-3'	PAX3c	532
		PAX3h	338
S14F	5'-GGCAGACCGAGATGAATCCTCA-3'		
S14R	5'-CAGGTCCAGGGTCTTGGTCC-3'	S14	143

Reaction tubes were centrifuged for 30 sec and placed in a thermal cycler programmed for 40 cycles to allow the amplification of low level expressed *PAX3* isoforms (95^{O}C for 1 min, 58^{O}C for 1min, and 72^{O}C for 1 min) and 72^{o}C for 10 min final incubation. Extracted total RNA from three specific *PAX3* positive controls of non-transfected JR1, RH30 and A375 cell lines cells known to be expressing the *PAX3* gene, with cDNA containing *PAX3* isoforms, were set alongside the experimental reaction tubes to monitor

the effectiveness of the PCR master mix reaction, PCR programme and to identify the various *PAX3* isoforms bands on agarose gel. A non-template negative control, set alongside the experimental reaction tubes containing 1µl nuclease free-water in lieu of cDNA was amplified in parallel to monitor contamination. A human ribosomal RNA *S14* housekeeping gene was included as an internal normalisation control and carried out alongside the *PAX3* experimental target genes to monitor the effectiveness of the reverse transcription reaction of extracted RNA into cDNA for RT-PCR analysis. The RT-PCR analysis for each sample was performed three times.

2.3.2.5. Agarose Gel Electrophoresis

1.5% agarose gels were prepared in 1 X TBE buffer (Invitrogen), boiled in a microwave at high power to completely dissolve the agarose powder at 100^{O}C, and allowed to cool to approximately 50^{O}C. The gel casting combs were inserted in the gel casting chambers and 45ml of the molten agarose solution was poured to about 1 mm thickness to create sample loading lanes without air bubbles and incubated at RT for 30 min to solidify at a gel thickness of 3.5 mm. The combs were carefully removed and the gels were transferred into an agarose gel electrophoresis running tank containing 450 ml 1 X TBE electrophoresis running buffer. Equal volumes (5µl) of sqRT-PCR products and 2 X orange G DNA loading buffer were mixed, briefly vortexed and loaded. A 100-1500bp Benchtop ladder was used as a sample tracking molecular weight marker and to determine the size of RT-PCR analysis amplicons of the various *PAX3* isoforms (**Table 2.2**). The gels were electrophoresed at 50-55mA for 45 min, stained in 0.5µg/ml ethidium bromide in ddH_2O for 30 min and visualised with a G-Box UV chemiluminescence transilluminator.

2.4. Microarray Analysis of Downstream Target of *PAX3* Gene

The microarray experimental work and analysis was carried out by Dr. Leo Zeef and colleagues at the microarray facility, University of Manchester, UK.

2.4.1. cDNA Synthesis

Total RNA was extracted using a Trizol RNA extraction kit as described in section section **2.3.2.1**). RNA quality was checked using the RNA 6000 Nano Assay, and analysed on an Agilent 2100 Bioanalyser. The RNA was quantified using a Nanodrop ultra-low-volume spectrophotometer. Approximately 100ng total RNA was used to synthesize cDNA. Synthesis was carried out using a Two-Cycled cDNA Synthesis Kit and a Gene Chip Sample Clean up Module kit was used for cDNA cleanup. The final elution step resulted in approximately 12µl cDNA.

2.4.2. Biotinylation and Fragmentation of Complementary RNA

Biotin labelling of complementary RNA (cRNA) was carried out using a Genechip IVT labelling kit. 12µl of cDNA was used and the resultant cRNA was purified using the GeneChip sample clean up module with a final elution volume of 19µl in RNase free water. Using the Nanodrop spectrophotometer, cRNA was quantified and 15µg cRNA was used for fragmentation. The reaction was carried out in 5 X fragmentation buffer at 94^{O}C for 35 min.

2.4.3. Hybridization

For each target, a hybridization cocktail was made using the standard array methodology as described in the Gene Chip Expression Analysis Technical Manual. The cocktail was hybridized to genome Mouse-4302 chips by incubating the Gene Chips in a rotisserie box in a 45^{O}C oven rotating at 60rpm. Following 16 hr hybridization, the chips were loaded onto a Fluidics station for washing and staining with R-phycoerythrin conjugated to streptavidin using the EukGe W S2v5 program controlled Affymetrix software, GCOS (V1.4).

2.4.4. Scanning

The chips were loaded onto the Agilent Gene Chip scanner 30009 and quality control checks for control hybridizations were performed, again using Affymetrix GCOS (V1.4) software. RNA quality was checked using the RNA 6000 Nano Assay, analysed on an

Agilent 2100 Bioanalyser and then quantified using a Nanodrop ultra-low-volume spectrophotometer. The Human genome U133 plus 2.0 Affymetrix GeneChips were run according to manufacturer's instructions.

2.4.5. Analysis

A technical quality control was performed with dChip (V2005) (www.dchip.org; Li and Wong, 2001) using the default settings. Background correction, quantile normalization, and gene expression analysis were performed using robust multiarray analysis in a bioconductor (Bolstad *et al.,* 2003). The principal component analysis was performed with Partek Genomics Solution (version 6.5, Copyright 2010). Differential expression analysis was performed using Limma functions lmFit and eBayes (Smyth, 2004). Gene lists of differentially expressed genes were controlled for false discovery rate and errors using the method of QVALUE (Storey and Tibshirani, 2003). Functional annotation of the genes was performed using DAVID NIH version 2 (Glynn *et al.,* 2003).

2.5. Reverse-Transcription Quantitative Polymerase Chain Reaction

Dr. Fiona Marriage and colleagues (Quantitative Polymerase Chain Reaction Facility, Manchester Institute of Biotechnology, University of Manchester, UK), performed the Reverse-Transcription quantitative Polymerase Chain Reaction (RT-qPCR) experimental work and analysis.

Extracted RNA was quantified using a NanoDrop ND-1000 UV-visible spectrophotometer. Before RNA measurements were taken, the ND-1000 was blanked by pipetting 1.2µl of Nuclease free water directly onto the optical pedestal, the lid was closed and using surface tension to hold a 1mm column of liquid in place, the background measurement was taken. The pedestal surface was then wiped clean and 1.2µl of undiluted RNA measured. The NanoDrop software displayed the concentration of RNA in ng/µl and assessed the OD of 260/280 and 260/230 purity ratios for the estimation of RNA purity. A 260/280 ratio between 1.9-2.1, and a 260/230 ratio around 2.0 indicates pure RNA. The RNA integrity was assessed using the Agilent 2100

Bioanalyser. RNA (1.5µl/sample) and 1.5µl RNA ladder were heat denatured at 70^{O}C for 2 min and placed on ice. The Eukaryote RNA 6000 nano-chip was filled with 9µl of gel dye mix into the appropriate well. The chip was placed onto a chip priming station and a plunger depressed for 30 sec to fill the chip with gel. A further 9µl of gel dye mix was placed into the two remaining gel dye mix wells. A gel matrix (5µl) was added to each of the sample wells and the ladder well. The denatured samples and RNA ladder (1µl) were then added to one of 12 sample wells. The chip was vortexed for 1 min and then run on the Agilent 2100 Bioanalyser. The 28s and 18s RNA peaks were seen at approximately 48 and 42 sec respectively for the extracted RNA. The Agilent 2100 Bioanalyser software assigned an RNA integrity number to each sample using a scale from 0 to 10, with a value of 0 meaning totally degraded and a value of 10 meaning highly intact.

2.5.1. DNAse Treatment

DNA Free Turbo was used to remove any contaminating genomic DNA present. Briefly, the RNA was diluted to give a greater volume, one-tenth volume of 10 X DNAse buffer and equal volume of DNAse and diluted RNA (1µl) were mixed and incubated at 37^{O}C for 30 min. One tenth volume of DNase inactivation buffer was added to each tube (or 2µl if the volume was low). The tubes were incubated at RT for 5 min, gently mixed at intervals and then spun at 10,000 x g for 90 sec. The RNA supernatant was collected.

2.5.2. Reverse Transcription

RNA (3µg/µl) was reverse transcribed using SuperScript III^{TM} RNase H reverse transcriptase following the manufacturer's guidelines. Briefly, 1µl Oligo $(dT)_{12-18}$ (0.5µg/µl), 3µg RNA and 1µl dNTP mix (10mM) were added to a nuclease-free micro-centrifuge tube, incubated at 65^{O}C for 5 min and then chilled on ice. The tubes were briefly centrifuged, and 4µl of 5 X first strand buffer, 1µl DTT (0.1M), 1µl RNaseOUT^{TM} and 1µl SuperScript III were added, gently mixed and the reaction tubes

were incubated at 50^{O}C for 60 min. The reaction was terminated by heating the samples to 70^{O}C for 15 min.

2.5.3. Quantitative PCR Measurement of Gene of Interest

The Human Universal Probe Library system (Mouritzen *et al*, 2003) employing proprietary locked nucleic acid analogues of fluorescence resonance energy transfer hydrolysis probes, was used for qRT-PCR to measure expression levels of genes of interest (GOI). Using the Roche online assay design centre, specific primers and an associated probe were selected for the gene of interest transcripts. The primers were submitted to a basic local alignment search Tool (BLAST®) (http://www.ncbi.nlm.nih.gov/BLAST/) to check for non-specific binding. Where primers showed homology to other regions within the human transcriptome, the assay was redesigned and the new primers submitted to BLAST again. Dual labelled DNA probes were from the Universal probe library. To compensate for variations in cell number, RNA isolation, reverse transcription and PCR amplification efficiency, two endogenous 'house-keeping' transcripts were chosen from a panel of eight 'house-keeping' genes (**Table. 2.3**) using the GeNorm algorithm.

Table 2.3 Gene of interest Oligonucleotide primers for RT-qPCR

Gene symbol	Forward (F) and Reverse (R) primers Sequence	Expected Fragments Size (bp)	Ta (°C)
PAX3	**F: CGTCTCCAAGATCCTGTGC** **R: CGTCAGGCGTTGTCACCT**	95	60
ADAM23	F: GCACAAGAGGAGTTGGTGTG R: GCCAGGCTCTGCGATAATAC	73	58
AEN	F: TGCAGACCGGAAGAGACAC R: GGAAGCCTGGGGAGTAATCT	89	60
AKT3	F: TTGCTTTCAGGGCTCTTAT R: CATAATTTCTTTTGCATCATCTGG	75	59
BCL2	F: CATCGCGGTATTCGGTTC R: GCTTTGCCATTTGGTCTT	132	60
BRCA1	F: CATCCCAGGAGGTGACGATTC R: GGGAGGCTCTGTGAATTGTC	98	60
CALM3	**F:** ATTGACTTCCCGGAGTTCCT **R:** GATGTAGCCATTCCCATCCTT	114	60
CAPRIN1	F**:** GGCAGAAACACAGTTCACCA R: AGGTTGCTGCTGGAGTGAAT	94	59
CASP3	F: TGGAATTGATGCGTGATG T R**:** TGGCTCAGAAGCACACAA AC	73	60
CCNBI	F: CGTCTCCAAGATCCTGTGCAAC R: CGTCAGGCGTTGTCACCTA	90	64
CCND3	**F:** ATCACTGGCACTGAAGTG GA **R:** CCTGAGGCTCTCCCTGAGT	75	59
CDC25B	F: TGCAGGTCTCTGCATGGAT R: GGATGGCCTGTTCAAACG	74	60
CDCA3	**F:** TGGTATTGCACGGACACCTA **R:** TGTTTCACCAGTGGGCTTG	63	60
CDK5	F: AATGACATCTGCCTTGACGAA R: GTAAATGCGTCGACGTTCAATC	79	58
C-MYC	**F:**GAACCAGAGAAACCTAACAGTGC **R:** CGAAGCAGCTCTATTTCTGGA	89	59
COL1A1	F: CTGGACCCCAGGGTCTTC R: CATCTGATCCAGGGTTTCCA	75	60
CXCR4	F: ATTGGGATCAGCATCGACTC R: CAAACTCACACCCTTGCTTG	61	60
E2F7	F: CAGGAAGCCTCCTTAGGAAAG R: GGGGCTGATCAGGTCTTTTA	68	59
E2F8	F**:** AATGACATCTGCCTTGACGA R**:** GTAAATGCGTCGACGTTCAA	95	60
ETS1	F: ACAAGCCTGTCATTCCTGCT R: GTAATTCCAGAAGAAACTGCCATAG	84	59
FOXO 1	F: AGGCTGAGGGTTAGTGAGCA R**:** TGAAAGACATCTTTGGACTGCTT	91	60
FOXO3	F: CTTCAAGGATAAGGGCGACA R: CGACTATGCAGTGACAGGTTG	87	60
GADD45B	F: CAGGAAGCCTCCTTAGGAAAGTC R: GGGGCTGATCAGGTCTTTTA	96	58
HES1	F: GAAGCACCTCCGGAACCT R: GTCACCTCGTTCATGCACTC	111	60
ID3	F: CATCTCCAACGACAAAAGGAG R: CTTCCGGCAGGAGAGGTT	90	63

Continued

ITGB5	F: GGAGTTTGCAAAGTTTCAGAGC R: TGTGCGTGGAGATAGGCTTT	89	60
JAM2	F: GCTATGCTCAGAGGAAAGGCTA R: GGATTTTGTGTGCTTGAAATCAT	110	60
JUN	F: CTGTCTCAAGGGGTGATTGCTC R: TTCGATAGGTCCATGTGCTG	95	54
MAP1A	F: ATTGGGATCAGCATCGACTCTCCG R: CAAACTCACACCCTTGCTTG	88	66
MCM3	F: TCACCACAGACCAGGAAACA R: CAAATTCATCAATGCAAACCA	90	60
MDM2	F: GGCAGAAACACAGTTCACCAGTC R: AGGTTGCTGCTGGAGTGAAT	89	58
MITF	F: AGAGTCTGAAGCAAGAGCACTG R: TGCGGTCATTTATGTTAAATCTTC	95	59
MMP23A	F: TTGCTTTCAGGGCTCTTATCCT R: CATAATTTCTTTTGCATCATCTGG	75	60
MRPL16	F: GAAGCACCTCCGGAACCTGTA R: GTCACCTCGTTCATGCACTC	88	58
MYOD1	F: CACTACAGCGGCGACTCC R: TAGGCGCCTTCGTAGCAG	116	60
MYOG4	F: CAGCTCCCTCAACCAGGAG R: GCTGTGAGAGCTGCATTCG	90	60
NDRG1	F: CGTCTCCAAGATCCTGTGCA R: CGTCAGGCGTTGTCACCTGC	95	60
NID 1	F: CAGTTTTCAGATGAGGGAACG R: TGAAGGCCAGTTTCACAGTAGTT	74	60
P21	F: CAGCTCCCTCAACCAGGAG R: GCTGTGAGAGCTGCATTCGTCC	86	68
PCDH18	F: AACCACGTGCCAGAGAATTT R: GAAAGAAGCTGAGAGACCTGCT	77	59
PCNA	F: TGGAGAACTTGGAAATGGAAA R: GAACTGGTTCATTCATCTCTATGG	109	60
POLA2	F: GACATTGTTTCCATTCAAGAGC R: GTGTGGTGTAAGAGTTCAAGAGGA	74	59
PTEN	F: CGAACTGGTGTAATGATATGTGC R: CGCCTCTGACTGGGAATAGT	131	59
RBBP4	F: CAGTTTTCAGATGAGGGAACGTCCG R: TGAAGGCCAGTTTCACAGTAGTTC	85	64
SENP5	F: TTTTGACGAGCCTTCAACAAG R: CTACAACCTGATGCGTCTGC	90	60
SKP2	F: CTGTCTCAAGGGGTGATTGC R: TTCGATAGGTCCATGTGCTG	104	60
SMAD2	F: AAAGGGTGGGGAGCAGAATA R: GAAGTTCAATCCAGCAAGGAT	64	60
SOX10	F: CATCCCAGGAGGTGACGA R: GGGAGGCTCTGTGAATTGTC	76	58
TFDP 2	F: CTGTCTCAAGGGGTGATTGCTGA R: TTCGATAGGTCCATGTGCTGC	102	60
TGFB3	F: AGTGCAGACACAACCCACAG R: GGTCCTCCCAACATAGTACAGG	129	59
TMBIM4	F: CTGTCTCAAGGGGTGATTGCTA R: TTCGATAGGTCCATGTGCTGAC	85	59
P53	F: CCTTGCTGCTCTACCTCCACGCC R: CCACTTCGTGATGATTCTGCAT	68	57
TRIB3C	F: CTGTCTCAAGGGGTGATTGC R: TTCGATAGGTCCATGTGCTG	67	60
VCAN	F: GCACCTGTGTGCCAGGATA R: CAGGGATTAGAGTGACATTCATA	70	60
VEGFA	F: CCTTGCTGCTCTACCTCCAC R: CCACTTCGTGATGATTCTGC	84	60

2.5.4. Reference Gene Screen Using GeNorm

A reference gene selection of 'ten patients spanning the age range' previously used in a related study of *PAX3* gene knockdown in neuroblastoma (Fang *et al.,* 2013), was applied in this study for screening the eight reference genes including glyceraldehyde 3 phosphate dehydrogenase (*GAPDH*), Beta-Actin (*ACTB*), Beta 2 microglobulin (*β2M*), hypoxanthine phosphoribosyl transferase 1 (*HPRT1*), ribosomal protein L32, (*RPL32*), Succinate dehydrogenase complex subunit A (*SDHA*), hydroxymethyl-bilane synthase (*HMBS*) and ribosomal protein L13a (*RPL13A*) (Using the GeNorm software, the two most stably expressed genes were selected and used for normalization) (**Table 2.4**).

Table 2.4 Selected housekeeping gene primers

Gene Symbol	Transcript length	Forward Primer	Reverse Primer	Probe ID	Probe Sequence
GAPDH	NM_002046	AGCCACATCGCTCAGACAC	GCCCAATACGACCAAATCC	60	TGGGGAG
ACTB	NM_001101	ATTGGCAATGAGCGGTTC	GGATGCCACAGGACTCCAT	11	CTTCCAC
β2M	NM_004048	TTCTGGCCTGGAGGCTATC	TCAGGAAATTTGACTTTCCATTC	42	CATCCAC
HPRT1	NM_000194	TGACCTTGATTTATTTTGCATACC	CGAGCAAGACGTTCAGTCCT	73	GCTGAGA
RPL32	NM_000994	GAAGTTCCTGGTCCACAACG	GCGATCTCGGCACAGTAAG	17	AGGAGCG
SDHA	NM_004168	AGAAGCCCTTTGAGGAGCA	CGATTACGGGTCTATATTCCAGA	69	CTTCCTCC
HMBS	NM_000190	AGCTATGAAGGATGGGCAAC	TTGTATGCTATCTGAGCCGTCTA	25	CTCCTCCA
RPL13A	NM_012423	GAGGCCCCTACCACTTCC	TGTGGGGCAGCATACCTC	28	CCAGCCGC

The algorithm worked out the stability of each transcript and sequentially removed the least stable transcript until the two most stable transcripts remained. The software compared the amount of each gene detected across all the samples. The threshold for the stability value M, was set at 0.4 and any value below 0.4 was considered stable (Anstaett *et al.,* 2010). In this current study, *HMBS* and *SDHA* demonstrated low stability values (as the most stable genes) and were chosen as reference normalization genes.

2.5.5. Quantitative RT-PCR Analysis

cDNA was diluted 1 in 40 with nuclease free water. Each reaction comprised 4µl diluted cDNA, 5µl 2 X Light Cycler 480 Probes Master, 0.1µl forward and reverse primer mix (20µM), 0.1µl Probe (10µM) and 0.8µl of nuclease free water. Samples were then amplified on a Light Cycler® 480 real time PCR machine on the following cycle 95^{O}C for 5 min, followed by 50 cycles of 95^{O}C for 10 sec and 60^{O}C for 30 sec. The amount of target genes expressed in a sample were normalised to the average of each of the two selected endogenous controls. This was given by ΔC_p, where ΔC_p was determined by subtracting the average endogenous gene C_p value from the average target gene C_p value. [C_p GOI – C_p average (endogenous gene)].

2.5.6. Sample Normalisation

In this study, sample data normalisation was performed to ensure the reliability of the RT-sqPCR, RT-qPCR and microarray experimental data, which compensates for sample-to-sample variations in these experiments, efficiency and sample quantification errors. The microarray and RT-PCR data were normalised to a selected invariant endogenous control reference 'house-keeping' genes including (*GAPDH, S14, SDHA* and *HMBS*). These four most commonly used housekeeping genes were selected as the optimal number of genes for validation, because they have been widely used as the most stable expressed house-keeping genes required for reliable normalization of RT-PCR data. They were used to eliminate gene expression inconsistencies and to allow appropriate comparison of data between the NC-siRNA and *PAX3*-siRNA transfected cells. Following adjustment of mean ratios of the 'house-keeping' genes to 1.0, the relative expression ratio of *PAX3*-siRNA and NC-siRNA was then used to obtain the normalised data (Gilsbach *et al.,* 2006).

2.6. Expression of PAX3 protein in Rhabdomyosarcoma and Melanoma Cells

2.6.1. Cell lysate extraction of total protein from transfected cell lines

96 hr after transfection with *PAX3*-siRNA and NC-siRNA, medium was discarded and the cells were washed three times with 0.5ml ice-cooled 1 X PBS to remove residual medium and possible contaminants. 0.2ml iced-cooled radioimmunoprecipitation assay buffer was added to the cells, incubated on ice for 30 min and the cells were removed with a cell scraper. The cell lysate was transferred into a sterile 1.5ml ice-cooled eppendorf tube and kept on ice for 20 min, vortexed 2 to 3 times to get a homogeneous mixture and then centrifuged at 1,2000 x g at 4^{O}C for 10 min. The supernatant lysate containing the cellular soluble protein was transferred to a new sterile ice-cooled eppendorf tube for measurement of protein concentration.

2.6.2. Bio-Rad Assay Estimation of Total Protein Concentration

The concentration of total protein in the extracted cell lysate was determined using the Bio-Rad protein estimation assay kit. A standard curve was made from bovine serum albumin (BSA) (1mg/ml) with increasing concentrations of BSA, ranging from (0 to 50µg/µl) in ddH_2O prepared in triplicate (**Table. 2.5**). 2ml of diluted Bio-Rad dye reagent (1:5 in ddH_20), was added to each 10µl diluted BSA or cell lysate concentration, mixed and then incubated for 20 min at RT. The cell lysate was treated in parallel with the BSA standards. The absorbance of both BSA and the cell lysate were measured at 585nm on an LKB spectrophotometer. The protein concentration of cell lysate was determined by comparison with the standard curve (**Fig. 2.1**). The cell lysate tube was stored at -20ºC.

Table 2.5. Preparation of BSA working concentrations

BSA(µg/µl)	0	10	20	30	40	50
BSA(µ1)	0	10µl	20µl	30µl	40µl	50µl
ddH_2O	100µl	90µl	80µl	70µl	60µl	50µl

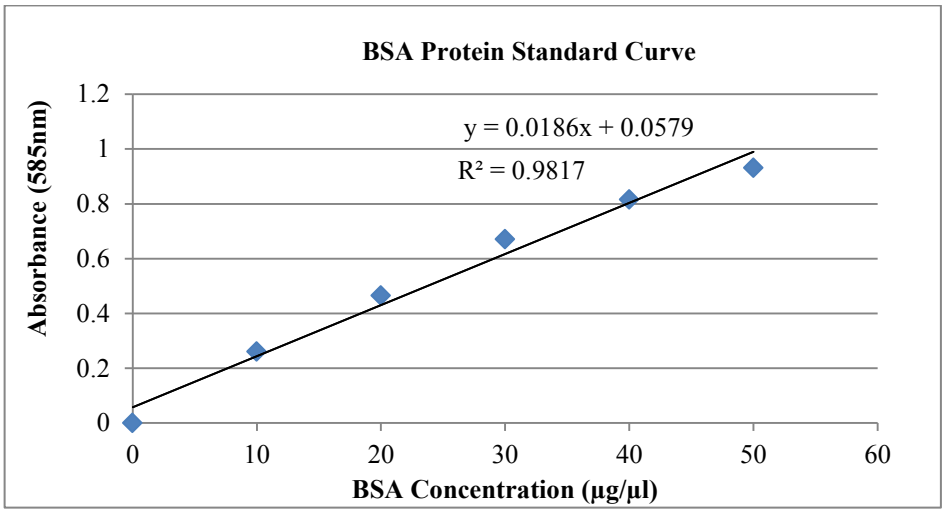

Figure 2.1 A typical BSA Protein Standard Curve for calculating protein sample concentration.

2.6.3. Western Blotting Analysis

Western blotting is a very powerful tool in identifying specific proteins (Kurien *et al*., 2011). This was used to investigate the effect of *PAX3* knockdown on protein expression levels of downstream targets. The technique utilises an electric field to separate charged protein molecules on a membrane based on their charge and size.

2.6.4. SDS Polyacrylamide Gel Electrophoresis

The use of **SDS-PAGE gel,** requires sample lysate solubilisation with an anionic detergent SDS, to coat membrane protein fragments with negatively charged particles. This was achieved by boiling a sample lysate with SDS for 15 min to disrupt protein-protein and protein-lipid complexes. Wells of freshly prepared polyacrylamide gel held

in between two glass plates, loaded with small samples of solubilised proteins, permits migration of protein molecules when an electrical potential is applied across the gel, with the positively charged anode attached to the bottom of the gel. This causes the negatively charged protein molecules to migrate towards the bottom end of the gel, each forming a discrete band. The rate of migration of each protein molecule down the gel is inversely proportional to its size and gel pore resistance, with the smallest protein molecules reaching the bottom as they easily migrate through the gel. The SDS-PAGE gel containing discrete protein molecules are then transferred onto a nitrocellulose membrane placed flat against the gel. Using an electric field, the protein molecules are then transferred from the gel to the membrane, where they remain in the same relative positions that they initially occupied in the gel. Using labelled antibodies known to bind to specific proteins of interest, the proteins from the gel are then identified and quantified

Separating and stacking gels for SDS polyacrylamide gel electrophoresis were prepared according to **table 2.6**.

Table 2.6 SDS-PAGE gel preparation

SDS-PAGE gels	Volume of 40% gel solution[1]	Volume of Buffer[2]	Volume of ddH_2O	Volume of 10% APS[3]	Volume of TEMED
Separation gel	3.3ml	2.5ml	4.2ml	100µl	10µl
Stacking gel	1.45ml	2.5ml	6.1ml	100µl	10µl

Note: 1. The gel solution was Acrylamide and N, N' methylene bis-acrylamide (37.5:1)

2. The buffers for separating gel and stacking gel were separating buffer and stacking buffer respectively.

3. APS: (Ammonium persulphate) freshly prepared.

The gels were prepared in sterile universal containers for two vertical dual casting-gel stand duplicate membranes using the table above. A bis-acrylamide separating gel was prepared by combining 3.3ml of 40% bis-acrylamide with 4.2ml ddH_2O and 2.5ml of

separating buffer in a sterile universal container, then 100µl of 100mg/ml ammonium persulphate was added and immediately followed by 10µl TEMED. As soon as the TEMED was added, the solution was swirled gently to mix and immediately 4.6ml of the prepared separating gel was poured into each vertical dual gel-casting stand, 100µl of isopropanol was added on the top of the separating gel to expel air pockets and incubated at RT for 15 min to polymerize. The isopropanol was discarded and the top of the gel immediately rinsed five times with ddH_2O to completely remove all traces of isopropanol. The ddH_2O was discarded and all traces of dd_2O were removed using 1mm Whatman blotting paper. A bis-acrylamide stacking gel was prepared by combining 1.4ml of 40% bis-acrylamide with 6.1ml ddH_2O and 2.5ml of stacking buffer in a sterile universal container, then 100µl of 100mg/ml APS was added followed by 10µl TEMED. As soon as the TEMED was added, the solution was swirled gently to mix and 4.5ml of the prepared stacking gel was poured on top of the resolving gel in each gel-casting stand to the brim of the glass plates. A pair of clean gel combs were carefully inserted without trapping air bubbles and incubated at RT for 15 min to polymerize. As soon as the stacking gel polymerized, the spacers were removed and the gel sandwiched glass plates were submerged in the electrophoresis tank and filled with 400ml-500ml electrophoresis buffer. The protein samples were mixed with 2 X protein loading buffer to stabilized the protein, then vortexed for 30 sec, boiled for 20 min and centrifuged in a microcentrifuge for a few sec at 800 x g. The total protein samples of known concentration were loaded at 20-40µg per lane alongside a MagicMark™ XP protein standard to determine the size of the target protein. In addition, a Novex® sharp pre-stained protein standard was used to allow the visualization of protein molecular weight ranges during electrophoresis and to evaluate western blot transfer efficiency. Electrophoresis was carried out at 60V for 45 min and the voltage was increased to 200V for another 45 min until the dye reached the bottom of the gel.

2.6.5. Blotting

Six pieces of 3mm Whatman chromatographic paper and 1 piece of Whatman nitrocellulose membrane were cut to about 1cm x 2cm and soaked in Towbin transfer buffer (PH 8.8) for 5 min. The separating gel was cut, placed on the soaked nitrocellulose membrane, sandwiched between 3 soaked chromatographic papers on a

Bio-Rad semidry electro-transfer machine. The proteins were transferred onto the nitrocellulose membrane at a current of 40mA/membrane for 30 min. The visible Novex® sharp pre-stained protein standard of varying protein molecular weight ranges was used to evaluate the western blot transfer efficiency.

2.6.6. Blocking

The nitrocellulose membranes containing the molecules of interest were blocked with 5% milk Blocking Buffer in TBS-Tween (PH 7.4) on a shaker at RT for 2 hr. The blocking buffer was discarded and a working solution of antibodies was prepared by dilution in 5% milk blocking buffer according to **table 2.7**.

Table 2.7 Antibodies used for western blotting

Primary Antibody	Host animal	Supplier	Working dilution	Predicted molecular Weight (KDa)
Monoclonal anti-GAPDH	Mouse	Abcam	1:1000	37
Monoclonal anti-PAX3	Mouse	Abcam	1:1000	53
Monoclonal anti-C-Myc	Mouse	Abcam	1:1000	49
Monoclonal anti-ITGβ5	Mouse	Abcam	1:250	88
Monoclonal anti-MyoD1	Mouse	Abcam	1:1000	35
Monoclonal anti-Bcl2	Mouse	Abcam	1:500	26
Monoclonal anti-P21	Mouse	Abcam	1:100	18
Monoclonal anti-P53	Mouse	Calbiochem	1:500	53
Monoclonal anti-Casp3	Mouse	Abcam	1:500	31
Secondary Antibody	-	-	-	-
Polyclonal Goat anti-mouse-IgG	Goat	Dako	1:1000	-

Antibodies were allowed to bind their cognate antigens by incubating at 4^{O}C overnight on a shaker. The following day, the membranes were washed with 10ml freshly prepared TBS-Tween (PH 7.4) five times for 10 min each on a shaker at RT. The horseradish peroxidise conjugated secondary antibody, Goat anti-Mouse IgG diluted at 1:1000 in 5% milk Blocking Buffer was hybridized with the membrane on a shaker at RT for 1 hr. The membranes were washed with 10ml freshly prepared TBS-Tween

5 times for 10 min each on a shaker at RT and kept briefly in 10ml freshly prepared TBS-Tween until developed.

2.6.7. Developing

The nitrocellulose membranes were incubated in 2ml combined ECL A and B working detection solutions in the dark room for approximately 5 min. The membranes were then covered with transparent cling film and exposed in a G-snap chemiluminescence UV transilluminator for capture of protein signal intensity and quantification.

2.7. Analysis of Rhabdomyosarcoma and Melanoma Cell Proliferation

Growth characteristics of JR1, RH30 and A375 cell lines, having a doubling time of 29 hr, 35 hr and 20 hr respectively, was used to determine cell proliferation. The cell proliferative potential of JR1, RH30 and A375 cells following inhibition of *PAX3* gene expression, was evaluated using both indirect and direct methods.

2.7.1. Indirect MTS Cell Proliferation Analysis

Indirect cell proliferation was measured using the tetrazolium salt (MTS) colorimetric CellTiter 96® AQueous Non-radioactive cell proliferation assay kit as a colorimetric method to determine the number of viable cells. This assay provided a rapid and convenient method of determining viable cell number. The principle of this assay is based on the conversion of the tetrazolium component of the dye solution into a formazan product by living cells. A solubilisation solution added to the culture was able to solubilize the formazan product. OD at 490nm was directly proportional to the number of viable cells. The viability of JR1, RH30 and A375 cells transiently transfected with *PAX3*-siRNA and NC-siRNA was determined by a trypan blue exclusion assay.

Prior to indirect cell proliferation analysis of transfected cells, a pre-transfection time course standard growth curve of JR1, RH30 and A375 cells was performed using the MTS cell proliferation kit, since different cell types have different levels of metabolic

activity which may affect the relationship between the number of viable cells and their relative absorption over a period of time. This was necessary to establish the optimal seeding density producing optimal gradual growth over a transfection period, yielding medial absorbance readings according to the manufacturer's instructions. JR1, RH30 and A375 cells were dispensed as 100µl aliquots into 96 well plates in triplicate at varying cell seeding densities of 5.0 X 10^4 cells/ml, 1.0 X 10^5 cells/ml, 1.5 X 10^5 cells/ml, 2.0 X 10^5 cells/ml, 2.5 X 10^5 cells/ml, 3.0 X 10^5 cells/ml and incubated over a 96 hour period at 37^{O}C in a humidified 5% CO_2 atmosphere. Following incubation, the MTS cell proliferation solution was allowed to equilibrate at RT for 1 hr, and then 15µl/well of the MTS solution was added and incubated for 4 hr at 37^{O}C. Following incubation, 100µl of the solubilization solution was added to each well and the plates were sealed with a cling film and incubated at RT overnight. The absorbance reading at 490nm was measured using the 96-well plate AScorn Eliza reader. The mean optical densities of three replicate measurements were used to plot against cell seeding densities. The correlation coefficient of JR1, RH30 and A375 cells showed a linear relationship between cell number and absorbance at 490nm indicated optimal cell growth at 5.0 X10^4 cells/well and this was selected as the seeding density for subsequent cell proliferation analysis. Cells in complete DMEM medium were seeded at a seeding density of 5.0 X 10^4 cells/ml by dispensing 100µl/ml of suspension cells into three replicate wells of 96 well plates for NC-siRNA and *PAX3*-siRNA transfection and then incubated for 24-96 hr at 37^{O}C in a humidified 5% CO_2 atmosphere. Following transfection, the MTS cell proliferation analysis was determined as previously described using the MTS assay.

2.7.2. Direct Cell Proliferation Analysis

Analysis of direct cell growth of siRNA transfected cells was carried out by directly counting the number of growing cells as an indicator of cell proliferation. Following a 96 hr *PAX3*-siRNA and NC-siRNA transfection of JR1, RH30 and A375 cell lines cells, the cells were trypsinized and seeded in triplicate in 12-well plates (1ml/well) at a concentration of 1.5 X 10^4 cells/ml of complete DMEM. After 24 hr incubation at 37^{O}C in 5% CO_2 humidified atmospheric temperature, the cell number in each well were counted directly for three consecutive days using a Bio-Rad coulter cell counter. The

mean percentage of viable cells was estimated as well. The experiment was repeated three times.

2.8. Preparation of Homogeneous Discrete Single Cell Suspension

For subsequent cellular functional analysis (**2.9-2.14**), a suspension of discrete single cells was prepared. After 24-96 hr transfection, cells were trypsinized, pelleted at 300 x g for 5min, resuspended in 1 x PBS and then centrifuged at 100 x g for 1 min. The supernatant PBS was transferred into a fresh sterile universal container, centrifuged at 300 x g for 5 min and the cell pellet was resuspended in 1ml complete medium to form a homogeneous suspension of single discrete cells.

2.9. Cell Cycle Analysis

To assess the stage of the cell cycle which a cell has reached, its DNA content can be measured by using DNA-binding fluorochrome dyes (e.g. Propidium iodide: PI) followed by flow cytometry. The interaction of fluorochrome and cellular DNA content leads to fluorochrome excitation by laser and trigger cell fluorescence. The binding of fluorochrome to the DNA and the amount of fluorescence of each cell is directly proportional to the amount of DNA in that cell. This assay was used to demonstrate the stage of the cell cycle distribution after *PAX3* gene expression was inhibited and to quantify the relative number of cells in the cell cycle phases.

2.9.1. Propidium Iodide Staining and Flow Cytomerty

After transfection, discrete single cells (as shown in section **2.8**) were resuspended in 1ml cold 70% ethanol, briefly vortexed and incubated at $4^{O}C$ for 3 hr. The cells were again centrifuged at 300 x g for 5 min and the cell pellet was resuspended in 437µl cold PBS, 13µl 0.8U/ml DNase-free RNase A, 40µg/ml PI (Sigma Aldrich) and then incubated at $37^{O}C$ for 1 hr. The cell fluorescence was analysed using a FACS-Calibur Flow cytometer (Becton Dickinson) at the Paterson Cancer Research Centre, Manchester, UK. The experiment was repeated three times.

2.10. Cell Migration Analysis

In vitro analysis of JR1, RH30 and A375 cell migration potential was carried out to measure the migration ability following PAX3-siRNA gene knockdown. The principle of the assay was that, a "wound gap" in a cell monolayer was created by a scratch, followed by monitoring the "healing" of this gap due to cell growth and migrating towards the centre of the gap, thereby filling up and decreasing the initial width of the gap. Factors that alter the growth and/or motility of the cell can lead to increased or decreased rate of "healing" of the gap.

2.10.1. Scratch Wound Healing Assay

Following 12-96 hr transfection, homogenous discrete cells (as shown in section **2.8**) were harvested and seeded in triplicate onto 13mm round glass Thermanox coverslips (Nalge Nunc International, USA) in 24-well plates at a cell concentration of 4 X 10^5 cells/well. The cells were then grown in serum-free DMEM medium for 24 hr incubation, at 37^{O}C in a humidified 5% CO_2 atmosphere to obtain a monolayer cell growth of about 70-80% confluence. Using a sterile 1ml pipette tip, the cell monolayer was gently and slowly scratched to form a linear straight scratch wound across the centre of the well. After scratching, the wells were gently washed three times with complete DMEM medium to remove the detached cells and fresh medium was added to the wells. Areas of wound were marked and photographed at various time-points with a phase-contrast microscope. The initial width of the gap between the two edges at the time of scratching (0 hr) was measured and the plates were incubated for 24 hr at 37^{O}C. The cells were washed three times with 1 x PBS, fixed with 70% ethanol for 30 min and then stained with 0.5% methylene blue for 30 min and rinsed in ddH_2O. The width of the stained monolayer wound healing gap was measured after 24 hr. The difference in width of the wound gaps between 0 hr and 24 hr represents the distance migrated by the cells. Cell migration was assessed using inverted phase contrast microscopy with a 20 X phase objective lens and photographed. The same configuration of the microscope was used when pictures were taken of different views of the stained monolayer. Using the ImagJ software, the mean width of wound gap and the individual cells migrated within

the wound gaps were quantitatively evaluated. To reduce variability in results, multiple views of each well were documented and each experiment was repeated thrice.

2.11. Cell Adhesion Analysis

In vitro analysis of JR1, RH30 and A375 cells adhesion potential was demonstrated by examining the extent of adhesion on various extracellular matrix (ECM) component proteins (Collagen I, Collagen II, Collagen IV, Fibronectin, Laminin, Tenascin, Vitronectin) following knockdown of *PAX3* gene expression.

2.11.1. Cell Adhesion Assay

After transfection, 100µl of the discrete single cell suspension (as shown in section **2.8**) was added into each ECM array plates and then incubated at 37^{O}C in a 5% CO_2 incubator for 3 hr. Subsequently the complete DMEM medium was gently discarded and each well was washed three times with 200µl assay buffer to remove unbound cells whilst leaving residual assay buffer on the adherent cells to prevent drying of cells. 100µl of 0.2% methylene blue cell staining solution was added to each well and incubated at RT for 10 min to fix and stain the cells. The plates were washed four times with deionized water and 100µl of extraction buffer was added to each strip of well, incubated at RT on a gentle rotating orbital shaker for 20 min until the cell-bound stain was completely solubilized. The strips of wells were placed on a multiskan Ascent micro plate reader and the average relative cell attachment OD at 540nm was measured. The OD reading was directly proportional to the attachment of cells to ECM coated proteins. The experiment was repeated three times.

2.12. Cell Invasion Analysis

This assay was employed for the measurement of the metastatic potential of rhabdomyosarcoma and melanoma cells following knockdown of *PAX3*. The BD BioCoat Matrigel Invasion Chambers (Becton Dickinson) provide cells with the conditions that allow evaluation of their invasive property *in vitro.* The BD BioCoat Matrigel Invasion Chambers consist of a BD Falcon™ TC Companion Plate with Falcon

Cell Culture Inserts containing an eight micron pore size PET membrane with a thin layer of MATRIGEL Basement Membrane Matrix. The Matrigel Matrix serves as a reconstituted basement membrane *in vitro*. The layer occludes the pores of the membrane, blocking non-invasive cells from migrating through the membrane. In contrast, invasive cells (malignant or non-malignant) are able to detach themselves from the basement membrane and invade through the Matrigel Matrix and the membrane pores.

2.12.1. Cell Invasion Assay

Matrigel Matrix invasion insert chambers stored at -20^{O}C, were carefully removed with sterile forceps into a 24-well plate and allowed to equilibrate at RT for 10 min. The 24-well plates with the insert chambers were rehydrated with 0.5ml complete medium and incubated at 37^{O}C in a humidified 5% CO_2 incubator for 2 hr. The medium was carefully removed from the chambers without disturbing the layer of the Matrigel^{TM} Matrix. The inserts were then transferred into empty wells of the BD falcon^{TM} TC Companion plate containing 5% foetal bovine serum complete DMEM medium. Immediately, 0.5ml of homogeneous transfected discrete single cell suspension (as shown in section **2.8**) (1.5 X 10^4 cells/well) was added to the chamber in triplicate and incubated for 24 hr in a humidified incubator at 37^{O}C with 5% CO_2 atmosphere. The complete medium was discarded and the inserts were washed three times with 0.5ml 1 X PBS. Non-invading cells were removed from the upper surface of the membrane by scrubbing three times with a cotton swab moistened with warm 1x PBS. The cells on the lower surface of the insert membrane were fixed with 4% paraformaldehyde for 20 min at RT, rinsed with 1 x PBS three times and then stained with 1% Giemsa for 2 min. The insert membranes were rinsed three times with ddH_2O, dehydrated in 70% ethanol for 2 min followed by complete dehydration in 100% ethanol and air dried at RT. The membrane was removed using a sharp scalpel blade and forceps onto a drop of immersion oil on a microscope slide. Oil immersion microscopy was used to examine cells. Several fields of view were counted to obtain the mean number of cells invading the insert membrane. The experiment was repeated three times.

2.13. Cell Transformation Analysis

Anchorage-independent growth is one of the hallmarks of cell transformation. *In vitro* cellular transformation detection assays are semi-quantitative and measure the morphological transformation of cell colonies induced by experimental conditions. The anchorage independent growth potential of rhabdomyosarcoma and melanoma was assayed by testing their ability to grow in soft agar cell culture®.

2.13.1. Cell Transformation Assay

Following transfection, a discrete single cell suspension (as shown in section **2.8**) was resuspended in 0.3% agar in complete DMEM pre-warmed at 35^{O}C in a water bath. The cells were seeded at a density of 2.0 X 10^3 cells/well onto a 0.8% agar base layer at the bottom of each well. The cell layers were allowed to solidify prior to incubation and 1ml of complete DMEM was added to the wells to completely cover the agar layers and then incubated at 37^{O}C in 5% CO_2 atmosphere for 28 days until colonies were formed. The complete DMEM medium was changed twice every week. Three weeks later, visible morphologically colonies were stained with 1% crystal violet staining solution and photographed under an inverted microscope at 40 X magnification. Colonies were counted in several microscopic fields to obtain the mean number of colonies per field. All experiments were performed in triplicate and repeated three times.

2.14. Apoptosis Assays

The biochemical products of apoptosis including caspases are essential determinants of induction of cellular apoptosis. Caspases are cysteine proteases that cleave their substrate after an aspartic acid residue and have a critical role in both the initiation and execution of apoptosis. This assay uses a proluminescent caspase-3/7 DEVD-aminoluciferin substrate and a thermo stable luciferase for the detection of caspase-3/7 activity to indicate induction of apoptosis. Addition of caspase-Glo™ 3/7 reagent in samples triggers cell lysis, followed by caspase cleavage of the substrate and this results in the liberation of free aminoluciferin which is then consumed by the luciferase to generate a "glow-type" luminescent signal. The signal is proportional to caspase-3/7

activity. The caspase-Glo® 3/7 assay was employed to demonstrate indirect induction of apoptosis following knockdown of *PAX3* in rhabdomyosarcoma and melanoma cells.

2.14.1. Indirect Caspase 3/7 Detection of Induction of Apoptosis

Following transfection, 100µl of homogeneous discrete cells in suspension (as shown in section **2.8**) was seeded at a density of 1.5 X 10^4 cells/well in 96-well white-walled plates with positive control and blank (negative control) wells. The plates were incubated overnight at 37ºC in a humidified CO_2 incubator. A non-transfected positive apoptotic control was set up alongside to be used for induction of apoptosis by a pro-apoptotic agent, staurosporine at an optimal working concentration (1µM/ml; 1µl/ml). Prior to the assay, the caspase-Glo™ 3/7 buffer and lyophilised caspase-Glo™ 3/7 substrate were allow to equilibrate to RT and then the working caspase-Glo® 3/7 reagent was freshly prepared by transferring the caspase-Glo™ 3/7 buffer into the lyophilised caspase-Glo™ 3/7 substrate amber bottle and mixed until all the lyophilised caspase-Glo™ 3/7 substrate was completely dissolved. Following a 24 hr incubation at 37^{O}C, the 96-well white-walled plates containing siRNA transfected cells, non-transfected cells and blank wells were removed from the incubator and allowed to equilibrate to RT for 5 min. The positive apoptotic control was first prepared by adding 100µl of staurosporine to the non-transfected cells and incubated at 37^{O}C in a humidified CO_2 incubator for 2 hr to induce apoptosis. To each well, 100µl of caspase-Glo® 3/7 working reagent was added, covered with a plate lid, gently mixed using a plate shaker at 300–500rpm for 3 min and then incubated at 37ºC in a humidified CO_2 incubator for 2 hr. The luminescence of each sample was measured in a plate-reading luminometer according to the manufacturer's instructions. The blank reading was subtracted from the corresponding NC-siRNA, *PAX3*-siRNA and positive control readings. Induction of cellular apoptosis was determined by comparing the average luminescence readings relating to induction of apoptosis in both *PAX3*-siRNA and NC-siRNA transfected cells with the average luminescence readings of induction of apoptosis in the 2 hr staurosporine treated cells. The experiment was repeated three times under the same experimental conditions.

2.14.2. Direct DeadEnd Fluorometric TUNEL detection of Induction of Cell Apoptosis

During apoptosis, cellular morphological features are important determinants, distinguishing apoptosis from other cell death pathways. The DeadEnd™ Fluorometric TUNEL System is a standard assay designed for the specific detection and quantitation of late apoptotic cells within a cell population (Doonan and Cotter, 2013). This assay quantifies nuclear DNA fragmentation, as an important morphological hallmark of apoptosis in many cell types, by catalytically incorporating fluorescein-12-dUTP at 3-OH DNA ends using the enzyme Terminal Deoxynucleotidyl Transferase (TdT), which forms a polymeric tail by (TdT-mediated dUTP Nick-End Labelling). The fluorescein-12-dUTP-labeled DNA can then be visualized directly by fluorescence microscopy. This assay was intended to directly detect apoptosis by comparing the morphological changes in NC-siRNA and *PAX3*-siRNA following knockdown of *PAX3* in rhabdomyosarcoma and melanoma cells, using a combined 96 hr *PAX3*-siRNA transfected cells and 2 hr staurosporine (1µM/ml; 1µl/ml) treated induced-cell apoptosis.

The experiment was designed as: non-transfected cells (staurosporine positive apoptosis control wells, PC); NC-siRNA transfected cells; *PAX3*-siRNA transfected cells and *PAX3*-siRNA with staurosporine treatment (1µM/ml; 1µl/ml). After transfection, 1ml of the homogeneous discrete single cell suspension (as shown in section **2.8**) was seeded on Thermanox glass coverslips in 24-well plates at a cell concentration of 1.5 X 10^4 cells/well in triplicate and incubated at 37^{O}C in a humidified CO_2 incubator for 24 hr. In this present study, staurosporine (1µM/ml) was employed to induced apoptosis because it has been widely used as a potent non-selective broad-spectrum protein kinase inhibitor of protein phosphorylation in cell functional and regulation studies (Nan *et al.,* 2014).

Following overnight incubation, the complete DMEM medium was discarded and the wells of both positive apoptosis control cells and one set of *PAX3*-siRNA transfected cells were first treated with 100µl pro-apoptotic agent staurosporine optimal working solution (1µM/ml; 1µl/ml) and incubated at 37^{O}C in a humidified CO_2 incubator for 2 hr. This combination criterion provides a strong support for comparison as cells were equally treated with the pro-apoptotic agent. The other set of *PAX3*-siRNA transfected

cells was without staurosporine treatment. The cells were washed three times with 500µl of 1 X PBS and then fixed with 250µl freshly prepared 4% Paraformaldehyde solution in PBS (pH 7.4) for 30 min at 4^{O}C. The fixed cells were washed three times with 500µl of 1 x PBS, incubated at RT for 5 min in each wash, permeabilized in 0.2% Triton® X-100 solution in PBS for 5 min and then rinsed three times in fresh PBS for 5 min at RT. At this point, the 24-well plate was placed in a humidified chamber and excess PBS was completely removed. The fixed cells were covered with 100µl equilibration buffer to equilibrate at RT for 20 min and blotted to remove most of the equilibration buffer whilst avoiding cells drying. The fixed cells were treated with 100µl freshly prepared rTdT working solution, covered with aluminium foil to protect from direct light and then incubated at 37^{O}C for 2 hr in a humidified 5% CO_2 incubator to allow the tailing reaction to occur. Excess rTdT working solution was removed from the fixed cells and the reaction was terminated with 100µl of 2 X SSC solution at RT for 20 min. The SSC solution was completely blotted and the fixed cells were washed three times in fresh 1 x PBS, incubated at RT for 5 min in each wash to completely remove unincorporated fluorescein-12-dUTP. The PBS solution was completely blotted and the fixed cells were stained with 200µl freshly prepared Hutchin stain in PBS for 15 min at RT in the dark, washed three times with 300µl ddH_2O and then incubated in 200µl ddH_2O for 5 min at RT. Using forceps, the Thermanox glass coverslips with the fixed stained cells were removed and excess water was drained off from the surrounding area of cells. Two drops of Anti-Fade solution was placed directly onto the Thermanox glass coverslips area containing the treated cells. With a clean glass slide, the Thermanox glass coverslips were gently picked up and immediately examined to demonstrate the morphological changes of apoptosis under a fluorescence microscope using a standard fluorescein filter set to view the green fluorescence of fluorescein at 520 ± 20nm and blue DAPI (diamidino-2-phenylindole) at 460nm. The Fluorescein-12-dUTP incorporation resulted in localized green fluorescence within the nucleus of apoptotic cells only and non-apoptotic cells showed DAPI blue nuclei. The mean number of apoptotic cells per microscopic field in the NC-siRNA, *PAX3*-siRNA and *PAX3*-siRNA transfected cells with 2 hr staurosporine (1µM/ml; 1µl/ml) treatment were compared with the 2 hr staurosporine (1µM/ml; 1µl/ml) treated induced-apoptosis positive control cells to evaluate the cellular induction of apoptosis. This comparison was to check if

there was apoptosis when *PAX3*-siRNA transfected cells was compared to NC-siRNA transfected cells and to evaluate the degree of apoptosis when *PAX3*-siRNA transfected cells were compared to both *PAX3*-siRNA transfected plus 2 hr staurosporine (1μM/ml; 1μl/ml) treated cells and the 2 hr staurosporine induced-apoptosis positive control cells. The experiment was repeated three times.

2.15. Statistical Analysis

Data representation in all the figures were statistically analysed using arithmetic means and standard deviations (SD). Results of all the figures were expressed as mean ± standard deviation (SD) of three independent experiments. The error bars denotes SD. The correlation coefficients between arithmetic means tested by the Student's t-test (where P means probability of false positive), were used to verify the statistical significance of the difference between *PAX3*-siRNA and NC-siRNA treated paired samples. Values obtained from the differences were considered statistically significant if $p \leq 0.05$ (*), $p \leq 0.01$ (**) and insignificant if $p > 0.05$, where '*' means degree of p value.

CHAPTER 3

INHIBITION OF *PAX3* IN HUMAN RHABDOMYOSARCOMA CELL LINES

CHAPTER 3. INHIBITION OF *PAX3* IN HUMAN RHABDOMYOSARCOMA CELL LINES

3. Results

PAX3 aberrant expression promotes tumourigenic characteristics of rhabdomyosarcoma whilst inhibition of *PAX3* in JR1 and RH30 cell line *in vitro* could probably reduce the tumourigenic activity of rhabdomyosarcoma.

3.1. Morphological Characteristics of Transfected Human Rhabdomyosarcoma Cell Lines

Transfection of rhabdomyosarcoma cell lines with *PAX3* siRNA targeting (*PAX3*-siRNA), showed variable cell morphological changes. Embryonal rhabdomyosarcoma cell line, JR1 (**Fig. 3.1**) and alveolar rhabdomyosarcoma cell line, RH30 (**Fig. 3.2**), transfected with a pre-designed siRNA targeting *PAX3* (*PAX3*-siRNA) or a scramled irrelevant non-targeting negative control siRNA (NC-siRNA) under the same experimental conditions, showed different morphological changes. The NC-siRNA transfected JR1 (**Fig. 3.1A, B**) and RH30 (**Fig. 3.2 A, B**) cells, showed cell growth and had thin intact and well-defined cell borders. This was suspected to be due to the inability of NC-siRNA to induce *PAX3* gene silencing. In contrast, the *PAX3*-siRNA induced different morphologies in JR1 (**Fig. 3.1C, D**) and RH30 (**Fig. 3.2C, D**) cells, which appeared thicker, with irregular thick cell borders and deep brownish transfection-complex attachment on cell surfaces (according to literature transfection kit).

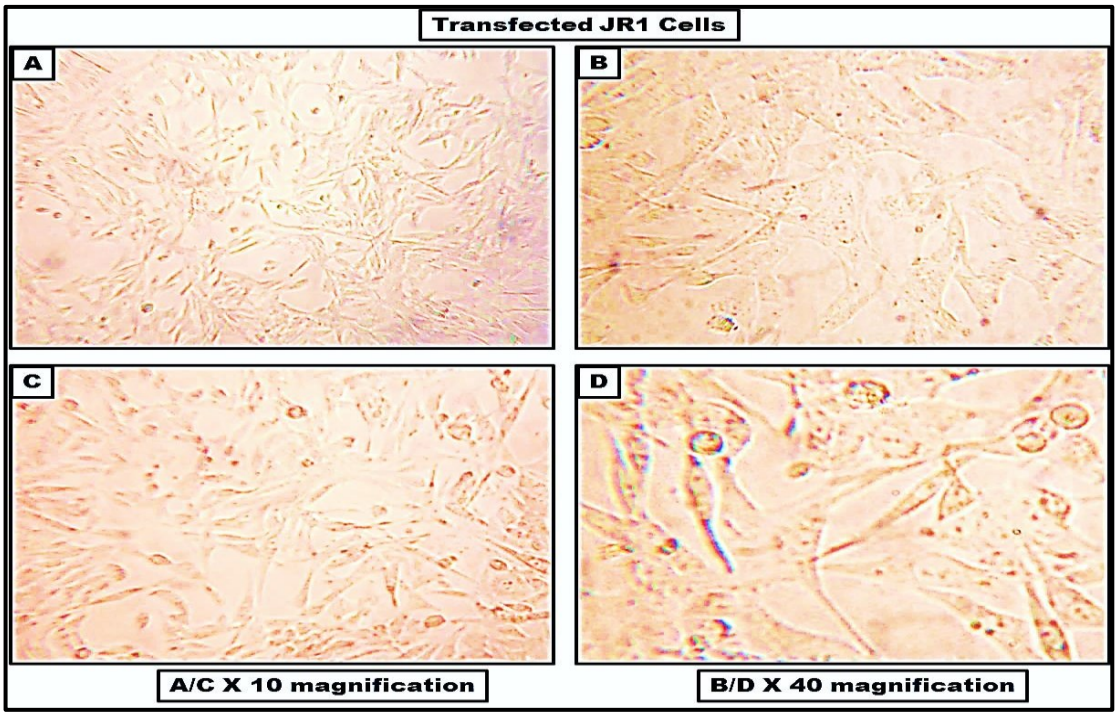

Figure 3.1 Phase contrast micrograph showing representative morphology of JR1 cells after 96 hr siRNA transfection. (**A, B**) NC-siRNA transfected JR1 cells. (**C, D**) *PAX3*-siRNA transfected JR1 cells. A/C, X 10 magnification and B/D, X 40 magnification.

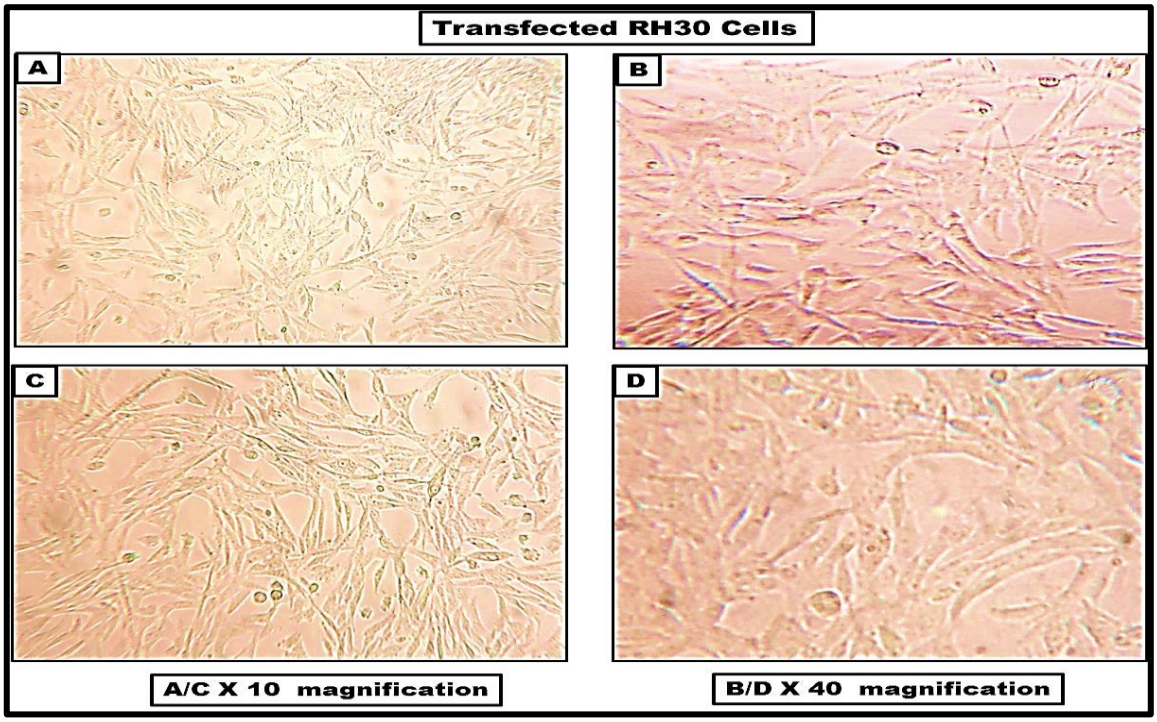

Figure 3.2 Phase contrast micrograph showing representative morphology of RH30 cells after 96 hr siRNA transfection. (**A, B**) NC-siRNA transfected RH30 cells (**C, D**) *PAX3*-siRNA transfected RH30 cells. A/C, X 10 magnification and (B/D), X 40 magnification.

3.2. *PAX3*-siRNA Knockdown in Human JR1 and RH30 Cell Lines

Table 3.1 Extracted total RNA purity and concentration

Sample	OD 260nm	OD 280nm	OD Ratio 260/280	RNA(µg/µl)
JR	-	-	-	-
C	0.338	0.185	1.82	3.38
T	0.255	0.135	1.88	2.55
RH30	-	-	-	-
C	0.488	0.260	1.87	4.88
T	0.377	0.206	1.83	3.77

OD: Denotes absorbance of extracted total RNA, where 260nm values determines the concentration of extracted RNA and 280nm values indicate purity of extracted RNA. High 260nm OD values signifies contamination of RNA with protein, peptides, carbohydrate, aromatic compounds and phenol. The ratio $OD_{260/280}$ indicates the degree of RNA purity (the range of RNA ratio value is between (1.6 - 2.0).

C: Represent OD of NC-siRNA indicating the purity and concentration of total RNA.
T: Represent OD of *PAX3*-siRNA signifying the purity and concentration of total RNA.

A pre-transfection analysis of *PAX3* gene expression, showed varying expression levels of the seven variants of *PAX3* mRNA and human ribosomal mRNA in both JR1 and RH30 cell lines (**Figs. 3.3 and 3.4**). *PAX3b, PAX3g* and *PAX3h* were weakly expressed in both JR1 and RH30 cell lines.

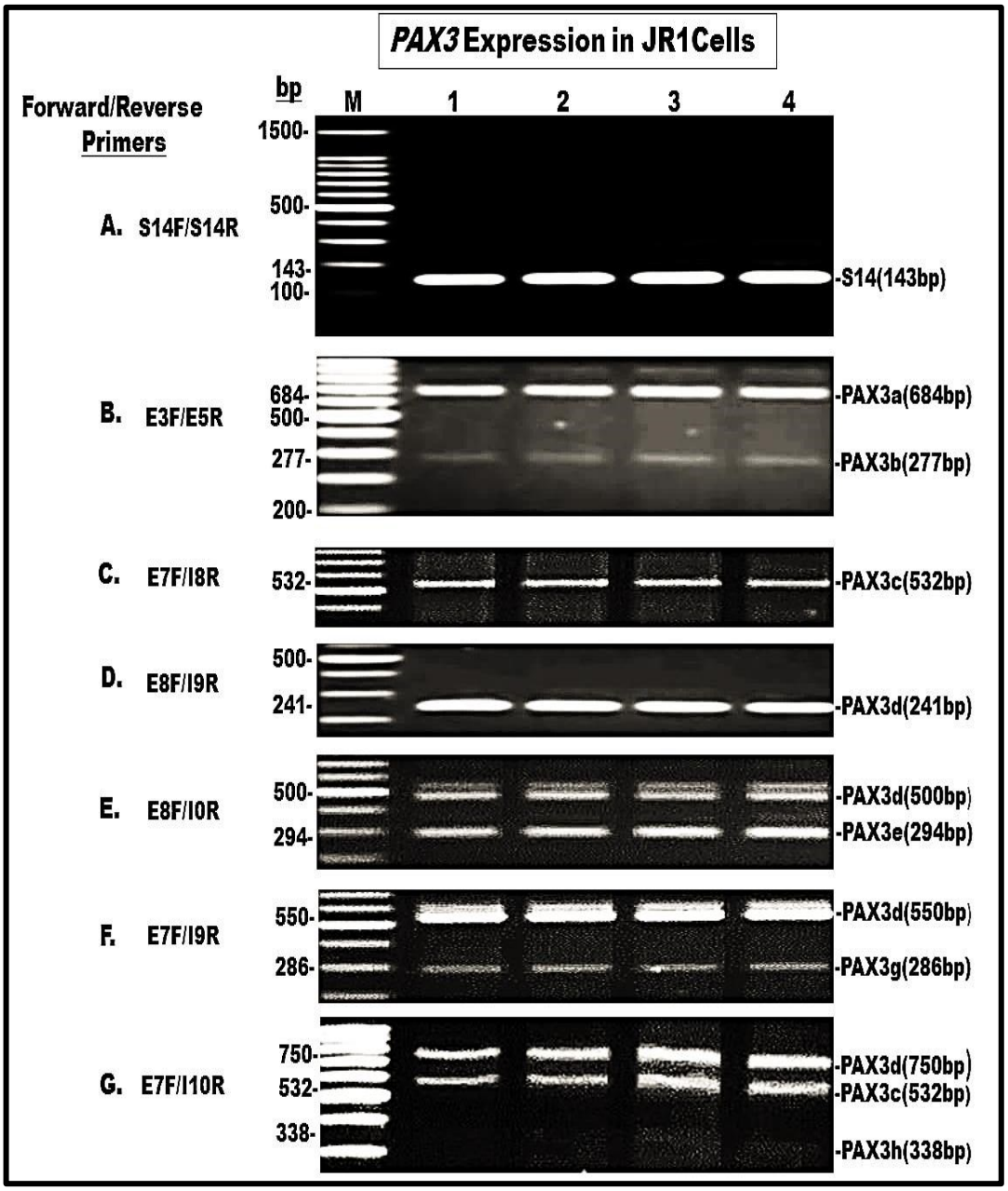

Figure 3.3 Semi-quantitative RT-PCR analysis of *PAX3* mRNA expression pattern in non-transfected JR1 cells. Lane M: 100bp benchtop DNA Marker (100-1500bp); Lanes 1-4: Replicate cDNA template from JR1 cells. (**A**) S14F/S14/R primer amplification of *S14* human ribosomal RNA; (**B**) E3F/E5R primer amplification of *PAX3a* and *PAX3b*; (**C**) E7F/I8R primer amplification of *PAX3c*; (**D**) E8F/I9R primer amplification of *PAX3d;* (**E**) E8F/10R primer amplification of *PAX3e* and *PAX3d;* (**F**) E7F/I9R primer amplification of *PAX3g* and *PAX3d;* (**G**) E7F/I10R primer amplification of *PAX3h,* faintly; *PAX3c* and *PAX3d.*

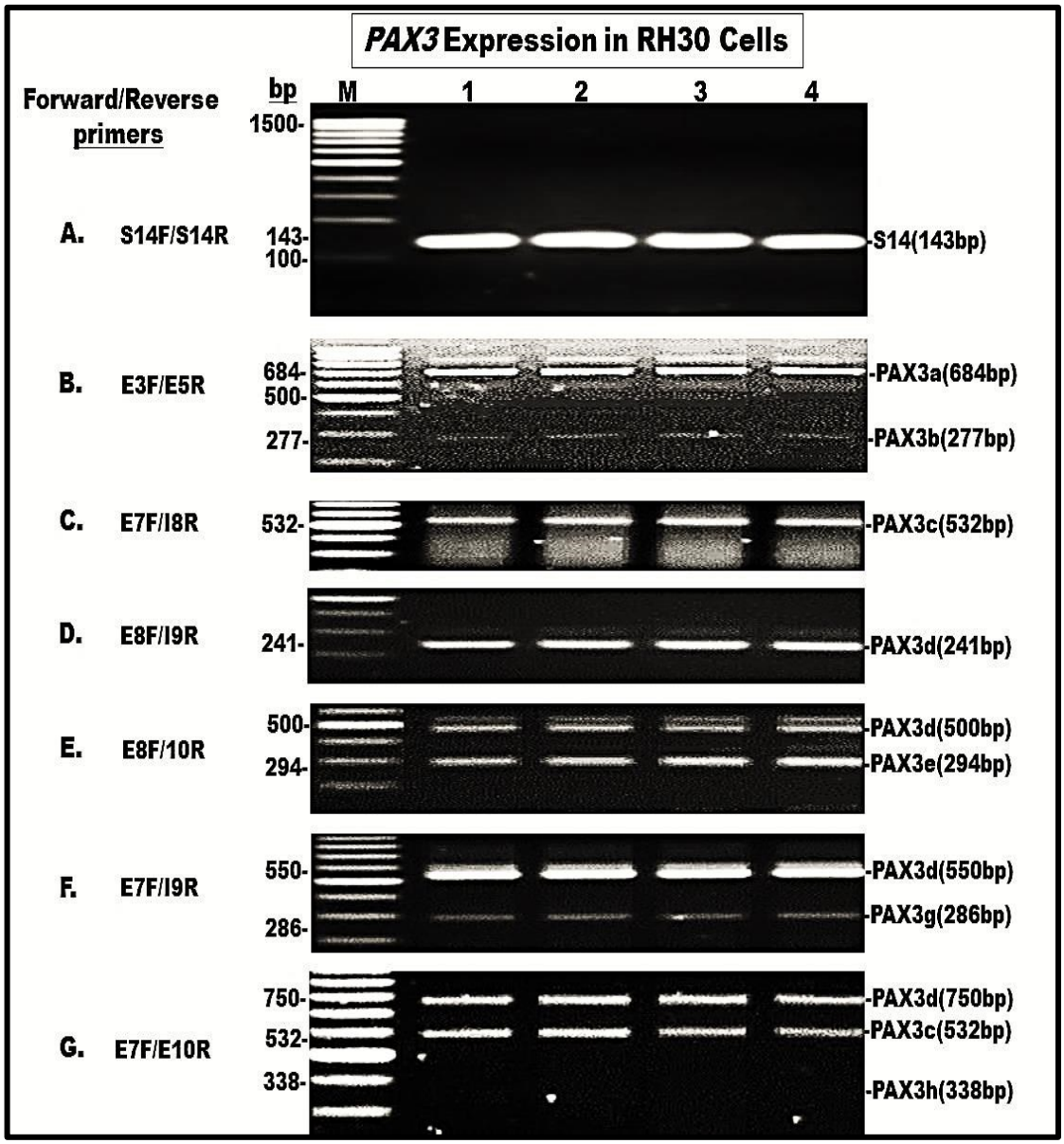

Figure 3.4 Semi-quantitative RT-PCR analysis of *PAX3* mRNA expression pattern in non-transfected RH30 cells. Lane M: 100bp benchtop DNA Marker (100-1500bp); Lanes 1-4: Replicate cDNA template from RH30 cells. (**A**) S14F/S14/R primer amplification of *S14* human ribosomal RNA; (**B**) E3F/E5R primer amplification of *PAX3a* and *PAX3b*; (**C**) E7F/I8R primer amplification of *PAX3c;* (**D**) E8F/I9R primer amplification of *PAX3d;* (**E**) E8F/10R primer amplification of *PAX3e* and *PAX3d*; (**F**) E7F/I9R primer amplification of *PAX3g* and *PAX3d*; (**G**) E7F/I10R primer amplification of *PAX3d, PAX3c* and faintly *PAX3h.*

To evaluate the degree of *PAX3* knockdown following siRNA treatment, *PAX3* mRNA expression in NC-siRNA negative control transfected cells (average of lanes 3-5) (**Fig. 3.5**) was compared with *PAX3* mRNA expression in *PAX3*-siRNA transfected cells (average of lanes 6-8) (**Fig. 3.5**).

Semi-quantitative RT-PCR analysis showed no change in expression pattern of S14 human ribosomal RNA, used as internal normalization control, (lanes 3-8 of **fig. 3.5A**). *PAX3*-siRNA induced significant high levels of knockdown of all *PAX3* isoform mRNAs in JR1 cells (**Fig. 3.5B-G**).

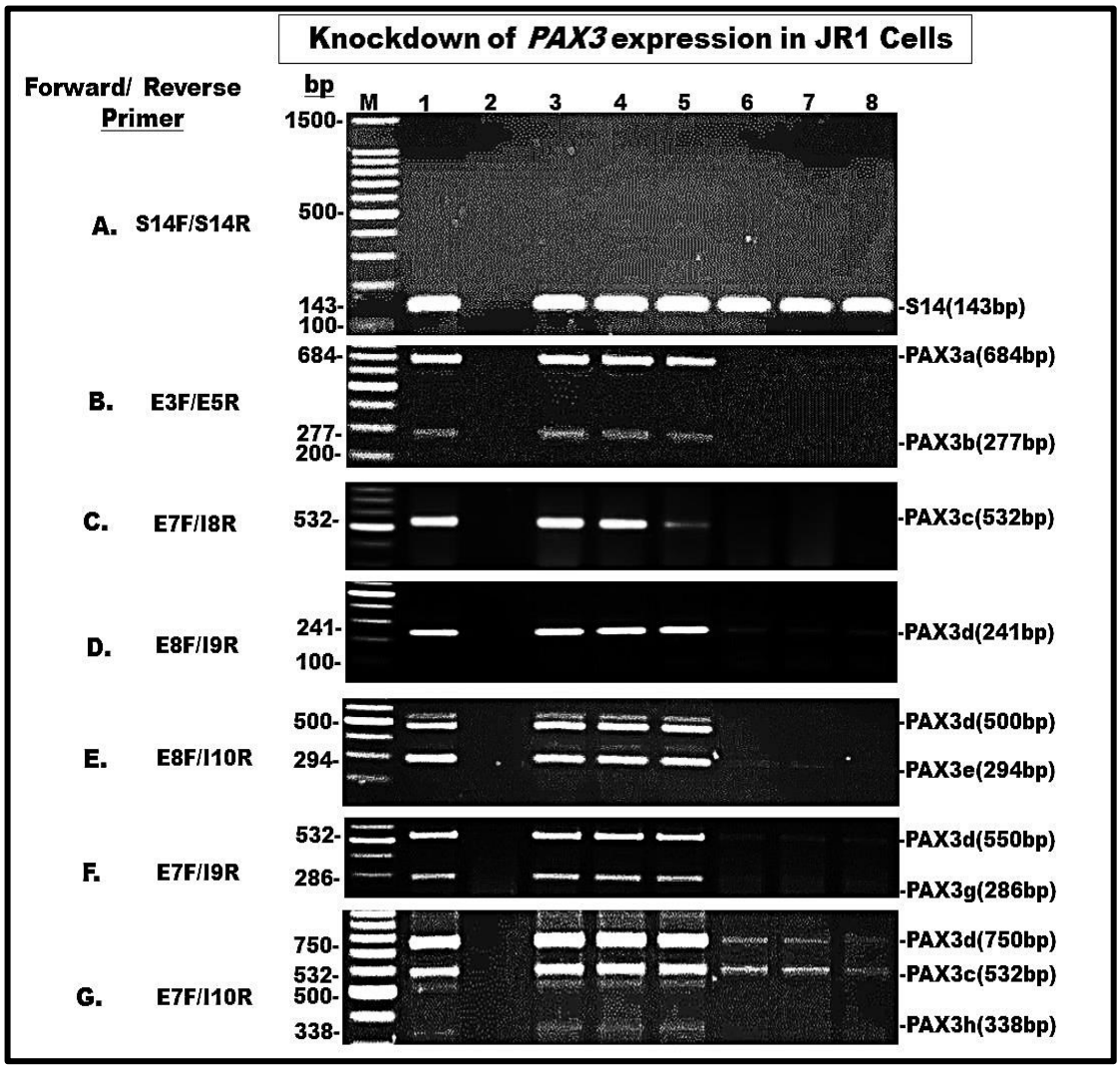

Figure 3.5 Semi-quantitative RT-PCR analysis of *PAX3* mRNA after 96 hr siRNA transfection of JR1 cells. Lane M: 100bp benchtop DNA Marker (100-1500bp); Lane 1: Untreated JR1 cell control; Lane 2: Negative control (no DNA); Lanes 3-5: Trilicate NC-siRNA tranfected JR cells as negative control;Lanes 6-8: Triplicate *PAX3*-siRNA transfected JR1 cells. (**A**) S14F/S14/R primer amplification of *S14* human ribosomal RNA internal normalization control; (**B**) E3F/E5R primer amplification of *PAX3a* and *PAX3b*; (**C**) E7F/I8R primer amplification of *PAX3c*; (**D**) E8F/I9R primer amplification of *PAX3d*; (**E**) E8F/10R primer amplification of *PAX3e* and *PAX3d;* (**F**) E7F/I9R primer amplification of *PAX3g* and *PAX3d;* (**G**) E7F/I10R primer amplification of *PAX3d; PAX3c* and *PAX3h*.

After 96 hr transfection, there was a significant reduction of *PAX3* gene expression in JR1 cells ($p < 0.01$): at least 93% knockdown of all variants of *PAX3* mRNA (**Fig. 3.6**). The level of *PAX3* gene expression remaining after PAX3-siRNA repression observed was *PAX3a* (2%); *PAX3b* (1%); *PAX3c* (2%); *PAX3d* (7%); *PAX3e* (2%); *PAX3g* (5%) and *PAX3h* (2%). The knockdown of *PAX3c* and *PAX3d* expression in JR1 cells was determined using **C** (**E7F/I8R**) and **D** (**E8F/I9R)** primer amplifications **in figure 3.5**, which are routinely used for the detection of only *PAX3c* and *PAX3d* respectively. However, E7F/I10R, that normally detects *PAX3h*, also identifies *PAX3c* and *PAX3d* in addition, which have also been knockeddown more than 90% (*PAX3c*) and 80% (*PAX3d*).

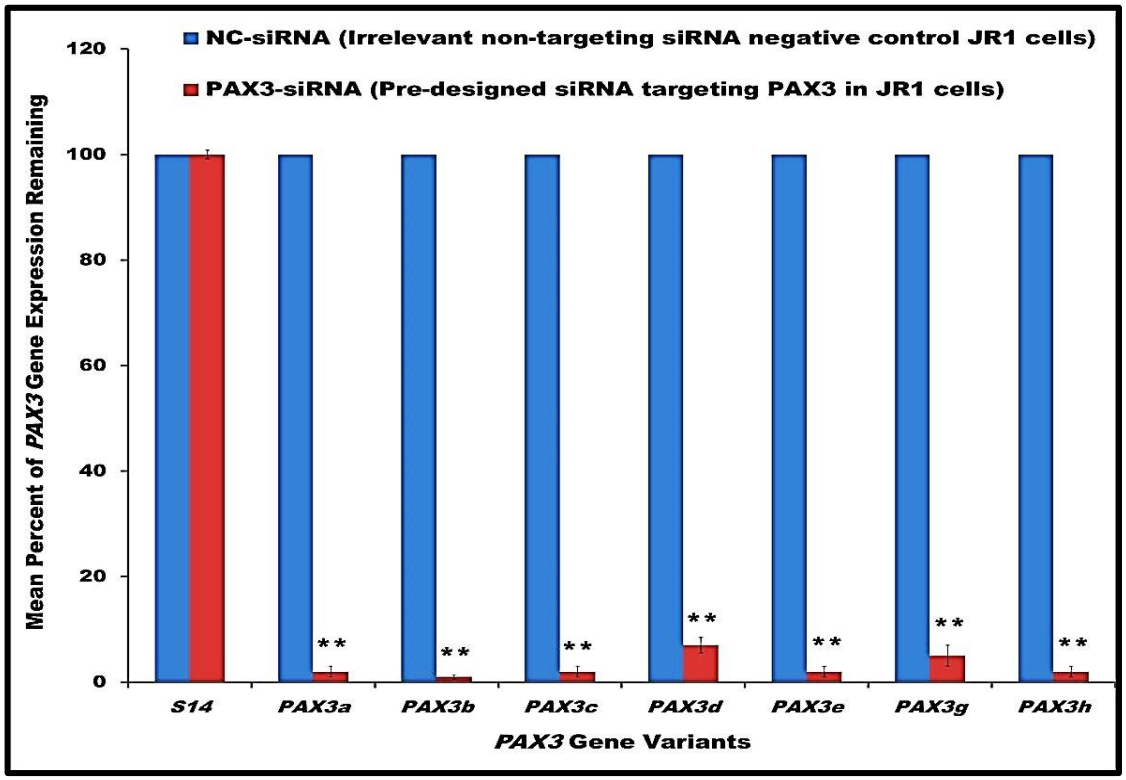

Figure 3.6 Mean percentages of *PAX3* gene expression as mRNA following 96 hr treatment with siRNA. The average *PAX3* gene expression in NC-siRNA transfected JR1 cells (blue columns) was compared with the average *PAX3* gene expression in *PAX3*-siRNA transfected JR1 cells (red columns) for each *PAX3* mRNA variant. The values are means of three measurements in three separate experiments (n = 9). (Values marked **; have a $p < 0.01$, Student's t-test).

A similar pattern of *PAX3*-siRNA gene knockdown was observed in the RH30 cell line after 96 hr transfection (see lanes 6, 7 and 8 of **fig. 3.7**).

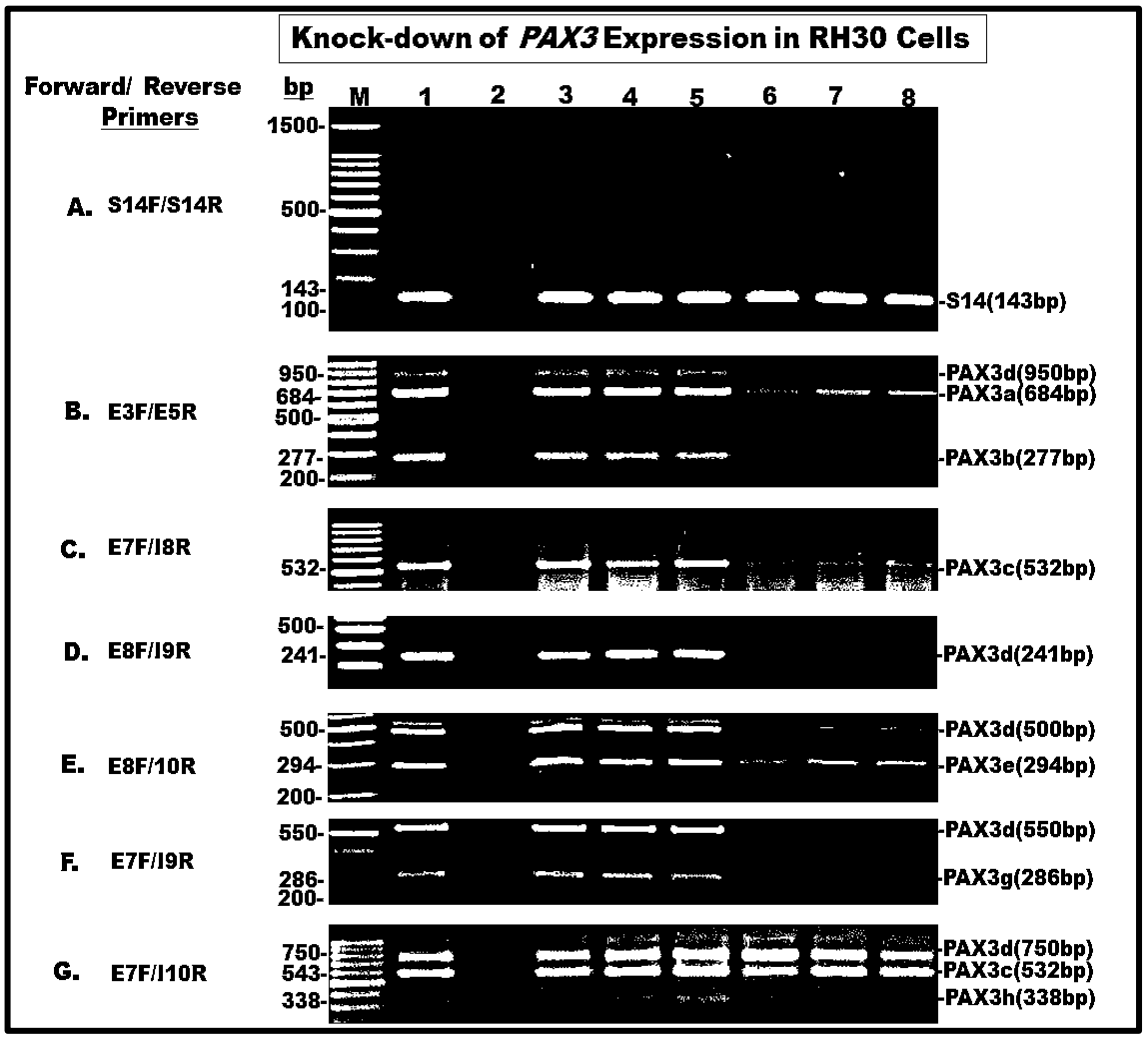

Figure 3.7 Semi-quantitative RT-PCR analysis of *PAX3* expression following 96 hr siRNA transfection of RH30 cells. Lane M: 100bp benchtop DNA Marker (100-1500bp); Lane 1: Untreated RH30 cell control; Lane 2: Negative control (no DNA); Lanes 3-5: Triplicate NC-siRNA treated RH30 cells as negative control; Lanes 6-8: Triplicate *PAX3*-siRNA transfected RH30 cells. (**A**) S14F/S14/R primer amplification of human ribosomal RNA S14 internal normalization control; (**B**) E3F/E5R primer amplification of *PAX3a* and *PAX3b;* (**C**) E7F/I8R primer amplification of *PAX3c;* (**D**) E8F/I9R primer amplification of PAX3d; (**E**) E8F/10R primer amplification of *PAX3e* and *PAX3d*; (**F**) E7F/I9R primer amplification of *PAX3g* and *PAX3d;* (**G**) E7F/I10R primer amplification of *PAX3d, PAX3c* and *PAX3h*.

High levels of *PAX3* gene expression were observed in NC-siRNA transfected RH30 cells compared to statistically significant low levels of *PAX3* gene expression in *PAX3*-siRNA transfected RH30 cells ($p < 0.01$). The suppression of *PAX3* mRNA detected in the RH30 cell line, indicated at least 90% *PAX3* knockdown across all *PAX3* mRNAs (**Fig. 3.8**), based on triplicate reading in three independent experiments (n = 9).

The levels of *PAX3* mRNA expression remaining after *PAX3*-siRNA transfection were: *PAX3a* (7%); *PAX3b* (3%); *PAX3c* (4%); *PAX3d* (10%); *PAX3e* (8%); *PAX3g* (5%) and *PAX3h* (4%). The knockdown of *PAX3c* and *PAX3d* expression in the RH30 cell line was determined using the primer combinations, **C** (**E7F/I8R**) and **D** (**E8F/I9R**) respectively in **figure 3.7**, which are unique for the amplification and identification of only *PAX3c* and *PAX3d* expression.

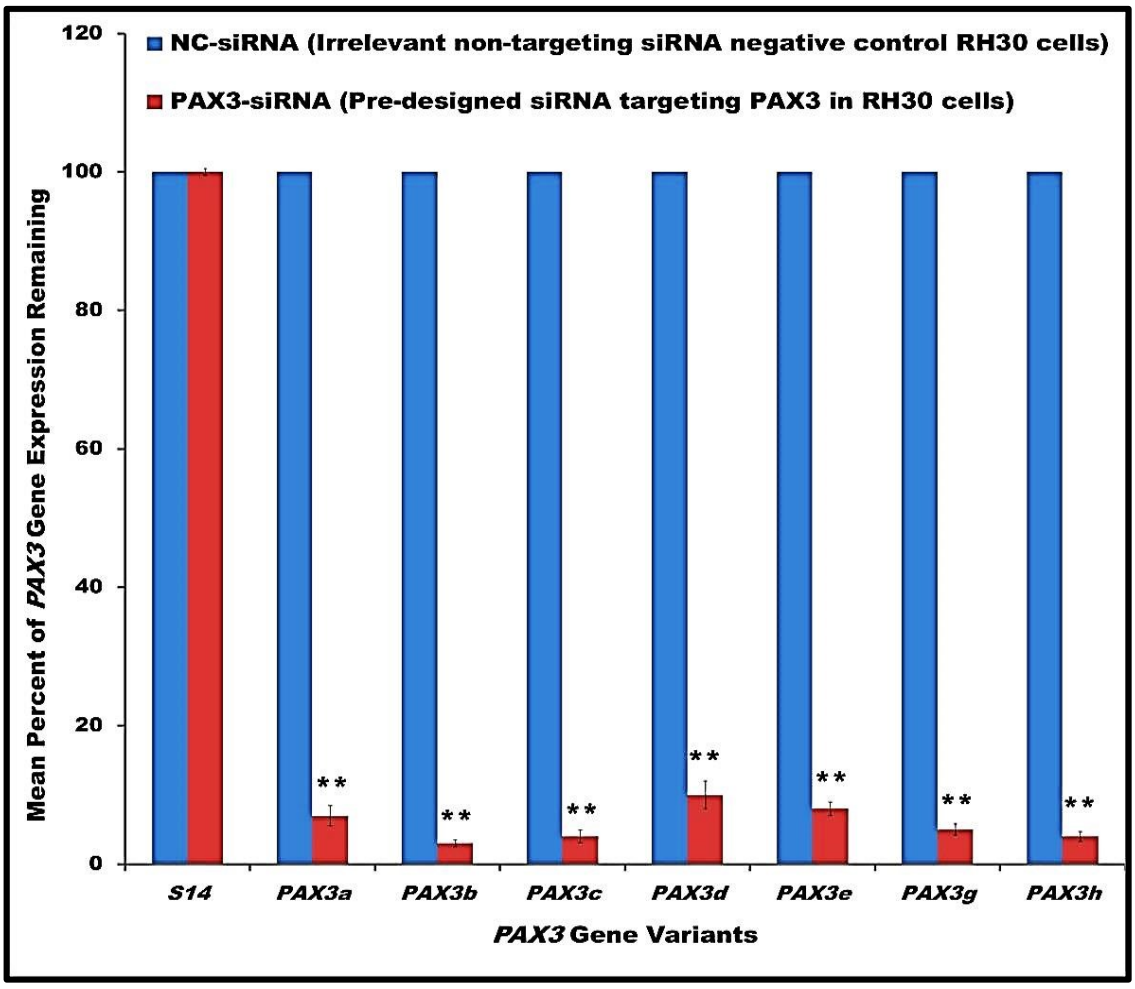

Figure 3.8 Mean percentages of *PAX3* gene expression as mRNA in RH30 cells following 96 hr siRNA transfection. The average *PAX3* gene expression in NC-siRNA transfected RH30 cells (blue columns) was compared with the average *PAX3* gene expression in *PAX3*-siRNA transfected RH30 cell (red columns). The values are means from three separate experiments (n = 9). Student's t-test showed statistically significant difference between blue and red columns for each *PAX3* gene variant (**; $p < 0.01$).

3.3. Effects of Inhibiting *PAX3* Gene Expression on Downstream Targets

The expression of the *PAX3* gene in rhabdomyosarcoma modulates the function of other target genes by either down-regulating or up-regulating them (Rescan *et al*, 2013). Microarray analysis was used to measure the degree of siRNA knockdown of *PAX3* gene expression in both JR1 and RH30 cell lines and the functional effects of this down-regulation on downstream targets. The mean normalized cDNA microarray gene expression profiling of NC-siRNA transfected cells was compared to that of *PAX3*-siRNA transfected cells. Prior to microarray analysis, the RNA integrity of JR1 and RH30 transfected cell lines was confirmed to be of high quality without degradation **(Fig. 3.9),** since reliable microarray data is dependent on the quality of RNA (**Fig. 3.10a**). The concentration of extracted RNA demonstrated a normal rRNA ratio of 1.6-2.0 in both NC-siRNA and *PAX3*-siRNA transfected cells (shown in **Table 3.1**).

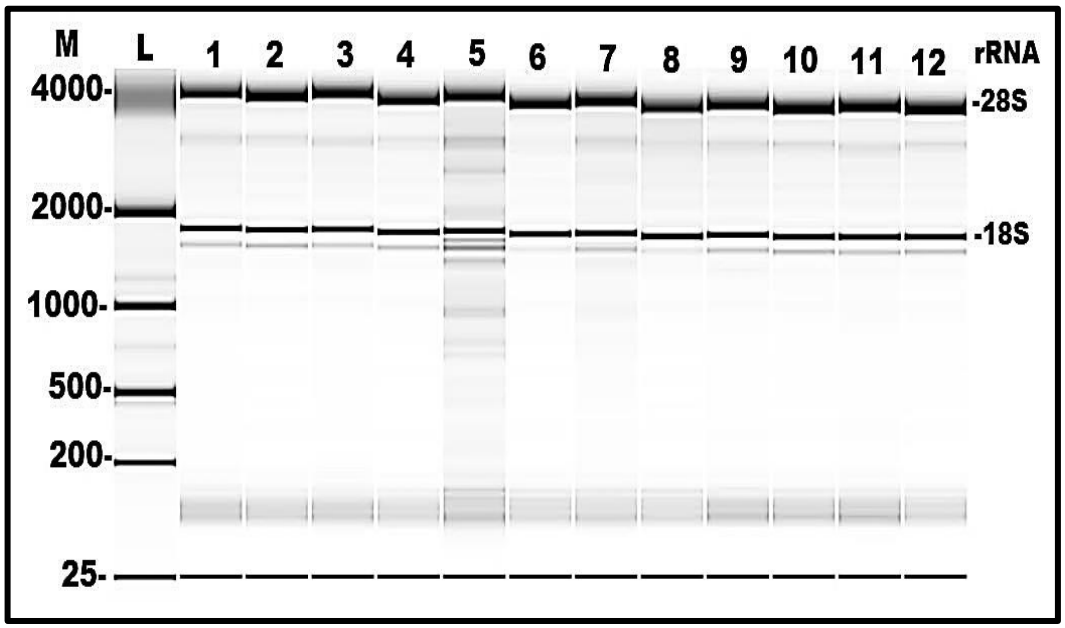

Figure 3.9 Electrophoresis of RNA from NC-siRNA and *PAX3*-siRNA transfected cell lines to determine the integrity of extracted RNA observed as ribosomal RNA (rRNA) bands, 28S (5kb) and 18S (2kb), with a 28S/18S ratio of intact RNA of 2:1 as a benchmark. Lane M: Marker size (25-4000bp); Lane L: Sample ladder (25-10,000bp); Lanes 1-3: NC-siRNA transfected JR1cells; Lanes 4-6: *PAX3*-siRNA transfected JR1cells; Lanes 7-9: NC-siRNA transfected RH30 cells; Lanes 10-12: *PAX3*-siRNA transfected RH30 cells. The above discrete separation of rRNA bands without smearing on the gel, showed high integrity and purity of the extracted RNA.

JR1 Cell mRNA

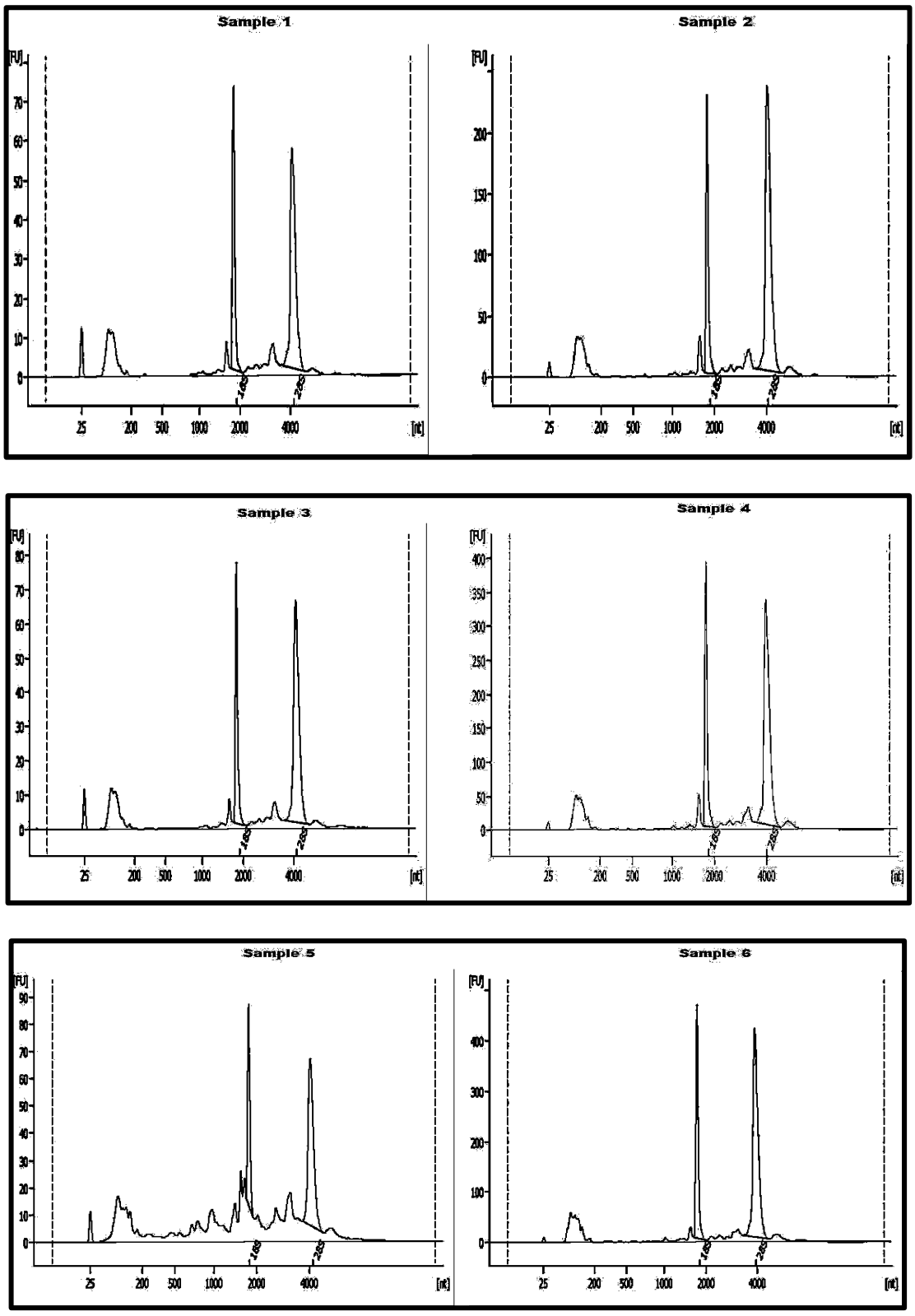

Figure 3.10a Quality of pooled RNA isolated from siRNA transfected JR1 cell line. A high relative absorbance fluorescence unit (FU) signal correlates with a high quality of rRNA in extracted RNA.

RH30 Cell mRNA

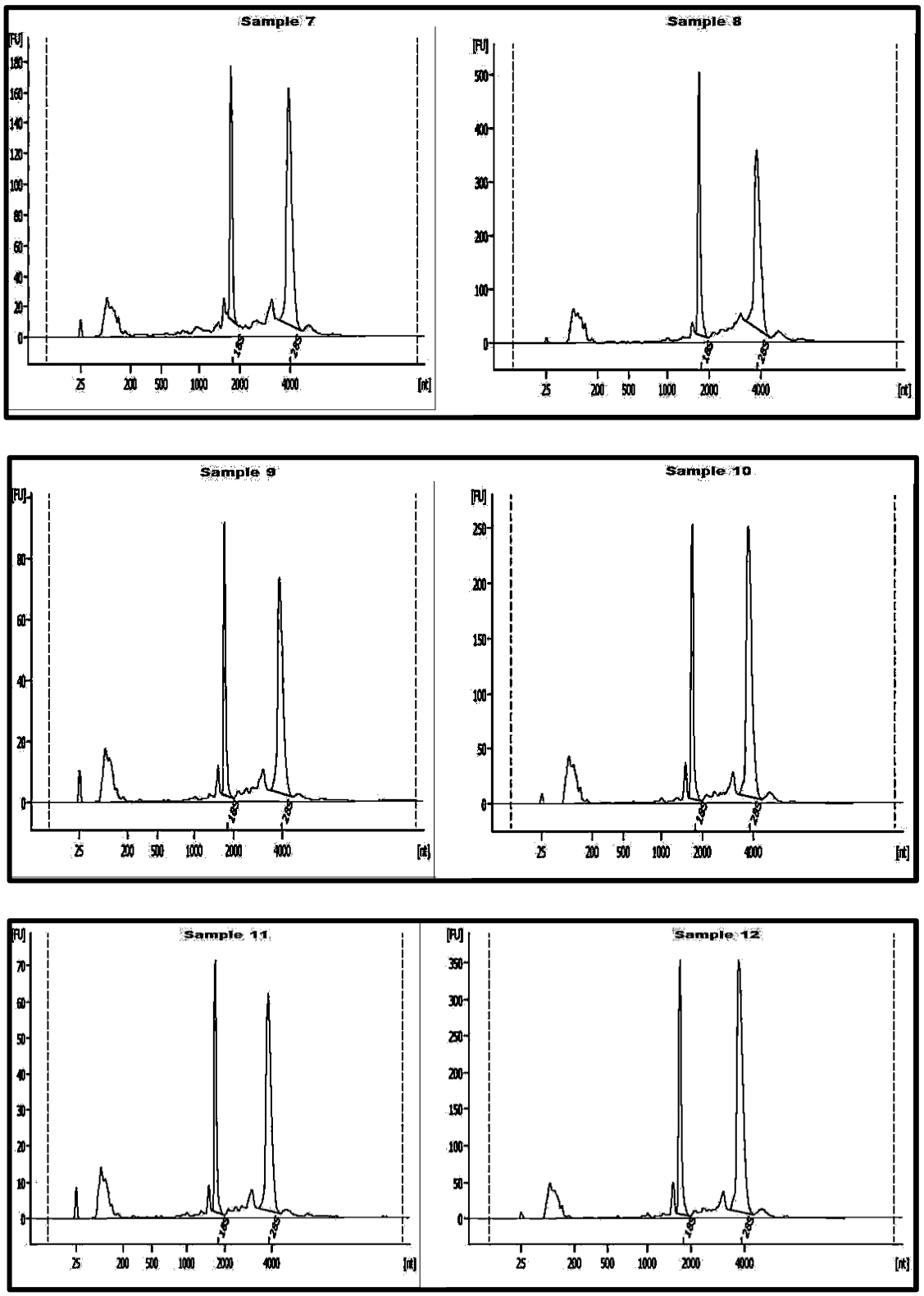

Figure 3.10b Quality of pooled RNA isolated from siRNA transfected RH30 cell line. A high relative absorbance fluorescence unit (FU) signal correlates with a high quality of rRNA in extracted **RNA**.

Table 3.2 Concentration and fragment rRNA ratios of extracted total RNA

SAMPLES	siRNA TRANSFECTED CELLS	TOTAL RNA CONCENTRATION (ng/µl)	RNA RATIO (28s/18s)
1	JR1 NC-siRNA	**200**	**1.6**
2	JR1 NC-siRNA	**650**	**2.0**
3	JR1 NC-siRNA	**214**	**1.8**
4	JR1 *PAX3*-siRNA	**1,003**	**1.7**
5	JR1 *PAX3*-siRNA	**461**	**1.8**
6	JR1 *PAX3*-siRNA	**1,201**	**1.7**
7	RH30 NC-siRNA	**619**	**1.9**
8	RH30 NC-siRNA	**1,460**	**1.6**
9	RH30 NC-siRNA	**275**	**1.7**
10	RH30 *PAX3*-siRNA	**757**	**1.9**
11	RH30 *PAX3*-siRNA	**224**	**1.8**
12	RH30 *PAX3*-siRNA	**999**	**2.0**

Affymetrix GCOS (V1.4) microarray analysis on the genechip, containing a 54,614 probe set, demonstrated a 4.15-fold and 2.61-fold reduction of *PAX3* expression in JR1 and RH30 cells respectively. Altered expression of 4,396 genes in JR1 and 5,877 genes in RH30 cells was observed (more than 1.5-fold) using the probability of positive log-ratio (PPLR < 0.1 or > 0.9). The mean knockdown of *PAX3* expression in *PAX3*-siRNA and NC-siRNA cells was compared after normalization to the housekeeping gene *GAPDH*. Using a 1.5-fold change of expression as a threshold in both JR1 and RH30 cell lines, 2,317 out of these 4,396 altered genes in JR1 cells were down-regulated following knockdown of *PAX3* expression, whilst 2,079 genes were up-regulated. Similarly, 3,456 out of these 5,877 altered genes in RH30 cells were down-regulated, whereas 2,421 genes were up-regulated. This present data revealed that some down-regulated genes in JR1 were up-regulated in RH30 cells. Genes of interest were classified into different groups according to their binding interactions with the *PAX3* gene and their main function in cells such as proliferation, migration, differentiation, adhesion, apoptosis and cell cycle (Farin *et al.,* 2008). 55 genes of interest including *PAX3* genes, which play critical roles in cancer cell developmental processes, were selected from the microarray data of 86 down-regulated genes (**Table 3.3**) and 54 up-

regulated genes (**Table 3.4**) for comparison with gene alteration pattern in qRT-PCR analysis under the same experimental condition.

Tables 3.3-3.7 show microarray expression analysis data on selected genes following 96 hr *PAX3*-siRNA knockdown in JR1 and RH30 cell lines. The selected genes in the Table below, as determined by the gene functional annotation tool DAVID NIH version 2, have important roles in cell proliferation (P), cell cycle (CC), migration (M), adhesion (AD), differentiation (DF), development (D) and apoptosis (AP). Some genes were selected based on their known regulation by *PAX3*.

Table 3.3 Microarray data showing genes down-regulated following *PAX3*-siRNA knockdown

The degree of gene down-regulation was denoted by varying shades of colour. Deep blue: gene expression down-regulated more than 2-fold; light blue: gene expression down-regulated between 1.5-2 fold.

			Fold change	
Gene symbol	**Gene description**	**Gene function**	**JR1**	**RH30**
PAX3	**Paired Box 3**	**D**	**-4.64**	**-2.61**
ADAM23	ADAM metallopeptidase domain 23	DF, M	-4.43	-4.87
ANAPC5	Anaphase promoting complex subunit 5	CC	-2.05	-2.55
BCL2	B-Cell lymphoma 2	AP	-4.37	-3.45
BIRC5	Baculoviral 1AP repeat containing 5	CC, P	-6.23	-3.45
BRCA1	Breast cancer 1	CC,P	-2.57	-2.86
BRCA1	Breast cancer 2	CC,P	-2.93	-2.45
CALM3	Calmodulin 3	P	-2.62	-2.20
CAPRIN1	Cell cycle associated protein 1	CC	-2.50	-9.84
CCNBI	Cyclin B1	CC	-2.90	-2.00
CCND1	Cyclin D1	CC	-10.00	-5.00
CCND3	Cyclin D3	CC	-3.68	-2.91
CCNE1	Cyclin E1	CC	-6.03	-5.45
CDC7	Cell division cycle 7 homolog	CC	-2.94	-3.83
CDC25A	Cell division cycle 25 homolog A	CC	-2.94	-1.96
CDC25B	Cell division cycle 25 homolog B	CC	-2.42	-1.57
CDC25C	Cell division cycle 25 homolog C	CC	-2.09	-2.18
CDC42EP3	CDC42 effector protein (Rho GTPase binding)	P	-1.83	-1.59

Continued

CDCA3	Cell division cycle association 3	CC	-5.84	-3.66
CDCA7	Cell division cycle association 7	CC	-2.34	-6.76
CDK2	Cyclin-dependant kinase 2	CC	-4.55	-2.02
CDK4	Cyclin-dependant kinase 4	CC,P	-2.59	-2.65
CDK5	Cyclin-dependent kinase 5	CC	-6.29	-4.72
CDKN3	Cyclin-dependent kinase inhibitor 3	CC	-2.32	-2.39
CDKN2C	Cyclin-dependent kinase inhibitor 2C (p18)	CC	-2.83	-2.65
CHEK1	CHK1 checkpoint homolog (S. pombe)	CC	-2.58	-1.83
CHEK2	CHK2 checkpoint homolog (S. pombe)	CC	-2.69	-2.50
C-MYC	C-myc binding protein	P	-5.85	-3.50
COL1A1	Collagen type I, alpha 1	AD, M	-10.48	-5.98
COL3A1	Collagen type III, alpha 1	AD, M	-15.66	-9.65
CYB5B	Cytochrome b5 type B	AP	-5.17	-4.84
DDB2	Damage-specific DNA binding protein 2, 48kDa	P	-2.93	-2.48
DHFR	Dihydrofolate reductase	P	-2.62	-4.57
E2F2	E2F transcription factor 2	P	-4.36	-2.21
E2F8	E2F transcription factor 8	P	-5.40	-3.74
EDN3	Endothelin 3	P	-29.01	-9.80
ENDRA	Endothelin receptor type A	M	-5.97	-2.86
FAIM	Fas apoptotic inhibitory molecule	AP	-6.78	-3.20
FGD4	FYVE, RhoGEF and PH domain containing 4	AD, M	-8.99	-2.16
FNDC5	Fibronectin containing sub-unit 5	AD, M	-4.46	-1.99
FSCN1	Fascin homolog 1, actin bunding protein	M	-3.27	-2.60
GINS1	GINS complex subunit 1(Psf1 homolog)	CC	-2.35	-3.16
GAS1	Growth arrest-specific 1	CC	-8.27	-4.23
HP1γ	Heterochromatin protein Lambda binding 1,	P, D	-2.94	-2.35
HMMR	Hyaluronic-mediated mobility receptor	P	-2.07	-1.52
ID3	Inhibitor of DNA binding 3	CC	-18.14	-17.48
ITGβ5	Integrin beta 5	AD, M	-6.06	-2.14
IPO13	Importin 13	P, D	-3.03	-2.04
LAMA1	Laminin alpha 1	AD, M	-4.43	-1.57
MAP1A	Microtubule-associated protein 1A	DF	-5.86	-6.65
MAPK 3	Mitogen-activated protein kinase 3	P	-3.05	-3.47
MAPK9	Mitogen-activated protein kinase 9	P	-3.08	-1.71
MCM3	Minichromosone maintenance complex 3	P	-5.84	-3.99
MMP2	Matrix metallopeptidase 2 A (pseudo)	M	-2.47	-1.98
MRPL16	Mitochondria ribosomal protein L16	P	-2.16	-2.59
MSH2	Muts homolog 2	M	-2.93	-2.47

Continued

MXRA7	Matrix-remodelling associated 7	M	-3.34	-2.81
MYOD1	Myogenic differentiation 1	D	-2.82	-4.65
MYOG4	Myogenin (myogenic factor 4)	D	-11.18	-2.54
NID1	Nidogen 1	AD,M	-2.39	-1.74
NUSAP1	Nucleolar and spindle associated protein 1	CC	-2.10	-1.61
P300	CREB binding protein E1A binding protein	P	-2.59	-1.67
PBK	PDZ binding kinase	CC	-2.56	-2.32
PCDH18	Protocadherin 18	AD, M	-35.19	-4.76
PCDH7	Proto cadherin 7	M	-12.88	-14.27
PCNA	Proliferating cell nuclear antigen	P	-3.75	-4.26
POLA2	Polymerase (DNA directed alpha 2)	P	-2.68	-2.11
PRM 2	Protein arginine methyltransferase 2	P	-3.54	-2.21
RAB27B	RAB27B, member RAS oncogene family	P	-9.09	-8.29
RB	Retinoblastoma	P	-7.66	-6.74
RBBP4	Retinoblastoma binding protein 4	P	-6.71	-3.64
RECK	Reversion-inducing-cysteine-rich protein K	M	-13.71	-3.22
RXA	Retinoid X receptor alpha	P	-4.22	-1.86
SHC4	Src homology 2 domain member 4	P	-2.33	-2.32
SKP2	S-phase kinase- Associated protein 2(p45)	CC	-3.99	-1.93
SELPLG	Selectin P ligand	AD	-6.26	-5.67
SMAD2	SMAD family member 2	P, M, D	-2.55	-2.06
SMC1	Structural maintenance of chromosomes 4	CC	-2.34	-1.68
SPCS3	Signal peptidase receptor complex subunit 3	CC	-3.27	-2.58
TFDP1	Transcription factor DP-1	P	-10.58	-4.36
TGFβ3	Transforming growth factor beta 3	P	-11.21	-6.22
TMBIM4	Transmembrane BAX inhibitor motif containing 4	AP	-2.55	-2.06
TNC	Tenascin	D, M	-3.52	-3.03
TNFRSF19	Tumour necrosis factor receptor superfamily member 19	AP	-15.52	-4.20
TUBB2C	Tubulin beta 2c	AP	-1.72	-3.03
VCAN	Versican	AD, M	-22.00	-2.96

A 1.50-fold change (light blue shade) was used as the threshold for down-regulation of gene expression.

Table 3.4 Microarray data of genes up-regulated following *PAX3*-siRNA knockdown

The degree of gene up-regulation was denoted by varying shades of colour. Red: gene expression up-regulated more than 2 fold; Orange: gene expression up-regulated 1.5-2 fold.

			Fold change	
Gene symbol	**Gene description**	**Gene function**	**JR1**	**RH30**
AEN	Apoptosis enhancing nuclease	AP	10.72	7.64
AKT3	V-AKTmurine thymoma viral oncogene homolog 3	P, AP	2.43	3.39
BAX	BCL2-associated X protein	AP	2.97	1.87
BNIP1	BCL2/adenovirus E1B 19kDa interacting protein 1	P	2.59	1.86
BNIP3	BCL2/adenovirus E1B19kDa interacting protein 3	AP	3.75	4.94
BTG2	B-cell translocation gene	CC, P	2.92	2.85
CASP3	Caspase3, apoptosis-related cysteine peptidase	AP	2.45	2.92
CASP4	Caspase 4, apoptosis-related cysteine peptidase	AP	3.36	1.62
CCNA	Cyclin A	CC	4.10	2.92
CCND2	Cyclin D2	CC	10.00	5.00
CDH2	Cadherin 2, type 1 N-cadherin (neuronal)	D	2.61	1.88
CDK6	Cyclin-dependent kinase 6	CC	7.66	6.99
CDKN1A	Cyclin-dependent kinase inhibitor 1A	CC	1.68	1.99
CGRRF1	Cell growth regulator with ring finger	CC, P	2.43	2.24
CITED2	Cbp/p300-interacting transactivator with Glu/Asp-rich carboxy-terminal domain 2,	P	3.66	4.75
CXCR4	Chemokine (C-X-C motif) receptor 4	P	4.73	2.88
DAXX	Death-domain associated protein	D	2.95	1.62
E2F7	E2F transcription factor 7	P	7.36	2.19
ETS1	V-ETS erythroblastosis virus E26	P	11.11	4.73
FOXO1	Forkhead box O1	P, D	3.51	2.04
GADD45B	Growth arrest and DNA- damage-inducible, beta	CC, P	5.23	3.40
H-RAS	V-Ha-ras Harvey rat sarcoma oncogene	M	5.82	9.40
HES1	Hairy and enhancer of split 1	P, D	6.69	2.92

Continued

HMOX1	Heme oxygenase 1	P, D	8.25	5.28
HUS1	Hus1 checkpoint homolog	P, M	4.58	2.94
ITGβ1	Integrin beta 1	P	4.84	3.64
JAK2	Janus kinase 2	P	2.47	2.50
JAM2	Junctional adhesion molecule 2	AD	4.04	2.93
JUN	Jun oncogene	P	6.66	1.89
KAP1	kinase A anchor protein 1	P, D	6.23	3.85
KITLG	Kit ligand	AP, M	27.30	5.86
LOC	Similar to C-Jun	P	6.09	2.24
MCL1	Myeloid cell leukemia sequence 1 (BCL2-related)	AP	4.63	3.70
MDM2	Mdm2 p53 binding protein homolog	P	2.49	2.12
MKNK2	MAP kinase interacting serine/threonine kinase2	P	2.42	2.21
MTSS1	Metastasis suppressor 1	M	10.33	8.48
MYC	V-myc myelocytomatosis viral oncogene	P	7.45	4.13
NAMPT	Nicotinamide phosphoribosyl transferase	P	4.66	4.46
NDRG1	N-myc downstream regulated 1	P	6.82	6.07
P15	Cyclin-dependent kinase inhibitor 2B	CC	9.08	4.84
P16	Cyclin-dependent kinase inhibitor 2A	CC	2.52	2.31
P21	Cyclin-dependent kinase inhibitor 1	P, CC	4.08	3.25
P53	Tumour protein p53 inducible protein	P, AP	3.51	3.77
PDRG1	P53 and DNA-damage regulated 1	CC	1.87	2.12
PTEN	Phosphatase and tensin homolog	P	2.87	2.77
RASA2	RAS p21 protein activator 2	P	2.67	2.07
ROCK2	Rho-associated, coiled-coil containing protein kinase 2	M	1.50	1.51
SENP5	SUMO1/sentrin specific peptidase	AP	4.61	3.88
SMEK1	SMEK homolog 1, suppressor of mek1	P, AP	2.02	1.90
TBX18	T-box 18	P, D	6.85	4.53
TRAF1	TNF receptor-associated factor 1	P	30.03	4.72
TRIB3C	Tribbles homolog 3	AP	10.33	11.97
VEGFA	Vascular endothelial growth factor A	P	6.02	2.70
ZEB2	Zinc finger E-box binding homolog 2	P, M	7.83	2.30

A 1.50-fold change (orange shade) was used as the threshold for up-regulation of gene expression.

Some of the affected genes were DNA binding interaction partners of *PAX3* (**Table 3.5**), acting as cofactor transcriptional modulators or functional modulators of *PAX3* (Boutet *et al.,* 2007).

Table 3.5 Microarray expression data of *PAX3* binding partners after *PAX3* inhibition

The degree of alteration in gene expression was denoted by varying shades of colour. Deep blue: gene expression down-regulated more than 2 fold; red: gene expression up-regulated more than 2 fold; orange: gene expression up-regulated 1.5-2 fold.

		Fold change	
Gene symbol	**Gene description**	**JR1**	**RH30**
PAX3	**Paired box3**	**-4.64**	**-2.61**
	***PAX3* Cofactor transcriptional modulators**		
HP1γ	Heterochromatin protein Lambda binding 1,	-2.94	-2.35
KAP1	kinase A anchor protein 1	6.23	3.85
TBX18	T-box 18	6.85	4.53
	PAX3 functional modulators		
BCL2	B-Cell lymphoma 2	-4.37	-3.45
DAXX	Death-domain associated protein	2.95	1.62
HES1	Hairy and enhancer of split 1	6.69	2.92
HMOX1	Heme oxygenase 1	8.25	5.28
IPO13	Importin 13	-3.03	-2.04
MSX1	Msh homeobox 1	2.22	-2.54
PTEN	Phosphatase and tensin homolog	2.87	2.77
RB	Retinoblastoma	-7.66	-6.74

+/- 1.50-fold change, down-regulation or up-regulation of expression was used as a threshold.

3.4. Quantitative RT-PCR Analysis of Downstream Targets

The microarray data of selected downstream targets in JR1 and RH30 cell lines were validated by quantitative RT-PCR analysis. Using a threshold of 0.4 as a cut-off point for stability showed that both *HMBS* and *SDHA* with a least mean value of stability were the most stable reference genes suitable for use to normalise both JR1 and RH30 cell lines **(Fig. 3.11**).

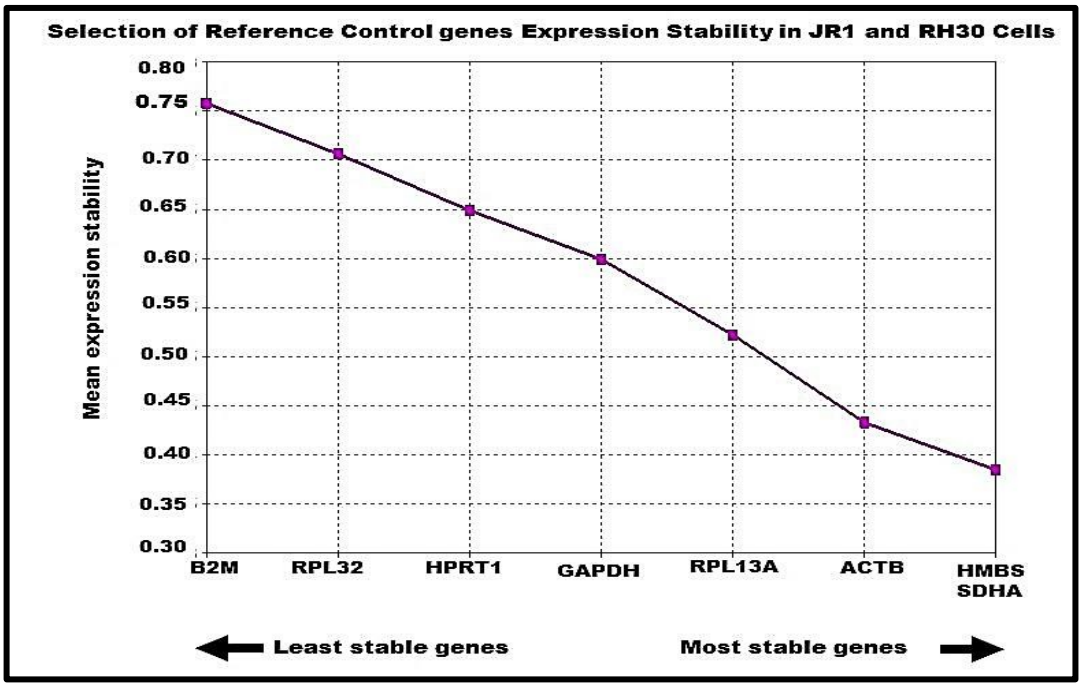

Figure 3.11 JR1 and RH30 cell lines GeNorm graph showing the mean expression stability values of eight selected reference sample genes. Each point shows the mean change of gene expression relative to fluorescence intensity at each PCR cycle. Both *HMBS* and *SDHA* genes with average stability value of (<0.4) were selected as the most stable housekeeping reference genes for normalization.

The quantification of cycle values (delta Cp), defined as cycle number at which the measured reporter fluorescence value past a fixed threshold above base line, was calculated for each gene. Generally, samples with higher message expression levels have lower delta Cp values. The microarray analysis results of 26 selected downstream target genes of interest together with *PAX3* in rhabdomyosarcoma cell lines were verified by the quantitative RT-PCR analysis. The genes were selected from the microarray analysis data based on their function including cell cycle, proliferation, migration, differentiation

and apoptosis. In addition to exceeding the q-value threshold of 1.50 and -1.50 for up-regulated and down-regulated genes respectively (based on 0.5 representing a 2-fold change in gene expression), the microarray analysis data of genes showing consistent changes in expression in both cell lines were selected. The microarray analysis data pattern of down-regulation of *PAX3* expression (-4.64-fold) in the JR1 cell line was confirmed by the qRT-PCR analysis data (-1.63-fold), whilst in the RH30 cell line, the pattern of *PAX3* down-regulation (-2.61-fold) confirmed by the qRT-PCR analysis was below 1.5-fold change (-1.37), (**Table 3.6**). Out of the 14 down-regulated genes of the microarray analysis data of 27 genes compared, the qRT-PCR analysis data confirmed the down-regulation of another 11 genes beyond 1.5-fold change (*ADAM23, BCL2, CAPRIN1, CCND3, CDCA3, COL3A1, C-MYC, E2F8, ITGβ5, MCM3* and *MYOG4*) (**Table 3.6**). However, the down-regulation of both *C-MYC* and *MYOD1* in RH30 cell line and *PCNA* expression in JR1 cell line verified by the qRT-PCR analysis was below 1.5-fold change whilst the down-regulation of JR1 *MYOD1* expression in the microarray data analysis was in contrast, up-regulated in the qRT-PCR analysis below 1.5-fold change (**Table 3.6**). The qRT-PCR analysis data further confirmed the microarray data of up-regulation of another 12 genes, in the JR1 cell line above 1.5-fold change (*AEN, AKT3, CASP3*, *CXCR4, E2F7, ETS1, FOXO1, JAM2, JUN, NDRG1, P21, P53* and *TRIB3C*) (**Table 3.6**)

Similarly, in the RH30 cell line, the qRT-PCR analysis data confirmed the down-regulation with at least 1.5-fold change of 10 genes out of the 14 genes down-regulated in the microarray analysis data (*ADAM23, BCL2, CAPRIN1, CCND3, CDCA3, COL3A1, E2F8, ITGβ5, MCM3* and *PCNA*) (**Table 3.6**). The qRT-PCR further validated the expression of another 4 down-regulated genes in the RH30 cell line below 1.5-fold (*PAX3, C-MYC, MYOD1* and *MYOG4*) (**Table 3.6**). Furthermore, the qRT-PCR analysis data has proved the up-regulation in the RH30 cell line of the expression of 12 genes (with at least 1.5-fold change) out of the 13 genes up-regulated in the microarray analysis data (*AEN, AKT3, CASP3, CXCR4, E2F7, ETS1, FOXO1, JAM2, JUN, NDRG1, P53* and *TRIB3C*) (**Table 3.6**), whilst the pattern of up-regulation of *P21* expression was confirmed as less than a 1.5-fold change in the qRT-PCR analysis data (**Table 3.6**).

Table 3.6 Microarray analyses gene alteration data compared to RT-qPCR analysis following *PAX3* silencing

The degree of gene up-regulation was denoted by varying shades of colour. Red: gene expression up-regulated more than 2 fold; Orange: gene expression up-regulated 1.5-2 fold; Deep blue: gene expression down-regulated more than 2 fold; light blue: gene expression down-regulated between 1.5-2 fold White non-shaded means gene expression < 1.5 fold (unchanged).

		Fold change			
		JR1		RH30	
Gene symbol	**Gene description**	**Micro-array**	**qRT-PCR**	**Micro-array**	**qRT-PCR**
PAX3	**Paired Box 3**	**-4.64**	-1.63	**-2.61**	**-1.37**
ADAM23	ADAM metallopeptidase domain 23	-4.34	-2.64	-4.87	-1.67
AEN	Apoptosis enhancing nuclease	10.72	3.72	7.64	3.82
AKT3	V-AKT murine homolog 3 oncogene	2.43	1.74	3.39	2.37
BCL2	B-Cell lymphoma 2	-4.37	-3.43	-3.45	-2.37
CAPRIN1	Cell cycle associated protein 1	-2.50	-1.57	-9.84	-2.27
CASP3	Caspase3, apoptosis related cysteine peptidase	2.45	1.56	2.92	1.68
CCND3	Cyclin D3	-3.68	-2.02	-2.91	-1.71
CDCA3	Cell cycle associated 3	-5.84	-1.54	-3.66	-1.50
COL3A1	Collagen type III, alpha 1	-15.66	-4.64	-9.65	-2.64
C-MYC	C-MYCBP C myc binding protein	-5.85	-2.62	-3.50	-1.12
CXCR4	Chemokine (C-X-C motif) receptor 4	4.73	2.15	2.88	1.55
E2F7	E2F7 Transcription factor	7.36	2.82	2.19	1.57
E2F8	E2F transcription factor 8	-5.40	-1.97	-3.74	-1.98
ETS1	V-ETS erythroblastosis virus 1	11.11	2.98	4.73	1.89
FOXO1	Forkhead box O1	3.51	1.58	2.04	1.52
ITGβ5	Integrin beta 5	-6.06	-1.76	-2.14	-1.52
JAM2	Junctional adhesion molecule 2	4.04	2.34	2.93	1.54
JUN	Jun oncogene	6.66	1.88	1.89	1.53
MCM3	Minichromosome maintenance 3	-5.84	-2.44	-3.99	-1.51
MYOD1	Myogenic differentiation	-2.82	1.02	-4.65	-1.34
MYOG4	Myogenin (myogenic factor 4)	-11.18	-2.20	-2.54	-1.14
NDRG1	N-myc downstream regulated 1	6.82	2.33	6.07	2.03
P21	Cyclin-dependent kinase inhibitor 1	4.08	1.56	3.25	1.45
P53	Tumour protein p53	3.51	1.55	3.77	2.05
PCNA	Proliferating cell nuclear antigen	-3.75	-1.30	-4.26	-2.54
TRIB3C	Tribbles homolog 3	10.33	2.02	11.97	2.52

The pattern of gene expressions alteration in the JR1 and RH30 rhandomyosarcoma cell lines after *PAX3* inhibition was compared with previous microarray data of *PAX3*-siRNA inhibition in the SH-EP1 and SH-SY5Y neuroblastoma cell lines (Fang *et al*., 2013). The microarray analysis and the qRT-PCR data analysis of 14 selected downstream target genes of interest together with *PAX3* in the rhabdomyosarcoma cell lines were compared with the microarray analysis and the qRT-PCR analysis data of neuroblastoma (**Table 3.7**). Out of the 14 genes compared, the expression of 5 genes showed similar pattern of down-regulation of expression in both microarray and qRT-PCR data analysis of both rhabdomyosarcoma cell lines and neuroblastoma cell lines (*PAX3, CALM3, CDCA3, SKP2* and *TFDP1*) (**Table 3.7**). Although the qRT-PCR analysis of another 2 genes failed (*BRCA1* and *POLA2*), after being repeated three times, their down-regulation of expression in the microarray data analysis of both rhabdomyosarcoma cell lines was comparable to the down-regulation of expression in the microarray data of both neuroblastoma cell lines (*BRCA1* and *POLA2*) (**Table 3.7**).

On the contrary, the down-regulation of expression of another 2 genes in both microarray analysis and the qRT-PCR data analysis of rhabdomyosarcoma cell lines, was in disparity with their up-regulation of expression in both microarray analysis and qRT-PCR data analysis of neuroblastoma cell lines (*NID1* and *SMAD2*) (**Table 3.7**). Likewise, with the exception of the qRT-PCR analysis data of down-regulation of the *MCM3* expression in SH-EP1 neroblastoma cell line, the down-regulation of *MCM3* expression in both microarray analysis and qRT-PCR data analysis of both rhabdomyosarcoma cell lines was different from both microarray and the qRT-PCR data analysis of the neuroblastoma cell lines (**Table 3.7**).

The expression of 2 genes in both rhabdomyosarcoma and neuroblastoma cell lines was comparably up-regulated in the microarray and qRT-PCR data analysis (*FOXO1* and *JUN*) (**Table 3.7**). The microarray and qRT-PCR data analysis of down-regulation of *BCL2* expression was only comparable to the SH-EP1 neuroblastoma cell line, in contrast to the up-regulation of *BCL2* in the SH-SY5Y neuroblastoma cell line (**Table 3.7**). Likewise, the up-regulation of *CASP3* in both microarray and qRT-PCR data analysis of rhabdomyosarcoma cell lines was only comparable to the SH-SY5Y

neuroblastoma cell line, in contrast to *CAPS3* down-regulation in the SH-EP1 neuroblastoma cell line(**Table 3.7**). The microarray and the qRT-PCR data analysis of down-regulation of *COL3A1* expression in both rhabdomyosarcoma cell lines were dissimilar to the up-regulation of *COL3A1* expression in both microarray and qRT-PCR data analysis of the neuroblastoma cell lines (**Table 3.7**).

Table 3.7 Comparison of *PAX3*-siRNA knockdown in rhabdomyosarcoma and neuroblastoma

The pattern of gene expression in rhabdomyosarcoma cell lines after *PAX3*-siRNA knockdown was comparable to both microarray and qRT-PCR data in a related PAX3-siRNA inhibition of neuroblastoma cells shown below. Gene expression up-regulated ≥ 1.50 fold is shown in red; gene expression down-regulated > 1.50 fold is shown in blue; ND means not detected.

	Rhabdomyosarcoma				**Neuroblastoma**			
	JR1		**RH30**		**SH-EP1**		**SH-SY5Y**	
Gene Symbol	**Micro-array**	**RT-qPCR**	**Micro-array**	**RT-qPCR**	**Micro-array**	**RT-qPCR**	**Micro array**	**RT-qPCR**
PAX3	**-4.64**	**-1.63**	**-2.61**	**-1.37**	**-2.89**	**-1.47**	**-2.56**	**-1.48**
BCL2	-4.37	-3.43	-3.45	-2.37	-1.14	-1.60	2.37	3.03
BRCA1	-2.57	ND	-2.86	ND	-9.88	-6.00	-1.34	-1.27
CALM3	-2.62	-2.32	-2.20	-1.53	-7.68	-1.71	-1.99	-1.03
CASP3	2.45	1.56	2.92	1.68	-2.02	-1.20	1.02	3.12
CDCA3	-5.84	-1.54	-3.66	-1.50	-31.74	-12.57	-1.76	-1.11
COL3A1	-15.66	-4.64	-9.65	-2.64	133.39	64.44	1.36	6.12
FOXO1	3.51	1.58	2.04	1.52	1.90	1.67	1.85	2.52
JUN	6.66	1.88	1.89	1.53	6.32	4.12	2.19	2.11
MCM3	-5.84	-2.44	-3.99	-1.51	4.59	-1.09	2.33	8.99
NID1	-2.39	-1.55	-1.74	-1.53	1.90	1.79	2.03	2.74
POLA2	-2.68	ND	-2.11	ND	-8.49	-4.15	-2.01	1.08
SKP2	-3.99	-1.57	-1.93	-1.56	-20.38	-6.33	-1.83	-1.61
SMAD2	-2.55	-1.67	-2.06	-1.76	2.48	3.01	1.81	2.07
TFDP1	-10.58	-2.55	-4.36	-1.58	-4.21	-2.91	-1.70	-1.33

1.50 fold change (light blue) gene expression was used as the threshold for significant down-regulation.

1.50 fold change (orange shade) gene expression was used as the threshold for significant up-regulation.

3.5. Effect of Inhibition of *PAX3* mRNA on Downstream Target Protein Expression

Western blotting analysis of non-transfected JR1 (**Fig. 3.12**) and RH30 cells (**Fig. 3.13**) demonstrated high levels of PAX3 protein as a base line.

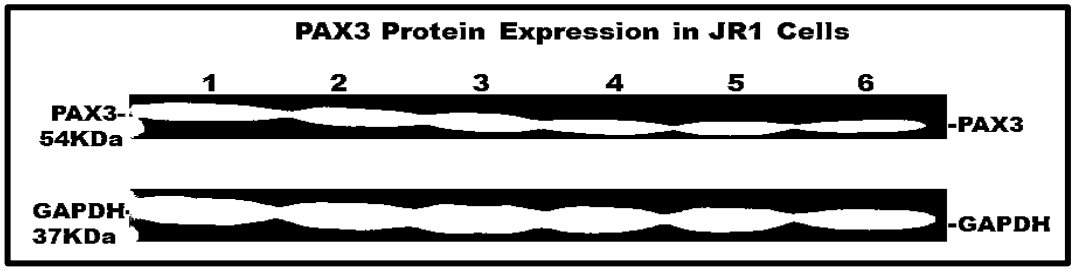

Figure 3.12 Pre-transfection determination of PAX3 protein in non-transfected JR1 cells. Lanes 1-6: Replicate JR1 PAX3 and GAPDH protein expression.

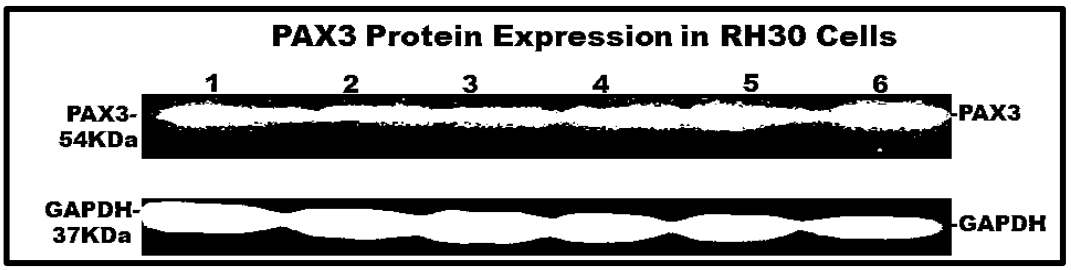

Figure 3.13 Pre-transfection determination of PAX3 protein in non-transfected RH30 cells. Lanes 1-6: Replicate RH30 PAX3 and GAPDH protein expression.

To assess the effect of *PAX3* knockdown on protein levels in JR1 and RH30 cells, immunoblotting was undertaken and *PAX3*-siRNA and NC-siRNA transfected cells were compared. Western blotting analysis demonstrated reduced PAX3 protein levels after *PAX3* knockdown. The NC-siRNA had no effect on PAX3 mRNA as shown in (lanes 3-5 of **Figs. 3.5 and 3.7**) and the cells showed high PAX3 protein expression (lanes 1-3 of **Figs. 3.14B and 3.16B**), whereas knockdown of *PAX3* mRNA in *PAX3*-siRNA transfected cells (see lanes 6-8 of **Figs. 3.5 and 3.7**), showed 2% of PAX3 protein (lanes 5-7 of **Figs. 3.14B and 3.16B**). Using human GAPDH as an internal normalization control, JR1 showed high levels of GAPDH in both NC-siRNA and *PAX3*-siRNA transfected cells (lanes 1-3 and 5-7 of **Fig. 3.14A**). This indicated that neither *PAX3*-siRNA nor NC-siRNA had any inhibitory effect on GAPDH protein expression. NC-siRNA had no inhibitory effects on *PAX3* expression and subsequently,

showed consistently high levels of PAX3. Western blotting validated genes of interest that were significantly altered in the microarray data. *PAX3*-siRNA knockdown gene of PAX3 expression resulted in down-regulation or up-regulation of its downstream targets, including a remarkable reduction of C-MYC (lanes 5, 6 and 7 of **Fig. 3.14C**) and completely decreased ITGβ5 (lanes 5, 6 and 7 of **Fig. 3.14D**). There was a reduction in MYOD1 (lanes 5, 6 and 7 of **Fig. 3.14E**), decreased BCL2 (lanes 5, 6 and 7 of **Fig. 3.14F**) and increase in P21 **(**lanes 5, 6 and 7 of **Fig. 3.14G**). P53 and phosphorylated P53 (lanes 5, 6 and 7 of **Fig. 3.14H**) and CASP3 (lanes 5, 6 and 7 of **Fig. 3.14I**) were all increased.

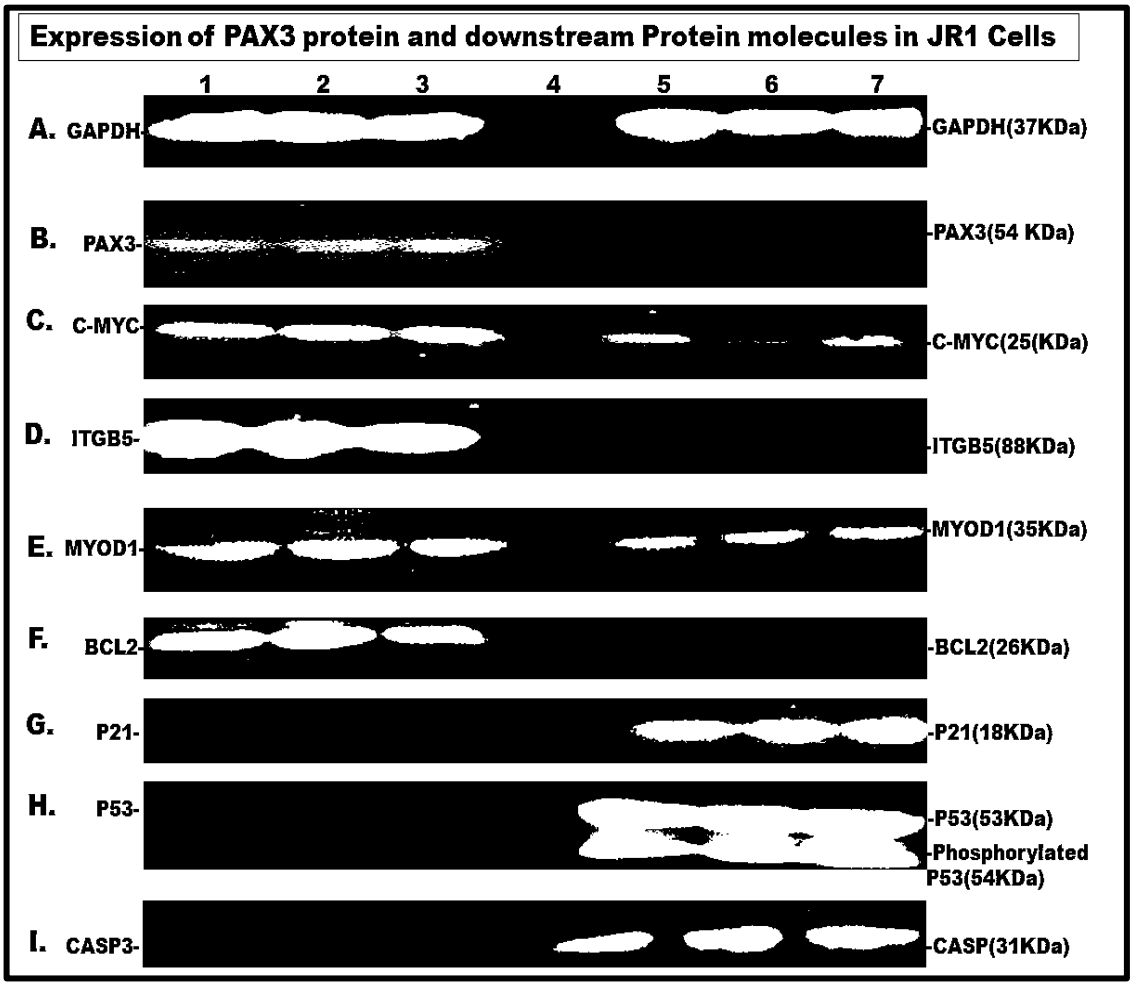

Figure 3.14 Western blotting of JR1 cell proteins following 96 hr transfection with *PAX3*-siRNA. Lanes 1-3: Triplicate NC-siRNA transfected JR1 cells; Lane 4: Blank; Lanes 5-7: Triplicate *PAX3*-siRNA transfected JR1 cells.

The effect of knockdown of *PAX3* mRNA on PAX3 protein and downstream target protein expression in JR1 cell line was statistically significant ($p < 0.01$). Following 96 hr transfection, the knockdown of *PAX3* resulted in PAX3 protein being reduced by a mean of 98% (n = 9) (**Fig. 3.15**). Downstream molecules down-regulated by PAX3 showing low levels of protein remaining were, C-MYC (8%); ITGβ5 (3%); MYOD1 (20%) and BCL2 (5%) (of expression relative to NC-siRNA). Likewise, up-regulated molecules downstream of PAX3 showing high levels of protein expression were, P21 (20 fold) P53 (15 fold) and CASP3 (30 fold).

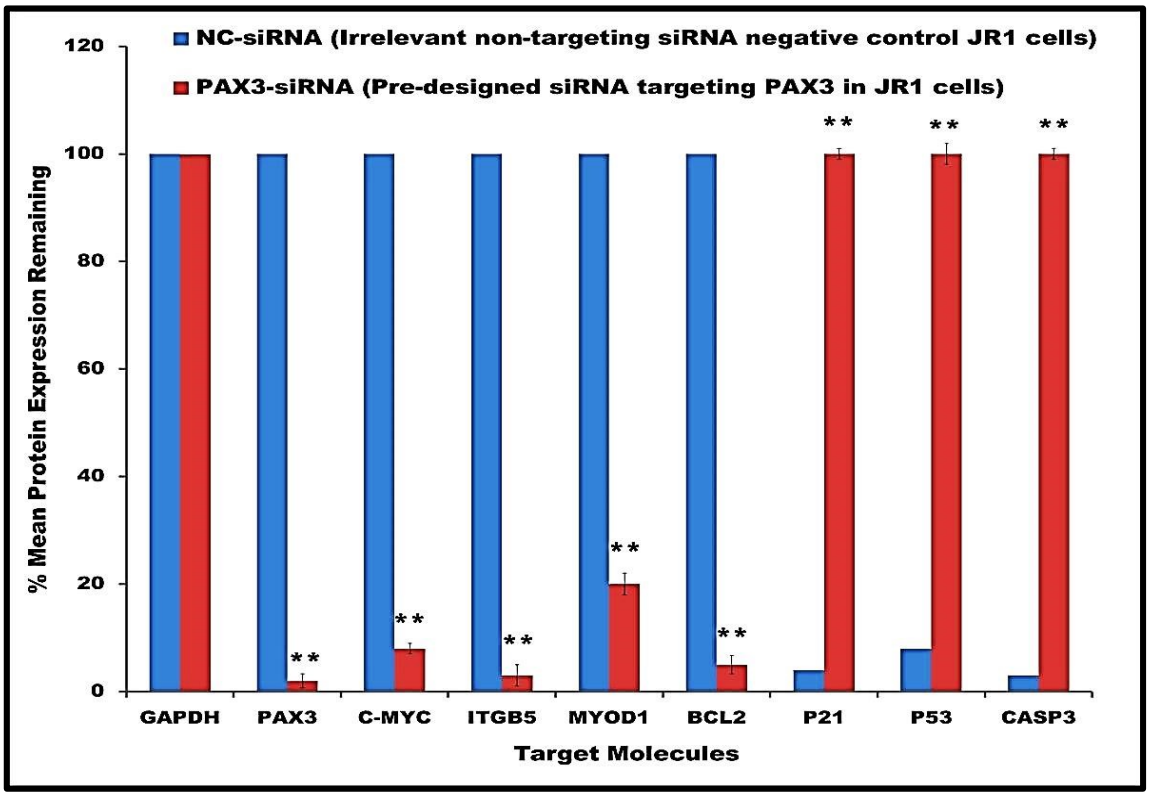

Figure 3.15 Mean percentages of protein expression after 96 hr siRNA transfection. The mean protein expression in NC-siRNA transfected JR1 cells (blue columns) was compared with mean protein expression in *PAX3*-siRNA transfected JR1 cells (red columns). Means of triplicate values in each of three separate experiments, (n = 9). Blue versus red column for each protein (Student's t-test), (**, $p < 0.01$).

Although a similar protein expression pattern was observed in RH30 cells, the protein expression levels in the RH30 cell line after knockdown of PAX3 were higher compared to the JR1 cell line in which some downstream target molecules were almost completely absent. NC-siRNA showed no effect on protein levels whilst *PAX3*-siRNA did. High

levels of GAPDH were observed in both NC-siRNA and *PAX3*-siRNA transfected cells (**Fig. 3.16**).

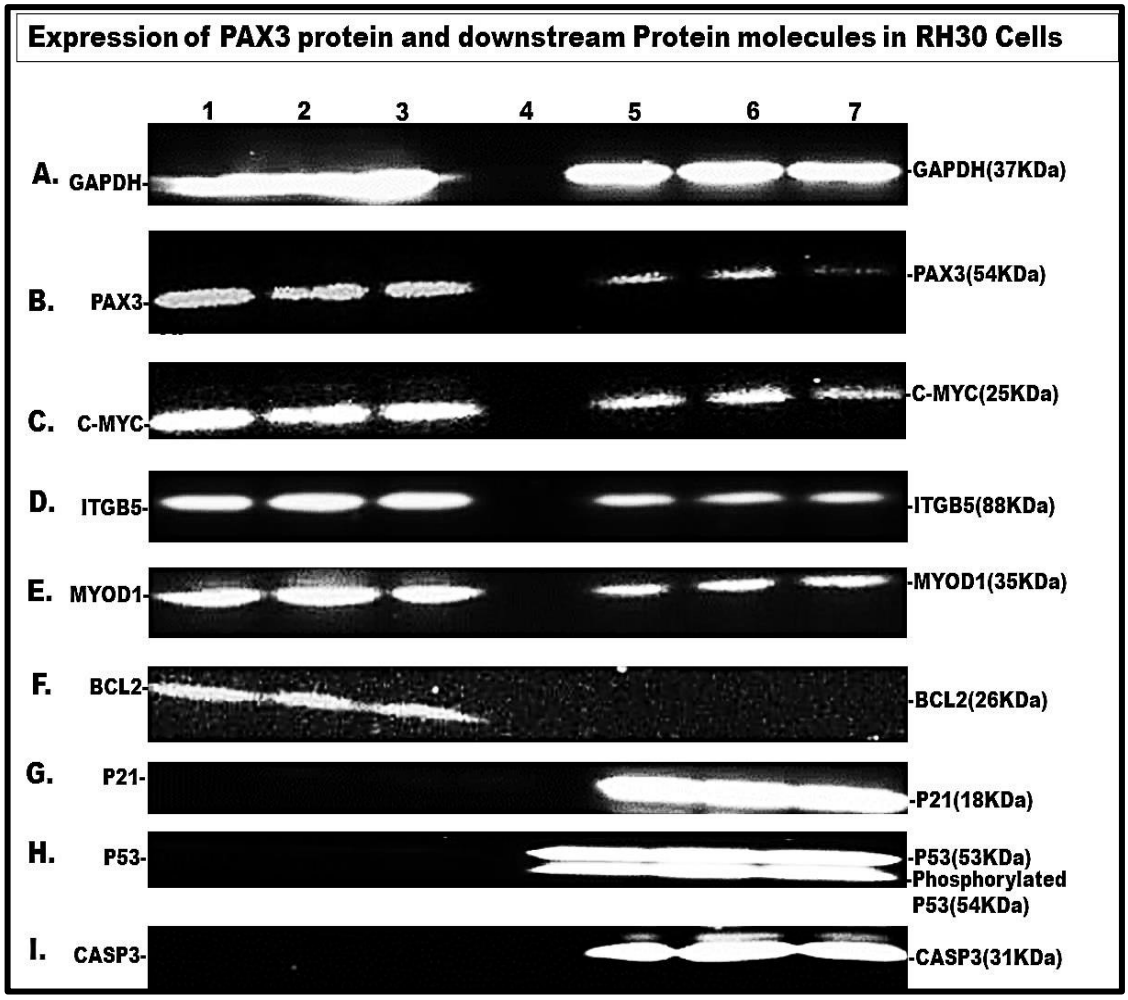

Figure 3.16 Western blotting of RH30 cell proteins following 96 hr trnafcetion with *PAX3*-siRNA results in both inhibition and induction of downstream targets. Lanes 1-3: Triplicate NC-siRNA transfected RH30 cells; Lane 4: Blank; Lanes 5-7: Triplicate *PAX3*-siRNA transfected RH30 cells.

RH30 cells transfected with NC-siRNA showed high levels of PAX3 relative to consistent reduction of PAX3 in *PAX3*-siRNA treated cells. Knockdown of PAX3 expression in RH30 cells caused up or down-regulation of some downstream targets including reduction of C-MYC (lanes 5, 6 and 7 of **Fig. 3.16C**), consistent reduction of ITGβ5 (lanes 5, 6 and 7 of **Fig. 3.16D**) compared to markedly decreased ITGβ5 expression in the JR1 cell line. There were a consistent reduction of MYOD1 (lanes 5, 6 and 7 of **Fig. 3.16E**) and decrease in BCL2 (lanes 5, 6 and 7 of **Fig. 3.16F**). Increase in

P21 expression (lanes 5, 6 and 7 of **Fig. 3.16G**) were higher compared to the JR1 cell line (lanes 5, 6 and 7 of **Fig. 3.14G**). The increased expression of P53 and its phosphorylated form in (lanes 5, 6 and 7 of **Fig. 3.16H**) is similar to that in JR1 cells (lanes 5, 6 and 7 of **Fig. 3.14H**). The increase in CASP3 expression (**Fig. 3.14I**) was higher than in JR1 cells (lanes 5, 6 and 7 of **Fig. 3.16I**).

After 96 hr transfection, the effect of knockdown of *PAX3* mRNA on PAX3 protein and downstream target protein expression in the RH30 cell line was statistically significant ($p < 0.01$). PAX3 protein levels were reduced by 92% (**Fig. 3.17**).

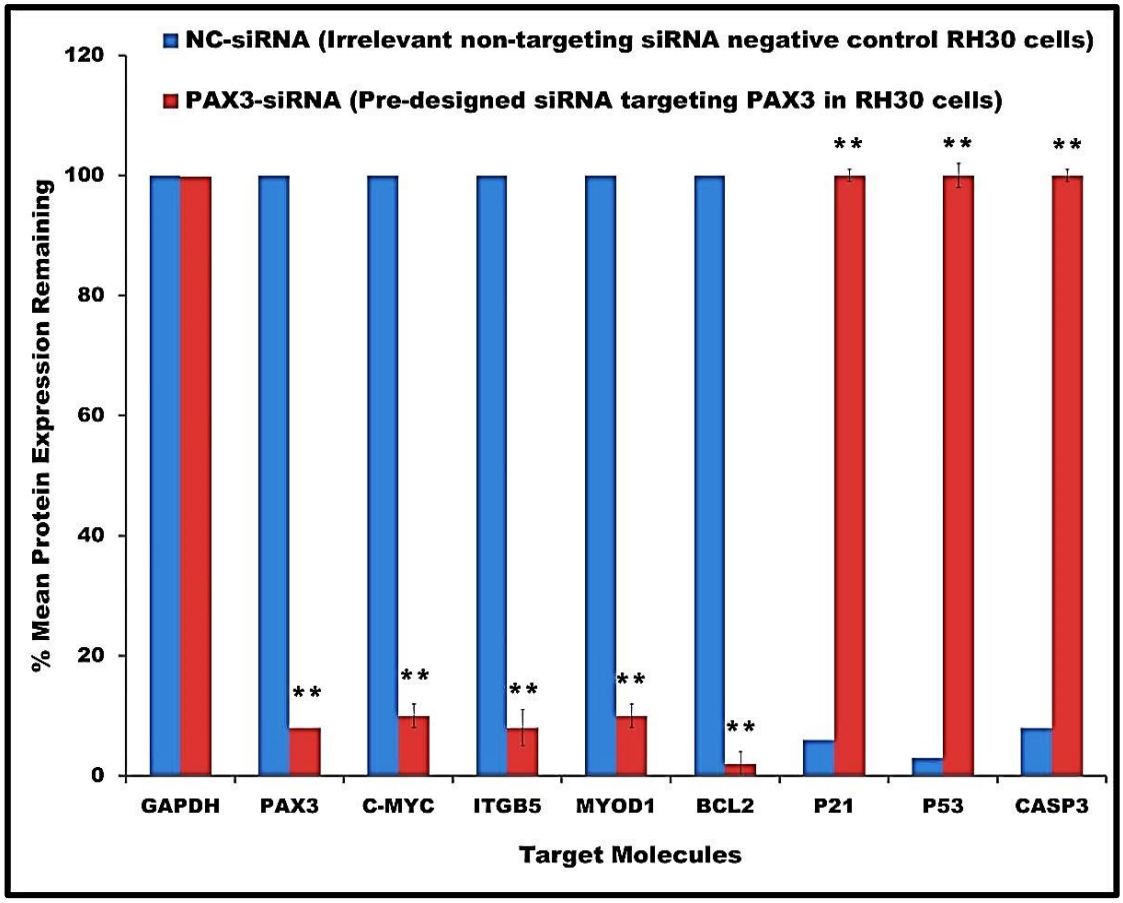

Figure 3.17 Mean percentages of protein expression after 96 hr siRNA transfection. The mean protein expression in NC-siRNA transfected RH30 cells (Blue columns) was compared with the mean protein expression in *PAX3*-siRNA transfected RH30 cells (Red columns). The histograms are means of three measurements in each of three separate experiments (n = 9). Blue versus red column for each protein (Student's t-test), (**, $p < 0.01$).

Following inhibition of *PAX3* gene expression, the levels of protein expression were PAX3 (8%); C-MYC (10%); ITGβ5 (8%); MYOD1 (10%) and BCL2 (2%). The approximate level of protein expression in downstream molecules up-regulated by PAX3 were, P21 (15 fold); P53 (30 fold) and CASP3 (10 fold).

3.6. Effect of *PAX3* Inhibition on Proliferation of Rhabdomyosarcoma Cell Lines

The purpose of this experiment was to study the growth potential for the determination of optimal cell seeding density over 96 hr transfection period. Standard growth curves for JR1 and RH30 (non transfected), cell lines where growth was proportional to starting density, demonstrated a linear growth (**Figs. 3.18 and 3.19**). A cell seeding density of 5.0 X10^4 cells/ well, that produced a steady optimal growth with mean ODs of 0.35 in the JR1 cells and 0.45 in the the RH30 cells, relating to a slow cell growth over a 96 hour time-course without over-growth and showing minimal cytotoxicity was selected for the cell proliferation analysis of JR1 and RH30 cells.

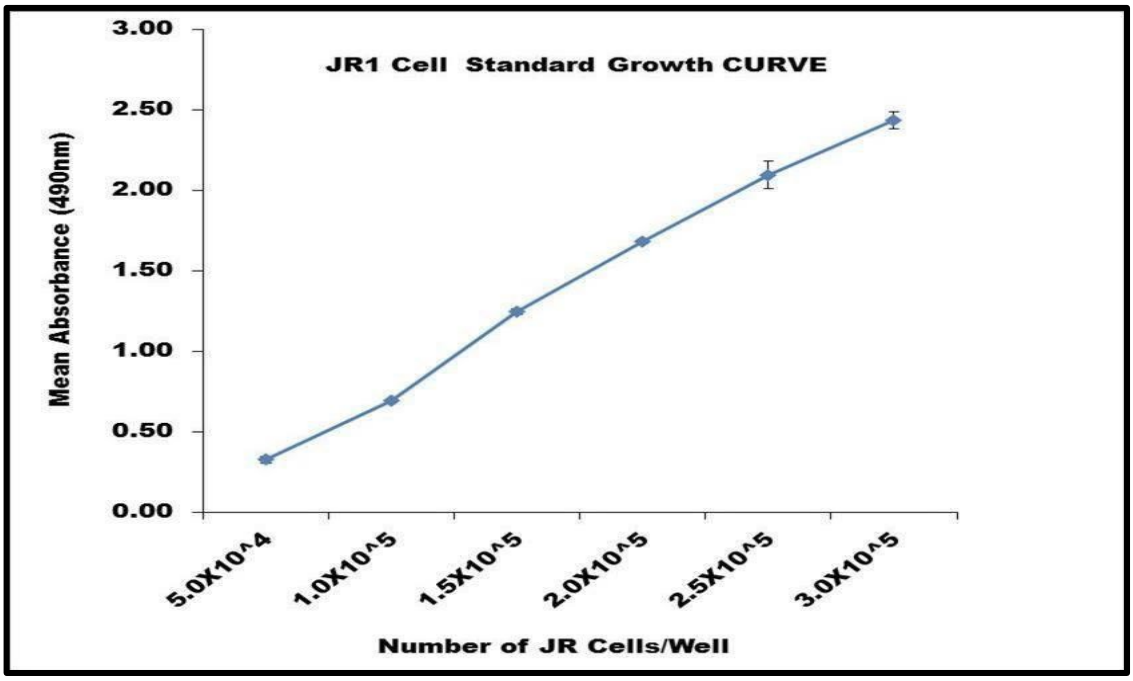

Figure 3.18 Pre-transfection standard curve of JR1 cells for selection of optimal cell seeding density in subsequent cell proliferation analyses. The OD readings of formazan produced are directly proportional to the number of proliferating cells. Each point represents the mean ± SD of three replicate measurements in each of three separate experiments (n = 9). Ninety-six hours was selected for the duration of the subsequent cell proliferation analysis and 5.0 X 10^4 cells/well chosen as the starting density.

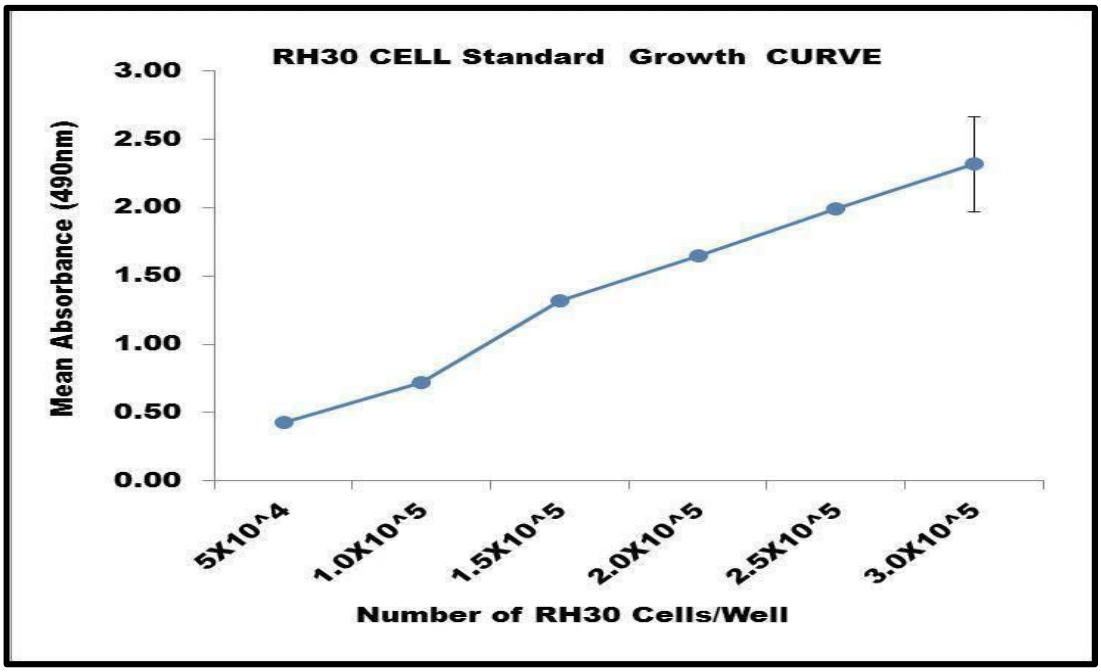

Figure 3.19 Pre-transfection standard growth curve of RH30 cells for selection of optimal cell seeding density in subsequent cell proliferation analyses. The OD readings of formazan produced are directly proportional to the number of proliferating cells. Each point represents the mean ± SD of three replicate measurements in each of three separate experiments (n = 9). Ninety-six hours was selected for the duration of the subsequent cell proliferation analysis and 5.0 X 10^4 cells/well chosen as the starting density.

To determine the effects of knockdown of *PAX3* gene expression over 12-96 hrs on proliferation of rhabdomyosarcoma cell lines, the mean OD relating to cell proliferation of NC-siRNA control cells were compared with that of *PAX3*-siRNA treated cells, using the Cell Titer non-radioactive MTS colorimetric time-course cell proliferation assay. In the indirect MTS cell proliferation analysis, mean large amounts of formazan product (OD) relating to a higher number of proliferating viable cells was observed in the NC-siRNA transfected cells compared to a smaller amount of formed formazan product in *PAX3*-siRNA transfected cells, indicating a lower number of proliferating viable cells. Following 96hr transfection, a lower mean OD of 0.25 demonstrated in *PAX3*-siRNA treated JR cells cells, signifies inhibition of cell proliferation compared to a corresponding higher mean OD of 1.83 in the NC-siRNA treated JR1 cells cells indicated high cell proliferation. These results were confirmed by direct Coulter counter analysis of the mean numbers of proliferating JR1 cells (**Fig. 3.20**).

A significant difference in cell proliferation was observed between NC-siRNA transfected JR1 cells and *PAX3*-siRNA transfected JR1 cells ($p < 0.01$). Thus, a significant inhibition of cell growth was observed in *PAX3*-siRNA transfected JR1 cells because of cell apoptosis.

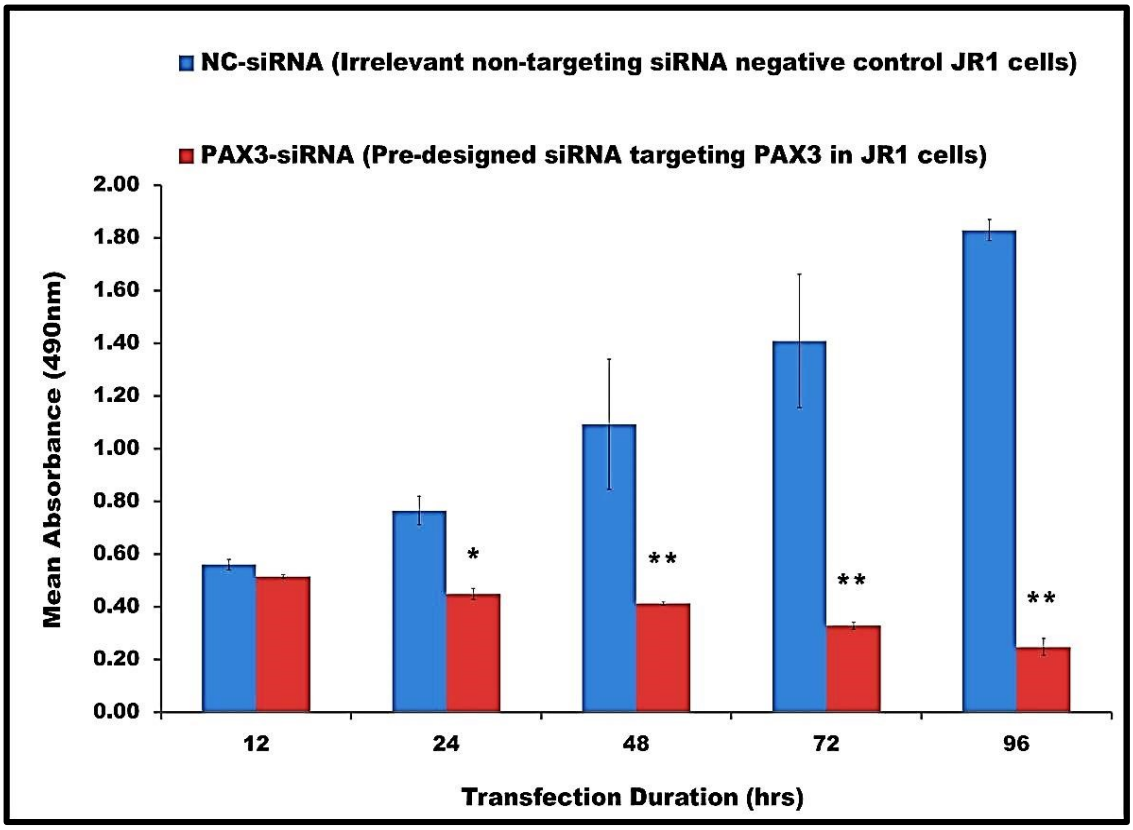

Figure 3.20 CellTiter 96® aqueous cell proliferation analyses for determination of inhibition of JR1 cell proliferation following 96 hr *PAX3*-siRNA transfection. The mean OD reading of NC-siRNA transfected JR1 cells (blue columns) was compared with the OD reading of *PAX3*-siRNA transfected JR1 cells (red columns) at each time point. A cell seeding density of 5.0 X 10^4 cells/well was initially seeded at the start of the experiment.
The histograms are means of three replicate measurements in each three separate experiments, (n = 9). (Student's t-test), (*, $p < 0.05$; **, $p < 0.01$).

Cell Coulter counter of cell growth measurements of 5.0 X 10^4 cells/ml initial cell seeding density confirmed a significant cell growth inhibition in *PAX3*-siRNA transfected JR1 cells compared to NC-siRNA transfected JR1 cells. Higher mean cell count over the 96hr transfection (253 X 10^4 cells) was observed in NC-siRNA transfected JR1 cells expressing the *PAX3* gene than in the corresponding significantly reduced number of cells at 96hr transfection (20 X 10^4 cells) in *PAX3*-siRNA transfected

JR1 cells with decreased *PAX3* gene expression ($p < 0.01$) caused cell apoptosis (**Fig. 3.21**).

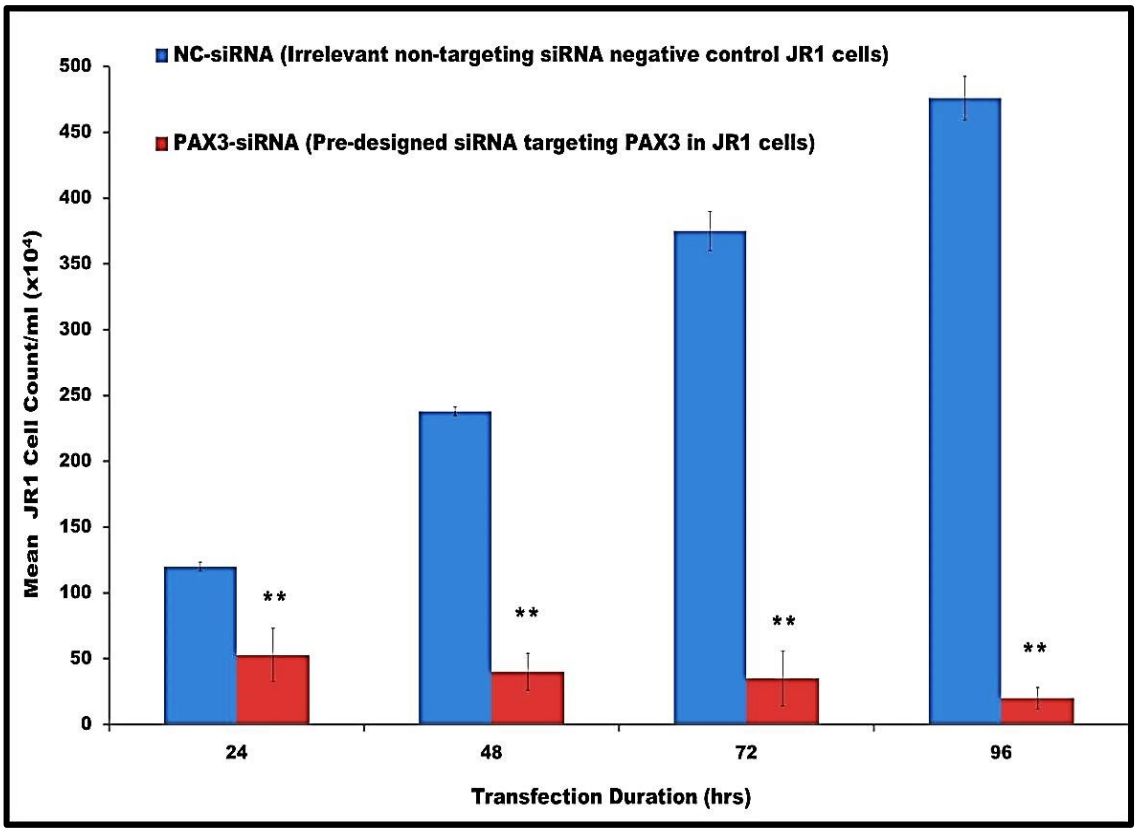

Figure 3.21 Coulter counter direct cell counts for determination of inhibition of JR1 cell proliferation following siRNA transfection. The mean number of JR1 cell count in NC-siRNA transfected cells (blue columns) was compared with the mean number of JR1 cell count in *PAX3*-siRNA transfected cells (red columns) at each transfection time point. At the start of the experiment, 5.0 X 10^4 cells/well was originally seeded. The histograms are means of three replicate cell counts in each of three separate repeated experiments, (n = 9). (Student's t-test), (**, $p < 0.01$).

Similarly, following a 96 hr transfection, a significant inhibition of cell growth of 5.0 X 10^4 cells/ml initial cell seeding density ($p < 0.01$) was observed in *PAX3*-siRNA transfected RH30 cells (with knockdown of *PAX3* gene expression) recording a mean OD of 0.34 compared to a correponding higher OD of 2.14 in the NC-siRNA transfected RH30 cell growth with high levels of *PAX3* gene expression (**Fig. 3.22**).

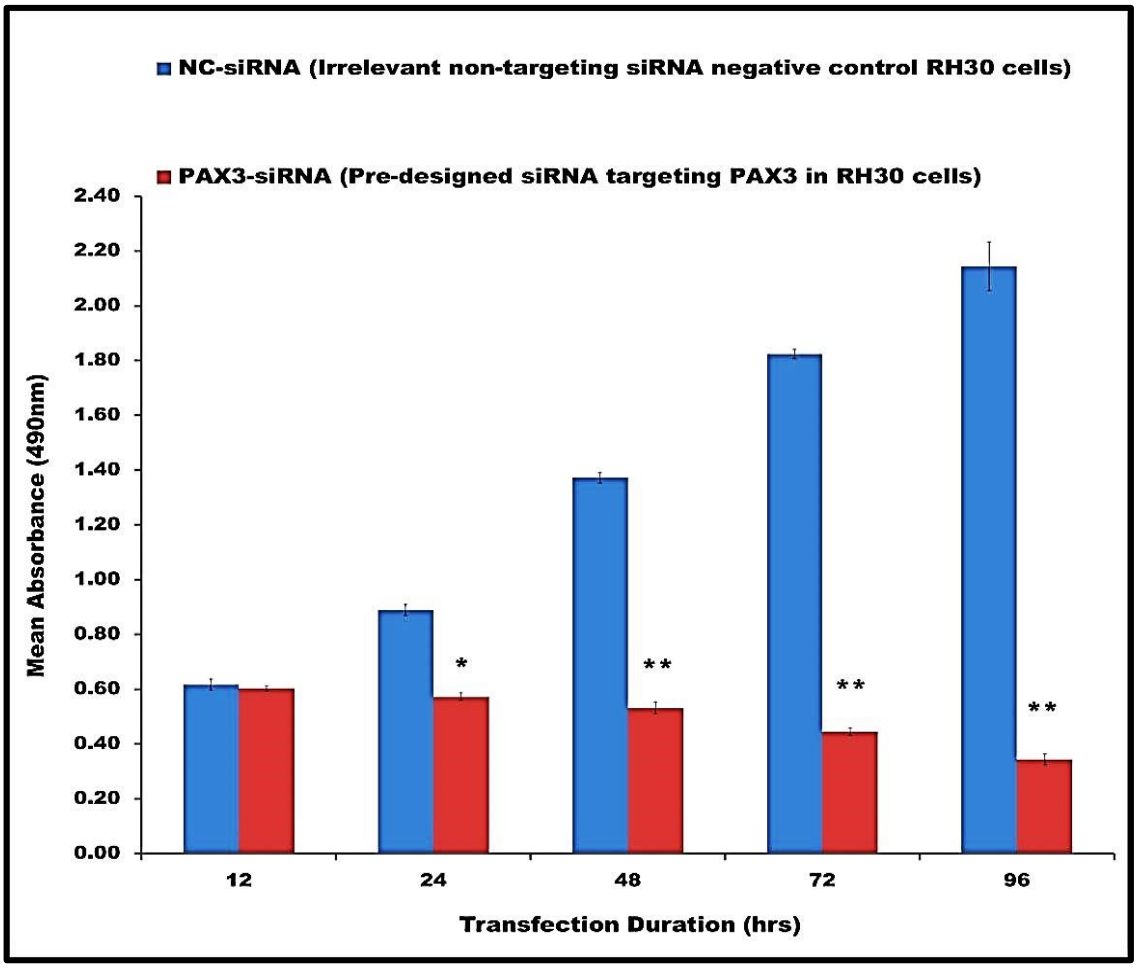

Figure 3.22 CellTiter 96® aqueous indirect cell proliferation analyses for determination of inhibition of RH30 cell proliferation following siRNA transfection. The mean OD readings of NC-siRNA transfected RH30 cells (blue columns) was compared with the mean OD readings of *PAX3*-siRNA transfected RH30 cells (in red columns) at each transfection time point. Cell seeding density was originally 5.0 X 10^4 cells/well at the start of the experiment.
The histograms are means of three replicate measurements in each of three separate experiments, (n = 9). (Student's t-test), (*, $p < 0.01$; **, $p < 0.01$).

In the direct Coulter counter proliferation analysis used to confirm the results of the MTS, the mean cell counts of 15 X 10^4 cells at 96 hr transfection in the *PAX3*-siRNA treated RH30 cells, demonstrated a significant cell growth inhibition of 5.0 X 10^4 cells/ml of initial cell seeding density compared to a higher mean cell count in the NC-siRNA treated RH30 cells of 220 X 10^4 cells observed at 96hr respectively ($p < 0.01$) becaused of cell apoptosis (**Fig. 3.23**).

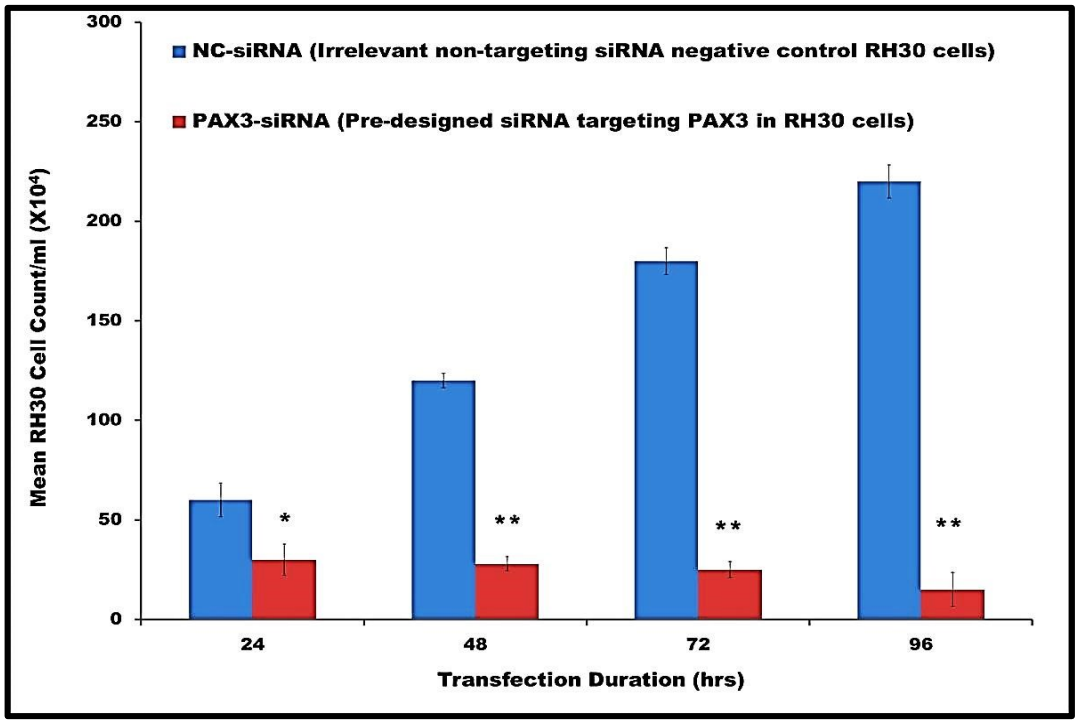

Figure 3.23 Coulter counter direct cell count for determination of inhibition of RH30 cell proliferation following 96 hr siRNA transfection. The mean number of RH30 cell count in NC-siRNA transfected cells (blue columns) was compared with the mean number of RH30 cell count in *PAX3*-siRNA transfected cells (red columns) at each time point. Original cell seeding density was 5.0 X 10^4 cells/well. The histograms are means of three replicate cell counts in each of three separate experiments, (n = 9). (Student's t-test), (*, $p < 0.05$; **, $p < 0.01$).

3.7. Effect of Knockdown of *PAX3* on the Cell Cycle of JR1 and RH30 Cells

PAX3 has a crucial role in the modulation of activity of downstream cell cycle genes. Since inhibition of *PAX3* gene expression in JR1 and RH30 cells led to significant inhibition of cell proliferation, it was important therefore, to investigate the impact on the phases of the cell cycle at which cell growth was arrested. Following 96 hr siRNA knockdown of *PAX3* gene expression, flow cytometry was used to analyse the DNA content of individual transfected cells. The mean number of PI stained cells among NC-siRNA transfected cells were compared with the average number of PI stained cells among *PAX3*-siRNA transfected cells. The amount of PI staining per cell determined the distribution of cells in each phase of the cell cycle (**Table 3.8**). The outcome of this analysis demonstrated a high proportion of G0/G1 phase cells among the *PAX3*-siRNA transfected cells compared with the NC-siRNA transfected control cells (62.5% versus 42.7%) arrested at the G0/G1 phase in JR1 cells (**Fig. 3.24**) and 70.3% versus 63.6% in

RH30 cells (**Fig. 3.25**). *PAX3* inhibition in JR1 cells reduced the cells in S phase from 13.1% to 7.4%. *PAX3* inhibition reduced RH30 cells in S from 9.8% to 7.4%. Although there can be a cell cycle check point in G2, the presence of cells in S phase signifies cell cycle progression and hence probably cell proliferation. Therefore, this result implies a lower cell proliferation rate in *PAX3*-siRNA transfected cells compared to a higher cell proliferation rate in the NC-siRNA transfected cells and agrees with the cell proliferation experiments mentioned earlier.

Table 3.8 Cell cycle distribution of JR1 and RH30 cells following 96 h siRNA knockdown of *PAX3* gene expression

Flow cytometry analysis of DNA content by propidium iodide incorporation. Each value is the percentage of cells at that stage.

Cell cycle Phase	JR1 CELLS		RH30 CELLS	
	NC-siRNA	*PAX3*-siRNA	NC-siRNA	*PAX3*-siRNA
G0/G1	42.7% ±3.6	62.5% ±2.2	63.6% ±2.1	70.3% ±2.7
S	13.1% ±2.4	7.4% ±1.1	9.8% ±1.2	7.4% ±1.4
G2/M	44.2% ±1.3	30.1% ±1.0	26.6% ±1.4	22.3% ±2.1

These values are mean of three measurements in two separate experiments, (n = 6); in all categories:- G0/G1, S and G2/M: $p < 0.05$; for NC-siRNA vs *PAX3*-siRNA (by Student's t-test).

The cell cycle results positively correlated with the western blotting results of increased P12 and P53 protein expression and a decreased in BCL2 protein expression.

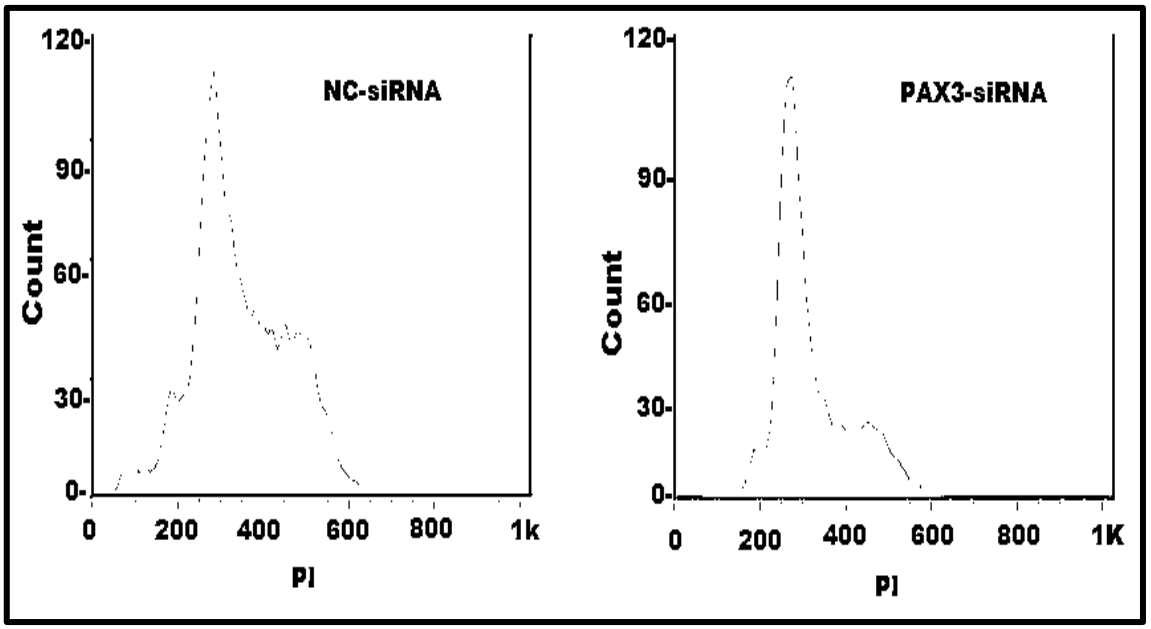

Figure 3.24 Flow cytometric cell cycle analysis of JR1 siRNA transfected PI stained cells after 96 hr transfection. This curve represents JR1 cells in one of two separate experiments.

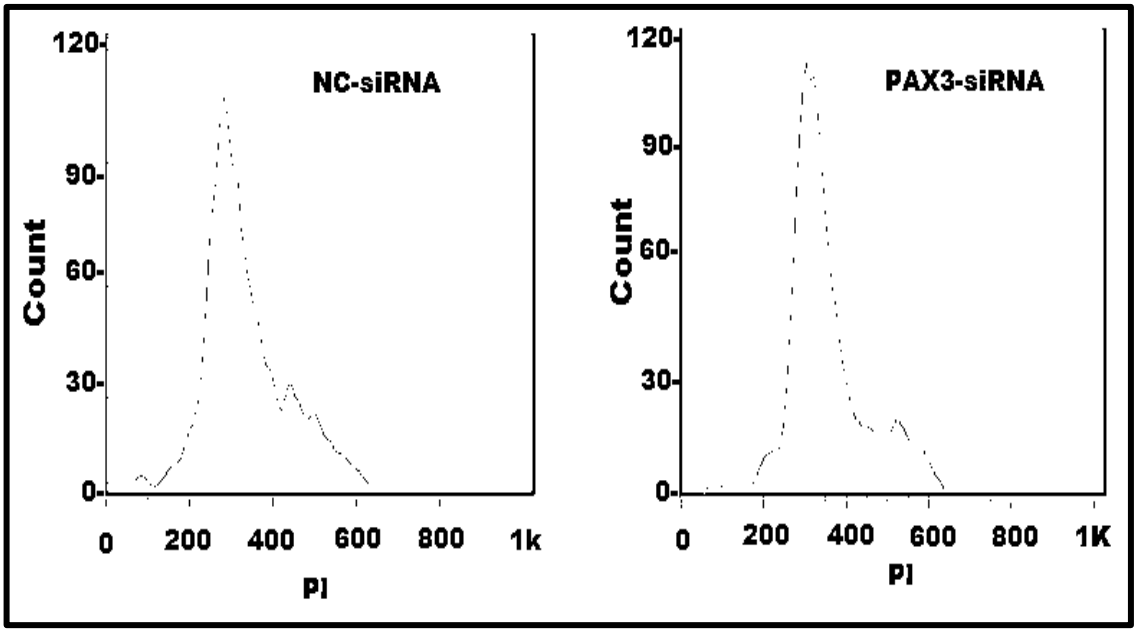

Figure 3.25 Flow cytometric cell cycle analysis of RH30 siRNA transfected PI stained cells after 96 hr transfection. This curve represents RH30 cells in one of two separate experiments.

3.8. Effect of Inhibition of *PAX3* on Cell Migration of Rhabdomyosarcoma Cell Lines

To study the impact that knockdown of *PAX3* gene expression might have on metastasis of rhabdomyosarcoma, a scratch wound healing assay was carried out to measure JR1 and RH30 cell migration *in vitro*. The difference between wound gaps as indicated by the arrows at 0 hr (**Fig. 3.26**) and the wound healing gaps at 24 hr (**Fig. 3.27**) represents the relative distance migrated by cells. To verify the distance migrated by siRNA treated cells after 24 hr migration, the mean relative distance of cell migration indicated by the closure of wound gaps in NC-siRNA treated cells was compared to that of *PAX3*-siRNA treated cells (**Fig. 3.27**).

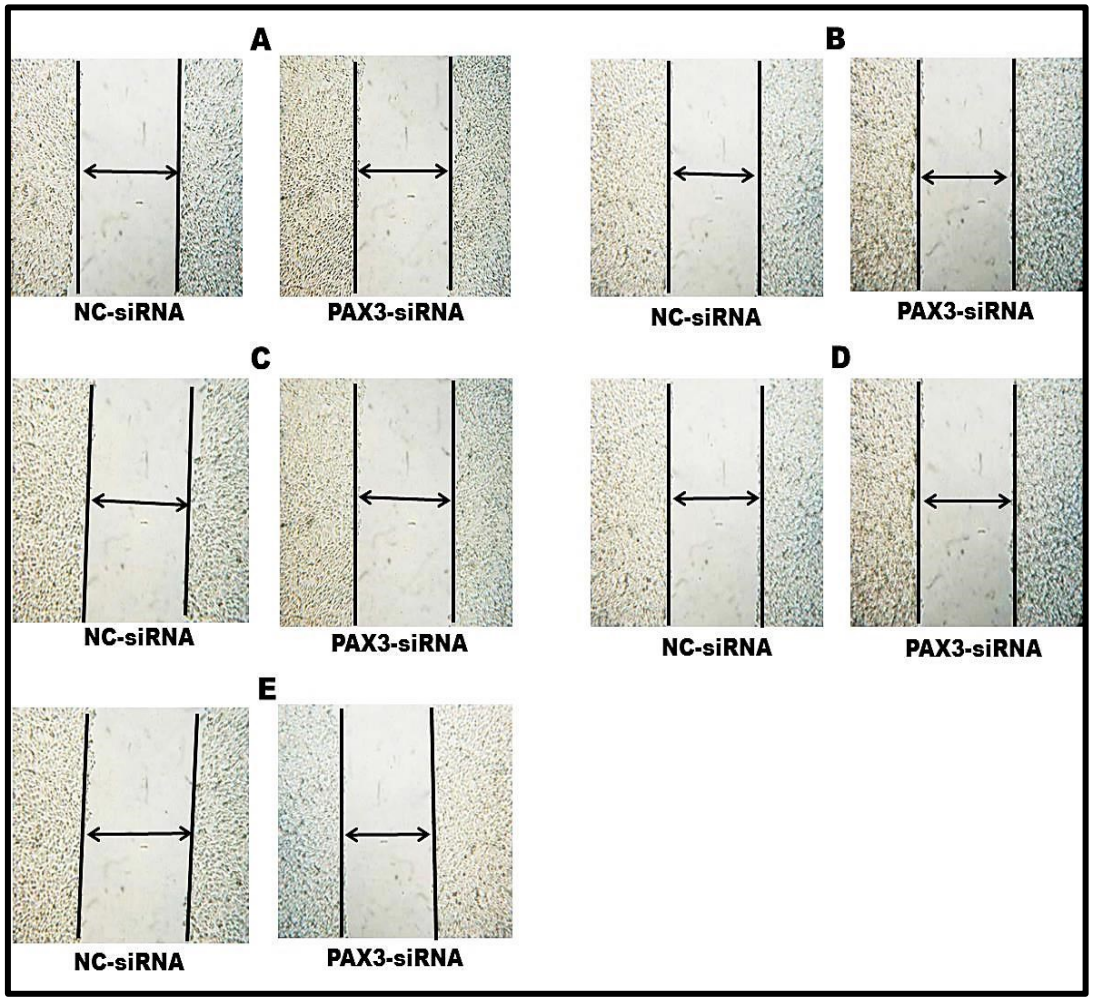

Figure 3.26 Width of JR1 cells scratched wound gap at 0 hr after 12-96 hr transfection duration, X 10 magnification. A (12 hr); B (24 hr); C (48 hr); D (72 hr); E (96 hr). The arrow represents the initial scratched wound width gap of NC-siRNA and *PAX3*-siRNA prior to 24 hr JR1 cell migration (wider arrows).

After 24 hr cell migration, the NC-siRNA treated JR1 cells demonstrated narrow wound gaps because of migration of cells from the wound edges into the wound gaps whereas wider wound gaps were observed in the *PAX3*-siRNA treated JR1 cells indicating inhibition of cell migration from the wound edges. The NC-siRNA transfected JR1 cells migrated over longer distances and gradually closed the width of wound gaps over 24 hr to maintain narrow wound gaps denoted by shorter arrows (**Fig. 3.27**). By contrast, *PAX3*-siRNA transfected JR1 cells, which hardly migrated over the 24 hr from the initial scratched wound gaps, retained larger wound gaps shown by longer arrows (**Fig. 3.27**).

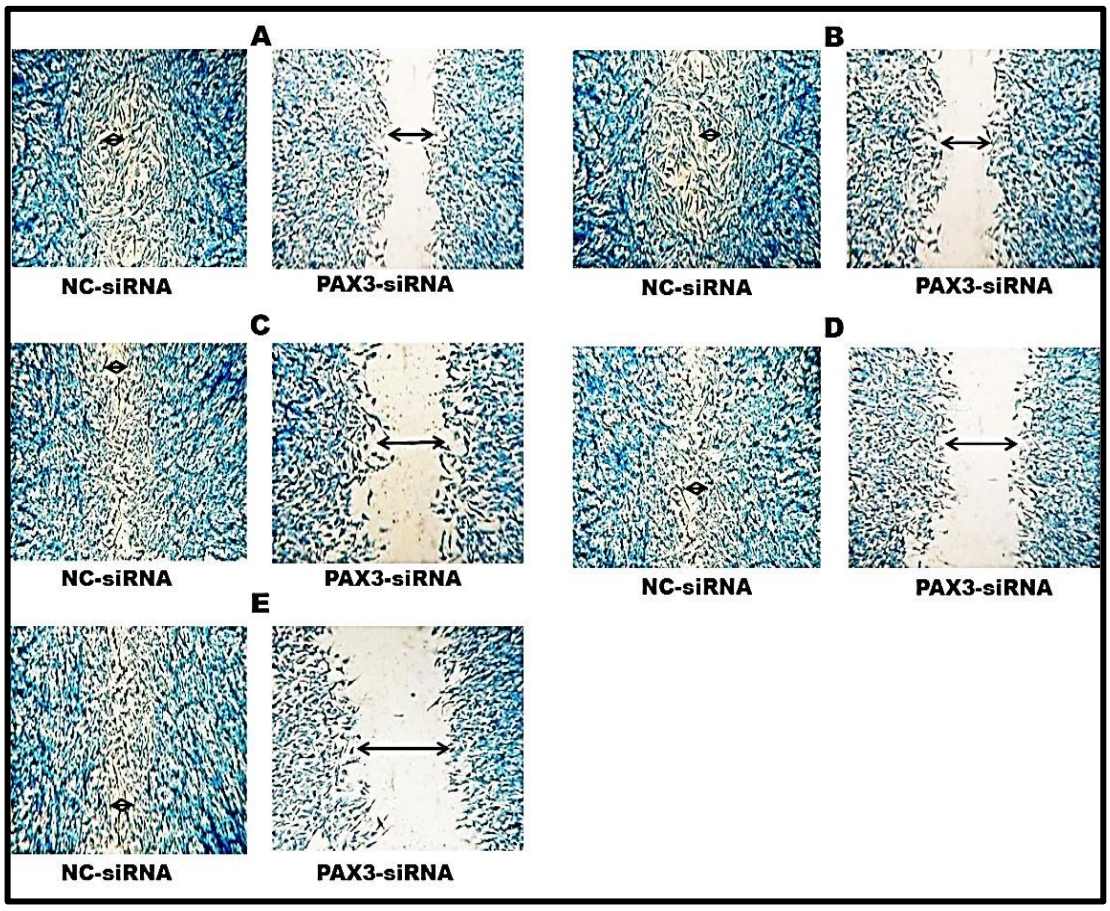

Figure 3.27, X 10 magnification in scratch wound healing assay of transfected JR1 cells after 24 hours. JR1 cells were stained with methylene blue. **A** (**12 hr**); **B** (**24 hr**); **C** (**48 hr**); **D (72 hr**); **E** (**96 hr**). Relative measurement of width of wound gap represents JR1 cell migrated distance. Wound healing by cell migration was related to measured distance in the 24 hr following 12 hr, 24 hr, 48 hr, 72 hr or 96 hr siRNA transfection of JR1 cells. NC-siRNA transfected JR1 cells showed a narrow wound gap from original wide wound gap at 0 hr due to high migration of JR1 cells (short arrows). *PAX3*-siRNA transfected JR1 cells showed a wide wound gap due to inhibition of JR1 cell migration resulting from JR1 cell apoptosis (long arrow).

A low relative mean of cell migration distance (4 units), observed at E, demonstrated in the *PAX3*-siRNA treated JR1 cells was significantly different from a high relative mean of cell migration distance of (70) at E in the NC-siRNA transfected JR1 cells ($p < 0.01$) (**Fig. 3.28**).

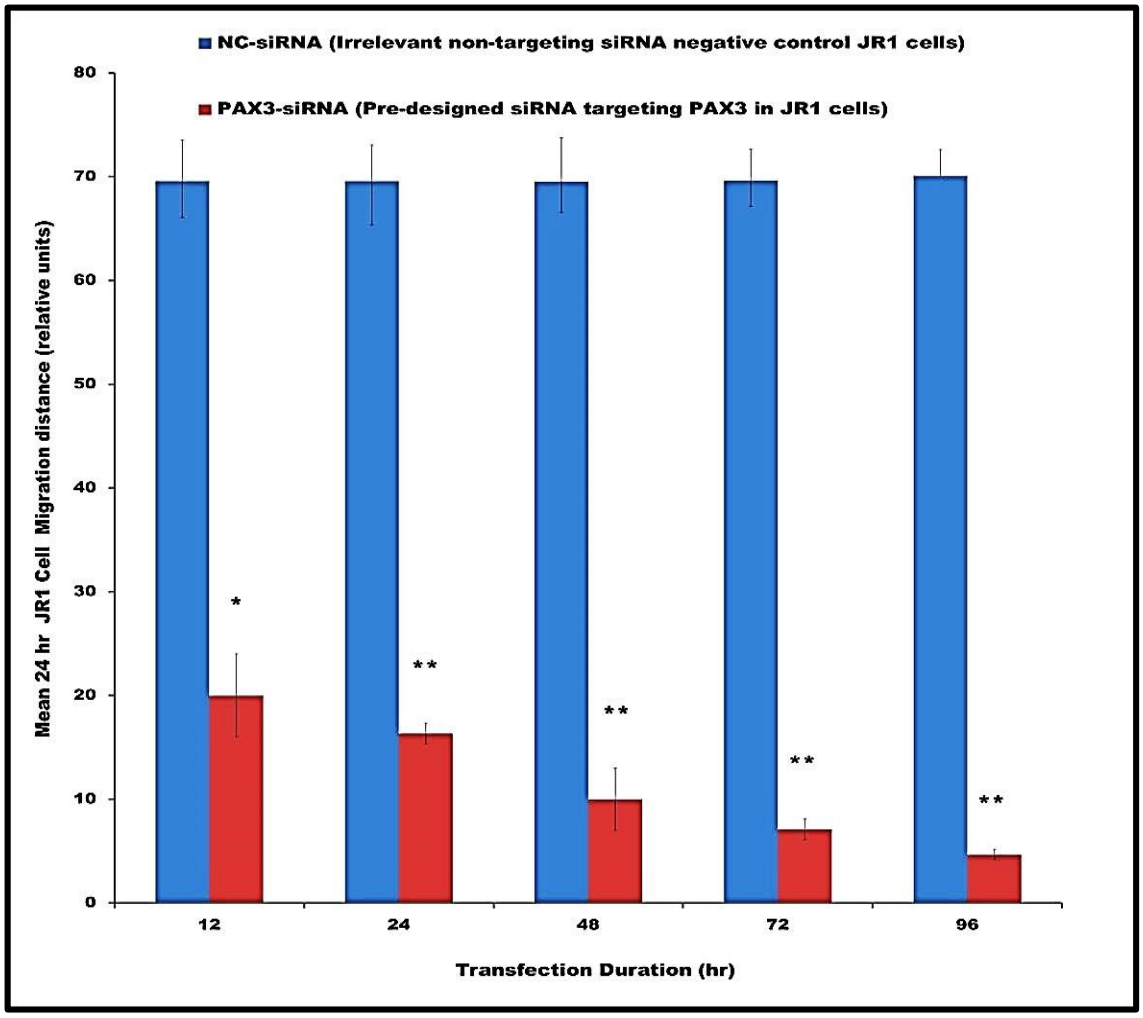

Figure 3.28 Relative JR1 cell migration over 24 hr after 12 hr, 24 hr, 48 hr, 72 hr or 96 hr siRNA transfection duration. The relative average migration distance of NC-siRNA transfected JR1 cells (blue columns) was compared with the relative average migration distance of P*AX3*-siRNA transfected JR1 cells (red columns) after 24 hr incubation. The mean values were derived from three measurements observed in three separate experiments (n = 9). Student's t-test, (*, $p < 0.05$; **, $p < 0.01$).

A similar cell migration inhibition pattern of the RH30 cell line was observed, but the extent of inhibition was not as high as that in JR1 cells. Likewise, the NC-siRNA

treated RH30 cells demonstrated more closure of wound gaps created at 0 hr (**Figs. 3.29**) after 24 hr cell migration (**Fig. 3.30**).

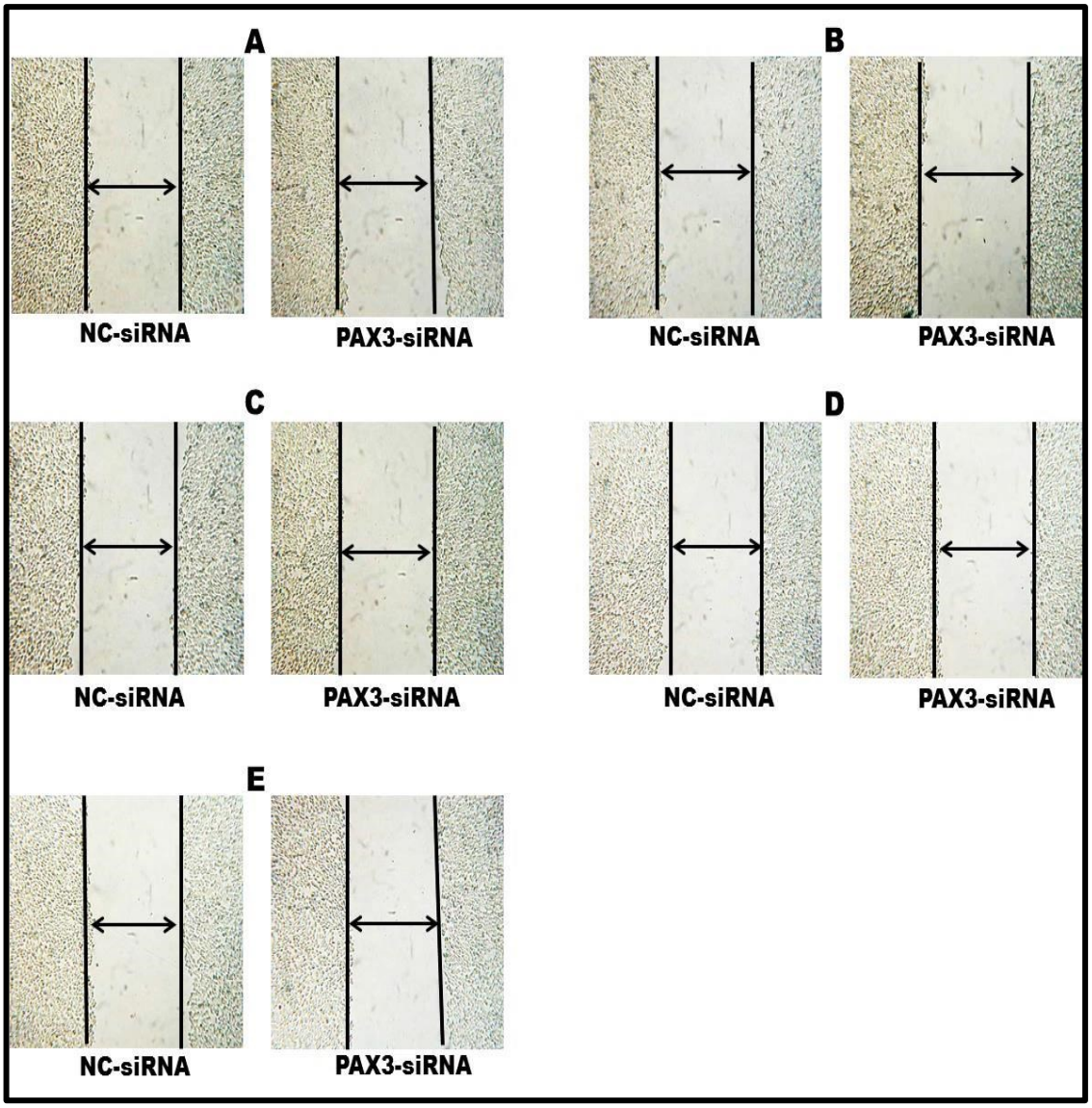

Figure 3.29, X 10 magnification of width of RH30 cells in scratched wound assay at 0 hr after 12-96 hr transfection duration. A (12 hr); **B (24 hr); C (48 hr**); **D (72 hr**); **E (96 hr**). The arrow represents the initial scratched wound gap of NC-siRNA and *PAX3*-siRNA at the start of RH30 cell migration experiment.

In the NC-siRNA treated RH30 cells, narrow wound gaps were observed owing to migration of cells. In contrast, wider wound gaps seen in the *PAX3*-siRNA treated RH30 cells revealed inhibition of cell migration. The NC-siRNA transfected RH30 cells migrated over long distances, gradually increasing over 24 hr to close the initial wound

gaps denoted by short arrows (**Fig. 3.30**). By contrast, *PAX3*-siRNA transfected RH30 cells showed significant inhibition of migration (shorter distances), over 24 hr to maintain broader wound gaps designated by wider arrows (**Fig. 3.30**).

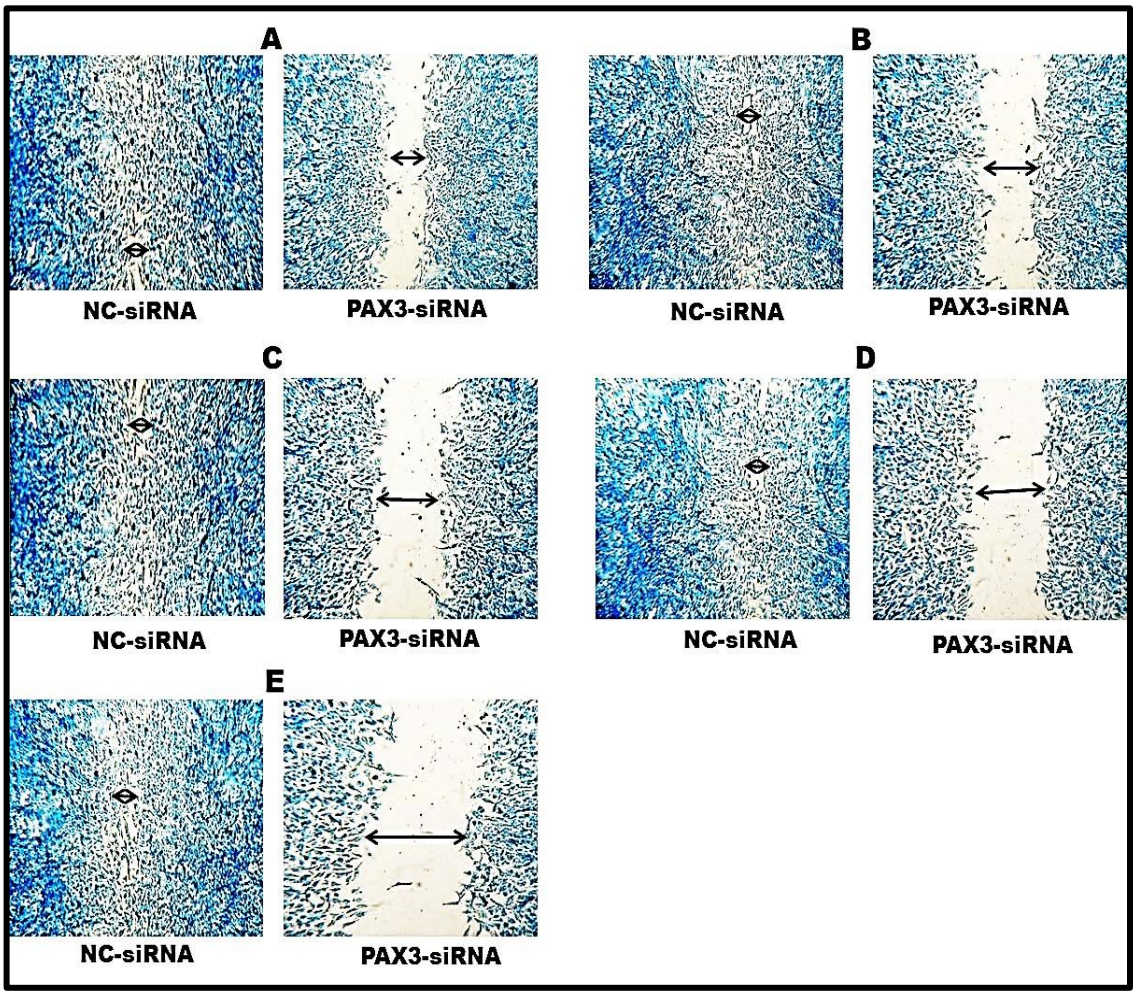

Figure 3.30, X 10 magnification in scratch wound 24 hr healing assay of transfected RH30 cells after 12-96 hr transfection duration. RH30 cells were stained with methylene blue. **A (12 hr); B (24 hr); C (48 hr); D (72 hr); E (96 hr)**. Measurement of wound gap distance represents cell distance migrated over 24 hr. Wound healing by cell migration related to measured distance in the 24 hr following 12 hr, 24 hr, 48 hr, 72 hr or 96 hr siRNA transfection. NC-siRNA transfected RH30 cells showed a narrow wound gap owing to high RH3 cell migration (shorter arrows). *PAX3*-siRNA transfected RH30 cells showed a wide wound gap owing to inhibition of RH30 cell migration as a result of RH30 cell apoptosis (longer arrows).

A minimal relative mean of cell migration distance (5 units) demonstrated in *PAX3*-siRNA treated cells at E was significantly different from an elevated relative mean of

cell migration distance at E (70) was exhibited in NC-siRNA transfected JR1 cells ($p <$ 0.01) because of cell apoptosis (**Fig. 3.31**).

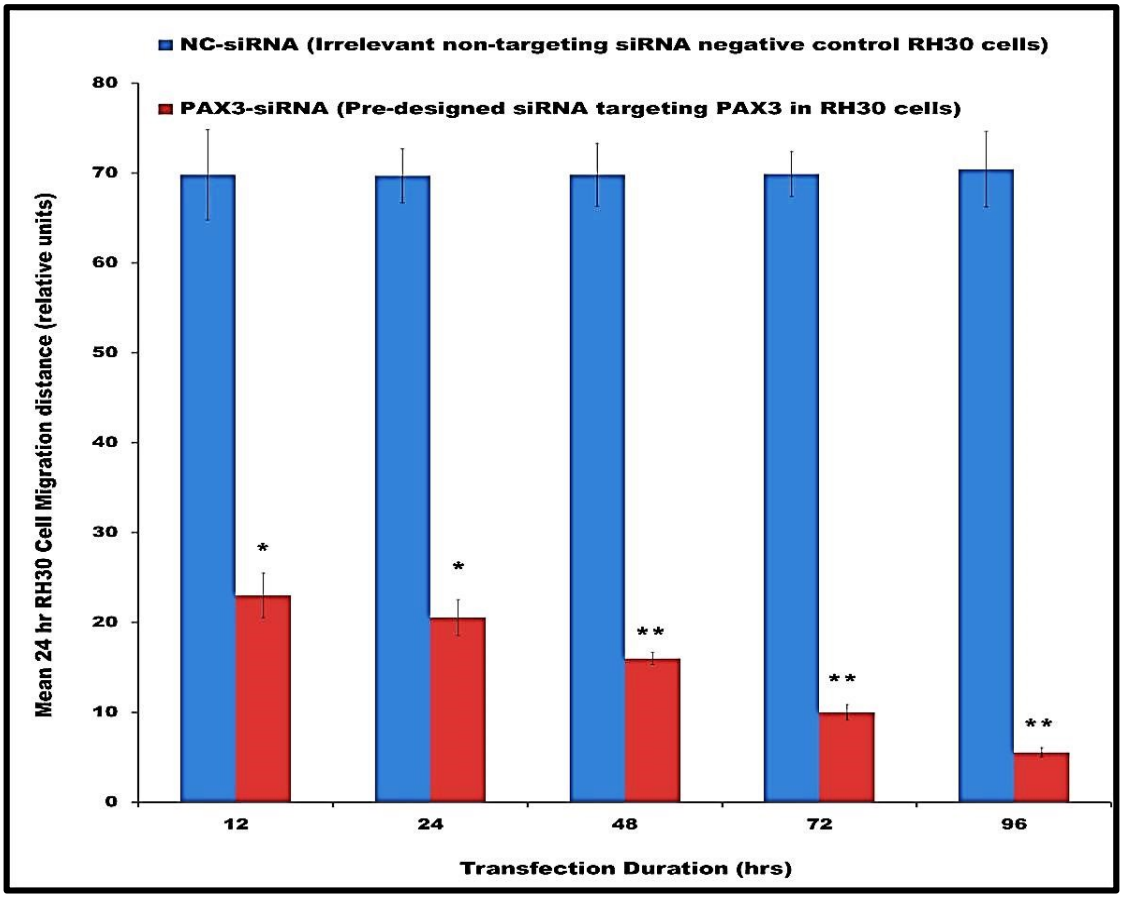

Figure 3.31 Relative migration of RH30 cells over 24 hr following 12 hr, 24 hr, 48 hr, 72 hr or 96 hr siRNA transfection duration. The relative average migration distance of NC-siRNA transfected RH30 cells (blue columns) was compared with the relative average migration distance of *PAX3*-siRNA transfected RH30 cells (red columns).The mean measurements were derived from three separate experiments (n = 9). Student's t-test; (*, $p < 0.05$; **, $p < 0.01$).

3.9. Effect of *PAX3* Expression Knockdown on Cell Adhesion to Extracellular Matrix Proteins

Cell adhesion to natural extracellular matrices (ECMs) plays a major role in cellular communication regulation and is of fundamental importance in the development and maintenance of tumourigenesis of JR1 and RH30 cells (Al-Ayoubi *et al,* 2012). The effect of silencing *PAX3* on inhibition of JR1 and RH30 adhesion to human ECM proteins, including collagen I, collagen II, collagen IV, fibronectin, laminin, tenascin and

vitronectin, previously coated on surfaces of plastic wells was demonstrated. The mean OD relating to the extent of NC-siRNA treated cell attachment to each ECM protein was compared to that of *PAX3*-siRNA treated cells following 96 hr transfection. The NC-siRNA transfected cells with high *PAX3* expression showed higher mean ODs corresponding to increased cell attachment to the various ECM proteins compared to lower mean ODs observed in *PAX3*-siRNA treated JR1 cells, which demonstrated weaker adhesion to all ECM proteins studied. At 96 hr transfection, lower mean ODs in the *PAX3*-siRNA treated JR1 cell inhibition of adhesion to Col I (0.04), Col II (0.03) and Col IV (0.03) were significantly different from the NC-siRNA JR1 treated cells attachment with higher mean ODs on Col I (0.62), Col II (0.41) and Col IV (0.26) ($p <$ 0.01) (**Fig. 3.32**).

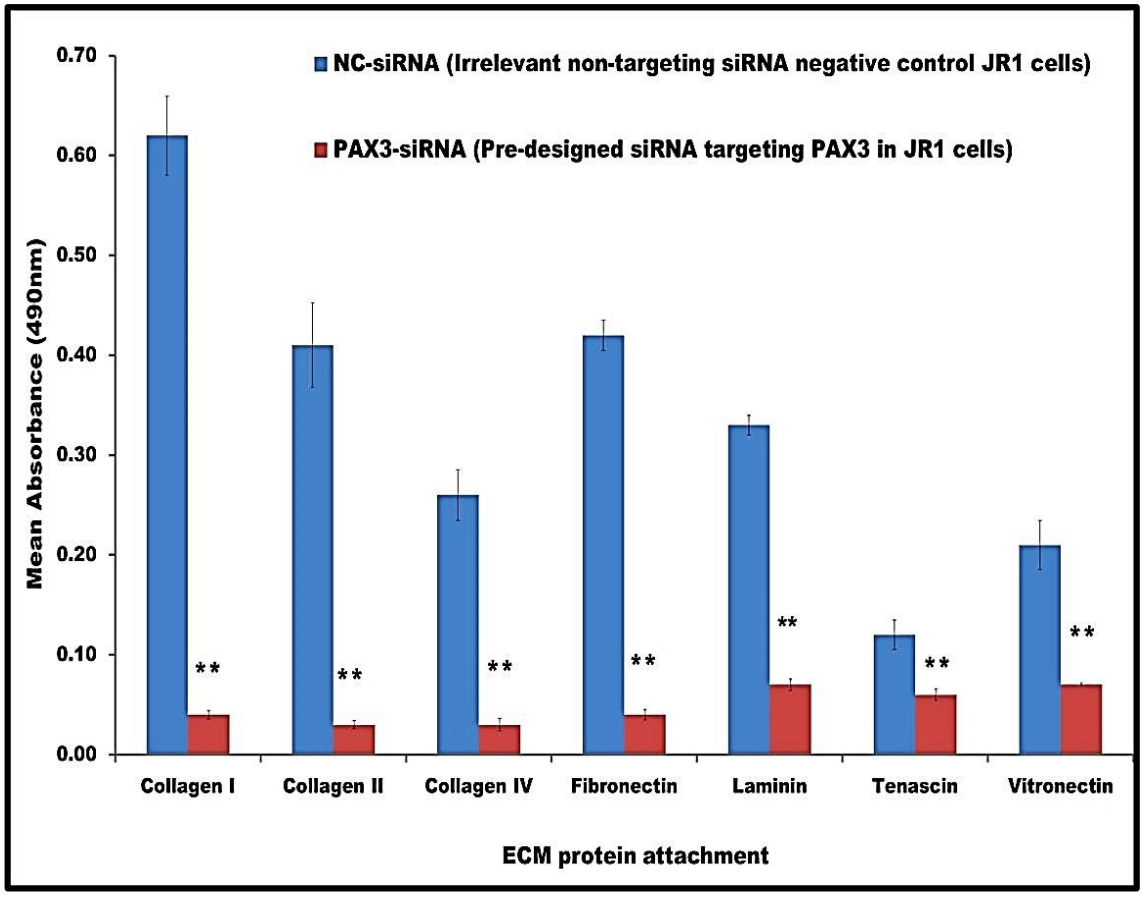

Figure 3.32 Inhibition of JR1 cell adhesion to ECM proteins following 96 hr siRNA transfection. The mean OD of JR1 cell adhesion in NC-siRNA transfected JR1 cells (blue columns) was compared with the mean OD of JR1 cell adhesion in *PAX3*-siRNA transfected JR1 cells (red columns). The means were derived from three measurements in each of two separate experiments (n = 6). Student's t-test, (**, $p < 0.01$).

Likewise, RH30 cells showed a similar cell adhesion inhibition pattern with the NC-siRNA treated RH30 cells adhering more strongly to the various ECM proteins (demonstrated higher mean ODs relating to increased cell attachment), while *PAX3*-siRNA transfected RH30 cells adhered much less strongly.

Following 96 hr transfection, *PAX3*-siRNA treated JR1 cells demonstrating lower mean ODs of cell attachment to Col I (0.05), Col II (0.04) and Col IV (0.04) which were significantly different from higher mean ODs in the NC-siRNA RH30 treated cell attachment to Col I (0.81), Col II (0.53) and Col IV ($p < 0.01$) (**Fig. 3.33**).

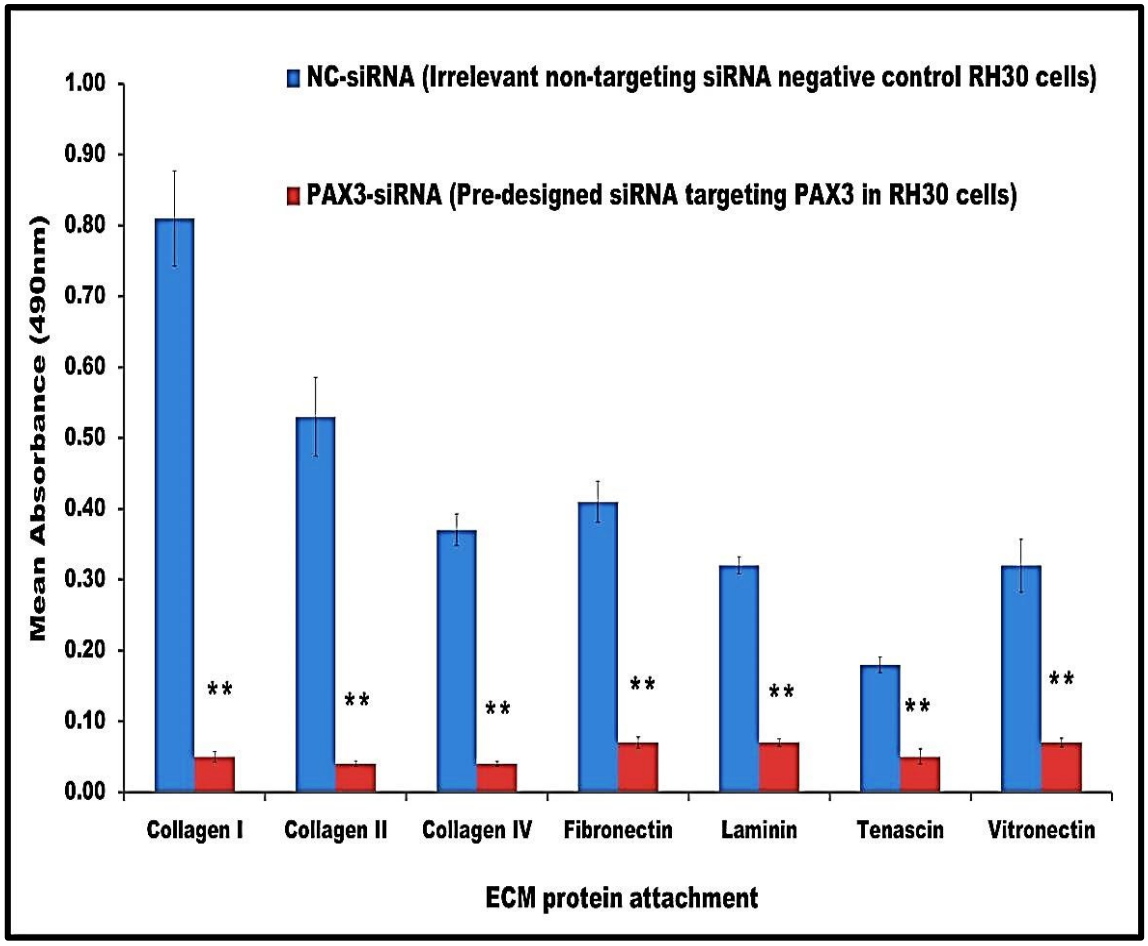

Figure 3.33 Inhibition of RH30 cell adhesion to ECM proteins following 96 hr siRNA transfection. The mean OD of JR1 cell adhesion in NC-siRNA transfected RH30 cells (blue columns) was compared with the mean OD of JR1 cell adhesion in *PAX3*-siRNA transfected RH30 cells (red columns). The means were derived from three measurements in each of two separate experiments (n = 6). Student's t-test, (**, $p < 0.01$).

3.10. Effect of Silencing *PAX3* on cell Invasion of JR1 and RH30 Cell Lines

To investigate the effects of silencing *PAX3* on JR1 and RH30 cell invasion *in vitro*, the mean numbers of cells invading a matrigel membrane among the NC-siRNA transfected cells were compared to the number of *PAX3*-siRNA transfected cells. One part of a microscopic field view (**Fig 3.34**), showed JR1 cell invasion after 96 hr transfection. In the JR1 cell line, among NC-siRNA transfected cells with high *PAX3* expression, a mean number of seventy cells per microscopic field were observed to invade matrigel membranes to indicate high cell invasive capacity in. On the contrary, a mean of fifteen *PAX3*-siRNA treated cells per microscopic field invaded the matrigel membranes (**Fig.3.35**).

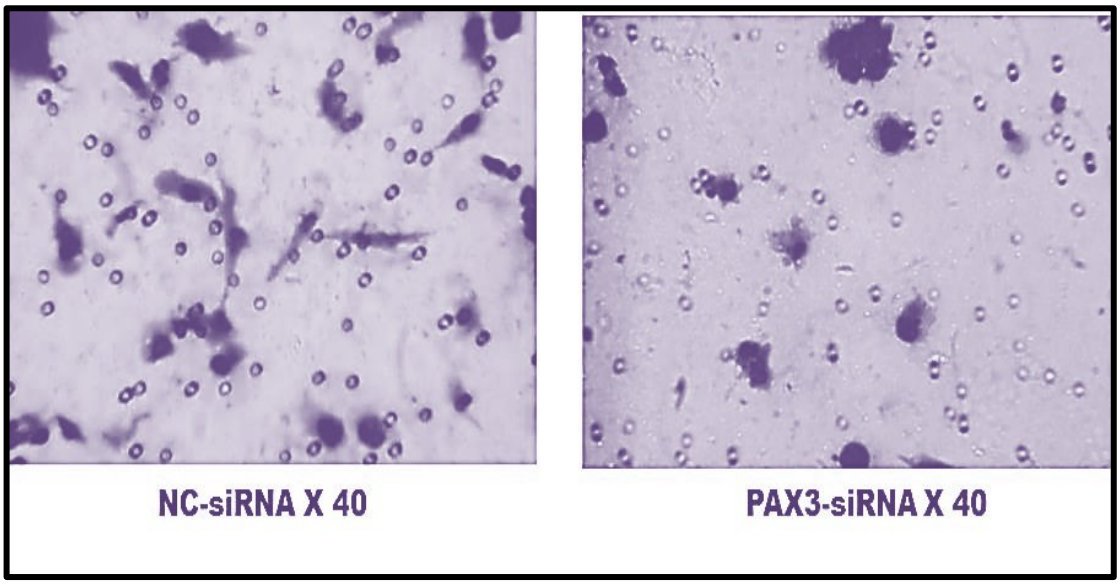

Figure 3.34 Inhibition of JR1 cell invasion of matrigel membrane following 96 hr siRNA transfection. Invaded JR1 cells were stained with Giemsa and viewed in a phase contrast microscope X 40. NC-siRNA transfected JR1 cells invaded the metri gel membrane in high numbers than *PAX3*-siRNA transfected JR1 cells invading in less numbers. Invaded JR1 cells were counted in five microscopic fields in each of three experiments.

Comparatively, a significantly reduced mean number of *PAX3*-siRNA transfected cells (15) invading the matrigel membrane, demonstrated a poorer cell invasive capacity ($p < 0.01$), in contrast to a higher mean number of JR1 cell invasion (70) in the NC-siRNA transfected cells (**Fig 3.35**). The low JR1 cell invasion observed in *PAX3*-siRNA transfected cells was significantly different from NC-siRNA treated invaded cells ($p < 0.01$).

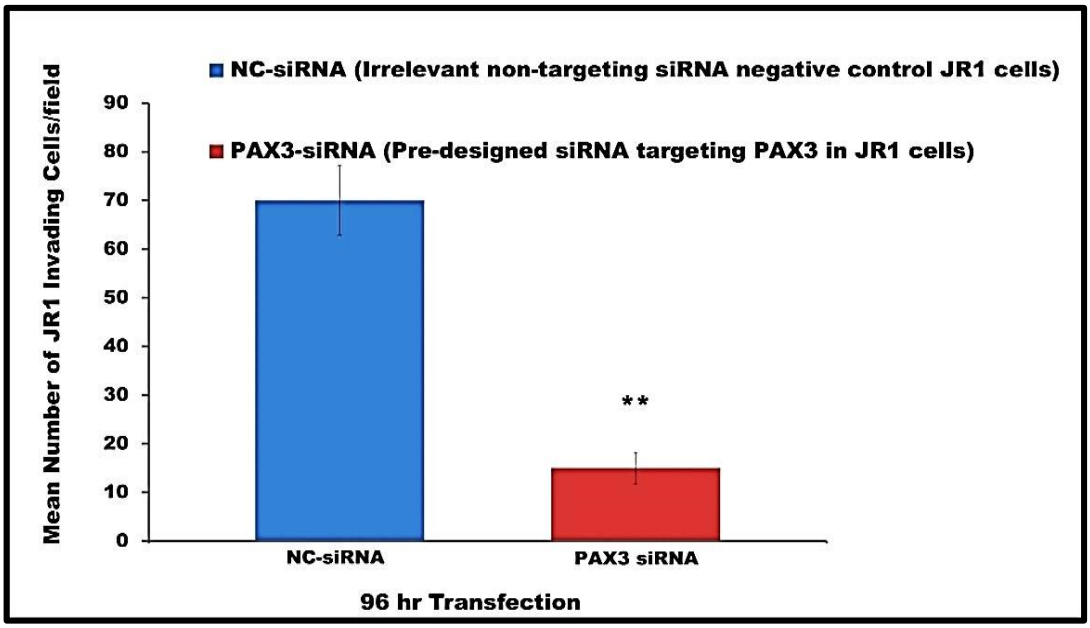

Figure 3.35 Mean inhibition of JR1 cell invasion. The mean number of JR1 cell invasion in NC-siRNA transfected JR1 cells (blue column) was compared with the mean number of JR1 cell invasion in *PAX3*-siRNA transfected JR1 cells (red column). The means were derived from five microscopic field measurements in each of three separate experiments (n = 15). (Student's t-test), (**, $p < 0.01$).

Similarly, a microscopic field view in an area (**Fig 3.36**), likewise showed higher RH30 cells invasion of the NC-siRNA treated cells than the *PAX3*-siRNA treated cells.

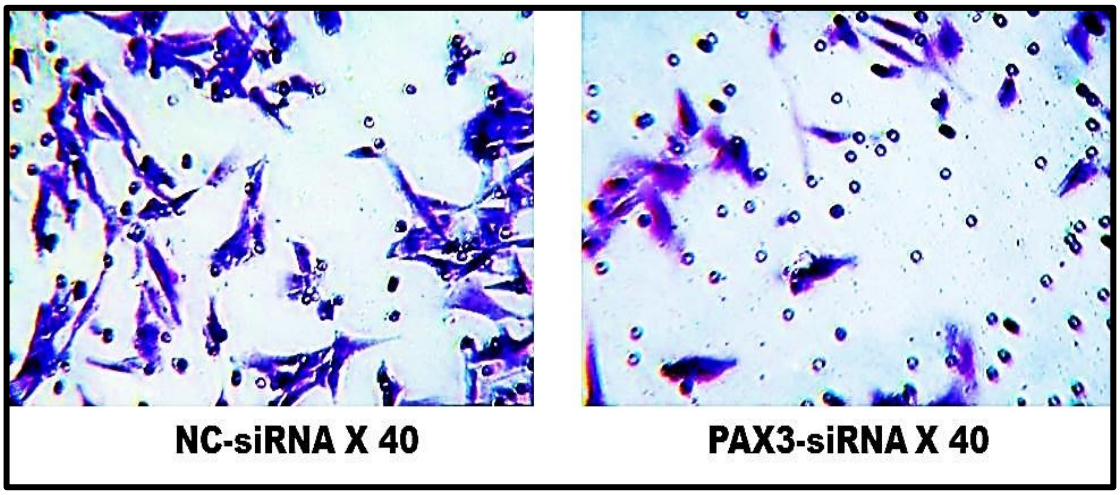

Figure 3.36 Inhibition of RH30 cell invasion of matrigel membrane after 96 hr siRNA transfection. RH30 cells were stained with Giemsa and viewed in a phase contrast microscope X 40. High number of NC-siRNA transfected RH30 cells invaded the metri gel membrane than *PAX3*-siRNA transfected RH30 cells invading in few numbers. Invaded RH30 cells were counted from five microscopic fields per experiment.

After 96 hr transfection, the NC-siRNA transfected cells with high *PAX3* gene expression were observed to invade a matrigel membrane in high numbers (75 cells/field), indicating a high cell invasive capacity. Comparatively, *PAX3*-siRNA transfected cells with *PAX3* gene knockdown invaded a matrigel membrane in significantly lower numbers (20 cells/field) indicating a reduced cell invasive capacity (**Fig 3.37**). The low RH30 cell invasion observed in *PAX3*-siRNA transfected cells was significantly different from NC-siRNA treated invaded cells ($p < 0.01$).

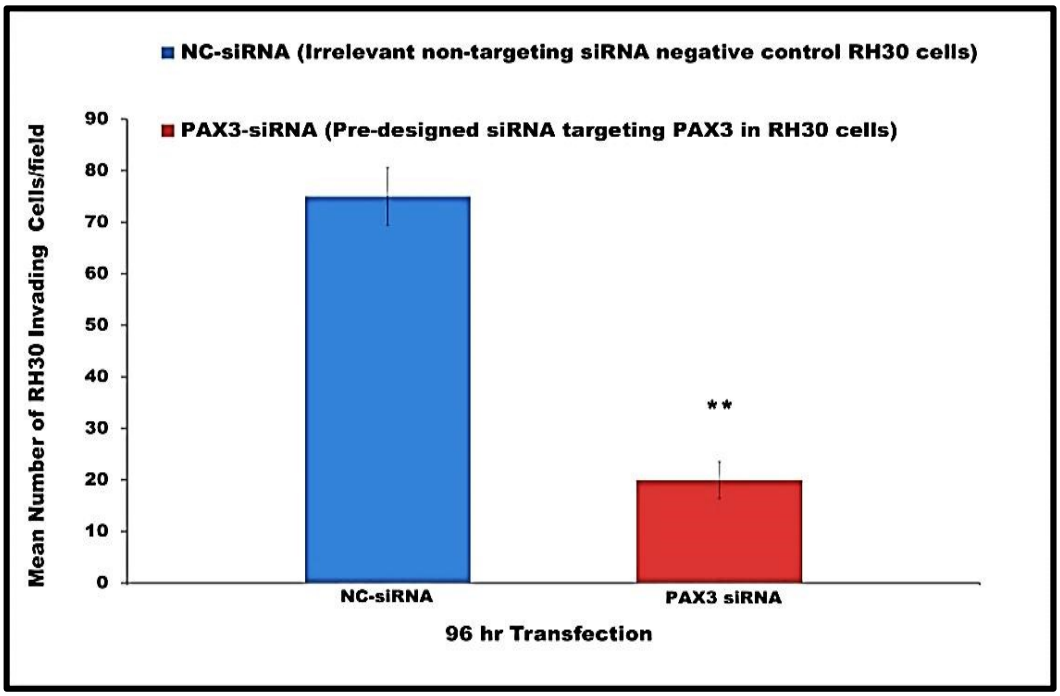

Figure 3.37 Mean inhibition of RH30 cell invasion. The mean number of RH30 cell invasion in NC-siRNA transfected RH30 cells (blue column) was compared with the mean number of RH30 cell invasion in *PAX3*-siRNA transfected RH30 cells (red column). The means were derived from five microscopic field measurements in each of three separate experiments (n = 15). Student's t-test, (**, $p < 0.01$).

3.11. Effect of Silencing *PAX3* on Clonogenicity of JR1 and RH30 Cells

The effect of knockdown of *PAX3* on JR1 and RH30 cell transformation was evaluated using an *in vitro* soft agar assay. This detects colony formation arising from morphological transformation of JR1 and RH30 cells, which might be changed by *PAX3*-siRNA transfection. The average number of visible large colonies in the gel

arising from NC-siRNA transfected cells was compared with those arising from *PAX3*-siRNA transfected cells.

Following 96 hr transfected, the NC-siRNA transfection JR1 cells with high *PAX3* gene expression produced an average of six large colonies of diameter greater than approximately 100µm as shown in one part of a microscopic field view (**Fig. 3.38**). In contrast, *PAX3*-siRNA treated JR1 cells formed small aggregates of apoptotic JR1 cells (according to the manufacturer's literature).

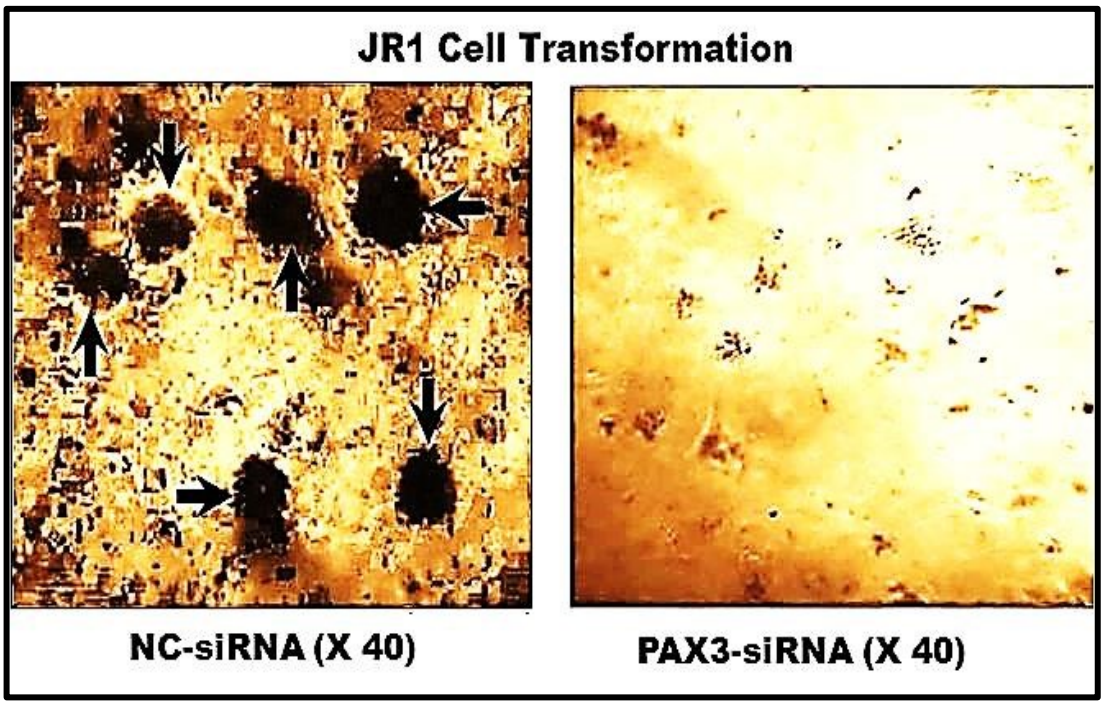

Figure 3.38 Inhibition of JR1 colony reproducibility in (soft agar) following 96 hr siRNA transfection. JR1 colonies were stained with crystal violet. Phase contrast X 40 micrograph of anchorage independent growth of JR1 cells in soft agar after 28 days incubation. The number of colonies in each of five microscopic fields was counted. NC-siRNA transfected JR1 cells formed seven large colonies (approximately 100µm) per part field than *PAX3*-siRNA transfected JR1 cells which produced apoptotic cells. Colonies greater than 100µm were counted in each five microscopic fields in each of three experiments.

The mean number of transformed colonies in the NC-siRNA transfected cells (seven per microscopic field) were significantly different from *PAX3*-siRNA treated cells ($p < 0.01$) (**Fig. 3.39**) because of cell apoptosis.

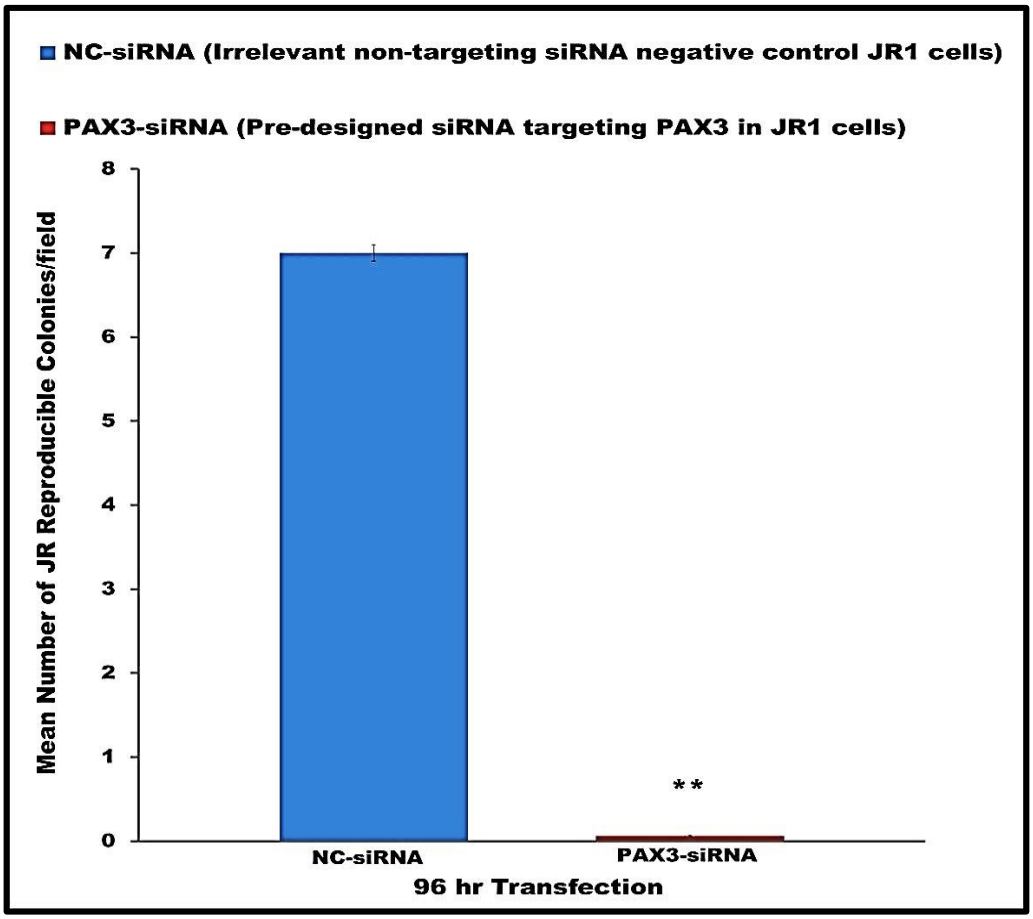

Figure 3.39 Mean inhibition of JR1 colony reproducibility. The mean number of reproducible colony in NC-siRNA transfected JR1 cells (blue column) was compared with the mean number of reproducible colony in *PAX3*-siRNA transfected JR1 cells (red column). The mean number of colonies were counted over five microscopic fields in each of three separate experiments and found to be statistically different, (n = 15). Student's t-test, (**, $p < 0.01$).

A similar pattern of colony reproducibility was observed in the RH30 cell line after 96 hr transfection. NC-siRNA transfected RH30 cells produced about sixteen large colonies diameter greater than 100μm as demonstrated in one microscopic field view (**Fig. 3.40**). By contrast, *PAX3*-siRNA transfected RH30 cells produced much smaller colonies that were suspected to be collections of apoptotic RH30 cells (according to the manufacturer's literature).

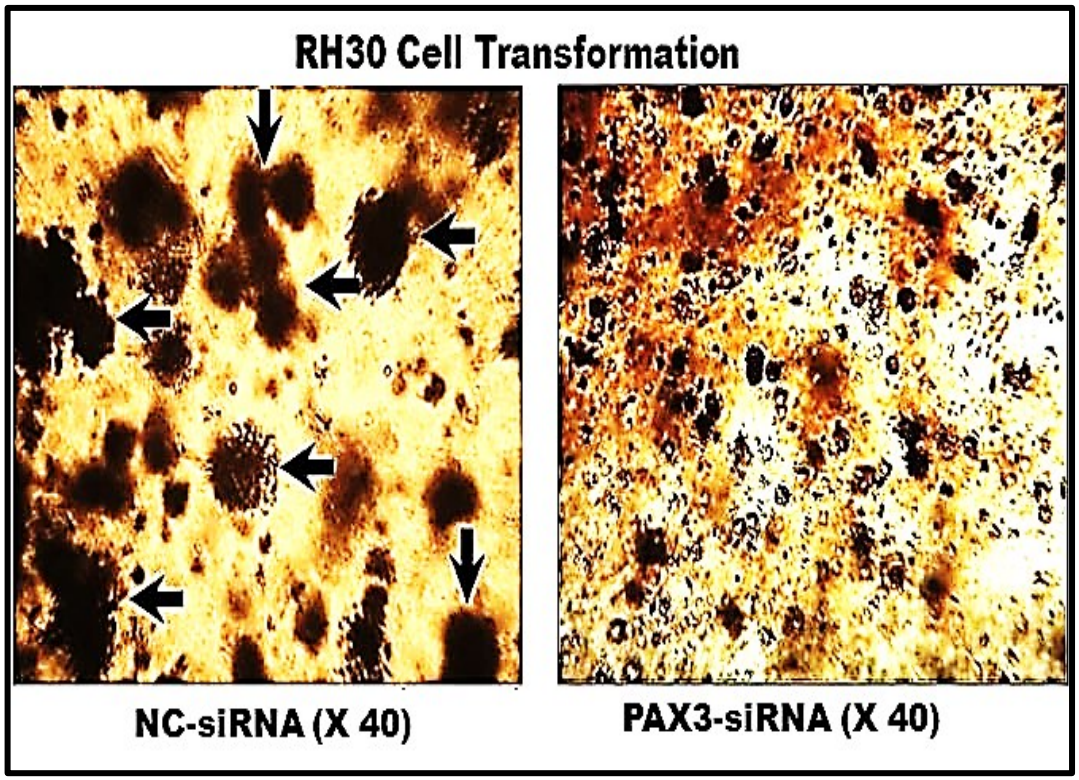

Figure 3.40 Inhibition of RH30 colony reproducibility in (soft agar) following 96 hr siRNA transfection. RH30 cells were stained with crystal violet. Phase contrast X 40 micrograph of anchorage independent growth of RH30 cell in soft agar after 28 days incubation. NC-siRNA transfected RH30 cells generated higher numbers of large colonies while *PAX3*-siRNA transfected RH30 cells produced apoptotic cells. Colonies greater than 100μm were counted in each five microscopic fields in each of three experiments.

There was significantly less number of colonies generated from *PAX3*-siRNA transfected RH30 cells (1 per field) than those generated from the NC-siRNA transfected cells (16 per field) ($p < 0.01$) **(Fig. 3.41)**.

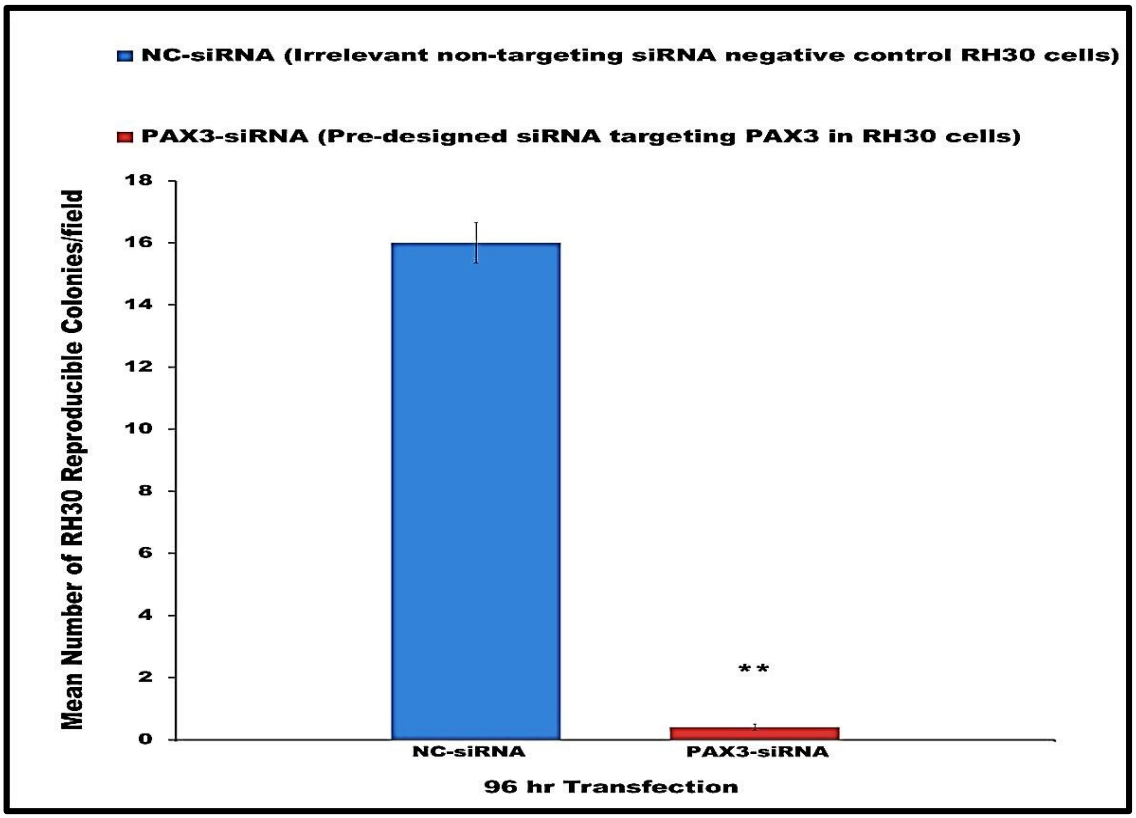

Figure 3.41 Mean inhibition of RH30 colony reproducibility. The mean number of reproducible colony in NC-siRNA transfected RH30 cells (blue column) was compared with the mean number of reproducible colony in *PAX3*-siRNA transfected RH30 cells (red column). The mean number of colonies were counted in five microscopic fields in each of three separate experiments and found to be statistically different, (n = 15). Student's t-test, (**, $p < 0.01$).

3.12. Effect of Silencing *PAX3* on Apoptosis of JR1 and RH30 Cells

To investigate the effect of knockdown of *PAX3* on apoptosis of JR1 and RH30 cells both indirect biochemical and direct morphological assessments of cell apoptosis were carried out. Using an indirect biochemical analysis, caspase 3/7 activities were determined, since high caspase 3/7 activation has been regarded as a universal marker of early apoptosis (Dieker *et al.,* 2012).

In the indirect biochemical analysis of early apoptosis, the mean measured relative luminescence unit (RLU) of caspase 3/7 activity was measured over a 60 min period in a 2 hr staurosporine (1µM/ml; 1µl/ml) induced-apoptosis of JR1 cells (positive control) which was compared to RLU caspase 3/7 activity in both NC-siRNA (negative control)

and *PAX3*-siRNA transfected JR1 cells. Following transfection, a high caspase 3/7 activity evidenced by a high mean luminescence of 325 X 10^4 RLU at 30 min was observed in the staurosporine induced-apoptotic JR1 cells (1µM/ml; 1µl/ml) (**Fig. 3.42A**). While at 30 min incubation, *PAX3*-siRNA JR1 cells demonstrated significant increased mean caspase 3/7 activity (180 X 10^4 RLU) ($p < 0.01$) (**Fig. 3.42B**), compared to the NC-siRNA transfected JR1 cells which had little caspase 3/7 activity at 30 min (60 X10^4 RLU) (**Fig. 3.42C**).

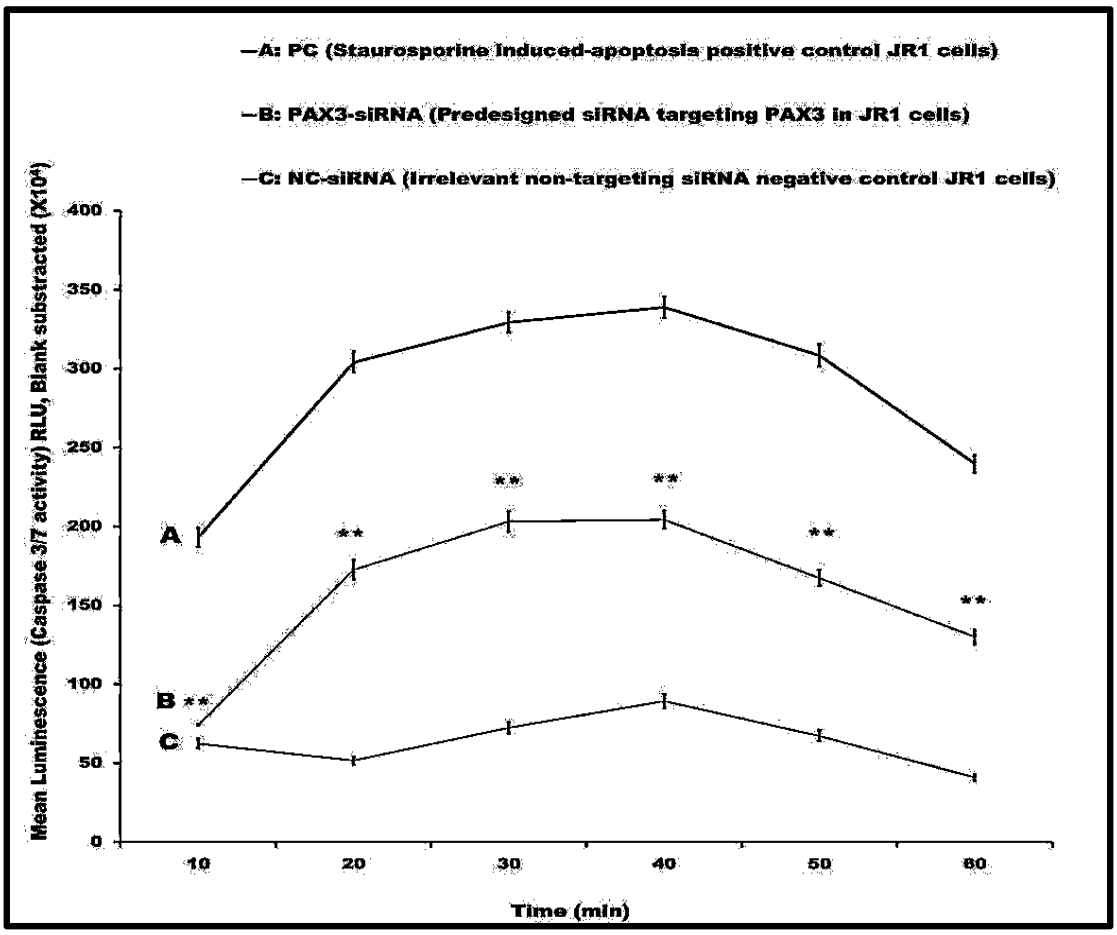

Figure 3.42 Caspase 3/7 activity in JR1 cells following 96 hr siRNA transfection and/ or 2 hr staurosporine induced-apoptosis (positive control). The mean caspase 3/7 activity in **A (**2 hr Staurosporine (1µM/ml; 1µl/ml) treated JR1 cells induced positive apoptosis control which pattern of curve indicate higher caspase 3/7 activity and induction of apoptosis), was compared with both **B (***PAX3*-siRNA transfected JR1 cells which showed similar pattern of curve to A, revealed high caspase 3/7 activity and induction of JR1 cell apoptosis) and **C** (NC-siRNA transfected JR1 cells showing dissimilar pattern of curve to A, indicates no apoptosis). The curves are representations of the mean of three replicate measurements in each of two separate experiments (n = 6). At 30 min the mean RLU measurement of **B** was statistically higher than that of C, Student's t-test, (**B** versus **C** **, $p < 0.01$).

The RH30 cell line showed a similar pattern of mean caspase 3/7 activity at 30 min after 96 hr transfection. The staurosporine (1µM/ml; 1µl/ml) induced apoptosis of RH30 cells (1µM/ml; 1µl/ml) (positive control) showed high caspase 3/7 activity (300 X 10^4 RLU) (**Fig. 3.43A**). The caspase 3/7 activity (175 X 10^4 RLU) of *PAX3*-siRNA transfected RH30 cells (**Fig. 3.43B**), was significantly higher than that of NC-siRNA transfected RH30 cells which showed little caspase 3/7 activity (30 X 10^4 RLU) (**Fig. 3.43C**) ($p < 0.01$).

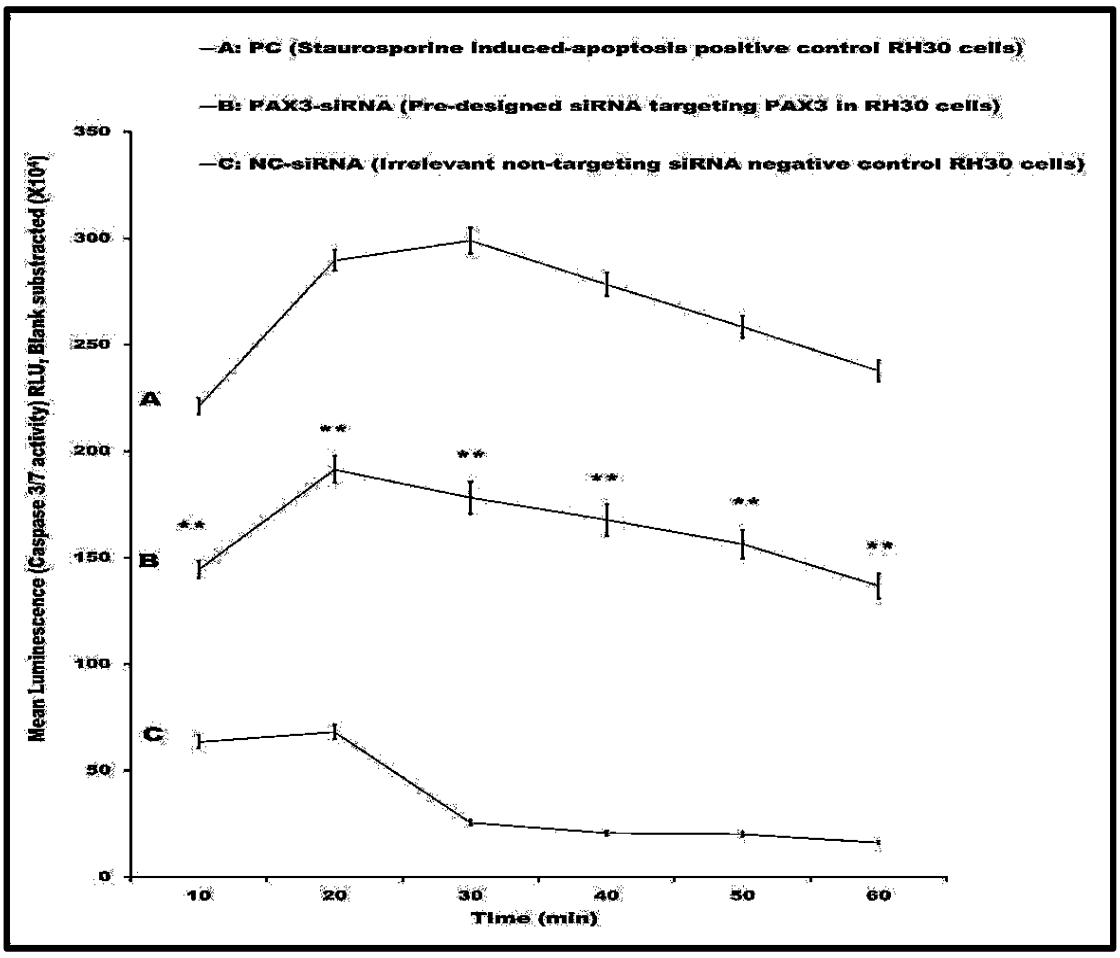

Figure 3.43 Caspase 3/7 activity in RH30 cells following 96 hr siRNA transfection and/ or 2 hr staurosporine induced-apoptosis (positive control). The mean caspase 3/7 activity in **A (**2 hr Staurosporine (1µM/ml; 1µl/ml) treated RH30 cells induced positive apoptosis control, which pattern of curve signifies higher caspase 3/7 activity and induction of apoptosis), was compared with both **B (***PAX3*-siRNA transfected RH30 cells which has similar pattern of curve to A, suggested high activity of caspase 3/7 and RH30 cell apoptosis) and **C** (NC-siRNA transfected RH30 cells having dissimilar pattern of curve to **A**, indicates no apoptosis). The curves are representations of the mean of three replicate measurements in each of two separate experiments (n = 6). At 30 min the mean RLU measurement of **B** was statistically higher than that of C, Student's t-test, (**B** versus **C** **, $p < 0.01$).

Direct detection of late apoptosis was performed using the DeadEnd™ Fluorometric TUNEL system for morphological detection of apoptosis. Staurosporine (1μM/ml; 1μl/ml) is highly permeable to cells and has a strong cytotoxicity effect on various mammalian tumour cell lines. It induce cell apoptosis by inhibiting the binding of ATP to kinases such as phospolipid/Ca2+ dependent and cyclic nucleotide dependent protein kinases.

The mean number of cells with fragmented DNA, indicative of apoptosis, induced by 96 hr *PAX3*-siRNA transfection of JR cells or combined 96 hr *PAX3*-siRNA transfection of JR cells plus 2 hr staurosporine (1μM/ml; 1μl/ml) treatment was compared to the DNA of NC-siRNA (negative control) or 2 hr staurosporine (1μM/ml; 1μl/ml) induced-apoptosis of JR1 cells (positive control). Part of a typical microscopic field showed fragmented DNA apoptotic nuclei in the PC, *PAX3*-siRNA or *PAX3*-siRNA-PC cells (**Fig. 3.44**).

The 2 hr staurosporine (1μM/ml; 1μl/ml) treated JR1 cells, PC (positive control), showed a mean of three localized green fluorescent nuclei per field (DNA fragmentation) (**Fig. 3.44)**. In the *PAX3*-siRNA treated cells, a mean of two fragmented DNA apoptotic nuclei was demonstrated compared to the mean of six fragmented DNA apoptotic nuclei shown in combined *PAX3*-siRNA-PC treated cells (**Fig. 3.44**).

By contrast, NC-siRNA transfected JR1 cells showed only blue DAPI stained nuclei and no localized green fluorescent nuclei (no DNA fragmentation).

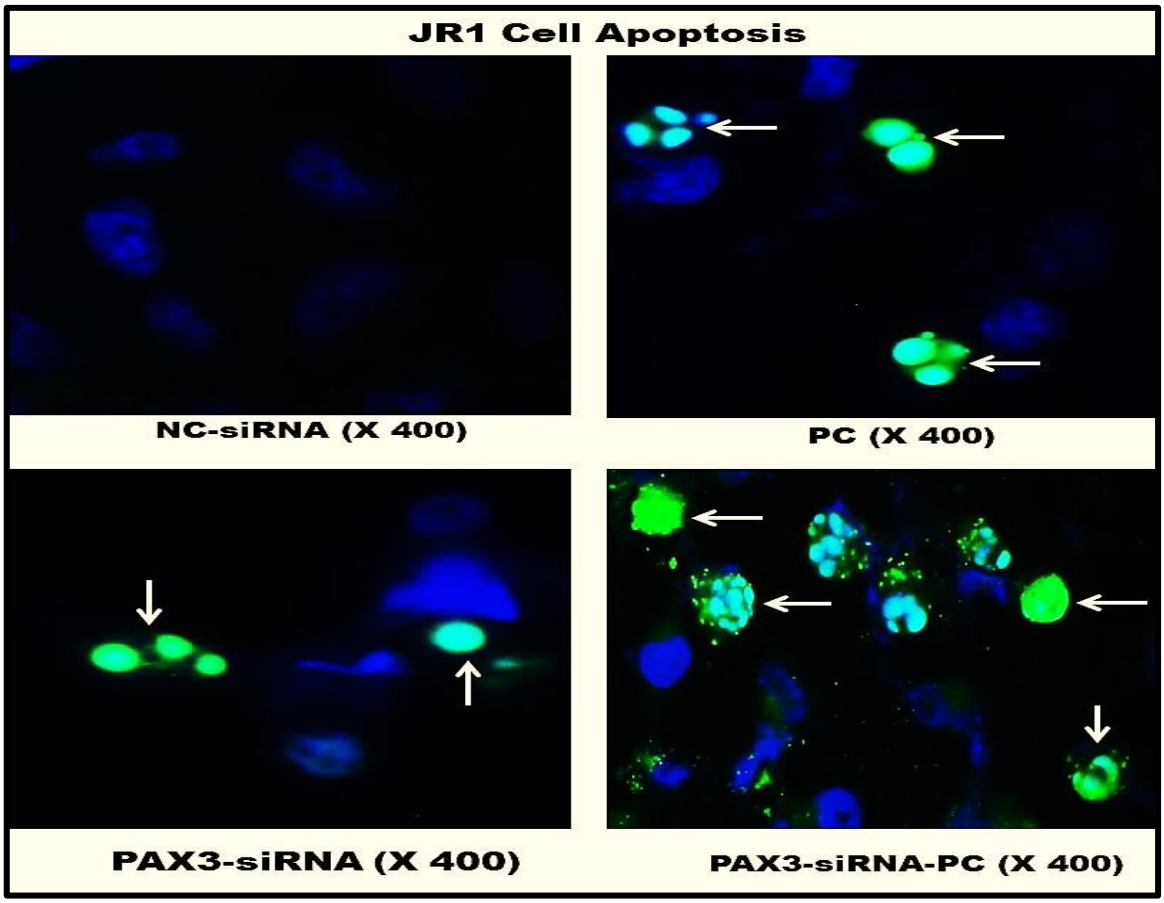

Figure 3.44 Direct detection of apoptosis in transfected JR1 cells by DeadEnd Fluorometric TUNEL system. X 400 fluorescence micrograph of apoptosis in JR1cells following 96 hr siRNA transfection. **NC-siRNA (**negative control transfected JR1cells showing non-apoptotic cell blue nuclei) (DAPI). **PC** (2 hr staurosporine (1µM/ml; 1µl/ml) treated JR1 cells positive apoptosis control revealed few green fluorescent fragmented apoptotic cell nuclei) (pointed arrows). ***PAX3*-siRNA (***PAX3*-siRNA transfected JR cells showed few green fluorescent apoptotic cell nuclei) (pointed arrows). ***PAX3*-siRNA-PC** (combined *PAX3*-siRNA transfected JR1 cells plus 2 hr staurosporine (1µM/ml; 1µl/ml) treatment displayed many green fluorescent apoptotic cell nuclei) (pointed arrows).

A mean of two localized green fluorescent nuclei per field was observed in the *PAX3*-siRNA treated cells against a mean of three localized green fluorescent nuclei in the 2 hr staurosporine (1µM/ml; 1µl/ml) treated positive control JR1 cells. Whereas a high mean number of localized green fluorescent nuclei, (six per microscopic field) indicative of DNA fragmentation was observed in the *PAX3*-siRNA plus 2 hr staurosporine (1µM/ml; 1µl/ml) treated JR1 cells. The number of localized green fluorescent nuclei (DNA fragmentation) observed in *PAX3*-siRNA or *PAX3*-siRNA-PC JR1 cells was significantly different from NC-siRNA transfected JR cells ($p < 0.01$) (**Fig. 3.45**).

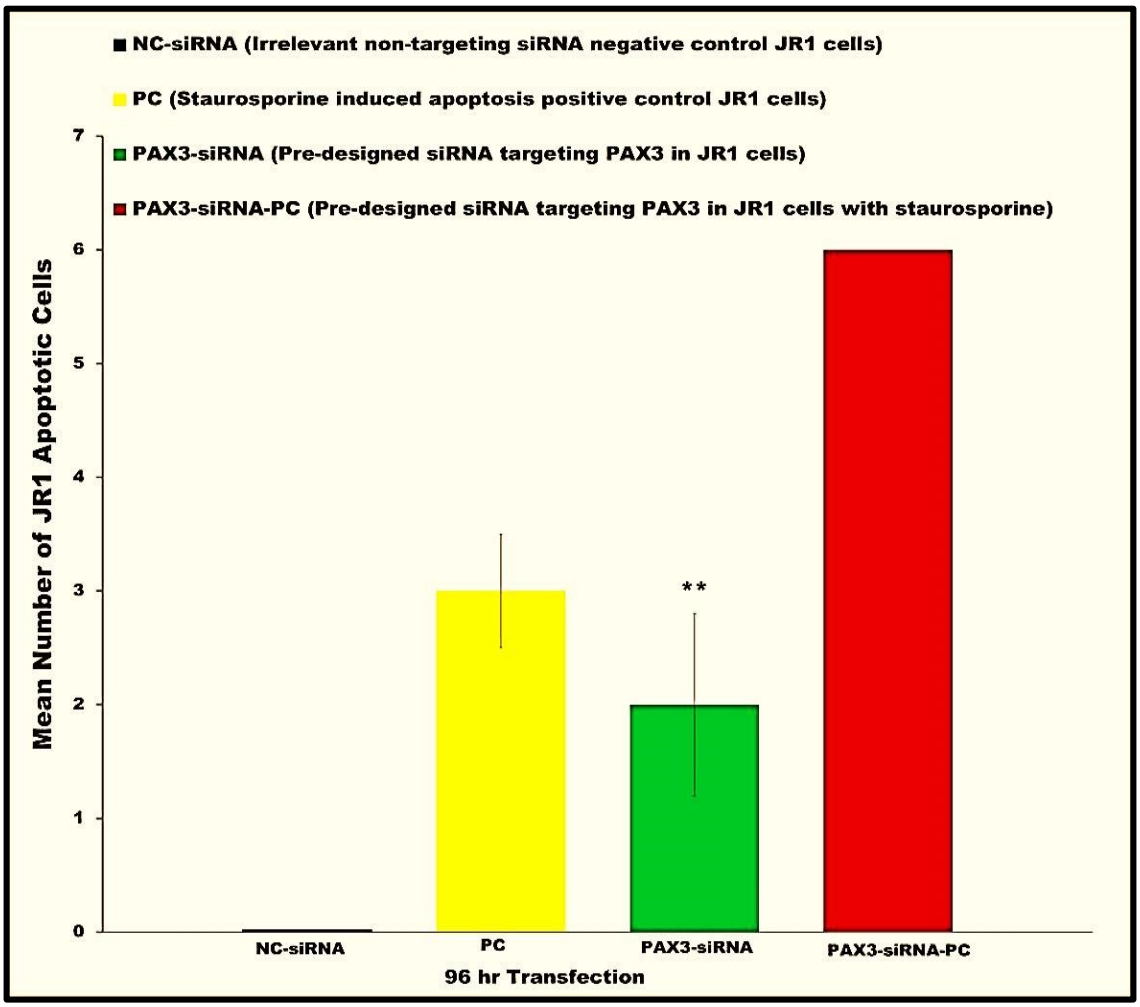

Figure 3.45 Mean numbers of transfcted JR1 apoptotic cells. The mean number of JR1 apoptotic cells in **NC-siRNA (**negative control transfected JR1 cells) (blue column) was compared with the mean number of apoptotic cells in both **PC** (2 hr staurosporine (1µM/ml; 1µl/ml) treated JR1 cells positive apoptosis control) (yellow column) and ***PAX3*-siRNA** transfected JR1 cells (green column) or ***PAX3*-siRNA-PC** (combined *PAX3*-siRNA transfected JR1 cells followed by 2 hr staurosporine (1µM/ml; 1µl/ml) treatment) (red column). The Mean number of apoptotic JR1 cells were counted from five microscopic fields in three separate experiments (n = 15). **PC** versus **NC** to demonstrate that positive control was working, (**NC** versus ***PAX3*-siRNA** or ***PAX3*-siRNA-PC**), Student's t-test *, $p < 0.01$).

A similar induction of apoptosis was detected in RH30 cells. Likewise, a field microscopic view (**Fig. 3.46**), showed localized green fluorescent nuclei (DNA fragmentation) in the 2 hr staurosporine (1µM/ml; 1µl/ml) treated RH30 cells (three per field), *PAX3*-siRNA transfection of RH30 cells (two per field) and *PAX3*-siRNA transfected plus 2 hr staurosporine (1µM/ml; 1µl/ml) treated RH30 cells (eight per

field). By contrast, NC-siRNA transfected RH30 cells showed only blue DAPI stained nuclei and no localized green fluorescent nuclei (no DNA fragmentation)

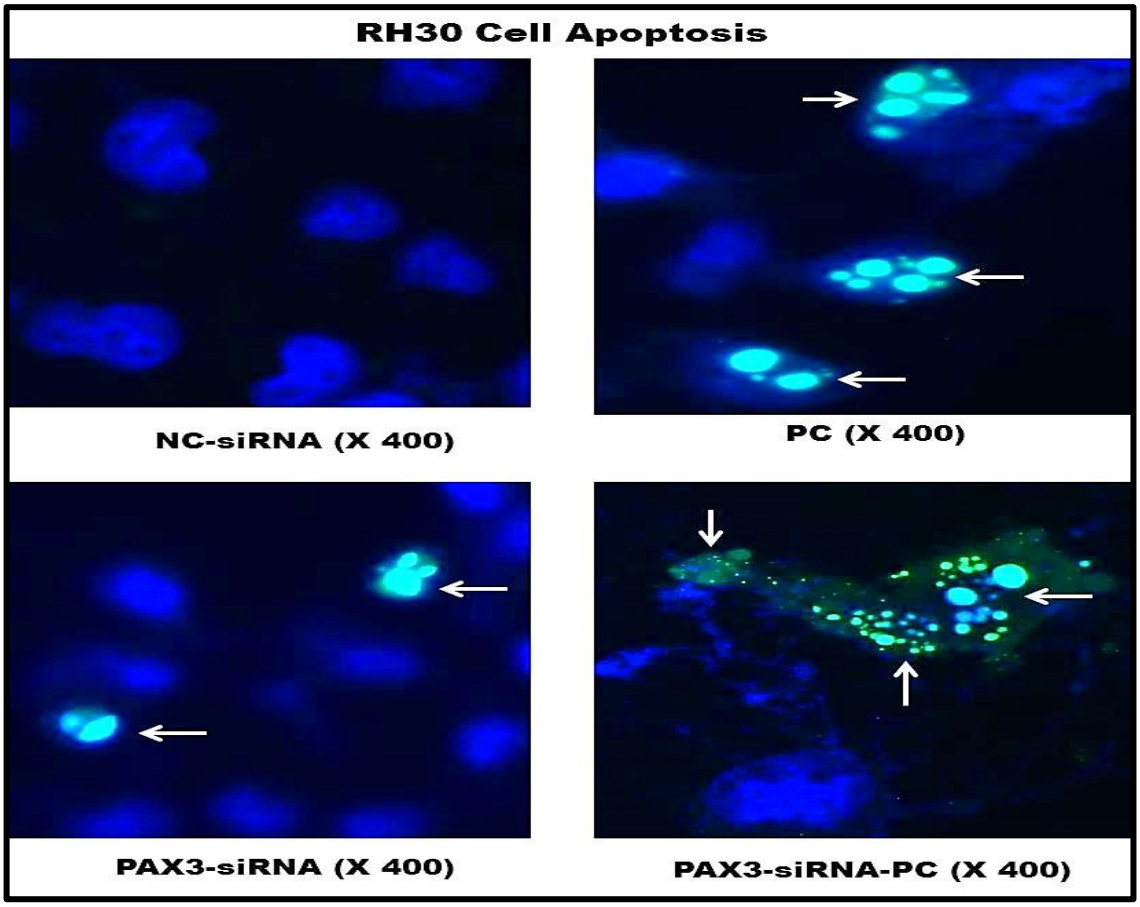

Figure 3.46 Direct detection of apoptosis in transfected RH30 cells by the DeadEnd Fluorometric TUNEL system. X 400 fluorescence micrograph of apoptosis in RH30 cells following 96 hr siRNA transfection. **NC-siRNA (**negative control transfected RH30 cells; exhibited blue nuclei non-apoptotic cells). **PC (**2 hr staurosporine (1µM/ml; 1µl/ml) treated RH30 cells positive apoptosis control showed green fluorescent fragmented apoptotic nuclei) (pointed arrows). ***PAX3*-siRNA (***PAX3*-siRNA transfected RH30 cells revealed green fluorescent apoptotic cell nuclei) (pointed arrows). ***PAX3*-siRNA-PC (**combined *PAX3*-siRNA transfected RH30 cells plus 2 hr staurosporine (1µM/ml; 1µl/ml) treatment displayed many fluorescent apoptotic cell nuclei).

The mean apoptotic RH30 cells observed in both ***PAX3*-siRNA** transfected RH30 cells (two per microscopic field) and ***PAX3*-siRNA** transfected plus 2 hr staurosporine (1µM/ml; 1µl/ml) treated RH30 cells (eight per microscopic field), indicate induction of apoptosis similar to the 2 hr staurosporine (1µM/ml; 1µl/ml) induced apoptosis of RH30 cells (**PC**) which also had a mean of three localized green fluorescent nuclei (DNA

fragmentation) (**Fig. 3.47**). Likewise a significant number of localized green fluorescent nuclei (DNA fragmentation) observed in *PAX3*-siRNA or *PAX3*-siRNA-PC RH30 cells was significantly different from NC-siRNA transfected RH30 cells ($p < 0.01$).

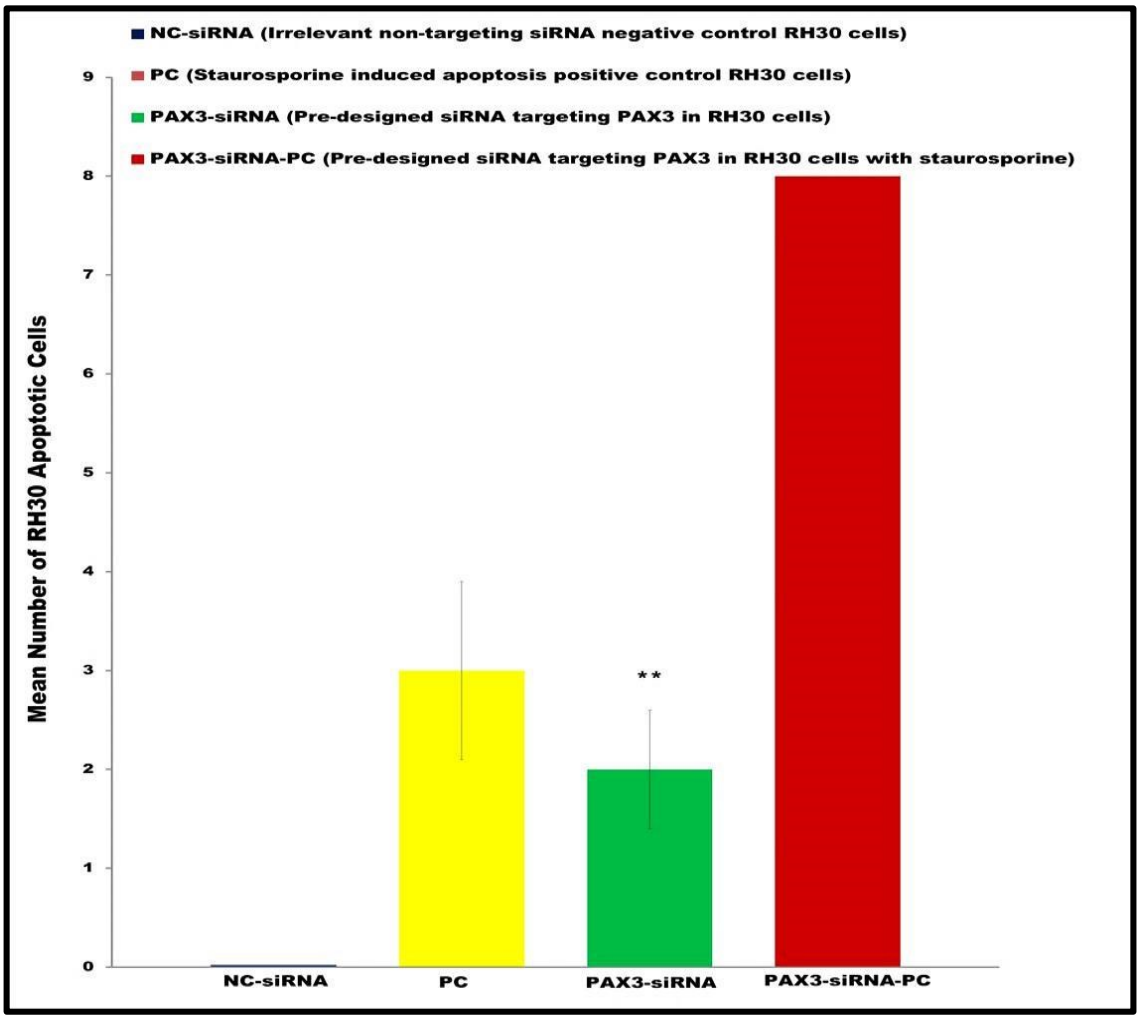

Figure 3.47 Mean numbers of transfected RH30 apoptotic cells. The mean number of RH30 apoptotic cells in **NC-siRNA (**negative control transfected RH30 cells) (blue column) was compared with the mean number of RH30 apoptotic cells in both **PC** (2 hr staurosporine (1µM/ml; 1µl/ml) treated RH30 cells positive apoptosis control (yellow column) and ***PAX3*-siRNA** *PAX3*-siRNA transfected RH30 cells (green column) or ***PAX3*-siRNA-PC** (combined *PAX3*-siRNA transfected RH30 cells plus 2 hr staurosporine (1µM/ml; 1µl/ml) treatment) (red column). The Mean number of apoptotic RH30 cells were counted from five fluorescence microscopic fields in three separate experiments (n = 15). **NC** versus ***PAX3*-siRNA** or ***PAX3*-siRNA-PC**, Student's t-test *, $p < 0.01$).

3.13. DISCUSSION

3.13.1. *PAX3*-siRNA Knockdown Modulates JR1 and RH30 Cellular Activity

During development and embryonic morphogenesis, the normal activities of cells including regulation of the cell cycle, proliferation, migration, adhesion, and induction of apoptosis are well coordinated by normal gene expression (De Crozé *et al.,* 2011; Jamiyandorj *et al.*, 2013). Cellular gene expression plays a central role in the control of functional activity of cells using several mechanisms (Yan[3] *et al.,* 2013). Aberrant gene expression may result in tumourigenesis, accompanied by induced inappropriate progression of the cell cycle, proliferation, migration, adhesion, invasion and prevention of apoptosis (Santarpia *et al.,* 2013).

This present study achieved a successful knockdown of *PAX3* gene expression, as microarray data analysis demonstrated a four-fold and two-fold knockdown of *PAX3* expression in human JR1 and RH30 cells respectively. A validation of the microarray data by quantitave RT-PCR analysis showed similar patterns of *PAX3* decreased expression in both human JR1 and RH30 cells. A semi-quantitative RT-PCR analysis indicated at least 93% knockdown of all variants of *PAX3* mRNA in human JR1 cells with a significantly decreased expression of *PAX3* compared to control cells ($p < 0.01$), (**Figs. 3.5 and 3.6**). Likewise, a minimum of 90% *PAX3* knockdown in all *PAX3* variants was demonstrated in human RH30 cells compared to negative control cells (**Figs. 3.7 and 3.8**) and resulted in significantly decreasd *PAX3* expression ($p < 0.01$).

Silencing of *PAX3* mRNA in the human JR1 cell line subsequently induced a 98% decrease in PAX3 protein, which consequently repressed the expression of key downstream target protein expression ($p < 0.01$), including C-MYC, ITGβ5, MYOD1 and BCL2 (**Figs. 3.14 and 3.15**). Other downstream targets demonstrating increased protein expression resulting from the knockdown of *PAX3* include P21, P53 and Casp3 (**Figs. 3.14 and 3.15**). Similarly, repression of *PAX3* in the RH30 cell line significantly reduced PAX3 protein by 92% ($p < 0.01$). This resulted in decreased expression of some downstream target proteins such as C-MYC, ITGβ5, MYOD1 and BCL2 whilst inducing increased expression of P21, P53, and Casp3 (**Figs. 3.16** and **3.17**).

Microarray data analysis revealed that *PAX3* silencing in both JR1 and RH30 cell lines, altered the expression of other genes of interest, which were classified into different groups according to their binding interactions with *PAX3* and their main function such as cell cycle regulation, proliferation, migration, adhesion, differentiation, myogenesis and apoptosis. The expression levels of DNA binding interaction partners of *PAX3;* acting as cofactor transcriptional modulators or functional modulators of the *PAX3* gene that were increased or decreased are shown in **Table 3.2**. For instance, HP1γ was down-regulated, whilst KAP1 and TBX18 were up-regulated. In both JR1 and RH30 cell lines, other *PAX3* DNA-binding partners including *BCL2, IPO13* and *RB* were down-regulated whilst *DAXX, HES1, HMOX1* and *PTEN* were up-regulated. The induced up-regulation of *PTEN* in particular, was in agreement with a previous study demonstrating high expression of *PTEN* following inhibition of *PAX3* expression in rhabdomyosarcoma (Li *et al.,* 2007). Intriguingly, *MSX1* was up-regulated in JR1 cells but down-regulated in RH30 cells. Most importantly, *PAX3* dual functional inhibition of apoptosis through repression of *PTEN* and increased expression of *BCL2* was demonstrated. Hence, here the up-regulation of *PTEN* and inhibition of *BCL2* induced human JR1 and RH30 cell apoptosis.

3.13.2. Suppression of *PAX3* Inhibits JR1 and RH30 Cell Cycle and Proliferation

Progression of cell cycle through the G1, S, or M phases in eukaryotic cells is regulated by fluctuation in the activities of cyclin-dependent kinases (CDKs) (Bose *et al*., 2013). The activity of CDK is controlled by recurrent synthesis and degradation of cyclins, as well as variations in the levels of CDK inhibitors (CKI) and reversible phosphorylation (Gomes *et al.,* 2013). Abnormal regulation of the cell cycle leads to uncontrolled growth, which may lead to tumour formation (Khammanivong *et al.,* 2013).

This present investigation was the first to demonstrate a substantial down-regulation of *PAX3* following *PAX3*-siRNA silencing in human rhabdomyosarcoma, which significantly inhibited *PAX3* cellular activities *in vitro*. Knockdown of *PAX3* drastically inhibited proliferation of both human JR1 ($p < 0.01$) and human RH30 cells ($p < 0.01$) by about 95% whilst maintaining cell viability and subsequently inducing apoptosis.

The pattern of inhibition of cell proliferation in both the CellTiter 96® aqueous cell proliferation and the Coulter counter direct cell counts were positively correlated (**Figs. 3.20, 3.21, 3.22** and **3.23**).

In conformity with the above studies, the microarray analysis in this current study revealed that other essential downstream targets of *PAX3* were either repressed or activated following knockdown of *PAX3* gene expression in both human JR1 and RH30 cell lines. Twenty nine genes that promote the cell cycle and cell proliferation were significantly down-regulated (**Table 3.3**) (*BIRC5, BRCA1, BRCA2, CALM, CAPRINI, CCNB1, CCND1, CCND3, CCNDE1, CDCA3, CDC7, CDC25A, CDC25B, CDC25C, CDK2, CDK4, CDK5, CDKN2C, CHK1, CHK2,C-MYC, ID3, MCM3, MSH2, PCNA, RB, RBBP4, SKP2* and *TGFβ3*.

On the contrary, twenty-one genes that inhibit cell cycle progression and cell proliferation were significantly up-regulated in both human JR1 and RH30 cell lines (*AKT, ATM, ATR, BTG2, CASP3, CDK1, CDK6, ETS1, HES1, FOXO3, GADD45B, HUS1, ITGβ3, MDM2, NOTCH2, P15, P16, P21, PTEN*, *P53* and *VEGFA*) (**Table 3.4**). Since inhibition of *PAX3* gene expression in both human JR1 and RH30 caused significant inhibition of cell proliferation, it was important therefore, to identify the phases of the cell cycle at which cell growth was arrested. To clarify this, a flow cytometry analysis of the cell cycle was used to identify the phase at which cell growth was halted.

In both human JR1 and RH30 cell lines, repression of *PAX3* triggered a cell cycle blockade in the G1 phase at an early stage of *PAX3* knockdown with subsequent induction of apoptosis. In the G1/G0 phase of the cell cycle, 62.5% of JR1 and 70.3% of RH30 *PAX3* siRNA treated cells were located, compared to 42% of JR1 and 63.6% of RH30 control cells (**Figs. 3.24 and 3.25**). Concurrently, there was a percentage reduction of cells in S phase (**Table 3.8**). Repression of *PAX3* in the JR1 cell line decreased the population of cells in S and G2/M phases from 13.1% to 7.4%, whereas in the RH30 cell line the population in S phase decreased from 9.8% to 7.4% signifying

that *PAX3* silencing inhibited cell entry into S phase. Correspondingly, the decreased expression of S phase and G2 phase checkpoint genes (*CHK1, CHK2, CDC25A, CDC25B* and *CDC25C*) indicate that neither JR nor RH30 cells were halted in S or G2 phases of the cell cycle. There was a lower percentage of cells observed in S phase in the current study. This indicates that the cell proliferation rate was slower in *PAX3*-siRNA transfected cells than in the negative control cells, which correlates with the cell proliferation experiments.

Analysis of the cell cycle results demonstrating a significant high proportion of human JR1 and RH30 cells in the G1 phase of the cell cycle showed that silencing of *PAX3* caused a G1 phase cell cycle growth arrest. The microarray data suggest that *PAX3* repression induced increased expression of six genes promoting G1 phase cell cycle arrest (*ATM, ATR, BTG2, GADD45B, P21*, and *P53*). By contrast, the four positive regulatory genes of G1 phase of the cell cycle (*RB, CCND1, CDK2,* and *CCNE1*) had substantially decreased expression. Likewise, G1 phase cell cycle arrest in other cells has been associated with decreased expression of five key genes (*CCNA, CCND1, CCNE1, CDK2* and *CDK4*).

The significant decrease in the number of JR1 and RH30 cells observed in the cell proliferation assays (**Figs. 3.20, 3.21, 3.22** and **3.23**), does not only demonstrate inhibition of JR1 and RH30 cell proliferation, but also indicates induction of JR1 and RH30 cell apoptosis induced by *PAX3* knockdown, which was remarkably high at 96 hr transfection. The pattern of JR1 and RH30 cell proliferation resulting from apoptosis, correlates with increased expression of apoptosis inducing genes (**Table 3.4**) and decreased expression of apoptosis inhibitory genes (**Table 3.3**).

This present microarray data was further analysed to determine the effects of *PAX3* down-regulation on the different regulatory pathways in JR1 and RH30 cell lines using the David NIH functional annotational bioinformatics KEGG-pathway analysis tool version 6.7. The KEGG-pathway analysis of this present microarray data indicates that *PAX3* silencing triggered the *P53* signaling pathway to halt both JR1 and RH30 cell

cycle in G1 via activation of the ATM/ATR signaling pathways. Inhibition of *PAX3* in both JR1 and RH30 cell lines induced activation of the *ATM/ATR* signaling pathways, which in turn trigger the *P53* pathway (**Figs. 3.48 and 3.49**).

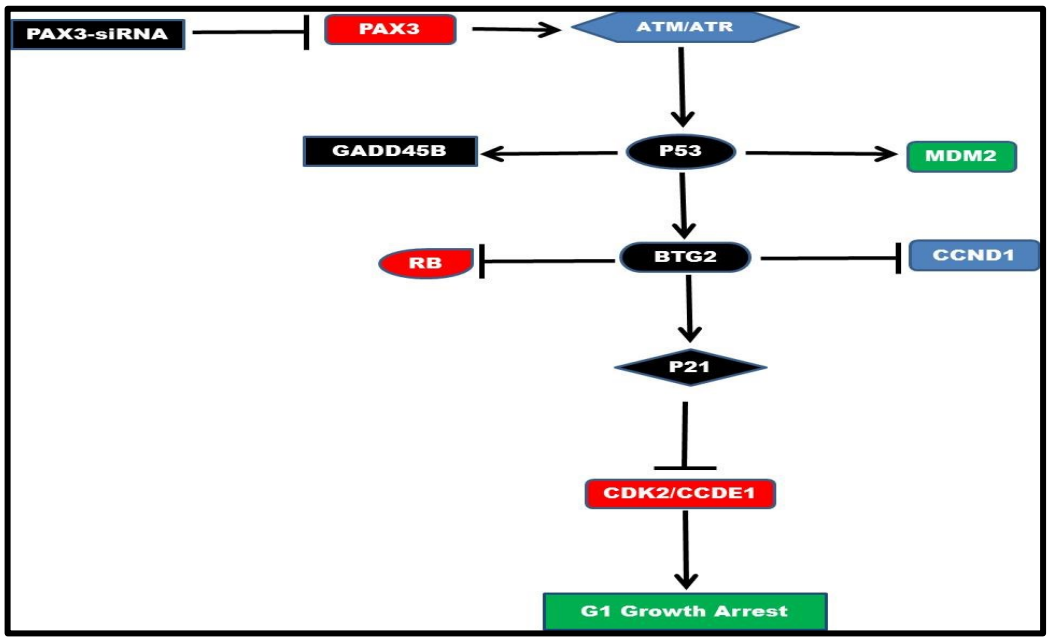

Figure 3.48 Schematic diagram of proposed induction of G1/S growth arrest induced by *PAX3* silencing in rhabdomyosarcoma. Activation of *ATM/ATR* by *PAX3*-siRNA knockdown induces the *P53* pathway. *BTG2* inhibits proliferation of both JR1 and RH30 cells by blocking the phosphorylation of *RB* and synthesis of CCND1. Activation of *P21* induces the blockage of synthesis of both CDK2 and CCDE1 to cause a G1 growth arrest.

Key: → Represents activation. ⊣ Designates inhibition/block

P53 activation of *BTG2* primarily induced the inhibition of *CCND1* and phosphorylation of *RB,* resulting in inhibition of JR1 and RH30 cell proliferation. Subsequently, *BTG2* activation of *P21* induced inhibition of *CDK2* and *CCDE1* to halt the JR1 and RH30 cell growth arrest at the G1 phase of the cell cycle. The microarray data showed increases in *BTG2* and *P53* after *PAX3* siRNA knockdown, which agrees with western blotting showing two equally large amounts of *P53* and phosphorylated *P53*. This leads to the activation of *P21* demonstrated by both microarray and western blotting with a consequential G1 phase cell cycle growth arrest. Likewise, the current microarray data supports the pattern of results seen in the inhibition of both JR1 and RH30 cell

proliferation and cell cycle (**Figs. 3.20-3.23**). This present study strongly suggests that inhibition of *PAX3* activity, as a potential target would perhaps be a promising avenue for developing a therapeutic regimen to effectively inhibit rhabdomyosarcoma tumour progression and growth.

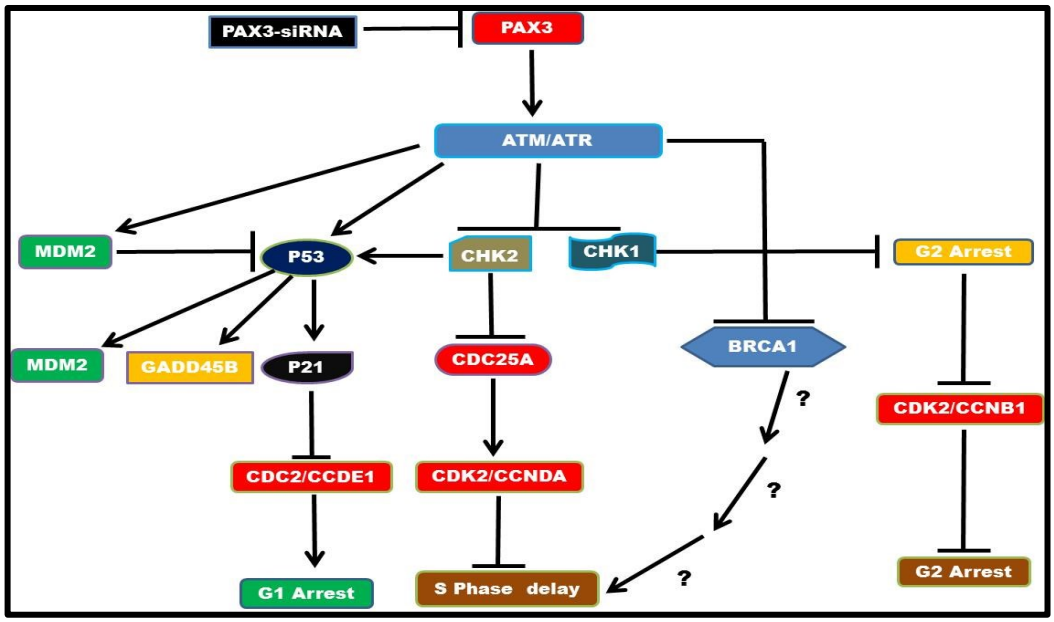

Figure 3.49 *PAX3* silencing modulates the main cell cycle checkpoint effectors of G1, G2 and S phases to halt progression of the cell cycle. *PAX3*-siRNA knockdown activates the *ATM/ATR* pathway to induce the activation of *P53* and *P21*, inhibits CDC2/CCDE1 to halt G1 phase arrest. The activation of *ATM/ATR* pathway also prevents the occurrence of cell growth arrest in both S and G2 phases of the cell cycle. Inhibition of the cell cycle checkpoint proteins CHK2 blocked CDC25A to activate CDK2 and CCNDA, promoting the progression of JR1 and RH30 cells into the S phase of the cells cycle. Likewise, inhibition of *BRCA1* by *ATM/ATR* may perhaps induce entry of cells into S phase through unknown mechanisms. Additionally, *ATM/ATR* inhibition of CHK2 directly allows JR1 and RH30 cell progression into G2 phase or indirectly inhibits CDK2 and CCNB1 to allow cell growth at the G2 phase of the cell cycle.

Key: → Denotes activation. ⊣ Signifies inhibition/block.

Question marks (**?**) indicate unclear mechanisms.

Comparatively, the outcome of this current cell cycle analysis demonstrating a G1 phase cell growth arrest, is in agreement with a related siRNA silencing of *PAX3* in neuroblastoma, in which cells were halted in G1 phase of the cell cycle after siRNA inhibition of *PAX3* in two neuroblastoma cell lines, whre a flow cytometry analysis

demonstrated that 61% of SH-SY5Y cells and 69% of SH-EP1 cells were arrested in G1 compared to 40% in control cells, whilst approximately 38% of SH-SY5Y cells and 33% SH-EP1 cells were observed in the S phase of the cell cycle (Fang *et al.,* 2013). *PAX3* knockdown in human neuroblastoma cell lines triggered cell cycle arrest followed by apoptosis. This indicates that *PAX3* re-expression in neuroblastoma might impair regulation of cell cycle checkpoints allowing tumour development, growth advantage and maintenance. Even though higher level of *PAX3* down-regulation in both human rhabdomyosarcoma JR1 and RH30 cell lines was observed in this present study, the pattern of *PAX3* repression was similar to *PAX3* inhibition and other downstream targets in neuroblastoma (Fang *et al.,* 2013).

3.13.3. Inhibition of Rhabdomyosarcoma Cell Metastasis

The intricate interactions between host stromal cells and tumour cells lead to the development of a tumour microenvironment, which subsequently contributes to tumour malignant characteristics, including increased cancer cell proliferation, angiogenesis, inflammation, invasiveness, metastasis, evasion of adaptive immunity and apoptosis (Suriyan *et al.,* 2012). The ECM is an important constituent of the tumour microenvironment that provides the physical microenvironment for the existence and maintenance of cells (He[2] *et al.,* 2013; Kucharzewska and Belting, 2013). It is a dense mixture of matrix molecules, comprising hyaluronan, glycoproteins, fibronectin, collagens, laminin, tenascin, vitronectin, proteoglycans, and growth factors (Gonzalez-Perez and Udina, 2013; Plantman, 2013. The ECM further transmits signals to cells, which alter cell proliferation, differentiation and apoptosis (Su[1] *et al.,* 2013). Adhesion of cell surface molecules to the ECM activates various intracellular signaling pathways to regulate progression of the cell cycle, growth, migration and differentiation (Campbell *et al.,* 2010). The most important feature of these metastatic processes is the alteration of tumour cell adhesive properties, mediated by variations in the expression of cell adhesion molecules (Jiang *et al.,* 2013).

3.13.3.1. Repression of *PAX3* Inhibits JR1 and RH30 Cell Migration *In Vitro*

This present investigation sought to ascertain whether *PAX3* affects the migration potential of rhabdomyosarcoma cells. Microarray analysis showed that silencing of *PAX3* in both JR1 and RH30 cells significantly decreased expression of eleven genes that positively regulate cell migration (*COL1A1, COL3A1, ENDRA, FNDC5, FSCNI, HCG, HMMR, MAP1A, MXRA7, MYO1B*, and *TGFβ3*) (**Table 3.3**). *PAX3* silencing on the other hand, induces increased expression of six other genes that negatively regulate cell migration (*H-RAS, KITL, RND3, ROCK2, VEGFA* and *ZEB2*) (**Table 3.4**).

Alteration of these genes may contribute negatively to inhibit cell migration. The pattern of alteration of gene expression shown in the microarray data correlates with the significant inhibition of cell migration demonstrated in the migration experiments (**Figs. 3.26-3.31**). Likewise, genes related to the promotion of myogenesis (*MYOD1* and *MYOG4*) as well as cell differentiation genes (*ADAM23* and *MAPA1*) were significantly down-regulated (**Table 3.3**).

In assessing the potential impact of *PAX3* expression on cell migration, the scratch cell migration wound-healing assay demonstrated significantly decreased *PAX3*-siRNA cell migration compare to negative control cells, which was monitored over 24 hr. This result demonstrates that the negative control cells with high expression of *PAX3* induced high migration of JR1 and RH30 cells across a demarcation line at the wound edges to close scratch wound gaps compare to initial wound gaps as indicated by the arrows. *PAX3* silencing in JR1 cell line induced significant inhibition of cell migration ($p < 0.01$) (**Figs. 3.26 and 3.29**). Likewise, inhibition of *PAX3* in RH30 cells significantly inhibited cell migration ($p < 0.01$) (**Figs. 3.26 and 3.29**).

The significant inhibition of cell migration (**Figs. 3.27, 3.28, 3.30 and 3.31**) observed, in which wider wound healing gaps remained after 96 hr inhibition of *PAX3*, is suggestive of induction of human JR1 and RH30 cell apoptosis as a result of *PAX3* knockdown. Since cells undergoing apoptosis lose their tumourigenic migration potential characteristics, they are unable to migrate, as demonstrated by broader wound gaps

remaining. Inhibition of JR1 and RH30 cell migration caused by apoptosis of JR1 and RH30 cells, relates to increased expression of apoptosis inducing genes (**Table 3.4**) and decreased expression of apoptosis inhibitory genes (**Table 3.3**).

In agreement with the above studies, David NIH bioinformatics database functional annotational tool version 6.7 analysis of this present microarray data in the KEGG-pathway indicate that *PAX3* repression inhibits cell migration possibly via activation of FAK/Rho/RAS/MAPK signaling pathways. Silencing *PAX3* in both JR1 and RH30 cells induced the activation of these signaling pathways. Induced activation of *VEGFA, ROCK2* and *RND3* caused inhibition of *TGFβ3*, *HMMR* and *FNDC5* with subsequent inhibition of cell migration (**Fig. 3.50**).

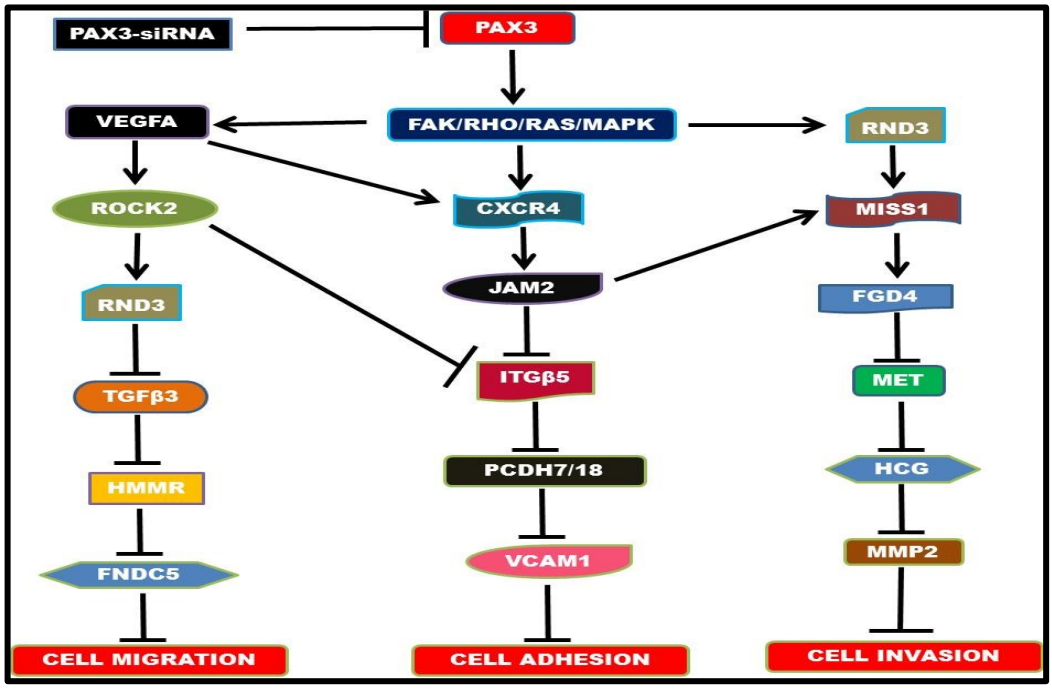

Figure 3.50 Schematic diagram of inhibition of JR1 and RH30 cell metastasis (derived from the KEGG-pathway analysis**.** Activation of the FAK/RHO/RAS/MAPK signaling pathways by *PAX3* repression stimulated the activation of *VEGFA*, with sequential activation of *ROCK2* and *RND3*, inducing inhibition of *TGFβ3, HMMR* and *FNDC5*, subsequently blocked migration of JR1 and RH30 cells. The successive activation of *CXCR4* and *JAM2* induced inhibition of *ITGβ5, PCDH7, PCDH18* and *VCAM1*, resulted in the inhibition of JR1 and RH30 cell attachment to the ECM. Knockdown of *PAX3* further induced progressive activation of *RND3* and *MISS1*, sequentially inhibited *FGD4, MET, HCG* and *MMP2*, induced blockage of JR1 and RH30 cell invasion.

Key: → Indicates activation. ⊣ Implies inhibition/block

These results strongly suggest that indeed *PAX3* expression plays a crucial role in promoting JR1 and RH30 cell migration during metastasis of rhabdomyosarcoma. Therefore, *PAX3* could be a suitable target for inhibiting rhabdomyosarcoma cell migration. Since cell migration involves cell adhesion to the ECM, this significant inhibition of rhabdomyosarcoma cell migration could imply impaired rhabdomyosarcoma cell adhesion to ECM proteins.

3.13.3.2. Knockdown of *PAX3* Inhibits JR1 and RH30 Cell Adhesion to the ECM

Cell adhesion plays a major role in metastatic invasion of rhabdomyosarcoma. Knockdown of *PAX3* in this present study, inhibited *NCAM* and ITGβ5 expression whilst up-regulating ITGβ1 in both human JR1 and RH30 cell lines.

The present microarray data established that the suppression of *PAX3* expression in both human JR1 and RH30 cells induced significant decreased expression of ten cell adhesion promoting genes (*FGD4, ICAM3, ITGβ5, LAMA1, NID1, PCDH7, PCDH18, SELPLG, VCAM1* and *VCAN*), which subsequently decreased JR1 and RH30 cell adhesion to ECM proteins *in vitro.* On the other hand, four cell adhesion inhibitory genes (*CXCR4, JAM2, RND3, ITGβ1* and *ROCK2*) were up-regulated when *PAX3* was inhibited. The changes in expression of these genes may negatively contribute to inhibit cell adhesion, especially the knockdown observed of the major cell surface adhesion molecules including *ICAM3, ITGβ5, LAMA1 VCAM1,* and *VCAN*. The influence of these cell adhesion regulatory proteins on JR1 and RH30 cell adhesion potential was evaluated. Cell–matrix assays demonstrated that the *PAX3* repression in *PAX3*-siRNA cells, indeed induced significant inhibition of JR1 ($p < 0.01$) and RH30 cell adhesion ($p < 0.01$) to seven selected ECM proteins (Collagen I, Collagen II, Collagen IV, Fibronectin, Laminin, Tenascin and Vitronectin) as shown in (**Fig. 3.32 and 3.33**). By contrast, high *PAX3* expression in NC-siRNA cells showed enhanced JR1 and RH30 cell adhesion to the various ECM proteins. The pattern of inhibition of cell adhesion to the various ECM proteins relates to the results of the microarray analysis showing knockdown of expression of cell adhesion regulatory genes (**Table 3.3**).

Microarray analysis suggests that reduced *PAX3* expression may perhaps decrease cell adhesion to ECM proteins through activation of the FAK/Rho/RAS/MAPK signaling pathway, since the major cell surface ECM receptors, including integrins are known to signal through the FAK signaling pathway (Han *et al.,* 2013). Knockdown of *PAX3* in both JR1 and RH30 cell lines cells activated the FAK/Rho/RAS/MAPK signaling pathway. The activation of *CXCR4* and *JAM2*, inhibiting *ITGβ5, PCDH7, PCDH18* and *VCAM1,* subsequently inhibits JR1 and RH30 cell adhesion to ECM proteins (see earlier **Fig.3.50**).

The present cell adhesion results established that *PAX3* could be an appropriate target for blocking rhabdomyosarcoma cell adhesion with consequential inhibition of tumour metastasis. Because a decreased interaction between cells and the ECM may alter cell functions, this significant inhibition of rhabdomyosarcoma cells to ECM proteins may impair tumour cell invasion.

3.13.3.3. Down-regulation of *PAX3* Blocked JR1 and RH30 Cell Invasion *In Vitro*

The functional involvement of *PAX3* in JR1 and RH30 cell metastasis was determined. Invasion of cells through the ECM is a critical step in tumour metastasis (Kikuchi *et al.,* 2013). Following migration and adhesion of cells to the ECM, the proteolytic activity of proteases then results in basement membrane degradation to allow invasion by malignant cells (Nowak *et al*., 2013; Sun[2] *et al.,* 2013).

In the present study, microarray analysis data demonstrated significantly decreased expression of six cell invasion promoting genes (*MMP2, RECK, MET*, *SMAD2, FGD4* and *HCG*), shown in **Table 3.3**. The expression of two cell invasion inhibitory genes was significantly increased (*RND3* and *MISS1*) (**Table 3.4**). The changes in expression of these genes may contribute negatively to inhibit cell invasion in cells with repressed *PAX3*.

In determining what effects these genes might have on JR1 and RH30 cell invasive potential, the Boyden chamber invasion analysis showed that *PAX3*-siRNA JR1 treated

cells had weak invasion potential, with significantly fewer cells than controls invading the ECM ($p < 0.01$), (**Figs**. **3.34** and **3.35**). Similarly, *PAX3*-siRNA RH30 treated cells had weak invasion potential, demonstrated by substantially fewer cells than controls invading the ECM ($p < 0.01$), (**Figs. 3.36** and **3.37**). This inhibition of ECM cell invasion correlates with the microarray data showing reduced expression of cell invasion promoting genes (**Table 3.3**). These results suggest that *PAX3* expression certainly promotes JR1 and RH30 cell invasive capacity. *PAX3* knockdown in *PAX3*-siRNA cells, also decreased expression of proteases, especially *MMP2,* which additionally decreased the invasion potential (Roomi *et al.,* 2013).

The current microarray data in David NIH bioinformatics database functional annotational tool KEGG-pathway analysis, imply that *PAX3* suppression in both JR1 and RH30 cell lines probably inhibits cell metastasis through activation of the FAK/RHO/RAS/MAPK signaling pathways. Silencing of *PAX3* activated the FAK/RHO/RAS/MAPK signaling pathways (see earlier **Fig. 3.50**). Activation of *RND3* and *MISS1* inhibited *FGD4, MET, HCG* and *MMP2* and blocked ECM invasion by JR1 and RH30 cell. Taken together, these findings strongly demonstrate that the above cell migration, adhesion and invasion regulatory genes are transcriptional targets of *PAX3* and affect metastasis. Since repression of *PAX3* in this study resulted in a consecutive inhibition of cell migration, adhesion and invasion, this suggests a suppression of rhabdomyosarcoma cell metastasis. Therefore, inhibition of *PAX3* as a tractable metastatic target could be an ideal therapeutic intervention in rhabdomyosarcoma. In brief, *PAX3* silencing inhibited the multiple steps involved in tumour metastasis, particularly proteins and pathways that determine the invasive potential of cells.

3.13.4. Effect of Repression of *PAX3* on Clonogenicity of JR1 and RH30 Cells

Accumulation of several genetic mutations that result in neoplastic transformation, permits uncontrolled cell proliferation and growth independent of normal homeostatic regulation (Bu *et al.,* 2013). Furthermore, up or down regulation of several genes can induce transformation of cells under unfavourable growth conditions (Gacche and Meshram, 2013).

The present investigation examined whether *PAX3* expression in rhabdomyosarcoma could induce transformation of JR1 and RH30 cell lines *in vitro*. In this present microarray analysis, silencing of *PAX3* expression in both JR1 and RH30 cell lines repressed two cell transformation-promoting genes, (*DCA7* and *TGFβ3*) (**Table 3.3**). However, the expression of five genes inhibiting cell transformation (H-*RAS, MYC, NDRG1*, *P21* and *P53*) was significantly increased (**Table 3.4**). Changes in the expression of these genes may directly or indirectly interfere with cell clonogenesity.

PAX3 colony reproducibility capacity was evaluated using the soft agar anchorage-independent growth assay for JR1 and RH30 cell lines. *PAX3*-siRNA JR1 cells showed no colony formation. RH30 cells produced a few small non-growing aggregates apoptotic cell (based on manufacturer's literature). On the contrary, NC-siRNA negative control cells with high *PAX3* expression demonstrated significant cell growth producing large colonies of both JR1 cells (**Figs. 3.38** and **3.39**) ($p < 0.01$) and RH30 cells (**Figs. 3.40** and **3.41**) ($p < 0.01$).

The pattern of inhibition of reproducibile colonies of human JR1 and RH30 cell lines, observed in *PAX3*-siRNA transfected cells (**Figs. 3.38 and 3.40**), indicates induction of cell apoptosis. This suggests that 96 hr knockdown of *PAX3* resulted in apoptosis of JR1 and RH30 cells, thereby, blocking their survival. Supression of colonal reproducibility in JR1 and RH30 cell induced by apoptosis, agree with the pattern of increased expression of apoptosis inducing genes (**Table 3.4**) and decreased expression of apoptosis inhibitory genes (**Table 3.3**).

The microarray results of David NIH functional annotation KEGG-pathway analysis presented here demonstrate that *PAX3* silencing probably inhibits the colony reproducibility of JR1 and RH30 cells *in vitro* by activating the RAS signaling pathway (**Fig.3.51**).

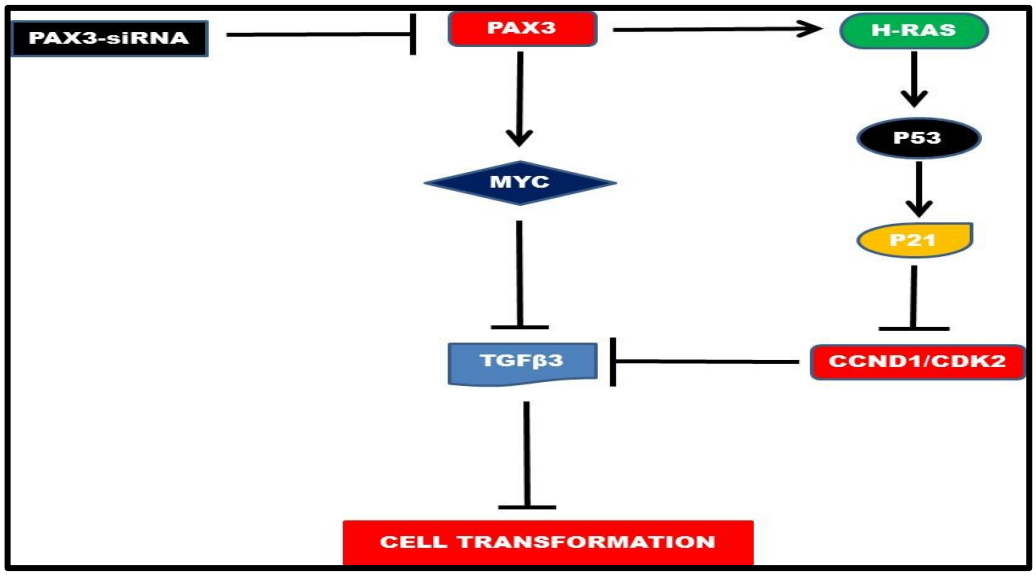

Figure 3.51 Schematic diagram of inhibition of JR1 and RH30 colony reproducibility (originated from the KEGG-pathway analysis)**.** Induced expression of *MYC* by *PAX3* silencing blocked *TGFβ3* to cause inhibition of JR1 and RH30 colony formation. Activation of *H-RAS*, *P53* and *P21* by *PAX3* repression induced blockage of *CCND1* and *CDK2* to block *TGFβ3* then inhibited JR1 and RH30 reproducible colonies.
Key: → Stand for activation. ⊣ Symbolizes inhibition/block

Down-regulation of *PAX3* primarily induced activation of *MYC* to inhibit *TGFβ3,* resulting in a block to JR1 and RH30 colony formation. Activation of *H-RAS* by *PAX3* silencing in this present study activated *P53* and *P21* to inhibit CCND1 and CDK2, which in turn inhibited *TGFβ3* to block JR1 and RH30 colony reproducibility. This finding indicates that *PAX3* is an appropriate target for the development of effective therapeutic agents to inhibit rhabdomyosarcoma clonogenesity.

3.13.5. Down-regulation of *PAX3* Induced JR1 and RH30 Cell Apoptosis *In Vitro*

Apoptosis is a highly regulated mechanism of programmed cell death that is essential in embryogenesis, maintenance of cellular and tissue homeostasis and host defence in multicellular organisms and is required for autodestruction of damaged and abnormal cells (Fuchs and Steller, 2011). Cells die in response to a variety of stimuli and during apoptosis, they do so in a controlled regulated fashion (Fietta, 2006). Defective apoptotic process is implicated in various diseases including cancer, and autoimmune disorders, neurodegenerative diseases and ischemic injuries (Fuchs and Steller, 2011).

Different cell types are triggered to undergo apoptosis through extracellular or intracellular signals (Galluzzi, *et al.,* 2012; Gholami *et al.,* 2013). Apoptotic cells exhibit a series of characteristic morphological changes, including plasma membrane blebbing, cell shrinkage and formation of membrane-bound apoptotic bodies, which are engulf by neighbouring healthy cells (Gholami *et al.,* 2013). Thus, during apoptosis, intracellular contents are not released, thus prevent potentially harmful inflammatory responses. Apoptosis is accompanied by certain biochemical changes including cleavage of various cellular proteins (Gholami *et al.,* 2013).

The microarray data of this present study show that five anti-apoptotic genes that negatively regulate apoptosis were down-regulated (*BCL2, CYB5B, FAIM, TMBIM4* and *TUBB2*) in *PAX3*- siRNA treated cells (**Table 3.3**). Fourteen genes that positively regulate apoptosis are up-regulated when *PAX3* is knocked down (*AEN, AKT, BNIP3, CASP3, CASP4, DAXX, GADD45B, KITL, MCL1, SMEK1, P53, PTEN, SENP5* and *TRIB3C*) (**Table 3.4**). The genes could have a potential role in inducing apoptosis of rhabdomyosarcoma cells.

An indirect biochemical apoptosis index analysis that has been used in previous studies (Zhang[1]*et al.,* 2013), was used in this present study to demonstrate that silencing *PAX3* can induce apoptosis in JR1 and RH30 cells. **Fig. 3.42A** shows a positive control for apoptosis in JR1 cells. Caspase 3/7 activity was higher in *PAX3*-siRNA treated JR1 cells than in NC-siRNA JR1 cells, which showed little caspase 3/7 activity ($p < 0.01$) (**Figs. 3.42B** and **3.42C**). Likewise, *PAX3*-siRNA treated RH30 cells showed a significant increase in caspase 3/7 activity compared with NC-siRNA treasted RH30 cells having insignificant caspase 3/7 activity ($p < 0.01$) (**Figs. 3.43B** and **3.43C**). A positive control for apoptosis in RH30 cells is shown in **Fig. 3.43A.** This result implies that *PAX3* silencing induced an early apoptosis of both JR1 and RH30 cells *in vitro* compared with controls (Scabini *et al*., 2011). Since non-apoptotic cells show a small but detectable level of caspase 3/7 activity, the morphological features of apoptosis were demonstrated to confirm the increased caspase 3/7 activity observed in JR1 and RH30 cells following *PAX3* silencing (**Figs. 3.44** and **3.46**). Induction of a persistent and prolonged apoptosis of tumours is a hallmark for the treatment and management of

cancer patients with combination therapeutic regimens (Abdelghany *et al.,* 2011; Marchal *et al.,* 2013; Waters *et al.,* 2013).

The findings of this present represent the first attempt to demonstrate that silencing of *PAX3* followed by a therapeutic regimen, for example staurosporine, could produce sustained apoptosis in rhabdomyosarcoma.

This study established the induction of late apoptosis of JR1 and RH30 cells indicated by fragmentated apoptotic nuclei in both *PAX3*-siRNA and staurosporine (1µM/ml; 1µl/ml) treatment **(Figs. 3.44** and **3.46**). The observed enhanced apoptotic DNA nuclie fragmentation in *PAX3*-siRNA and staurosporine (1µM/ml; 1µl/ml) combined treatment compared to either staurosporine or *PAX3*-siRNA alone, demonstrates the efficacy of a combine therapeutic regimen in the treatment of cancer. In the JR1 cell line, the combination treatment of *PAX3*-siRNA followed by staurosporine (*PAX3*-siRNA-PC) demonstrated significantly higher numbers of apoptotic nuclei induced ($p < 0.01$) **(Figs. 3.44** and **3.45**). Likewise, a significantly higher number of induced apoptotic nuclei of RH30 cells was observed after combined *PAX3*-siRNA and staurosporine treatment (*PAX3*-siRNA-PC) ($p < 0.01$) (**Figs. 3.46** and **3.47**). By contrast, NC-siRNA transfection of both JR1 and RH30 cells failed to induce apoptosis since these cells showed DAPI stained blue nuclei but no green fluorescent apoptotic nuclei (DNA fragmentation) **(Figs. 3.44** and **3.45**) and (**Figs. 3.46** and **3.47**).

This present study showed that *PAX3* expression is essential for prevention of apoptosis and the survival of human rhabdomyosarcoma cells. For instance, the induction of JR1 and RH30 cell apoptosis following *PAX3* knockdown, resulted in marked inhibition of cell proliferation and cell cycle. Increased P53 expression inhibited proliferation of JR1 and RH30 cells, whilst increased P21 expression halted their cell cycle and a decreased BCL2 expression resulted in apoptosis of JR1 and RH30 cells. This was confirmed by the significant reduction in the number of proliferating JR1 and RH30 cells (**Figs. 3.20, 3.21, 3.22** and **3.23**) after 96 hr knockdown of *PAX3*. Furthermore, the observed presence of cells in the sub-G1 phase of the cell cycle (**Figs. 3.24 and 3.25**) and the

increased P21 expression, was suggestive of cell apoptosis. Significant inhibition of migration and colony reproducibility of JR1 and RH30 cells induced by apoptosis, also correlates with increased expression of apoptosis inducing genes (**Table 3.4**) and decreased expression of apoptosis inhibitory genes (**Table 3.3**).

Following 96 hr *PAX3* knockdown in JR1 and RH30 cell lines with subsequent induction of JR1 and RH30 cell apoptosis, resulted in remarkable inhibition of proliferation of JR1 and RH30 cells (Figs. **3.20, 3.21, 3.22 and 3.23**). The induction of JR1 and RH30 cell apoptosis led to wider wound healing gaps as dead cells failed to migrate (**Figs. 3.27 and 3.30**). Similarly, a significant inhibition of reproducibility of JR1 and RH30 cell colony formation, was induced by apoptosis of transformed JR1 and RH30 cells (**Figs. 3.38 and 3.40**). This significant effects of apoptosis on the tumourigenic activities of JR1 and RH30 cell lines, confirmed the pattern of increased expression of apoptosis promoting genes (**Fig. 3.4**) and decreased expression of apoptosis inhibiting genes (**Fig. 3.3**), proved induction of JR1 and RH30 cell apoptosis as shown by the presence of apoptotic morphologic features (**Fig. 3.44 and 3.46**).

Taken together, in support of this current investigation of apoptosis, the functional annotational KEGG-pathway analysis of the microarray data in the David NIH bioinformatics tool database, suggests that inhibition of *PAX3* expression might induce apoptosis through both the mitochondrial apoptotic pathway of caspase activation and the P53-dependent apoptotic pathway via the Bcl-2 family. In the KEGG-pathway analysis, P*AX3* silencing caused mitochondrial release of cytochrome C, which subsequently induced caspase activation and resulted in cell apoptosis (**Fig. 3.52**). Likewise, the direct activation of *P53* after *PAX3* silencing, either induced activation of caspase 3 or directly blocked *BCL2* expression or activated *BAX* expression to block *BCL2,* resulting in cell apoptosis (**Fig. 3.52**). Interestingly, *PAX3* silencing induced increased expression of its binding partiner, *PTEN*, which activated expression of *BAX* to induce a block of *BCL2* expression, resulting in cell apoptosis (**Fig. 3.52**). This study strongly demonstrates that targeting *PAX3* in a combination treatment, probably could

enhance and sustain apoptosis for effective treatment and management of rhabdomyosarcoma.

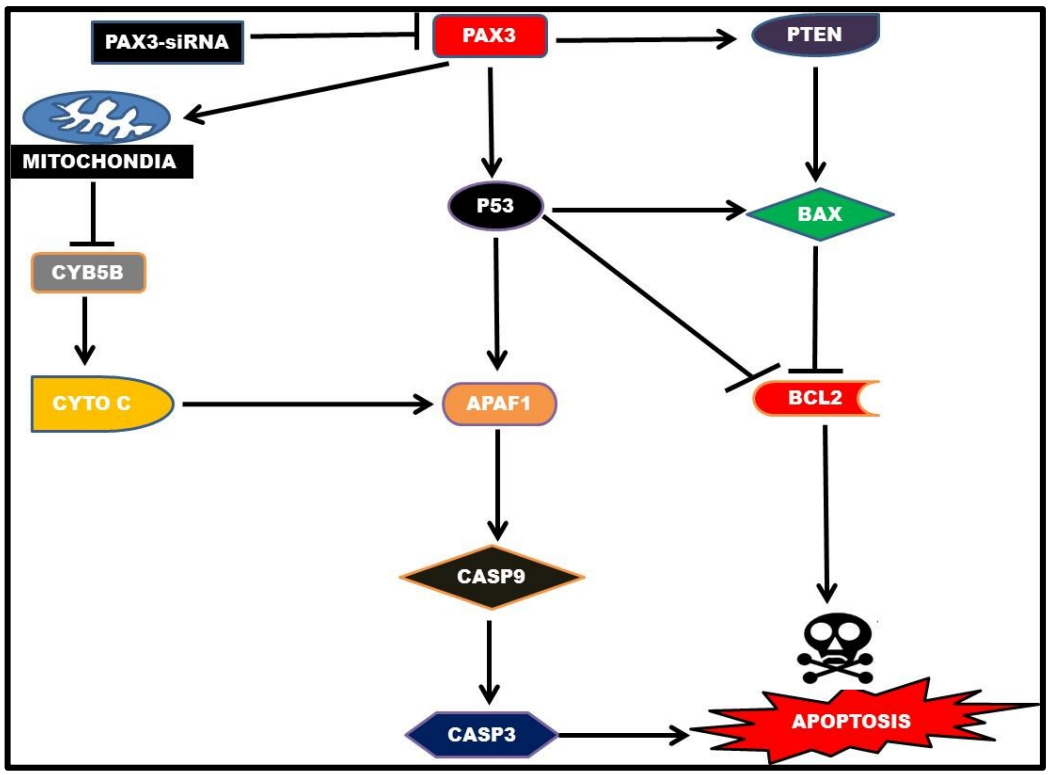

Figure 3.52 Schematic diagram of induction of JR1 and RH30 cell apoptosis. Suppression of *PAX3* principally induced successive activation of *P53, APAF1, CASP9* and C*ASP3* to induce apoptosis via the P53 pathway. Inhibition of *PAX3* partly induced mitochondrial membrane blockage of *CYB5B* and induced the activation of CYTO C to induce apoptosis through caspase activation via the activation of A*PAF1*. Suppression of *PAX3* activated the apoptosis repressor *PTEN,* which in turn activated *BAX and* blocked *BCL2* to induce apoptosis.

Key: → Indicate activation. ⊣ Show inhibition/block

In summary, these findings demonstrate that the re-expression of *PAX3* as an embryonic morphogenic developmental transcription factor, following embryonic development, plays a pivotal role in the onset and regulation of the oncogenic potential of rhabdomyosarcoma. Undoubtedly, this current study strongly supports the various previous studies implicating *PAX3* in the development of rhabdomyosarcoma. Apparently, the crucial transcriptional and cellular functional roles of *PAX3* during embryonic development, which include regulation of cell cycle and proliferation,

migration, adhesion and cell survival, have been used repeatedly in rhabdomyosarcoma. These oncogenic mechanisms of *PAX3* activities were demonstrated by comparing the negative control cells with high *PAX3* activity with *PAX3*-siRNA cells having decreased *PAX3* activity. This present study demonstrates that re-expression of *PAX3* is essential for the development of rhabdomyosarcoma.

CHAPTER 4

INHIBITION OF *PAX3* IN A HUMAN MALIGNANT MELANOMA CELL LINE

CHAPTER 4. siRNA INHIBITION OF *PAX3* IN A HUMAN MALIGNANT MELANOMA CELL LINE

Expression of *PAX3* in maglignant melanoma play a crucial role progressing cellular tumourigenic activity of melanoma and interruption of *PAX3* in human A375 melanoma cell line *in vitro*, may suppress melanoma.

4. Results

4.1. Morphological Characteristics of the Human Malignant A375 Melanoma Cell Line

Transient transfection of the A375 melanoma cell line with non-targeting siRNA negative control (NC-siRNA) or pre-designed siRNA targeting *PAX3* (*PAX3*-siRNA) aimed at suppressing *PAX3* mRNA expression, presented variable morphological alterations. The NC-siRNA transfected A375 cells showed thin, intact, well-defined cell borders (**Fig. 4.1**). In contrast, *PAX3*-siRNA treated A375 cells appeared thicker, with irregular thick cell borders and attachment of deep brownish transfection-complexes to cell surfaces (**Fig. 4.1**) (according to the manufacturer's transfection literature).

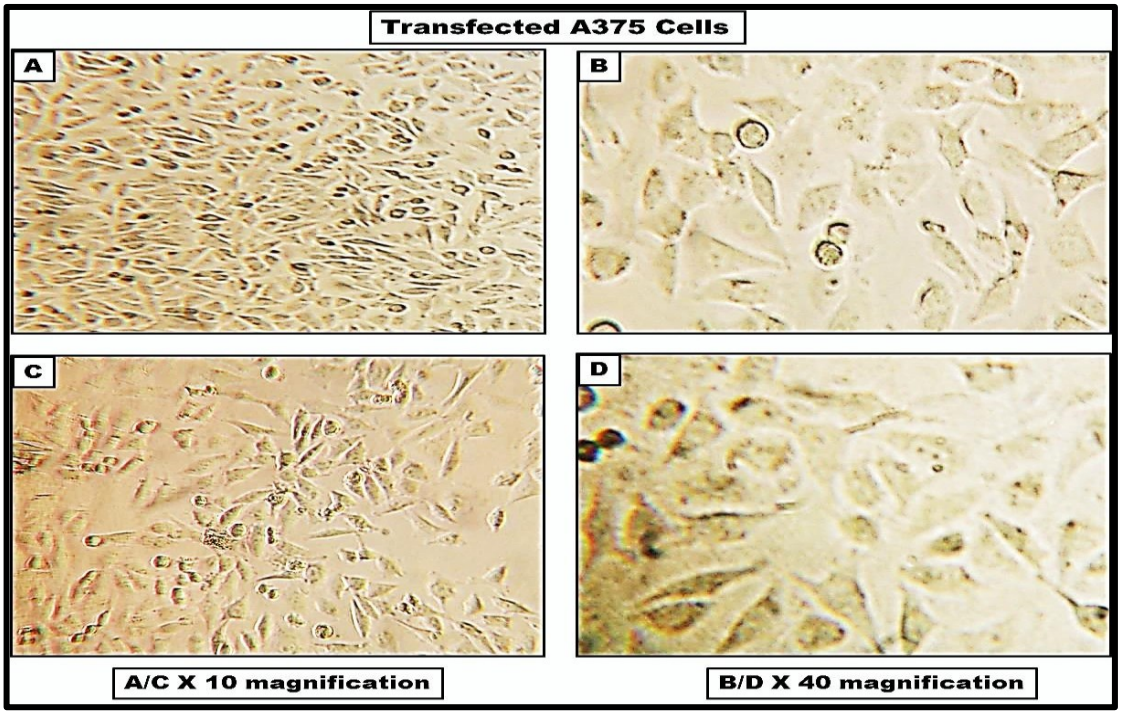

Figure 4.1 Phase contrast micrograph showing representative morphology of A375 cells following 96 hr siRNA treatment (**A, B**) NC-siRNA transfected A375 cells. (**C, D**) *PAX3*-siRNA transfected A375cells. A/C, X 10 magnification and B/D, X 40 magnification.

4.2. Inhibition of *PAX3* Gene Expression in the A375 melanoma Cell Line

Table 4.1 Extracted total RNA purity and concentration

Sample	OD 260nm	OD 280nm	OD Ratio 260/280	RNA(µg/µl)
A375	-	-	-	-
C	0.568	0.303	1.9	5.68
T	0.468	0.261	1.8	4.68

OD: Designates absorbance of extracted total RNA, where 260nm values verifies the concentration of extracted RNA and 280nm values indicates purity of extracted RNA. High 260nm OD values indicates contamination of RNA with protein, peptides, carbohydrate, aromatic compounds and phenol. The ratio $OD_{260/280}$ indicates the degree of RNA purity (the range of RNA ratio value is between (1.6 - 2.0)**.**

C: Representative OD of NC-siRNA indicating the purity and concentration of total RNA.
T: Representative OD of *PAX3*-siRNA signifying the purity and concentration of total RNA.

Analysis of *PAX3* gene expression in the A375 cell line pre-transfection demonstrates expression levels of the seven *PAX3* isoforms. Human *S14* ribosomal mRNA was used as a measure of the amount of mRNA in each sample (**Fig. 4.2**). *PAX3a* and *PAX3g* were weakly expressed in the A375 cell lines. This study revealed that *PAX3a* is more highly expressed in the rhabdomyosarcoma cell lines (**Fig. 3.2**) than in the A375 melanoma cell line, which demonstrates high expression levels of *PAX3b* in contrast to its low level in rhabdomyosarcoma cell lines.

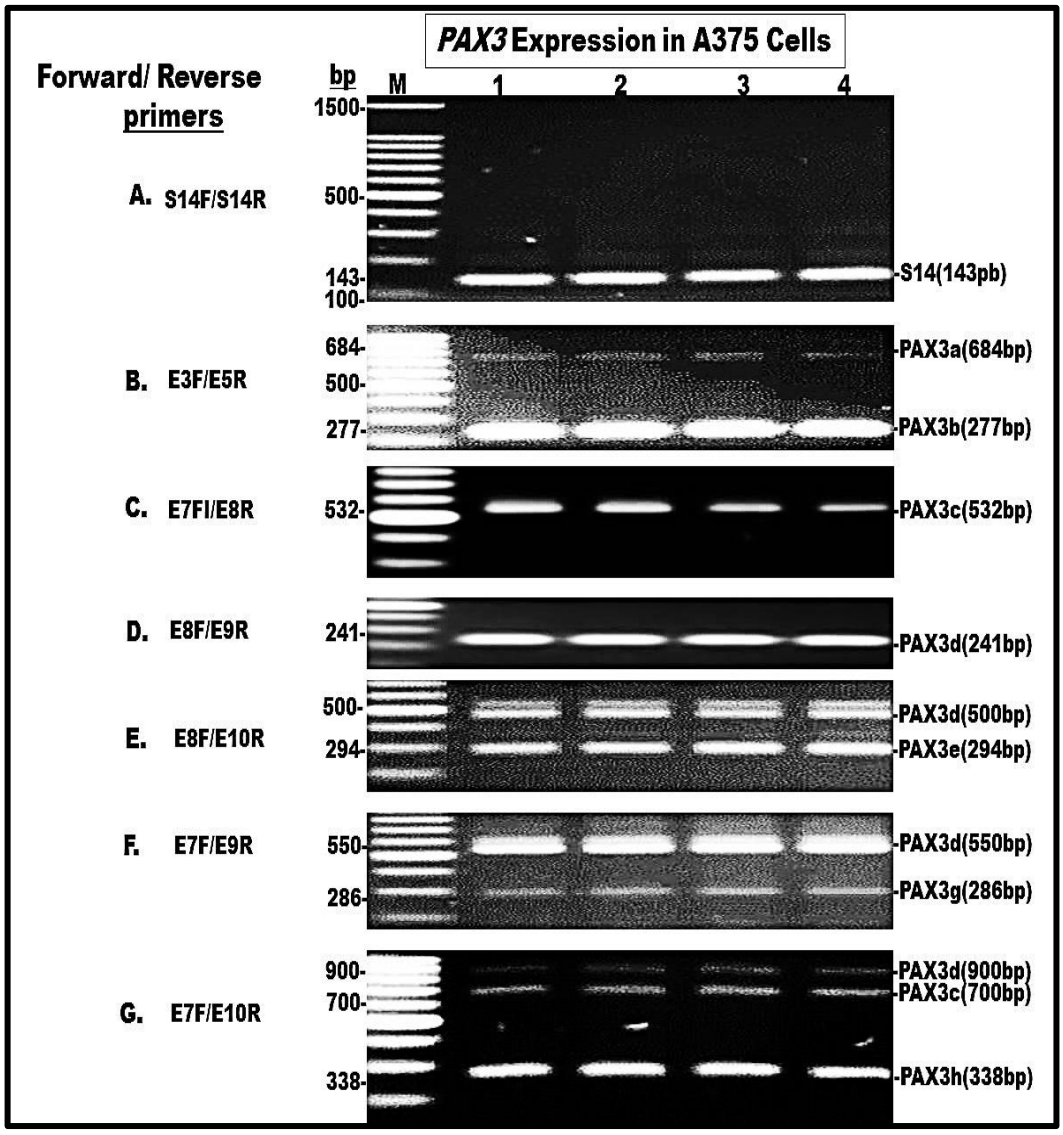

Figure 4.2 Semi-quantitative RT-PCR analysis of *PAX3* mRNA expression pattern in non-transfected A375 cells on a 1.5% agarose gel to verify base line of *PAX3* gene expression. Lane M: 100bp benchtop DNA Marker (100-1500bp); Lanes 1-4: replicate *PAX3* mRNA expression in non-transfected A375 cells. (**A**) S14F/S14/R primer amplification of S14 human ribosomal protein mRNA; (**B**) E3F/E5R primer amplification of *PAX3a* and *PAX3b;* (**C**) E7F/I8R primer amplification of *PAX3c*; (**D**) E8F/I9R primer amplification of *PAX3d; (**E**)* E8F/10R primer amplification of *PAX3e* and *PAX3d;* (**F**) E7F/I9R primer amplification of *PAX3g* and *PAX3d;* (**G**) E7F/I10R primer amplification of *PAX3h, PAX3c* and faintly *PAX3d* respectively.

To assess the degree of inhibition of *PAX3* resulting from siRNA treatment, the mean *PAX3* gene expression in A375 cells transfected with *PAX3*-siRNA was compared with the mean expression of *PAX3* in A375 cells treated with NC-siRNA. Semi-quantitative RT-PCR analysis indicated that the human ribosomal RNA *S14* housekeeping gene, used

as an internal normalization control, showed no change of gene expression whether treated with *PAX3*-siRNA or NC-siRNA. High levels of down-regulation of *PAX3* in the *PAX3*-siRNA treated A375 cells (lanes 6, 7 and 8 of **Fig. 4.3**) was evident without corresponding gene inhibitory effects in the NC-siRNA treated A375 cells (lanes 3, 4and 5 of **Fig. 4.3**) when compared with *PAX3* in untreated A375 cells (lane 1 of **Fig. 4.3**).

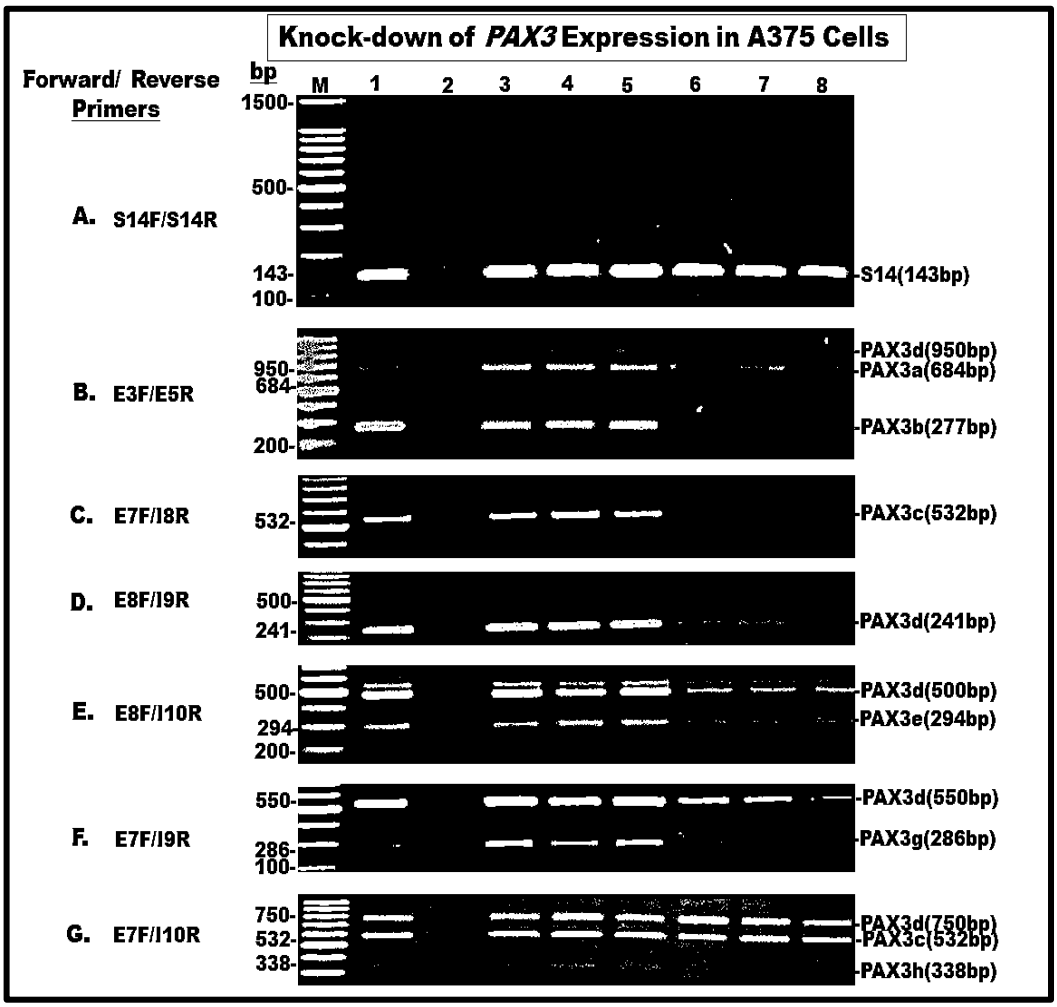

Figure 4.3 Semi-quantitative RT-PCR analysis of *PAX3* mRNA after 96 hr siRNA treatment in A375 cells. Lane M: 100bp benchtop DNA Marker (100-1500bp); Lane 1: A375 control PCR cells; Lane 2: Non-template negative control PCR (no DNA); Lanes 3-5: Triplicate NC-siRNA treated negative control; Lanes 6-8: Triplicate *PAX3*-siRNA treated. (A) S14F/S14/R primer amplification of *S14* human ribosomal RNA as an internal normalization control; (B) E3F/E5R primer amplification of *PAX3a* and *PAX3b*; (C) E7F/I8R primer amplification of *PAX3c;* (D) E8F/I9R primer amplification of *PAX3d*; (E) E8F/10R primer amplification of *PAX3e* and *PAX3d;* (F) E7F/I9R primer amplification of *PAX3g* and *PAX3d;* (G) E7F/I10R primer amplification of *PAX3d; PAX3c* and *PAX3h*.

The knockdown of *PAX3c* and *PAX3d* expression in the above figure, was determined using the primer combination in **C** (**E8F/I8R**) and **D** (**E8F/I10R**), which only amplify *PAX3c* and *PAX3d* respectively. There was considerably decreased gene expression, (approximately 90% knockdown) in all *PAX3* isoforms after *PAX3*-siRNA transfection in A375 cells. The residual gene expressions were; *PAX3a* (7%); *PAX3b* (4%); *PAX3c* (8%); *PAX3d* (10%); *PAX3e* (10%); *PAX3g* (9%) and *PAX3h* (8%). The reduced *PAX3* mRNA expression in *PAX3*-siRNA treated cells was significantly different ($p < 0.01$) from the high expression of *PAX3* in NC-siRNA treated cells (**Fig. 4.4**).

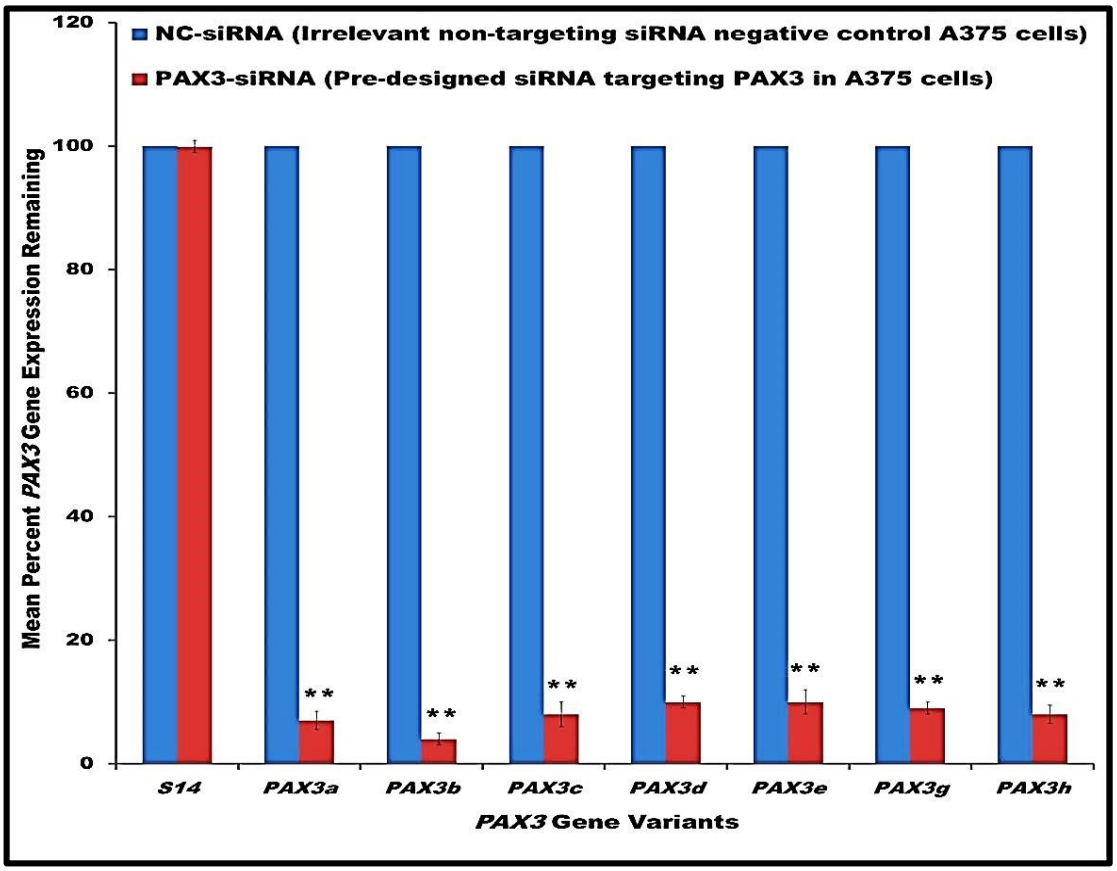

Figure 4.4 Mean percentages of *PAX3* isoforms remaining following 96 hr siRNA treatment. The mean *PAX3* gene expression in NC-siRNA transfected A375 cells (blue columns) was compared with the mean *PAX* gene expression in *PAX3*-siRNA transfected A375 cells (red columns). The mean values were derived from triplicate measurements in each of three separate experiments (n = 9). The difference between red and blue columns for each isoform was statistically significant (Student's t-test **, $p < 0.01$).

4.3. Inhibitory Effects of *PAX3* Gene Expression on Potential Downstream Targets

High quality extracted RNA (data not shown) obtained from the A375 cell line (260/280 ratio 1.6-2.0) as well as the RNA concentrations (**Table 4.2**), was similar to the patterns of extracted RNA observed in JR1 and RH30 cell lines (**Figs. 3.9 and 3.10**)

Table 4.2 Concentration and rRNA fragment ratios of total RNA extracted from A375 cells

SAMPLES	siRNA TREATED CELLS	TOTAL RNA CONCENTRATION (ng/µl)	RNA RATIO (28s/18s)
1	A375 NC-siRNA	**346**	**1.9**
2	A375 NC-siRNA	**679**	**1.7**
3	A375 NC-siRNA	**545**	**2.0**
4	A375 *PAX3*-siRNA	**965**	**1.9**
5	A375 *PAX3*-siRNA	**1,379**	**2.0**
6	A375 *PAX3*-siRNA	**935**	**1.8**

Microarray data analysed using Affymetrix GCOS (V1.4) on the genechip, containing a 54,614 probe set, showed an 8.95-fold knockdown of *PAX3* in *PAX3*-siRNA treated A375 cells compared with *PAX3* in NC-siRNA treated cells (**Table 4.3**). The inhibition of *PAX3* in A375 cells resulted in the alteration of 8,520 genes (more than 1.5-fold), using the probability of positive log-ratio (PPLR < 0.1 or > 0.9). After normalization to the housekeeping gene *GAPDH*, the alteration of expression of these 8,520 genes in *PAX3*-siRNA and NC-siRNA treated cells was compared. Out of these genes, 6,220 were down-regulated following knockdown of *PAX3* expression, whilst 2,300 genes were up-regulated.

Tables 4.3-4.7 showed microarray analysis data of selected gene expression alteration patterns after 96 hr *PAX3*-siRNA knockdown of *PAX3* gene in A375 cell line. These genes were determined by the gene functional annotation tool DAVID NIH, version 2, to play an essential role in cell proliferation (P), cell cycle (CC), migration (M), adhesion (AD), differentiation (DF), development (D) or apoptosis (AP).

Values are means of three experiments expressed separately on a microarray. (n = 3), (**; $p < 0.01$), (Student's t-test). Important genes of interest including *PAX3* were selected from the microarray data for verification by qRT-PCR data analysis. Down-regulated genes (**Table 4.3**) that are essential in cell developmental processes such as proliferation, migration, differentiation and apoptosis were selected for verification by qRT-PCR data analysis under the same experimental conditions.

Table 4.3 Genes down-regulated in the A375 melanoma cell line following *PAX3* inhibition

A -1.50-fold change was used as the threshold for down-regulation of gene expression. The degree of gene down-regulation was denoted by distinct shades of colour. Deep blue: gene expression down-regulated more than 2 fold; light blue: gene expression down-regulated between 1.5-2 fold.

Gene Symbol	Gene description	Gene Function	Fold change
PAX3	**Paired Box 3**	D	-8.95
ADAM23	ADAM metallopeptidase domain 23	DF	-2.51
BCL2	B-Cell lymphoma 2	AP	-6.17
BNIP3	BCL2/adenovirus E1B19kDa interacting protein 3	AP	-4.17
CALM3	Calmodulin 3	P	-1.71
CAPRINI	Cell cycle associated protein 1	CC	-1.57
CCND2	Cyclin D2	CC	-1.62
CCND3	Cyclin D3	CC	-1.82
CDC25C	Cell division cycle 25 homolog C (S. pombe)	CC	-1.88
CDCA3	Cell cycle associated 3	CC, P	-1.80
CDK2	Cyclin-dependent Kinase 2	CC, P	-1.68
CDK4	Cyclin-dependent Kinase 4	CC, P	-3.04
CDK5	Cyclin-dependent kinase 5	CC	-1.61
CIB1	Calcium and integrin binding 1	M	-1.66
CITED2	Cbp/p300-interacting transactivator with Glu/Asp-rich carboxy-terminal domain,	P	-2.35
CDKN2C	Cyclin-dependent kinase inhibitor 2C (p18)	CC	-1.51
C-MYC	C-myc binding protein	P	-1.54
COL3A1	Collagen type III, alpha 1	AD, M	-72.08
CXCR4	Chemokine (C-X-C motif) receptor	AD, M	-11.87
FAIM	Fas apoptotic inhibitory molecule	AP	-1.95
FGD4	FYVE, Rho GEF and PH domain containing 4	AD, M	-1.65
FOXO1	Forkhead box O1	D, P	-2.82
FSCN1	Fascin homolog 1, actin binding protein	M	-1.86

Continued

GTSE1	G-2 and S-phase expressed 1	CC	-2.97
HES1	Hairy and enhancer of split 1	P	-4.25
ID3	Inhibitor of DNA binding 3	CC	-1.62
HUS1	Hus1 checkpoint homolog	P, M	-1.58
IGFβP3	Insulin-like growth factor binding protein 3	P	-5.00
IGFβP5	Insulin-like growth factor binding protein 5	P	-23.25
ITGβ5	Integrin beta 5	AD, M	-2.26
JAM2	Junctional adhesion molecule 2	AD	-12.24
LOC	Similar to C-Jun	P	-3.41
MCAM	Melanoma cell adhesion molecule	AD, M	-4.25
MITF	Microphthalmia associated transcription factor	D, P	-6.15
MKNK2	MAP kinase interacting serine/threonine kinase 2	P	-1.81
MMP2	Matrix metallopeptidase 2 A (pseudo)	M	-3.53
MXRA7	Matrix-remodelling associated 7	M	-1.73
MYOD1	Myogenic differentiation1	D	-2.42
MYOG4	Myogenin (myogenic factor 4)	D	-4.83
NDRG1	N-myc downstream regulated 1	P	-5.85
NID1	Nidogen 1	AD,M	-2.76
PCDH18	Proto cadherin 18	AD, M	-1.65
PCDH7	Proto cadherin 7	AD, M	-3.79
RECK	Reversion-inducing-cysteine-rich protein K	M	-2.00
RXA	Retinoid X receptor alpha	P	-1.56
SOSTDC1	Slerostin domain containing 1	P, D	-1.53
SMAD2	SMAD family member 2	P, M, D	-2.23
SOX10	Sex determining region-box 10	D, P	-2.23
TAZ	Tafazzin	P, D	-4.41
TBX18	T-box 18	CC, P	-1.50
TGFβ2	Transforming growth factor, beta 2	P, D	-7.26
TGFβ3	Transforming growth factor, beta 3	P, D	-3.11
TNFRSF19	Tumour necrosis factor receptor superfamily, member 19	AP	-3.90
TUBB2 C	Tubulin beta 2c	AP	-4.96
VCAN	Versican	AD, M	-3.31
VEGFA	Vascular endothelial growth factor A	P	-3.39

Similarly, up-regulated genes (**Table 4.4**) that are important in cell developmental processes including: proliferation, migration, differentiation and apoptosis were selected for verification by qRT-PCR data analysis under the same experimental conditions.

Table 4.4 Genes up-regulated in the A375 melanoma cell line following *PAX3* inhibition

A 1.50-fold change was used as the threshold for up-regulation of gene expression. The degree of gene up-regulation was denoted by different shades of colour. Red: gene expression up-regulated more than 2 fold; Orange: gene expression up-regulated 1.5-2 fold.

Gene symbol	Gene description	Gene function	Fold change
AEN	Apoptosis enhancing nuclease	AP	2.80
ANAPC5	Anaphase promoting complex subunit 5	CC	2.29
AKT	V-AKTmurine thymoma viral homolog 3 oncogene	P	2.52
BIRC5	Baculoviral IAP repeating containing 5 (survivin)	P	3.33
BRCA1	Breast cancer 1	P	1.92
BRCA2	Breast cancer 1	P	2.34
BUB1	Budding uninhibited by benzimidazoles 1	P	1.73
CASP3	Caspase 3, apoptosis-related cysteine peptidase	AP	2.53
CASP4	Caspase 4, apoptosis-related cysteine peptidase	AP	1.79
CASP7	Caspase 7, apoptosis-related cysteine peptidase	AP	2.23
CCNA2	Cyclin A2	CC	1.69
CDC25A	Cell division cyclin 25 homolog A	CC	3.20
CDC25B	Cell division cycle25 homolog B (S. pombe)	CC	3.53
CDC42SE1	CDC42 small effector 1	CC	1.55
CDH2	Cadherin 2, type 1 N-cadherin (neuronal)	D	1.65
CDK1	Cyclin-dependent kinase 1	CC	2.00
CDK6	Cyclin-dependent kinase 6	CC	2.02
CDKN1A	Cyclin-dependent kinase inhibitor 1A	CC	2.29
CHEK1	CHK1 checkpoint homolog (S. pombe)	CC	1.75
CHEK2	CHK2 checkpoint homolog (S. pombe)	CC	2.53
DHFR	Dihydrofolate reductase	P	2.20
E2F7	E2F transcription factor 7	P, CC	1.50
E2F8	E2F8 transcription factor 8	P, CC	1.57
EDN3	Endothelin 3	P	3.27
ENDRA	Endothelin receptor type A	M	3.26
ETS1	V-ETS erythroblastosis virus E26 oncogene	P	3.68
FNDC5	Fibronectin containing sub-unit 5	AD,M	2.40
GADDβ45	Growth arrest and DNA-damage-inducible, beta	CC, P	5.59
GINS1	GINS complex subunit 1(Psf1 homolog)	CC	1.98
GRK6	G protein coupled receptor 6 kinase	P	4.91
HIRA	HIR histone cell cycle regulation defective homolog	P	5.07
HMOX1	Heme oxygenase decycling 1	CC, P	2.13
ITGβ1	Integrin beta 1	P	5.23
JAK2	Janus kinase 2	P	2.20

Continued

JUN	Jun oncogene	P	7.59
KITLG	Kit ligand	P, AP, M	3.58
LAMA1	Laminin alpha 1	AD, M	3.89
MCL1	Myeloid cell leukemia sequence 1(BCL2-related)	AP	1.77
MCM3	Minichromosone maintenance 3 complex b	P	2.29
MDM2	Mdm2 p53 binding protein homolog	P	4.48
MELK	Maternal Embryonic leucine zipper kinase	P	1.81
MSH2	Muts homolog 2	M	1.83
MSX1	MSH homeobox 1	CC, P	1.57
MTSS1	Metastasis suppressor 1	M	2.71
NCAPH	Barren homolog 1	P	2.85
P21	PAK protein (Cdc42/Rac)-associated kinase	P,CC	1.83
PBK	PDZ binding kinase	CC, P	1.61
PCNA	Proliferating cell nuclear antigen	P	2.29
POLA2	Polymerase (DNA directed alpha 2)	P	1.61
PTEN	Phosphatase and tensin homolog	P	3.99
RB	Retinoblastoma	P	2.03
RBBP4	Retinoblastoma binding protein 4	p	3.04
SENP5	SUMO1/sentrin specific peptidase	AP	1.81
SKP2	S-phase kinase- Associated protein 2(p45)	CC	15.03
SELPLG	Selectin P ligand	AD	3.10
SPCS3	Signal peptidase receptor complex subunit 3	CC	1.54
TFDP1	Transcription factor DP-1	P	2.36
P53	Tumour protein p53 inducible protein	P, AP	4.43
TRIB3C	Tribbles homolog 3	AP	1.50

Some of the altered genes had been identified previously as DNA binding interaction partners or cofactor transcriptional modulators of *PAX3* or as having a main role in cell proliferation, migration,differentiation or apoptosis (**Table 4.5**) (Boutet *et al.,* 2007; Li *et al.,* 2007).

Table 4.5 Alteration of *PAX3* interaction partners following *PAX3* knockdown in A375 cells

A -1.50 fold change in gene expression (Deep blue/light blue) indicates significant down-regulation. A 1.50 fold change in gene expression (red/orange) indicates significant up-regulation.

The level of gene alteration was denoted by varying shades of colour. Deep blue: gene expression down-regulated more than 2 fold; light blue: gene expression down-regulated between 1.5-2 fold; red: gene expression up-regulated more than 2 fold; orange: gene expression up-regulated 1.5-2 fold; non-shaded white: gene expression unchanged 1-1.5 fold.

Gene symbol	Gene description	Fold change
PAX3	**Paired box3**	**-8.95**
	***PAX3* Cofactor transcriptional modulators**	
SOX10	Sex determining region Y-box 10	-2.23
TBX18	T-box 18	-1.50
	***PAX3* functional modulators**	
BCL2	B-Cell lymphoma 2	-6.17
CIB1	Calcium and integrin binding 1	-1.66
HES1	Hairy and enhancer of split 1	-4.25
HMOX1	Heme oxygenase 1	2.13
MSX1	Msh homeobox 1	1.57
MITF	Microphthalmia-associated transcription factor	-6.15
MYOD1	Myogenic differentiation1	-2.42
MYOG4	Myogenin (myogenic factor 4)	-4.83
PTEN	Phosphatase and tensin homolog	3.99
SOSTDC1	Sclerostin domain containing 1	-1.53

4.4. Quantitative RT-PCR Analyses of Potential Downstream Targets of *PAX3*

The microarray data of potential downstream targets of *PAX3* were validated by qRT-PCR analysis in the A375 cell line. Using a threshold of 0.4 as a cut-off point for stability, demonstrated that *HMBS* and *SDHA,* having the lowest stability values were more stable and were selected as reference genes for normalisation of the qRT-PCR data from the cell line (**Fig 4.5**).

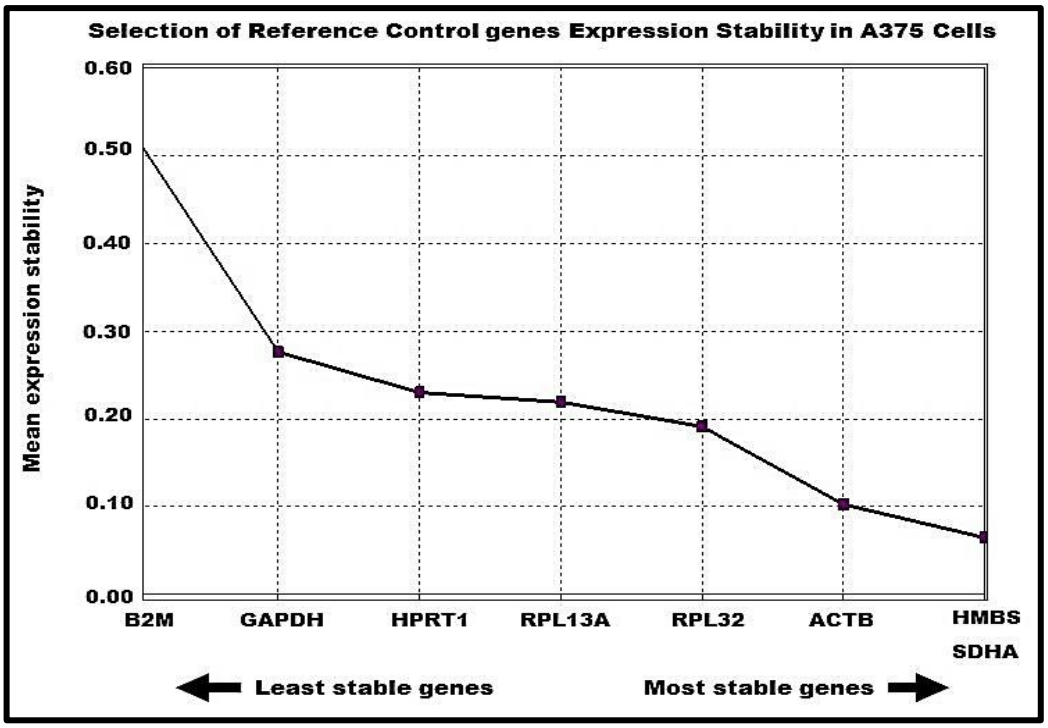

Figure 4.5 A375 cell line GeNorm graph showing the mean expression stability values of eight selected reference sample genes. Each point shows mean change in the fluorescence intensity at each PCR cycle. Both *HMBS* and *SDHA* genes with average stability values of (<0.40) were selected as the most stable housekeeping reference genes for normalisation.

The quantification of cycle values (delta Cp), is defined as the cycle number at which the measured reporter fluorescence value past a fixed threshold above base line, was calculated for each gene. Generally, samples with higher expression levels have lower delta Cp values. The genes of interest from the microarray data were selected for verification by qRT-PCR analysis, based on the role they play in cellular processess including: cell cycle, proliferation, migration, differentiation, or apoptosis, in addition to exceeding the thresholds of 1.5 and -1.50 for up-regulation and down-regulation

respectively. The inhibition of *PAX3* in the A375 cell line (8.95-fold down-regulation) in *PAX3*-siRNA treated A375 cells was further confirmed by the qRT-PCR analysis. Although low levels of gene expression were observed in the qRT-PCR data analysis, 25 genes including *PAX3*, which were validated by the qRT-PCR analysis, showed that the pattern of down-regulation of 16 genes of the 25 genes investigated was comparable to their down-regulation in the microarray data analysis. The down-regulation of 3 genes of the 16 genes analysed by the qRT-PCR analysis, confirmed the down-regulation of the microarray data analysis (*PAX3*, *COL3A1* and *CXCR4)* (**Table 4.6**). However, the down-regulation of another 13 genes expression pattern verified by the qRT-PCR data analysis was less than a -1.5 fold-change (*ADAM23, BCL2, CALM3, CAPRIN1, CCND3, CDCA3, C-MYC, FOXO1, ITGβ5, JAM2, MITF, MYOD1* and *NDRG1)* (**Table 4.6**). The down-regulation of 4 genes in the qRT-PCR data analysis was in contrast to their up-regulation in the microarray data analysis (*E2F7, E2F8, MCM3* and *PCNA*) (**Table 4.6**). The qRT-PCR analysis confirmed the pattern of up-regulation of 5 genes in the microarray analysis data. Two of the 5 up-regulated genes were confirmed above a 1.5 fold-change in the qRT-PCR analysis *(AEN* and *P21*) (**Table 4.6**) while the up-regulation of another 3 genes validated in the qRT-PCR data analysis was less than a 1.5 fold-change (*AKT3, CASP3* and *P53*) (**Table 4.6**).

The alteration of gene expression in the microarray analysis data of the A375 cell line was partly confirmed by the qRT-PCR data analysis. However, the qRT-PCR validated less alteration in expression of the majority of genes compared to the microarray data and this was perceived to be partly due to the low levels of expression of these genes in A375 cells.

Table 4.6 A microarray data analysis of alterations in gene expression compared with qRT-PCR analysis of those genes in A375 cells

A 1.50 fold change in gene expression (light blue) was used as the threshold for significant down-regulation. A 1.50 fold change in gene expression (orange) was used as the threshold for significant up-regulation. The degree of gene alteration was denoted by varying shades of colour. Dark blue: gene expression down-regulated more than 2 fold; Light blue: gene expression down-regulated 1.5 to 2 fold; Red: gene expression up-regulated more than 2 fold; orange : gene expression up-regulated 1.5-2 fold; non-shaded white: gene expression unchanged 1-1.5 fold.

		Fold change	
Gene symbol	**Gene description**	**Microarray**	**qRT-PCR**
PAX3	**Paired Box 3**	-8.95	-2.04
ADAM23	ADAM metallopeptidase domain 23	-2.51	-0.98
AEN	Apoptosis enhancing nuclease	2.80	1.80
AKT3	V-AKTmurine thymoma viral homolog 3 oncogene	2.52	1.08
BCL2	B-Cell lymphoma 2	-6.17	-1.10
CASP3	Caspase3, apoptosis related cysteine peptidase	2.53	1.29
CALM3	Calmodulin 3	-1.71	-0.93
CAPRIN1	Cell cycle associated protein 1	-1.57	-1.33
CCND3	Cyclin D3	-1.82	-1.34
CDCA3	Cell cycle associated 3	-1.80	-1.33
C-MYC	C-myc binding protein	-1.54	-1.25
COL3A1	Collagen type III, alpha 1	-72.08	-1.80
CXCR4	Chemokine (C-X-C motif) receptor 4	-11.87	-3.56
E2F7	E2F transcription factor 7	1.50	-1.75
E2F8	E2F transcription factor 8	1.57	-1.26
FOXO1	Forkhead box O1	-2.82	-1.28
ITGβ5	Integrin beta 5	-2.26	-1.31
JAM2	Junctional adhesion molecule 2	-12.24	-1.20
MCM3	Minichromosome maintenance 3	2.29	-1.64
MITF	Microphthalmia-associated transcription factor	-6.15	-1.01
MYOD1	Myogenic differentiation 1	-2.42	-1.48
NDRG1	N-myc downstream regulated 1	-5.85	-0.95
P21	Cyclin-dependent kinase inhibitor 1	1.83	1.68
PCNA	Proliferating cell nuclear antigen	2.29	-1.30
P53	Tumour protein P53 inducible protein	4.43	1.44

The microarray and the qRT-PCR data analysis of gene up/down-regulation were comparable in both rhabdomyosarcoma and melanoma cell lines. The qRT-PCR data analysis however, showed smaller changes in gene expression of the majority of the genes compared (**Table 4.7**). The microarray and the qRT-PCR data analysis of down-regulation of 11 of 24 genes were comparable in the A375 cell line and in both JR1 and RH30 cell lines (*PAX3, ADAM23, BCL2, CALM3, CAPRIN1, CCND3, CDCA3, C-MYC, COL3A1, ITGβ5* and *MYOD1*) (**Table 4.7**). The down-regulation of another 4 genes expression in both the microarray and the qRT-PCR data analysis of the A375 melanoma cell line, was in contrast, up-regulated in both microarray and qRT-PCR data analysis of both JR1 and RH30 rhabdomyosarcoma cell lines (*CXCR4, FOXO1, JAM2* and *NDRG1*) (**Table 4.7**).

Additionally, the pattern of up-regulation of 5 of the 24 genes compared were similar in the A375, JR1 and RH30 cell lines (*AEN, AKT3, CASP3, P21* and *P53*) (**Table 4.7**). However, the pattern of down-regulation of another 3 genes was in contrast to their up-regulation in only the microarray data analysis of A375 cells (*E2F7, E2F8* and *PCNA*) (**Table 4.7**). The up-regulation of 4 genes in the microarray analysis data of A375 cells was in disagreement with the down-regulation of these genes in the qRT-PCR data analysis (*E2F7, E2F8, MCM3* and *PCNA*) (**Table 4.7**).

Table 4.7 Comparison of selected gene expression after *PAX3* down-regulation melanoma and rhabdomyosarcoma cell lines by microarray and qRT-PCR analyses

Gene expression up-regulated ≥ 1.50 fold is shown in orange; ≥ 2.0 in red; gene expression down-regulated ≥ 1.50 fold is shown in light blue; ≥ 2.0 in dark blue; gene expression less than 1.50 up-regulated / down-regulated is shown in white.

	A375 fold change		JR1 fold change		RH30 fold change	
Gene symbol	**Microarray**	**qRT-PCR**	**Microarray**	**qRT-PCR**	**Microarray**	**qRT-PCR**
PAX3	-8.95	-2.04	**-4.64**	**-1.63**	**-2.61**	**-1.37**
ADAM23	-2.51	-0.98	-4.34	-2.34	-4.87	-1.67
AEN	2.80	1.80	10.72	3.72	7.64	3.82
AKT3	2.52	1.08	2.43	1.74	3.39	2.37
BCL2	-6.17	-1.10	-4.37	-3.43	-3.45	-2.27
CALM3	-1.71	-0.93	-2.62	-2.32	-2.20	-1.53
CAPRIN1	-1.57	-1.33	-2.50	-1.57	-9.84	-2.27
CASP3	2.53	1.29	2.45	1.56	2.92	1.68
CCND3	-1.82	-1.34	-3.68	-2.02	-2.91	-1.71
CDCA3	-1.80	-1.33	-5.84	-1.54	-3.66	-1.50
C-MYC	-1.54	-1.25	-5.85	-2.62	-3.50	-1.12
COL3A1	-72.80	-1.80	-15.66	-4.64	-9.65	-2.64
CXCR4	-11.87	-3.56	4.73	2.15	2.88	1.55
E2F7	1.50	-1.75	7.36	2.82	2.19	1.57
E2F8	1.57	-1.26	-5.40	-1.97	-3.74	-1.98
FOXO1	-2.82	-1.28	3.51	1.58	2.04	1.52
ITGβ5	-2.26	-1.31	-6.06	-1.76	-2.14	-1.52
JAM2	-12.24	-1.20	4.04	2.34	2.93	1.54
MCM3	2.29	-1.64	-5.84	-2.44	-3.99	-1.51
MYOD1	-2.42	-1.48	-2.82	-1.02	-4.65	-1.34
NDRG1	-5.85	-0.95	6.82	2.33	6.07	2.03
PCNA	2.29	-1.30	-3.75	-1.30	-4.26	-2.54
P21	1.83	1.68	4.08	1.56	3.25	1.45
P53	4.43	1.44	3.51	1.55	3.77	2.05

4.5. Effect of *PAX3* down-regulation on Potential Downstream Target Protein Expression

Western blotting analysis of pre-transfected A375 cells revealed high levels of PAX3 and GAPDH expression (**Fig.4.6**).

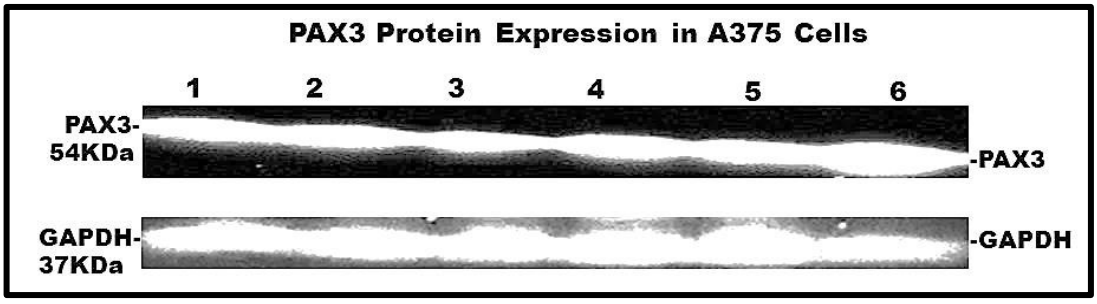

Figure 4.6 Pre-transfection analysis of PAX3 protein expression pattern in A375 cells. Lanes 1-6: Replicate PAX3 and GAPDH proteins in non-transfected A375 cells.

To evaluate the effect of *PAX3*-siRNA inhibition of *PAX3* protein levels in A375 melanoma cells, immunoblotting of *PAX3*-siRNA and NC-siRNA transfected cells was carried out. Western blotting analysis of *PAX3* and selected genes of interest confirmed the pattern of alteration of gene expression observed in the microarray data. PAX3 protein expression in *PAX3*-siRNA treated A375 cells was compared with the protein expression in NC-siRNA treated A375 cells. Human GAPDH was used as an internal normalisation control (lanes 1, 2, 3, 5, 6 and 7 of **Fig. 4.7A**). The NC-siRNA treated cells showed high PAX3 protein expression (see lanes 1-3 of **Fig. 4.7B**), while inhibition of *PAX3* mRNA in *PAX3*-siRNA treated cells resulted in a consistent reduction of PAX3 protein (see lanes 5-7 of **Fig. 4.7B**).

Significant knockdown of PAX3 protein by siRNA targeting *PAX3* without a corresponding effect in the NC-siRNA transfected negative control was observed. *PAX3*-siRNA knockdown caused both down-regulation and up-regulation of potential downstream molecules of PAX3 including a significantly decreased C-MYC **(**lanes 5, 6 and 7 of **Fig. 4.7C**), completely decreased ITGβ5 **(**lanes 5, 6 and 7 of **Fig. 4.7D),** decreased MYOD1 (lanes 5, 6 and 7 of **fig. 4.7E**) and almost completely diminished BCL2 **(**lanes 5, 6 and 7 of **Fig. 4.7F),** consistent induction of P21 protein (lanes 5, 6 and

7 of **Fig. 4.7G**), increased P53 protein expression as well as phosphorylation **(**lanes 5, 6 and 7 of **Fig. 4.7H)** and increased CASP3 **(**lanes 5, 6 and 7 of **Fig. 4.7I**).

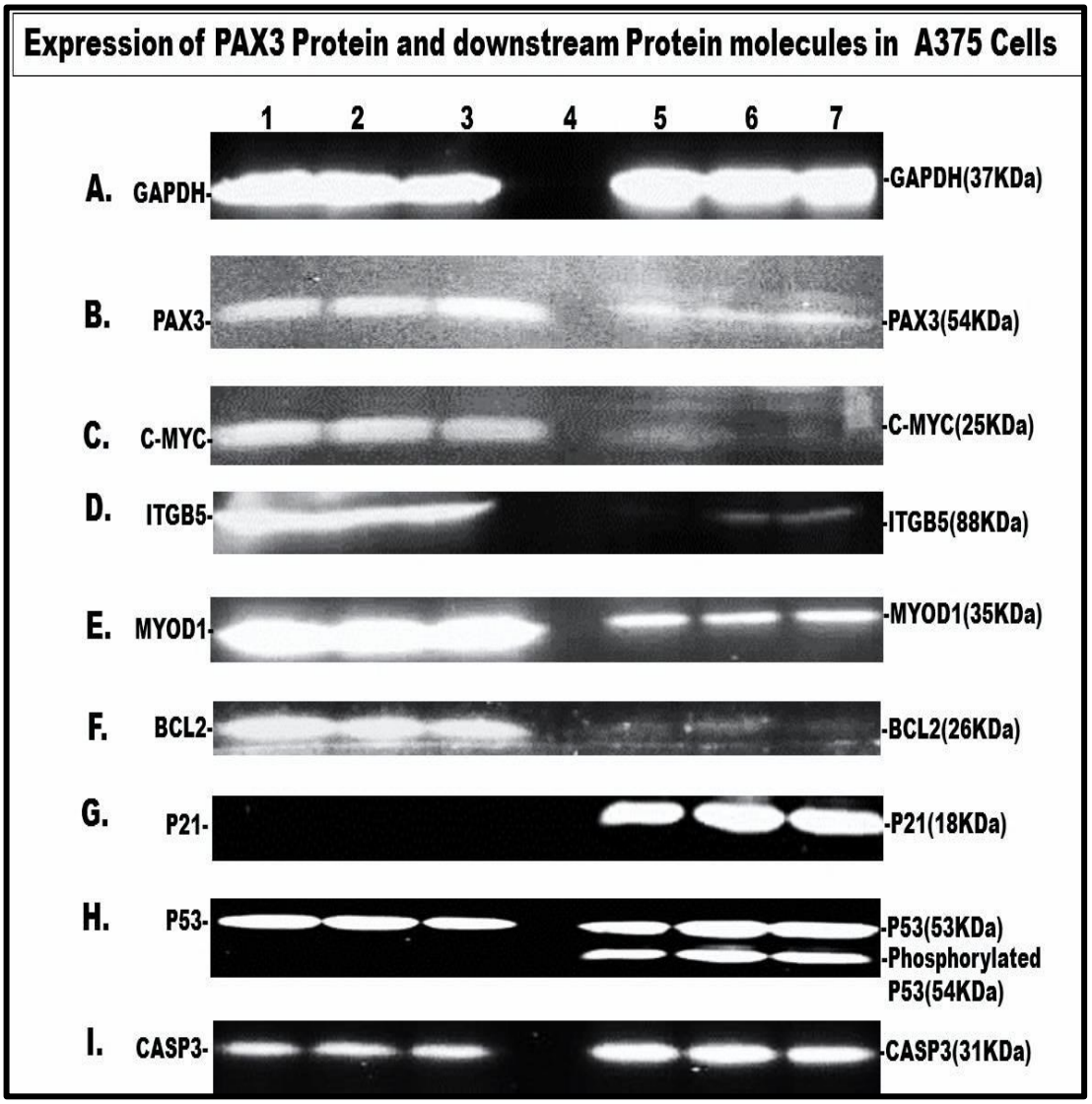

Figure 4.7 Western blotting of A375 cell protein expression after 96 hr *PAX3*-siRNA inhibition. Lanes: 1-3: Triplicate NC-siRNA treated A375 cells. 4: Blank. 5-7: Triplicate *PAX3*-siRNA treated A375 cells.

The mean percentage of PAX3 protein expression remaining after *PAX3*-siRNA treatment was 10% ($p < 0.01$) (**Fig. 4.8**). The percentages remaining of downstream proteins were: C-MYC (6%); ITGβ5 (8%); MYOD1 (15%) and BCL2 (7%). Likewise, other downstream targets of PAX3 had induced increased expression: P21 (20 fold), P53 (2.5 fold) and CASP3 (2.9 fold).

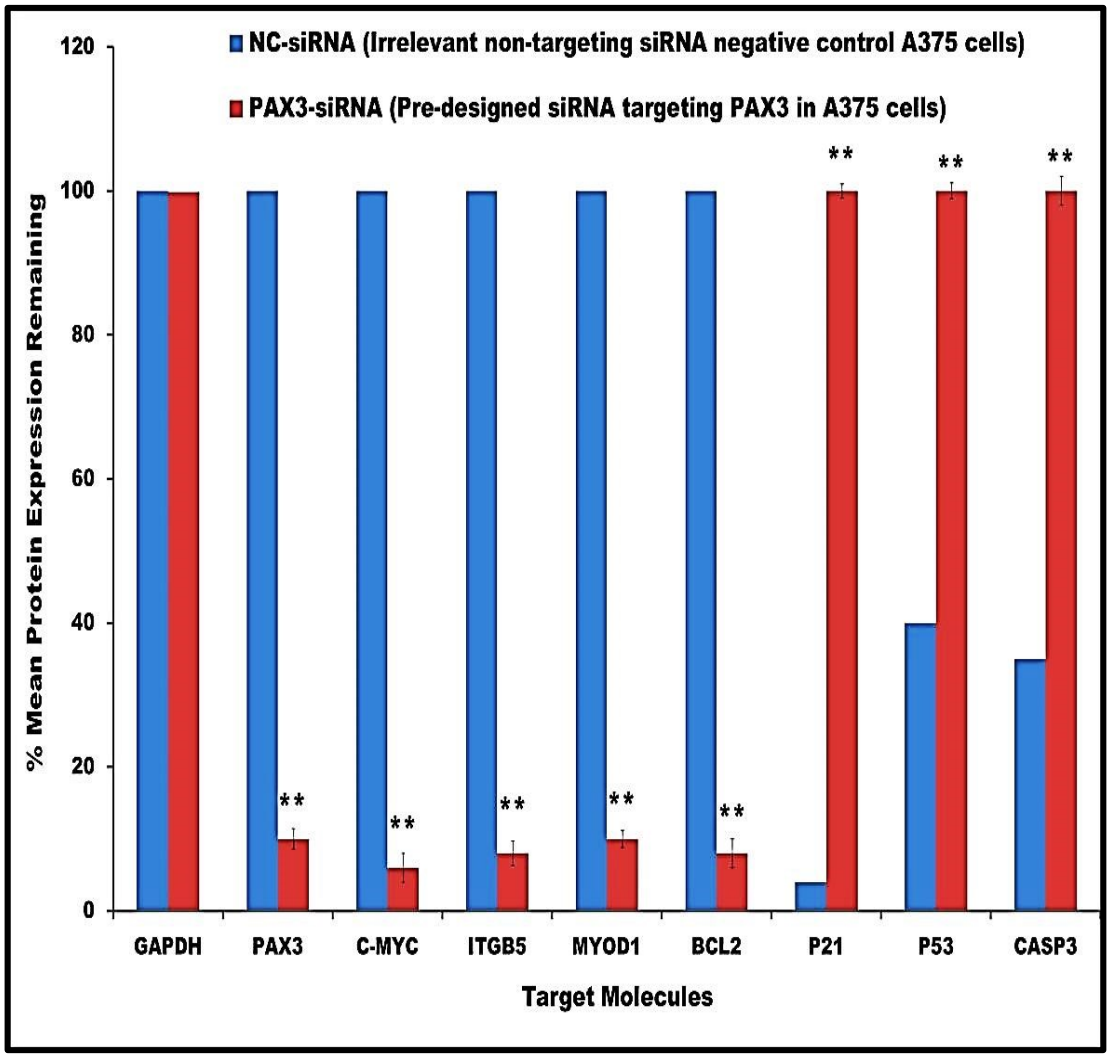

Figure 4.8 Mean percentages remaining of A375 cells of protein expression after 96 hr siRNA transfection. The mean protein expression in NC-siRNA transfected cells (blue columns) was compared with the mean protein expression in *PAX3*-siRNA transfected A375 cells (red colunms). The histograms are means of triplicate measurements in each of three separate experiments (n = 9). (Student's t-test), (**, $p < 0.01$).

4.6. Effect of Knockdown of *PAX3* on Cell Proliferation of A375 Melanoma Cell Line

A standard curve of the pre-transfected melanoma A375 cell line using various cell seeding densities/well, was established (**Fig. 4.9**), where linear growth was proportional to initial cell density. An initial cell seeding density of 5.0 X 10^4 cells/well that produced a steady optimal growth over a 96 hr time-course without over-growth and with minimal cytotoxicity was chosen for the investigation of A375 cell proliferation.

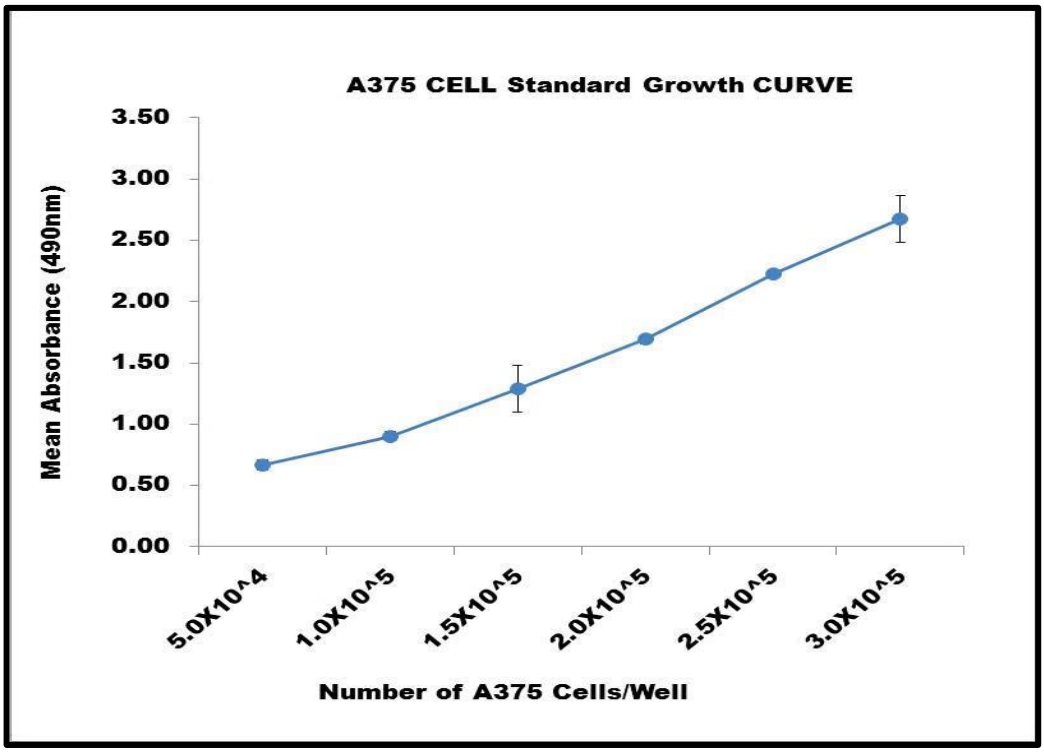

Figure 4.9 CellTiter 96 aqueous assay of pre-transfection standard curve for the selection of optimal A375 cell seeding density in successive cell proliferation analyses. Initial cell seeding density was 5.0 X 10^4 cells/well. Using an ELISA plate reader at 490nm, the OD readings of formazan produced are directly proportional to the number of proliferating A375 cells. Each point represents the mean of triplicate measurements (± SD) of three separate experiments performed (n = 9).

To establish the effects of *PAX3* inhibition on proliferation of the A375 melanoma cell line by the CellTiter non-radioactive MTS colorimetric assay, the mean OD reading relating to the number of proliferating viable cells among both NC-siRNA and *PAX3*-siRNA treated cells were compared (**Fig. 4.10**) and the results were further confirmed directly using the Coulter cell counter (**Fig. 4.11**).

Higher mean ODs produced by the NC-siRNA transfected cells relating to a greater number of proliferating viable cells were noticed, in contrast to lower OD values produced by *PAX3*-siRNA transfected cells at 24, 48 72 and 96-hr time points. This was particularly apparent in the cells transfected for 96 hrs, when the OD of *PAX3*-siRNA treated A375 was 0.49 and the NC-siRNA was 2.31. Consequently, a significant

inhibition of cell growth was observed in *PAX3*-siRNA transfected A375 cells after inhibition of *PAX3* ($p < 0.01$). (**Fig.4.10**).

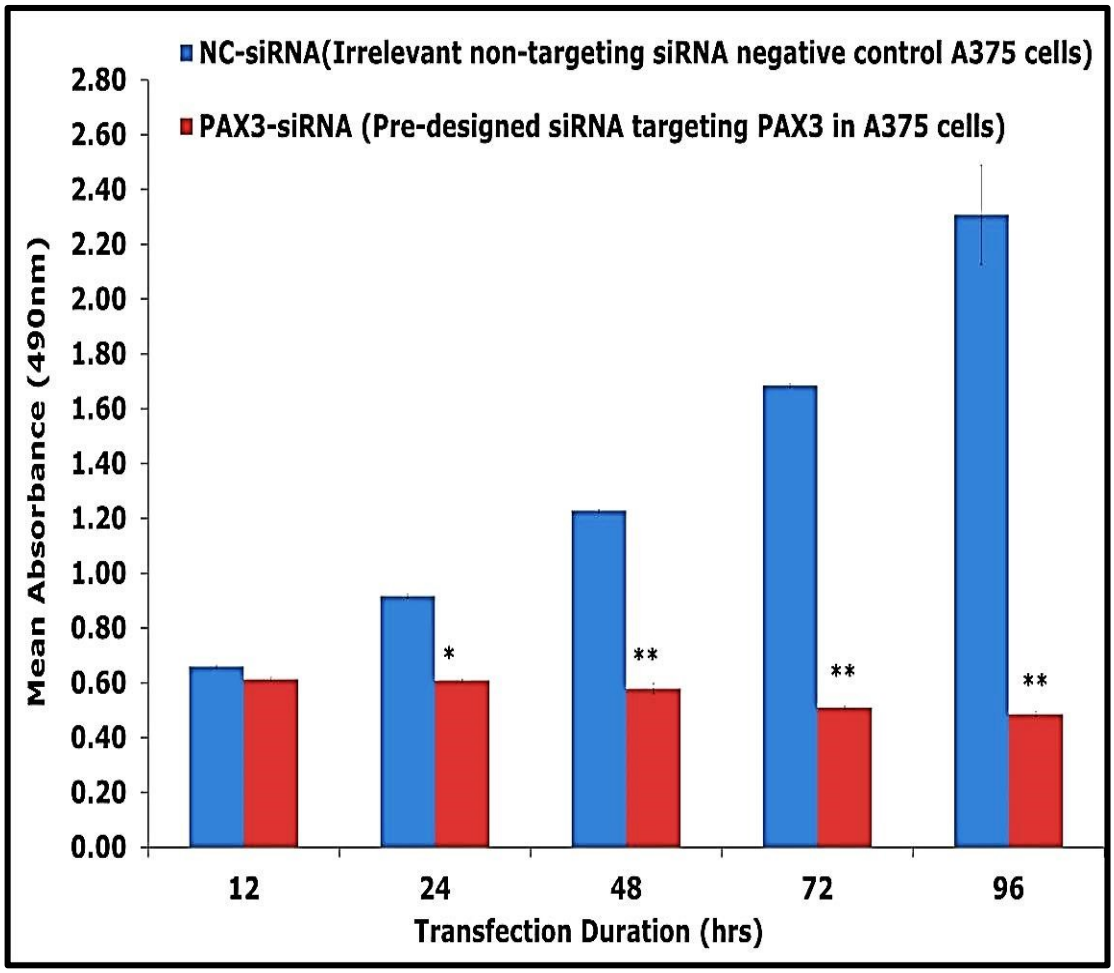

Figure 4.10 CellTiter 96 aqueous indirect cell proliferation analyses for determination of inhibition of A375 cell proliferation following 96 hr siRNA transfection. Cells were initially seeded at 5.0 X 10^4 cells/well. The mean OD of NC-siRNA transfected A375 cells (blue columns) was compared with the mean OD of *PAX3*-siRNA transfected A375 cells (red columns) at each time point. The histograms are means of three separate measurements in experiments carried out in triplicate, (n = 9). (Student's t-test), (*, $p < 0.05$; **, $p < 0.01$).

Direct coulter counter cell proliferation analysis was used to confirm the results of the MTS assay and equally demonstrated significant cell growth inhibition of an initial 5.0 X 10^4 cells/ml in *PAX3*-siRNA transfected A375 cells ($p < 0.05$ at 24 hrs and $p < 0.01$ at 48, 72, 96 hrs) compared to high cell numbers in NC-siRNA transfected A375 cells (**Fig. 4.11**).

The mean cell count (589 X 10^4/cells) after 96 hr transfection observed in NC-siRNA treated A375 cells was much higher than *PAX3*-siRNA treated A375 cells (20 X 10^4/cells). The decreased number of proliferating cells observed in *PAX3*-siRNA transfected cells was because of cell apoptosis.

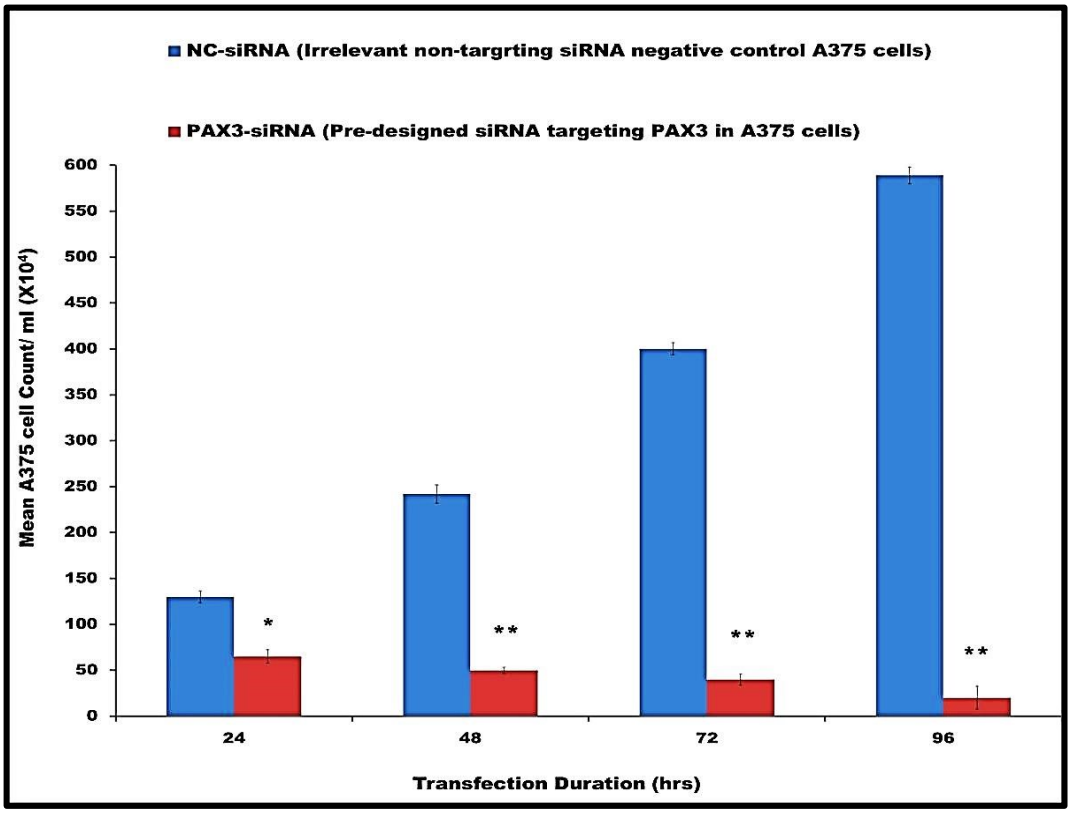

Figure 4.11 Coulter counter direct cell counts for determination of inhibition of A375 cell proliferation after *PAX3*-siRNA transfection. Original cell seeding density was 5.0 X 10^4 cells/well. The mean number of cell count in NC-siRNA transfected A375 cells (blue columns) was compared with the mean number of cell count in *PAX3*-siRNA transfected A375 cells (red columns) at each time point. The histograms are means of triplicate cell counts in three separate experiments (n= 9). (Student's t-test); (*, $p < 0.05$; **, $p < 0.01$).

4.7. Effect of Knockdown of *PAX3* on the Cell Cycle of A375 Melanoma Cells

Since inhibition of *PAX3* in A375 cells significantly suppressed cell proliferation, it was imperative to assess the influence of *PAX3* inhibition on the cell cycle and to distinguish the phases of the cell cycle at which cell growth was halted. After 96 hr siRNA knockdown of *PAX3* gene expression, the DNA content of individual transfected cells was analysed by flow cytometry. The mean numbers of PI stained cells amomg the NC-

siRNA treated A375 cells was compared with the numbers of PI stained cells among *PAX3*-siRNA treated A375 cells. The amount of PI staining per cell established the distribution of that cell in a particular phase of the cell cycle. A typical flow cytometry analysis is shown in **Fig. 4.12.**

Flow cytometry analyses of A375 cells following 96 hr siRNA inhibition of *PAX3* gene expression.

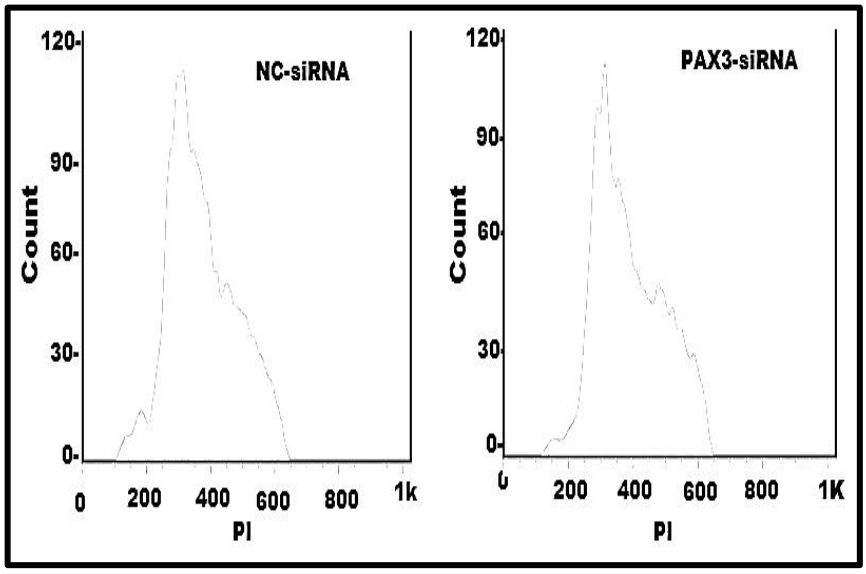

Figure 4.12 A typical cell cycle pattern of NC-siRNA and *PAX3*-siRNA of A375 siRNA treated PI stained cells after 96 hr transfection. The mean percentages of cells at different stages of the cell cycle are shown in (**Table 4.9)**.

Table 4.8 Cell cycle distribution of A375 cells after 96 h siRNA knockdown of PAX3. Flow cytometry analysis of DNA content by Propidium iodide incorporation. Each value is the percentage of cells at a particular cell cycle stage.

Cell cycle phase	A375 cells treated with NC-siRNA	A375 cells treated with *PAX3*-siRNA
G0/G1	59.6% ±2.1	57.6% ±1.2
S	7.9% ±1.2	5.3% ±2.2
G2/M	32.5% ±1.2	36.7% ±1.3

These values are means of three cell counts in each of two separate experiments, (n = 6); $p < 0.05$; for NC-siRNA vs *PAX3*-siRNA (by Student's t-test).

This analysis revealed a lower percentage of cells among G0/G1 *PAX3*-siRNA treated A375 cells compared with the NC-siRNA treated cells: ± 57.6% of *PAX3*-siRNA treated cells versus ± 59.6% NC-siRNA treated A375 control cells were arrested at the G0/G1 phase. NC-siRNA transfected cells showed ± 7.9% in S phase compared to ± 5.3% of *PAX3*-siRNA transfected cells. The occurrence of cells in S phase suggests cell cycle progression and hence is probably related to cell proliferation. This result therefore, indicates a slower cell proliferation rate in *PAX3*-siRNA treated A375 cells compared to a higher cell proliferation rate in the NC-siRNA treated A375 cells and corresponds with the cell proliferation experiments described previously. Cells in which *PAX3* had been down-regulated, appeared to be halted more in G2/M phase than the NC-siRNA treated controls (36.7 ± 1.3% versus 32.5 ± 1.2 % respectively: $p < 0.05$), thus more *PAX3*-siRNA treated cells were accumulating at the well-known cell cycle checkpoint in the G2/M.

4.8. Effect of *PAX3* Down-regulation on Migration of A375 Melanoma Cells

A scratch wound healing assay was analysed to evaluate the migratory ability *in vitro* (and possible metastatic potential) of A375 melanoma cells. The initial relative mean width of scratch wound gaps of NC-siRNA treated A375 cells and *PAX3*-siRNA treated A375 cells at 0 hr (**Fig. 4.13**), was compared with the relative mean width of scratch wound healing of A375 cells after 12, 24, 48, 72 and 96 hr transfection. The NC-siRNA treated A375 cells with high expression of *PAX3* migrated long distances to close wound gaps, better than *PAX3*-siRNA treated cells, which migrated only short distances.

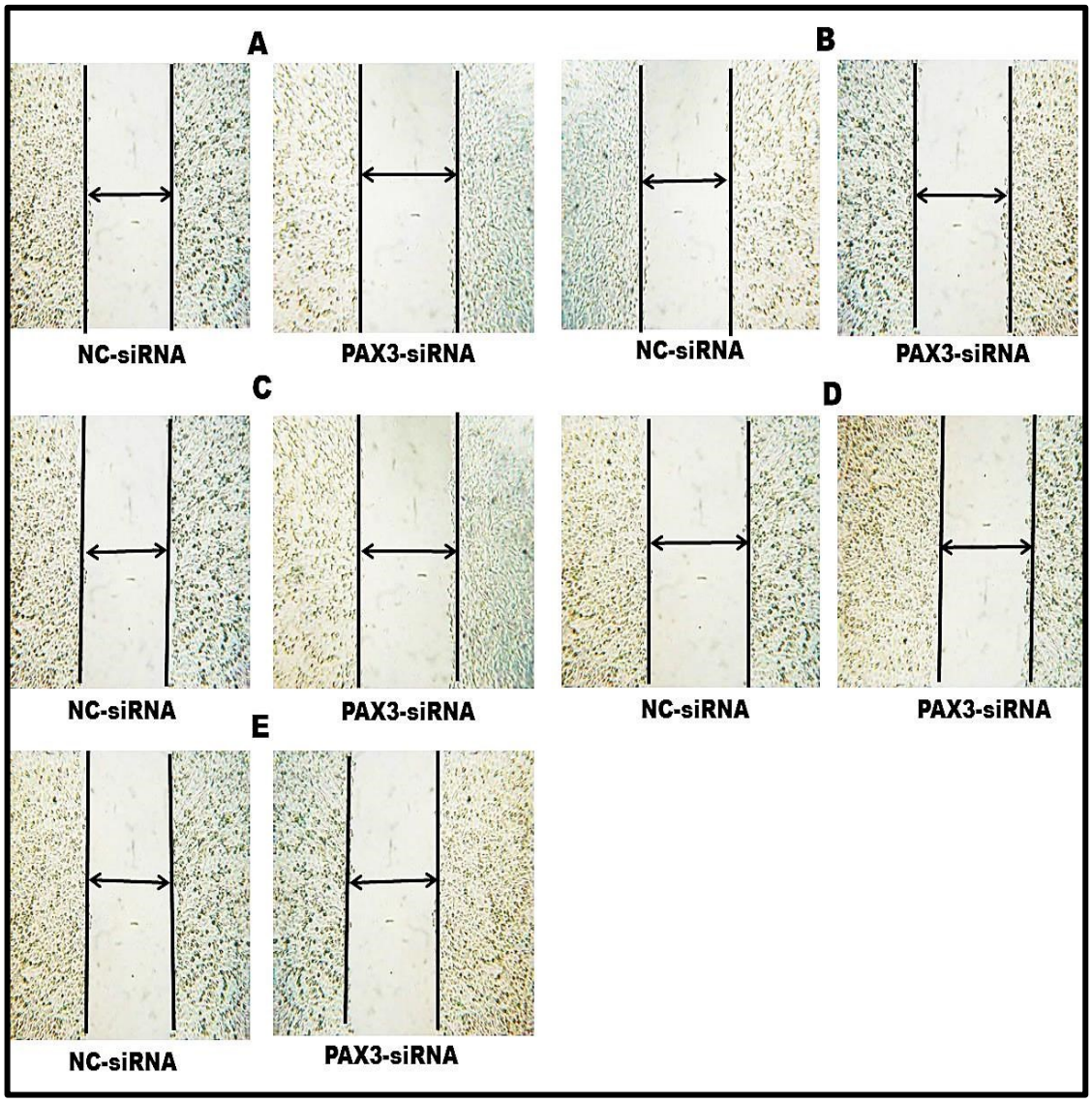

Figure 4.13, X 10 magnification of width of A375 cells scratched wound gap at 0 hr after 12- 96 hr transfection duration. A (12 hr); B (24 hr); C (48 hr); D (72 hr); E (96 hr) transfected cells. The arrows represent the initial widths of scratch wound gaps measured in monolayers of NC-siRNA and *PAX3*-siRNA transfected A375 cells before 24 hr cell migration.

Following 24 hr cell migration, the NC-siRNA treated A375 cells exhibited narrow wound gaps due to migration the wound edges to close wound gaps, whereas broader wound gaps were detected in the *PAX3*-siRNA treated A375 cells, representing less cell migration. (**Figure 4.14**) (long arrows indicate wound gaps).

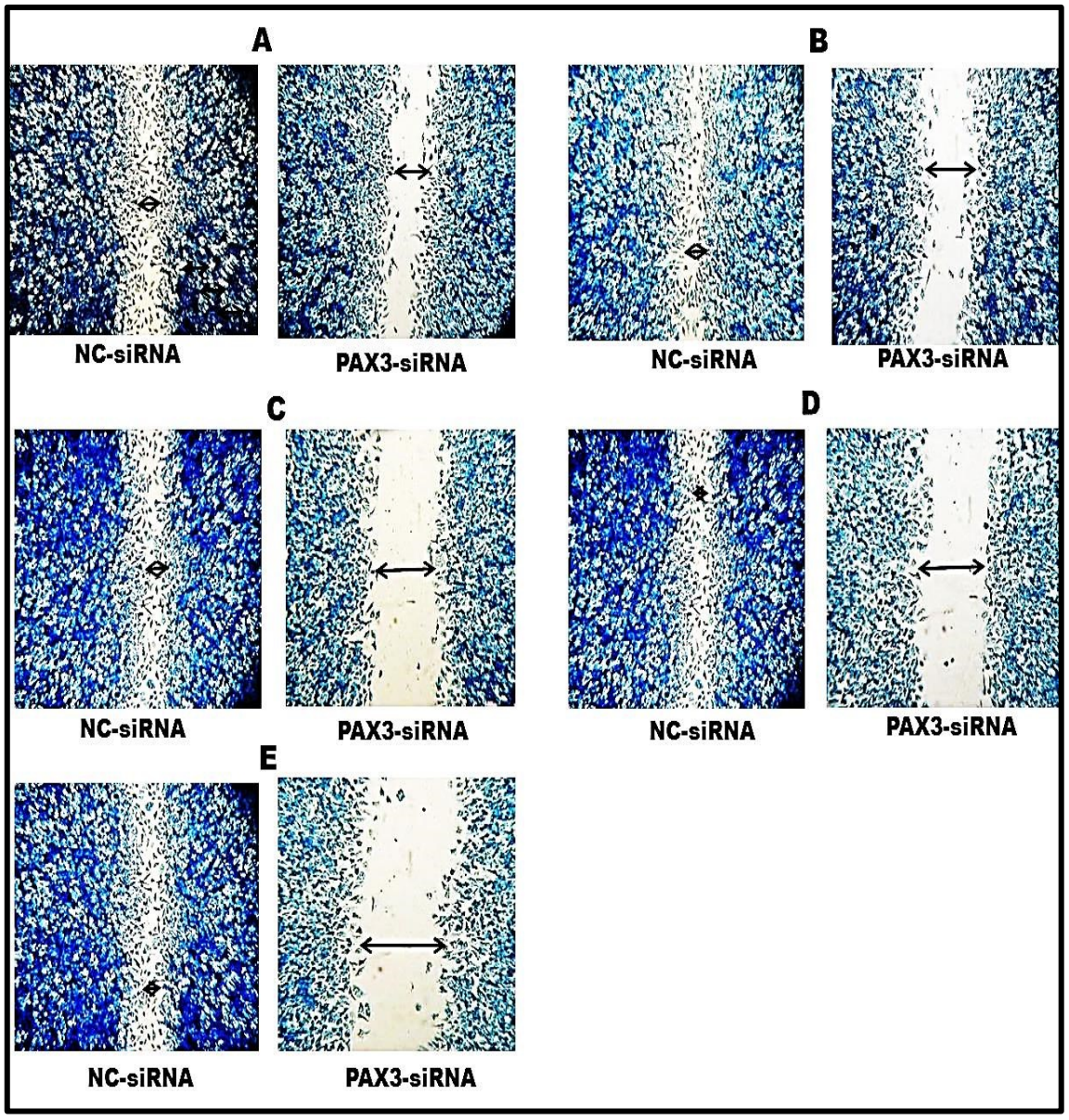

Figure 4.14, X 10 magnification in scratch wound healing assay of transfected A375 cells after 24 hours. A375 cells were stained with methylene blue**. A (12 hr)**; **B (24 hr)**; **C (48 hr)**; **D (72 hr)**; **E (96 hr) transfection durations.** Relative measurement of wound gap distance indicates A375 cell migration distance. Wound healing corresponds to measured distance in 24 hr cell migration after 12 hr, 24 hr, 48 hr, 72 hr or 96hr siRNA transient transfection of A375 cells. NC-siRNA transfected A375 cells displayed narrow wound gaps, signifying high cell migration. *PAX3*-siRNA transfected A375 cells showed wider wound gaps, because of inhibition of cell migration as a result of A375 cell apoptosis.

The relative mean cell migration distance in the 96 hr *PAX3*-siRNA treated cells of (10 units) was significantly different from the relative mean cell migration distance in the 96 hr NC-siRNA treated cells which was (75 units), ($p < 0.01$) as shown in (**Fig. 4.15)**.

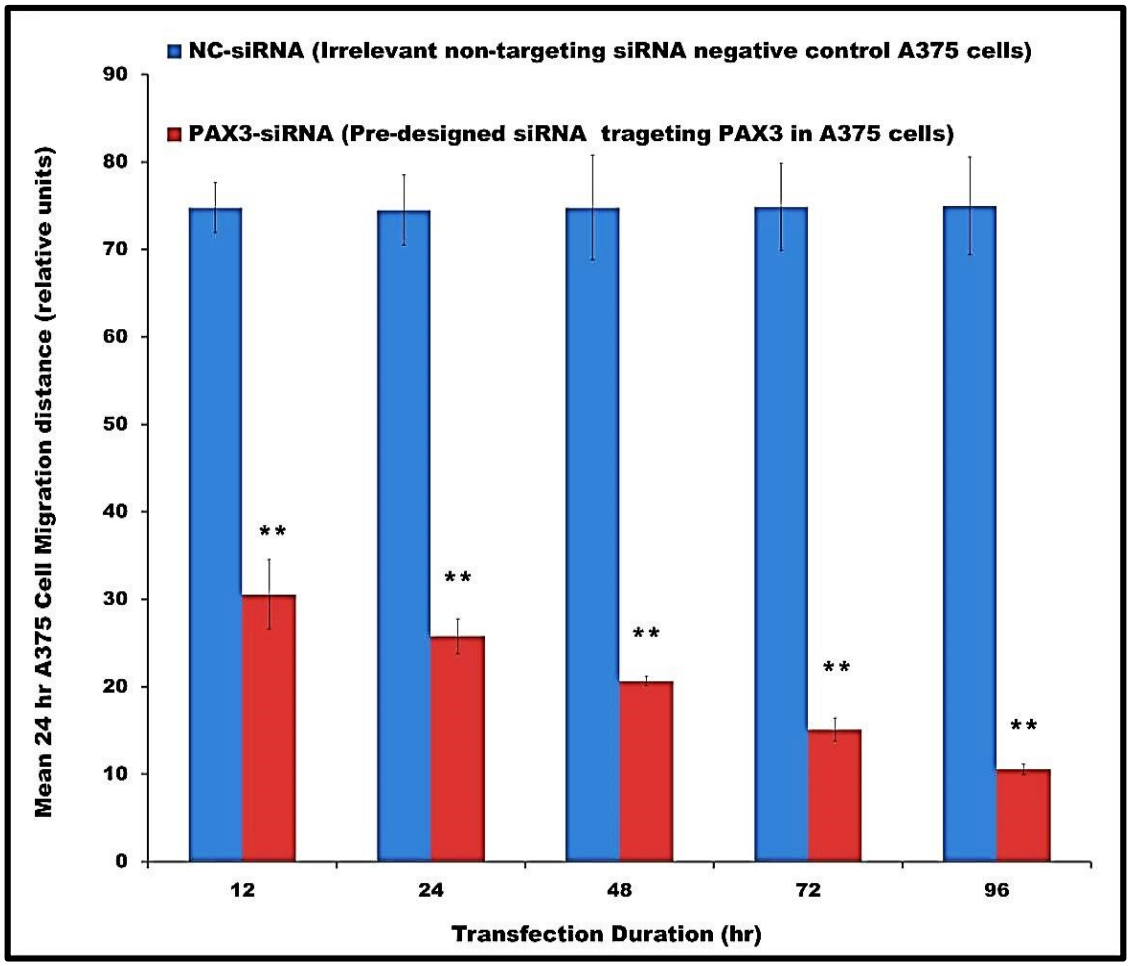

Figure 4.15 Relative migration of A375 cells over a 24 hr period after 12 hr, 24 hr, 48 hr, 72 hr or 96 hr siRNA transfection duration. The relative cell migration distance of NC-siRNA treated A375 cells (blue columns) was compared with the relative cell migration distance of *PAX3*-siRNA transfected A375 cells (red columns). Mean values were derived from three measurements in each of three separate experiments (n = 9). Student's t-test; **, $p < 0.01$.

4.9. Effect of *PAX3* Down-regulation on A375 Cell Adhesion to ECM Proteins

Cell attachment to natural ECMs is essential in cell communication and regulation of growth and is of central importantance in the advancement and continuation of tumourigenesis of A375 cells (Wang *et al*. 2013). The effect of suppressing *PAX3* on the inhibition of A375 cell adhesion to human ECM components was investigated using collagen I, collagen II, collagen IV, fibronectin, laminin, tenascin and vitronectin, previously coated onto the surfaces of plastic wells. Following 96 hr transfection, the mean cell adhesion to the various ECM proteins in the NC-siRNA transfected A375 cells was compared with that of *PAX3*-siRNA treated A375 cells. In each well, the OD

was proportional to the number of adherent stained cells. *PAX3*-siRNA treated A375 cells with knockdown of *PAX3* displayed lower mean ODs, relating to a weaker cell adhesion to collagen I (0.06), collagen II (0.05), collagen IV (0.05), fibronectin (0.14), laminin (0.13), tenascin (0.09) and vitronectin (0.06) was significantly different from higher means of ODs in NC-siRNA JR1 treated cell adhesion to Col I (0.45), Col II (0.37), Col IV (0.41), fibronectin (0.62),laminin (0.52) tenascin (0.36) and vitronectin (0.34) ($p < 0.01$) (**Fig. 4.16**).

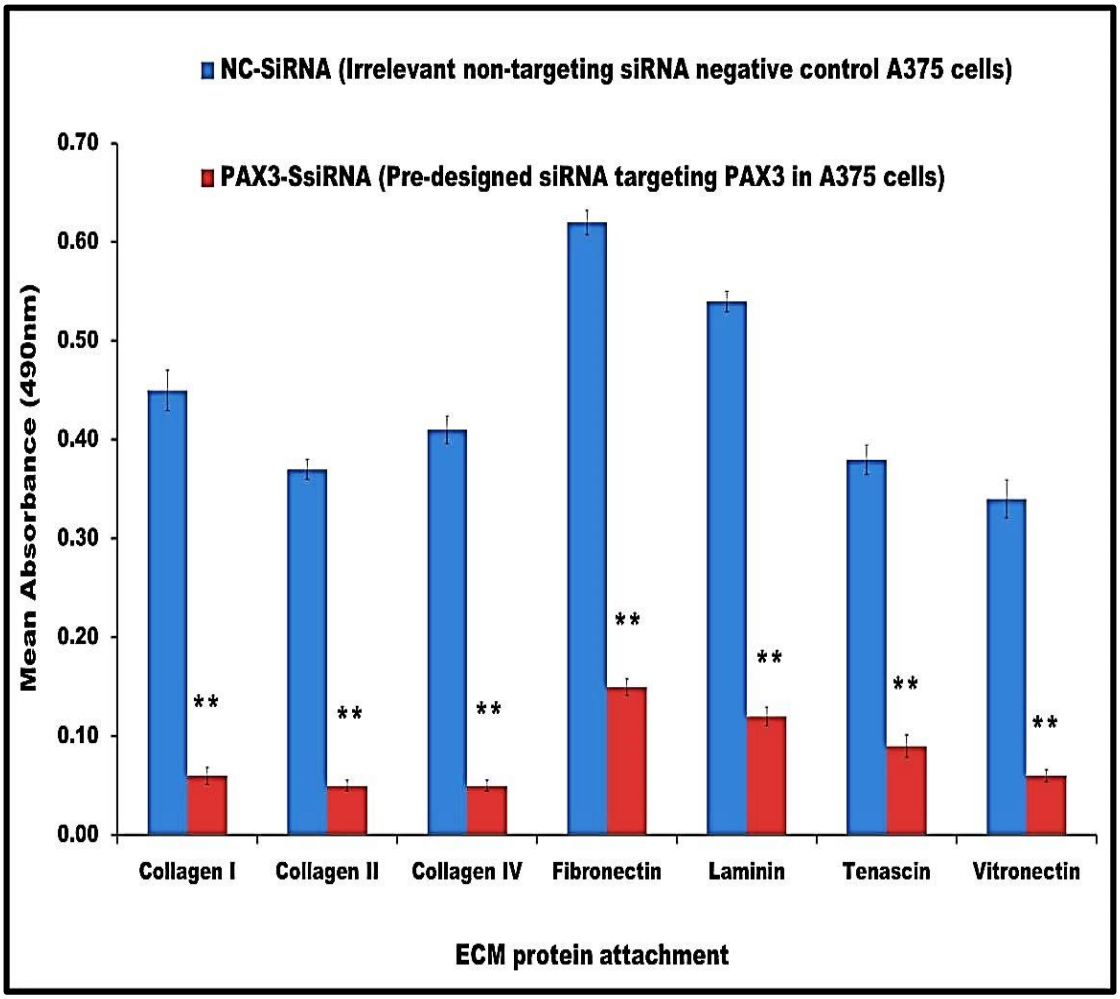

Figure 4.16 Inhibition of A375 cell adhesion to ECM after 96 hr siRNA transfection. The mean OD of A375 cell adhesion in NC-siRNA transfected A375 cells (blue columns) was compared with the mean OD of A375 cell adhesion in *PAX3*-siRNA transfected cells (red columns). Three measurements were derived from each of two separate experiments (n = 6). Student's t-test; **, $p < 0.01$.

4.10. Influence of Silencing *PAX3* on Invasion of A375 Cells

Cell invasion is fundamental in the metastasis of these tumours. To examine the effects of 96 hr down-regulation of *PAX3* on A375 cell invasion *in vitro*, the mean numbers of NC-siRNA transfected A375 cells invading a basement membrane were compared to the mean numbers of *PAX3*-siRNA transfected A375 cells. Representative microscopic images of invading cells from both NC-siRNA transfected and *PAX*-siRNA transfected cells are shown under the same magnification (**Figs. 4.17**). A mean of 80 NC-siRNA transfected A375 cells per field were detected to invade the matrigel membranes, indicating significant cell invasive ability, compared to a mean number of 22 *PAX3*-siRNA transfected A375 cells per field invading the matrigel membranes ($p < 0.01$) (**Fig. 4.18**).

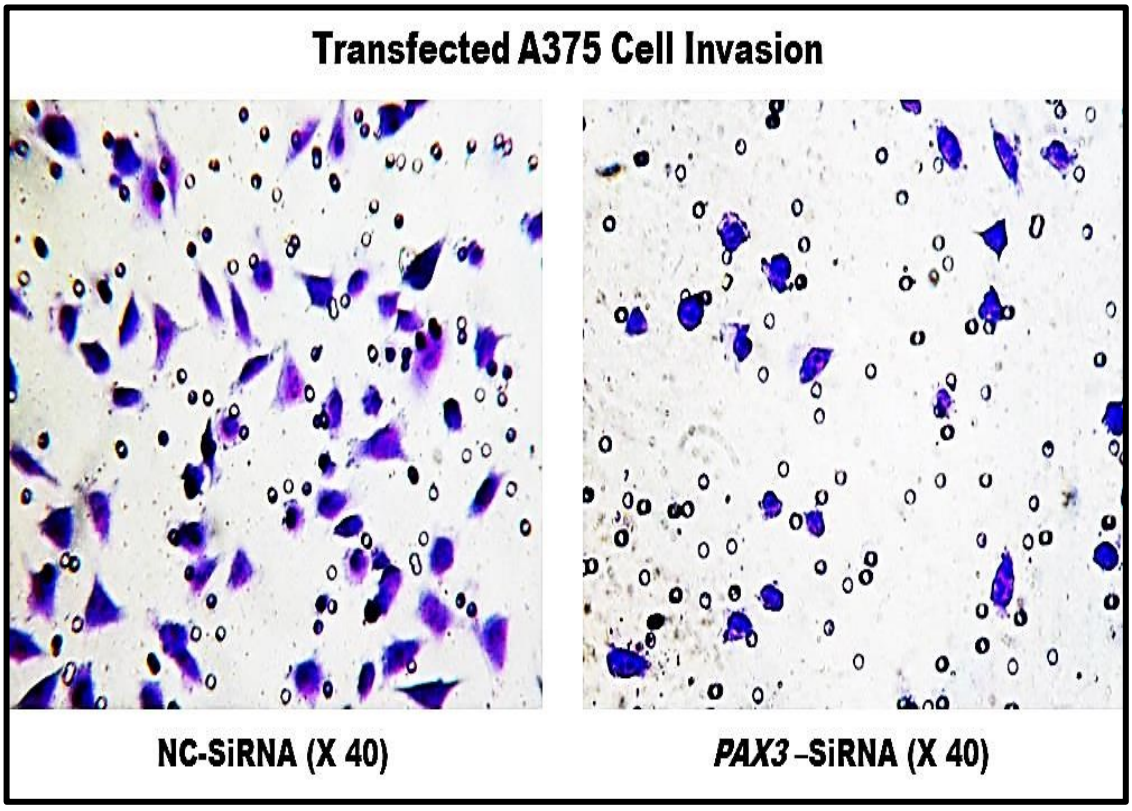

Figure 4.17 Inhibition of A375 cell invasion of matrigel membrane following 96 hr transient siRNA transfection. Invaded A375 cells were stained with Giemsa and viewed in a phase contrast microscope X 40. NC-siRNA transfected A375 cells averagely invaded in high numbers while *PAX3*-siRNA transfected A375 cells showed less cell invasion.

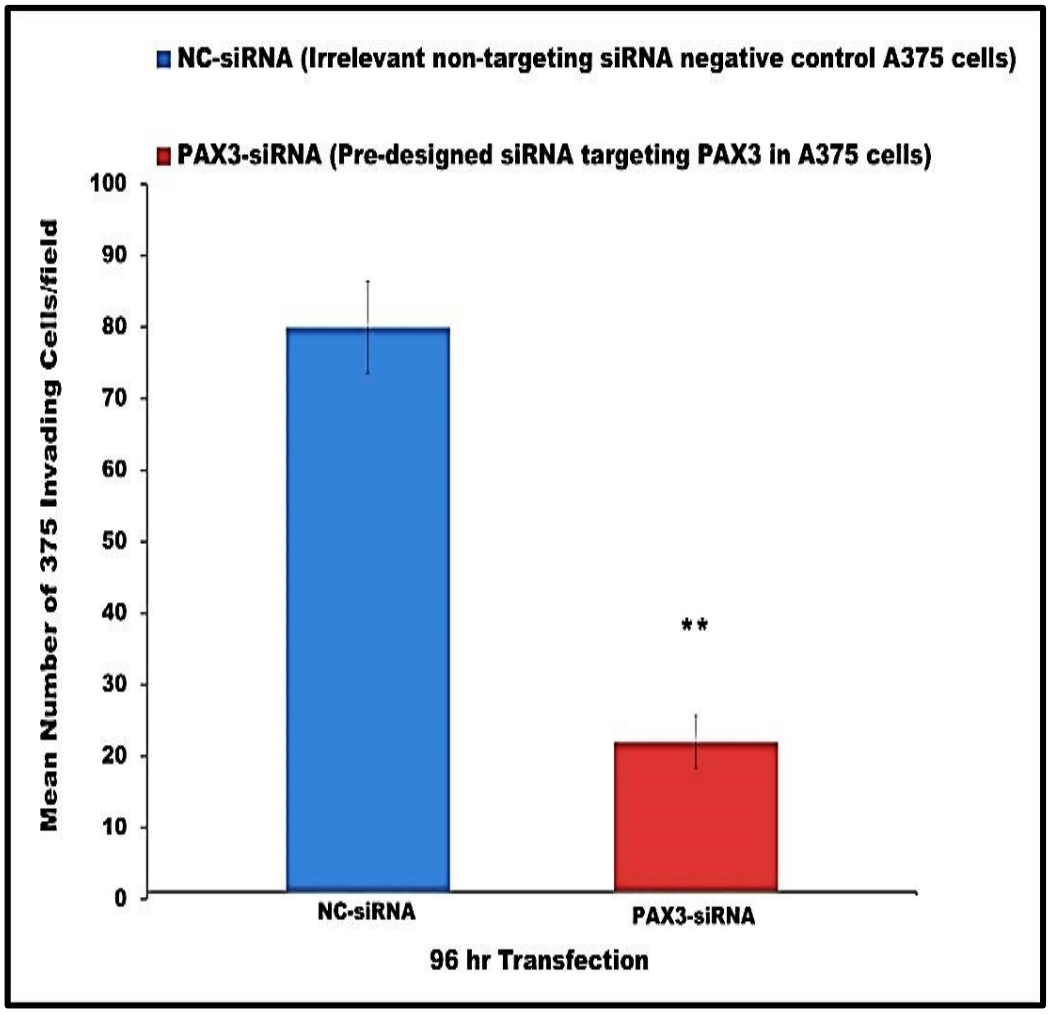

Figure 4.18 Mean numbers of A375 cell invasion. The mean number of invading cells in NC-siRNA transfected A375 cells (blue column) was compared with the mean number of invading cells in *PAX3*-siRNA transfected A375 cells (red column). Invading A375 cells were counted in five microscopic fields per experiment. The columns represent the mean number of A375 cells invading a matrigel membrane as a mean of three separate experiments (n = 15). (Student's t-test), (**, $p < 0.01$).

4.11. Effect of Knockdown of *PAX3* on Clonogenicity of A375 Cells

The inhibitory effect of *PAX3* repression on A375 cell colony reproducibility was evaluated by an *in vitro* soft agar assay following 96 hr transfection with NC-siRNA or*PAX3*-siRNA. This experiments demonstrated that colony formation of A375 cells was reduced by *PAX3* inhibition in *PAX3*-siRNA transfected cells when compared with NC-siRNA transfected counterparts. NC-siRNA transfected A375 cells generated many large colonies of diameter greater than 100µm in contrast to smaller colonies generated

of diameter much less than 100µm from *PAX3*-siRNA transfected A375 cells (**Fig. 4. 19**). The small colonies were expected to be aggregates of apoptotic A375 cells (according to the soft agar assay manufacturer's literature).

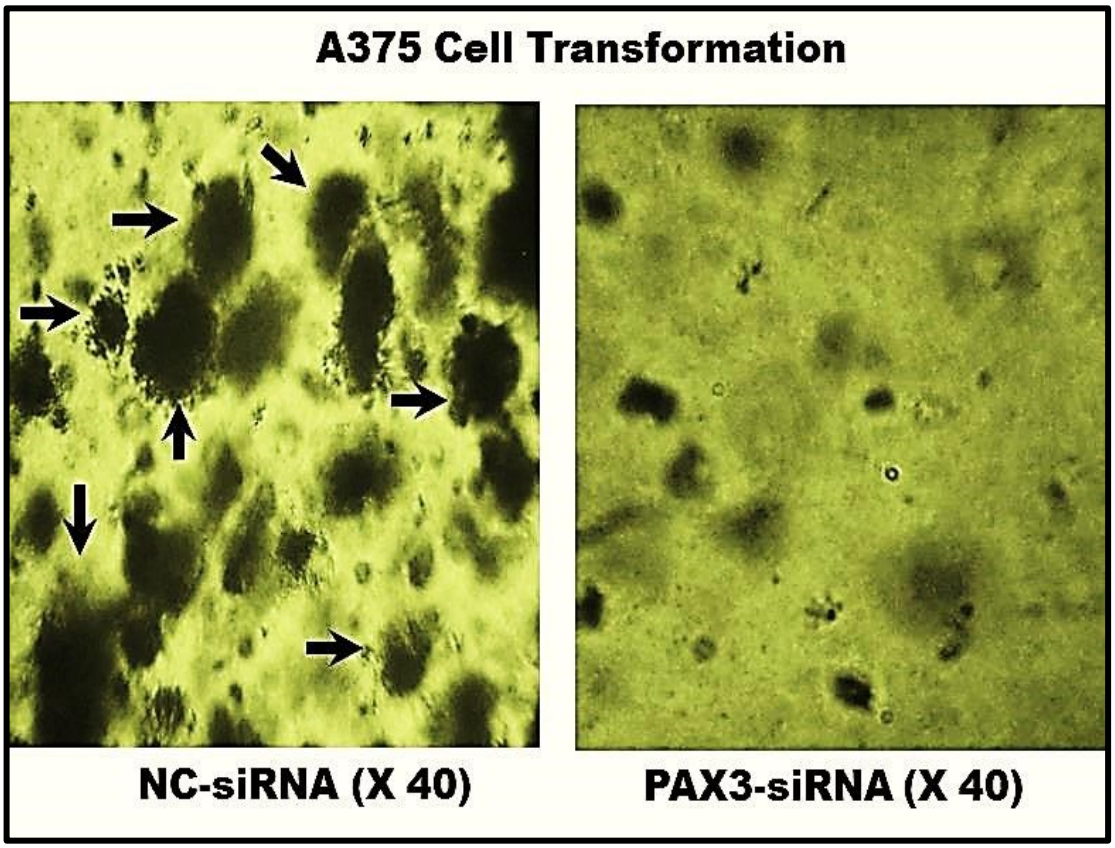

Figure 4.19 A375 cell soft agar colony reproducibility following 96 hr transient siRNA transfection. X 40 magnification phase contrast micrograph of anchorage independent growth of A375 cell colonies in soft agar after 28 days incubation. A375 colonies were stained with crystal violet. NC-siRNA transfected A375 cells produced larger colonies (>100µm). *PAX3*-siRNA transfected A375 cells showed smaller colonies. Colonies were counted over five fields in each of three experiments.

The mean number of 15 colonies in NC-siRNA transgected A375 cells was significantly different from the mean number of 1 colony in *PAX3*-siRNA transfected cells ($p < 0.01$) because of apoptosis of A375 cells (**Fig.4.20**).

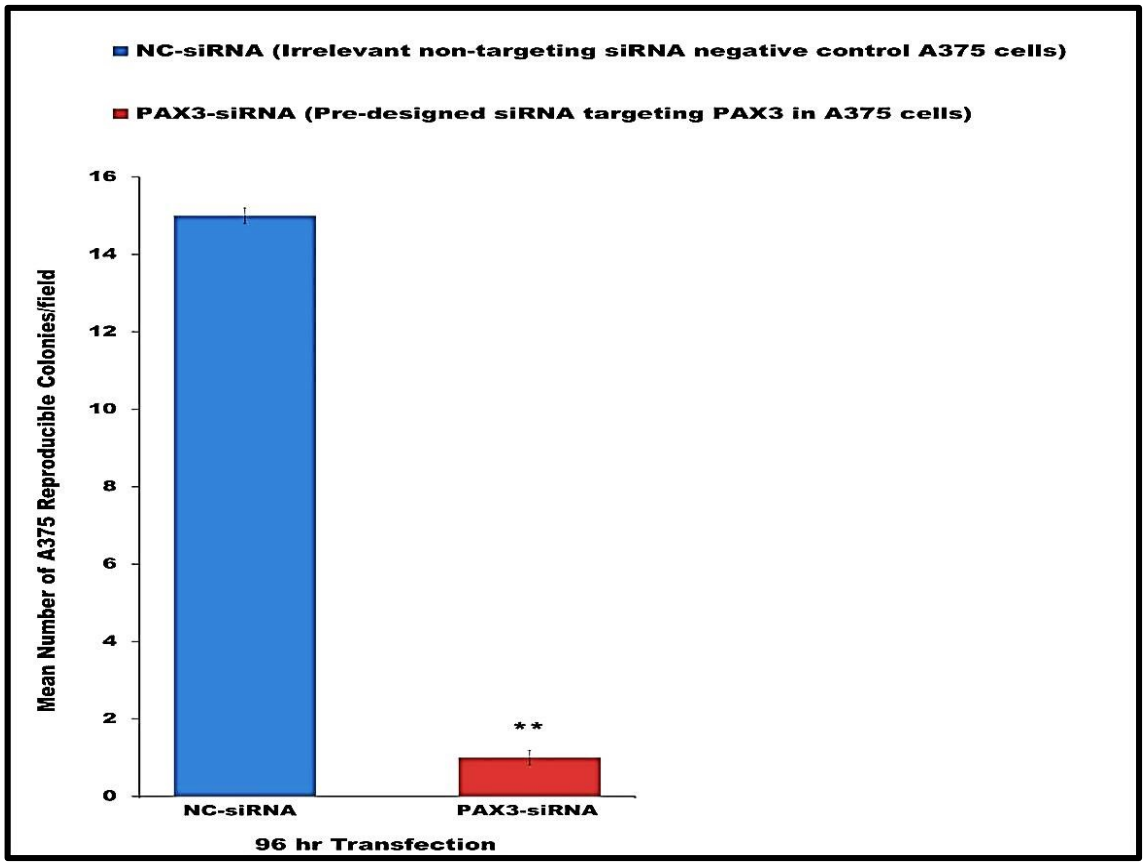

Figure 4.20 Mean numbers of A375 reproducible colonies. The mean number of reproducible colony in NC-siRNA treated A375 cells (blue column) was compared with the mean number of reproducible colony in *PAX3*-siRNA transfected cells (red column). The mean values were derived from three separate experiments and found to be statistically different, (n = 15). Student's t-test; **, $p < 0.01$.

4.12. Effect of *PAX3* Down-regulation on Inhibition of Apoptosis of A375 Cells

Both indirect biochemical and direct morphological assessments of cell apoptosis were undertaken to determine the effect of *PAX3* down-regulation on apoptosis of the A375 cell line. The caspase 3/7 activities in both 96 hr *PAX3*-siRNA and NC-siRNA treated A375 cells were measured by indirect biomedical analysis. The caspase 3/7 activity in the staurosporine (1µM/ml; 1µl/ml) treated A375 cells was used as positive control. At 30 min, the mean caspase 3/7 activities in *PAX3*-siRNA treated A375 cells of 210 X 10^4 RLU (**Fig. 4.21B**) was significantly higher ($p < 0.01$) than 75 X 10^4 RLU produced in NC-siRNA treated cells (**Fig. 4.21C**). The staurosporine positive apoptosis control yielded 380 X10^4 RLU (**Fig. 4.21A**).

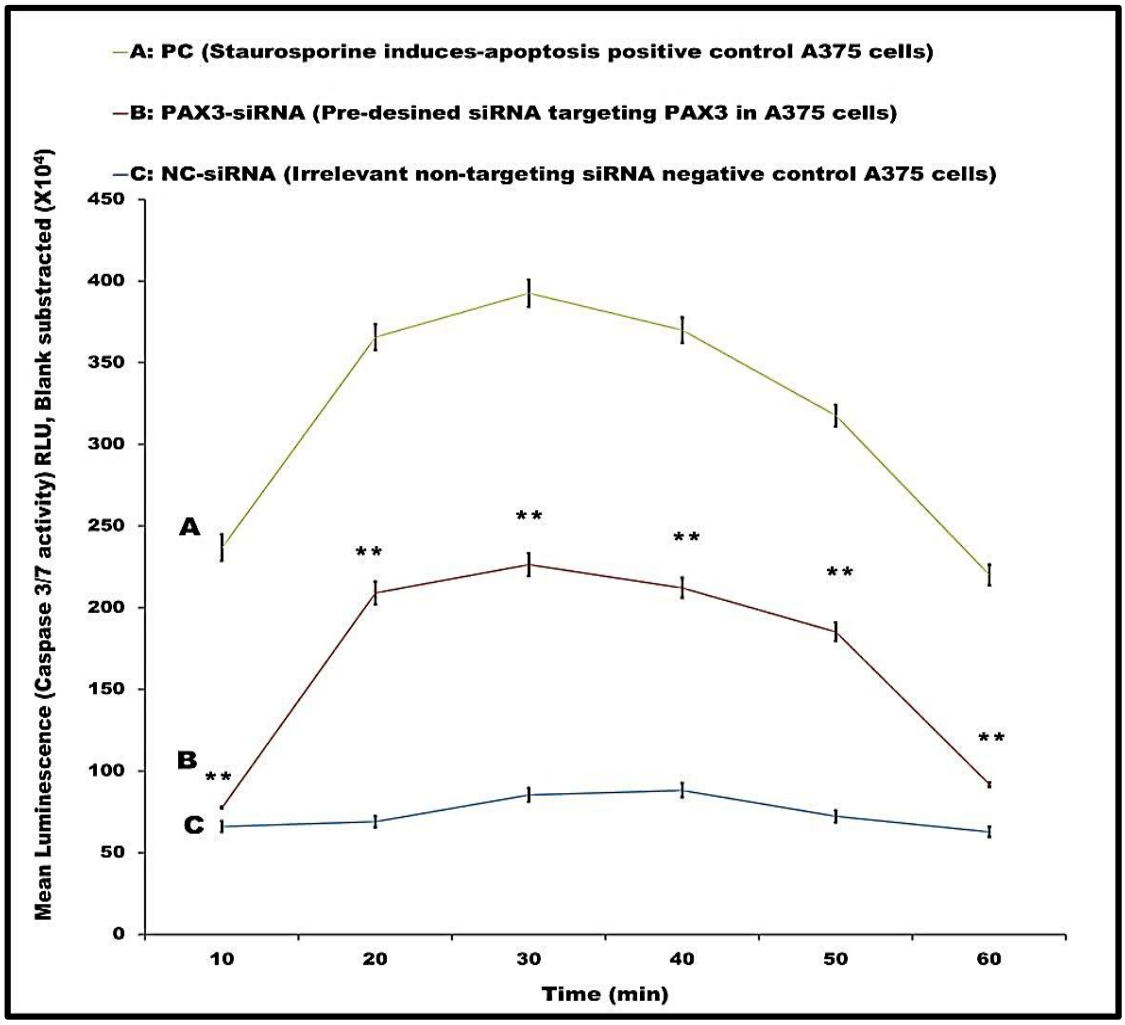

Figure 4.21 Indirect Caspase 3/7 activity in A375 cells following 96 hr siRNA transfection and/ or 2 hr staurosporine induced-apoptosis (**positive control**). The mean caspase 3/7 activity in **A (**2 hr Staurosporine (1µM/ml; 1µl/ml) treated A375 cells positive apoptosis control, which pattern of curve signify increased caspase 3/7 activity and induction of apoptosis), was compared with both **B (***PAX3*-siRNA transfected A375 cells which presented similar pattern of curve to **A** indicated increased caspase 3/7 activity and induction of A375 cell apoptosis), and **C** (NC-siRNA transfected A375 cells, showing dissimilar pattern of curve to **A** showed no induction of apoptosis). The curves are representation of mean of three replicate measurements in two separate experiments (n = 6). At 30 min the mean RLU measurement of **B** was statistically higher than that of C, Student's t-test, (**B** versus **C** **, $p < 0.01$).

Direct detection of delayed apoptosis of A375 cells was performed by the DeadEnd™ Fluorometric TUNEL system after 96 hr A375 cell transfection. DNA fragments with green fluorescence-staining were rarely observed in NC-siRNA A375 cells in a typical fluorescence microscopic field. However, they were observed in both staurosporine-

treated (PC), *PAX3*-siRNA transfected as well as *PAX3*-siRNA transfected plus PC treated cells (**Fig. 4.22**).

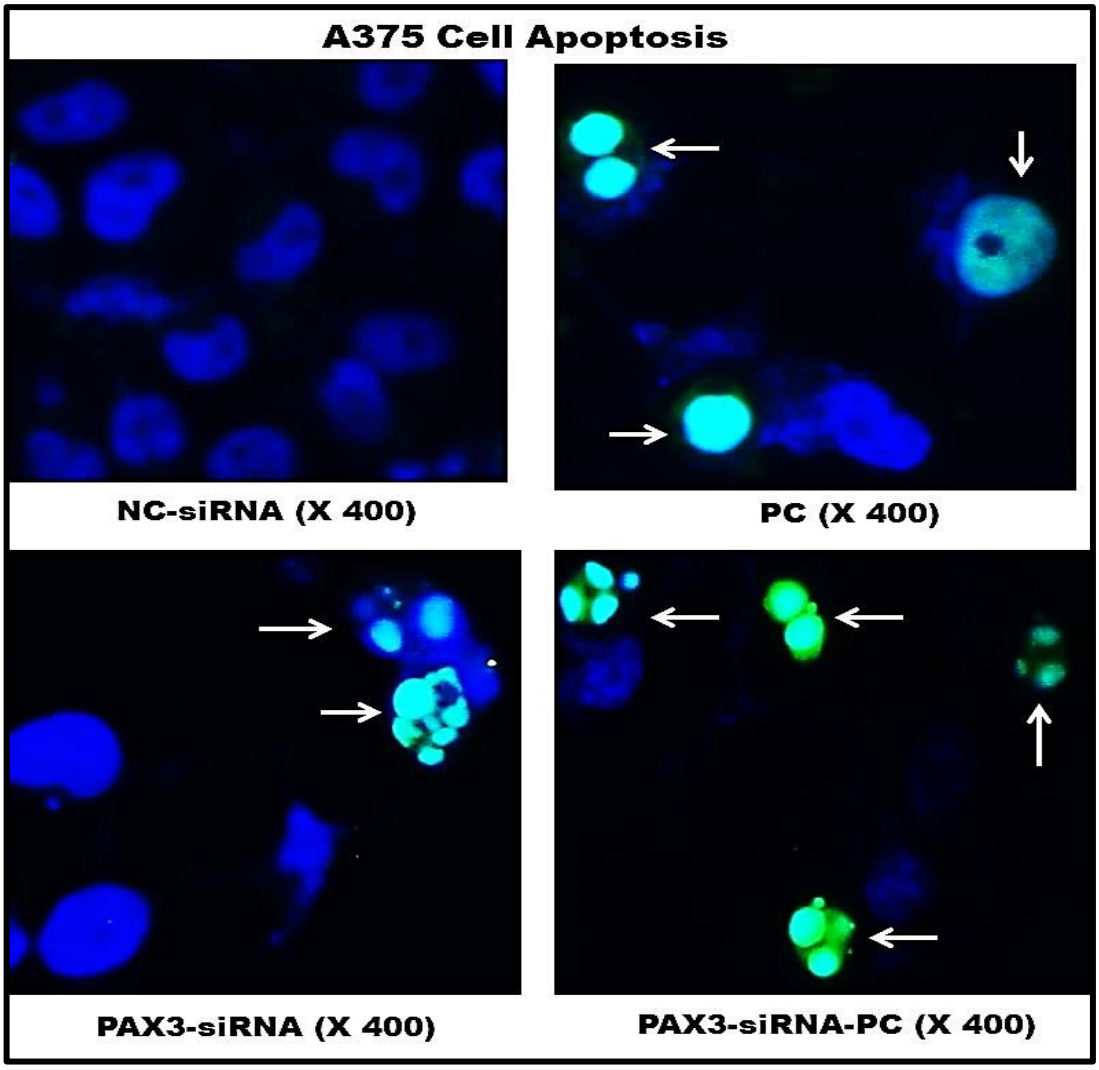

Figure 4.22 Direct detection of apoptosis in transfected A375 cells by the DeadEnd Fluorometric TUNEL System. X 400 fluorescence micrographs of apoptosis in A375 cells following 96 hr siRNA transfection. **NC-siRNA** (negative control transfected A375 cells showed blue nuclei non-apoptotic cells (DAPI). **PC** (2hr staurosporine (1μM/ml; 1μl/ml) treated A375 cells positive apoptosis control exhibited few green fluorescent apoptotic cell nuclei (pointed arrows). ***PAX3*-siRNA** (*PAX3*-siRNA transfected A375 cells displayed few green fluorescent apoptotic cell nuclei (pointed arrows). ***PAX3*-siRNA-PC** (combined *PAX3*-siRNA transfected A375 cells plus 2 hr staurosporine treatment revealed many green fluorescent apoptotic cell nuclei) (pointed arrows).

The conclusion is that *PAX3* down-regulation added to the apoptosis caused by staurosporine (1μM/ml; 1μl/ml) in A375 cells, which had been transfected with *PAX3*-

siRNA plus treated for 2 hr with staurosporine (1µM/ml; 1µl/ml). Moreover *PAX3* siRNA alone could induce apoptosis. There was a significant difference in the mean number of observed apoptotic cells amongst the PC (3 per field), *PAX3*-siRNA (2 per field), *PAX3*-siRNA-PC treated (7 per field) compared to NC-siRNA treated cells ($p < 0.01$). The mean number of apoptotic cells in the *PAX3*-siRNA-PC sample was higher than *PAX3*-siRNA treated A375 cells or A375 cells treated with staurosporine (1µM/ml; 1µl/ml) alone (**Fig. 4.23**).

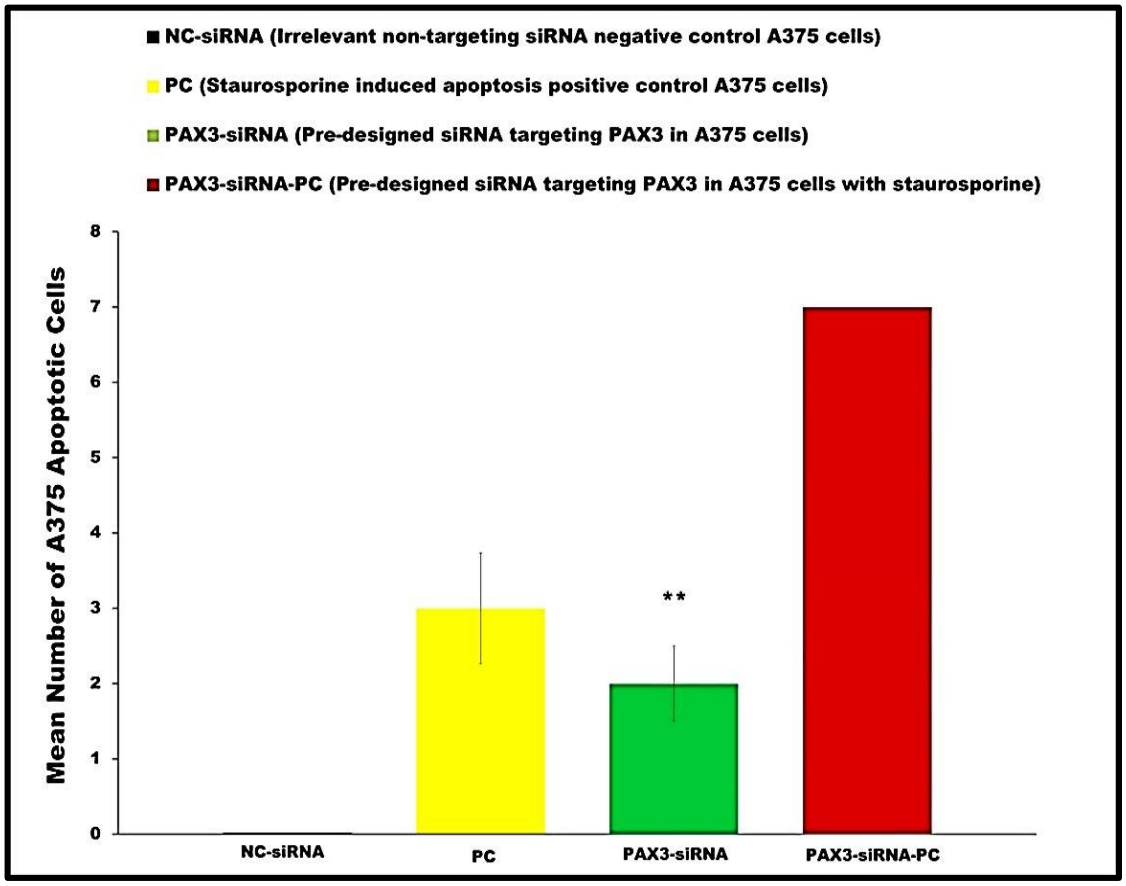

Figure 4.23 Mean numbers of transfected A375 apoptotic cells. The mean number of A375 apoptotic cells in **NC-siRNA** (negative control transfected A375 cells (blue column) was compared with the mean number of apoptotic A375 cells in both **PC** (2 hr staurosporine (1µM/ml; 1µl/ml) treated A375 cells positive apoptosis control (yellow column) and ***PAX3*-siRNA (** *PAX3*-siRNA transfected A375 cells) (green column) or ***PAX3*-siRNA-PC**, (combine *PAX3*-siRNA transfected A375 cells followed by 2 hr staurosporine (1µM/ml; 1µl/ml) treatment (red column). The Mean number of apoptotic A375 cells were counted from five fluorescence microscopic fields in three separate experiments (n = 15). PC vs NC demonstrates that positive control was working. (**NC** vs ***PAX3*-siRNA** or **NC** vs ***PAX3*-siRNA–PC**), Student's t-test; **, $p < 0.01$.

4.13. DISCUSSION

4.13.1. Down-regulation of *PAX3* Expression in Melanoma A375 Cells Modulates Downstream Targets

PAX3 as a transcription factor is essential for the development of melanocytes by regulating melanocyte differentiation, proliferation, migration and inhibition of apoptosis during embryogenesis. The regulatory activities of *PAX3* isoforms in melanocytes have been demonstrated (Wang *et al.,* 2007). The functional activities of *PAX3* in melanocyte development seem to be observed also in melanoma cells (Medic *et al.,* 2011; Milet *et al*., 2013). *PAX3* expression in metastatic melanoma of a transgenic mouse model has been demonstrated alongside *MITF* (Makhzami *et al*., 2012). Recently, the expression of *PAX3* and *MCAM* in peripheral blood have been identified as biomarkers in recurrent aggressive metastatic melanoma (Dye *et al*., 2013).

Collectively, the above studies implicate *PAX3* involvement in melanoma. Since *PAX3* has been demonstrated to regulate melanocyte development as well as the metastatic activity of melanoma, repression of *PAX3* will probably inhibit melanoma progression

This present study has achieved a significant down-regulation of *PAX3* in the A375 melanoma cell line. Analysis of microarray data revealed a 8.95-fold knockdown of *PAX3* expression in the A375 cell line following 96 hr *PAX3*-siRNA transfection, which subsequently altered the expression patterns of numerous downstream targets of *PAX3* (**Tables 4.3 and 4.4**). Likewise, semi-quantitative RT-PCR analysis demonstrated a minimum of 90% knockdown in expression of the various *PAX3* isoforms in *PAX3*-siRNA transfected A375 cells, which was significantly different from the NC-siRNA transfected negative control A375 cells ($p < 0.01$), (**Figs. 4.3 and 4.4**). Western blotting analysis validation of the knockdown of *PAX3* mRNA, demonstrated a significant reduction in PAX3 protein expression and changes in its downstream targets. Suppression of PAX3, induced significant inhibition of C-MYC, ITGβ5, MYOD1 and BCL2 protein expression, whereas increased protein expression of P21, P53 and CASP3 was demonstrated (**Figs. 4.7 and 4.8**).

Microarray analysis data further demonstrated that silencing of *PAX3* expression in A375 cells, significantly modulated the expression patterns of some *PAX3* binding partners (**Table 4.5**). For example, *BCL2, CIB1, HES1, MITF, SRY10, MYOD1, MYOG, SOSTDC1* and *TBX18* were down-regulated, whilst *PTEN, HMOX1* and *MSX1* were up-regulated. Once again, the increased expression pattern of *PTEN* agreed with a previous study of the induced expression of *PTEN* in rhabdomyosarcoma (Li *et al.,* 2007). The suppression of *PTEN* and increased *BCL2* expression after *PAX3* down-regulation can inhibit apoptosis. Fascinatingly, the present study demonstrates that up-regulation of *PTEN* and decreased expression of *BCL2* certainly induced A375 cell apoptosis. The effect of *PAX3*-siRNA inhibition of *PAX3* mRNA and protein in A375 melanoma cells was comparable to the pattern of inhibition of *PAX3* demonstrated in the JR1 and RH30 rhabdomyosarcoma cell lines.

Additionally, inhibition of *PAX3* in the A375 melanoma cell line induced both suppression and activation of downstream regulatory genes that facilitate *PAX3* activities in the regulation of A375 cell cycle, proliferation, migration, adhesion, and apoptosis. This current study demonstrates that some of the potential tumourigenic activities of *PAX3* were interrupted following *PAX3*-siRNA knockdown, including the significant inhibition of A375 cell proliferation ($p < 0.01$), (**Figs. 4.10 and 4.11**). This significant decreased in cell proliferation indicate that A375 cells were undergoing apoptosis after 96 hr inhibition of *PAX3* as shown in the microarray results of increasing expression of apoptosis ptomoting genes (**Table 4.4**) and decreasing expression of apoptosis inhibitotry genes (**Table 4.3**).

4.13.2. Inhibition of *PAX3* Expression Suppressed A375 Cell Cycle Progression and cell Proliferation

Expression of *PAX3* promotes both melanocyte proliferation during melanogenesis and proliferation of melanoma cells (Kubic *et al.,* 2012; Milet *et al.,* 2013). The impact of *PAX3* down-regulation on A375 melanoma cell growth and proliferation was investigated. The present microarray analysis demonstrated that 28 selected key genes involved in regulating the cell cycle and cell proliferation were significantly down-

regulated (**Table 4.3**: *CALM, CAPRINI, CCNB1, CCND2, CCND3, CDCA3, CDC25C, CDK2, CDK4, CDK5, CDKN2C, CIB1, CITED2, C-MYC, GTSE1, HES1, HUS1, ID3, IGFβP3, IGFβP5, LOC, NDRG1, SMAD2, TAZ, TBX18, TGFβ2, TGFβ3* and *VEGFA*). By contrast, 35 other selected genes which inhibit cell cycle progression and cell proliferation were significantly up-regulated following *PAX3* repression in A375 cells (**Table 4.4**); (*ANAPC5, AKT, BIRC5, BRCA1, BRCA2, BUB1, CDC25A, CDC25B, CDK1, CDK6, CDKN1A, EDN3, DHFR, CHK1, CHK2, ETS1, GADDβ45, GINS1, GRK6, HIRA, HMOX1, ITGβ1, JAK2, JUN, SKP2, MCM3, MDM2, MSX1, MELK, RB, P21, P53, PCNA, PTEN* and *TFDP1*).

The KEGG-pathway functional annotational tool of David NIH bioinformatics database analysis of the present microarray data suggest that inhibition of *PAX3* in A375 cells induces the activation of AKT/P53/PTEN signaling pathways resulting in G2 cell cycle arrest and induction of apoptosis.

PAX3 silencing induces A375 cell cycle arrest, which subsequently inhibits cell proliferation. Flow cytometry cell cycle analysis following *PAX3* knockdown, indicates that fewer A375 cells (57.6% ±) were in the G0/G1 phase relative to negative control cells (59.6% ±) and 5.3% ± of A375 cells were in the S phase compared to 7.9% ± in the NC-siRNA negative control, demonstrating the inhibitory effects of *PAX3*-siRNA on cell cycle progression (**Fig. 4.12**) (**Table 4.8**). A375 cells seemed to accumulate in the G2/M checkpoints after *PAX3* down-regulation. Repression of *PAX3* after 96 hr markedly inhibited A375 cell proliferation (**Figs. 4.10 and 4.11**), as a result of apoptosis of A375 cells. This pattern of inhibition reflected the increased expression of cell apoptosis promoting genes caspase 3 (**Fig. 4.4**) including and the decreased expression of apoptosis inhibiting genes including BCL2 (**Fig. 4.3**).

David NIH functional annotational bioinformatics KEGG-pathway analysis tool version 6.7, was used to determine the effects of *PAX3* down-regulation on the various regulatory pathways of the A375 cell line in this present microarray data. Following *PAX3* inhibition, the microarray data demonstrated increased expression of *PCNA,*

BIRC5, BRCA1, BRCA2, JAK2, JUN, ITGβ1 and *TFDP1,* indicating A375 cell viability with a decreased proliferation rate. Alterations in the expression patterns of these genes in the microarray data showed a strong relationship with the cell proliferation experiments. Similarly, the increased expression of *P21, P53* as well as the checkpoint genes (*CHK1, CHK2, CDC25A* and *CDC25B*) indicates that the suppression of *PAX3* possibly induced a G2 phase cell cycle arrest of A375 cells through the CHK1/CHK2/CDC25C pathways. Furthermore, a close evaluation of the microarray data demonstrating increased expression of the key G2 phase cell cycle arrest-promoting genes including (*ANAPC5, AKT, CHK1, CHK2, CDC25A, CDC25B, CDK1, CDK6, GADDβ45, P21* and *P53*) indicating that suppression of *PAX3* induced a G2 phase A375 cell cycle growth arrest. By contrast, the decreased expression levels observed in the five key positive regulators of G1 phase of the cell cycle (*CCNA, CCND1, CDC25C, CDK2* and CDK4), demonstrates that A375 cells were not arrested at the G1 phase after *PAX3* knockdown.

The KEGG-pathway analysis of this present microarray data demonstrates that down-regulation of *PAX3* in A375 cells induced activation of the AKT signaling pathway, which in turn stimulated the P53 signaling pathway to block cell cycle at the G2 growth phase and subsequently inhibited cell proliferation (**Fig. 4.24**). Inhibition of *PAX3* expression caused increased AKT expression, which resulted in the activation of the checkpoint kinases 1/2 to induce activation of CDC25A/CDC25B to block CDK2/CCNB1 and arrest A375 melanoma cell growth at the G2 phase of the cell cycle (**Fig. 4.24**). Similarly, *PAX3* down-regulation induced increased P53 expression which stimulated *P21* and *GADD45B* expression to block CDK2/CCNB1 and resulted in G2 phase A375 melanoma cell arrest (**Fig. 4.24**).

The activation of P53 correlates with the western blotting results showing increased P53 phosphorylation and decresed BCL2 expression induced A375 cell apoptosis. This implies that suppression of *PAX3* is a suitable therapeutic target and would possibly inhibit melanoma tumour growth and progression. By comparison, silencing *PAX3* in JR1 and RH30 cell lines activated the ATR/ATM signalling pathway to induce JR1 and RH30 cell arrest at the G1 phase of the cycle resulted in JR1 and RH30 cell apoptosis.

Repression of *PAX3* in A375 cells induces activation of the AKT signalling pathway to halt A375 cells at the G2 phase of the cell cycle also resulted in A375 cell apoptosis. These diverging activities of *PAX3* demonstrate that *PAX3* could use different pathways in its cell regulatory mechanisms, according to the cell type in which it acts.

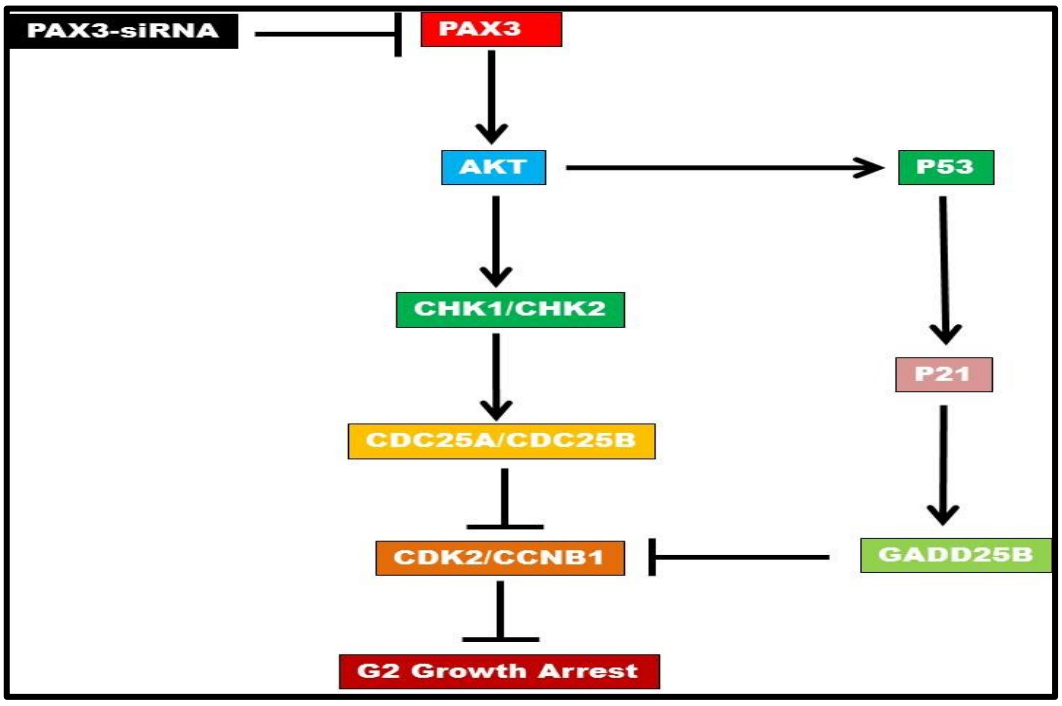

Figure 4.24 Schematic diagram of A375 melanoma cell cycle arrest. **Knockdown of *PAX3* induced a G2 growth arrest of A375 cells via activation of AKT signaling.** Induced activation of checkpoints kinases 1/2 induced activation of CDC25A/CDC25B, which in turn blocked CDK2/CCNB1 to arrest melanoma A375 cell growth at the G2 phase of the cell cycle. Likewise, activation of P53 induced the activation of P21 and GADD45B, which in turn block CDK2/CCNB1 to cause a G2 phase cell growth arrest.

Key: → Denote activation. ⊣ Indicate inhibition/block.

4.13.3 Knockdown of *PAX3* Induced Metastatic Inhibition of A375 Cell Migration

Migration of A375 cells is crucial for melanocyte migration and proliferation as well as metastatic melanoma (Berlin *et al.,* 2012; Milet *et al.,* 2013). *PAX3* knockdown in melanoma has been demonstrated to inhibit cell migration (Wouters *et al.,* 2013). The present study examined the effect of *PAX3* suppression on the migratory ability of melanoma A375 cells. The microarray analysis demonstrates that silencing *PAX3* in

A375 cells induced significantly diminished expression of 17 selected genes regulating cell migration (**Table 4.3**: *ADAM23, CIB1, COL3A1, CXCR4, FGD4, FSCNI, HUS1, MCAM, MMP2, MXRA7, PCDH18, PCDH7, RECK, VCAN, TGFβ2, TGFβ3* and *VEGFA*). Conversely, *PAX3* inhibition induces increased expression of six negative regulatory genes for cell migration (*ENDRA, FNDC5, JUN, LAMA1, MSH2* and *MTSS1*) (**Table 4.4**). The change in expression of all of these genes probably inhibits A375 cell migration. The microarray analysis of these gene alterations shows a strong correlation with the substantial suppression of A375 cell migration exhibited in the migration experiments (**Figs. 4.14 and 4.15**).

The effect of *PAX3* down-regulation on A375 cell migration was demonstrated using a scratch wound healing assay, which showed a significant decrease in the P*AX3*-siRNA transfected A375 cell migration relative to the NC-siRNA transfected A375 cells ($p < 0.01$) (**fig. 4.15**). The higher level of A375 cell migration observed in the negative control A375 cells was correlated with a higher level of P*AX3* expression, which induces A375 cell migration, resulting in a significant closure of the wound gaps (**Figs. 4.13 and 4.14**). Comparatively, *PAX3*-siRNA maintained wider wound gaps to indicate inhibition of A375 cell migration caused by diminished *PAX3* activity. Inhibition of *PAX3* induced A375 cell apoptosis which resulted remarkable inhibition of A375 cell migration. This was demonstrated in microarray data of increasing expression of apoptosis ptomoting genes (**Table 4.4**), and decreasing expression of apoptosis inhibitotry genes (**Table 4.3**).

The microarray analysis in the KEGG-pathway demonstrated increased expression of *ENDRA* and *FNDC5* that induced inhibition of *TGFβ3, VEGFA, FGD4* and *FSCNI* expression, suggesting that *PAX3* probably activates the FAK/Rho/RAS/MAPK signaling pathways to inhibit A375 cell migration (**Fig. 4.25**). The cell migration assay, demonstrating that the presence of *PAX3* in A375 cells induces migration, indicates that *PAX3* expression is probably essential for metastatic melanoma A375 cell migration. Hence, *PAX3* could be an appropriate target for inhibition of melanoma cell migration. In the metastatic processes, adhesion of cells to the ECM may depend on the migratory ability of cells. Therefore, this markedly decreased A375 melanoma cell migration may perhaps impair adhesion of A375 melanoma cell to ECM proteins.

4.13.4. Repression of *PAX3* Expression Blocked A375 Cell Adhesion

Expression of cell surface adhesion molecules is essential for the promotion of metastatic melanoma since decreased cell adhesion inhibits metastasis (Sil *et al.,* 2010; Nishibaba *et al.,* 2012).

Following repression of PAX3 in A375 melanoma cells, microarray analysis demonstrates that expression of ten cell adhesion genes was decreased *COL3A1, CXCR4, FGD4, ITGβ5, JAM2, NID1, MCAM, PCDH7, PCDH18,* and *VCAN*) which inhibited A375 cell adhesion to ECM proteins *in vitro* (**Table 4.3**). On the contrary, three cell adhesion inhibitory genes (*FNDC5, SELPLG,* and *LAMA1*) were up-regulated (**Table 4.4**). The alterations in expression of these genes will possibly interfere with A375 cell adhesion during metastatic melanoma.

In assessing the impact of inhibition of these cell surface adhesion molecules on A375 cell adhesion ability, cell–matrix assays indicated that *PAX3* silencing induced significantly decreased adhesion of A375 cells to all of the seven selected ECM proteins (Collagen I, Collagen II, Collagen IV, Fibronectin, Laminin, Tenascin and Vitronectin) relative to negative control cells ($p < 0.01$) (**Fig. 4.16**). The observed inhibition of A375 cell adhesion strongly correlates with the microarray analysis showing suppression of cell adhesion regulatory genes. The KEGG-pathway analysis of this present microarray data implies that silencing of *PAX3* probably decreases A375 cell adhesion to the ECM, via activation of the FAK/Rho/RAS/MAPK signaling pathway. The activation of *FNDC5* and *SELPLG,* suppressed *ITGβ5, PCDH7, PCDH18* and *MCAM*, which consequently induced inhibition of A375 cell adhesion to ECM proteins (**Fig. 4.25**). Particularly, *MCAM* as a downstream target of *PAX3,* plays a crucial role in promoting A375 cell adhesion.

The outcome of this current cell adhesion assay confirmed that *PAX3* is crucial in the promotion of A375 cell adhesion. Therefore, *PAX3* would be a suitable target for inhibition of A375 cell adhesion, which could possibly block metastatic melanoma. Since contact between cells and the ECM modulates cellular functional activities, the

observed marked block of A375 cell adhesion to the ECM could probably impede tumour cell invasion.

4.13.5. *PAX3* Silencing Inhibits A375 Cell Invasion

The expression of *PAX3* has been implicated in promoting invasion of melanoma through modulation of downstream targets (Makhzami *et al.,* 2012; Dye *et al.,* 2013).

In this present study, microarray analysis demonstrates significantly decreased expression of four cell invasion promoting genes (*FGD4, MMP2, RECK* and *SMAD2*) (**Table 4.3**). On the contrary, the expression of two cell invasion inhibitory genes was significantly increased (*ENDRA* and *MTSS1*) (**Table 4.4**). The observed changes in gene expression could possibly influence A375 melanoma cell invasion and metastatic potential. *PAX3*-siRNA significantly decreased A375 cell invasion compare to the NC-siRNA ($p < 0.01$) as demonstrated using the Boyden chamber invasion assay (**Figs. 4.17 and 4.18**). The inhibition of A375 cell invasion demonstrated here, correlates with the microarray analysis showing altered expression of genes related to cell invasion. The outcome of this cell invasion analysis demonstrates that *PAX3* induces A375 melanoma cell invasion by activating the FAK/RHO/RAS/MAPK signaling pathways as shown in the KEGG-pathway analysis. Activation of *ENDRA* and *MISS1* blocked *MMP2* and its ability to induced A375 cell invasion of ECM (**Fig. 4.25**). Silencing of *PAX3* therefore, is a possible therapeutic target for inhibition of metastatic melanoma.

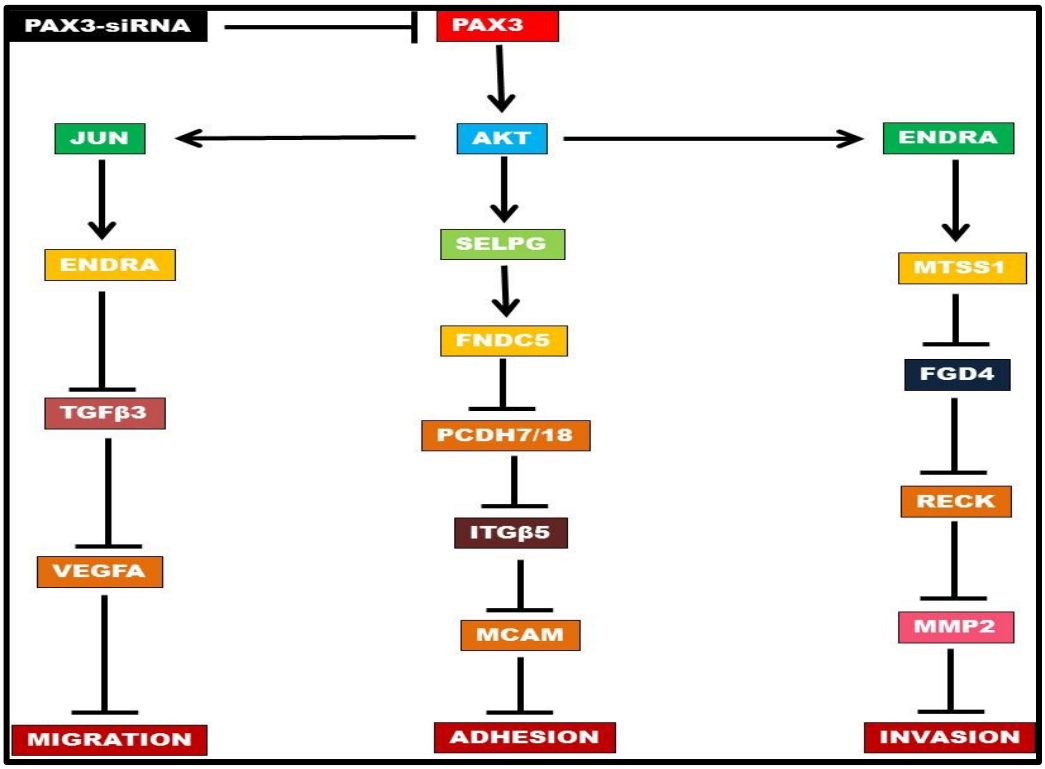

Figure 4.25 Inhibition of metastatic A375 melanoma cells via activation of AKT signaling (created from the KEGG-pathway analysis**).** *PAX3* silencing induced activation of the AKT signaling pathway, which activated *JUN* and *ENDRA* to inhibit *TGFβ3* and *VEGFA*, which in turn induced inhibition of A375 melanoma cell migration. *AKT* activation of *SELPG* and *FNDC5* blocked *PCDH7/18, ITGβ5*, and *MCAM* to induce inhibition of A375 melanoma cell adhesion. *AKT* activation of *ENDRA* and *MTSS1* blocked *FGD4, RECK* and *MMP2* to induce inhibition of A375 melanoma cell invasion.

4.13.6. Knockdown of *PAX3* Inhibited A375 Cell Clonogenicity in Soft Agar

Melanocyte transformation into melanomas (demonstrated *in vitro*) is one of the tumourigenic activities of *PAX3* (Berlin *et al.*, 2013).

In this present study, the potential of *PAX3* to inhibit transformed cell growth was demonstrated following inhibition of *PAX3* in melanoma A375 cells. Analysis of microarray data showed a significantly reduced expression of one cell transformation gene (*TGFβ3*) (**Table 4.3**) and markedly increased expression of two cell transformation inhibitory genes (*P21* and *P53*) (**Table 4.4**). The observed alterations in the expression of these genes could probably stimulate the ability of transformed A375 melanoma cells to grow in soft agar.

The potential of *PAX3* to allow transformed cell growth (of A375 melanoma cells) was investigated using the soft agar anchorage-independent assay. *PAX3*-siRNA transfected A375 cells produced a few insignificant colonies compared to the large colonies demonstrated in the NC-siRNA transfected cells ($p < 0.01$) (**Figs. 4.19 and 4.20**). This indicates that the expression of *PAX3* in the NC-siRNA transfected cells allows A375 melanoma cell growth in soft agar, whilst inhibition of *PAX3* expression in *PAX3*-siRNA transfected cells blocked it. Analysis of this current microarray data in the KEGG-pathway, demonstrate that inhibition of transformed A375 melanoma cell growth could possibly have occurred through the activation of the P53 signaling pathway (**Fig. 4.26**).

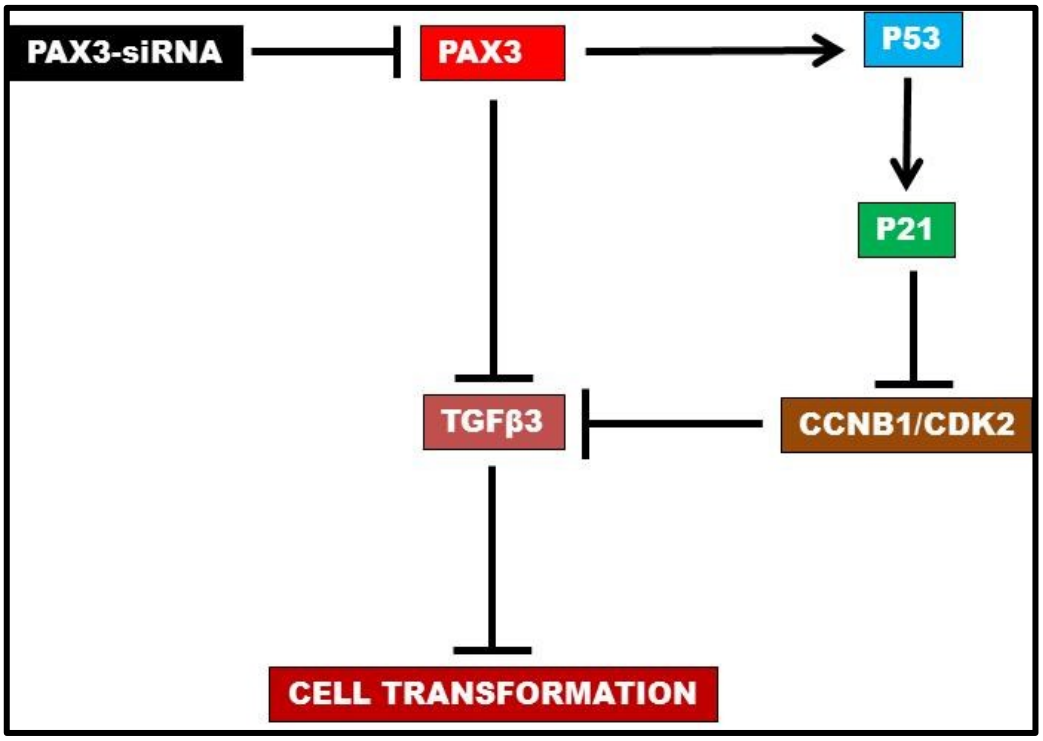

Figure 4.26 Inhibition of A375 melanoma colony formation via P53 signaling pathway (drived from the KEGG-pathway analysis). Silencing of *PAX*3 activation of P53 and P21 to block CCNB1/CDK2, which in turn can prevent TGFβ3 from inhibiting transformed A375 melanoma cell growth in soft agar. Likewise, *PAX3* silencingdirectly inhibits *TGFβ3* and prevents its block of A375 melanoma cell growth in soft agar.

Inhibition of A375 colony reproducibility resulting from apoptosis of A375 cells relates to the increasing expression of apoptosis inducing genes (**Table 4.4**) and decreasing expression of apoptosis inhibitotry genes (**Table 4.3**) of the microarray data.

Knockdown of *PAX3* probably induced direct inhibition of *TGFβ3* expression to block the growth of transformed A375 melanoma cells. Likewise, *PAX3* silencing also induced increased *P53* expression, which in turn up-regulated *P21* expression to block *CCNB1/CDK2*, which in turn blocked TGFβ3, resulting in the inhibition of transformed A375 melanoma cell growth. This discovery is suggestive of *PAX3* being a suitable therapeutic target for inhibiting transformed (melanoma) cells. These experiments show that *PAX3* is possibly acting more as a survival factor for transformed cells.

4.13.7. Suppression of *PAX3* Induced A375 Cell Apoptosis

Evasion of apoptosis is one of the mechanisms used by *PAX3* for the benefit of melanoma. Following knockdown of *PAX3*, the microarray analysis data demonstrates decreased expression of five apoptosis inhibitory genes *(BCL2, BNIP3, FAIM, TNFRSF19* and *TUBB2C*) (**Table 4.3**). On the contrary, increased expression of ten apoptosis promoting genes was shown (*AEN, CASP3, CASP4, CASP7, KITLG, MCL1, P53, PTEN, SENP5* and *TRIB3C*) (**Table 4.4**). The observed variations in the expression of these genes may perhaps play contributory roles in induction of A375 melanoma cell apoptosis.

After *PAX3* knockdown, assessment of the role of *PAX3* in the induction of A375 melanoma cell apoptosis using the indirect caspase 3/7 activity assay, demonstrated significant high caspase 3/7 activity in the *PAX3*-siRNA transfected cells compared to a low caspase 3/7 activity in the NC-siRNA transfected A375 cells ($p < 0.01$) (**Fig. 4.21**). The direct apoptosis DeadEnd™ Fluorometric TUNEL assay verified the above experiments. The *PAX3*-siRNA transfected cells in combination with staurosporine, demonstrated significantly greater numbers of apoptotic nuclei compared to either the NC-siRNA transfected cells (negative control) the staurosporine induced apoptotic cells (positive control) ($p < 0.01$) (**Figs. 4.22 and 4.23**). This result firstly demonstrates that inhibition of *PAX3* in *PAX3*-siRNA treated cells plays a crucial role in the induction of A375 melanoma cell apoptosis and secondly indicates that *PAX3* uses two different pathways in both induction and inhibition of apoptosis. *PAX3* expression was inversely correlated with the expression of some of its downstream targets. For instance, in regulating cell apoptosis, the up-regulation of *PAX3* expression decreases *PTEN* and

increases *BCL2* expression to inhibit cell apoptosis. In contrast to this present study, the down-regulation of *PAX3* expression decreases *BCL2* and increases *PTEN* expression to induce apoptosis. In the *PAX3*-siRNA transfected A375 cells, *PAX3* utilised the *PTEN* pathway to induce apoptosis. Thus, knockdown of *PAX3* induced increased expression of *PTEN* resulting in A375 melanoma cell apoptosis. On the other hand, in the NC-siRNA transfected A375 cells, *PAX3* used the *BCL2* pathway to inhibit apoptosis by maintaining high expression of *BCL2*. In this manner knockdown of *PAX3* decreased expression of *BCL2,* which subsequently resulted in apoptosis of the A375 melanoma cells. The KEGG-pathway analysis of this present microarray data indicate that suppression of *PAX3* induced activation of both PTEN and P53 pathways which in turn blocked *BCL2* to induced melanoma A375 cell apoptosis (**Fig. 4.27**).

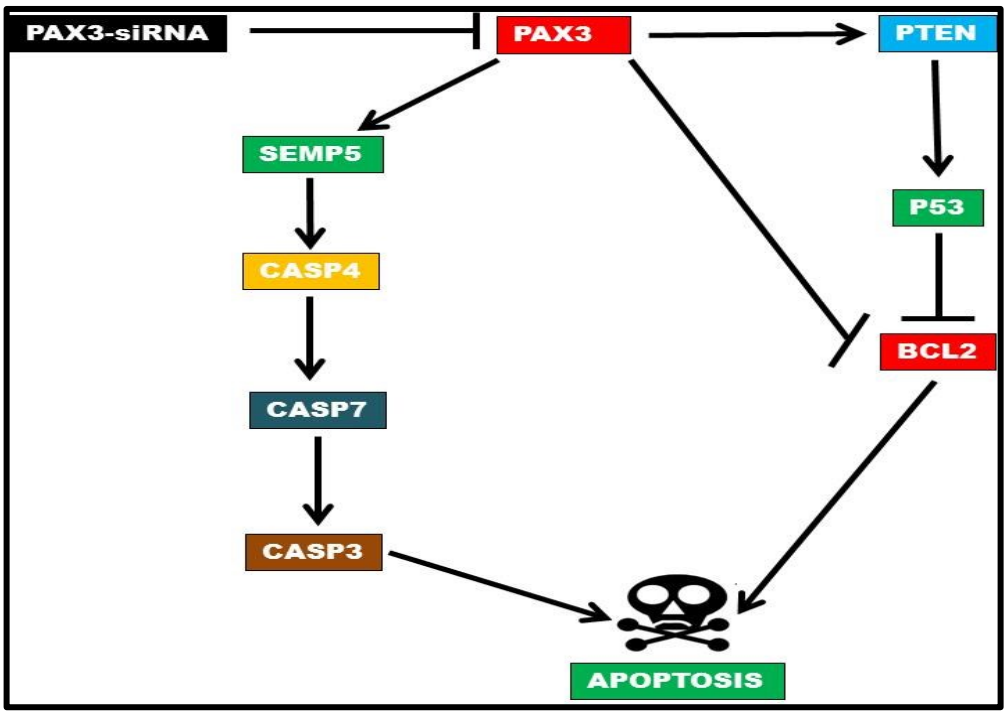

Figure 4.27 Induction of A375 melanoma cell apoptosis through P53 pathway and caspase activation cascade. Silencing of *PAX3* induced activation of *PTEN*, which in turn induced the P53 pathway to inhibit *BCL2* and induced A375 melanoma cell apoptosis. *PAX3* knockdown further activated *SEMP5,* which in turn activated *CASP3* to induced apoptosis. Equally, repression of *PAX3* induces activation of *SEMP5,* which in turn induces caspase activation cascade, which finally activate *CASP3* to induce A375 melanoma cell apoptosis.

The observed significant apoptosis of A375 cell (**Fig. 4.22**), confirmed by the increased expression of apoptosis promoting genes **(Fig. 4.4)** and decreased expression of

inhibitory genes of apoptosis (**Fig. 4.3**). This affected the tumourigenic characteristics of malignant melanoma A375 cells and induced significant reduction in prolifetation of A375 cells, resulting from cell death caused by *PAX3* inhibition (**Fig. 4.11**). Additionally, migration of A375 cells was significantly inhibited (**Fig. 4.14**) as non-proliferative cells continually unergoe apoptosis. Furthermore, colony reproducibility of malignant melanoma A375 cells was inhibited (**Fig. 4.19**), because of apoptosis of A375 cells.

In summary, melanoma is one of the most aggressive tumours with high metastatic potential (Helfrich *et al.,* 2014). This present study demonstrates that the expression of *PAX3* plays a crucial role in A375 metastatic melanoma. In this regard, *PAX3* could promote the development of melanoma and maintain its tumourigenic activities.

The techniques of siRNA-silencing, microarray analysis, semi-quantitative RT-PCR and western blotting demonstrated significant inhibition of expression of both *PAX3* mRNA and protein in A375 melanoma cells and this subsequently inhibited the cellular activities of *PAX3*. Silencing of *PAX3* inhibited melanoma A375 cell cycle and proliferation that progressively interrupted the metastatic process melanoma and induction of apoptosis. Additionally, in this study for the first time, *PAX3* knockdown in A375 melanoma cells induced remarkable alterations in expression of wide range of downstream targets of *PAX3*, which subsequently negatively affected a number of signaling pathways. Suppression of *PAX3* expression in melanoma A375 cells reduced *PAX3* activities resulting in a marked inhibition of the cell cycle progression. Melanoma A375 cell growth was arrested at the G2 phase of the cell cycle resulting in an extensive inhibition of proliferation of A375 cells.

PAX3 down-regulation decreased A375 melanoma cell attachment to various ECM proteins (because of repression of cell surface adhesion molecules) with a consequent inhibition of cell migration. During the metastatic processes of melanoma, migration of A375 cells requires the expression of cell surface adhesion molecules, which were remarkably inhibited after *PAX3* knockdown. This successively decreased the metastatic

invasive potential of A375 cells. Intriguingly, in this study for the first time, *PAX3* silencing induced tremendous inhibition of A375 melanoma cells to grow in soft agar and induced enormous apoptosis of A375 cells (hallmarks of inhibition of melanoma tumourigenesis). Additionally, the combination treatment approach adapted for demonstrating significant apoptosis of A375 melanoma cells indicates a therapeutic window for malignant melanoma that could target all *PAX3* spliced variants. This present study indeed demonstrated that *PAX3* is vital for the survival of melanoma and inhibition of *PAX3* induced cell apoptosis. In conclusion, taken together this current study demonstrates that the *PAX3* signaling pathway, which interacts with multiple pathways could possibly be suitable target for a novel therapeutic treatment for melanoma.

CHAPTER 5

GENERAL CONCLUSION AND FUTURE WORK

CHAPTER 5. GENERAL CONCLUSION AND FUTURE WORK

5.1. General Conclusion

Human rhabdomyosarcoma is the most frequent and highly metastatic aggressive childhood soft tissue sarcoma accounting for approximately 5% of all malignant paediatric tumours (Annavarapu *et al.,* 2013; Roomi *et al.,* 2013). Paediatric rhabdomyosarcoma continues to be associated with poor patient prognosis owing to its morphological and genetically heterogeneous malignant nature (Jacob *et al.,* 2013). The invasive and metastatic potential of rhabdomyosarcoma are the main concern in the treatment and survival of patients (Oue *et al.,* 2013). Likewise, human melanoma is an equally highly metastatic and aggressive tumour that can affect all age groups (Dye *et al*., 2013).

The oncogenic activities of *PAX3/Pax3* have been well demonstrated, playing a significant role in contributing to the establishment, maintenance and aggressiveness of several tumours. Early studies showed that P*AX3* expression contributes to several tumours, including rhabdomyosarcoma, malignant melanoma, neuroblastoma and Ewing's sarcoma (Rodeberg *et al*., 2006). Apart from ARMS, the expression of PAX3-FKHR has been identified to promote Ewing's sarcoma, synovial sarcoma and neuroectodermal tumours (Oda and Tsuneyoshi, 2009).

In the past, several attempts have been made to provide knowledge concerning *PAX3/Pax3* in cancer and currently, more scientific efforts are underway to broaden our understanding of the cancer biology of *PAX3/Pax3* (Kojima *et al.,* 2012; Dummer *et al.,* 2013). Although *PAX3/Pax3* has been identified to be strongly involved in the tumourigenesis of rhabdomyosarcoma, melanoma, neuroblastoma, Ewing's sarcoma and medulloblastoma (Barone *et al.,* 2012; Van Gaal *et al*., 2013), the development of effective therapeuties targeting *PAX3/Pax3* still poses a challenge to medical research, as patients' treatment response rates are poor (Capovilla, 2013; Raciborska *et al.,* 2013). Hence, this present study was undertaken in an attempt to address some of the drawbacks of *PAX3/Pax3* inhibition, which could perhaps be developed further in identifying specific biomarkers with a high predictive response, to comprehend

mechanisms of resistance and finally but not least, to explore strategic combination therapeutic regimens for a good prognostic response.

Histology demonstrates that the biological activity of *PAX3* in RMS cells also presents difficulties in morphological identification and classification of variants of RMS (Rudzinski *et al.,* 2013). In recent times, ERMS has been found to harbour one PAX3-NCOA2 translocation. The tumourigenic activity of ERMS, has been demonstrated in murine C2C12 myoblasts by transfecting the PAX3-NCOA2 translocated gene. This characteristic of ERMS is comparable with the PAX3-FOXO1 observed in ARMS (Yoshida *et al.,* 2013).

The formation of chimeric proteins resulting from the translocation of PAX3/Pax3 and its interaction with other multiple downstream molecules enhances the oncogenic activities of *PAX3*, especially in the aggressive tumours (Parham and Barr, 2013). Clinically, PAX3-FOXO1 contributes to the poor prognosis for ARMS patients (Skapek *et al.,* 2013). In ARMS cells, thapsigargin induced inhibition of tumourigenic activity of PAX3-FOXO1, via the AKT signaling pathway as a presumed therapeutic target, resulted in apoptosis (Jothi *et al*., 2013). PAX3-FOXO1 chimeric proteins augment the tumourigenic activity of *PAX3,* which has the potential for increasing expression of downstream targets including myogenic markers such as *MYOD* and *MYOG* (Yuan *et al*., 2013). In ARMS cells, PAX3-FOX01 modulates its downstream targets by increasing expression of *MYOD1, DAPK1* and *GREM1*. Decreased expression of *HEY1* caused up-regulation of *MYCN* (Ahn, 2013). The chimeric protein of PAX3-FOXO1A transfected into murine satellite cells inhibited terminal differentiation of those cells through repression of myogenin (Calhabeu *et al.,* 2013).

In primary myoblasts and RH30 ARMS cells, increased expression of *NOXA* expression induced apoptosis following up-regulation of PAX3-FOXO1 expression (Marshall *et al.,* 2013). *In vivo* suppression of IGFBP2 as a downstream target of *PAX3* in an IGF1R antibody-resistant rhabdomyosarcoma cell model, induced inhibition of both the IGF signaling pathway and AKT activation (Kang *et al.,* 2013). Repression of *Rb1* in a

rhabdomyosarcoma mouse model, modified tumour progression and enhanced both anaplasia and pleomorphism, making identification of rhabdomyosarcoma variants difficult (Kikuchi *et al.,* 2013). The tumourigenic activity of PAX3-FOXO1 in ARMS cells has been identified to be augmented by increased expression of EZH2, whilst repression of EZH2 inhibits the cellular activities of PAX3-FOXO1 and induces apoptosis (Ciarapica *et al.,* 2013). Increased expression of anaplastic lymphoma kinase enhanced PAX3/7-FOXO1 tumourigenic activities in cells of patients with rhabdomyosarcoma resulting in unfavourable outcomes (Bonvini *et al.,* 2013). In a related study, histology of Asian patients with metastatic rhabdomyosarcoma, demonstrated high expression of anaplastic lymphoma kinase as a diagnostic marker of metastatic rhabdomyosarcoma (Lee[3] *et al*., 2013).

In ARMS, neuroblastoma and Ewing's sarcoma cells, fenretinide effectively interrupted PAX3-FOXO1 tumourigenic activity and induced apoptosis (Herrero *et al.,* 2013). Lately in RH30 ARMS cells, the expression of FKHR-PAX3 as a reciprocal gene of PAX3-FOXO1, increases expression of PAX3-FKHR, does not only contribute to ARMS but also promotes its tumourigenic activity by augmenting proliferation, migration, invasion and transformation ability (Hu *et al.,* 2013). Most cases of metastatic rhabdomyosarcoma are associated with chemoresistance to multiple chemotherapeutic agents such as doxorubicin, ifosfamide, dacarbazine; gemcitabine, paclitaxel; vincristine, actinomycin D, cyclophosphamide and gemcitabine-paclitaxel resulting in patients' death (Haider *et al.,* 2013). Since there is a poor event-free survival rate for recurrent ARMS, a therapeutic combination regime with using vincristine, irinotecan and temozolomide has been tried recently (Mixon *et al.,* 2013). In chemoresistant metastatic recurrent Ewing's sarcoma, a combination treatment regimen consisting of vincristine, irinotecan and temozolomide gave a good prognosis (Raciborska *et al.,* 2013).

PAX3 regulates melanocyte development and it is involved in the maintenance and survival of melanoma through induced increased expression of *TBX2* as a direct downstream target (Liu[2] *et al.,* 2013). In melanoma, increased *PAX3* expression induced cell proliferation and inhibition of apoptosis through downstream modulation of the mitogen activated protein kinase pathway (Smith *et al.,* 2013). *PAX3/Pax3* can induce

melanoma cell proliferation and invasion through downstream regulation of *Brn-2* (Bonvin *et al.,* 2012). Recently in melanoma patients, circulating tumour cells have been identificated in addition to *PAX3* as a biomarker for the determination of prognosis (Kiyohara *et al.,* 2013). In mouse primary melanoma, high *PAX3* expression has been identified in addition to *CCND1, STAT3, MITF* and *TYR* as diagnostic indicators (Makhzami *et al.,* 2012). The expression of *PAX3* plays a contributory role in melanoma chemoresistance to chemotherapeutic regimes. Particularly, *PAX3* increased expression of *STAT3* to promote melanoma resistance to vemurafenib treatment, which resulted in a good prognosis during initial treatment (Liu[1] *et al*., 2013). In human medulloblastoma cells, expression of murine *Pax3* induced adhesion through increased expression of neural cell adhesion molecules (Mayanil *et al.,* 2000). *PAX3* expression promoted glioma cell proliferation whilst knockdown of PAX3 inhibited proliferation, invasion and induction of glioma cell apoptosis (Xia *et al*., 2013).

Neuroblastoma has been characterized generally as having a poor prognosis, although metastatic neuroblastoma is more common in older children. Usually, the age of a patient and the stage of tumour progression are commonly used as prognostic indicators for neuroblastoma (Maris, 2010). Recently, high expression of *Sam68* observed in neuroblastoma, which correlates with metastatic neuroblastoma appeared to be a valuable diagnostic prognostic tool (Zhao[2] *et al.,* 2013). In the treatment of neuroblastoma, the chemotherapeutic regimens presently used are aimed at inducing apoptosis through the activation of important elements in the apoptosis signaling pathways (Van Noesel and Versteeg 2004; Fangusaro *et al.,* 2006). However, aggressive neuroblastoma can use dysregulation of these pathways as a self-defence against broad chemotherapeutic agents. Defects in the key elements of the apoptotic pathways, including caspases, *P53*, *BCL-2,* survivin and aberrant *MYCN* expression are the main contributory factors in chemoresistant neuroblastoma (Goldsmith *et al.,* 2012; Barone *et al.*, 2013). Treatment of neuroblastoma has been associated with a poor prognosis, because patients respond briefly to therapeutic agents, after which recurrence occurs with a fatal chemoresistant neuroblastoma (Modesto *et al.,* 2013; Fang *et al.,* 2014). The survival rate of high-risk neuroblastoma patients is less than 30%, even though rigorous

effective multimodal therapies are being used (Fechete *et al*., 2011; Goldsmith *et al.,* 2012;).

This present study investigated the oncogenic potential role of *PAX3* in the two main subtypes of human rhabdomyosarcoma embryonal rhabdomyosarcoma the JR1 cell line and the alveolar RH30 cell line, as well as in an A375 melanoma cell line and possible potential strategic therapeutic targets.

The expression of *PAX3* was down-regulated in JR1, RH30 and A375 cell lines utilising siRNA technology. *PAX3*-siRNA transient transfection induced significant inhibition of *PAX3* mRNA expression in JR1, RH30 and A375 cell lines, and demonstrated that the different spliced variants of *PAX3* present unique biological functions in rhabdomyosarcoma and melanoma, which may perhaps require different therapeutic interventions. Pre-designed *PAX3*-siRNA transient transfection induced a continual 95% and 98% inhibition of JR1 cell line *PAX3* mRNA and PAX3 protein expression respectively for four days. Similarly, a persistent 90% and 92% repression of *PAX3* mRNA and PAX3 protein expression respectively was observed in the RH30 cell line. Whereas in the A375 cell line, 90% inhibition of both *PAX3* mRNA and protein expression was demonstrated.

Semi-quantitative RT-PCR demonstrating the seven spliced variants of *PAX3* (*PAX3a-h*) showed evidently different *PAX3* mRNA expression patterns in both JR1 and RH30 cell lines. Overall, JR1 cell line cells anticipated to be less aggressive showed higher inhibition of *PAX3* compared to the expected highly aggressive rhabdomyosarcoma RH30 cell line and the A375 malignant melanoma cell line. Interestingly, the expressions of the various *PAX3* variants in the JR1 cell line was almost completely inhibited compared to RH30 and A375 cell lines. In the JR1 cell line, a decreasing order of residual expression pattern of *PAX3* spliced transcript variants were demonstrated; *PAX3d, PAX3g, (PAX3a, PAX3c PAX3e* and *PAX3h*) and *PAX3b.* Whereas in the RH30 and A375 cell lines; *PAX3d, PAX3e, PAX3a*, (*PAX3c* and *PAX3h*) and *PAX3b* in decreasing order of residual expression was observed. Likewise, the parallel inhibition

of PAX3 protein in JR1, RH30 and A375 cell lines demonstrated by western blotting, conformed the patterns of inhibition of *PAX3* mRNA. Additionally, this study indeed demonstrates *PAX3* functional modulation of crucial downstream targets including P53, P21, C-MYC, MYOD1, ITGβ5, CASP3 and BCL2 as proven by the western blotting.

This present study confirmed the primary activity of *PAX3* in the regulation of cell cycle and proliferation as one of the control mechanisms, used in promoting rhabdomyosarcoma and melanoma tumour growth and maintenance as previously established in various investigations. However, this study further demonstrates that down-regulation of *PAX3* impedes the cell cycle and proliferation regulatory mechanisms as well as inhibition of other cellular oncogenic control activities of *PAX3* including metastatic rhabdomyosarcoma and melanoma cell migration, adhesion, invasion and induction of apoptosis.

Knockdown of *PAX3* expression in JR1, RH30 and A375 cell lines, impaired *PAX3* activities by a drastic blockage of the cell cycle progression with a consequential inhibition of proliferation in the pre-designed *PAX3*-siRNA transfected JR1, RH30 and A375 cell lines, compared to the negative control siRNA transfected cells. A G1 phase growth arrest in the cell cycle ensued a markedly inhibition of proliferation of JR1, and RH30 cell lines and a G2 arrest occurred in the A375 cell line. The extent of inhibition of cell proliferation was evident in the microarray data of down-regulation of several interacting molecules, which are being used by *PAX3* to regulate diverse aspects of the cell proliferation and cell cycle pathways.

Knockdown of *PAX3* prominently diminished JR1, RH30 and A375 cell line adhesion potential to a number of ECM proteins because of inhibition of cell surface adhesion molecule expression. The latter are utilised by *PAX3* to regulate different aspects of the metastatic pathway and this subsequently impaires cell migration. Since mobility of cells requires attachment of cell surface molecules to epithelial surfaces, JR1, RH30 and A375 cell migration was tremendously inhibited following *PAX3* knockdown, which subsequently impaired the metastatic invasive potential of JR1, RH30 and A375 cell

lines. In view of the fact that migration of cells is central in the metastatic process, inhibition of cell migration through endothelial surfaces has debilitating consequences on invasion. Intriguingly, knockdown of *PAX3* enormously inhibited JR1, RH30 and A375 cell lines invasion. Fascinatingly, for the first time, the down-regulation of *PAX3* increased apoptosis in JR1, RH30 and A375 cell line (as a hallmark of cancer treatment), subsequently resulted in significant inhibition of cell proliferation, cell cycle, cell migration and colony reproducibility.

Analysis of the Affymetrix GeneChip human genome microarray demonstrated variations in gene expression patterns between *PAX3* knockeddown rhabdomyosarcoma cells and negative control siRNA transient transfected cells. Remarkably, the array discovered that over two hundred signalling pathways were extensively altered following *PAX3* knockdown in rhabdomyosarcoma and melanoma cells. Interestingly, most of the major affected signalling pathways were cell cycle and cell proliferation related, emphasising that inhibition of *PAX3* negatively regulated these altered signaling pathways, and confirming that *PAX3* is certainly associated with regulation of the cell cycle and proliferation. Quantitative PCR and western blotting validated a selected number of microarray data. The array data further revealed other *PAX3* target genes that have not been investigated in embryonic developmental studies, which implies that *PAX3* may perhaps employ additional unusual signaling pathways to facilitate its cellular functional activities for tumour growth progression and maintenance.

This current study demonstrates for the first time that *PAX3* is vital for the development of rhabdomyosarcoma and melanoma by modulating several essential signaling pathways, which signifies that *PAX3* may have other functional characteristics that may be a possible novel therapeutic target for the treatment of rhabdomyosarcoma and melanoma. Expression of *PAX3* is mainly observed during embryogenesis as well as in malignant cells, and is absent in adult differentiated tissues. This implies that in rhabdomyosarcoma and melanoma, anti-PAX3 therapeutic regimens that are perhaps formulated to avoid cytotoxicity effects on normal cells, can be selectively targeted at cancer cells. Additionally, several presumed *PAX3* downstream target genes, which perhaps augment *PAX3* tumourigenic activity including, *CDC25A, CDC25B, CDK2,*

CCDE1, BRCA1, MYCN, RB, TGFβ3, ITGβ5, MMP2, MET, REC, PCDH18, BCL2, CYB5B and *FAIM,* which have oncogenic potential and which could induce therapeutic resistance would be promising targets for the development of novel therapeutic schemes. Consequently, anti-PAX3 therapeutic regimes for the treatment of tumours, which have the capacity to target the activities of multiple oncogenes including suppression of tumour intrinsic networks, are therefore, more potent, effective and promising therapeutic strategies in oncology.

Conversely, other vital therapeutic questions concerning treatment of aggressive rhabdomyosarcoma and melanoma continue to present a clinical challenge concerning the spliced variants of *PAX3*. Each *PAX3* spliced variant presents a unique oncogenic attribute in rhabdomyosarcoma and melanoma and counteract to effective treatment. This problem requires intensive research on selective therapeutic target schemes specific for targeting the signaling pathways connected to individual *PAX3* spliced variants.

Furthermore, this study represents an *in vitro* inhibition of *PAX3*. Hence, *in vivo* assessment of the anti-cancer effect of *PAX3* inhibition will be vital to establish the therapeutic potential. Since, the expression of *PAX3* has been observed in specific stem cells such as muscle satellite cells and melanocyte cells, it is unclear whether anti-PAX3 therapy, particularly long-term therapeutic schemes will have a consequential effect on the viability of these normal stem cells and tissue regeneration.

The combination strategy of inducing apoptosis, which has been tried in this study, seems to target both *PAX3* and its downstream genes, which facilities *PAX3* cellular activities. The induced apoptosis observed in this study affirms the effectiveness of combination chemotherapeutics that are currently underway in several studies. A collective analysis of this present study regarded the *PAX3* signaling pathway as a possible target for the development of effective and potent therapeutic regimes for rhabdomyosarcoma and melanoma treatment. The microarray analysis data of this present study showed very many significantly up/down-regulated genes, demonstrating the importance of *PAX3* in regulating the majority of genes expressed in these cell types

(ARMS, ERMS and melanoma). An interesting aspect of this study was that all the results were positively correlated and very consistent with one another with the exception of some qRT-PCR analysis results.

The pattern of gene expression in the microarray analysis data corroborated all the results of the functional assays. Even though the microarray data demonstrated a high level of *PAX3* knockdown in the melanoma A375 cells compared to the relatively lower *PAX3* knockdown in the rhabdomyosarcoma JR1 and RH30 cell lines, a higher number of significantly down-regulated genes was revealed in the rhabdomyosarcoma JR1 and RH30 cell lines than in the melanoma A375 cells. A higher number of cell proliferation and cell cycle promoting genes were down-regulated in the rhabdomyosarcoma JR1 and RH30 cell lines compared to the melanoma A375 cell line. Likewise, a higher number of genes that promote cell migration, adhesion and invasion were down-regulated in the rhabdomyosarcoma cell lines than in the melanoma cell line. Fascinatingly, the apoptosis inhibitory genes were equally down-regulated in both melanoma and rhabdomyosarcoma cell lines and this confirmed the patterns of increased cell apoptosis in all the cell lines observed in this present study.

This study demonstrates that, *PAX3* utilises various molecular pathways in regulating the tumourigenic activities of rhabdomyosarcoma, melanoma and neuroblastoma. This was evident by different pattern of alterations of molecules in the microarray data of the rhabdomyosarcoma, melanoma and neuroblastoma cell lines after *PAX3* down-regulation. The myogenic differention factor, *SMAD2,* was inhibited in both rhabdomyosarcoma and melanoma cell lines, as opposed to the activation of *SMAD2* in the neuroblastoma cell lines. This showed that the repression of *SMAD2* possibly influenced the inhibition of cell proliferation and apoptosis observed in the rhabdomyosarcoma and melanoma cell lines, but did not in the neuroblastoma cell lines. Interestingly, *PAX3* silencing induced the activation of *FOXO1* in both rhabdomyosarcoma and neuroblastoma cell lines, compared to the inhibition of *FOXO1* in melanoma cell line. This implies that, the inhibition of *PAX3* could possibly suppress the myogenic differentiation activity of *FOXO1* in the melanoma cell line, (which presupposes that the myogenic activities of both *PAX3* and *FOXO1* depend on each

other), whereas inhibition of *PAX3* in both rhabdomyosarcoma and neuroblastoma cell lines, enhances the myogenic differentiation activity of *FOXO1* in these cell lines. Similarly, the activation of *HES1* expression in both JR1 and RH30 rhabdomyosarcoma cell lines, compared to the inhibition of *HES1* in the A375 cell line, indicates that the perhaps the myogenic differentiation activity of *HES1* in the A375 melanoma cell line depends on *PAX3*, whereas the myogenic activity of *HES1* in the JR1 and RH30 rhabdomyosarcoma cell lines is possibly enhanced by *PAX3* inhibition. Intriguingly, the inhibition of *ADAM23*, *MYOD1* and *MYOG4* expression *in* both rhabdomyosarcoma and melanoma cell lines, demonstrates that the differentiation and myogenic activities of these genes might be influenced by *PAX3* in these cell lines. The down-regulation of two tumour metastatasis molecules, *COL3A1* and *NID1* in both rhabdomyosarcoma and melanoma cell lines was in contrast to the up-regulation of *COL3A1* and *NID1* in the neuroblastoma cell lines. This indicates that, the suppression of C*OL3A1* and *NID1* in the rhabdomyosarcoma and melanoma cell lines, possibly contributed directly to the metastatic inhibition observed in these cell lines. By contrast, the inhibition of neuroblastoma metastatasis might not be induced directly by *COL3A1* and *NID1*.

Similarly, activation of caspase 3 in the rhabdomyosarcoma and melanoma cell lines as well as in the SH-SY5Y neuroblastoma cell line, was in contrast to caspase 3 inhibition in the SH-EP1 neuroblastoma cell line. This suggests that, with the exception of the SH-EP1 neuroblastoma cell line, caspase 3 possibly promoted apoptosis unequivocally as observed in these cell lines. Likewise, the inhibition of *BCL2* in the rhabdomyosarcoma and melanoma cell lines as well as the SH-EP1 neuroblastoma cell line, was in contrast to the actication of *BCL2* in the SH-SY5Y neuroblastoma cell line. These inconsistencies established that BCL2 expression does not perhaps influence apoptosis of the SH-SY5Y neuroblastoma cell line, but may influence apoptosis of the JR1, RH30, A375 and SH-EP1 cell lines.

Interestingly, the patterns of gene expression verified by the qRT-PCR analysis were similar to the microarray analysis data with the exception of few inconsistencies. For instance, a few genes that were down-regulated in the microarray data of JR and RH30 rhabdomyosarcoma cell lines such as *MCM3* and *PCNA*, were up-regulated in the

microarray data of A375 melanoma cell line. Likewise, *CXCR4* and *JAM2* expression were down-regulated in both microarray and qRT-PCR data of A375 melanoma cell line, whilst up-regulated in both microarray and qRT-PCR data of the JR1 and RH30 rhabdomyosarcoma cell lines. In the A375 cell line, the expression of *MCM3, E2F7, E2F8* and *PCNA* were up-regulated in the microarray data and down-regulated in the qRT-PCR data. Generally, the microarray data demonstrated higher fold-change of gene expression than the qRT-PCR data in both rhabdomyosarcoma and melanoma cell lines. Most of the qRT-PCR data of the A375 melanoma cell line were less than 1.5-fold changed compared to the JR1 and RH30 rhabdomyosarcoma cell lines, which showed higher than 1.5-fold changes.

Even though this current study demonstrated a coherent result pattern between the various methodologies, its main drawback was the failure of the qRT-PCR analysis in confirming the expression of *BRCA1* and *POLA2*, out of the 55 selected genes from the microarray analysis data for verification by the qRT-PCR analysis. In attempt to rectify this shortcoming, different freshly ordered primers, which were used also failed after three repetitions. The observed limitation in the qRT-PCR analysis of these genes was attributed probably to a poor primer quality from manufacturers. To address this inadequacy in the future work, primers from different manufacturers could be tried.

In summary, this present study significantly down-regulated *PAX3* in both JR1 and RH30 rhabdomyosarcoma cell lines and the A375 melanoma cell line. The cellular activity of *PAX3* was substantially inhibited. For instance, *PAX3* siRNA-silencing inhibited JR1, RH30 and A375 cell growth and proliferation, which was indicative of inhibition of progression of these tumours. The metastatic activity of *PAX3* was inhibited in these cell lines, which was demonstrated by the inhibition of cell migration, adhesion and invasion. At this stage, both rhabdomyosarcoma and melanoma were blocked from progressing and metastatic invasion of distant sites. The siRNA inhibition further exerted its effects on the apoptotic signaling pathways (usually regulated by *PAX3* to maintain the survival of these tumours) by inhibiting apoptosis. Interestingly, a block of *PAX3* in these tumour cell lines induced both extrinsic and intrinsic apoptotic

pathways as the hallmarks of cancer treatment. In conclusion, targeting of *PAX3* in this manner may provide a perfect mode of inhibiting rhabdomyosarcoma and melanoma.

The results of this study, which implicates *PAX3* involvement in rhabdomyosarcoma and melanoma, suggest that down-regulation of tumourigenic activities of *PAX3 in vivo* using chemotherapeutic agents will perhaps enhance effective treatment of both rhabdomyosarcoma and melanoma. It is intended to further analyse the results of our larger group study where *PAX3* down-regulation in rhabdomyosarcoma is compared with up-regulation in myoblasts, *PAX3* down-regulation in melanoma is compared with up-regulation in melanocytes and *PAX3* down-regulation in neuroblastoma is compared with up-regulation in neural stem cells. However, this meta-analysis is beyond the scope of this study.

5.2. Future Work

PAX3 expression provides both protective and survival mechanisms for rhabdomyosarcoma and melanoma and could prevent long-term chemotherapeutic effectiveness, with consequential patient mortality. Conversely, down-regulation of *PAX3* expression with subsequent monitoring of cellular function, will invariably promote tumour cell apoptosis improving patients' survival. It is essential therefore, to carry out a series of monitoring experiments following *PAX3* down-regulation, which could be suitable as an effective monitor during chemotherapy as, outlined below.

1. To stably transfect *PAX3*-pBABE HAER inducible plasmid vector DNA into murine myoblast cell line C2C12. The pBABE retroviral plasmid DNA vector backbone, which has been widely used for reliable transfer and maintenance of stable exogenous gene expression in human cell lines as an advantage over small interference messenger RNA (siRNA), since it can then be silenced using siRNA, to decrease the expression of target genes both *in vitro* and *in vivo* (Patel *et al.,* 2012).

2. To identify the *PAX3/Pax3* variants in a *PAX3*-pBABE HAER plasmid vector previously extracted from competent transformed *E. coli DH5α* cells (See **appendix A**).

3. To confirm *PAX3/Pax3* variants in a murine C2C12 myoblasts cell line and subsequently down-regulate *PAX3* expression using siRNA silencing.

4. To determine the effects of *PAX3* siRNA knockdown in murine C2C12 myoblasts on downstream targets using microarray analysis.

5. To evaluate the effects of *PAX3* knockdown on cell growth and proliferation, cell migration, adhesion, invasion, transformation and cell apoptosis.

6. To carry out *in vivo* tamoxifen treatment studies on cultured *PAX3*-pBABE HAER clones after switch off or on of *PAX3* gene expression using the optimized siRNA silencing methodology. A vector can be switched on or off easily (more easily than doing transfection studies). A vector is more stable for few months than siRNA, which only lasts for few days. Tamoxifen, which has been widely used as anti-oestrogen metabolite in previous studies, effectively antagonizes oestrogen and oestrogen receptors, thereby inhibiting cell growth with consequent effects on downstream gene expression (Ishiguro *et al.,* 2012; Li[3] *et al.,* 2013).

7. To determine the effects of tamoxifen induced *PAX3* inhibition on cell proliferation, migration, adhesion, invasion, transformation and apoptosis.

8. To perform microarray analysis of tamoxifen induced *PAX3* inhibition in the C2C12 murine myoblast cell line.

9. To compare the results of *PAX3*-pBABE HAER vector tamoxifen down-regulation of *PAX3* expression in murine myoblasts with the results of siRNA down-regulation of *PAX3* expression in rhabdomyosarcoma, melanoma and neuroblastoma cell lines.

10. Once the PAX3-pBABE HAER vector system is established, it will be very easy to understand the mechanism of action of drugs against these tumours.

REFERENCES

Abdelghany, S. M., Schmid, D., Deacon, J., Jaworski, J, Fay, F., *et al.,* (2011). 'Enhanced antitumour activity of the photosensitizer meso-Tetra (N-methyl-4-pyridyl) porphine tetra tosylate through encapsulation in antibody-targeted chitosan/alginate nanoparticles'. *Biomacro molecules, vol. 14, issue 2, pp. 302-10.*

Ahn, E. H. (2013). 'Regulation of target genes of PAX3-FOXO1 in alveolar rhabdomyosarcoma'. *Anticancer Research, vol. 33, issue 5, pp. 2029-35.*

Agoston, Z., Li, N., Haslinger, A., Wizenmann, A., Schulte, D. (2012). 'Genetic and physical interaction of *Meis2, Pax3* and *Pax7* during dorsal midbrain development'. *BMC. Developmental Biology, vol. 12, p. 10.*

Aggarwal, S., Jinda, W., Limwongse, C., Atchaneeyasakul, L. O., Phadke, S. R. (2011). 'Run-on mutation in the *PAX6* gene and chorioretinal degeneration in autosomal dominant aniridia'. *Molecular Vision, vol. 17, pp. 1305-9.*

Alan, J. K., Lundquist, E. A. (2013). 'Mutationally activated Rho GTPases in cancer'. *Small GTPases, vol. 4, issue 3.*

Ambesajir, A., Kaushik, A., Kaushik, J. J., Petros, S. T. (2012). 'RNA interference: A futuristic tool and its therapeutic applications'. *Saudi Journal of Biological Science, vol.19, issue 4, pp. 395-403.*

Amstutz, R., Wachte, M., Troxler, H., Kleinert, P., Ebauer, M., *et al.,* (2008). 'Phosphorylation regulates transcriptional activity of PAX3/FKHR and reveals novel therapeutic possibilities'. *Cancer Research, vol. 68, issue 10, pp. 3767-76.*

Annavarapu, S. R., Cialfi, S., Dominici, C., Kokai, G. K., Uccini, S., Ceccarelli, S., *et al.,* (2013). 'Characterization of Wnt/β-catenin signaling in rhabdomyosarcoma'. *Laboratory Investigation, vol. 93, issue 10, pp. 1090-9.*

Anstaett, O. L., Brownlie, J., Collins, M. E., Thomas, C. J. (2010). 'Validation of endogenous reference genes for RT-qPCR normalisation in bovine lymphoid cells (BL-3) infected with Bovine Viral Diarrhoea Virus (BVDV)'. *Vetinary Immunology and Immunopathology, vol. 137, issue 3-4, pp. 201-7.*

Apuzzo, S., Gros, P. (2006). 'The paired domain of Pax3 contains a putative homeodomain interaction pocket defined by cysteine scanning mutagenesis'. *Biochemistry, vol. 45, issue 23, pp. 7154-61.*

Aradhya, S., Smaoui, N., Marble, M., Lacassie, Y. (2011). 'De novo duplication 11p13 involving the *PAX6* gene in a patient with neonatal seizures, hypotonia, microcephaly, developmental disability and minor ocular manifestations'. *American Journal of Medical Genetics, vol. 155A, issue 2, pp. 442-4.*

Arozarena, I., Goicoechea, I., Erice, O., Ferguson, J., Margison, G. P., Wellbrock. C. (2014). 'Differential chemosensitivity to antifolate drugs between RAS and BRAF melanoma cells'. *Molecular Cancer, vol. 13, issue 1, p. 154.*

Armeanu-Ebinger, S., Bonin, M., Häbig, K., Poremba, C., Koscielniak, E., *et al.,* (2011). 'Differential expression of invasion promoting genes in childhood rhabdomyosarcoma'. *International Journal of Oncology, vol. 38, issue 4, pp. 993-1000.*

Ashworth, M. T., Daud, A.I. (2014). 'Combinatorial Approach to Treatment of Melanoma'. *Hematology/Oncology Clinics of North America, vol. 28, issue 3, pp.601-612.*

Bae, C. J., Park, B. Y., Lee, Y. H., Tobias, J. W., Hong, C. S., Saint-Jeannet, J. P. (2013). 'Identification of *Pax3* and *Zic1* targets in the developing neural crest'. *Developmental Biology, pii: S0012-1606(13)00656-8.*

Bai, S. W., Li, B., Zhang, H., Jonas, J. B., Zhao, B. W., Shen, L., Wang, Y. C. (2011). *'Pax6* regulates proliferation and apoptosis of human retinoblastoma cells'. *Investigative Ophthalmology and Visual Science, vol. 52, issue 7, pp. 4560-70.*

Bánusz, R., Váradi, Z., Varga, E., Jakab, Z., Garami, M., Csóka, M. (2014). 'Diagnosis and treatment of childhood soft tissue sarcomas'. *Magy Onkol, vol. 58, issue 1, pp. 59-64.*

Barembaum, M., Bronner-Fraser, M. (2010). '*Pax2* and *Pax3* synergize to activate a novel regulatory enhancer for spalt4 in the developing ear'. *Developmental Biology, vol. 340, issue 2, pp. 222-31.*

Barone, G., Anderson, J., Pearson, A. D., Petrie, K., Chesler, L. (2013). 'New strategies in neuroblastoma: Therapeutic targeting of MYCN and ALK'. *Clinical Cancer Research, vol. 19, issue 21, pp. 5814-21.*

Barr, F. G. (2001). 'Gene fusions involving *PAX* and *FOX* family members in alveolar rhabdomyosarcoma'. *Oncogene, vol. 20, issue 40, pp. 5736-46.*

Barraud, P., Seferiadis, A. A., Tyson, L. D., Zwart, M. F., Szabo-Rogers, H. L., *et al*., (2010). 'Neural crest origin of olfactory ensheathing glia'. *Proceedings of the National Academy of Sciences, vol. 107, issue 49, pp. 21040 -21045.*

Beaudin, A. E., Abarinov, E. V., Noden, D. M., Perry, C. A., Chu, S., *et al.,* (2011). 'Shmt1 and de novo thymidylate biosynthesis underlie folate-responsive neural tube defects in mice'. *American Journal of Clinical Nutrition, vol. 93, issue 4, pp. 789-98.*

Belay, E., Mátrai, J., Acosta-Sanchez, A., Ma, L., Quattrocelli, M., Mátés, L., *et al*., (2010). 'Novel hyperactive transposons for genetic modification of induced pluripotent and adult stem cells: a nonviral paradigm for coaxed differentiation'. *Stem Cells, vol. 28, issue 10, pp. 1760-71.*

Berlin, I., Denat, L., Steunou, A. L., Puig, I., Champeval, D., Colombo, S., *et al.,* (2012). 'Phosphorylation of BRN2 modulates its interaction with the Pax3 promoter to control melanocyte migration and proliferation'. *Molecular Cell Biology, vol. 32, issue 7, pp. 1237-47.*

Betters, E., Liu, Y., Kjaeldgaard, A., Sundström, E., García-Castro, M. I. (2010). 'Analysis of early human neural crest development'. *Developmental Biology, vol. 344, issue 2, pp. 578-92.*

Bhattacharya, S., Macdonald, S. T., Farthing, C. R. (2006). 'Molecular mechanisms controlling the coupled development of myocardium and coronary vasculature'. *Clinical Science, vol. 111, issue 1, pp. 35-46.*

Biamonti, G., Bonomi, S., Gallo, S., Ghigna, C. (2012). 'Making alternative splicing decisions during epithelial-to-mesenchymal transition (EMT)'. *Cellular and Molecular Life Science, vol. 69, issue 15, pp. 2515-26.*

Bilodeau, S., Roussel-Gervais, A., Drouin, J. (2009). 'Distinct developmental roles of cell cycle inhibitors p57Kip2 and p27Kip1 distinguish pituitary progenitor cell cycle exit from cell cycle re-entry of differentiated cells'. *Mol. Cell Biol., vol. 29, issue 7, pp. 1895-908.*

Birrane, G., Soni, A., Ladias, J. A. (2009). 'Structural basis for DNA recognition by the human PAX3 homeodomain'. *Biochemistry, vol. 48, issue 6, pp. 1148-55.*

Blake, J., Ziman, M. R. (2003). 'Aberrant *PAX3* and *PAX7* expression. A link to the metastatic potential of embryonal rhabdomyosarcoma and cutaneous malignant melanoma?' *Histology and Histopathology, vol. 18, issue 2, pp. 529-39.*

Bolstad, B. M., Irizarry, R. A., Astrand, M. Speed, T.P. (2003). 'A comparison of normalization methods for high density oligonucleotide array data based on variance and bias'. *Bioinformatics, vol. 19, pp. 185-193*.

Bondurand, N., Dastot-Le Moal, F., Stanchina, L., Collot, N., Baral, V., *et al.,* (2007). 'Deletions at the SOX10 gene locus cause Waardenburg syndrome types 2 and 4'. *American Journal of Human Genetics, vol. 81, issue 6, pp. 1169-85.*

Bonvin, E., Falletta, P., Shaw, H., Delmas, V., Goding, C. R. (2012). 'A phosphatidylinositol 3-kinase-Pax3 axis regulates Brn-2 expression in melanoma'. *Molecular Cell Biology, vol. 32, issue 22, pp. 4674-83.*

Bonvini, P., Zin, A., Alaggio, R., Pawel, B., Bisogno, G., Rosolen, A. (2013). 'High ALK mRNA expression has a negative prognostic significance in rhabdomyosarcoma'. *British Journal of Cancer, vol. 109, issue 12, pp. 3084-91.*

Bork, K., Hoffmann, M., Horstkorte, R. (2013). 'ATP interferes with neural cell adhesion molecule-induced neurite outgrowth'. *NeuroReport, vol. 24, issue 11, pp. 616-9.*

Bose, P., Simmons, G. L., Grant, S. (2013). 'Cyclin-dependent kinase inhibitor therapy for hematologic malignancies'. *Expert Opinion Investigational Drugs, vol. 22, issue 6, pp. 723-38.*

Boshnjaku, V., Ichi, S., Shen, Y. W., Puranmalka, R., Mania-Farnell, B., *et al*., (2011). 'Epigenetic regulation of sensory neurogenesis in the dorsal root ganglion cell line ND7 by folic acid'. *Epigenetics, vol. 6, issue 10, pp. 1207-16.*

Bosserhoff, A. K., Ellmann, L., Kuphal, S. (2011). 'Melanoblasts in culture as an in vitro system to determine molecular changes in melanoma'. *Experimental Dermatology, vol. 20, issue 5, pp. 435-40.*

Bouchard, M., de Caprona, D., Busslinger, M., Xu, P., Fritzsch, B. (2010). '*Pax2* and *Pax8* cooperate in mouse inner ear morphogenesis and innervation'. *BMC. Developmental Biology, vol. 10, pp. 89.*

Boutet, S. C., Biressi, S., Iori, K., Natu, V., Rando, T. A. (2010). *'Taf1* regulates *Pax3* protein by monoubiquitination in skeletal muscle progenitors'. *Molecular Cell, vol. 40, issue 5, pp. 749-61.*

Boutet, S. C., Disatnik, M. H., Chan, L. S., Iori, K., Rando, T. A. (2007). 'Regulation of *Pax3* by proteasomal degradation of monoubiquitinated protein in skeletal muscle progenitors'. *Cell, vol. 130, issue 2, pp. 349-62.*

Bower, M., Salomon, R., Allanson, J., Antignac, C., Benedicenti, F., *et al.,* (2012). 'Update of *PAX2* mutations in renal coloboma syndrome and establishment of a locus-specific database'. *Human Mutation, vol. 33, issue 3, pp. 457-66.*

Bradshaw, L., Chaudhry, B., Hildreth, V., Webb, S., Henderson, D. J. (2009). 'Dual role for neural crest cells during outflow tract septation in the neural crest-deficient mutant Splotch (2H).' *Journal of Anatomy, vol. 214, issue 2, pp. 245-57.*

Brauchle, E., Noor**,** S**.**, Holtorf**,** E**.**, Garbe**,** C**.**, Schenke-Layland**,** K**.**, Busch, C. (2014). 'Raman spectroscopy as an analytical tool for melanoma research'. *Clinical and Experimental Dermatology, vol. 39, issue 5, pp. 636-45.*

Brook, A. H., Elcock, C., Aggarwal, M., Lath, D. L., Russell, J. M., *et al*., (2009). 'Tooth dimensions in hypodontia with a known *PAX9* mutation'. *Archives of Oral Biology, vol. 54 Suppl 1, pp. S57-62.*

Brun, T, Duhamel, D. L., Hu, H. K. H., Wollheim, C. B., Gauthier, B. R. (2007). 'The transcription factor *PAX4* acts as a survival gene in INS-1E insulinoma cells'. *Oncogene, vol. 26, issue 29, pp. 4261-71.*

Brun, T., Hu, H. K. H., Lupi, R., Boehm, B., Wojtusciszyn, A., *et al.,* (2008). 'The diabetes-linked transcription factor *Pax4* is expressed in human pancreatic islets and is activated by mitogens and GLP-1'. *Human Molecular Genetics, vol. 17, issue 4, pp. 478-89.*

Brunelli, S., Relaix, F., Baesso, S., Buckingham, M., Cossu, G. (2007). 'Beta catenin-independent activation of MyoD in presomitic mesoderm requires PKC and depends on Pax3 transcriptional activity'. *Developmental Biology, vol. 304, issue 2, pp. 604-14.*

Brzóska, E., Przewoźniak, M., Grabowska, I., Jańczyk-Ilach, K., Moraczewski, J. (2009). '*Pax3* and *Pax7* expression during myoblast differentiation in vitro and fast and slow muscle regeneration in vivo'. *Cell Biology International, vol. 33, issue 4, pp. 483-92.*

Bu, W., Zhang, X., Dai, H., Huang, S., Li, Y. (2013). 'Mammary Cells with Active Wnt Signaling Resist ErbB2-Induced tumourigenesis'. *PLoS One, vol. 8, issue 11, e78720.*

Buchberger, A., Freitag, D., Arnold, H. H. (2007). 'A homeo-paired domain-binding motif directs Myf5 expression in progenitor cells of limb muscle'. *Development, vol. 134, issue 6, pp. 1171-80.*

Buckingham[1], M. (2007). 'Skeletal muscle progenitor cells and the role of *Pax* genes.' *Comptes Rendus Biologies, vol. 330, issue 7, pp. 530-3.*

Buckingham[2], M., Relaix, F. (2007). 'The role of *Pax* genes in the development of tissues and organs: Pax3 and Pax7 regulate muscle progenitor cell functions.' *Annual Review Cell Developmental Biology, vol. 23, pp. 645-73.*

Burger, M. C., Brucker, D. P., Baumgarten, P., Ronellenfitsch, M. W., Wanka, C., *et al.*, (2012). *'PAX2* is an antiapoptotic molecule with deregulated expression in medulloblastoma'. *International Journal of Oncology, vol. 41, issue 1, pp. 235-41.*

Cabrera[1], R. M., Finnell, R. H., Zhu, H., Shaw, G. M., Wlodarczyk, B. J. (2012). 'Transcriptional analyses of two mouse models of spina bifida'. *Birth Defects Research Part A: Clinical and Molecular Teratology, vol. 94, issue 10, pp. 782-9.*

Cairns, D. M., Liu, R., Sen, M., Canner, J. P., Schindeler, A., Little, D. G., Zeng, L. (2012). 'Interplay of *Nkx3.2, Sox9* and *Pax3* regulates chondrogenic differentiation of muscle progenitor cells'. *PLoS One, vol. 7, issue 7, e39642*.

Calhabeu, F., Hayashi, S., Morgan, J. E., Relaix, F., Zammit, P. S. (2013). 'Alveolar rhabdomyosarcoma-associated proteins PAX3/FOXO1A and PAX7/FOXO1A suppress the transcriptional activity of MyoD-target genes in muscle stem cells'. *Oncogene, vol. 32, issue 5, pp. 651-62.*

Campbell, N. E., Kellenberger, L., Greenaway, J., Moorehead, R. A., Linnerth-Petrik, N. M., Petrik, J. (2010).'Extracellular Matrix Proteins and Tumour Angiogenesis'. *Journal of Oncology, vol. 2010, p. 586905.*

Cao, L., Yu, Y., Bilke, S., Walker, R. L., Mayeenuddin, L. H., *et al.,* (2010). 'Genome-wide identification of PAX3-FKHR binding sites in rhabdomyosarcoma reveals candidate target genes important for development and cancer'. *Cancer Research, vol. 70, issue 16, pp. 6497-508.*

Cao, X., Kambe, F., Lu, X., Kobayashi, N., Ohmori, S., Seo, H. (2005). 'Glutathionylation of two cysteine residues in paired domain regulates DNA binding activity of Pax-8'. *Journal of Biological Chemistry vol. 280, issue 27, pp. 25901-6.*

Capellini, T. D., Handschuh, K., Quintana, L., Ferretti, E., Di Giacomo, G., *et al.,* (2011). 'Control of pelvic girdle development by genes of the *Pax* family and *Emx2*'. *Developmental Dynamics, vol. 240, issue 5, pp. 1173-89.*

Capellini, T. D., Vaccari, G., Ferretti, E., Fantini, S., He, M., *et al.,* (2010). 'Scapula development is governed by genetic interactions of *Pax1* with its family members and with *Emx2* via their cooperative control of *Alx1'. Development, vol. 137, issue 15, pp. 2559-69.*

Capovilla, M. (2013). 'Cellular and molecular mechanisms of carcinogenic side effects and resistance to *BRAF* inhibitors in metastatic melanoma with BRAFV600 mutation: State of the knowledge'. *Annals of Diagnostic Pathology, vol. 33, issue 6, pp. 375-85.*

Carlson, A. L., Florek, C. A., Kim, J. J., Neubauer, T., Moore, J. C., Cohen, R. I., et al., (2012). 'Microfibrous substrate geometry as a critical trigger for organization, self-renewal, and differentiation of human embryonic stem cells within synthetic 3-dimensional microenvironments'. *FASEB Journal, vol. 26, issue 8, pp. 3240-3251.*

Carlson, B. (2013). 'Master the concepts you need to know with Human Embryology and Developmental Biology'. *Gene Expression Patterns, 5th edition, pp. 1-520,*

Carrillo, C. M., Corrêa, F. N., Lopes, N. N., Fava, M., Filho, V. O. (2014). 'Dental anomalies in children submitted to antineoplastic therapy'. *Clinics, vol. 69, issue 6, pp.433-437.*

Carney, E. M., Banerjee, P., Ellis, C. L., Albadine, R., Sharma, R., *et al*., (2011). '*PAX2*(-)/*PAX8*(-)/inhibin A(+) immunoprofile in hemangioblastoma: A helpful combination in the differential diagnosis with metastatic clear cell renal cell carcinoma to the central nervous system'. *American Journal of Surgical Pathology, vol. 35, issue 2, pp. 262-7.*

Castellino, S. M., Martinez-Borges, A. R., McLean, T. W. (2009). 'Paediatric genitourinary tumours'. *Current Opinion in Oncology, vol. 21, issue 3, pp. 278-83.*

Castranio, T., Mishina, Y. (2009). 'Bmp2 is required for cephalic neural tube closure in the mouse.' *Developmental Dynamics, vol. 238, issue 1, pp. 110-22.*

Chao, T. K., Ke, F. Y., Liao, Y. P., Wang, H. C., Yu, C. P., Lai, H. C. (2013). 'Triage of cervical cytological diagnoses of atypical squamous cells by DNA methylation of paired boxed gene 1'. *Diagnotics Cytopathology, vol. 41, issue 1, pp. 41-6.*

Chappell, J. H. Jr, Wang, X. D., Loeken, M. R. (2009). 'Diabetes and apoptosis: neural crest cells and neural tube'. *Apoptosis, vol 14, issue 12, pp. 1472-83.*

Charytonowicz, E., Matushansky, I., Castillo-Martin, M., Hricik, T., Cordon-Cardo, C., Ziman, M. (2011). 'Alternate PAX3 and PAX7 C-terminal isoforms in myogenic differentiation and sarcomagenesis'. *Clinical and Translational Oncology, vol. 13, issue 3, pp. 194-203.*

Chen, E. Y., Langenau, D. M. (2011). 'Zebra fish Models of Rhabdomyosarcoma' *Methods in Cell Biology, vol. 105, pp. 383- 402.*

Chen, J., Ezzeddine, N., Waltenspiel, B., Albrecht, T. R., Warren, W. D., *et al.,* (2012). 'An RNAi screen identifies additional members of the Drosophila Integrator complex and a requirement for cyclin C/Cdk8 in snRNA 3'-end formation'. *RNA, vol. 18, issue 12, pp. 2148-56.*

Chen[1], H., Suo, K., Cheng, Y., Zheng, B., Xu, L. (2013). 'Vascular endothelial growth factor C enhances cervical cancer migration and invasion via activation of focal adhesion kinase'. *Gynecological Endocrinology, vol. 29, issue 1, pp. 20-4.*

Chen[5], Q., Ganapathy, S., Singh, K. P., Shankar, S., Srivastava, R. K. (2010). 'Resveratrol induces growth arrest and apoptosis through activation of FOXO transcription factors in prostate cancer cells'. *PLoS One, vol. 5, issue 12, e15288.*

Chen, Y., Takita, J., Mizuguchi, M., Tanaka, K., Ida, K., *et al.,* (2007). 'Mutation and expression analyses of the *MET* and *CDKN2A* genes in rhabdomyosarcoma with emphasis on MET overexpression'. *Genes Chromosomes Cancer, vol. 46, issue 4, pp. 348-58.*

Chen, Y. J., Campbell, H. G., Wiles, A. K., Eccles, M. R., Reddel, R. R., *et al.,* (2008). *'PAX8* regulates telomerase reverse transcriptase and telomerase RNA component in glioma'. *Cancer Research, vol. 68, issue 14, pp. 5724-32.*

Chen[1], H., Jiang, L., Xie, Z., Mei, L., He, C., *et al.,* (2010). 'Novel mutations of *PAX3*, *MITF* and *SOX10* genes in Chinese patients with type I or type II Waardenburg syndrome'. *Biochemical and Biophysical Research Communications, vol. 397, issue 1, pp. 70-4*.

Chen[2], L., Zhang, Q. J., Wang, W., Wang, Y. Q. (2010). 'Spatiotemporal expression of *Pax* genes in amphioxus: insights into Pax-related organogenesis and evolution'. *Science China Life Sciences, vol. 53, issue 8, pp. 1031–1040.*

Chen[3], Q., DeGraff, D. J., Sikes, R. A. (2010). 'The developmental expression profile of *PAX2* in the murine prostate'. *Prostate, vol. 70, issue 6, pp. 654-65.*

Chia, W. K., Sharifah, N. A., Reena, R. M., Zubaidah, Z., Clarence-Ko, C. H., *et al.,* (2010). 'Fluorescence in situ hybridization analysis using PAX8- and PPARG-specific probes reveals the presence of PAX8-PPARG translocation and 3p25 aneusomy in follicular thyroid neoplasms'. *Cancer Genet Cytogenetics, vol. 196, issue 1, pp. 7-13.*

Chishti, M. A., Kaya, N., Binbakheet, A. B., Al-Mohanna, F., Goyns, M. H., Colak, D. (2013). 'Induction of cell proliferation in old rat liver can reset certain gene expression levels characteristic of old liver to those associated with young liver'. Age, vol. 35, issue 3, pp. 719-32.

Chivukula, M., Dabbs, D. J., O'Connor, S., Bhargava, R. (2009). '*PAX2*: a novel Müllerian marker for serous papillary carcinomas to differentiate from micropapillary breast carcinoma'. *International Journal of Gynecological Pathology, vol. 28, issue 6, pp. 570-8.*

Christova, T., Mojtahedi, G., Hamel, P. A. (2010). 'Lymphoid enhancer factor-1 mediates loading of *Pax3* to a promoter harbouring lymphoid enhancer factor-1 binding sites resulting in enhancement of transcription'. *International Journal of Biochem and Cell Biology, vol. 42, issue 5, pp. 630-40.*

Chuang, S, F., Su, L. H., Cho, C. C., Pan, Y. J., Sun, C. H. (2012). 'Functional redundancy of two Pax-like proteins in transcriptional activation of cyst wall protein genes in Giardia lamblia'. *PLoS One, vol. 7, issue 2, pp. e30614.*

Ciarapica, R., De Salvo, M., Carcarino, E., Bracaglia, G., Adesso, L., *et al.,* (2013). 'The Polycomb group (PcG) protein EZH2 supports the survival of PAX3-FOXO1 alveolar rhabdomyosarcoma by repressing FBXO32 (Atrogin1/MAFbx)'. *Oncogene, doi: 10.1038/onc.2013.471.*

Cocas, L. A., Georgala, P. A., Mangin, J. M., Clegg, J. M., Kessaris N., *et al.,* (2011). 'Pax6 is required at the telencephalic pallial-subpallial boundary for the generation of neuronal diversity in the postnatal limbic system'. *Journal of Neuroscience, vol. 31, issue 14, pp. 5313-24.*

Collombat, P., Xu, X., Ravassard, P., Sosa-Pineda, B., Dussaud, S., *et al.,* (2009). 'The ectopic expression of *Pax4* in the mouse pancreas converts progenitor cells into alpha and subsequently beta cells'. *Cell, vol. 138, issue 3, pp. 449-62.*

Conrad, A. H., Albrecht, M., Pettit-Scott, M., Conrad, G. W. (2009). 'Embryonic corneal Schwann cells express some Schwann cell marker mRNAs, but no mature Schwann cell marker proteins'. *Investigative Ophthalmological and Vision Science, vol. 50, issue 9, pp. 4173-84.*

Corry, G. N., Hendzel, M. J., Underhill, D. A. (2008). 'Subnuclear localization and mobility are key indicators of PAX3 dysfunction in Waardenburg syndrome.' *Human Molecular Genetics, vol. 17, issue 12, pp. 1825-37.*

Corry, G. N., Raghuram, N., Missiaen, K. K., Hu, N., Hendzel, M. J., Underhill, D. A. (2010). 'The PAX3 paired domain and homeodomain function as a single binding module *in vivo* to regulate subnuclear localization and mobility by a mechanism that requires base-specific recognition'. *Journal of Molecular Biology, vol. 402, issue 1, pp. 178-93.*

Curchoe, C. L., Maurer, J., McKeown, S. J., Cattarossi, G., Cimadamore, F., *et al.,* (2010).'Early acquisition of neural crest competence during hESCs neuralization'. *PLoS One, vol.5, issue 11, e13890.*

Daneshi, A., Hassanzadeh, S., Farhadi, M. (2005). 'Cochlear implantation in children with Waardenburg syndrome'. *Journal of Laryngol Otology, vol. 119, issue 9, pp. 719-23.*

Daubas, P., Buckingham, M. E. (2013). 'Direct molecular regulation of the myogenic determination gene *Myf5* by *Pax3*, with modulation by Six1/4 factors, is exemplified by the 111 kb-Myf5 enhancer'. *Developmental Biology, vol. 376, issue 2, pp. 236-44.*

Davidson, C. E., Li, Q., Churchill, G. A., Osborne, L. R., McDermid, H. E. (2007). 'Modifier locus for exencephaly in Cecr2 mutant mice is syntenic to the 10q25.3 region associated with neural tube defects in humans'. *Physiological Genomics, vol. 31, issue 2, pp. 244-51.*

Davis, J. L., Matsumura, L., Weeks, D. A., Troxell, M. L. (2011). '*PAX2* expression in Wilms tumours and other childhood neoplasms'. *American Journal of Surgical Pathology, vol. 35, issue 8, pp. 1186-94.*

Davicioni, E., Anderson, M. J., Finckenstein, F. G., Lynch, JC, Qualman, S. J., *et al.,* (2009). 'Molecular classification of rhabdomyosarcoma--genotypic and phenotypic determinants of diagnosis: a report from the Children's Oncology Group'. *American Journal of Pathology, vol. 174, issue 2, pp. 550-64.*

Davis, J. R., Mossalam, M., Lim, C. S. (2013). 'Controlled access of p53 to the nucleus regulates its proteasomal degradation by MDM2'. *Molecular Pharmacology, vol. 10, issue 4, pp. 1340-9.*

De Crozé, N., Maczkowiak, F., Monsoro-Burq, A. H. (2011). 'Reiterative AP2a activity controls sequential steps in the neural crest gene regulatory network'. *Proceedings of the National Academy of Sciences. U S A., vol. 108, issue 1, pp. 155-60.*

Dedeic, Z., Cetera, M., Cohen, T. V., Holaska, J. M. (2011). 'Emerin inhibits Lmo7 binding to the *Pax3* and *MyoD* promoters and expression of myoblast proliferation genes'. *Journal of Cell Science, vol. 124, issue 10, pp. 1691-702.*

Degenhardt, K. R., Milewski, R. C., Padmanabhan, A., Miller, M., *et al.,* (2010). 'Distinct enhancers at the *pax3* locus can function redundantly to regulate neural tube and neural crest expressions'. *Developmental Biology, vol. 339, issue 2, pp. 519-527.*

Demirci, G. T., Atıs, G., Altunay, I. K. (2011). 'Waardenburg Syndrome type 1: A case report'. *Dermatology Online Journal, vol. 17, issue 11, p. 3.*

Deries, M., Schweitzer, R. Duxson, M., J. (2010). 'Developmental fate of the mammalian myotome'. *Developmental Dynamics, vol. 239, issue 11, pp. 2898-910.*

Deshmane, V., Kalloli, M., Chikaraddi, S., Keerthi, B., Krishnappa, R. (2014). 'Predictive factors for loco regional recurrence and distant metastasis following primary surgical treatment of cutaneous melanoma'. *Indian Journal of Dermatology, vol. 59, issue 3, pp. 241-6.*

Devi, Y. S., Shehu, A., Halperin, J., Stocco, C., Le, J., Seibold, A. M., Gibori, G. (2009). 'Prolactin signaling through the short isoform of the mouse prolactin receptor regulates DNA binding of specific transcription factors, often with opposite effects in different reproductive issues'. *Reproductive Biological Endocrinololgy, vol. 7, p. 87.*

Dieker, J., Iglesias, G. V., Décossas, M., Stevenin, J., van der, Vlag J., Yuste, V. J., Muller, S. (2012). 'Early apoptotic reorganization of spliceosomal proteins involves caspases, CAD and rearrangement of NuMA'. *Traffic, vol.13, issue 2, pp. 257-72.*

Dietz, K. N., Miller, P. J., Hollenbach, A. D. (2009). 'Phosphorylation of serine 205 by the protein kinase CK2 persists on Pax3-FOXO1, but not Pax3, throughout early myogenic differentiation'. *Biochemistry, vol. 48, issue 49, pp. 11786-95.*

Dietz, K. N., Miller, P. J., Iyengar, A. S., Loupe, J. M., Hollenbach, A. D. (2011). 'Identification of serines 201 and 209 as sites of Pax3 phosphorylation and the altered phosphorylation status of Pax3-FOXO1 during early myogenic differentiation'. *International Journal of Biochemistry and Cell Biology, vol. 43, issue 6, pp. 936-45*.

Djian-Zaouche, J., Campagne, C., Reyes-Gomez, E., Gadin-Czerw, S., Bernex, F., *et al.*, (2012). '*Pax3* (GFP) a new reporter for the melanocyte lineage, highlights novel aspects of *PAX3* expression in the skin'. *Pigment Cell Melanoma Research, vol. 25, issue 5, pp. 545-54.*

Demetri, G. D. (2011). 'Sarcomas of soft tissue and bone, and other neoplasms of connective tissue'. In: Goldman, L., Schafer, A. I., editions. *Cecil Medicine, 24th edition. Philadelphia, P. A: Saunders Elsevier, chap 209.*

Doddrell, R. D., Dun, X. P., Moate, R. M., Jessen, K. R., Mirsky, R., et al., (2012). 'Regulation of Schwann cell differentiation and proliferation by the Pax-3 transcription factor'. Glia, vol. 60, issue 9, pp. 1269-78.

Domingo, R., Chibale, K., Sturrock, E. D. (2011). 'The significance of the C(α) substituent in the selective inhibition of matrix metalloproteinases 1 and 9'. *Biological Chemistry, vol. 392, issue 11, pp. 1003-10.*

Donahue, R. N., Duncan, B. B., Fry, T. J., Jones, B., Bachovchin, W. W., Kiritsy, C. P., *et al.,* (2014). 'A pan inhibitor of DASH family enzymes induces immunogenic modulation and sensitizes murine and human carcinoma cells to antigen-specific cytotoxic T lymphocyte killing: implications for combination therapy with cancer vaccines'. *Vaccine, vol. 32, issue 26, pp. 3223-31.*

Dong[1], D., Jiang, M., Xu, X., Guan, M., Wu, J., Chen Q., Xiang, L. (2012). 'The effects of NB-UVB on the hair follicle-derived neural crest stem cells differentiating into melanocyte lineage in vitro'. *Journal of Dermatological Science, vol. 66, issue 1, pp. 20-8.*

Dong[2], L., Li, Y., Cao, J., Liu, F., Pier, E., Chen, J., *et al.,* (2012). *'FGF2* regulates melanocytes viability through the STAT3-transactivated *PAX3* transcription'. *Cell Death and Differentiation, vol. 19, issue 4, pp. 616-22.*

Dong, M., Hu, N., Hua, Y., Xu, X., Kandadi, M. R., *et al*., (2013). 'Chronic Akt activation attenuated lipopolysaccharide-induced cardiac dysfunction via Akt/GSK3β-dependent inhibition of apoptosis and ER stress'. *Biochimistry and Biophysical Activities, vol. 1832, issue 6, pp. 848-63.*

Doonan, F., Cotter, T. G. (2013). 'Detection of DNA fragmentation in retinal apoptosis by TUNEL'. *Methods in Molecular Biology, vol. 935, pp. 207-13.*

Du, S., Lawrence, E. J., Strzelecki D., Rajput P., Xia S. J. *et al.,* (2005). 'Co-expression of alternatively spliced forms of PAX3, PAX7, PAX3-FKHR and PAX7-FKHR with distinct DNA binding and transactivation properties in rhabdomyosarcoma'. *International Journal of Cancer, vol. 115, issue 1, pp. 85-92.*

Dummer, R., Goldinger, S. M., Turtschi, C. P., Eggmann, N. B., Michielin, O., *et al.,* (2013). 'Vemurafenib in patients with BRAFV600 mutation-positive melanoma with symptomatic brain metastases: Final results of an open-label pilot study'. *European Journal of Cancer. pii: S0959-8049(13)00979-9.*

Dumont, S. N., Lazar, A. J., Bridge, J. A., Benjamin, R. S., Trent, J. C. (2012). 'PAX3/7-FOXO1 fusion status in older rhabdomyosarcoma patient population by fluorescent in situ hybridization'. *Journal of Cancer Research and Clinical Oncology, vol. 138, issue 2, pp. 213-20.*

Durbin, A. D., Somers, G. R., Forrester, M., Pienkowska, M., Hannigan, G. E., Malkin, D. (2009). 'JNK1 determines the oncogenic or tumour-suppressive activity of the integrin-linked kinase in human rhabdomyosarcoma'. *Journal of Clinical Investigations, vol. 119, issue 6, pp. 1558-70.*

Dye, D. E., Medic, S., Ziman, M., Coombe, D. R. (2013). 'Melanoma Biomolecules: Independently Identified but Functionally Intertwined'. *Fronters in Oncology, vol. 3, pp. 252.*

Edgar, R., Mazor, Y., Rinon, A., Blumenthal, J., Golan, Y., Buzhor, E., Livnat, I., *et al*., (2013). 'LifeMap Discovery™: the embryonic development, stem cells, and regenerative medicine research portal'. *PLoS One, vol. 8, issue 7, e66629*.

Egas-Bejar, D., Huh, W. W. (2014). 'Rhabdomyosarcoma in adolescent and young adult patients: current perspectives'. *Adolescent Health, Medicine and Therapeutics, vol. 5, pp.115-25.*

Eigelshoven, S., Kameda, G., Kortüm, A. K., Hübsch, S., Angerstein, W., *et al*., (2009). 'Waardenburg syndrome type I with heterochromia iridis and circumscribed hypopigmentation of the skin.' *Pediatrics Dermatology, vol 26, issue 6, pp. 759-61.*

Fang, W. H., Wang, Q., Li, H. M., Ahmed, M., Kumar, P., Kumar, S. (2014). '*PAX3* in neuroblastoma: oncogenic potential, chemosensitivity and signalling pathways'. *Journal of Cellular and Molecular Medicine, vol.18, issue 1, pp. 38-48.*

Fang, W. H., Ahmed, M., Wang, Q., Li, H.M., Kumar, P., Kumar, S. (2013). '*PAX3* promotes tumour progression via CD105 signaling'. *Microvascular Research, vol. 86, pp. 42-3.*

Fangusaro, J. R., Caldas, H., Jiang, Y., Altura, R. A. (2006). 'Survivin: an inhibitor of apoptosis in pediatric cancer'. *Pediatrics Blood Cancer, vol. 47, issue 1, pp. 4-13.*

Farin, H. F., Mansouri, A., Petry, M., Kispert, A. (2008). 'T-box protein Tbx18 interacts with the paired box protein Pax3 in the development of the paraxial mesoderm'. *Journal of Biological Chemistry, vol. 283, issue 37, pp. 25372-80.*

Fechete, R., Barth, S., Olender, T., Munteanu, A., Bernthaler, A., Inger, A., *et al*., (2011). 'Synthetic lethal hubs associated with vincristine resistant neuroblastoma'. *Molecular Biosystems, vol. 7, issue 1, pp. 200-14.*

Fenby, B. T., Fotaki, V., Mason, J. O. (2008). *'Pax3* regulates *Wnt1* expression via a conserved binding site in the 5' proximal promoter'. *Biochimistry and Biophysical Activities, vol. 1779, issue 2, pp. 115-21.*

Fernandez, K., Serinagaoglu, Y., Hammond, S., Martin, L. T., Martin, P. T. (2010). 'Mice lacking dystrophin or alpha sarcoglycan spontaneously develop embryonal rhabdomyosarcoma with cancer-associated p53 mutations and alternatively spliced or mutant Mdm2 transcripts'. *Americal Journal of Pathology, vol. 176, issue 1, pp. 416-34.*

Fernández, R. M., Núñez-Ramos, R., Enguix-Riego, M. V., Román-Rodríguez, F. J., Galán-Gómez, E. (2014). 'Waardenburg syndrome type 4: Report of two new cases caused by SOX10 mutations in Spain'. *Americal Journal of Medical Genetics part A, vol. 164A, issue 2, pp. 542-7.*

Fietta, P. (2006). 'Many ways to die: passive and active cell death styles'. *Riview Biology, vol. 99, issue 1, pp. 69-83.*

Firtina, S., Sayitoglu, M., Hatirnaz, O., Erbilgin, Y., Oztunc, C., *et al*., (2012). 'Evaluation of *PAX5* gene in the early stages of leukemic B cells in the childhood B cell acute lymphoblastic leukemia.' *Leukeamia Research, vol. 36, issue 1, pp. 87-92.*

Froehlich, J. M., Galt, N. J., Charging, M. J., Meyer, B. M., Biga, P. R. (2013). 'In vitro indeterminate teleost myogenesis appears to be dependent on *Pax3*'. *In Vitro Cell Developmental Biological Animal, vol. 49, issue 5, pp. 371-85.*

Fuchs, Y., Steller, H. (2011). 'Programmed cell death in animal development and disease'. *Cell, vol. 147, pp. 742–758.*

Fujita, T., Fujii, H. (2011). 'Species-specific 5'-genomic structure and multiple transcription start sites in the chicken *Pax5* gene'. *Gene, vol. 477, issue 2, pp. 24-31.*

Gacche, R. N., Meshram, R. J. (2013).'Targeting tumour micro-environment for design and development of novel anti-angiogenic agents arresting tumour growth'. *Progress in Biophysics & Molecular Biology, vol. 113, issue 2, pp. 333-54.*

Gad, A., Laurino, M., Maravilla, K. R., Matsushita, M., Raskind, W. H. (2008). 'Sensorineural deafness, distinctive facial features, and abnormal cranial bones: a new variant of Waardenburg syndrome'? *American Journal of Medical Genetics part A, vol. 146A, issue 14, pp. 1880-5.*

Gajda, M., Kaminska-Winciorek, G. (2014). 'Do not let to be late: overview of reasons for melanoma delayed diagnosis'. *Asian Pacific journal of cancer prevention, vol. 15, issue 9, pp. 3873-7.*

Gallego, Melcón, S., Sánchez, de Toledo, Codina, J. (2007). 'Molecular biology of rhabdomyosarcoma.' *Clinical and Translational Oncology, vol. 9, issue 7, pp. 415-9.*

Galluzzi, L., Vitale, I., Abrams, J. M., Alnemri, E. S., Baehrecke, E. H., *at al*., (2012). 'Molecular definitions of cell death subroutines: recommendations of the Nomenclature Committee on Cell Death 2012'. *Cell Death and Differentiation, vol. 19, issue 1, pp. 107-20.*

Gee, S. T., Milgram, S. L., Kramer, K. L., Conlon, F. L., Moody, S. A. (2011). 'Yes-associated protein 65 (YAP) expands neural progenitors and regulates *Pax3* expression in the neural plate border zone'. *PLoS One, vol. 6, issue 6, e20309.*

Gholami, O., Jeddi-Tehrani, M., Iranshahi, M., Zarnani, A. H., Ziai, S. A. (2013). 'Umbelliprenin from Ferula szowitsiana Activates both Intrinsic and Extrinsic Pathways of Apoptosis in Jurkat T-CLL cell line'. *Iranian Journal of Pharmaceutical Research, vol. 12, issue 3, pp. 371-6.*

Gianakopoulos, P. J., Mehta, V., Voronova, A., Cao, Y., Yao, Z., *et al.,* (2011). 'MyoD directly up-regulates premyogenic mesoderm factors during induction of skeletal myogenesis in stem cells'. *Journal of Biological Chemistry, vol. 286, issue 4, pp. 2517-25.*

Gilsbach, R., Kouta, M., Bönisch, H., Brüss, M. (2006). 'Comparison of in vitro and in vivo reference genes for internal standardization of real-time PCR data'. *Biotechniques, vol. 40, issue 2, pp. 173-7.*

Glynn, D., Brad, T. S., Douglas, A, H., Jun, Y., Wei, G. H. C. Richard, A. L. (2003). *'Genome Biology', vol. 4: R60doi:10.1186.*

Goding, C. (2008). 'Genesis and NEMESIS'. *Pigment Cell Melanoma Research, vol. 21, issue 6, pp. 591.*

Goldsmith, K. C., Gross, M., Peirce, S., Luyindula, D., Liu, X., *et al*., (2012). 'Mitochondrial Bcl-2 family dynamics define therapy response and resistance in neuroblastoma'. *Cancer Research, vol. 72, issue 10, pp. 2565-77.*

Goljanek-Whysall, K., Sweetman, D., Abu-Elmagd, M., Chapnik, E., Dalmay, T., *et al*., (2011). 'MicroRNA regulation of the paired-box transcription factor *Pax3* confers robustness to developmental timing of myogenesis'. *Proceedings of the National Academy of Sciences U S A., vol. 108, issue 29, pp. 11936-41.*

Gomes, H., Romeiro, N. C., Braz, G. R., de, Oliveira, E. A., Rodrigues, C., *et al*., (2013). 'Identification and Structural-Functional Analysis of Cyclin-Dependent Kinases of the Cattle Tick Rhipicephalus (Boophilus) microplus'. *PLoS One, vol. 8, issue 10, e76128.*

Gonzalez-Perez, F., Udina, E., Navarro, X. (2013). 'Extracellular matrix components in peripheral nerve regeneration'. *International Review of Neurobiology, vol. 108, pp. 257-75.*

Gonzalez-Reyes, S., Fernandez-Dumont, V., Calonge, W. M., Martinez, L., Tovar, J. A. (2006). 'Vitamin A improves Pax3 expression that is decreased in the heart of rats with experimental diaphragmatic hernia'. *Journal of Pediatric Surgery, vol. 41, issue 2, pp. 327-30.*

Grabellus, F., Konik, M. J., Worm, K., Sheu, S. Y., van de Nes, J. A., *et al.,* (2010). 'MET overexpressing chordomas frequently exhibit polysomy of chromosome 7 but no MET activation through sarcoma-specific gene fusions'. *Tumour Biology, vol. 31, issue 3, pp. 157-63.*

Graveley, B. R. (2009). 'Alternative splicing: regulation without regulators'. *Nature Structural & Molecular Biology, vol. 16, issue 1, pp. 13–15.*

Greene, N. D., Massa, V., Copp, A. J. (2009). 'Understanding the causes and prevention of neural tube defects: Insights from the splotch mouse model.' *Birth Defects Research part: A Clinical and Molecular Teratology, vol. 85, issue 4, pp. 322-30.*

Gregory, S., Barlow, K. F., McLay, K. E., Kaul, R., Swarbreck, D., *et al.,* (2006). 'The DNA sequence and biological annotation of human chromosome 1'. *Nature, vol. 441, issue 7091, pp. 315-21.*

Griffith, A. V., Cardenas, K., Carter, C., Gordon, J., Iberg, A., *et al.,* (2009). 'Increased thymus and decreased parathyroid-fated organ domains in Splotch mutant embryos'. *Developmental Biology, vol. 327, issue 1, pp. 216-27.*

Grill, C., Bergsteinsdóttir, K., Ogmundsdóttir, M. H., Pogenberg, V., Schepsky, A., *et al.,* (2013). 'MITF mutations associated with pigment deficiency syndromes and melanoma have different effects on protein function'. *Human Molecular Genetics, vol. 22, issue 21, pp. 4357-67.*

Gutkovich, Y. E., Ofir, R., Elkouby, Y. M., Dibner, C., Gefen, A., Elias, S., Frank, D. (2010). 'Xenopus Meis3 protein lies at a nexus downstream to Zic1 and Pax3 proteins, regulating multiple cell-fates during early nervous system development'. *Developmental Biology, vol. 338, issue 1, pp. 50-62.*

Hager, T., Walter, H. S., Seitz, B., Käsmann-Kellner, B. (2010). 'Visual diagnosis: Waardenburg syndrome'. *Ophthalmologe, vol. 107, issue 7, pp. 660-2.*

Haider, N., Nadim, M. S., Piracha, M. N. (2013). 'Primary embryonal rhabdomyosarcoma of the liver in a young male'. *Journal College of Physicians Surgeons of Pakistan, vol. 23, issue 10, pp. 750-1.*

Haldeman-Englert, C. R., Biser, A., Zackai, E. H., Ming, J. E. (2012). 'A 223-kb *de novo* deletion of *PAX9* in a patient with oligodontia'. *Journal Craniofacial Surgery, vol. 23, issue 2, e149-51.*

Han, H. Y., Zhang, J. P., Ji, S. Q., Liang, Q. M., Kang, H. C., *et al.,* (2013). 'αv and β1 integrins mediate Aβ-induced neurotoxicity in hippocampal neurons via the FAK signaling pathway'. *PLoS One, vol. 8, issue 6, e64839*.

Hansen, L., Kreiborg, S., Jarlov, H., Niebuhr, E., Eiberg, H. (2007). 'A novel nonsense mutation in *PAX9* is associated with marked variability in number of missing teeth'. *European Journal of Oral Science, vol. 115, issue 4, pp. 330-3.*

Hata, S., Hamada, J., Maeda, K., Murai, T., Tada, M., Furukawa, H., *et al.,* (2008). '*PAX4* has the potential to function as a tumour suppressor in human melanoma'. *International Journal of Oncology, vol. 33, issue 5, pp. 1065-71.*

Hauswirth, R., Haase, B., Blatter, M., Brooks, S. A., Burger D*., et al*., (2012). 'Mutations in *MITF* and *PAX3* cause "splashed white" and other white spotting phenotypes in horses'. *PLoS Genetics, vol. 8, issue 4, e1002653.*

Hawkins, R. D., Hon, G. C., Ren, B. (2010). 'Next-generation genomics: an integrative approach'. *Nature Reviews Genetics, 11, issue 7, pp. 476-486.*

Hayashi, S., Rocancourt, D., Buckingham, M., Relaix, F. (2011). 'Lack of *in vivo* functional compensation between Pax family groups II and III in rodents'. *Molecular Biology Evolution, vol. 28, issue 10, pp. 2787-98.*

Hazan, F., Ozturk, A. T., Adibelli, H., Unal, N., Tukun, A. (2013). 'A novel missense mutation of the paired box 3 gene in a Turkish family with Waardenburg syndrome type 1'. *Molecular Vision, vol. 19, pp. 196-202.*

He[2], G., Kuang, J., Khokhar, A. R., Siddik, Z. H. (2011). 'The impact of S and G2 checkpoint response on the fidelity of G1-arrest by cisplatin and its comparison to a non-cross-resistant platinum (IV) analog'. *Gynecologic Oncology, vol. 122, issue 2, pp. 402-9.*

He[1], S., Li, C. G., Slobbe, L., Glover, A., Marshall, E., *et al*., (2011). '*PAX3* knockdown in metastatic melanoma cell lines does not reduce *MITF* expression'. *Melanoma Research, vol. 21, issue 1, pp. 24-34.*

He[2], X., Zhou, A., Lu, H., Chen, Y., Huang, G., Yue, X., Zhao, P., Wu, Y. (2013). 'Suppression of mitochondrial complex I influences cell metastatic properties'. *PLoS One, vol. 8, issue 4, e61677.*

Hebert, D. N., Molinari, M. (2007). 'In and out of the ER: protein folding, quality control, degradation, and related human diseases'. *Physiological Review, vol. 87, issue 4, pp. 1377-408.*

Hecker, R. M., Amstutz, R. A., Wachtel, M., Walter, D., Niggli, F. K., Schäfer, B. W. (2010). 'p21 Downregulation is an important component of PAX3/FKHR oncogenicity and its reactivation by HDAC inhibitors enhances combination treatment.' *Oncogene, vol. 29, issue 27, pp. 3942-52.*

Helfrich, I., Ullrich, N., Zigrino, P., Schadendorf, D. (2014). 'Primary Tumor versus Metastasis: New experimental Models for Studies on Cancer Cell Homing and Metastasis in Melanoma'. *'Pigment Cell Melanoma Research, vol., 27, issue 2, pp. 309-16.*

Heltemes-Harris, L. M., Willette, M. J., Ramsey, L. B., Qiu, Y. H., Neeley E. S., *et al*., (2011). '*Ebf1* or *Pax5* haploinsufficiency synergizes with *STAT5* activation to initiate acute lymphoblastic leukemia'. *Journal of Experimental Medicine, vol. 208, issue 6, pp. 1135-49.*

Herbeck, R., Teodorescu, B, D., Giubelan, M., Lazăr, E., Dema, A., Ioniţă, H. (2011). 'B-cell transcription factors *Pax-5, Oct-2, BOB.1, Bcl-6,* and *MUM1* are useful markers for the diagnosis of nodular lymphocyte predominant Hodgkin lymphoma'. *Romanian Journal of Morphology and Embryology, vol. 52, issue 1, pp. 69-74.*

Herrero., M. D., Boro, A., Schäfer, B. W. (2013). 'Cell-based small-molecule compound screen identifies fenretinide as potential therapeutic for translocation-positive rhabdomyosarcoma'. *PLoS One, vol. 8, issue 1, e55072.*

Himeda, C. L., Barro, M. V., Emerson, C. P. Jr. (2013). '*Pax3* synergizes with *Gli2* and *Zic1* in transactivating the *Myf5* epaxial somite enhancer'. *Developmental Biology, vol. 383, issue 1, pp. 7-14.*

Higgins, I, H. W., Lee, K. C., Leffell, D. J. (2014). 'Point of care cutaneous imaging technology in melanoma screening and mole mapping'. *F1000Prime Reports, vol. 6, p. 34.*

Hirai, H., Verma, M., Watanabe, S., Tastad, C., Asakura, Y., Asakura, A. (2010). '*MyoD* regulates apoptosis of myoblasts through microRNA-mediated down-regulation of *Pax3'. Journal of Cell Biology, vol. 191, issue 2, pp. 347-65.*

Hoffmeier, A., Sindermann, J. R., Scheld, H. H., Martens, S. (2014). 'Cardiac tumours-diagnosis and surgical treatment'. *Deutsches Ärzteblatt International, vol. 111, issue 12, pp. 205-11.*

Holland, L. Z., Short, S. (2010). 'Alternative splicing in development and function of chordate endocrine systems: a focus on *Pax* genes'. *Integrative and Comparative Biology, vol. 50, issue 1, pp. 22–3.*

Hong, C. S., Saint-Jeannet, J. P. (2007). 'The activity of *Pax3* and *Zic1* regulates three distinct cell fates at the neural plate border'. *Molecular Biology of the Cell*, *vol. 18, issue 6, pp. 2192-202*.

Hong, G. M., Bain, L. J. (2012). 'Arsenic exposure inhibits myogenesis and neurogenesis in P19 stem cells through repression of the β-catenin signaling pathway'. *Toxicological Sciences, vol. 129, issue 1, pp. 146-56.*

Hoshimoto, S., Faries, M. B., Morton D. L., Shingai, T., Kuo, C., *et al.,* (2012). 'Assessment of prognostic circulating tumour cells in a phase III trial of adjuvant immunotherapy after complete resection of stage IV melanoma'. *Annals of Surgery, vol. 255, issue 2, pp. 357-62.*

Hosoyama, T., Aslam, M. I., Abraham, J., Prajapati, S. I., Nishijo, K., *et al.,* (2011). 'IL-4R drives dedifferentiation, mitogenesis, and metastasis in rhabdomyosarcoma'. *Clinical Cancer Research, vol. 17, issue 9, pp. 2757-66.*

Hou, L., Pavan, W. J. (2008). 'Transcriptional and signaling regulation in neural crest stem cell-derived melanocyte development: do all roads lead to Mitf?' *Stem Cell Research, vol. 18, issue 12, pp. 1163-76.*

Hsieh, M. J., Yao, Y. L., Lai, I. L., Yang, W. M. (2006). 'Transcriptional repression activity of PAX3 is modulated by competition between corepressor KAP1 and heterochromatin protein 1'. *Biochemical and Biophysical Research Communications, vol. 349, issue 2, pp. 573-81*.

Hsu, D. S., Acharya, C. R., Balakumaran, B. S., Riedel, R. F., Kim, M. K., *et al*., (2011). 'Characterizing the developmental pathways TTF-1, NKX2-8, and PAX9 in lung cancer'. *Proceedings of the National Academy of Sciences U S A., vol. 108, issue 35, pp. 14705*.

http//AtlasGeneticsOnchology.org/Genes/Foxo1ID83ch13q14.html

http://discovery.lifemapsc.com/'Neural crest development.

http://david.niaid.nih.gov/david/version2/index.htm.

http://www.ncbi.nlm.nih.gov/BLAST/

http://www.dchip.org

http://ghr.nlm.nih.gov/

Hu, H., K. H., Lorenzo, P. I., Brun, T., Jimenez, M., C. M., Aeberhard D., *et al.,* (2011). 'In vivo conditional Pax4 overexpression in mature islet β-cells prevents stress-induced hyperglycemia in mice'. *Diabetes, vol. 60, issue 6, pp. 1705-15.*

Hu[2], Q., Wu, D., Chen, W., Yan, Z., Shi, Y. (2013). 'Proteolytic processing of the caspase-9 zymogen is required for apoptosome-mediated activation of caspase-9'. *Journal of Biological Chemistry, vol. 288, issue 21, pp. 15142-7.*

Hu[1], Q., Yuan, Y., Wang, C. (2013). 'Structural and functional studies of FKHR-PAX3, a reciprocal fusion gene of the t(2;13) chromosomal translocation in alveolar rhabdomyosarcoma'. *PLoS One, vol. 8, issue 6, e68065.*

Hu, Y., Hartmann, A., Stoehr, C., Zhang, S., Wang, M., *et al.,* (2012). '*PAX8* is expressed in the majority of renal epithelial neoplasms: an immunohistochemical study of 223 cases using a mouse monoclonal antibody'. *Journal of Clinical Pathology, vol. 65, issue 3, pp. 254-6.*

Hutcheson, D. A., Zhao, J., Merrell, A., Haldar, M., Kardon, G. (2009). 'Embryonic and fetal limb myogenic cells are derived from developmentally distinct progenitors and have different requirements for beta-catenin'. *Genes Development, vol. 23, issue 8, pp. 997-1013.*

Ichi[1], S., Boshnjaku, V., Shen, Y. W., Mania-Farnell, B., Ahlgren, S., *et al.,* (2010). 'Role of *Pax3* acetylation in the regulation of *Hes1* and *Neurog2'. Molecular Biological Cell, vol. 22, issue 4, pp. 503-12.*

Ichi[2], S., Costa, F. F., Bischof, J. M., Nakazaki, H., Shen, Y., *et al.,* (2010). 'Folic acid remodels chromatin on Hes1 and Neurog2 promoters during caudal neural tube development'. *Journal of Biological Chemistry, vol. 285, issue 47, pp. 36922-32.*

Inami, Y., Yoshikai, T., Ito, S., Nishio, N., Suzuki, H., Sakurai, H., Isobe, K. (2011) 'Differentiation of induced pluripotent stem cells to thymic epithelial cells by phenotype'. *Immunology and Cell Biology, vol. 89, issue 2, pp. 314-21.*

Inoue, Y., Hasegawa, S., Yamada, T., Date, Y., Mizutani, H., *et al*., (2013). 'Analysis of the effects of hydroquinone and arbutin on the differentiation of melanocytes'. *Biological and Pharmaceutical Bulletin, vol. 36, issue 11, pp. 1722-30.*

Ishiguro, T., Ishiguro, R., Ishiguro, M., Iwai, S. (2012). 'Co-treatment of dichloroacetate, omeprazole and tamoxifen exhibited synergistically antiproliferative effect on malignant tumours: in vivo experiments and a case report'. *Hepatogastroenterology, vol. 59, issue 116, pp. 994-6.*

Iyengar, A. S., Loupe, J. M., Miller, P. J., Hollenbach, A. D. (2012). 'Identification of CK2 as the kinase that phosphorylates *Pax3* at Ser209 in early myogenic differentiation'. *Biochemical and Biophysical Research Communications, vol. 428, issue 1, pp. 24-30.*

Jacob, A. G., O'Brien, D., Singh, R. K., Comiskey, D. F. Jr., Littleton, R. M., Mohammad, F., *et al.,* (2013). 'Stress-induced isoforms of MDM2 and MDM4 correlate with high-grade disease and an altered splicing network in pediatric rhabdomyosarcoma'. *Neoplasia, vol. 15, issue 9, pp. 1049-63.*

Jain, R., Engleka, K. A., Rentschler, S. L., Manderfield, L. J., Li, L., *et al*., (2011). 'Cardiac neural crest orchestrates remodelling and functional maturation of mouse semilunar valves'. *Journal of Clinical Investigations, vol. 121, issue 1, pp. 422-30.*

Jamiyandorj, U., Bae, J. S., Noh, S. J., Jachin, S., Choi J. E., *et al*., (2013). 'Expression of peptidyl-prolyl isomerase PIN1 and its role in the pathogenesis of extrahepatic cholangiocarcinoma'. *Oncology Letters, vol. 6, issue 5, pp. 1421-1426*.

Jia, H., Tao, H., Feng, R., Li, M., Bai, J., Sun, T., Wen, J., Hu, Q. (2011). '*Pax6* regulates the epidermal growth factor-responsive neural stem cells of the subventricular zone'. *NeuroReport, vol. 22, issue 9, pp. 448-52*.

Jiang, M., Wang, C. Y., Huang, S., Yang, T., Dong, Z. (2009). 'Cisplatin-induced apoptosis in p53-deficient renal cells via the intrinsic mitochondrial pathway'. *American Journal of Renal Physiology, vol. 296, pp. 983-993.*

Jiang[1], L., Chen, H., Jiang, W., Hu, Z., Mei, L., *et al*., (2011). 'Novel mutations in the SOX10 gene in the first two Chinese cases of type IV Waardenburg syndrome'. *Biochemical and Biophysical Research Communications, vol. 408, issue 4, pp. 620-4.*

Jiang, W., Crossman, D. K., Mitchell, E. H., Sohn, P., Crowley, M. R., Serra, R. (2013). '*WNT5A* inhibits metastasis and alters splicing of Cd44 in breast cancer cells'. *PLoS One, vol. 8, issue 3, e58329*.

Jiao, Z., Zhang, Z. G., Hornyak, T. J, Hozeska, A., Zhang, R. L., *et al.,* (2006). 'Dopachrome tautomerase (*Dct*) regulates neural progenitor cell proliferation'. *Developmental Biology, vol. 296, issue 2, pp. 396-408.*

Jo, W., Endo, M., Ishizu, K., Nakamura, A., Tajima, T. (2011). 'A novel *PAX4* mutation in a Japanese patient with maturity-onset diabetes of the young'. *Tohoku Journal of Experimental Medicine, vol. 223, issue 2, pp. 113-8.*

Johnson, S. A., Harmon, K. J., Smiley, S. G., Still, F. M., Kavaler, J. (2011). 'Discrete regulatory regions control early and late expression of *D-Pax2* during external sensory organ development'. *Developmental Dynamics, vol. 240, issue 7, pp. 1769-78.*

Jothi, M., Nishijo, K., Keller, C., Mal, A. K. (2012). 'AKT and PAX3-FKHR cooperation enforces myogenic differentiation blockade in alveolar rhabdomyosarcoma cell'. *Cell Cycle, vol. 11, issue 5, pp. 895-908.*

Jothi, M., Mal, M., Keller, C., Mal, A. K. (2013). 'Small Molecule Inhibition of PAX3-FOXO1 through AKT Activation Suppresses Malignant Phenotypes of Alveolar Rhabdomyosarcoma'. *Molecular Cancer Therapeutics, vol. 12, issue 12, pp. 2663-74.*

Kaneko, K. J., Kohn, M. J., Liu, C., DePamphilis, M. L. (2007). 'Transcription factor TEAD2 is involved in neural tube closure.' *Genesis, vol.45, issue 9, pp. 577-87.*

Kang, H. J., Kawasawa, Y. I., Cheng, F., *et al.,* (2011). 'Spatio-temporal transcriptome of the human brain'. *Nature, 478, issue 7370, pp. 483-489.*

Kang, J. S., Krauss, R. S. (2010). 'Muscle stem cells in developmental and regenerative myogenesis.' *Current Opinion in Clinical Nutrition and Metabolic Care, vol.13, issue 3, pp. 243-248*.

Kang, Z., Yu, Y., Zhu, Y. J., Davis, S., Walker, R., Meltzer, P. S., Helman, L. J., Cao, L. (2013). 'Downregulation of IGFBP2 is associated with resistance to IGF1R therapy in rhabdomyosarcoma'. *Oncogene, doi: 10.1038/onc.2013.509.*

Kapadia, H., Frazier-Bowers, S., Ogawa, T., D'Souza, R. N. (2006). 'Molecular characterization of a novel *PAX9* missense mutation causing posterior tooth agenesis'. *European Journal of Human Genetics, vol. 14, issue 4, pp. 403-9.*

Kapoor, S., Bindu, P. S., Taly, A. B., Sinha, S., Gayathri, N., *et al.,* (2012). 'Genetic analysis of an Indian family with members affected with Waardenburg syndrome and Duchenne muscular dystrophy'. *Molecular Vision, vol., 18, pp. 2022-32.*

Karafin, M., Parwani, A. V., Netto, G. J., Illei, P. B., Epstein, J. I. *et al.,* (2011). 'Diffuse expression of *PAX2* and *PAX8* in the cystic epithelium of mixed epithelial stromal tumor, angiomyolipoma with epithelial cysts, and primary renal synovial sarcoma: evidence supporting renal tubular differentiation'. *American Journal of Surgical Pathology, vol. 35, issue 9, pp. 1264-73.*

Kaufman, H. L., Ruby, C. E., Hughes, T., Slingluff, C. L. Jr. (2014). 'Current status of granulocyte-macrophage colony-stimulating factor in the immunotherapy of melanoma'. *Journal of Immunotherapy of Cancer. vol. 2, issue 11.*

Kazi A, Sun J, Doi K, Sung SS, Takahashi Y, Yin H., *et al*., (2011). 'The BH3 alpha-helical mimic BH3-M6 disrupts Bcl-X(L), Bcl-2, and MCL-1 protein-protein interactions with Bax, Bak, Bad, or Bim and induces apoptosis in a Bax- and Bim-dependent manner'. *Journal of Biological Chemistry, vol. 286, issue11, pp. 9382-92.*

Kennedy, K. A., Porter, T., Mehta, V., Ryan, S. D., Price, F., *et al.,* (2009). 'Retinoic acid enhances skeletal muscle progenitor formation and bypasses inhibition by bone morphogenetic protein 4 but not dominant negative beta-catenin'. *BMC Biology, vol. 7, p. 67.*

Khammanivong, A., Wang, C., Sorenson, B. S., Ross, K. F., Herzberg, M. C. (2013). 'S100A8/A9 (calprotectin) negatively regulates G2/M cell cycle progression and growth of squamous cell carcinoma'. *PLoS One, vol. 8, issue 7, e69395.*

Kikuchi, K., Taniguchi, E., Chen, H. I., Svalina, M. N., Abraham, J., Huang, E. T., *et al*., (2013). 'Rb1 loss modifies but does not initiate alveolar rhabdomyosarcoma'. *Skeletal Muscle, vol. 3, issue 1, p. 27.*

Kist, R., Watson, M., Wang, X., Cairns, P., Miles, C., Reid, D. J., Peters, H. (2005). 'Reduction of *Pax9* gene dosage in an allelic series of mouse mutants causes hypodontia and oligodontia'. *Human Molecular Genetics, vol. 14, issue 23, pp. 3605-17.*

Kiyohara, E., Hata, K., Lam, S., Hoon, D. S. (2013). 'Circulating tumour cells as prognostic biomarkers in cutaneous melanoma patients'. *Methods in Molecular Biology, vol. 1102, pp. 513-22.*

Kohli, S., Saxena, R., Verma, I. C. (2010). 'Novel human pathological mutations. Gene symbol: *PAX3*. Disease: Waardenburg syndrome'. *Human Genetics, vol. 127, issue 4, p. 485.*

Kojima, Y., Hashimoto, K., Ando, M., Yonemori, K., Yamamoto, H., *et al.,* (2012). 'Comparison of dose intensity of vincristine, d-actinomycin, and cyclophosphamide chemotherapy for child and adult rhabdomyosarcoma: a retrospective analysis'. *Cancer Chemotherapy Pharmacology, vol. 70, issue 3, pp. 391-7.*

Kong, M., Muñoz, N., Valdivia, A., Alvarez, A., Herrera-Molina, R., *et al*., (2013). 'Thy-1-mediated cell-cell contact induces astrocyte migration through the engagement of αVβ3 integrin and syndecan-4'. *Biochimitry and Biophysical Activitie., vol. 1833, issue 6, pp. 1409-20.*

Kozawa, M., Kondo, H., Tahira, T., Hayashi, K., Uchio, E. (2009). 'Novel mutation in *PAX3* gene in Waardenburg syndrome accompanied by unilateral macular degeneration.' *Eye, vol. 23, issue 7, pp. 1619-21.*

Krskova, L., Augustinakova, A., Drahokoupilova, E., Sumerauer, D., Mudry, P., Kodet, R. (2011). 'Rhabdomyosarcoma: molecular analysis of Igf2, MyoD1 and Myogenin expression'. *Neoplasma, vol. 58, issue 5, pp. 415-23.*

Kubic, J. D., Mascarenhas, J. B., Iizuka, T., Wolfgeher, D., Lang, D. (2012). 'GSK-3 promotes cell survival, growth, and PAX3 levels in human melanoma cells'. *Molecular Cancer Research, vol. 10, issue 8, pp. 1065-76.*

Kubic, J. D., Young, K. P., Plummer, R. S., Ludvik, L. D. (2008). 'Pigmentation *PAX*-way: The role of pax in melanogenesis, melanocyte stem cell maintenance and disease'. *Pigment Cell Melanom, vol. 21, issue 6, pp. 627-645*.

Kucharzewska, P., Belting, M. (2013). 'Emerging roles of extracellular vesicles in the adaptive response of tumour cells to microenvironmental stress'. *Journal of Extracellular Vesicles, vol. 2, 10. doi: 10.3402/jev.v2i0.20304.eCollection 2013*.

Kumar, S. D., Dheen, S. T., Tay, S. S. (2007). 'Maternal diabetes induces congenital heart defects in mice by altering the expression of genes involved in cardiovascular development'. *Cardiovascular Diabetology, vol. 6, p. 34.*

Kumar, V., Abbas, A., Aster, J. (2009). 'Robbin and Cotran Pathologic basis of disease. *Soft tumours' 8th edition, pp. 1321-1322, Saunders, Elseivier*.

Kurien, B. T., Dorri, Y., Dillon, S., Dsouza. A., Scofield, R. H. (2011). 'An overview of Western blotting for determining antibody specificities for immunohistochemistry'. *Methods in Molecular Biology, vol. 717, pp. 55-67.*

Kusakabe, R., Kuraku, S. Kuratani, S. (2011). 'Expression and interaction of muscle-related genes in the lamprey imply the evolutionary scenario for vertebrate skeletal muscle, in association with the acquisition of the neck and fins'. *Developmental Biology, vol. 350, issue 1, pp. 217-27.*

Lacosta, A. M., Canudas, J., Gonzalez, C., Muniesa, P., Sarasa, M., Dominguez, L. (2007). '*Pax7* identifies neural crest, chromatophore lineages, and pigment stem cells during zebrafish development'. *International Journal of Devevelopmental Biology, vol. 51, issue 4, pp. 327-31.*

Lagha, M., Mayeuf-Louchart, A., Chang, T., Montarras D., Rocancourt, D., *et al.,* (2013). 'Itm2a is a *Pax3* target gene, expressed at sites of skeletal muscle formation *in vivo'. PLoS One, vol. 8, issue 5, e63143.*

Lagha, M., Sato, T., Regnault, B., Cumano A., Zuniga A., *et al.,* (2010). 'Transcriptome analyses based on genetic screens for *Pax3* myogenic targets in the mouse embryo'. *BMC Genomics, vol. 11, p. 696.*

Lagutina, I., Conway, S. J., Sublett, J., Grosveld, G. C. (2002). 'Pax3-FKHR knock-in mice show developmental aberrations but do not develop tumours'. *Molecular Cell Biology, vol. 22, issue 20, pp. 7204-16.*

La Greca, M., Grasso, G., Antonelli, G., Russo, A. E., Bartolotta, S., *et al.,* (2014). 'Neoadjuvant therapy for locally advanced melanoma: new strategies with targeted therapies'. *OncoTargets and Therapy, vol. 7, pp. 1115-21.*

Lai, I. L., Lin, T. P., Yao, Y. L., Lin, C. Y., Hsieh, M. J., Yang, W. M. (2010). 'Histone deacetylase 10 relieves repression on the melanogenic program by maintaining the deacetylation status of repressors'. *Journal of Biological Chemistry, vol. 285, issue 10, pp. 7187-96.*

Lange, M., Koulova, A., Kang, S., Griffin, M. J., Lassaletta, A. D., Erat, A., *et al.* (2014). 'Arterial territory-specific phosphorylated retinoblastoma protein species and CDK2 promote differences in the vascular smooth muscle cell response to mitogens'. *Cell Cycle, vol. 13, issue 3.*

Lasfar, A., Cohen-Solal, K. A. (2010). 'Resistance to transforming growth factor β-mediated tumour suppression in melanoma: are multiple mechanisms in place?' *Carcinogenesis, vol. 31, issue 10, pp. 1710-7.*

Lassiter, R. N., Ball, M. K., Adams, J. S., Wright, B. T., Stark, M. R. (2010). 'Sensory neuron differentiation is regulated by notch signaling in the trigeminal placode'. *Developmental Biology, vol. 344, issue 2, pp. 836-48.*

Laurenz, S., Tamara, S., Oliver, I., Christoph L.,Martin, R., Edgar, D. (2013). 'Eruptive Nevi Mimicking Wart-Like Lesions under Selective BRAF Inhibition in a 37-Year-Old Female Melanoma Patient'. *Case Reports in Dermatology, vol. 5, issue 1, pp. 69–72.*

Lazzi, S., Bellan, C., Onnis, A., De Falco, G., Sayed, S., Kostopoulos, I., *et al.,* (2009). 'Rare lymphoid neoplasms coexpressing B- and T-cell antigens. The role of *PAX5* gene methylation in their pathogenesis'. *Human Pathology, vol. 40, issue 9, pp. 1252-61.*

Lee[1], A. S., Harris, J., Bate, M., Vijayraghavan, K., Fisher, L., *et al.,* (2013). 'Initiation of primary myogenesis in amniote limb muscles'. *Development Dynamics, vol. 242, issue 9, pp. 1043-55.*

Lee[2], D. J., Kang, D. H., Choi, M., Choi, Y. J., Lee, J. Y., *et al.,* (2013). 'Peroxiredoxin-2 represses melanoma metastasis by increasing E-Cadherin/β-Catenin complexes in adherens junctions'. *Cancer Research, vol. 73, issue 15, pp. 4744-57.*

Lee, I. S., Choi, W. H., Kim, J. Y., Jeong, J. Y., Kim, M. J., *et al.,* (2008). 'Transcriptional regulation of the murine 1-cys peroxiredoxin gene by the B cell-specific activator protein, Pax5'. *Journal of Cellular Biochemistry, vol. 104, issue 2, pp. 465-76.*

Lee[3], J. S., Lim, S. M., Rha, S. Y., Roh, J. K., Cho, Y. J., Shin, K. H., *et al*., (2013). 'Prognostic implications of anaplastic lymphoma kinase gene aberrations in rhabdomyosarcoma; an immunohistochemical and fluorescence in situ hybridisation study'. *Journal of Clinical Patholology doi: 10.1136/jclinpath-2013-201655.*

Leon, T. Y., Ngan, E. S., Poon, H. C., So, M. T., Lui, V. C, *et al.,* (2009). 'Transcriptional regulation .of *RET* by *Nkx2-1, Phox2b, Sox10,* and *Pax3'. Journal of Pediatric Surgery, vol. 44, issue 10, pp. 1904-12.*

Li, B, Kuriyama, S., Moreno, M., Mayor, R. (2009). 'The posteriorizing gene *Pax2* is a direct target of Wnt signalling and the earliest factor in neural crest induction.' *Development, vol. 136, issue 19, pp. 3267-78.*

Li[3], Y., Chen, Y., Zhu, Z. X., Liu, X. H., Yang, L., Wan, L., *et al.,* (2013). 4-Hydroxytamoxifen-stimulated processing of cyclin E is mediated via G protein-coupled receptor 30 (GPR30) and accompanied by enhanced migration in MCF-7 breast cancer cells'. *Toxicology, vol. 309, pp. 61-5.*

Li, C., Wong, W., H. (2001). 'Model-based analysis of oligonucleotide arrays: Expression index computation and outlier detection', *Proceedings of the National Academy of Sciences, vol. 98, PP. 31-36.*

Li, H. G., Wang, Q., Li, H. M., Kumar, S., Parker, C., Slevin, M., Kumar, P. (2007). 'PAX3 and PAX3-FKHR promote rhabdomyosarcoma cell survival through downregulation of PTEN'. *Cancer Letters, vol. 253, issue 2, pp. 215-23.*

Li[4], L., Sarver, A. L., Alamgir, S., Subramanian, S. (2012). 'Downregulation of microRNAs miR-1, -206 and -29 stabilizes *PAX3* and *CCND2* expression in rhabdomyosarcoma'. *Laboratory Investigations, vol. 92, issue 4, pp. 571-83.*

Li[1], C. G., Eccles, M. R. (2012). '*PAX* Genes in Cancer; Friends or Foes?' *Fronters in Genetics, vol. 3, p. 6.*

Li[1], C. G., Nyman, J. E., Braithwaite, A. W., Eccles, M. R. (2011). '*PAX8* promotes tumour cell growth by transcriptionally regulating E2F1 and stabilizing RB protein'. *Oncogene, vol. 30, issue 48, pp. 4824-34.*

Li[2], L., Li, B., Zhang, H., Bai, S., Wang, Y., Zhao, B., Jonas, J. B. (2011). 'Lentiviral vector-mediated *PAX6* overexpression promotes growth and inhibits apoptosis of human retinoblastoma cells'. *Innvestigative Ophthalmology and Visual Science, vol. 52, issue 11, pp. 8393-400.*

Li[3], Y., Zhu, X., Yang, L., Li, J., Lian, Z., Li, N., Deng, X. (2011). 'Expression and network analysis of genes related to melanocyte development in the Silky Fowl and White Leghorn embryos'. *Molecular Biology Reports, vol. 38, issue 2, pp. 1433-41.*

Li[4], S. Q., Cheuk, A. T., Shern, J. F., Song, Y. K., Hurd, L., Liao, H., *et al.,* (2013). 'Targeting Wild-Type and Mutationally Activated FGFR4 in Rhabdomyosarcoma with the Inhibitor Ponatinib'. *PLoS One, vol. 8, issue 10, e76551.*

Liang, C. L., His, E., Chen, K. C., Pan, Y. R., Wang, Y. S., Juo, S. H. (2011). 'A functional polymorphism at 3'UTR of the PAX6 gene may confer risk for extreme myopia in the Chinese'. *Investigative Ophthalmology and Visual Science, vol. 52, issue 6, pp. 3500-5.*

Liao, H., Wang, Q., Xu, D., Qiu, X., Yu, L., Ouyang, J. (2009). '*Pax7* and depletion of satellite cell pool in prolonged denervated skeletal muscles of adult rats'. *Zhongguo Xiu Fu Chong Jian Wai Ke Za Zhi, vol. 23, issue 1, pp. 92-6.*

Linardic, C. M., Naini, S., Herndon, J. E., Kesserwan, C., Qualman, S. J., Counter, C. M. (2007). 'The PAX3-FKHR fusion gene of rhabdomyosarcoma cooperates with loss of p16INK4A to promote bypass of cellular senescence'. *Cancer Research, vol. 67, issue 14, pp. 6691-9.*

Lingling, L., Jing, W., Su, S. O., Taosheng, C. (2013). 'Cyclin-Dependent Kinase 4 Phosphorylates and Positively Regulates PAX3-FOXO1 in Human Alveolar Rhabdomyosarcoma Cells'. *PLoS One, vol. 8, issue 2, e58193.*

Liu[1], F., Cao, J., Wu, J., Sullivan, K., Shen, J., Ryu, B., *et al*., (2013). 'Stat3-targeted therapies overcome the acquired resistance to vemurafenib in melanomas'. *Journal of Investigative Dermatology, vol. 133, issue 8, pp. 2041-9.*

Liu[2], F., Cao, J. Lv, J., Dong, L., Pier, E., Xu, G. X., *et al.*, (2013). 'TBX2 expression is regulated by PAX3 in the melanocyte lineage'. *Pigment Cell Melanoma Research, vol. 26, issue 1, pp. 67-77.*

Liu, L., Chen, L., Chung, J., Huang, S. (2008). 'Rapamycin inhibits F-actin reorganization and phosphorylation of focal adhesion proteins'. *Oncogene, vol. 27, issue 37, pp. 4998-5010.*

Liu, S., Liu, F., Schneider, A. E., St Amand, T., Epstein, J. A., Gutstein, D. E. (2006). 'Distinct cardiac malformations caused by absence of connexin 43 in the neural crest and in the non-crest neural tube'. *Development, vol. 133, issue 10, pp. 2063-73.*

Liu, W., Liu, Y., Lai, X., Kuang, S. (2012). 'Intramuscular adipose is derived from a non-Pax3 lineage and required for efficient regeneration of skeletal muscles'. *Developmental Biology, vol. 361, issue 1, pp. 27-38.*

Liu[1], J., Guzman, M. A., Pezanowski, D., Patel, D., Hauptman, J., *et al.,* (2011). 'FOXO1-FGFR1 fusion and amplification in a solid variant of alveolar rhabdomyosarcoma'. *Modern Pathology, vol. 24, issue 10, pp. 1327-35.*

Liu[2], W., Xue, L. (2011). 'Functional conservation of the *Drosophila gooseberry* gene and its evolutionary alleles'. *PLoS One, vol.7, issue 1, e30980.*

Looi, C. Y., Moharram, B., Paydar, M., Wong, Y. L., Leong, K. H., *et al.,* (2013). 'Induction of apoptosis in melanoma A375 cells by a chloroform fraction of Centratherum anthelminticum seeds involves NF-kappaB, p53 and Bcl-2-controlled mitochondrial signaling pathways'. *BMC Complement Alternative Medicine Review, vol. 13, pp. 166.*

Lorain, S., Lécluse, Y., Scamps, C., Mattéi, M. G., Lipinski, M. (2001). 'Identification of human and mouse HIRA-interacting protein-5 (HIRIP5), two mammalian representatives in a family of phylogenetically conserved proteins with a role in the biogenesis of Fe/S proteins'. *Biochimical and Biophysical Activities, vol. 1517, issue 3, pp. 376-83.*

Lozano-Velasco, E., Contreras, A., Crist, C., Aránega, A. E., *et al.,* (2011). '*Pitx2c* modulates *Pax3+/Pax7+* cell populations and regulates Pax3 expression by repressing miR27 expression during myogenesis'. *Developmental Biology, vol. 357, issue 1, pp. 165-78.*

Lupo, P. J., Danysh, H. E., Skapek ,S. X., Hawkins, D. S., Spector, L. G., Zhou, R., *et al.*, (2014). 'Maternal and birth characteristics and childhood rhabdomyosarcoma: a report from the Children's Oncology Group'. *Cancer Causes Control, vol. 25, issue 7, pp.905-13.*

Maciej, T., Katarzyna, G., Rui, L., Joanna, T., Justyna, D., *et al.,* (2010). 'Human Rhabdomyosarcomas secrete *MIF* that modulates metastatic behaviour of tumour cells and inhibits recruitment of Cancer Associated Fibroblasts'. *Molecular Cancer Research, vol. 8, issue 10, pp. 1328-1343.*

Macones, G. A., Odibo, A., Cahill, A., Stamilio, D. L. *et al.,* (2011). 'Discussion: 'Testing for biomarkers after ASC-US Pap smears'. *American Journal of Obstetrics and Gynecology, vol. 204, issue 1, e12-3.*

Maczkowiak, F., Matéos, S., Wang, E., Roche, D., Harland, R., Monsoro-Burq, A. H. (2010). 'The *Pax3* and *Pax7* paralogs cooperate in neural and neural crest patterning using distinct molecular mechanisms, in Xenopus laevis embryos'. *Developmental Biology, vol. 340, issue 2, pp. 381-96.*

Magli, A., Schnettler, E., Rinaldi, F., Bremer, P., Perlingeiro, R. C. (2013). 'Functional dissection of *Pax3* in paraxial mesoderm development and myogenesis'. *Stem Cells, vol. 31, issue 1, pp. 59-70.*

Makawita, S., Ho, M., Durbin, A. D., Thorner, P. S., Malkin, D., Somers, G. R. (2009). 'Expression of insulin-like growth factor pathway proteins in rhabdomyosarcoma: IGF-2 expression is associated with translocation-negative tumours. *Pediatrics Developmental Pathology, vol. 12, issue 2, pp. 127-35.*

Makhzami, S., Rambow, F., Delmas, V., Larue, L. (2012). 'Efficient gene expression profiling of laser-microdissected melanoma metastases'. *Pigment Cell Melanoma Research, vol. 25, issue 6, pp. 783-91.*

Marchal, J. A., Carrasco, E., Ramirez, A., Jiménez, G., Olmedo, C., *et al.,* (2013). 'Bozepinib, a novel small antitumour agent, induces PKR-mediated apoptosis and synergizes with IFNα triggering apoptosis, autophagy and senescence'. *Drug Design, Development and Therapy*, *vol. 7, pp. 1301-13.*

Marchetti, G., Pinotti, M., Lunghi, B., Casari, C., Bernardi, F. (2012). 'Functional genetics'. *Thrombosis Research, vol. 129, issue 3, pp. 336-40.*

Marie, B., Pym, E., Bergquist, S., Davis, G. W. (2010). 'Synaptic homeostasis is consolidated by the cell fate gene gooseberry, a Drosophila pax3/7 homolog.' *Journal of Neuroscience, vol. 30, issue 24, pp. 8071-82.*

Maris, J., M. (2010). 'Recent Advances in Neuroblastoma'. *New England Journal of Medicine, vol. 362, pp. 2202-2211.*

Marshall[1], A. D., Lagutina, I., Grosveld, G. C. (2011). 'PAX3-FOXO1 induces cannabinoid receptor 1 to enhance cell invasion and metastasis'. *Cancer Resreseach, vol. 71, issue 24, pp. 7471-80.*

Marshall, A. D., Picchione, F., Geltink, R.I., Grosveld, G. C. (2013). 'PAX3-FOXO1 induces up-regulation of Noxa sensitizing alveolar rhabdomyosarcoma cells to apoptosis'. *Neoplasia, vol. 15, issue 7, pp. 738-48.*

Marshall[2], A. D., van der Ent. M. A., Grosveld, G. C. (2012). 'PAX3-FOXO1 and FGFR4 in alveolar rhabdomyosarcoma'. *Molecular Carcinogenesis, vol. 51, issue 10, pp. 807-15.*

Mascarenhas, J. B., Littlejohn, E. L., Wolsky, R. J., Young, KP., Nelson, M., Salgia, R., Lang, D. (2010). *'PAX3* and *SOX10* activate *MET* receptor expression in melanoma'. *Pigment Cell Melanoma Research, vol. 23, issue 2, pp. 225-37.*

Masià, A., Almazán-Moga, A., Velasco, P., Reventós, J., Torán, N. (2012). 'Notch-mediated induction of N-cadherin and α9-integrin confers higher invasive phenotype on rhabdomyosarcoma cells'. *British Journal of Cancer, vol. 107, issue 8, pp. 1374-83.*

Mayanil, C. S., George, D., Mania-Farnell, B., Bremer, C. L., McLone, D. G., Bremer, E. G. (2000). 'Overexpression of murine Pax3 increases NCAM polysialylation in a human medulloblastomacell line'. *Journal of Biological Chemistry, vol. 275, issue 30, pp. 23259-66.*

Mavropoulos, J. C., Wang, T. S. (2014). 'Managing the skin toxicities from new melanoma drugs'. *Current Treatment Options in Oncology, vol. 15, issue 2, pp. 281-301.*

Mayanil, C. S., Pool, A., Nakazaki, H., Reddy, A. C., Mania-Farnell B., *et al.,* (2006). 'Regulation of murine *TGFbeta2* by *Pax3* during early embryonic development.' *Journal of Biological Chemistry*, *vol. 281, issue 34, pp. 24544-52.*

McCabe, K. L., Bronner-Fraser, M. (2008). 'Essential role for PDGF signaling in ophthalmic trigeminal placode induction'. *Development, vol. 135, issue 10, pp. 1863-74.*

McLean, T. W., Castellino, S. M. (2008). 'Pediatric genitourinary tumours.' *Current Opinion in Oncology, vol. 20, issue 3, pp. 315-20.*

Medic, S., Rizos, H., Ziman, M. (2011). 'Differential *PAX3* functions in normal skin melanocytes and melanoma cells'. *Biochemical and Biophysical Research Communications, vol. 411, issue 4, pp. 832-7.*

Medic[1], S., Ziman, M. (2010). *'PAX3* across the spectrum: from melanoblasts to melanoma.' *Critical Reviews in Biochemistry and Molecular Biology, vol. 44, issue 2-3, pp. 85-97.*

Medic[2], S., Ziman, M. (2010). *'PAX3* expression in normal skin melanocytes and melanocytic lesions (naevi and melanomas).' *PLoS One, vol.5, issue 4, e9977.*

Megahed, A., Faulhaber, P., Phillips, T., Koon, H. (2014). 'Delayed response in ipilimumab therapy'. *Journal of Community and Supportive Oncology, vol. 12, issue 3, pp. 109-10.*

Mendoza-Fandino, G. A., Gee, J. M., Ben-Dor, S., Gonzalez-Quevedo, C., Lee, K., *et al.,* (2011). 'A novel g.-1258G>A mutation in a conserved putative regulatory element of *PAX9* is associated with autosomal dominant molar hypodontia'. *Clinical Genetics, vol. 80, issue 3, pp. 265-72.*

Kilic-Eren, M., Boylu, T., Tabor, V. (2013). 'Targeting PI3K/Akt represses Hypoxia inducible factor-1α activation and sensitizes Rhabdomyosarcoma and Ewing's sarcoma cells for apoptosis'. *Cancer Cell International, vol. 13, p. 36.*

Michael, J. M., Kirsten, M., Allie, H. G., Joshua, D., Schiffman, R., *et al.,* (2012). 'Microsatellites with Macro-Influence in Ewing Sarcoma'. *Genes, vol. 3, issue 3, pp. 444-460.*

Michael, R. E., Shujie H., Antonio, A., Lynn, J. S., Aaron, R. J., Han-Seung, Y., Carlson, B., C. (2013). '*MITF* and *PAX3* Play Distinct Roles in Melanoma Cell Migration; Outline of a "Genetic Switch" Theory Involving *MITF* and *PAX3* in Proliferative and Invasive Phenotypes of Melanoma'. *Fronters in Oncology, vol. 3, p. 229.*

Milet, C., Maczkowiak, F., Roche, D. D., Monsoro-Burq, A. H. (2013). *'Pax3* and *Zic1* drive induction and differentiation of multipotent, migratory, and functional neural crest in Xenopus embryos'. *Proceedings of the National Academy of Sciences, U S A., vol. 110, issue 14, pp. 5528-33.*

Militi D, Militi A, Cutrupi MC, Portelli M, Rigoli L, Matarese G, Salpietro DC. (2011). 'Genetic basis of non syndromic hypodontia: a DNA investigation performed on three couples of monozygotic twins about PAX9 mutation'. *European Journal of Paediatric Dentistry, vol. 12, issue 1, pp. 21-4*

Miller, K. A., Barrow, J., Collinson, J. M., Davidson, S., Lear, M., *et al.,* (2007). 'A highly conserved Wnt-dependent TCF4 binding site within the proximal enhancer of the anti-myogenic Msx1 gene supports expression within Pax3-expressing limb bud muscle precursor cells'. *Developmental Biology, vol. 311, issue 2, pp. 665-78.*

Miller, P. J., Dietz, K. N., Hollenbach, A. D. (2008). 'Identification of serine 205 as a site of phosphorylation on Pax3 in proliferating but not differentiating primary myoblasts'. *Protein Science, vol.17, issue 11, pp. 1979-86.*

Minchin, J. E., Hughes, S. M. (2008). 'Sequential actions of Pax3 and Pax7 drive xanthophore development in zebrafish neural crest'. *Developmental Biology, vol. 317, issue 2, pp. 508-22.*

Minchin, J. E., Williams, V. C., Hinits, Y., Low, S., Tandon, P., et al., (2013). 'Oesophageal and sternohyal muscle fibres are novel Pax3-dependent migratory somite derivatives essential for ingestion'. *Development, vol. 140, issue 14, pp. 2972-84.*

Missiaglia, E., Williamson, D., Chisholm, J., Wirapati, P., Pierron, G., *et al.,* (2012). 'PAX3/FOXO1 fusion gene status is the key prognostic molecular marker in rhabdomyosarcoma and significantly improves current risk stratification'. *Journal of Clinical Oncology, vol. 30, issue 14, pp. 1670-7.*

Mixon, B. A., Eckrich, M. J., Lowas, S., Engel, M. E. (2013). 'Vincristine, irinotecan, and temozolomide for treatment of relapsed alveolar rhabdomyosarcoma'. *Journal of Pediatric Hematology Oncology, vol. 35, issue 4, e163-6.*

Miyachi, M., Kakazu, N., Yagyu, S., Katsumi, Y., Tsubai-Shimizu, S., *et al*., (2009). 'Restoration of p53 pathway by nutlin-3 induces cell cycle arrest and apoptosis in human rhabdomyosarcoma cells'. *Clinical Cancer Research, vol. 15, issue12, pp. 4077-84.*

Modesto, A., Blanchard, P., Tao, Y. G., Rives, M., Janot, F., *et al.,* (2013). 'Multimodal treatment and long-term outcome of patients with esthesioneuroblastoma'. *Oral Oncology, vol. 49, issue 8, pp. 830-4.*

Moelans, C. B., Verschuur-Maes, A. H., van Diest, P. J. (2012). 'Frequent promoter hypermethylation of *BRCA2, CDH13, MSH6, PAX5, PAX6* and *WT1* in ductal carcinoma in situ and invasive breast cancer'. *Journal of Pathology, vol. 226, issue 1, p. 143.*

Monte, N. M., Webster, K. A., Neuberg, D., Dressler, G. R., Mutter, G. L. (2010). 'Joint loss of PAX2 and PTEN expression in endometrial precancers and cancer. *Cancer Research, vol.70, issue 15, pp. 6225-32.*

Moretti, L., Medeiros, L. J., Kunkalla, K., Williams, M. D., Singh, R. R., Vega, F. (2012). 'N-terminal PAX8 polyclonal antibody shows cross-reactivity with N-terminal region of *PAX5* and is responsible for reports of *PAX8* positivity in malignant lymphomas'. *Modern Pathology, vol. 25, issue 2, pp. 231-6.*

Morgan, S. C., Lee, H.Y., Relaix, F., Sandell, L. L., Levorse, J. M. Loeken, M.R. (2008). 'Cardiac outflow tract septation failure in Pax3-deficient embryos is due to p53-dependent regulation of migrating cardiac neural crest'. *Mechanisms of Development, vol. 125, issue 10, pp. 757-67.*

Moran, D. M., Gawlak, G., Jayaprakash, M. S., Mayar, S., Maki, C. G. (2008). 'Geldanamycin promotes premature mitotic entry and micronucleation in irradiated p53/p21 deficient colon carcinoma cells'. *Oncogene, vol.27, issue 42, pp. 5567-77.*

Moscow, J. A., Cowan, K. H. (2011). 'Biology of cancer'. *In Goldman L, SchaferAI, eds. Cecil Medicine.Cecil Medicine. 24th ed. Philadelphia, chap 185, Pa: Saunders, Elsevier.*

Mouritzen, P.1., Nielsen, A. T., Pfundheller, H. M., Choleva, Y., Kongsbak, L., Møller, S. (2003). 'Single nucleotide polymorphism genotyping using locked nucleic acid (LNA)'. *Expert Review of Molecular Diagnostics, vol. 3, issue 1, pp. 27-38.*

Mousavi, K., Jasmin, B. J. (2006). 'BDNF is expressed in skeletal muscle satellite cells and inhibits myogenic differentiation'. *Journal of Neuroscience, vol. 26, issue 21, pp. 5739-49.*

Mudge, J. M., Frankish, A., Fernandez-Banet, J., *et al.* (2011). 'The origins, evolution and functional potential of alternative splicing in vertebrates'. *Molecular Biology and Evolution, 28, issue 10, pp. 2949-2959.*

Munde, A., Juvekar, M. V., Karle, R. R., Wankhede, P. (2014). 'Malignant melanoma of the oral cavity: Report of two cases'. *Contemporary Clinical Dentistry, vol. 5, issue 2, pp. 227-30.*

Mues, G., Kapadia, H., Wang, Y., D'Souza, R. N. (2009). 'Genetics and human malformations'. *Journal of Craniofacial Surgery, vol. 2, pp. 1652-4.*

Murdoch, B., Delconte, C., García-Castro, M. I. (2012). 'Pax7 lineage, issue contributions to the Mammalian neural crest'. *PLoS One, vol. 7, issue 7, e41089.*

Murko, C., Lagger, S., Steiner, M., Seiser, C., Schoefer, C., Pusch, O. (2013). 'Histone deacetylase inhibitor Trichostatin A induces neural tube defects and promotes neural crest specification in the chicken neural tube'. *Differentiation, vol. 85, issue 1-2, pp. 55-66.*

Myron, S. I., Eleanor, C., Natalie, M. E., Adam, F., Inês, M. T., *et al*., (2012). 'In vivo imaging of tumour-propagating cells, regional tumour heterogeneity, and dynamic cell movements in embryonal rhabdomyosarcoma'. *Cancer Cell, vol. 21, issue 5, pp. 680-693.*

Nabarro, S., Himoudi, N., Papanastasiou, A., Gilmour, K., Gibson, S., Sebire, N., *et al.* (2005). 'Coordinated oncogenic transformation and inhibition of host immune responses by the PAX3-FKHR fusion oncoprotein'. *Journal of Experimental Medicine, vol. 202, issue 10, pp. 1399-410.*

Nagoshi, N., Shibata, S., Nakamura, M., Matsuzaki,Y.,Toyama,Y., Okano, H. (2009). 'Neural crest-derived stem cells display a wide variety of characteristics'. *Journal of Cellular Biochemistry, vol. 107, issue 6 pp. 1046-1052.*

Nakazaki, H., Shen, Y. W., Yun, B., Reddy, A., Khanna, V., *et al.,* (2009). 'Transcriptional regulation by Pax3 and TGFbeta2 signaling: a potential gene regulatory network in neural crest development'. *International Journal of Developmental Biology, vol. 53, issue 1, pp. 69-79.*

Nakib, G., Calcaterra, V., Goruppi , I., Romano, P., Raffaele, A., Schleef, J., Pelizzo, G. (2014). 'Robotic-assisted surgery approach in a biliary rhabdomyosarcoma misdiagnosed as choledochal cyst'. *Rare Tumors, vol. 6, issue 1, 5173.*

Nan, Y. N., Zhu, J. Y., Tan, Y, Zhang, Q., Jia, W., Hua, Q. (2014). 'Staurosporine induced apoptosis rapidly downregulates TDP- 43 in glioma cells'. *Asian Pacific journal of cancer prevention vol.15, issue 8, pp. 35759.*

Narayansingh, R., Ouellette, R. J. (2011). 'Paired box gene 5 may modulate Proviral Integration of Moloney virus 2 gene and protein expression in mature B-cells'. *Leukaemia and Lymphoma, vol. 52, issue 5, pp. 887-95.*

Narumi, S., Muroya, K., Asakura, Y., Adachi, M., Hasegawa, T. (2010). 'Transcription factor mutations and congenital hypothyroidism: systematic genetic screening of a population-based cohort of Japanese patients'. *Journal of Clinical Endocrinology and Metabolism, vol. 95, issue 4, pp. 1981-5.*

Negrisolo, S, Benetti, E, Centi, S, Della, V. M, Ghirardo, G., *et al.* (2011). *'PAX2* gene mutations in pediatric and young adult transplant recipients: kidney and urinary tract malformations without ocular anomalies'. *Clinical Genetics, vol. 80, issue 6, pp. 581-5.*

Nelms, B. L., Pfaltzgraff, E. R., Labosky, P. A. (2011). 'Functional interaction between Foxd3 and Pax3 in cardiac neural crest development'. *Genesis, vol. 49, issue 1, pp. 10-23.*

Nguyen, T. H., Bertrand, M. J., Sterpin, C, Achouri, Y., De Backer, O. R. (2010). 'Maged1, a new regulator of skeletal myogenic differentiation and muscle regeneration'. *BMC Cell Biology, vol. 11, pp. 57.*

Nicholl, M. B., Elashoff, D., Takeuchi, H., Morton, D. L., Hoon, D. S. (2011). 'Molecular upstaging based on paraffin-embedded sentinel lymph nodes: ten-year follow-up confirms prognostic utility in melanoma patients'. *Annals of Surgery, vol. 253, issue 1, pp. 116-22.*

Nie, X., Deng, C. X., Wang, Q., Jiao, K. (2008). 'Disruption of Smad4 in neural crest cells leads to mid-gestation death with pharyngeal arch, craniofacial and cardiac defects'. *Developmental Biology, vol. 316, issue 2, pp. 417-30.*

Nishibaba, R., Higashi, Y., Su, J., Furukawa, T, Kawai, K., Kanekura, T. (2012). 'CD147-targeting siRNA inhibits cell-matrix adhesion of human malignant melanoma cells by phosphorylating focal adhesion kinase'. *Journal of Dermatology, vol. 39, issue 1, pp. 63-7.*

Nishimura, E. K. (2011). 'Melanocyte stem cells: a melanocyte reservoir in hair follicles for hair and skin pigmentation'. *Pigment Cell Melanoma Research, vol. 24, issue 3, pp. 401-10.*

Nitzan, E., Pfaltzgraff, E. R., Labosky, P. A., Kalcheim, C. (2013). 'Neural crest and Schwann cell progenitor-derived melanocytes are two spatially segregated populations similarly regulated by Foxd3'. *Proceedings of the National Academy of Sciences, U S A., vol. 110, issue 31, pp. 12709-14.*

Nowak, E., Galilejczyk, A., Sypniewski, D., Bednarek, I. (2013). 'MMP-9 directed shRNAs as relevant inhibitors of matrix metalloproteinase 9 activity and signaling'. *Postepy High Medical Dosw, vol. 67, pp. 742-9.*

O'Connor, R., Barr, F. G. (2008). 'FOXO1 (Forkhead box O1)'. *Atlas of Genetics/ Cytogenetics Oncology and Haematology.*

Oda, Y., Tsuneyoshi, M. (2009). 'Recent advances in the molecular pathology of soft tissue sarcoma: implications for diagnosis, patient prognosis, and molecular target therapy in the future'. *Cancer Science, vol. 100, issue 2, pp. 200-8.*

Oesch, S., Walter, D., Wachtel, M., Pretre, K., Salazar, M., *et al.,* (2009). 'Cannabinoid receptor 1 is a potential drug target for treatment of translocation-positive rhabdomyosarcoma'. *Molecular Cancer Therapy, vol. 8, issue 7, pp. 1838-45.*

Ognjanovic. S., Carozza, S. E., Chow, E. J., Fox, E. E., Horel, S., McLaughlin, C. C., *et al.,* (2010). 'Birth characteristics and the risk of childhood rhabdomyosarcoma based on histological subtype'. *British Journal of Cancer, vol. 102, issue 1, pp.227-31.*

Okamoto, Y., Sawaki, A., Ito, S., Nisolhida, T., Takahashi, T., *et al.,* (2012). 'Aberrant DNA methylation associated with aggressiveness of gastrointestinal stromal tumour'. *Gut, vol. 61, issue 3, pp. 392-401.*

Olaopa, M., Zhou, H. M., Snider, P., Wang, J., Schwartz, R. J., *et al.,* (2011). '*Pax3* is essential for normal cardiac neural crest morphogenesis but is not required during migration nor outflow tract septation'. *Developmental Biology, vol.356, issue 2, pp. 308-22.*

Olguín, H. C., Patzlaff, N. E., Olwin, B. B. (2011). 'Pax7-FKHR transcriptional activity is enhanced by transcriptionally repressed MyoD'. *Journal of Cellular Biochemistry, vol. 112, issue 5, pp. 1410-7.*

Olguín, H. C., Pisconti, A. (2012). 'Marking the tempo for myogenesis: Pax7 and the regulation of muscle stem cell fate decisions'. *Journal of Cellular Biochemistry, vol. 16, issue 5, pp. 1013-25.*

Onisto, M., Slongo, M. L., Gregnanin, L., Gastaldi, T., Carli, M., Rosolen, A. (2005). 'Expression and activity of vascular endothelial growth factor and metalloproteinases in alveolar and embryonal rhabdomyosarcoma cell lines'. *International Journal of Oncology, vol. 27, issue 3, pp. 791-8.*

Otręba, M., Miliński, M., Buszman, E., Wrześniok, D., Beberok, A. (2013). 'Hereditary hypomelanocytoses: the role of PAX3, SOX10, MITF, SNAI2, KIT, EDN3 and EDNRB genes'. *Postepy High Medical Dosw, vol.67, pp. 1109-18.*

Oue, T., Uehara, S., Yamanaka, H., Nomura, M., Usui, N. (2013). 'Hedgehog signal inhibitors suppress the invasion of human rhabdomyosarcoma cells'. *Pediatric Surgery International, vol. 29, issue 11, pp. 1153-8.*

Ozcan, A., Liles, N., Coffey, D., Shen, S. S., Truong, L. D. (2011). *'PAX2* and *PAX8* expression in primary and metastatic müllerian epithelial tumours: a comprehensive comparison'. *American Journal of Surgical Pathology, vol. 35, issue 12, pp. 1837-47.*

Padanad, M. S., Riley, B. B. (2012), 'Pax2/8 proteins coordinate sequential induction of otic and epibranchial placodes through differential regulation of foxi1, sox3 and fgf24'. *Developmental Biology, vol. 363, issue 1, p. 331.*

Pallafacchina, G., François, S., Regnault, B., Czarny, B., Dive, V., *et al*., (2010). 'An adult tissue-specific stem cell in its niche: a gene profiling analysis of in vivo quiescent and activated muscle satellite cells'. *Stem Cell Research, vol. 4, issue 2, pp. 77-91.*

Parham, D. M., Barr, F. G. (2013). 'Classification of rhabdomyosarcoma and its molecular basis'. *Advances in Anatomic Pathology, vol. 20, issue 6, pp. 387-97.*

Park, J. H., Ryu, J. M., Han, H. J. (2011). 'Involvement of caveolin-1 in fibronectin-induced mouse embryonic stem cell proliferation: role of FAK, RhoA, PI3K/Akt, and ERK 1/2 pathways'. *Journal of Cellular Physiology, vol. 226, issue 1, pp. 267-75.*

Park, M. A., Hwang, K. A., Lee, H. R., Yi, B. R., Jeung, E. B., Choi, K. C. (2013). Benzophenone-1 stimulated the growth of BG-1 ovarian cancer cells by cell cycle regulation via an estrogen receptor alpha-mediated signaling pathway in cellular and xenog mouse models'. *Toxicology, vol. 305, pp. 41-8.*

Parker, C. J., Shawcross, S. G., Li, H., Wang, Q. Y., Herrington, C. S., Kumar, S., Kumar, P., *et al.,* (2004). 'Expression of *PAX3* alternatively spliced transcripts and identification of two new isoforms in human tumours of neural crest origin'. *International Journal of Cancer, vol. 108, pp. 314-320.*

Patel, A., Muñoz, A., Halvorsen, K., Rai, P. (2012). 'Creation and validation of a ligation-independent cloning (LIC) retroviral vector for stable gene transduction in mammalian cells'. *BMC Biotechnology, vol. 12, issue 3.*

Paternoster, L., Zhurov, A. I., Toma, A. M., Kemp, J. P., St Pourcain, B., *et al*., (2012). 'Genome-wide association study of three-dimensional facial morphology identifies a variant in PAX3 associated with nasion position'. *American Journal of Human Genetics, vol. 90, issue 3, pp. 478-85.*

Patterson, S. E., Bird, N. C., Devoto, S. H. (2010). 'BMP regulation of myogenesis in zebrafish'. *Developmental Dynamics, vol 239, issue 3, pp. 806-17.*

Pham, T. V., Hartomo, T. B., Lee, M. J., Hasegawa, D., Ishida, T., *et al*., (2012). 'Rab15 alternative splicing is altered in spheres of neuroblastoma cells'. *Oncology Reports, vol. 27, issue 6, pp. 2045-9.*

Pingault, Ente, D., Dastot-Le, Moal, F. (2010). 'Review and update of mutations causing Waardenburg syndrome'. *Human Mutation, vol. 4, pp. 391-406.*

Plantman, S. (2013). 'Proregenerative Properties of ECM Molecules'. *Biomedical Research International, vol. 2013, p. 981695.*

Plengvidhya, N., Kooptiwut, S., Songtawee, N., Doi, A., Furuta, H., *et al*., (2007). '*PAX4* mutations in Thais with maturity onset diabetes of the young'. *Journal of Clinical Endocrinology Metabolism, vol. 92, issue 7, pp. 2821-6.*

Plummer, R. S., Shea, C. R., Nelson, M., Powell, S. K., Freeman, D. M., Dan C. P., Lang, D. (2008). *'PAX3* expression in primary melanomas and nevi'. *Modern Pathology, vol. 21, issue 5, pp. 525-30.*

Proulx, M., Cayer, M. P., Drouin, M., Laroche, A., Jung, D. (2010). 'Overexpression of PAX5 induces apoptosis in multiple myeloma cells'. *International Journal of Hematology, vol. 92, issue 3, pp. 451-62.*

Qiu, Z., Miao, C., L, J., Lei, X., Liu, S., Guo, W., Cao, Y., Duan, E. K. (2010). 'Skeletal myogenic potential of mouse skin-derived precursors.' *Stem Cells Development, vol. 19, issue 2, pp. 259-68.*

Quick, C. M., Gokden, N., Sangoi, A. R., Brooks, J. D., McKenney, J. K. (2010). 'The distribution of *PAX-2* immunoreactivity in the prostate gland, seminal vesicle, and ejaculatory duct: comparison with prostatic adenocarcinoma and discussion of prostatic zonal embryogenesis'. *Human Pathology, vol. 41, issue 8, pp. 1145-9.*

Quick[2], C. M., Ning, G., Bijron, J., Laury, A., Wei, T. S., Chen, E.Y., *et al*., (2012). '*PAX2*-null secretory cell outgrowths in the oviduct and their relationship to pelvic serous cancer'. *Modern Pathology, vol. 25, issue 3, pp. 449-55.*

Raciborska, A., Bilska, K., Drabko, K., Chaber, R., Pogorzala, M., *et al*., (2013). 'Vincristine, irinotecan, and temozolomide in patients with relapsed and refractory Ewing sarcoma'. *Pediatrics Blood Cancer, vol. 60, issue 10, pp. 1621-5.*

Rafei, M., Hsieh, J., Fortier, S., Li, M., Yuan, S., Birman, E., *et al.,* (2008). 'Mesenchymal stromal cell-derived CCL2 suppresses plasma cell immunoglobulin production via STAT3 inactivation and *PAX5* induction'. *Blood, vol. 112, issue 13, pp. 4991-8.*

Raghunandhakumar, S., Paramasivam, A., Senthilraja, S., Naveenkumar, C., Asokkumar, S, *et al*., (2013). 'Thymoquinone inhibits cell proliferation through regulation of G1/S phase cell cycle transition in N-nitrosodiethylamine-induced experimental rat hepatocellular carcinoma'. *Toxicol Letters, vol. 223, issue 1, pp. 60-72.*

Rapa, E., Hill, S. K., Morten, K. J., Potter, M., Mitchell, C. (2012). 'The over-expression of cell migratory genes in alveolar rhabdomyosarcoma could contribute to metastatic spread'. *Clinical and Experimental Metastasis, vol. 29, issue 5, pp. 419-29.*

Rath, M. F., Bailey, M.J., Kim, J. S., Coon, S. L., Klein, D. C., Møller, M. (2009). 'Developmental and daily expression of the Pax4 and Pax6 homeobox genes in the rat retina: localization of Pax4 in photoreceptor cells'. *Journal of Neurochemistry, vol. 108, issue 1, pp. 285-94.*

Ravasi, T., Suzuki, H., Cannistraci, C. V., Katayama, S., Bajic, V.B., *et al.,* (2010). 'An atlas of combinatorial transcriptional regulation in mouse and man'. *Cell, vol. 140, issue 5, pp. 744-52.*

Rees, H., Williamson, D., Papanastasiou, A., Jina, N., Nabarro, S., Shipley, J., Anderson, J. (2006). 'The MET receptor tyrosine kinase contributes to invasive tumour growth in rhabdomyosarcomas'. *Growth Factors, vol. 24, issue 3, pp. 197-208.*

Rescan, P. Y., Montfort, J., Fautrel, A., Rallière, C., Lebret, V. (2013). 'Gene expression profiling of the hyperplastic growth zones of the late trout embryo myotome using laser capture microdissection and microarray analysis'. *BMC Genomics, vol. 14, p. 173.*

Ricotti, F., Giuliodori, K., Cataldi, I., Campanati, A., Ganzetti, G., Ricotti, G., Offidani, A. (2014). 'Electrochemotherapy: an effective local treatment of cutaneous and subcutaneous melanoma metastases'. *Dermatology and Therapy, 27, issue 3, pp. 148-52.*

Reichek, J. L., Duan, F., Smith, L. M., Gustafson, D. M., O'Connor, R., S.*, et al*., (2011). 'Genomic and clinical analysis of amplification of the 13q31 chromosomal region in alveolar rhabdomyosarcoma: a report from the Children's Oncology Group'. *Clinical Cancer Research, vol.17, issue 6, pp. 1463-73.*

Relaix, F., Rocancourt, D., Mansouri, A., Buckingham, M. (2005). 'A Pax3/Pax7-dependent population of skeletal muscle progenitor cells'. *Nature, vol. 435, issue 7044, pp. 948-53.*

Ren, Y. X., Finckenstein, F. G., Abdueva, D. A., Shahbazian, V., Chung, B., *et al.,* (2008). 'Mouse mesenchymal stem cells expressing PAX-FKHR form alveolar rhabdomyosarcomas by cooperating with secondary mutations'. *Cancer Research, vol. 68, issue 16, pp. 6587-97.*

Robson, E. J., He, S. J., Eccles, M. R. (2006). 'A PANorama of *PAX* genes in cancer and development'. *Nature Review Cancer, vol. 6, issue 1, pp. 52-62.*

Rodeberg, D. A., Nuss, R. A., Elsawa, S. F., Erskine, C. L., Celis, E. (2006). 'Generation of tumouricidal PAX3 peptide antigen specific cytotoxic T lymphocytes'. *International Journal of Cancer, vol. 119, issue 1, pp. 126-32.*

Roeb, W., Boyer, A., Cavenee, W. K., Arden, K, C. (2007). 'PAX3-FOXO1 controls expression of the p57Kip2 cell-cycle regulator through degradation of EGR1'. *Proceedings of the National Academy of Sciences, U S A., vol. 104, issue 46, pp. 18085-90.*

Roomi, M. W., Kalinovsky, T., Monterrey, J., Rath, M., Niedzwiecki, A. (2013). 'In vitro modulation of MMP-2 and MMP-9 in adult human sarcoma cell lines by cytokines, inducers, and inhibitors'. *International Journal of Oncology, vol. 43, issue 6, pp. 1787-98.*

Rowan, S., Siggers, T., Lachke, S. A., Yue, Y., Bulyk, M. L., Maas, R. L. (2010). 'Precise temporal control of the eye regulatory gene *Pax6* via enhancer-binding site affinity'. *Genes Development, vol. 24, issue 10, pp. 980-5.*

Rudzinski, E. R., Teot, L. A., Anderson, J. R., Moore, J., Bridge, J. A., *et al.,* (2013). 'Dense pattern of embryonal rhabdomyosarcoma, a lesion easily confused with alveolar rhabdomyosarcoma: a report from the Soft Tissue Sarcoma Committee of the Children's Oncology Group'. *American Journal of Clinical Pathology, vol. 140, issue 1, pp. 82-90.*

Ruzickova, J., Piatigorsky, J., Kozmik, Z. (2009). 'Eye-specific expression of an ancestral jellyfish PaxB gene interferes with *Pax6* function despite its conserved *Pax6/Pax2* characteristics'. *International Journal of Developmental Biology, vol. 53, issue 4, pp. 469-82.*

Ryu, B., Kim, D. S., Deluca, A. M., Alani, R. M. (2007). 'Comprehensive expression profiling of tumor cell lines identifies molecular signatures of melanoma progression'. *PLoS One, vol. 2, issue 7, e594.*

Sambasivan, R., Gayraud-Morel, B., Dumas, G., Cimper, C., Paisant S., Kelly, R. G, Tajbakhsh, S. (2009). 'Distinct regulatory cascades govern extraocular and pharyngeal arch muscle progenitor cell fates'. *Developmental Cell, vol. 17, issue 1, p. 150.*

Sambrook, J., David, W. R. (2002). 'Molecular cloning laboratory manuals', *3rd edition, vol. 1.116-1.122, Cold Spring Harbor Laboratory.*

Samimi, S., Antignac, C., Combe, C., Lacombe, D., Renaud, R. M. B., Korobelnik, J. F. (2008). 'Bilateral macular detachment caused by bilateral optic nerve malformation in a papillorenal syndrome due to a new PAX2 mutation'. *European Journal of Ophthalmology, vol. 18, issue 4, pp. 656-8.*

Sanchez-Ferras, O., Coutaud, B., Djavanbakht, S. T., Tremblay I., Souchkova O., Pilon N. (2012). 'Caudal-related homeobox (Cdx) protein-dependent integration of canonical Wnt signaling on paired-box 3 (Pax3) neural crest enhancer'. *Journal of Biological Chemistry, vol. 287, issue 20, pp. 16623-35.*

Santarpia, L., Calin, G. A., Adam, L., Ye L., Fusco, A., Giunti, S., *et al.,* (2013). 'A miRNA signature associated with human metastatic medullary thyroid carcinoma'. *Endocrine-Related Cancer, vol. 20, issue 6, pp. 809-23.*

Sarkar, S., Rajput, S., Tripathi, A. K., Mandal, M. (2013). 'Targeted therapy against EGFR and VEGFR using ZD6474 enhances the therapeutic potential of UV-B phototherapy in breast cancer cells'. *Molecular Cancer, vol. 12. Issue 1, p. 122.*

Scabini, M., Stellari, F., Cappella, P., Rizzitano, S., Texido, G., Pesenti, E. (2011). 'In vivo imaging of early stage apoptosis by measuring real-time caspase-3/7 activation. *Apoptosis, vol. 16, issue 2, pp. 198-207.*

Schmidt, C., McGonnell, I., Allen, S., Patel, K. (2008). 'The role of Wnt signalling in the development of somites and neural crest'. *Advances in Anatomy, Embryology and Cell Biology, vol. 195, pp. 1-64.*

Scuoppo, C., Riess, I., Schmitt-Ney, M., Allegra, P., Forni, P. E., *et al.,* (2007). 'The oncogenic transcription factor PAX3-FKHR can convert fibroblasts into contractile myotubes'. *Experimental Cell Research, vol. 313, issue 11, pp. 2308-17.*

Sergio, A., Philippe, G. (2007). 'Cooperative interaction between the two DNA binding Domains of pax3: Helix 2 of the paired Domain is the proximity of the Amino Terminus of the Homeodomain'. *Biochemistry, vol.46, issue 11, pp. 2984-2993.*

Sevick-Muraca, E. M., King, P. D. (2014). 'Lymphatic vessel abnormalities arising from disorders of Ras signal transduction'. *Trends in Cardiovascular Medicine, vol. 1738, issue 13, pp. 141-2.*

Shen, X. X., Yu, L., Bi, R., Yang, W. T. (2011). 'Clinicopathologic study and immunohistochemistry comparison of Pax2, p53 and Ki-67 in low- and high-grade ovarian serous carcinomas'. *Zhonghua Bing Li Xue Za Zhi, vol. 40, issue 8, pp. 511-6.*

Shi, J., Zhang, L., Shen, A., Zhang, J., Wang, Y., *et al.,* (2010). 'Clinical and biological significance of forkhead class box O3a expression in glioma: mediation of glioma malignancy by transcriptional regulation of p27kip1'. *Journal of Neuro-Oncology, vol. 98, issue 1, pp. 57-69.*

Shin, J., McFarland, D. C., Velleman, S. G. (2012). 'Heparan sulfate proteoglycans, syndecan-4 and glypican-1, differentially regulate myogenic regulatory transcription factors and paired box 7 expression during turkey satellite cell myogenesis: implications for muscle growth'. *Poultry Science, vol. 91, issue 1, pp. 201-7.*

Shirley, S. H., Greene, V. R., Duncan, L. M., Torres, Cabala, C. A., Grimm, E. A., Kusewitt, D. F. (2012). 'Slug expression during melanoma progression'. *American Journal of Pathology, vol. 180, issue 6, pp. 2479-89.*

Short, S., Holland, L. Z. (2008). 'The evolution of alternative splicing in the *Pax* family: the view from the basal chordate amphioxus'. *Journal of Molecular Evolution, vol. 66, issue 6, pp. 605-620.*

Shukla, N., Ameur, N., Yilmaz, I., Nafa, K., Lau, C. Y., Marchetti, A., *et al.,* (2012). 'Oncogene mutation profiling of paediatric solid tumours reveals significant subsets of embryonal rhabdomyosarcoma and neuroblastoma with mutated genes in growth signaling pathways'. *Clinical Cancer Research, vol. 18, issue 3, pp. 748-57.*

Sidhu, A., Miller, P. J., Hollenbach, A. D. (2010). 'Isolation of putative FOXO1 genomic elements using an improved in vitro technique to isolate genomic regulatory sequences'. *Gene, vol. 458, issue 2, pp. 45-53.*

Sil, H., Sen, T., Moulik, S., Chatterjee, A. (2010). 'Black tea polyphenol (theaflavin) downregulates MMP-2 in human melanoma cell line A375 by involving multiple regulatory molecules'. *Journal of Environmental Pathology, Toxicology, and Oncology, vol., 29, issue 1, pp. 55-68.*

Silberstein, G. B., Van Horn, K., Hrabeta-Robinson, E., Compton, J. (2006). 'Estrogen-triggered delays in mammary gland gene expression during the estrous cycle: evidence for a novel timing system'. *Journal of Endocrinology, vol. 190, issue 2, pp. 225-39.*

Simone, H., Amy, J, W. (2010). 'Muscling in: Uncovering the origins of rhabdomyosarcoma'. *Nature Medicine, vol. 16, pp. 171-173.*

Singh, N., Trivedi, C. M., Lu, M., Mullican, S. E., Lazar, M. A., Epstein, J. A. (2011). 'Histone deacetylase 3 regulates smooth muscle differentiation in neural crest cells and development of the cardiac outflow tract'. *Circulation Research, vol. 109, issue 11, pp. 1240-9.*

Skapek, S. X., Anderson, J., Barr, F. G., Bridge, J. A., Gastier-Foster, J. M., Parham, D. M., *et al.,* (2013). 'PAX-FOXO1 fusion status drives unfavourable outcome for children with rhabdomyosarcoma: a children's oncology group report'. *Pediatric Blood Cancer, vol. 60, issue 9, pp. 1411-7.*

Smith, M. P., Ferguson, J., Arozarena, I., Hayward, R., Marais, R., *et al*., (2013). 'Effect of SMURF2 targeting on susceptibility to MEK inhibitors in melanoma'. *Journal of National Cancer Institude, vol. 105, issue 1, pp. 33-46.*

Smith[1], W. M., Lange, J. M., Sturm, A. C., Tanner, S. M, Mauger T. F. (2012). 'Familial peripheral keratopathy without *PAX6* mutation'. *Cornea, vol. 31, issue 2, pp. 130-3.*

Smoller B, R. (2006). 'Histologic criteria for diagnosing primary cutaneous malignant melanoma'. Modern Pathology, *5th edition, vol. 19, pp. 34-40, Elseiver. doi:10.1038/modpathol.3800508.*

Smyth, G. K. (2004). 'Linear models and empirical Bayes for assessing differential expression in microarray experiments'. *Statistical Applications in Genetics and Molecular Biology, vol.3, issue 1, Article 1.*

Snider, P., Olaopa, M., Firulli, A. B., Conway, S. J. (2007). 'Cardiovascular development and the colonizing cardiac neural crest lineage'. *Scientific World Journal, vol. 7, pp. 1090-113.*

Soleimani, V. D., Punch, V. G., Kawabe, Y., Jones, A. E., Palidwor, G. A., *et al.,* (2012). 'Transcriptional dominance of Pax7 in adult myogenesis is due to high-affinity recognition of homeodomain motifs'. *Development Cell, vol. 22, issue 6, pp. 1208-20.*

Sommer, A., Bartholomew, D. W. (2003). 'Craniofacial-deafness-hand syndrome revisited'. *American Journal of Medical Genetics part A, vol. 123A, issue 1, pp. 91-4.*

Sommer, L. (2011). 'Generation of melanocytes from neural crest cells'. *Pigment Cell Melanoma Research, vol.24, issue 3, pp. 411-21.*

Sondak, V. K., Gibney, G. T. (2014). 'Surgical Management of Melanoma'. *Hematology/Oncology Clinics of North America, vol. 28, issue 3, pp. 455-470.*

Sonnesen, L., Nolting, D., Kjaer, K. W., Kjaer, I. (2008). 'Association between the development of the body axis and the craniofacial skeleton studied by immunohistochemical analyses using collagen II, Pax9, Pax1 and Noggin antibodies'. *Spine, vol. 33, issue 15, pp. 1622-6.*

Sousa-Victor, P., Muñoz-Cánoves, P., Perdiguero, E. (2011). 'Regulation of skeletal muscle stem cells through epigenetic mechanisms'. *Toxicology Mechanisms and Methods, vol. 21, issue 4, pp. 334-42.*

Stegmaier, S., Poremba, C., Schaefer, K. L., Leuschner, I., Kazanowska, B., *et al.,* (2011). 'Prognostic value of PAX-FKHR fusion status in alveolar rhabdomyosarcoma: a report from the cooperative soft tissue sarcoma study group (CWS)'. *Pediatric Blood Cancer, vol. 57, issue 3, pp. 406-14.*

Stoller, J. Z., Degenhardt, K. R., Huang, L., Zhou, D. D., Lu, M. M., Epstein, J. A. (2008). 'Cre reporter mouse expressing a nuclear localized fusion of GFP and beta-galactosidase reveals new derivatives of *Pax3*-expressing precursors'. *Genesis, vol. 46, issue 4, pp. 200-4.*

Su[1], H., Si, X. Y., Tang, W. R., Luo, Y. (2013). 'The regulation of anoikis in tumour invasion and metastasis'. *Yi Chuan, vol. 35, issue 1, pp. 10-6.*

Su[3], T. R., Lin, J. J., Tsai, C. C., Huang, T. K., Yang, Z. Y., Wu, M. O., *et al*., (2013). 'Inhibition of melanogenesis by gallic acid: possible involvement of the PI3K/Akt, MEK/ERK and Wnt/β-catenin signaling pathways in B16F10 cells'. *International Journal of Molecular Sciences, vol. 14, issue 10, pp. 20443-58.*

Suda, N., Ogawa, T., Kojima, T., Saito, C., Moriyama, K. (2011). 'Non-syndromic oligodontia with a novel mutation of *PAX9'. Journal of Dental Research, vol. 90, issue 3, pp. 382-6.*

Sull, J. W, Liang, K. Y., Hetmanski, J. B., Fallin, M. D., Ingersoll, R. G., *et al.,* (2009). 'Maternal transmission effects of the *PAX* genes among cleft case-parent trios from four populations'. *European Journal of Human Genetics, vol. 17, issue 6, pp. 831-9.*

Sultana, H, Verma, S, Mishra, R. K. A. (2011). 'BEAF dependent chromatin domain boundary separates myoglianin and eyeless genes of Drosophila melanogaster'. *Nucleic Acids Research, vol. 39, issue 9, pp. 3543-57.*

Sumegi, J., Streblow, R., Frayer, R. W., Dal, Cin, P., Rosenberg, A., Meloni-Ehrig, A., Bridge, J. A. (2010). 'Recurrent t(2;2) and t(2;8) translocations in rhabdomyosarcoma without the canonical PAX-FOXO1 fuse PAX3 to members of the nuclear receptor transcriptional coactivator family'. *Genes Chromosomes Cancer, vol. 49, issue 3, pp. 224-36.*

Sumerauer, D., Vicha, A., Zuntova, A., Stejskalova, E., Krskova, L., Kabickova, E., Kodet, R., Eckschlager, T. (2006). 'Teratoma in an adolescent with malignant transformation into embryonal rhabdomyosarcoma: case report'. *Journal of Pediatric Hematology and Oncology, vol. 28, issue 10, pp. 688-92.*

Sun[2], X, Gao, X, Zhou, L, Sun, L, Lu, C. (2013). 'PDGF-BB-induced MT1-MMP expression regulates proliferation and invasion of mesenchymal stem cells in 3-dimensional collagen via MEK/ERK1/2 and PI3K/AKT signaling'. *Cell Signal, vol. 25, issue 5, pp. 1279-87.*

Suriyan, P., Shanmugam, P. S., Shikhar, M.,T., K., Ashley, J S., *et al.,* (2012). 'Communication between host organism and cancer cells is transduced by systemic sphingosine kinase 1/sphingosine 1-phosphate signalling to regulate tumour metastasis'. *EMBO Molecular Medicine, vol.4, issue 8, pp. 761-775.*

Stacey, D. W. (2010). 'Three Observations That Have Changed Our Understanding of Cyclin D1 and p27Kip1 in Cell Cycle Control'. *Genes Cancer, vol. 1, issue 12, pp. 1189-1199.*

Storey, J. D., Tibshirani, R. (2003). 'Statistical significance for genomewide studies'. *Proceedings of the National Academy of Sciences, vol. 100, issue 16, pp. 9440-9445.*

Tarnowski, M., Schneider, G., Amann, G., Clark, G., Houghton, P., Barr, F. G., *et al.,* (2012). 'RasGRF1 regulates proliferation and metastatic behavior of human alveolar rhabdomyosarcomas'. *International Journal of Oncology, vol. 41, issue 3, pp. 995-1004.*

Tatlidil, C., Parkhill, W. S., Giacomantonio, C. A., Greer, W. L., Morris, S. F., Walsh N. M. (2011). 'Detection of tyrosinase mRNA in the sentinel lymph nodes of melanoma patients is not a predictor of short-term disease recurrence'. *Biochemical and Biophysical Research Communications, vol. 411, issue 4, pp. 832-7.*

Taylor, A. C., Schuster, K., McKenzie, P. P., Harris, L. C. (2006). 'Differential cooperation of oncogenes with p53 and Bax to induce apoptosis in rhabdomyosarcoma'. *Molecular Cancer, vol. 5, p. 53.*

Tedesco, F. S., Dellavalle, A., Diaz-Manera, J., Messina, G., Cos, su, G. (2010). 'Repairing skeletal muscle: regenerative potential of skeletal muscle stem cells.' *Journal of Clinical Investigations, vol. 120, issue 1, pp. 11-9.*

Thomas, A. J., Erickson, C. A. (2009). 'FOXD3 regulates the lineage switch between neural crest-derived glial cells and pigment cells by repressing MITF through a non-canonical mechanism'. *Development, vol. 136, issue 11, pp. 1849-58.*

Thompson, J. A., Zembrzycki, A., Mansouri, A., Ziman, M. (2008). '*Pax7* is requisite for maintenance of a subpopulation of superior collicular neurons and shows a diverging expression pattern to *Pax3* during superior collicular development'. *BMC Developmental Biology, vol. 8, p. 62.*

Thoumine, O. (2008). 'Interplay between adhesion turnover and cytoskeleton dynamics in the control of growth cone migration'. *Cell Adhesion and Migration, vol. 2, issue 4, pp. 263-7.*

Thuault, S., Hayashi, S., Lagirand-Cantaloube, J., Plutoni, C., Comunale, F., *et al.,* (2013). 'P-cadherin is a direct PAX3-FOXO1A target involved in alveolar rhabdomyosarcoma aggressiveness'. *Oncogene, vol. 32, issue 15, pp. 1876-87.*

Thun, M. J., Jemal, A. (2011). 'Epidemiology of cancer'. In Goldman L, Schafer AI, eds. *Cecil Medicine, 24th edition. Philadelphia, Saunders Elsevier, chapter 183.*

Tishler, R. B. (2014). 'Increased clarity on the use of radiotherapy in the management of desmoplastic melanoma'. *Cancer, vol. 120, issue 9, pp.1315-8.*

Tonelli, R., McIntyre, A., Camerin, C., Walters, Z. S., Di, Leo, K., Selfe, J., *et al*., (2012).'Antitumour activity of sustained N-myc reduction in rhabdomyosarcomas and transcriptional block by antigene therapy'. *Clinical Cancer Research, vol. 18, issue 3, pp. 796-807.*

Tshori, S., Gilon, D., Beeri, R., Nechushtan, H., Kaluzhny, D., Pikarsky, E., Razin, E. (2006). 'Transcription factor MITF regulates cardiac growth and hypertrophy'. *Journal of Clinical Investigations, vol. 116, issue 10, pp. 2673-81.*

Tsumagari, K., Baribault, C., Terragni, J., Varley, K. E., Gertz, J., *et al*., (2013). 'Early *de novo* DNA methylation and prolonged demethylation in the muscle lineage'. *Epigenetics, vol. 8, issue 3, pp. 317-32.*

Uchida, H., Arita, K., Yunoue, S., Yonezawa, H., Shinsato, Y. (2011). 'Role of sonic hedgehog signaling in migration of cell lines established from CD133-positive malignant glioma cells'. *Journal of Neuro-oncology, vol. 104, issue 3, pp. 697-704.*

Underwood, T. J., Amin, J., Lillycrop, K. A., Blaydes, J. P. (2007). 'Dissection of the functional interaction between p53 and the embryonic proto-oncoprotein *PAX3'. FEBS Letters, vol. 581, issue 30, pp. 5831-5.*

Upson, K., Allison., K. H., Reed, S. D., Jordan, C. D., Newton., K. M., *et al.,* (2012). 'Biomarkers of progestin therapy resistance and endometrial hyperplasia progression'. *American Journal of Obstetrics and Gynecology, vol. 207, issue 1, p. 36, e1-8.*

Ushida, H., Koizumi, S., Katoh, K., Okabe, H., Okada, Y., Okamoto, K. (2013). 'Recurrent rhabdomyosarcoma after adjuvant chemotherapy for stage I non-seminomatous germ cell tumor with malignant transformation'. *International Journal of Urology, vol. 20, issue 5, pp. 544-6.*

Van Gaal, J. C., Roeffen, M. H., Flucke, U. E., Van der Laak, J. A., Van der Heijden, G., *et al*., (2013). 'Simultaneous targeting of insulin-like growth factor-1 receptor and anaplastic lymphoma kinase in embryonal and alveolar rhabdomyosarcoma: a rational choice'. *European Journal of Cancer, vol. 49, issue 16, pp. 3462-70.*

Van Noesel, M. M., Versteeg, R. (2004). 'Pediatric neuroblastomas: genetic and epigenetic 'danse macabre'. *Gene, vol. 325, pp. 1-15.*

Version 6.5, Copyright 2010, Partek Inc., St. Charles, MO, USA.

Wahlbuhl, M., Reiprich, S., Vogl, MR., Bösl, MR., Wegner, M. (2012). 'Transcription factor Sox10 orchestrates activity of a neural crest-specific enhancer in the vicinity of its gene'. *Nucleic Acids Research, vol. 40, issue 1, pp. 88-101.*

Wai, W. C., Dye, D. E., Coombe, D. R. (2012). 'The role of immunoglobulin superfamily cell adhesion molecules in cancer metastasis'. *International Journal of Cell Biology, vol. 2012, p. 340296.*

Walter, D., Satheesha, S., Albrecht, P., Bornhauser, B. C., D'Alessandro, V., *et al.,* (2011). 'CD133 positive embryonal rhabdomyosarcoma stem-like cell population is enriched in rhabdospheres'. *PLoS One, vol. 6, issue 5, e19506.*

Wan, P., Hu, Y., He, L. (2011). 'Regulation of melanocyte pivotal transcription factor MITF by some other transcription factors'. *Molecular and Cellular Biochemistry, vol. 354, issue 2, pp. 241-6.*

Wang, D., Claus, C. L., Rajkumar, P., Braunstein, M., Moore, A. J., Sigvardsson, M., Anderson, M. K. (2010). 'Context-dependent regulation of hematopoietic lineage choice by HEBAlt'. *Journal of Immunology, vol. 185, issue 7, pp. 4109-17.*

Wang[3], H., Zhu, Y., Zhao, M., Wu, C, Zhang, P., *et al.,* (2013). 'miRNA-29c suppresses lung cancer cell adhesion to extracellular matrix and metastasis by targeting integrin β1 and matrix metalloproteinase2 (MMP2)'. *PLoS One, vol. 8, issue 8, e70192.*

Wang, L. M., Ying, M., Wang, X., Wang, Y. C., Hao, P., Li, N. D. (2009). 'R240X mutation of the PAX6 gene in a Chinese family with congenital aniridia'. *Zhonghua Yi Xue Yi Chuan Xue Za Zhi., vol. 26, issue 5, pp. 546-9.*

Wang, Q., Kumar, S., Mitsios, N., Slevin., M., Kumar, P. (2007). 'Investigation of downstream target genes of *PAX3c, PAX3e* and *PAX3g* isoforms in melanocytes by microarray analysis'. *International Journal of Cancer, vol. 120, issue 6, pp. 1223-31.*

Wang, W., Slevin, M., Kumar, S., Kumar, P. (2005). 'The cooperative transforming effects of PAX3-FKHR and IGF-II on mouse myoblasts'. *International Journal of Oncology, vol. 27, issue 4, pp. 1087-96.*

Wang[1], E. T., Sandberg, R., Luo, S. J., *et al.,* (2008). 'Alternative isoform regulation in human tissue transcriptomes'. *Nature, vol. 456, issue 7221, pp. 470-476.*

Wang[2], J., Kazmi, S. A. (2011). 'Teratoma with Malignant Transformation: A Case Report with Pathological, Cytogenetic and Immunohistochemistry Analysis'. *Sarcoma, vol. 2011, p. 450743.*

Wang[2], Q., Fang, W. H., Krupinski, S., Slevin, M., Kumar, P. (2008). '*PAX* genes in embryogenesis and oncogenesis'. *Journal of Cellular and Molecular Medicine, vol. 12, issue 6A, pp. 228-2294.*

Wang[2], X. D., Morgan, S. C., Loeken, M. R. (2011). '*Pax3* stimulates *p53* ubiquitination and degradation independent of transcription'. *PLoS One, vol. 6, issue 12, e29379.*

Waters, K. M., Sontag, R. L., Weber, T. J. (2013). 'Hepatic leukemia factor promotes resistance to cell death: implications for therapeutics and chronotherapy'. *Toxicology and Applied Pharmacology, vol. 268, issue 2, pp. 141-8.*

Wei, K., Chen, J., Akrami, K., Sekhon, R., Chen, F. (2007). 'Generation of mice deficient for Lbx2, a gene expressed in the urogenital system, nervous system, and Pax3 dependent tissues'. *Genesis, vol. 45, issue 6, pp. 361-8.*

Wentzel, P., Eriksson, U. J. (2011). 'Altered gene expression in rat cranial neural crest cells exposed to a teratogenic glucose concentration in vitro: paradoxical downregulation of antioxidative defense genes'. *Birth Defects Research Part B Developmental and Reproductive Toxicology, vol. 92, issue 5, pp. 487-97.*

White, R. B., Ziman, M. R. (2008). 'Genome-wide discovery of Pax7 target genes during development'. *Physiological Genomics, vol. 33, issue1, pp. 41-9.*

Wiese, C. B., Ireland, S., Fleming, N. L., Yu, J., Valerius, M. T., Georgas, K., Chiu, H. S., *et al.*, (2012). 'A genome-wide screen to identify transcription factors expressed in pelvic Ganglia of the lower urinary tract'. *Fronters in Neuroscience, vol. 6, p. 130.*

Wiggan, O., Shaw, A. E., Bamburg, J. R. (2006). 'Essential requirement for Rho family GTPase signaling in Pax3 induced mesenchymal-epithelial transition'. *Cell Signal, vol. 18, issue 9, pp. 1501-14.*

Wildhardt, G., Zirn, B., Graul-Neumann, L. M., Wechtenbruch, J., Suckfüll, M., *et al.,* (2013). 'Spectrum of novel mutations found in Waardenburg syndrome types 1 and 2: implications for molecular genetic diagnostics'. *BMJ Open, vol. 3, issue 3. e001917.*

Wollnik, B., Tukel, T., Uyguner, O., Ghanbari, A., Kayserili, H., *et al.,* (2003). 'Homozygous and heterozygous inheritance of PAX3 mutations causes different types of Waardenburg syndrome'. *American Journal of Medical Genetics, vol. 122A, issue 1, pp. 42-5.*

Wong[1], J., Mehta, V., Voronova, A., Coutu, J., Ryan, T., Shelton, M., Skerjanc, I. S. (2013). 'β-catenin is essential for efficient in vitro premyogenic mesoderm formation but can be partially compensated by retinoic acid signalling'. *PLoS One, vol. 8, issue 2, e57501.*

Woodruff, J. B., Mitchell, B. J., Shankland, M. (2007). 'Hau-Pax3/7A is an early marker of leech mesoderm involved in segmental morphogenesis, nephridial development, and body cavity formation'. *Developmenta Biology, vol. 306, issue 2, pp. 824-37.*

Wouters, J., Stas, M., Gremeaux, L., Govaere, O., Van den Broeck, A., *et al.,* (2013). 'The Human Melanoma Side Population Displays Molecular and Functional Characteristics of Enriched Chemoresistance and Tumorigenesis'. *PLoS One, vol. 8, issue 10, e76550.*

Wu, M., Li, J., Engleka, KA., Zhou, B., Lu, M. *et al.,* (2008). 'Persistent expression of Pax3 in the neural crest causes cleft palate and defective osteogenesis in mice'. *Journal of Clinical Investigations, vol.118, issue 6, pp. 2076-87.*

Xao, X. T., Hiroyuki, S. (2013). 'Clinical Implications of Neuroblastoma Stem Cells, Neuroblastoma, *ISBN: 978-953-51-1128-3, InTech, DOI: 10.5772/56254.*

Xia, L., Huang, Q., Nie, D., Shi, J., Gong, M., Wu, B. (2013). '*PAX3* is overexpressed in human glioblastomas and critically regulates the tumourigenicity of glioma cells'. *Brain Research, vol. 1521, pp. 68-78.*

Xia, S. J., Holder, D. D., Pawel, B. R., Zhang, C., Barr, F. G. (2009). 'High expression of the PAX3-FKHR oncoprotein is required to promote tumorigenesis of human myoblasts'. *American Journal of Pathology, vol. 175, issue 6, pp. 2600-8.*

Xia, S. J., Rajput, P., Strzelecki, D. M., Barr, F. G. (2007). 'Analysis of genetic events that modulate the oncogenic and growth suppressive activities of the PAX3-FKHR fusion oncoprotein'. *Laboratory Investigations, vol. 87, issue 4, pp. 318-25.*

Xu, B., Hariharan, A., Rakshit, S., Dressler, G. R., Wellik, D. M. (2012). 'The role of Pax2 in mouse prostate development'. *Prostate, vol. 72, issue 2, pp. 217-24.*

Xynos, A., Corbella, P., Belmonte, N., Zini, R., Manfredini, R., Ferrari, G. (2010). 'Bone marrow-derived hematopoietic cells undergo myogenic differentiation following a Pax-7 independent pathway'. *Stem Cells, vol., 28, issue 5, pp. 965-73.*

Yamaguchi, K., Koga, Y., Suminoe, A., Saito, Y., Matsuzaki, A., *et al*., (2007). 'Alveolar rhabdomyosarcoma of unknown origin mimicking acute leukemia at the initial presentation'. *Rinsho Ketsueki, vol. 48, issue 4, pp. 315-20.*

Yamaguchi[1], Y., Hearing, V. J. (2009). 'Physiological factors that regulate skin pigmentation'. *Biofactors, vol. 35, issue 2, pp. 193-9.*

Yamauchi[2], J. (2009). 'Signaling mechanism underlying myelination in peripheral nervous system'. *Seikagaku, vol. 81, issue 7, pp. 565-80.*

Yan[3], R., Peng, X., Yuan, X., Huang, D., Chen, J., *et al*., (2013). 'Suppression of growth and migration by blocking the Hedgehog signaling pathway in gastric cancer cells'. *Cellular Oncology, vol. 36, issue 5, pp. 421-35.*

Yang, F., Jove, V., Xin, H., Hedvat, M., Van Meter, T. E., Yu, H. (2010). 'Sunitinib induces apoptosis and growth arrest of medulloblastoma tumour cells by inhibiting STAT3 and AKT signaling pathways'. *Molecular Cancer Research, vol. 8, issue 1, pp. 35-45.*

Yang, G., Li, Y., Nishimura, E. K., Xin, H., Zhou, A., *et al*., (2008). 'Inhibition of *PAX3* by *TGF-beta* modulates melanocyte viability'. *Molecular Cell*, *vol. 32, issue 4, pp. 554-63.*

Yang[1], J., Zheng, Z., Yan, X., Li, X., Liu, Z., Ma, Z. (2013). 'Integration of autophagy and anoikis resistance in solid tumours'. *Anatomical Record, vol. 296, issue 10, pp. 1501-8.*

Yang[2], T., Li, X., Huang, Q., Li, L., Chai, Y., *et al.,* (2013). 'Double heterozygous mutations of MITF and PAX3 result in Waardenburg syndrome with increased penetrance in pigmentary defects'. *Clinical Genetics, vol. 83, issue 1, pp. 78-82.*

Yang[1], D., Lai, D., Huang, X., Shi, X., Gao, Z., Huang, F., Zhou, X., Geng, Y. J. (2012). 'The defects in development and apoptosis of cardiomyocytes in mice lacking the transcriptional factor Pax-8'. *International Journal of Cardiology, vol. 154, issue 1, pp. 43-51.*

Yang[2], X. L., Zhang, S. C., Zhang, S. W., Wang, H. (2012). 'Detection of PAX3/PAX7-FKHR fusion transcripts in rhabdomyosarcoma and other small round cell tumours by 1-step reverse transcriptase polymerase chain reaction: a novel tool for diagnosis and differentiation'. *Annals of Diagnostic Pathology, vol. 138, pp. 213-220.*

Ying, M., Wang, S., Sang, Y., Sun, P., Lal, B., *et al.,* (2011). 'Regulation of glioblastoma stem cells by retinoic acid: role for Notch pathway inhibition'. *Oncogene, vol. 30, issue 31, pp. 3454-67.*

Yoo, Y. D., Huang, C. T., Zhang, X., Lavaute, T. M., Zhang, S. C. (2011). 'Fibroblast growth factor regulates human neuroectoderm specification through ERK1/2-PARP-1 pathway'. *Stem Cells, vol. 29, issue 12, pp. 1975-82.*

Yoshida, H., Miyachi, M., Sakamoto, K., Ouchi, K., Yagyu, S., Kikuchi, K., *et al*., (2013). 'PAX3-NCOA2 fusion gene has a dual role in promoting the proliferation and inhibiting the myogenic differentiation of rhabdomyosarcoma cells'. *Oncogene, doi: 10.1038/onc.2013.491.*

Yu[2], Z., Kelsey, A., Alaggio, R., Parham, D. (2012). 'Clinical utility gene card for: Alveolar rhabdomyosarcoma'. *European Journal of Human Genetics, vol. 20, issue 1. doi: 10.1038/ejhg.2011.147.*

Yuan, H., Qin, F., Movassagh, M., Park, H., Golden, W., Xie, Z., *et al.,* (2013). 'A chimeric RNA characteristic of rhabdomyosarcoma in normal myogenesis process'. *Cancer Discovery, vol. 3, issue 12, pp. 1394-403.*

Yvernogeau, L., Auda-Boucher, G., Fontaine-Perus, J. (2012). 'Limb bud colonization by somite-derived angioblasts is a crucial step for myoblast emigration'. *Development, vol. 139, issue 2, pp. 277-87.*

Zebda, N., Tian, Y., Tian, X., Gawlak, G., Higginbotham, K., *et al.,* (2013). 'Interaction of p190RhoGAP with C-terminal domain of p120-catenin modulates endothelial cytoskeleton and permeability'. *Journal of Biological Chemistry, vol. 288, issue 25, pp. 18290-9.*

Zeng, F. Y., Cui, J., Liu, L., Chen, T. (2009). 'PAX3-FKHR sensitizes human alveolar rhabdomyosarcoma cells to camptothecin-mediated growth inhibition and apoptosis'. *Cancer Letters, vol. 284, issue 2, pp. 157-64.*

Zhang[1], H., Chen, H., Luo, H., An, J., Sun, L., Mei, L., *et al.,* (2012). 'Functional analysis of Waardenburg syndrome-associated *PAX3* and *SOX10* mutations: report of a dominant-negative *SOX10* mutation in Waardenburg syndrome type II'. *Human Genetics, vol. 131, issue 3, pp. 491-503.*

Zhang[2], L., Yuan, G., Liu, H., Lin, H., Wan, C., Chen, Z. (2012). 'Expression pattern of Sox2 during mouse tooth development'. *Gene Expression Patterns, vol. 12, issue 8, pp. 273-281.*

Zhang[1], J., Wang, X., Cui, W., Wang, W., Zhang, H., Liu, L., *et al*., (2013). 'Visualization of caspase-3-like activity in cells using a genetically encoded fluorescent biosensor activated by protein cleavage'. *Nature Communications, vol. 4, issue 2157.*

Zhang, Y., Wang, C. (2011). 'Nephroblastoma overexpressed (NOV/CCN3) gene: a paired-domain-specific PAX3-FKHR transcription target that promotes survival and motility in alveolar rhabdomyosarcoma cells'. *Oncogene, vol. 30, issue 32, pp. 3549-62.*

Zhang[1]. Y., Liu. X. H. (2009). 'Expression of nNOS, Pax3 and Cx43 proteins in early developing posterior horn of embryonic and fetal human spinal cord'. *Nan Fang Yi Ke Da Xue Xue Bao, vol. 29, issue 8, pp. 1651-3.*

Zhang[2], Z., Xin, D., Wang, P., *et al.,* (2009). 'Noisy splicing, more than expression regulation, explains why some exons are subject to nonsense-mediated mRNA decay'. *BMC Biology, vol. 7, issue 23.*

Zhang[3], X., Liu, L., Chen, C., Chi, Y. L., Yang, X. Q., Xu, Y., *et al*., (2013). 'Interferon regulatory factor-1 together with reactive oxygen species promotes the acceleration of cell cycle progression by up-regulating the cyclin E and *CDK2* genes during high glucose-induced proliferation of vascular smooth muscle cells'. Cardiovasc Diabetol., vol. 12, issue 11, pp.147.

Zhao, J. L., Chen, Y. X., Bao, L., Wu, T. J., Zhou, L. (2005). 'Functional analysis of novel mutations in PAX9 associated with familial oligodontia'. *Zhonghua Yi Xue Yi Chuan Xue Za Zhi., vol. 22, issue 4, pp. 419-22.*

Zhao, J., Hu, Q., Chen, Y., Luo, S., Bao, L., Xu, Y. (2007). 'A novel missense mutation in the paired domain of human *PAX9* causes oligodontia'. *American Journal of Medical Genetics, vol. 143A, issue 21, pp. 2592-7.*

Zhao[3], T., Gan, Q., Stokes, A., Lassiter, R. N., Wang, Y., Chan, J., *et al*., (2013). 'β-catenin regulates Pax3 and Cdx2 for caudal neural tube closure and elongation'. *Development, vol. 141, issue 1, pp. 148-57.*

Zhao, W., Dai, F., Bonafede, A., Schafer, S., Jung, M., *et al.,* (2009). 'Histone deacetylase inhibitor, trichostatin A, affects gene expression patterns during morphogenesis of chicken limb buds in vivo'. *Cells Tissues Organs, vol. 190, issue 3, pp. 121-34.*

Zhao[2], X., Li, Z., He, B., Liu, J., Li, S., Zhou, L., *et al.,* (2013). 'Sam68 is a novel marker for aggressive neuroblastoma'. *Journal of OncoTargets and Therapy, vol. 6, pp. 1751-60.*

Zhou, H. M., Wang, J., Rogers, R., Conway, S. J. (2008). 'Lineage-specific responses to reduced embryonic *Pax3* expression levels'. *Developmental Biology, vol. 315, issue 2, pp. 369-82.*

Zhu, J., Yang, X., Zhang, C., Ge, L., Zheng, S. (2012). 'A novel nonsense mutation in PAX9 is associated with sporadic hypodontia'. *Mutagenesis, vol. 27, issue 3, pp. 313-7.*

Zibat, A., Missiaglia, E., Rosenberger, A., Pritchard-Jones, K., Shipley, J., *et al.,* (2010). 'Activation of the hedgehog pathway confers a poor prognosis in embryonal and fusion gene-negative alveolar rhabdomyosarcoma'. *Oncogene, vol. 29, issue 48, pp. 6323-30.*

Zohn I., E. (2012). 'Mouse as a model for multifactorial inheritance of neural tube defects'. *Birth Defects Research Part C: Embryo Today: Reviews, vol. 96, Issue 2, pp. 193-205.*

Zong, X., Yang, H., Yu, Y., Zou, D., Ling, Z., He, X., Meng, X. (2011). 'Possible role of Pax-6 in promoting breast cancer cell proliferation and tumorigenesis'. *BMB Reports, vol. 44, issue 9, pp. 595-600.*

Zutter, M. M. (2007). 'Integrin-mediated adhesion: tipping the balance between chemosensitivity and chemoresistance'. *Advances in Experimental Medicine and Biology, vol. 608, pp. 87-100.*

Appendix A : Map of Inducible PAX3-PBabe HAER plasmid vector

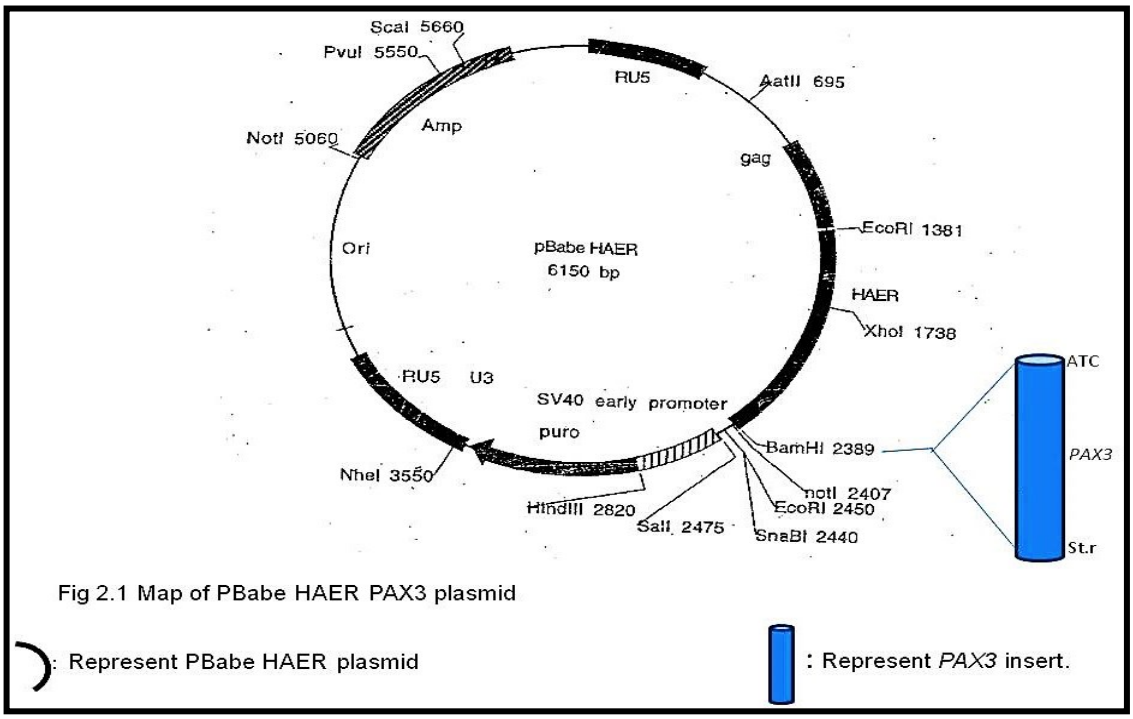

PAX3-PBabe-HAER plasmid vector DNA and PBabe-HAER empty plasmid vector were constructed by Kristian Helin and Karin Holm of the Biotech Research and Innovation Centre (BRIC). The PBabe puro backbone plasmid was cloned with a modified oestrogen receptor (ER) and *PAX3* gene HA-tag. *PAX3*-PBabe-HAER plasmid of a reading frame of GGA TCC was then cloned into the BamH site to put ORFs with an HA-tagged ER on the N-terminus.

Appendix B: *PAX3*-PBabe HAER Plasmid DNA and empty vector PBabe HAER plasmid DNA

Both *PAX3*-PBabe-HAER and empty vector PBabe-HAER plasmid DNA were recovered from a whatman filter paper and then used to transform a competent *E.coli DH5α* strain cells that were previously prepared using the calcium chloride protocol (Sambrook and Russel, 2002). Triplicates extracted *PAX3*-PBabe-HAER plasmid DNA (test) and empty vector plasmid DNA (negative control) showed three consistent non-degraded DNA bands of different sizes, consist of an open circular DNA (~23,130bp) undergoing DNA synthesis (**Fig A-A**), relaxed open circular DNA (~20000bp) (**Fig A-B**) and a super coiled DNA with *PAX3* insert (~6500bp) (**Fig A-C**). Extracted triplicate empty vector plasmid DNA also showed two consistent non-degraded DNA bands made up of relaxed open circular DNA(~20000bp) (**Fig A-D)** and super coiled DNA (~4361bp) (**Fig A-E**).

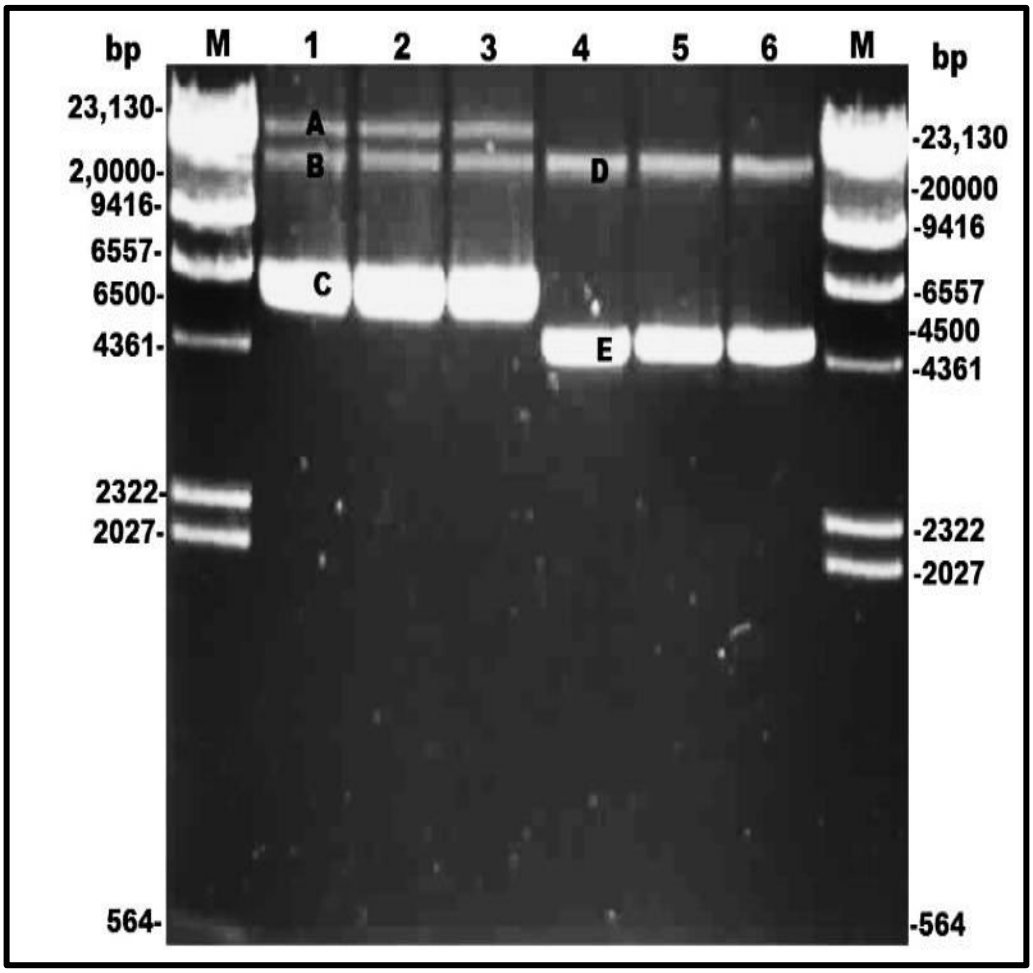

Figure A 0.8% Agarose gel, ethidium bromide stained of extracted *PAX3*-PBABE HAER plasmid DNA. Lane **M:** Lambda DNA HindIII marker (125bp-23.1 kb); Lanes **1-3:** *PAX3*-PBabe HAER Plasmid DNA; Lanes **4-6:** Empty plasmid DNA. **A.** *PAX3*-PBabe HAER plasmid DNA consists of open circular DNA undergoing DNA synthesis (~23,130bp). **B.** Relaxed open circular DNA (~20000bp) and C. Super coiled DNA with *PAX3* insert (~6500bp). **D.** Extracted empty plasmid vector DNA consist of relaxed open circular DNA (~20000bp) and **E.** Super coiled DNA without PAX3 insert (~4500bp)

APPENDIX C: PREPARATION OF WORKING SOLUTIONS

Sample Buffer

Tris-base	1.51g
SDS	4g
DDH_2O	25ml
Glycerol	20ml
PH	6.8
2-mercaptoethanol	10ml
Bromophenol blue	0.004g
H_2O	100ml

Filtered and freeze until used

1.51g Tris-base and 4g SDS were weighed and dissolved in 25ml ddH_2O with a magnetic stirrer in a clean 200ml beaker. 20ml glycerol was added, mixed with a magnetic stirrer to form homogenous mixture and PH adjusted to 6.8. 10ml 2-mercaptoethanol, 0.004g bromophenol blue and 100ml ddH_2O was added and stirred to mix well. The mixture was filtered and aliquots were frozen until used.

Separation Buffer

SDS	1g
Tris-base	45.4g
DDH_2O	250ml
PH	8.8

Store at RT

1g SDS and 45.4g Tris-base were weighed and dissolved in 250ml ddH_2O with a magnetic stirrer in a clean 250ml beaker to form homogenous mixture and PH adjusted to 8.8. The mixture was stored at RT until used

Stucking Buffer

SDS	1g
Tris-base	15g
H_2O	250ml
PH	6.8

Store at RT

1g SDS and 15g Tris-base were weighed and dissolved in 250ml ddH_2O with a magnetic stirrer in a clean 250ml beaker to form homogenous mixture and PH adjusted to 6.8. The mixture was stored at RT until used

Electrode Buffer

Tris-base	12.02g
SDS	4g
Glycine	57.68g
H_2O	2L
Store at	RT

12.02g Tris-base, 4g SDS and 57.68g glycine were weighed and dissolved in 2L ddH_2O with a magnetic stirrer in a clean beaker to form homogenous mixture. The mixture was stored at RT until used.

Towbin Buffer

Tris-base	1.5g
SDS	0.167g
Glycine	7.2g
Methanol	75ml
H_2O	500ml
PH	8.3
Store at RT	

1.5g Tris-base, 0.167g SDS and 7.2g glycine were weighed and dissolved in 75ml methanol with a magnetic stirrer in a clean beaker to form homogenous mixture. 500lm ddH_2O was added, well mixed and PH adjusted to 8.3. The mixture was stored at RT until used.

Persulphate

APS	100mg
ddH_2O	1ml
Store at	4°C

100mg APS was weighed, dissolved 1ml ddH_2O and stored at 4°C until used.

TBS-Tween

Tris-base	2.422g
Nacl	16.36g
H_2O	2L
Tween	2ml
PH	7.4
Store at	RT for 10 days

2.422g Tris-base and 16.36g SDS were weighed and dissolved in 2L of ddH_2O with a magnetic stirrer in a clean beaker. 2ml tween 20 added, well mixed and PH adjusted to 7.4. The mixture was stored at RT for 10 days.

1% Bovine Serum Albumin

BSA	1g
TBS-tween	100ml
PH	7.4
Store at	4°C

1g BSA was weighed, dissolved in 100ml TBS-tween and PH adjusted to 7.4. The mixture was stored at 4°C until used

5% Milk

Dry non-fat milk	5g
TBS-Tween	100ml
PH	7.4
Store at	4°C for 1 week

5g dry milk was weighed, dissolved in 100ml TBS-tween and PH adjusted to 7.4. The mixture was stored at 4°C for 1 week until used.

ECL Working Solution

ECL solution A	1ml
ECL solution B	1m

Equal volumes of ECL solutions A and B were mixed and used immediately.

0.8 % Agarose

Agarose	0.8g
1 in 10 TBE	100ml

1.5% Agarose

Agarose	1.5g
1 in 10 TBE	100ml

0.8g or 1.5g agarose powder was weighed into a cleaned beaker containing 100ml of diluted TBE buffer and microwaved at 1 horsepower for 2 min to completely dissolve the agarose powder. The mixture was allow to cool to 60º at RT and then agarose gels were casted and allowed to cool at RT for 30 min.

5% Stock Agar

Agar	5g
DDH_2O	100ml

5g agar powder was dissolved in 100ml of ddH_2O in sterile bottle and microwaved at 1 horsepower for 2 min to completely dissolve the agar powder. The mixture was tightly closed, allowed to cool to 50ºC at RT for 30 min and the stored at 4ºC until used.

0.8% Agar base

5% Stock Agar	0.8ml
DDH_2O	99.2ml

In a safety cabinet, 99.2ml sterile ddH_2O was mixed with 0.8ml stock ager and 5ml of the mixture dispensed into 38 well plates and the stored at 4ºC until used.

0.3% top Agar

5% stock Agar	0.3ml
DMEM suspension cells	99.7ml

In a safety cabinet, 99.7ml DMEM discrete suspension a cell was mixed with 0.3ml warmed stock ager (at 37ºC). 0.5ml of the mixture was dispensed onto the 0.8% ager base in 38 well plates previously warmed at 37 ºC in the incubator. The cells were allowed to settle for 10 min and then incubated at 37 ºC.